Evaluating the Role of 3D Visualisation in Colorectal Cancer Surgery Decision Making

PhD Thesis

Jordan Fletcher

BSc (Hons) MbChB (Hons) Med

Department of Surgery and Cancer

Imperial College London

St Mark's Hospital and Academic Institute, London UK

Supervisors

Mr Danilo Miskovic PhD

Department of Colorectal Surgery, St Mark's Hospital

Department of Surgery and Cancer, Imperial College London

Dr Phillip Lung MBBS FRCR

Department of Radiology, St Mark's Hospital

Professor George Hanna

Department of Surgery and Cancer, Imperial College London

Declaration

I hereby declare that I am the sole author of this thesis and that all work within it is my own. All else and any individuals who carried out any collaborative work are appropriately credited and referenced.

Copyright Declaration

The copyright of this thesis rests with the author. Unless otherwise indicated, its contents are licensed under a Creative Commons Attribution-Non-Commercial 4.0 International Licence (CC BY-NC). Under this licence, you may copy and redistribute the material in any medium or format. You may also create and distribute modified versions of the work. This is on the condition that: you credit the author and do not use it, or any derivative works, for a commercial purpose. When reusing or sharing this work, ensure you make the licence terms clear to others by naming the licence and linking to the licence text. Where a work has been adapted, you should indicate that the work has been changed and describe those changes. Please seek permission from the copyright holder for uses of this work that are not included in this licence or permitted under UK Copyright Law.

Ethics

Ethical approval for the research studies presented in this thesis was obtained from the Wales Research Ethics Committee (REC) 6 and the Health Research Authority. These approvals cover the relevant components of the work under REC reference 19/WA/0332 (IRAS ID: 263892) and IRAS ID: 266848. Local research governance approvals were also secured from the Research and Development departments at each participating site, including London North West University Healthcare NHS Trust (United Kingdom), Ikazia Hospital (Rotterdam, The Netherlands), and the Mater Misericordiae University Hospital (Dublin, Ireland). All participants provided written informed consent prior to inclusion in the relevant studies. All research activities were conducted in accordance with the ethical principles set out in the Declaration of Helsinki, with strict adherence to data confidentiality and participant anonymity throughout.

Thesis abstract

Recent advancements in three-dimensional (3D) visualisation show promise for enhancing anatomical understanding and surgical precision, particularly in procedures such as complete mesocolic excision (CME) and pelvic exenteration for advanced rectal cancer. Despite potential benefits in preoperative planning, intraoperative guidance, and patient education, routine adoption remains limited. The absence of well-defined frameworks for systematic evaluation and integration contributes to variable uptake and hinders consensus on best practice. Further research is required to standardise implementation and appraisal methodologies, enabling broader adoption and robust clinical evidence generation.

This thesis addresses these limitations by developing, evaluating, and integrating patient-specific 3D anatomical models into the continuum of advanced colorectal cancer surgery. The research spans four domains: (1) technical innovation and validation of scalable workflows for generating high-quality models from standard imaging; (2) establishment of standardised frameworks for assessing accuracy, educational impact, and clinical utility; (3) evaluation of clinical feasibility in CME; and (4) application in improving patient comprehension and decision-making for pelvic exenteration. Methods include advanced image segmentation and mesh processing, systematic reviews of evaluation methods, and mixed-methods studies with surgical trainees, expert CME surgeons, and patients.

Key findings show that 3D reconstructions achieve high accuracy in predicting mesenteric vascular anatomy, significantly improve surgeons' anatomical understanding, and enhance inter- and intra-rater reliability for CME planning. Patient-centred applications demonstrated improved understanding of surgical procedures, reduced decisional conflict, and support for shared decision-making. Surgeons reported practical value in both preoperative and intraoperative settings.

This work provides validated technical workflows, proposes evaluation frameworks, and demonstrates educational and clinical benefits. Findings establish a foundation for future research, including automated model generation and large-scale trials to assess long-term clinical outcomes. Addressing both technical and patient-centred dimensions, this thesis underscores the role of 3D visualisation in advancing surgical precision, safety, and collaborative decision-making in advanced colorectal cancer care.

Abbreviations

API	Application programming interface
AR	Augmented reality
ASPDV	Anterior superior pancreaticoduodenal vein
BJ	Binding jet
CCC	Complex cancer clinic
CME	Complete mesocolic excision
CNN	Convolutional neural network
CT	Computed tomography
DCS	Decisional conflict score
DICOM	Digital imaging and communication in medicine
EM	Electromagnetic
FBX	Film box 3D file format
FDM	Fused deposition modelling
FFF	Fused filament fabrication
GEV	Gastroepiploic vein
GPU	Graphical processing unit
HU	Hounsfield intensity
ICA	Ileocaecal artery
ICV	Ileocaecal vein
LPLND	Lateral pelvic lymph node dissection
LPSW	Lateral pelvic sidewall
MCA	Middle colic artery
MCV	Middle colic vein
MKV	Matrsoska
MLP	Multi-layer perceptron
MRI	Magnetic resonance imaging
OBJ	Wavefront 3D file format
PBR	Physically based rendering
PJ	Polyjet
RCA	Right colic artery
RCV	Right colic vein
RCT	Randomised controlled Trial
RRC	Recurrent rectal cancer
SLA	Stereolithography
SLS	Selective laser scintering
SMA	Superior mesenteric artery
SMV	Superior mesenteric vein
SRCV	Superior right colic vein
STL	Stereolithography 3D file format
TME	Total mesorectal excision
UC	Ulcerative colitis

UI	User interface
UX	User experience
VATS	Video assisted thorascopic surgery
ViT	Visual transformer
VR	Virtual reality

Peer reviewed publications and presentations

Poster presentations

- **Fletcher J**, Lung P, Van Eetvelde, Bertelsen, Stearns, Storli K, Miskovic D. Inter-rater and Intra-rater Reliability of Multi-Slice CT and 3D Reconstructed Imaging Analysis of Mesenteric Vascular Anatomy for Planning and Performing Complete Mesocolic Excision. ACPGBI, Wales 2024
- Iqbal N, **Fletcher J**, Hart A, Lung P, Tozer P. The clinical utility of 3D printed anal fistula models for patient understanding and decision-making: Results from a randomised controlled pilot study. Association of Coloproctology of Great Britain and Ireland (ACPGBI) Annual Meeting July 2022.
- **Fletcher J**, Gould L, Pring, T, Burling D, Miskovic D, Lung P, Jenkins J.
- Fletcher J, Lung P, Burling D, Burns E, Miskovic D, Jenkins JT. Development of patient specific 3D models for planning beyond-TME resections in advanced rectal cancer. ESCP, Vienna. September 2019

Oral Presentations

- **Fletcher J**, Drami I, Lung P, Burling D, Burns E, Miskovic D, Jenkins JT. Personalised 3D imaging enhances comprehension and Decision making in Pelvic Exenteration Surgery. BJS Prize Session ACPGBI 2024 and Brunschwig Prize Session PelvEx 2024.
- **J Fletcher**, T Heinze, T Wedel, D Miskovic. Digital Human Project: 3D Photogrammetry for Human Cadaveric Pelvic Specimens: An Innovation in Colorectal Anatomical Education. ESCP 2020

Invited presentations

- **J Fletcher** Image guided surgery and augmented reality for colorectal cancer. Champalimaud Colorectal Cancer Conference 2023.
- **J Fletcher** Image Guided Surgery in Pelvic exenteration. PelvEx Bordeaux 2023
- **J Fletcher** 3D modelling and machine learning in Colorectal Surgery. BASO 2021

- **J Fletcher** Role of 3D visualisation and printing techniques in Colorectal Surgery- ESCP 2019

Publications

- **Fletcher J,** Corr A, Drami I, Taylor C, Hona T, Burling D, Lung P, Burns E, Jenkins JT. Enhancing decision-making and patient comprehension in complex rectal cancer surgery through personalised three- dimensional imaging: randomised feasibility study. *BJS*, Volume 112, Issue 6, June 2025. https://doi.org/10.1093/bjs/znaf116
- **Fletcher J**, Lung P, Van Eetvelde, Bertelsen, Stearns, Storli K, Miskovic D. Inter-rater and Intra-rater Reliability of Multi-Slice CT and 3D Reconstructed Imaging Analysis of Mesenteric Vascular Anatomy for Planning and Performing Complete Mesocolic Excision. *Colorectal Dis*. 2025; 27:e70025. https://doi.org/10.1111/codi.70025
- **Fletcher J,** Miskovic D. Computer-Generated modelling in surgery. Seminars in Colon and Rectal Surgery. 2024 Mar; 35(1) https://doi.org/10.1016/j.scrs.2024.101003
- Iqbal N, **Fletcher J**, Basset P, Hart A, Lung P, Tozer P. Exploring methods of improving patient understanding and communication in a complex anal fistula clinic: results from a randomized controlled feasibility study. Colorectal Dis. 2024 Mar; 26(3): 518-526.
- **Fletcher J**, Ilangovan R, Hanna G, Miskovic D, Lung P. The impact of three-dimensional reconstruction and standardised CT interpretation (AMIGO) on the anatomical understanding of mesenteric vascular anatomy for planning complete mesocolic excision surgery: A randomised crossover study. Colorectal Dis. 2022 Apr;24(4):388-400. doi: 10.1111/codi.16041. Epub 2022 Feb 3. PMID: 34989089.
- Corr, **J. Fletcher**, J.T. Jenkins, D. Miskovic. Image-guided pelvic exenteration-preoperative and intraoperative strategies. European Journal of Surgical Oncology. https://doi.org/10.1016/j.ejso.2022.08.002
- Przedlacka A, Pellino G, **Fletcher J**, Bello F, Tekkis PP, Kontovounisios C. Current and future role of three-dimensional modelling technology in rectal cancer surgery: A systematic review. World J Gastrointest Surg. 2021 Dec 27;13(12):1754-1769. doi: 10.4240/wjgs.v13.i12.1754. PMID: 35070078; PMCID: PMC8727188.
- **Fletcher J**, Behrenbruch C, Lung P, Miskovic D. Robotic right complete mesocolectomy with patient-specific three-dimensional modelling for planning and intra-operative navigation - a video vignette. Colorectal Dis. 2021 Aug;23(8):2211-2212. doi: 10.1111/codi.15738. Epub 2021 Jul 27. PMID: 33991393.

Other publications involving 3D models:

- Heinz T, **Fletcher JA**, Miskovic D, Stelzner S, Bayer A, Wedel T. The middle rectal artery- revisited anatomy and surgical implications of a neglected blood vessel. Diseases of the Colon and Rectum.2023 Mar 1;66(3):477-485. doi: 10.1097/DCR.0000000000002531.
- Heinze T**, Fletcher J**, Miskovic D, Benz S, Heimke M, Stelzner S, and Wedel T. The retrocolic fascial system revisited for right hemicolectomy with complete mesocolic excision based on anatomical terminology. Do we need the eponyms Toldt, Gerota, Fredet, and Treitz? Colorectal Disease. 2022 PMID: 36457274 DOI: 10.1111/codi.16436
- **Fletcher J**, Miskovic D. The mesentery in complete mesocolic excision. Clin Colon Rectal Surg. Aug 22. PMID: 35966980 PMCID: PMC9365457 DOI: 10.1055/s-0042-1743430

Book chapters

- **Fletcher J**, Miskovic D. Chapter 25- Digital and 3D models for Surgical Planning from Digital Surgery. Springer Surgery. 2020.

- **Fletcher J**- Methods and Applications of 3D Patient-Specific Virtual Reconstructions in Surgery. P53-71. Biomedical Visualisation vol.12 part of Advances in Experimental Medicine and Biology Series. Springer. 2022.

Contributors and collaborators

Development and Validation of a 3D Modelling Pipeline for Surgical Planning and Patient Education

Dr Lorenz Berger & Dr Matt Gibb (Innersight Labs) Provided technical/code input with respect to automated surface rendered model workflow.

Systematic Review of Evaluation Methodologies for 3D Models in Surgical Planning

Nusrat Iqbal, Anna Sayers, Anna Przedlacka, Laura Gould (Clinical research fellows, St Marks Hospital). Second reviewers for screening and data extraction and bias assessments.

Impact of 3D Reconstructions on Understanding of Mesenteric Vascular Anatomy (Trainees and Experts)

Anders Bertelsen (Consultant Colorectal Surgeon Copenhagen University Hospital – North Zealand, Hillerød, Denmark), Ellen Van Eetvelde (Consultant Surgeon- University Hospital UZ Brussel, Jette, Belgium) , Kristian Storli (Consultant Colorectal Surgeon, Haraldsplass Deaconess Hospital, University of Bergen, Bergen, Norway) and Adam Stearns (Consultant colorectal Surgeon Norfolk and Norwich University Hospitals NHS Foundation Trust, Norwich, UK). Conducted CT Imaging and 3D model interpretation.

Paul Basset (Statsconsultancy Ltd.) statistical input regarding the interrater reliability study Innersight Labs for access to their 3D visualisation platform for the interrater reliability study.

Feasibility and Early Clinical Integration of 3D Models for Complete Mesocolic Excision (CME)

Dr Boudwijn Toorenvliet, Dr Joost Nooner (Consultant Colorectal Surgeons- Ikazia Hospital Rotterdam, Netherlands), Professor Ronan Cahill (Colorectal Surgeon,Mater Hosptial Dublin)- patient recruitment and study participants.

Patient-Centred Communication and Decision-Making: The Role of 3D Models in Pelvic Exenteration for Advanced Colorectal Cancer

Ioanna Drami (Clinical research fellow, St Marks Consultant)- qualitative interview second coder, data collection, Dr Claire Taylor (Cancer Nurse Consultant, St Marks Hospital complex cancer clinic)- study protocol review and patient recruitment

Table of Contents

Introduction to Three-Dimensional Visualisation in Surgical Practice 26

Overall Aim and Scope of Thesis: 28

Key challenges motivating this research: 28

Philosophical and Methodological Foundations: 29

Chapter 1: Literature review of 3D reconstruction and visualisation methods, applications in Colorectal Surgery 31

Chapter 2: Development and Validation of a 3D Modelling Pipeline for Surgical Planning and Patient Education 31

Chapter 3: Systematic Review of Evaluation Methodologies for 3D Models in Surgical Planning 32

Chapter 4: Impact of 3D Reconstructions on Understanding of Mesenteric Vascular Anatomy (Trainees and Experts) 33

Chapter 5: Feasibility and Early Clinical Integration of 3D Models for Complete Mesocolic Excision (CME) 34

Chapter 6: Patient-Centered Communication and Decision-Making: The Role of 3D Models in Pelvic Exenteration for Advanced Colorectal Cancer 35

Chapter 7: Discussion 36

1 Literature review of 3D reconstruction and visualisation methods, applications in Colorectal Surgery 37

1.1 Technical Foundations 37

1.1.1 Medical Image Processing 37

1.2 Segmentation Approaches 41

1.2.1 Manual Segmentation 41

1.2.2 Automated Segmentation in Abdominal-Pelvic Imaging: Challenges and Limitations of Classical Techniques 44

1.3 Deep Learning and Segmentation 47

1.3.1 Neural Networks: Theoretical Underpinnings 47

1.3.2 . Advanced Architectures for Segmentation 48

1.3.3 U-Net and Its Variants 52

1.3.4 Transformer-Based Architectures 55

1.4 Rendering Methods in 3D visualisation 57

1.4.1 Volumetric Rendering 57

1.4.2 Surface Rendering 60

1.4.3 Surface rendering methods 63

1.4.4 Advanced 3D modelling techniques 66

1.5 Visualisation methods 71
1.5.1 WebGL and Three.js 71
1.5.2 Game Engines 72
1.5.3 Specialised Commercial Software 73
1.5.4 3D printing 73
1.6 3D models in surgical practice 76
1.6.1 Preoperative planning 76
1.6.2 3D model surgical navigation 83
1.6.3 3D models in surgical patient education 87
1.7 The Application of Three-Dimensional Modelling in Colorectal Surgery 89
1.7.1 Three-Dimensional Modelling in Preoperative Planning 89
1.7.2 Three-Dimensional Modelling in Rectal Cancer Surgery 92
1.7.3 Three-Dimensional Modelling in Inflammatory bowel disease 95
1.7.4 Impact on Surgical Education and Training 98
2 Development of Advanced 3D Visualisation Tools for Complex Colorectal Cancer Surgery 99
2.1 Introduction 99
2.2 Background and requirements 100
2.2.1 Clinical context 100
2.2.2 Needs analysis. 100
2.3 Research Aims and Objectives 103
2.3.1 Primary Aim 103
2.3.2 Specific Objectives 103
2.4 Methodology Overview 104
2.4.1 Development Philosophy 104
2.5 Technical approach 108
2.5.1 Automated Visualisation Framework for Complete Mesocolic Excision 108
2.5.2 Patient-Specific Educational Models for Pelvic Exenteration 108
2.6 Technical implementation: Image segmentation 110
2.6.1 Complete mesocolic excision 110
2.6.2 Pelvic exenteration 111
2.7 Technical Implementation: CME Visualisation 112
2.7.1 Mesh Extraction 112
2.7.2 Mesh optimisation and processing. 117
2.7.3 3D model file format exports 125
2.8 Web-Based Visualisation application 128
2.8.1 Architectural Overview 128

2.9 Technical implementation: Patient education models for Pelvic exenteration 131
2.9.1 Model Production Workflow 131
2.9.2 Texturing Workflow 136
2.9.3 Online Model Visualisation and Interactive Interface 140
2.10 Quality Assurance and Validation of Mesh Processing Pipeline 142
2.10.1 Mean Surface Distance Change 143
2.10.2 Hausdorff Distance 143
2.10.3 Edge Length Ratio 143
2.11 Discussion 150
2.11.1 Limitations and Challenges 150
2.11.2 Web Platform Implementation and Interface Design 151
2.11.3 Integration Challenges and Future Directions 151
2.12 Conclusion 152
3 Systematic review of the use and evaluation of 3D patient-specific model for pre-operative surgical planning 153
3.1 Background 153
3.2 Rationale. 154
3.3 Objective 154
3.4 Methods 154
3.4.1 Protocol 154
3.4.2 Eligibility criteria 155
3.4.3 Information sources 156
3.4.4 Search Strategy 156
3.4.5 Study selection process. 157
3.4.6 Data collection process 157
3.4.7 Data items 158
3.4.8 Data synthesis 159
3.4.9 Risk of Bias in Individual Studies 160
3.4.10 Effect measures. 160
3.4.11 Data analysis 160
3.5 Results 161
3.5.1 Study selection. 161
3.5.2 General Summary 167
3.5.3 Study Characteristics 167
3.5.4 Colorectal Surgery 173
3.5.5 Hepatobiliary Surgery 173
3.5.6 Oral Maxillofacial Surgery and ENT 176

3.5.7 Trauma and Orthopaedics 177
3.5.8 Neurosurgery 178
3.5.9 Urology 179
3.5.10 Upper GI 184
3.5.11 Cardiac and Thoracic surgery 184
3.5.12 Bias assessments 185
3.6 Discussion 188
4 Impact of 3D Reconstructions on Understanding of Mesenteric Vascular Anatomy 199
4.1 Background 199
4.2 The impact of three-dimensional reconstruction and standardised CT interpretation (AMIGO) on the anatomical understanding of mesenteric vascular anatomy for planning complete mesocolic excision surgery. A randomised cross-over study. 201
4.2.1 Methods 201
4.2.2 Results 207
4.3 Inter and intra-rater reliability of multi-slice CT and 3D Reconstructed Imaging Analysis of Mesenteric Vascular Anatomy for Planning and Performing Complete Mesocolic Excision 214
4.3.1 Study Aims 214
4.3.2 Method 214
4.3.3 Results 217
4.4 Discussion 236
4.4.1 Summary of Key Findings 236
4.4.2 Interpretation and Analysis of Results 237
4.4.3 Study Limitations 239
4.5 Conclusions 240
5 Feasibility and Early Clinical Integration of 3D Models for Complete Mesocolic Excision 242
5.1 Aims 242
5.2 Study Population and Recruitment: 243
5.2.1 Surgeon Characteristics: 243
5.2.2 3D model workflow 243
5.2.3 Pre-operative Review and Intra-operative Use: 244
5.3 Outcome measures 244
5.3.1 Primary Outcomes: 244
5.3.2 Feasibility Assessment of Clinical Data Points: 245

5.4 Sample size and patient recruitment. 246
5.5 Results 246
5.5.1 Clinical Summary 246
5.5.2 Intraoperative haemorrhage events 248
5.5.3 Morbidity and mortality 248
5.5.4 Feasibility of intraoperative assessment of performance using recorded video 250
5.5.5 Imaging and Segmentation time summary 251
5.6 Anatomical Configuration of Mesenteric Vessels 253
5.6.1 Ileocolic Vein and Artery 253
5.6.2 Right Colic Artery 253
5.6.3 Middle Colic Veins 253
5.6.4 Henle's Trunk 254
5.7 Accuracy of Reconstructions 258
5.7.1 Anatomical Understanding of Participating Surgeon CT versus 3D 272
5.7.2 Time spent on imaging interpretation. 282
5.7.3 Subjective model feedback 284
5.8 Discussion 285
5.8.1 Accuracy of 3D Reconstructions 285
5.8.2 Anatomical Understanding 287
5.8.3 Subjective Model Feedback 288
5.9 Conclusion and Future Research Directions: 289
6 The Role of Personalised 3D Imaging in Enhancing Patient Comprehension and Decision-Making in Advanced Colorectal Cancer Treatment 290
6.1 Background 290
6.1.1 Context 290
6.1.2 Contemporary Challenges in Surgical Consent and Patient Instruction 291
6.1.3 Evaluation of Patient-Specific 3D Models in Enhancing Patient Understanding and Decision-Making 293
6.2 Methods 294
6.2.1 Study Design 294
6.2.2 3D patient-specific model reconstruction 294
6.2.3 Patient recruitment 295
6.2.4 Randomisation and Interventions 296
6.2.5 Outcome measures 296
6.2.6 Data Analysis 299
6.2.7 Sample size. 300
6.3 Results 303
6.3.1 Intended Exenteration Procedures 305

6.3.2 Treatment and decision making preferences 310
6.3.3 Decisional conflict score 316
6.3.4 Patient knowledge questionnaire 317
6.3.5 Subjective feedback 320
6.4 Interview data 324
6.4.1 Understanding 324
6.4.2 Personalisation 328
6.4.3 Communication and Engagement 330
6.4.4 Emotional Impact 332
6.4.5 Decision Making 334
6.5 Discussion 339
6.5.1 Conclusion 342
7 Discussion 343
7.1 Overview 343
7.1.1 Synthesis of Key Findings in Context 344
7.1.2 Integration of Findings Across Studies 344
7.2 Technical Innovation and implementation 345
7.3 Clinical Impact and Educational Value 347
7.4 Critical Analysis of Research Limitations 348
7.4.1 Technical Implementation Limitations 348
7.4.2 Clinical Validation Limitations 349
7.4.3 Methodological limitations 350
7.4.4 Unmeasured Impact of Imaging Acquisition Parameters on 3D Model Fidelity 352
7.5 Next steps and direction for future research 354
7.5.1 Clinical Validation Studies 354
7.5.2 Evidence-Based Imaging Protocols 355
7.5.3 Educational Impact Assessment 356
7.5.4 Machine learning approach to automated segmentation 356
7.5.5 Implementation research and technical developments 358
7.6 Summary conclusion 359
8 Bibliography 361
9 Appendices 395
9.1.1.1.1.1.9 Appendix 6.4 Pelvic Exenteration Lexicon definitions 426

List of Figures

Figure 1-1 diagram of vector, matrix, and 3D tensor. Cross sectional imaging can be considered a 3D tensor consisting of a stack of 2D matrix comprised of pixels corresponding to a numerical value. ... 39

Figure 1-2 Slice of CT scan demonstrating each slice can be considered a 2D array of pixels. 39

Figure 1-3 Overview of convolutional neural network. The network consists of the following key components. 50

Figure 1-4 Architecture of 3D CNN with U-net design. The network accepts 3D imaging data (3D tensor) and subsequently down and up samples the input data. The final probability map predicts the likelihood that a given voxel belongs to the training labelling data. 53

Figure 1-5 Demonstrating the effect of different levels of decimation. 65

Figure 1-6 Tri to Quad retopology 68

Figure 2-1 Example segmentation of pelvic MRI in ITK SNAP 111

Figure 2-2 Relative shifts of each anatomical mesh with initial mesh extraction and transformation method. 115

Figure 2-3 Python code implementation of 3D mesh extraction from segmentation file with affine transformation and scene centring and rotation to ensure correct relative positioning 116

Figure 2-4 Python implementation of decimation using decimation submodule from the Trimesh library. The implementation decimated different labels to ensure adequate fidelity in the final mesh (Label 1= artery, 2=Vein, 3= Stomach/Duodenum, 4= Colon, 5= Pancreas, 6=Tumour). 118

Figure 2-5 Effect of different degrees of decimation on overall model topology. Each mesh can be decimated to 90% without any significant distortions. 119

Figure 2-6 Laplacian mesh smoothing with illustration of mesh shrinkage and ‘dotted-line’ artefact. 120

Figure 2-7 Heat map plot demonstrating the effect of smoothing and decimation on the mean surface distance in comparison to the unprocessed meshes for each anatomical structure across the 111 patient data set. Such metrics allowed selection of appropriate processing parameters to achieve predetermined levels of mesh accuracy. 122

Figure 2-8 Visual comparison of the effect on mesh topology for combinations of smoothing and decimation. As decimation increases (and vertices count reduce) the model will tolerate less smoothing before unacceptable alterations in mesh topology occur. The model in the bottom left corner representing 90% decimation with 20 iterations of smoothing with a coefficient of 0.3 demonstrates the significant degradation in model fidelity that occur. 123

Figure 2-9 Visual illustration of the effects of model processing and subsequent shrink wrapping. The shrink wrap function restores the original topology of the unprocessed high polygon mesh derived from the segmentation file..... 125

Figure 2-10 Segmentation upload page. Users can drag and drop the file or upload via file directories. 130

Figure 2-11 Interactive colour coded 3D model derived from user uploaded segmentation file. Transparency controls are in the upper right corner of the screen. 130

Figure 2-12 Process of topologizing complex anatomical mesh structures using pen and polygrouping. The model is manually divided into different polygroups which then serve to determine the quad remeshing algorithm. 133

Figure 2-13 UV unwrapping using polygroups to determine seam placement. 134

Figure 2-14 UV grid map applied to unwrapped sacrum to demonstrate how 2D texture images are applied to 3D model. 135

Figure 2-15 3D mesh with multiple subdivision levels. 136

Figure 2-16 Example texture mapping components of low polygon sacrum mesh. The workflow show baking the normal map and the subsequent PBR texture maps that result in the final photorealistic bone texture (far right). 139

Figure 2-17 Advanced rectal cancer PBR rendered model derived from MR and CT imaging. The two extracted mesh were visually paired in the 3D software to enable the advantages of each imaging modality. 140

Figure 2-18 PBR Rendered model with custom UI allowing control over each component's transparency and material properties. 142

Figure 2-19 Box plot displaying the mean surface distance change (mm) after decimation only for different anatomical structures, including arteries, veins, tumour, colon, stomach/duodenum, and pancreas. 146

Figure 2-20 Box plot displaying the mean surface distance change (mm) after decimation and smoothing for different anatomical structures, including arteries, veins, tumour, colon, stomach/duodenum, and pancreas. 147

Figure 2-21 Box plot illustrating the mean edge length ratio (mm) across different anatomical structures, including arteries, veins, tumour, colon, stomach/duodenum, and pancreas. Each box represents the interquartile range, with the median indicated by a horizontal line within the box. Whiskers extend to the minimum and maximum values within 1.5 times the interquartile range, providing an overview of the mesh quality for each anatomical structure. Lower mean edge length ratios are observed for arteries, veins, and tumours, indicating a more uniform triangulation in these

structures, while the colon, stomach/duodenum, and pancreas exhibit higher mean edge length ratios, reflecting greater variability in mesh element quality. 148

Figure 2-22 Box plots for each mesh component demonstrating vertices counts before and after decimation 149

Figure 3-1 Prisma Diagram 162

Figure 3-2: Number of 3D planning studies published per year from 2008 -2020 163

Figure 3-3 Number of 3D planning studies published by specialty between 2008-2020 163

Figure 3-4 Number of 3D planning studies published by country 164

Figure 3-5 A-0 Radar plots summarising outcome measures used in all studies by surgical specialty 165

Figure 3-6 A-B Breakdown of specific planning applications for virtual and printed models. 168

Figure 3-7 radar plot summarising outcome measures used to evaluate 3D planning. Time and blood loss where the most common outcome measures employed in the included studies. 171

Figure 3-8 Summary of outcome measures used by each study. 172

Figure 3-9 Metanalysis of the effect of 3D models on operative time (mins) of Hepatectomy 175

Figure 3-10 Meta-analysis of the effect of 3D models on operative time (min) of partial nephrectomy for renal cell carcinoma 181

Figure 3-11 Metanalysis of the studies evaluating the effect of 3D models on intra-operative blood loss (ml) in partial nephrectomy for renal cell carcinoma 183

Figure 3-12 Bias Assessments of non-randomised studies using ROBBINS-2 assessment tool 186

Figure 3-13 Bias assessment of randomised studies using ROB 2 bias assessment tool. 187

Figure 4-1 3D vs. AMIGO study flow diagram 203

Figure 4-2 AMIGO CT interpretation checklist 206

Figure 4-3 Mean scores for all candidates at baseline and using AMIGO method versus 3D models; B- Mean scores for group 1 at baseline and using AMIGO method versus 3D models; C- Mean scores for group 2 at baseline and using 3D models versus AMIGO 209

Figure 4-4 A) Mean scores for baseline testing versus AMIGO versus 3D model by case number; B) Mean scores for baseline testing versus AMIGO versus 3D model by the candidate; C) Percentage of correct responses by the question at baseline versus AMIGO versus 3D model 211

Figure 4-5 Distribution of Time Required for 3D Model Generation. Histogram showing the frequency of cases by segmentation duration (minutes). 218

Figure 4-6 Box Plot Analysis of Average Correct Response Rates by Imaging Modality. This box plot contrasts the distribution of the average percentage of correct responses for each rater using CT (shown in blue) and 3D imaging modalities (shown in orange). The central line in each box represents the median percentage, the box itself shows the interquartile range (IQR), and the whiskers extend to the range of data points. 222

Figure 4-7 Box Plot Distribution of Rater Accuracy Using CT and 3D Imaging Modalities. The correct response for raters 1-4. Each rater has a pair of box plots where the blue box represents the distribution of correct responses when using CT imaging, and the orange box corresponds to 3D imaging. The central line in each box indicates the median accuracy, the box limits represent the interquartile range (IQR), and the whiskers extend to the furthest point within 1.5 times the IQR from the box. Outliers are represented as individual points outside the whiskers. 223

Figure 4-8 Differential Rater Performance in Correct Responses Using CT Imaging Versus 3D Models for Round 1. The bar chart illustrates the average absolute percentage difference in correct responses for each case, with the green bars representing the aggregated data. The overlaid scatter plot depicts individual rater performance, with each rater denoted by a unique colour and symbol. 225

Figure 4-9 Differential Rater Performance in Correct Responses Using CT Imaging Versus 3D Models for Round 2. The bar chart illustrates the average percentage difference in correct responses for each case, with the green bars representing the aggregated data. The overlaid scatter plot depicts individual rater performance, with each rater denoted by a unique colour and symbol 226

Figure 4-10 Individual Rater Accuracy Comparison by Case in ROUND 1 Using CT and 3D Models. This series of line graphs illustrates the percentage of correct responses for each case by four separate raters in the second evaluation round. The accuracy is compared between two diagnostic tools: CT imaging (depicted in blue) and 3D modelling (depicted in orange). Each graph corresponds to one of the four raters, with the x-axis representing individual cases and the y-axis showing the accuracy percentage. Data points on the lines indicate the accuracy achieved by the respective rater for each case using the specified imaging modality. 227

Figure 4-11 Individual Rater Accuracy Comparison by Case in ROUND 2 Using CT and 3D Models. This series of line graphs illustrates the percentage of correct responses for each case by four separate raters in the second evaluation round. The accuracy is compared between two diagnostic tools: CT imaging (depicted in blue) and 3D modelling (depicted in orange). Each graph corresponds to one of the four raters, with the x-axis representing individual cases and the y-axis showing the accuracy percentage. Data points on the lines indicate the accuracy achieved by the respective rater for each case using the specified imaging modality. 228

Figure 4-12 Average correct responses by question using CT and 3D models. 231

Figure 4-13 Comparative Analysis of Correct Response Rates by Imaging Modality Across Anatomical Variations. This paired bar chart displays the mean percentage of correct diagnoses by all evaluators, contrasting results obtained using 3D imaging (orange bars) with those from CT imaging (blue bars).

Each pair of bars corresponds to a different anatomical variation as specified on the x-axis. The number of cases (n) featuring each anatomical variant is indicated atop the respective bars, reflecting the sample size for each question category. 234

Figure 4-14 Box and whisker plots comparing the average correct responses for Henle's trunk using 3D and CT imaging modality by the number of constituent vessels. No statistical difference was found between the magnitude of the improvement of 3D over CT for the number of vessels as assessed by the Kruskall-Wallis test. 235

Figure 5-1 Histogram of segmentation times (minutes) per scan. 252

Figure 5-2 Histogram depicting the distribution of measured distances (in millimetres) between the ileocolic artery and the middle colic artery trunk. The most frequent range of measurements is between 20–30 mm. 256

Figure 5-4 Histogram illustrating the distribution of measured distances (in millimetres) between the origin of the MCA and its bifurcation into right and left branches. 256

Figure 5-5 Histogram representing the distribution of measured distances (in millimetres) between the ileocolic vein and Henle’s trunk. The most frequent distances fall within the 35–40 mm range. 257

Figure 5-6 Histogram showing the distribution of measured distances (in millimetres) between the ileocolic vein and the middle colic vein. 257

Figure 5-6 Example case 1 3D model predictions versus intraoperative findings. A-B ICA passes anteriorly over SMV. MCA origin off SMA with bifurcation into right and left branches 261

Figure 5-7 Example case 6- dissection of atypical colonic veins. Patient possessed 3 separate venous branches draining right and proximal transverse colon directly into the SMV (vessels 1-3) as predicted by 3D model. Each vessel was dissected and ligated. 262

Figure 5-8 Published video abstract demonstrating intra-operative use of 3D model in case 7. The bottom image demonstrates a jejunal vein passing over SMV just caudal to the origin on the MCA. The 3D model helped identify this variant, avoid iatrogenic injury during D3 lymphadenectomy and help target dissection of the MCA trunk. 263

Figure 5-9 Case 12- two separate MCV veins draining directly into SMV as predicted by 3D reconstruction. 264

Figure 5-10 Case 12- Henle’s Trunk comprised of GEV and ASPDV 265

Figure 5-11 Case 49- One MCV trunk inserting into SMV. Henle’s Trunk was comprised of SRCV, GEV and SRCV. 266

Figure 5-12 Case 69- Views demonstrating the MCA trunk and MCV trunk. Intraoperative findings were accurately predicted by the 3D model both in terms of number of trunks and their relative spatial relationships. Henle’s trunk was ligated at its origin. 267

Figure 5-13 Case 85- Sequential intraoperative dissection views alongside 3D reconstruction. ICV can be viewed draining into SMV at same level as jejunal/ileal vein as can viewed on the 3D model. ICA passes posterior to SMV. The MCA trunk can be visualised with bifurcation into left and right branches. 268

Figure 5-14 Case 85 Henle's trunk comprised of SRCV and ASPDV. GEV separate vessel draining into SMV directly. 269

Figure 5-15 Case 87- Atypical anatomy with early bifurcation of SMV with the ICA passing between the two (star and Asterix). Model accurately predicted the vessel configuration allowing confident dissection and ligation. 270

Figure 5-16 Case 87 (continued). MCV draining into SMV in proximity with the trunk of Henle with proximal drainage of GEV close to SMV. Confluence of two colonic vessels draining the hepatic flexure (SRCV) and ASPDV form the other constituent vessels of Henle. 271

Figure 5-17 Box plot comparing the percentage of correct responses for identifying mesenteric vessel configuration using CT scans (blue) and 3D reconstructions (orange). The median percentage correct for 3D reconstructions is higher than for CT, with reduced variability and fewer outliers, indicating improved consistency and accuracy in identification with the 3D modality. 274

Figure 5-18 A-H Comparison of correct responses for mesenteric vessel identification using CT (blue) and 3D (orange) imaging modalities for multiple raters. Each figure (A–I) presents data for one rater who performed at least three cases. For each rater, a box-and-whisker plot compares the average percentage of correct responses between CT and 3D and a line plot shows the percentage of correct responses by case, displayed chronologically. These figures highlight both the overall improvement in accuracy with 3D reconstructions and the case-by-case variability in performance. 275

Figure 5-19 Bar chart illustrating the absolute percentage difference in correct responses between CT and 3D imaging modalities for each case. Positive values indicate better performance with 3D, while negative values (in pink) represent cases where CT performed better. Most cases show improved accuracy with 3D, with only a small subset exhibiting a preference for CT. 279

Figure 5-20 Average correct responses by question using CT and 3D models 280

Figure 5-21 Time spent on interpretation of CT scans and 3D models to determine mesenteric vascular anatomy 282

Figure 5-22 Diverging bar chart of surgeon responses to Likert scale questionnaire relating to use of 3D model. 284

Figure 6-1 A-H Example patient specific 3D reconstructions. 301

Figure 6-2 I-P Example patient specific 3D reconstructions. 302

Figure 6-3 Patient recruitment flow chart. 303

Figure 6-4 Education level of Standard and 3D groups. No statistical difference between groups 311

Figure 6-5 Pre-consultation treatment preferences for Standard and 3D groups. 311

Figure 6-6 Stated decision making preferences for Standard and 3D groups. 312

Figure 6-7 Quality and Length of life preference for Standard and 3D groups. 312

Figure 6-8 Treatment priorities: Stated importance of Avoiding Stoma- 3D versus Standard groups.313

Figure 6-9 Treatment priorities: Stated importance of retaining control of bowel function 3D versus Standard Groups. 313

Figure 6-10 Treatment priorities Stated importance of maintaining independence 3D versus Standard Groups. 314

Figure 6-11 Treatment priorities: Stated importance of Minimising pain- 3D versus Standard groups. 314

Figure 6-12 Treatment priorities Stated importance of getting back to work- 3D versus Standard groups 315

Figure 6-13 Box plot adjusted DCS score pre and post consultation for 3D and STANDARD groups. 316

Figure 6-14 3D model subjective Likert scale questionnaire responses. 322

Figure 6-15 General consultation Likert scale questionnaire responses from Standard and 3D group 323

List of Tables

Table 1-1 Segmentation software programmes 42

Table 1-2 Common texture maps used in PBR rendering. 70

Table 2-1 Comparison of different 3D file formats 127

Table 2-2 A-D Quality metrics for 3D reconstructions derived from 111 segmentation files (corresponding to 111 patient cases). 145

Table 3-1 Summary of procedures by specialty in which 3D planning was used 166

Table 3-2 Summary of study designs 166

Table 3-3 Segmentation software utilised in studies 168

Table 3-4 Summary of 3D methods, printer models and print material used for planning 170

Table 3-5 Summary of study design and 3D interventions in Colorectal Surgery 191

Table 3-6 Summary of study design and 3D interventions in Hepatobiliary Surgery 191

Table 3-7 Summary of study design and 3D interventions in Upper Gastrointestinal Surgery 192

Table 3-8 Summary of study design and 3D interventions in Urology 192

Table 3-9 Summary of study design and 3D interventions in Thoracic Surgery 193

Table 3-10 Summary of study design and 3D interventions in Neurosurgery 194

Table 3-11 Summary of study design and 3D interventions in Oral maxillofacial surgery 194

Table 3-12 Summary of study design and 3D interventions in Gynaecological Surgery 195

Table 3-13 Summary of study design and 3D interventions in Trauma and Orthopaedics 196

Table 3-14 Summary of study design and 3D interventions in Plastic/Breast Surgery 197

Table 3-15 Summary of study design and 3D interventions in cardiac surgery 198

Table 4-1 3D vs AMIGO Participant demographics 207

Table 4-2 Summary of test scores overall and by study group at baseline and using AMIGO and 3D models (SD – standard deviation, maximum score = 14) 208

Table 4-3 Trainee subjective rating of ease of identifying colonic vessels using CT and 3D models 213

Table 4-4: CME experience and preoperative planning practices of participating surgeons 217

Table 4-5: Segmentation times summary as per scan protocol and slice thickness 218

Table 4-6: Comparative Inter-Rater Reliability Measured by Fleiss' Kappa for CT and 3D Imaging Modalities During Round 1. This table enumerates the Fleiss' Kappa statistics for each anatomical question, assessing raters' agreement when using CT and 3D imaging techniques. Colour key for Fleiss' Kappa values: RED: κ = 0-<0.2 (poor agreement) ORANGE: κ = 0.21-0.40 (fair agreement) YELLOW: κ = 0.41-0.60 (moderate agreement) LIGHT GREEN: κ = 0.61-0.80 (good agreement) GREEN: κ= 0.81-1.00 (very good agreement)..... 219

Table 4-7: Intra-Rater Reliability Assessment Using Cohen's Kappa for CT Versus 3D Imaging Across Anatomical Questions. This table quantifies the consistency of each rater's responses between rounds 1 and 2 by presenting Cohen's Kappa values for both CT and 3D imaging modalities. *Colour key for Fleiss' Kappa values: RED: κ = 0-<0.2 (poor agreement) ORANGE: κ = 0.21-0.40 (fair agreement) YELLOW: κ = 0.41-0.60 (moderate agreement) LIGHT GREEN: κ = 0.61-0.80 (good agreement) GREEN: κ= 0.81-1.00 (very good agreement)* 220

Table 4-8 Mean percentage of correct responses for CT and 3D imaging modalities by rater. Box and whisker plots depicting the distribution of correct responses percentages for each rater are provided in Figure 1-7..... 221

Table 4-9: Number(n) and per cent correct responses (%) for each anatomical questionnaire item for CT and 3D..... 230

Table 4-10 Rater-Specific Diagnostic Accuracy for Anatomical Variants Using CT and 3D Imaging. This table presents a detailed breakdown of the correct response rates for each rater across various anatomical variants using CT and 3D imaging modalities. The 'Total' column indicates the number of cases for each anatomical feature, while subsequent columns provide each rater's counts (n) and percentages (%) of correct diagnoses for the two imaging methods. 232

Table 5-1 Patient demographic and clinical characteristics summary 246

Table 5-2 Morbidity and mortality data..... 249

Table 5-3 Summary table of segmentation times by scan type and slice thickness 251

Table 5-4 Summary of imaging protocols utilised..... 252

Table 5-5 Measured distances between mesenteric vessels landmarks..... 255

Table 5-6 Reconstruction Accuracy in Predicting Vascular Anatomy: Sensitivity, Specificity, and Predictive Values Compared to Intraoperative Findings..... 258

Table 5-7 Confusion matrix for prediction and presence of middle colic artery 259

Table 5-8 Confusion matrix for prediction and presence of middle colic veins 259

Table 5-9 3D Reconstruction Accuracy in Predicting Henle Trunk Vascular Anatomy: Sensitivity, Specificity, and Predictive Values Compared to Intraoperative Findings..... 260

Table 5-10 Summary statistic for percentage correct responses for each participating surgeon using CT scans and 3D models. 273

Table 5-11 Comparative Percentage Differences in Correct Responses Between 3D Models and CT scans 278

Table 5-12 Average correct response by vessel using CT and 3D 281

Table 5-13 Summary statistics for time spent on imaging modality interpretation. 283

Table 6-1 Patient demographics summary 304

Table 6-2 Detailed Demographic Characteristics and Planned Exenteration Procedures in the 3D Group 306

Table 6-3 Detailed Demographic Characteristics and Planned Exenteration Procedures in the STANDARD Group 308

Table 6-4: Breakdown of agreement/discrepancies between patient and surgeon response by anatomical structure for the 3D GROUP 318

Table 6-5: Breakdown of agreement/discrepancies between patient and surgeon response by anatomical structure for the STANDARD GROUP 319

Table 6-6 Summary of the average agreement for functional outcomes in 3D and STANDARD groups 320

Introduction to Three-Dimensional Visualisation in Surgical Practice

Surgery stands at the threshold of a digital revolution. The convergence of advanced imaging technologies, computational processing capabilities, and novel visualisation methods is fundamentally transforming surgical practice. Three-dimensional (3D) visualisation and computer-generated modelling have emerged as potentially transformative tools, revolutionising the planning and execution of complex surgical procedures. This technological evolution promises to enhance surgical precision, improve patient outcomes, and facilitate better communication between healthcare providers and patients.

The ability to precisely visualise patient-specific anatomy before surgery represents a significant advancement from traditional approaches that relied heavily on surgeons' ability to mentally reconstruct three-dimensional relationships from two-dimensional imaging data. Modern surgical practice increasingly demands precise preoperative planning and intraoperative navigation, particularly for complex oncological procedures where achieving complete resection while preserving critical structures is paramount. The Royal College of Surgeons' 'Future of Surgery' review (2018) identified 3D visualisation as one of the key technologies likely to impact surgical practice significantly in the coming decade (1).

Three-dimensional reconstruction, a cornerstone of computer-generated modelling in surgery, entails creating detailed virtual models of anatomical structures from two-dimensional image data. This process typically begins with acquiring medical imaging data, such as computed tomography (CT) scans, magnetic resonance imaging (MRI), or ultrasound images. Through sophisticated computational methods, this data can be transformed into comprehensive 3D representations of patient anatomy. These reconstructions have evolved from basic renderings to highly sophisticated models with exceptional detail and accuracy, enabling unprecedented visualisation of complex anatomical relationships (2).

The applications of such technology in surgical practice are diverse and expanding. Surgeons utilise these models for preoperative planning, allowing precise visualisation of the operative field before making any incisions. This capability may improve surgical accuracy and efficiency, reduce intraoperative risks, and ultimately enhance patient outcomes. In complex procedures, such as craniofacial reconstruction or organ transplantation, 3D models provide unprecedented detail, aiding surgeons in navigating critical structures. Furthermore, these models serve as valuable tools for surgical education and training, offering safe environments for skill development without risk to patients.

However, despite this promising potential, significant challenges remain in the widespread adoption and validation of 3D visualisation technologies in surgical practice. Technical hurdles include the time-intensive nature of model creation, the need for specialised expertise, and the challenge of integrating these tools into existing clinical workflows. Moreover, while initial studies suggest benefits in surgical planning and execution, robust evidence demonstrating improved patient outcomes remains limited in many surgical specialties (3–5).

The field of colorectal cancer surgery presents challenges that may benefit from advanced visualisation techniques. Complete mesocolic excision (CME) for colon cancer, requires precise understanding of complex mesenteric vascular anatomy. Although potentially offering superior oncological outcomes technique's adoption has been limited partly due to concerns about the technical complexity and risk of vascular injury during central dissection (6). Three-dimensional visualisation could potentially address these challenges by providing clearer understanding of patient-specific vascular anatomy and facilitating precise surgical planning.

The interaction between surgeon and patient also stands to benefit from these technological advances. Traditional methods of explaining complex surgical procedures to patients often fall short in conveying the full scope and implications of proposed interventions (7). Patient-specific 3D models may enhance understanding and facilitate shared decision-making, particularly in cases involving extensive resections such as pelvic exenteration for advanced rectal cancer (8).

This thesis examines the role of 3D visualisation in colorectal cancer surgery decision-making, with particular focus on its application in complete mesocolic excision and patient education for complex pelvic surgery. Through systematic evaluation of existing evidence and novel research, it aims to establish the utility of these technologies in improving surgical planning, execution, and patient communication.

The technological foundation of surgical 3D visualisation encompasses various methods and approaches, from image segmentation and reconstruction techniques to advanced

visualisation platforms and augmented reality systems. Understanding these technical aspects is crucial for evaluating their potential impact on surgical practice. The following chapters will explore these foundations in detail before examining specific applications in colorectal cancer surgery.

Overall Aim and Scope of Thesis:

The overarching aim of this thesis is to develop, implement, and evaluate patient-specific three-dimensional (3D) anatomical models as an integrated decision-support system throughout the continuum of advanced colorectal cancer surgery. This goal encompasses four interrelated domains: (1) technical innovation and validation of workflows for generating high-quality, patient-specific 3D models from standard imaging data; (2) the establishment of standardised frameworks and metrics to evaluate model accuracy, educational impact, and clinical utility; (3) the assessment of clinical feasibility and early integration of these models into complete mesocolic excision (CME) procedures, informing the design of future comparative trials; and (4) the exploration of patient-centred applications, particularly how these visualisations can enhance patient comprehension, informed consent, and shared decision-making processes in complex surgical interventions such as pelvic exenteration.

By systematically addressing these four domains, the thesis aims not only to consolidate the technical foundations and methodological rigor underlying 3D visualisation but also to illuminate the practical, humanistic, and educational dimensions that influence its adoption and effectiveness in improving patient care.

Key challenges motivating this research:

First, the technical requirements for generating clinically useful patient-specific models from standard medical imaging are not well defined. Current approaches often rely on proprietary software and manual processes that limit widespread adoption. There is a clear need for standardized, efficient workflows that can be integrated into routine clinical practice.

Second, the evidence base supporting surgical 3D visualisation suffers from methodological limitations and heterogeneity in outcome measures. A systematic analysis of evaluation approaches is needed to establish robust frameworks for assessing utility and clinical impact.

Third, while complete mesocolic excision may offer oncological advantages, concerns about technical complexity and vascular injury risk have limited its adoption. The potential for 3D visualisation to address these challenges through enhanced anatomical understanding and surgical planning requires rigorous investigation. This project seeks to ascertain if models can be feasibly used within this context as judged by model production time and anatomical accuracy and whether key outcome measures can be recorded to inform future work.

Finally, patient understanding of complex surgical procedures often remains poor despite current education methods. The role of patient-specific 3D models in improving comprehension and facilitating shared decision-making warrants careful examination.

Philosophical and Methodological Foundations:

This thesis adopts a pragmatist paradigm, drawing on both quantitative and qualitative methods to address the multifaceted challenges of integrating patient-specific three-dimensional (3D) anatomical models into colorectal surgical practice. Pragmatism, with its emphasis on the practical utility and contextual relevance of knowledge, provides a flexible framework that aligns closely with the clinical and educational objectives of the research. Rather than adhering to a single epistemological stance, a pragmatist outlook allows the integration of positivist, interpretivist, and constructivist elements as warranted by the research questions at hand. Within this paradigm, methodological pluralism is encouraged, facilitating a robust and comprehensive exploration of the value and impact of 3D reconstructions in surgical care.

Central to this approach is the use of mixed methods, combining objective, quantitative evaluations of accuracy, fidelity, and clinical efficacy with qualitative inquiries into user experiences, cognitive processes, and patient perceptions. Quantitative measures—such as congruence between the 3D model and intraoperative findings, improvements in anatomical understanding scores, or operative/clinical outcome measures—provide objective evidence of effectiveness. Concurrently, qualitative techniques—such as semi-structured interviews with surgeons and patients, thematic analyses of decision-making processes—offer insight

into the subjective, contextual, and experiential dimensions that influence how these models are understood, employed, and valued.

In addition, the developmental phase of this work draws on principles of action research, an approach that actively involves end-users and stakeholders—surgeons, trainees, patients, radiologists, and IT specialists—in the design and iterative refinement of the 3D modelling pipeline. By engaging these participants in the research cycle of planning, acting, observing, and reflecting, the study ensures that the resulting solutions are both contextually grounded and practically implementable. Action research not only expedites the refinement of technical workflows but also helps tailor visualisations to the cognitive and informational needs of diverse user groups. This participatory, iterative process enhances ecological validity and supports the translation of research findings into improved patient care and decision-support practices.

To systematically evaluate the utility and effectiveness of the 3D models, the thesis adapts Kirkpatrick's hierarchy of training evaluation as a guiding conceptual framework. By progressing through four levels of assessment, it offers a structured approach to understanding the models' influence on surgical education, practice, and patient care:

- **Level 1 (Reaction):** Assessing surgeon and patient satisfaction, as well as perceived usefulness of the 3D models.
- **Level 2 (Learning):** Measuring improvements in anatomical knowledge and spatial understanding attributable to the 3D visualisations.
- **Level 3 (Behaviour):** Evaluating the influence of the models on surgical planning processes, procedural strategies, and technical performance.
- **Level 4 (Results/Outcomes):** Determining the models' ultimate impact on clinical outcomes, patient decision-making quality, and the broader healthcare delivery context (9).

The combination of pragmatism, mixed methods, and action research thus establishes a philosophical and methodological foundation capable of capturing the complexity of surgical decision-making, the intricacies of patient-provider communication, and the diversity of stakeholder expectations. By attending to both objective metrics and subjective experiences—while simultaneously involving end-users in shaping the intervention—this

thesis aspires to produce knowledge that is empirically sound, contextually meaningful, and readily adaptable to evolving clinical environments.

Chapter 1: Literature review of 3D reconstruction and visualisation methods, applications in Colorectal Surgery

- **Objectives:**
    - Outline the technical aspects of 3D visualisation of medical imaging including imaging segmentation, rendering and visualisation methods.
    - Introduce the theoretical grounding of 3D visualisation, its historical development, and emergent applications in surgical training, planning, and patient education.
    - Present the conceptual rationale for integrating 3D models into routine practice and how this aligns with the broader aims of improving quality of care and shared decision-making in advanced colorectal cancer.

Expected Contributions:
This chapter situates the thesis in the existing literature and justifies the need for a structured, evidence-based approach to the development and evaluation of 3D models.

Chapter 2: Development and Validation of a 3D Modelling Pipeline for Surgical Planning and Patient Education

- **Core Research Question:** What methods and techniques can be utilized to design a novel, scalable, and efficient pipeline for creating patient-specific 3D models from standard medical imaging data?
- **Objectives:**
    1. **Technical Innovation:**

- Develop a semi-automated segmentation protocol integrated into open source/ standardised platforms.
- Implement advanced mesh processing and texturing techniques that preserve anatomical detail, emphasising mesenteric vasculature and critical landmarks.

Quality Assurance and Validation:

- Define and employ robust criteria for evaluating surface mesh accuracy, anatomical fidelity, and rendering quality.
- Validate models against expert anatomical references, ensuring reproducibility and reliability.

Patient Education Focus:

- Adapt the pipeline to produce simplified yet anatomically accurate models for patient education, incorporating interactive features and intuitive visual cues.
- Integrate physically-based rendering (PBR) techniques to enhance realism, aiding patient comprehension.

Expected Contributions:
This chapter lays the foundation for subsequent research by delivering a validated, high-quality modelling pipeline suitable for both surgical teams and patients, thereby facilitating downstream evaluations.

Chapter 3: Systematic Review of Evaluation Methodologies for 3D Models in Surgical Planning

- **Core Research Question:** What evaluation methods have been employed to assess 3D models in surgical planning, and what is the current strength of the evidence base?
- **Objectives:**

- Identify and characterise the types of 3D modelling and printing techniques reported in the literature for surgical planning, focusing on colorectal and related surgical domains.
- Assess the heterogeneity of outcomes measures (e.g., anatomical comprehension tests, operative metrics, patient-reported understanding) and study designs used to evaluate effectiveness.
- Critically appraise the methodological quality and level of evidence, identifying gaps and proposing a standardised evaluation framework that can be applied in subsequent chapters.

Expected Contributions:
By delineating current practices, this chapter provides a methodological roadmap for standardised evaluation in the following empirical studies. The review will highlight best practices, thus informing the design of the studies on CME feasibility and patient education.

Chapter 4: Impact of 3D Reconstructions on Understanding of Mesenteric Vascular Anatomy (Trainees and Experts)

- **Core Research Question:** In what ways, and to what extent, do 3D models enhance the comprehension and interpretation of mesenteric vascular anatomy compared to traditional CT-based methods?
- **Study 1 (Trainees):**
  - **Aim:** Evaluate whether trainees gain a significantly improved understanding of mesenteric vascular anatomy using 3D models versus standardised CT interpretation protocols (AMIGO).
  - **Methodology:** A controlled educational intervention using objective assessments of anatomical knowledge and spatial cognition. Pre- and post-intervention tests will measure accuracy, speed, and confidence in vascular identification.
  - **Hypothesis:** Exposure to 3D models will yield statistically higher objective assessment scores compared to standard CT interpretation.

- **Study 2 (Experts):**
    - **Aim:** Examine inter- and intra-rater reliability among experienced CME surgeons using 3D models versus CT imaging for vascular interpretation.
    - **Methodology:** Multiple expert raters will evaluate vascular variants and critical anatomical relationships on both 3D and CT datasets. Reliability coefficients (Cohen's kappa) will quantify inter and intra rater consistency.
    - **Hypotheses:**
        1. Expert surgeons will exhibit higher inter/intra-rater reliability with 3D models than with CT alone.
        2. Accuracy of anatomical identification will be significantly enhanced using 3D visualisations.

Expected Contributions:
This chapter will provide empirical evidence on the educational and interpretive value of 3D models, informing their potential to improve anatomical understanding and ultimately facilitate pre-operative planning and subsequent operative performance.

Chapter 5: Feasibility and Early Clinical Integration of 3D Models for Complete Mesocolic Excision (CME)

- **Core Research Question:** Are 3D reconstructions feasible, accurate, and practically useful when integrated into the clinical planning and execution of CME for right-sided colon cancer?
- **Study Design (Multicentre, International Feasibility Study):**
    - **Objectives:**

1) Assess the accuracy of 3D preoperative models in predicting intraoperative findings of mesenteric vessel anatomy.
2) Gather structured surgeon feedback to determine usability, influence on preoperative planning, and real-time intraoperative decision-making.

3) Evaluate feasibility metrics for data collection—operative times, video recordings, operative and complication rates, and short-term surgical outcomes—to inform future large-scale trials.

4) Generate a validated, labelled dataset that can be leveraged to develop automated segmentation algorithms (e.g., using deep learning neural networks).

    - **Methods:**
      Quantitative measures of anatomical congruence will be paired with qualitative surgeon feedback. Feasibility endpoints will ensure practical applicability in routine workflows.

    - **Hypothesis**

      3D models accurately predict intraoperative anatomy, surgeons find model subjectively useful, key outcome measures can be reliably collected.

- **Expected Contributions:**
  This chapter offers critical early-stage evidence of real-world clinical utility and assesses whether key outcome measures can be recorded to inform potential future randomised controlled trials. The work also seeks to generate a validated 3D model dataset for future segmentation research.

Chapter 6: Patient-Centered Communication and Decision-Making: The Role of 3D Models in Pelvic Exenteration for Advanced Colorectal Cancer

- **Core Research Question:** How do patient-specific 3D anatomical reconstructions influence patient comprehension, engagement, and decision-making quality in the context of highly complex surgical procedures such as pelvic exenteration?

- **Objectives:**

    - Compare patient understanding of surgical anatomy, extent of resection, and potential complications when using interactive 3D models versus standard CT images and conventional verbal explanations.

    - Investigate whether 3D models enhance informed consent processes and support more effective shared decision-making, using validated decision quality and health literacy instruments.
    - Explore patient perceptions through qualitative interviews to capture experiential and subjective elements of the decision-making process.
- **Hypothesis**
    - Personalised 3D models improve patient understanding of their disease and proposed surgical intervention and reduces decisional conflict.
- **Expected Contributions:**
  This chapter extends the utility of 3D models beyond the surgical team, demonstrating their potential to improve patient comprehension, reduce decisional conflict, and facilitate truly patient-centred care.

Chapter 7: Discussion

- **Aims:**
    - Integrate findings from technical development, methodological standardisation, training studies, clinical feasibility assessments, and patient-centred evaluations.
    - Reflect on the initial pragmatist stance, examining how the mixed-methods approach facilitated actionable insights.
    - Position the findings within existing theoretical and clinical frameworks, offering a comprehensive conceptual model for integrating 3D visualisation into routine surgical practice.
- **Outcomes and Future Directions:**
    - Propose guidelines and best practices for implementing 3D modelling pipelines in colorectal surgery and potentially other surgical domains.
    - Identify areas requiring further research, including randomised controlled trials to establish definitive clinical outcomes and ongoing efforts to automate segmentation using convolutional neural networks.

1 Literature review of 3D reconstruction and visualisation methods, applications in Colorectal Surgery

1.1 Technical Foundations

1.1.1 Medical Image Processing

The creation of patient-specific three-dimensional models for surgical applications necessitates a sophisticated understanding of medical image processing fundamentals. This process encompasses a complex pipeline from image acquisition through to final visualisation, with each step critically influencing the accuracy and utility of the resultant models. This section examines the technical foundations underlying these processes, with particular emphasis on their implications for surgical planning and intervention.

1.1.1.1 DICOM Data Structure and Properties

Digital Imaging and Communications in Medicine (DICOM) represents the international standard for medical imaging data management. The format's hierarchical structure encompasses both image data and critical metadata essential for accurate spatial reconstruction. This standardisation facilitates interoperability whilst maintaining the fidelity of spatial and patient-specific information necessary for clinical applications (10).

The DICOM hierarchy comprises multiple organisational levels, each serving distinct purposes in data management and spatial reconstruction. At the highest level, patient metadata provides demographic information and unique identifiers. Study-specific information describes the imaging encounter, while series parameters detail specific

acquisition protocols. At the most granular level, individual slice data contains both pixel information and spatial metadata critical for accurate three-dimensional reconstruction (11).

Spatial reconstruction relies on several key DICOM parameters. Pixel spacing defines the physical distance between adjacent pixels in the image plane, while slice thickness and spacing characterise the through-plane resolution. The Image Position Patient (IPP) and Image Orientation Patient (IOP) parameters enable precise spatial localisation within the patient coordinate system. These parameters collectively enable accurate volumetric reconstruction, with the Frame of Reference UID ensuring spatial consistency across multiple acquisitions (10).

Cross-sectional imaging data can be mathematically represented as a three-dimensional tensor (w x h x d). Each voxel contains an intensity value corresponding to local tissue properties. This mathematical framework provides the foundation for subsequent processing and analysis (see figures 1-1 and 1-2).

Figure 1-1 diagram of vector, matrix, and 3D tensor. Cross sectional imaging can be considered a 3D tensor consisting of a stack of 2D matrix comprised of pixels corresponding to a numerical value.

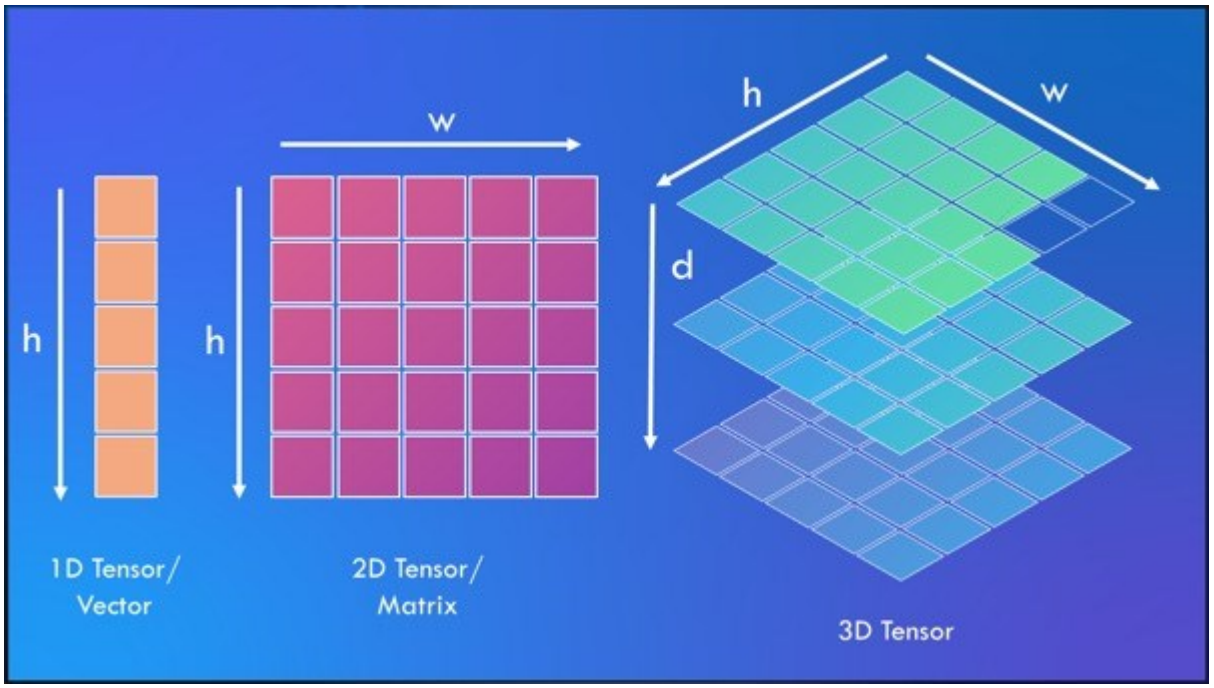
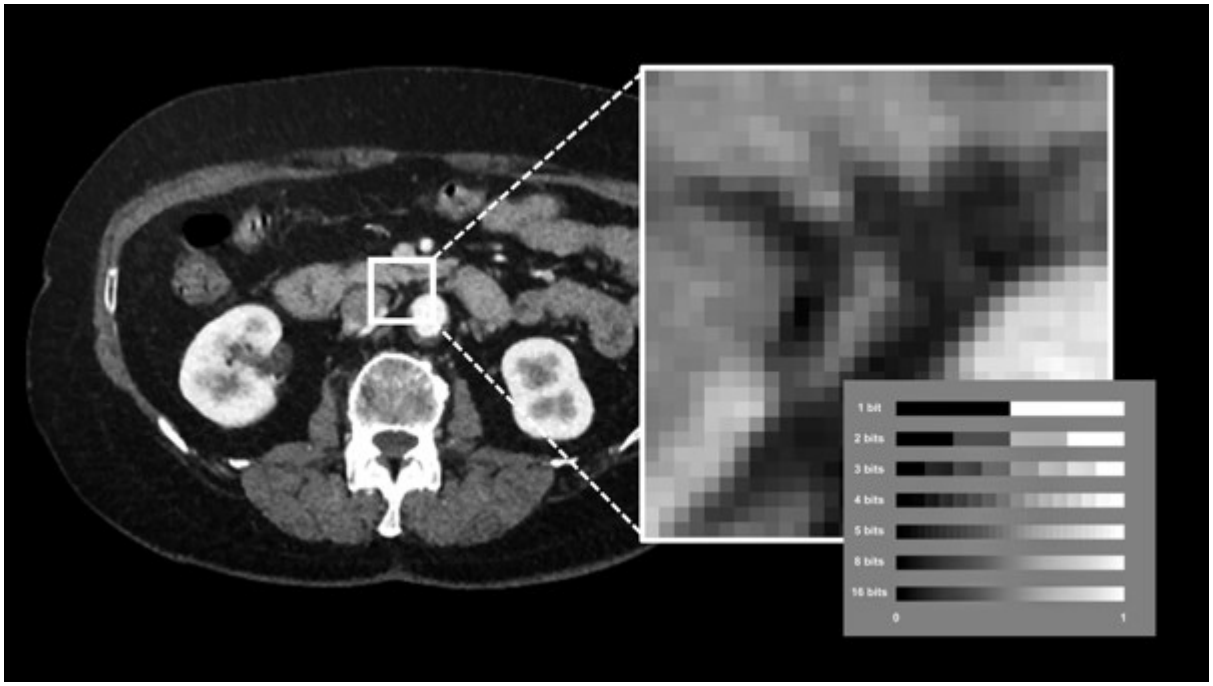


Figure 1-2 Slice of CT scan demonstrating each slice can be considered a 2D array of pixels.



1.1.1.2 Computed Tomography Principles

Computed Tomography (CT) generates cross-sectional images by measuring X-ray attenuation through tissue. The attenuation coefficient μ quantifies a material's X-ray penetrability, with denser tissues exhibiting higher attenuation. These measurements are standardised using the Hounsfield Unit (HU) scale, defined by:

$$HU = 1000 \times (\mu \text{ tissue} - \mu \text{ water}) / \mu \text{ water} - \mu \text{ air}$$

This standardisation enables consistent tissue identification across different scanners and protocols, with air approximately -1000 HU, water at 0 HU, and dense cortical bone exceeding +1000 HU. This quantitative nature of CT imaging proves particularly advantageous for automated processing and segmentation tasks (12).

1.1.1.3 Magnetic Resonance Imaging Characteristics

Magnetic Resonance Imaging (MRI) utilises magnetic fields and radiofrequency pulses to generate detailed soft tissue images without ionising radiation. The technique exploits the magnetic properties of hydrogen nuclei to create images weighted according to different tissue properties. T1-weighted sequences emphasise anatomical detail, T2-weighted sequences highlight fluid content, and proton density weighting reflects hydrogen concentration (13).

Unlike CT, MRI intensity values are relative rather than absolute, varying with acquisition parameters and magnetic field strength. This inherent variability necessitates additional pre-processing steps for consistent image analysis. The superior soft tissue contrast of MRI proves particularly valuable for rectal cancer (14), though the lack of standardised intensity values presents unique challenges for automated processing.

1.2 Segmentation Approaches

Image segmentation represents a fundamental process in medical image analysis, whereby volumetric imaging data is partitioned into distinct anatomical regions. This involves categorising image data into distinct structures and assigning labels to each voxel based on its membership to a particular anatomical structure (15).

This prerequisite step bridges the gap between raw imaging data and clinically meaningful three-dimensional reconstructions. The segmentation methodology significantly influences the accuracy of anatomical representations and the efficiency of the overall workflow (16).

Segmentation methodologies can be broadly categorised based on the degree of human intervention required, ranging from fully manual approaches to automated algorithms. Each methodology presents distinct advantages and limitations that must be carefully considered in the context of specific clinical applications and accuracy requirements.

1.2.1 Manual Segmentation

Manual segmentation remains the cornerstone of medical image analysis, particularly in scenarios demanding high precision or involving complex anatomical variations. This approach systematically delineates anatomical structures using specialised software interfaces by trained operators. The process typically proceeds on a slice-by-slice basis through the imaging volume, with operators defining structure boundaries based on their anatomical knowledge and interpretation of image features (17).

Table 1-1 Segmentation software programmes

Materialise Mimics	IntelliSpace Portal
Materialise Pro plan	HepaVision
3D Slicer	MEDICAL Imaging Three Divisional Visualisation System
ITK-SNAP	iPlan CMF
MI-3DVS	MI-3DVS
Synapse Vincent	Innersight Labs
Hisense CAS	VirSSPA
Osirix X	Leonardo InSpace
IQQA-Liver	SuperImage Ortho edition
Ziostation	M3DICS
MITK ReLiver	HipPlan (Symbiosis)
Amira 4.1	3D Plus Body Visible System
M3D MedGraphics	Visible Patient
Zed-Trauma	Maxilim
iNtellect Cranial Navigation	FreeForm Modeling System
Imascap	

The principal advantage of manual segmentation lies in its flexibility and capacity to accommodate suboptimal imaging, anatomical variants, and pathological changes. Expert operators can apply contextual knowledge and pattern recognition skills to resolve ambiguous boundaries and interpret complex anatomical relationships. This proves particularly valuable in abdominopelvic imaging, where tissue interfaces lack clear contrast differentiation, or normal anatomical relationships have been distorted by pathology (18).

Manual segmentation presents several limitations. It is time-consuming, often requiring hours of work. This time requirement is especially problematic in acute clinical scenarios where rapid processing is crucial. Moreover, the reliability of manual segmentation heavily relies on the operator's expertise and consistency, leading to a need for more standardisation and reproducibility. Studies have shown significant variations in segmentation results between operators and even within repeated segmentations by the same operator (16,19).

Manual segmentation often serves as the reference standard against which semi-automated and automated approaches are validated. However, this "gold standard" status must be considered in the context of inherent operator variability and the potential for systematic bias (19). The method's time efficiency and reproducibility limitations have driven the development of more automated approaches, particularly for routine clinical applications.

Practical implementation of manual segmentation typically involves specialised software platforms providing tools such as:

- Brush and eraser tools for regional painting
- Contour drawing with spline interpolation.
- Threshold-based region growing with manual correction.
- Multi-planar reconstruction views for three-dimensional context
- Real-time volume rendering for segmentation verification (20)

These tools aim to optimise the efficiency and accuracy of manual delineation while maintaining operator control over the segmentation process. The selection of appropriate tools and visualisation methods can significantly affect the speed and quality of manual segmentation results.

Despite its limitations, manual segmentation remains essential in several contexts:

1. Validation of automated methods
2. Complex anatomical regions where automated approaches consistently fail.
3. Novel anatomical applications where automated algorithms have not been developed.
4. Research applications requiring the highest possible accuracy.
5. Training data generation for machine learning algorithms

The role of manual segmentation continues to evolve with advancing technology. Modern approaches often incorporate manual segmentation within hybrid workflows, where expert human input guides and refines automated processes. This synthesis aims to leverage the advantages of manual segmentation while mitigating its practical limitations.

1.2.2 Automated Segmentation in Abdominal-Pelvic Imaging: Challenges and Limitations of Classical Techniques

Fully automated segmentation remains a highly desirable goal owing to the time pressures of modern medicine. With ‘one click’ the whole task would be implemented accurately and reliably from start to finish.

Key requirements of automatic segmentation include:

1) Accuracy- relevant structures should be correctly identified and delineated precisely if results are to be used in clinical decision making.
2) Speed- results should be sufficiently quick to enable integration into current clinical workflows.
3) Reproducibility- results should be similar for different users analysing the same data.
4) Robust- methods should be applicable in a wide range of scenarios (15).

However, automated segmentation of abdominal and pelvic is challenging due to the complex anatomy, low tissue contrast, and imaging artefacts. This section critically examines the fundamental challenges inherent in abdominopelvic automated segmentation and analyses how these challenges impact the performance of classical segmentation techniques, including threshold-based, region-based, edge-based, and atlas-based approaches.

1.2.2.1 Fundamental Challenges in Abdomino-Pelvic Automated Segmentation

1.2.2.1.1 Anatomical Variability

A primary challenge in abdominopelvic segmentation is the significant anatomical variability between patients. Intraabdominal structures exhibit considerable variation in size, position [1](21). This variability is further compounded by congenital anomalies/variations, post-surgical changes, and tumours or lesions [2] (21).

1.2.2.1.2 Tissue Characteristics and Partial Volume Effects

The abdominopelvic region is characterised by soft tissues with similar radiodensities, leading to minimal differentiation in Hounsfield Units (HU) between adjacent structures in computed tomography (CT) images (22). For example, the HU values of the colon, duodenum, mesenteric vessels, and pancreas often overlap, complicating the task of distinguishing these organs based solely on intensity values [4]. Partial volume effects exacerbate this issue, occurring when a single voxel encompasses multiple tissue types,

resulting in averaged intensity values that do not accurately represent any constituent tissue (23). This effect is particularly pronounced at tissue interfaces and in small structures (e.g. small calibre blood vessels), making accurate segmentation challenging.

1.2.2.1.3 Imaging Artefacts

Motion-related artefacts introduce significant complexity into the segmentation process. Respiratory movement, cardiac pulsation, and peristalsis can cause image distortion and blurring, leading to inaccuracies in boundary delineation (23). For instance, respiratory motion during image acquisition can cause misalignment of anatomical structures between successive slices. Technical artefacts, including beam hardening—especially pronounced in the presence of metallic implants—scatter radiation, and reconstruction errors, further degrade image quality. The variability of these artefacts across different imaging protocols and patient characteristics necessitates segmentation methods that can handle inconsistent image quality (23).

1.2.2.1.4 Contrast and Resolution Limitations

Limitations inherent in imaging modalities also affect segmentation efforts. In CT imaging, balancing radiation dose with image quality often results in lower resolution images that may not capture fine anatomical details (24). Magnetic resonance imaging (MRI), while offering superior soft tissue contrast, can suffer from lower spatial resolution and longer acquisition times (25). Variable contrast enhancement due to differing timing and distribution of contrast agents can affect tissue differentiation, further complicating segmentation (26)

1.2.2.2 Limitations of Classical Segmentation Techniques in Abdominal-Pelvic Imaging

1.2.2.2.1 Threshold-Based Methods

Threshold-based segmentation classifies pixels or voxels based on their intensity values relative to predefined thresholds. While effective for distinguishing structures with significant intensity differences, this method struggles in the abdominopelvic region due to the homogeneity of tissue intensity between adjacent structures (27). Partial volume effects further compromise thresholding by producing averaged intensities at tissue boundaries (16). Consequently, threshold-based methods often yield inaccurate and fragmented segmentations in abdominopelvic imaging. Furthermore, adjusting thresholds manually for each patient is impractical and counteracts the benefits of automation. Moreover, pathological conditions can alter tissue intensities, rendering standard thresholds ineffective (28).

1.2.2.2.2 Region-Based Approaches

Region-based methods, such as region growing, consider both intensity and spatial connectivity by expanding regions from seed points based on similarity criteria (28). The effectiveness of region-based methods is limited by the homogeneity assumptions inherent in their design. Abdominal-pelvic structures often have heterogeneous internal structures and share similar intensities with neighbouring tissues (28).

Consequently, region-based approaches are susceptible to "leakage" in areas with gradual intensity transitions (29). Noise and artefacts further disrupt the homogeneity criteria, leading to erroneous region expansion. For example, when segmenting the pancreas, region growth may inadvertently include adjacent structures like the duodenum due to similar intensities and proximity (21). Extensive manual intervention may be required to correct these errors, reducing the practicality of these methods in clinical settings (21).

1.2.2.2.3 Edge-Based Methods

Edge-based segmentation focuses on detecting boundaries by identifying significant changes in intensity gradients (28). In the abdominopelvic region, however, soft tissue interfaces often exhibit gradual intensity transitions rather than sharp edges, making edge detection unreliable. Imaging artefacts and noise can produce false edges or obscure true boundaries (30). These limitations make edge-based methods insufficient for reliable abdominopelvic segmentation without significant pre-processing or post-processing corrections (30).

1.2.2.2.4 Atlas-Based Approaches

Atlas-based segmentation employs pre-labelled anatomical templates registered to patient images to transfer segmentation labels (31). While promising in theory, atlas-based methods face challenges due to significant anatomical variability in the abdominopelvic region (28). Differences in organ morphology, pathological changes, and motion artefacts can hinder accurate registration between the atlas and patient images (21).

Even advanced non-rigid registration techniques may struggle to accommodate the complex deformations caused by respiratory motion and peristalsis (32). Misregistration leads to incorrect label transfer and inaccurate segmentation, limiting the utility of atlas-based methods in clinical practice [. Additionally, creating comprehensive atlases that account for all anatomical variations is impractical (28,31).

A critical evaluation of commonly employed segmentation techniques in abdominopelvic imaging uncovers inherent limitations that hinder their effectiveness. These limitations stem not from implementation deficiencies but rather from these methods' underlying assumptions

about image and anatomical characteristics. Threshold-based approaches falter due to overlapping tissue intensities while region-growing methods struggle with complex tissue interfaces. Edge detection proves unreliable given gradual tissue transitions, and atlas-based techniques face challenges with anatomical variability (28).

The inherent complexity of abdominal anatomy, combined with technical imaging constraints, suggests that more sophisticated approaches are required. Future methods must address three key challenges:

1. Contextual Understanding: The ability to interpret anatomical relationships beyond simple intensity or gradient characteristics.
2. Adaptive Processing: Robust handling of anatomical variants and imaging artefacts
3. Knowledge Integration: Incorporation of prior anatomical understanding while maintaining flexibility for patient-specific variations

These requirements point toward machine learning approaches, which offer the potential to learn complex patterns from data while maintaining robustness to anatomical and technical variations. The following section examines these advanced techniques and their potential to overcome the limitations identified in classical approaches.

1.3 Deep Learning and Segmentation

1.3.1 Neural Networks: Theoretical Underpinnings

Neural networks, inspired by the architecture of biological neural systems, have emerged as powerful tools for approximating complex functions. The universal approximation theorem posits that a feedforward network with a single hidden layer containing a finite number of neurons can approximate any continuous function under certain conditions (33). This theoretical foundation underscores the potential of neural networks to model complex patterns within data, a capability crucial for tasks such as medical image segmentation.

Despite their theoretical versatility, classical multilayer perceptron (MLP) architectures exhibit significant limitations in processing image data. MLPs treat inputs as flat vectors, thereby disregarding the spatial relationships inherent in images (34). This lack of spatial awareness leads to inefficiencies:

- **Parameter Explosion**: High-dimensional inputs result in an exponential increase in the number of parameters, making the networks computationally infeasible and prone to overfitting (35).
- **Inability to Exploit Local Features**: MLPs fail to capture local spatial patterns essential for recognizing and segmenting anatomical structures (36).
- **Lack of Translational Invariance**: MLPs cannot generalise features across different spatial locations within an image (36).

These limitations necessitated the development of architectures capable of leveraging the spatial hierarchies and local connectivity of image data.

1.3.2 . Advanced Architectures for Segmentation

1.3.2.1 Convolutional Neural Networks (CNNs)

Convolutional neural networks (CNNs) are specialised neural networks that have become a dominant technique for medical image segmentation.

Convolutional Neural Networks (CNNs) address the fundamental shortcomings of MLPs by incorporating architectural innovations tailored to image processing (37). CNNs exploit spatial hierarchies through local connectivity, weight sharing, and pooling operations, thereby reducing the number of parameters and enhancing the ability to capture local and global features (37).

CNNs contain three primary types of layers: convolutional, pooling, and activation layers (figure 1-3).

1.3.2.1.1 Convolutional Layers

Convolutional layers perform feature extraction by applying learnable filters (kernels) across local regions of the input image. These filters capture spatially localised patterns, enabling the network to detect features such as edges, textures, and shapes (38). During training, backpropagation optimises the kernel weights so the network can identify task-relevant features effectively (39). Convolution is thus a dynamic feature extraction procedure, converting visual inputs into analytical data critical for tasks like classification and segmentation (40).

Considerations and Limitations:

- **Kernel Size and Depth**: The choice of kernel size affects the receptive field and the network's ability to capture features at various scales (41).

- **Data Biases**: Learned filters may inadvertently capture biases present in the training data, necessitating careful dataset curation (42).
- **Overfitting**: With insufficient data, convolutional layers may overfit, highlighting the importance of regularisation techniques (43).

1.3.2.1.2 Pooling Layers

Pooling layers are employed to reduce the spatial dimensions of feature maps, aggregating information and providing translational invariance (44). Common pooling operations include max pooling, which selects the maximum value within a local neighbourhood, and average pooling, which computes the average value. By reducing the spatial resolution, pooling layers decrease the computational load and the number of parameters in subsequent layers, helping to prevent overfitting. They also provide a degree of spatial invariance, allowing the network to recognise features regardless of their exact location in the input. However, pooling can discard fine details critical for identifying subtle pathological features (45).

1.3.2.1.3 Activation Functions

Activation functions introduce non-linearity, enabling the network to model complex patterns. The Rectified Linear Unit (ReLU) is widely used due to its computational efficiency and mitigation of the vanishing gradient problem (46,47). However, alternatives like the Gaussian Error Linear Unit (GELU) and Swish have shown superior performance in certain contexts (48,49).

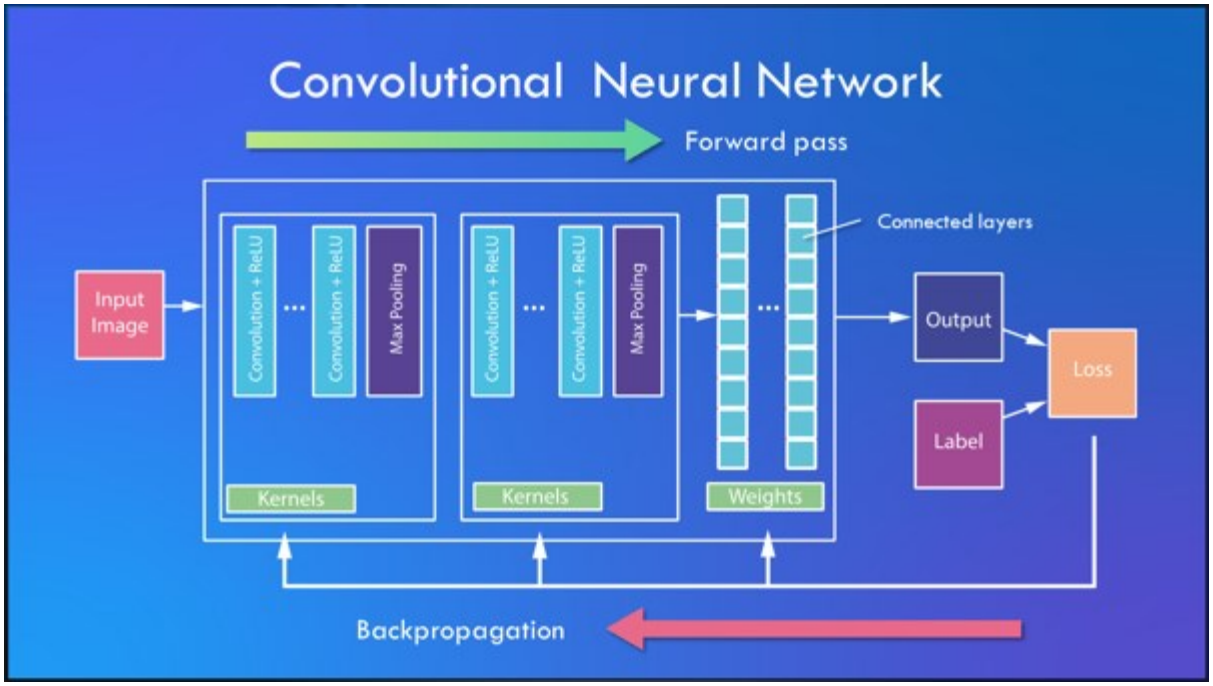


Figure 1-3 *Overview of convolutional neural network. The network consists of the following key components.*

- ***Input Image****: This is the raw image that is fed into the CNN for processing.*
- ***Convolution + ReLU****: These blocks represent the convolutional layers where the input image is convolved with various kernels (also known as filters) to detect features such as edges, corners, etc. The ReLU (Rectified Linear Unit) function introduces non-linearity into the system, allowing the network to learn complex patterns.*
- ***Max Pooling****: Following convolution layers, max pooling layers are used to reduce the spatial dimensions (width and height) of the input volume for the next convolution layer. It helps to reduce the computational load, memory usage, and helps to make the detection of features invariant to scale and orientation.*
- ***Connected Layers****: After several convolution and pooling layers, the high-level reasoning in the neural network is done via fully connected layers. Neurons in a fully connected layer have full connections to all activations in the previous layer.*
- ***Output****: This is the final layer that provides the predictions of the network. It typically has several units corresponding to the number of classes for a classification task.*
- ***Loss****: The loss function calculates how far the network's prediction is from the actual label. It's a measure of the error and is used during training to update the weights through a process known as backpropagation.*
- ***Label****: This represents the true classification of the input image, used during training to compute the loss.*
- ***Forward Pass****: This arrow signifies the direction of data flow during the prediction phase, from the input image through the different layers up to the output.*
- ***Backpropagation****: This process involves calculating the gradient of the loss function with respect to each weight by the chain rule, moving backwards through the layers to update the weights and minimize the loss function.*

Training Dynamics and Loss Functions in Medical Image Segmentation

- The training process for CNN-based medical image segmentation employs sophisticated loss functions and optimisation strategies tailored to the unique challenges of anatomical delineation. Segmentation-specific loss functions play a crucial role in guiding the network's learning process, with two predominant approaches emerging in medical applications (50).
- The Dice similarity coefficient loss function specifically addresses the common challenge of class imbalance in medical imaging, where regions of interest often occupy a small fraction of the total image volume. This loss function quantifies the spatial overlap between predicted and ground truth segmentations, providing a more meaningful measure of segmentation accuracy than traditional pixel-wise metrics (51).
- Weighted cross-entropy loss functions incorporate spatial context by applying varying weights to different regions of the image. This approach proves particularly valuable for emphasizing boundary regions, where segmentation accuracy is often most critical. The weighting scheme can be adapted to prioritize clinically relevant regions or account for varying levels of uncertainty in the ground truth annotations (52).
- The optimisation process follows a structured sequence of operations during each training iteration. Initially, the network performs a forward pass, generating predicted segmentation masks from input images. These predictions undergo comparison with expert-annotated ground truth segmentations using the chosen loss function. The backpropagation algorithm then computes gradients through the network using the chain rule, determining how each network parameter contributed to the prediction error (43).
- Parameter updates occur through carefully chosen optimisation algorithms, typically variants of stochastic gradient descent (53). These optimisers dynamically adjust the magnitude of parameter updates based on the historical behaviour of gradients, helping to navigate the complex loss landscapes characteristic of deep neural networks.

1.3.3 U-Net and Its Variants

1.3.3.1 The U-Net Architecture

The U-Net architecture, initially proposed by Ronneberger et al. (52) represents a paradigmatic advancement in medical image segmentation methodology. Its distinctive characteristic lies in its symmetric encoder-decoder framework augmented by skip connections, facilitating simultaneous contextual information extraction and precise spatial localisation (54) (see figure 1-5). The architecture's fundamental components are as follows:

- **Encoder Pathway (Contracting Path)**: This pathway implements progressive down sampling operations through successive convolutional and pooling layers, facilitating hierarchical feature abstraction. Each down sampling step typically doubles the number of feature channels, enabling the network to capture increasingly complex semantic information while reducing spatial dimensionality (54).
- **Decoder Pathway (Expanding Path)**: The decoder systematically restores spatial resolution through transposed convolutions or up sampling operations. This progressive spatial reconstruction is crucial for generating detailed segmentation maps at the original image resolution. Each up sampling operation is accompanied by a corresponding reduction in feature channels (52).
- **Skip Connections**: These connections establish direct pathways between corresponding encoder and decoder levels, facilitating the integration of high-resolution features with contextual information. This architectural element is particularly crucial for preserving fine structural details that might otherwise be lost during the encoding process (45).

The architecture has demonstrated efficacy across diverse medical imaging applications (45). Its success can be attributed to its ability to maintain a balance between global contextual understanding and local structural precision.

An important evolution of the U-Net architecture is the 3D U-Net, designed specifically to handle volumetric medical imaging modalities such as magnetic resonance imaging (MRI) and computed tomography (CT) scans. Proposed by Çiçek et al. (2016), the 3D U-Net extends the original 2D U-Net to three dimensions, enabling the network to learn volumetric features directly from the data (45).

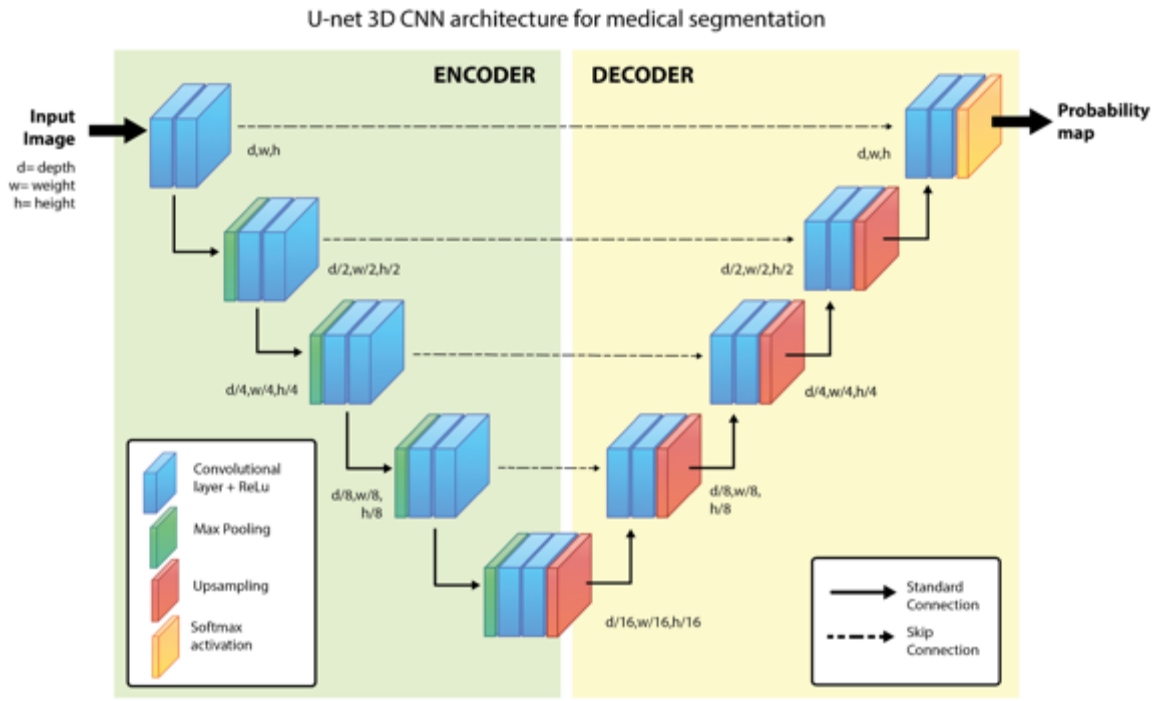


Figure 1-4 *Architecture of 3D CNN with U-net design. The network accepts 3D imaging data (3D tensor) and subsequently down and up samples the input data. The final probability map predicts the likelihood that a given voxel belongs to the training labelling data.*

1.3.3.2 U-Net Limitations and Enhancements

Despite its widespread adoption, the original U-Net architecture exhibits several limitations that have prompted the development of various enhancements.

Limitations:

- **Computational Inefficiency:**

The concatenation of feature maps via skip connections leads to a substantial increase in memory usage and computational cost, particularly when processing high-resolution 3D medical images (55) This inefficiency can hinder the network's scalability and applicability in resource-constrained environments.

- **Architectural Rigidity:**

The fixed topology of the U-Net does not readily adapt to varying image resolutions or scales of anatomical structures, potentially limiting its effectiveness across different imaging modalities and clinical applications.

- **Feature Redundancy:**

Uncontrolled propagation of features through skip connections may result in redundant or irrelevant information being passed to the decoder. This redundancy can contribute to overfitting and unnecessary computational overhead without proportional gains in performance (56).

Contemporary Architectural Variants:

To address these limitations, several variants of the U-Net architecture have been proposed, incorporating novel mechanisms and design principles.

1.3.3.3 V-Net Architecture:

The V-Net, introduced by Milletari et al., extends the U-Net architecture to three-dimensional (3D) medical image segmentation tasks (50). Designed specifically for volumetric data, the V-Net employs volumetric convolutions and deconvolutions, enabling end-to-end learning from 3D input images to 3D output segmentation maps.

Key features of the V-Net include:

- **Residual Connections:**
  Unlike the original U-Net, which uses concatenation in skip connections, V-Net incorporates residual connections inspired by ResNet architectures (57). These connections add the input of a layer to its output, facilitating the training of deeper networks by alleviating the vanishing gradient problem (this arises when gradients of the loss function become very small as they are backpropagated through multiple layers of the network. This issue hampers effective weight updates in the earlier layers, leading to suboptimal learning) (50).

- **Dice Loss Function:**
  V-Net utilizes the Dice similarity coefficient as the loss function during training. This choice directly optimizes the metric of interest in segmentation tasks, especially when dealing with imbalanced datasets where the foreground objects occupy a small fraction of the volume (54).

The V-Net has demonstrated superior performance in segmenting anatomical structures in volumetric data, such as prostate MRI and cardiac CT images (50). Its design addresses the computational challenges associated with processing 3D data by efficiently managing memory usage and computational resources.

1.3.4 Transformer-Based Architectures

1.3.4.1 Vision Transformers (ViT)

In recent years, transformer-based architectures have emerged as a powerful alternative to convolutional neural networks (CNNs) for various computer vision tasks (58). Originally introduced in the context of natural language processing (NLP) (59), transformers have been adapted for image analysis through models such as the Vision Transformer (ViT) (60). The ViT architecture leverages self-attention mechanisms to capture global dependencies within the data, offering a novel approach to image segmentation that addresses some of the inherent limitations of CNNs (60).

Mechanism of Vision Transformers

The core of transformers lies in the self-attention mechanism, which allows the model to weigh the relevance of different parts of the input data relative to each other. In the context of image analysis, the ViT processes an image as a sequence of patches rather than as a grid of pixels) (60). The following steps outline how a transformer operates on image data:

The transformer architecture comprises four essential components:

- Patch Embedding: The initial image undergoes division into a sequence of non-overlapping patches. These patches are flattened and projected into a lower-dimensional space through a learnable linear transformation. This crucial step transforms the grid-structured image data into a sequence format suitable for transformer processing.
- Positional Encoding To preserve spatial relationships within the image, positional information is embedded alongside the patch data. This encoding ensures the model retains awareness of each patch's original location in the image, which is vital for accurate spatial analysis.
- Transformer Encoder The core processing occurs in the transformer encoder, which consists of alternating layers of:

- Multi-head self-attention: Computes relationships between all patches simultaneously, enabling the capture of both local and global image features.
- Feed-forward networks: Process each position independently through fully connected layers, adding non-linear transformations to the model.

- Output Processing The final output represents a comprehensive embedding of the input image, capturing both local features and global contextual relationships. This output can be adapted for various tasks, including classification and segmentation.

1.3.4.2 Advantages of Vision Transformers in Medical Imaging

The self-attention mechanism enables Vision Transformers to model interactions between distant regions of an image effectively, providing a global contextual understanding that is particularly valuable in medical imaging. Pathological features in medical images often exhibit complex spatial relationships that may not be adequately captured by the local receptive fields of CNNs. The ViT's ability to consider the entire image context allows it to recognize patterns and dependencies that span large spatial extents.

Furthermore, the ViT offers a flexible representation capable of processing variable-sized inputs and focusing on salient features without being constrained by the locality bias inherent in convolutional operations. This flexibility can be advantageous when dealing with medical images of different resolutions or when the scale of anatomical structures varies significantly.

1.3.4.3 Challenges and Limitations

Despite these advantages, several challenges arise when applying Vision Transformers to medical image segmentation. One significant limitation is the substantial data requirement for training transformers effectively. Transformers lack the inductive biases present in CNNs, such as translation invariance and locality, which help CNNs generalize well from limited data. As a result, transformers often require large-scale datasets to learn meaningful representations, a condition that is difficult to meet in medical imaging due to the scarcity of annotated data (58).

Additionally, the computational complexity of the self-attention mechanism, which scales quadratically with the input sequence length (i.e., the number of patches), poses practical challenges. High-resolution medical images result in many patches, leading to increased memory consumption and longer training times. This computational demand can limit the applicability of ViTs in settings where resources are constrained (58).

1.4 Rendering Methods in 3D visualisation

We can broadly divide two rendering approaches to 3D medical visualisation:

1) Volumetrically (direct) rendered models.
2) Surface (indirect) rendered models.

1.4.1 Volumetric Rendering

Volumetric or direct volume rendering is one of the two primary techniques for visualising medical imaging data in its raw, unprocessed form (61). This approach bypasses any intermediate representation, projecting volumetric data directly onto the viewing plane via sophisticated optical models that simulate light interaction with materials (62).

Volumetric or direct volume rendering is one of the two primary techniques for visualising medical imaging data in its raw, unprocessed form (61). This approach bypasses any intermediate representation, projecting volumetric data directly onto the viewing plane via sophisticated optical models that simulate light interaction with materials (62).

1.4.1.1 Theoretical foundations

At the core of volume rendering lies the simulation of light interaction within a participating medium—a medium where light is absorbed, emitted, and potentially scattered as it travels through it. The physical principles governing this interaction are based on radiative transfer theory, which models the behaviour of light as it propagates through a volume. However, solving the full radiative transfer equation is computationally intensive due to the complexity of accounting for all possible interactions of light within the medium, including scattering in multiple directions.
To render the computational requirements manageable for clinical applications, various architectural optimisations and methodological constraints are frequently implemented.

The simplest approach, absorption-only model, assumes light within the volume can only be absorbed, neglecting emission and scattering effects. While computationally efficient, this model produces limited depth cues and tissue differentiation capabilities.

A widely adopted model in volume rendering is the **emission-absorption model**, which focuses solely on absorption and emission phenomena while neglecting scattering effects. This model assumes that as light travels through the medium, it is attenuated due to absorption and augmented by emission from the medium itself. The cumulative effect of

these interactions along a viewing ray determines the intensity of light reaching the observer (63).

1.4.1.2 Transfer Functions and Data Classification in Volume Rendering

Transfer functions serve as a critical component in volume rendering by establishing the mapping between raw imaging data and visual properties. In medical imaging, the scalar values typically represent tissue-specific physical properties - Hounsfield Units (HU) in computed tomography or signal intensities in magnetic resonance imaging (64).
Transfer functions map these scalar values to optical properties through several approaches:

1.4.1.2.1 One-dimensional Transfer Functions

The simplest approach maps scalar values directly to colour (RGB) and opacity (α) values. While computationally efficient, these functions struggle to differentiate structures with overlapping intensity ranges. For instance, differentiating adjacent soft tissues with similar HU values presents a significant challenge.

1.4.1.2.2 Multi-dimensional Transfer Functions

Multi-dimensional transfer functions represent a more sophisticated approach to volume classification by incorporating derived measures beyond simple scalar values (63). These functions leverage first derivatives, particularly gradient magnitude, to effectively identify tissue boundaries and transitional regions (65). Second derivatives enable the detection of subtle structural changes, while statistical measures facilitate texture-based tissue differentiation (66) The incorporation of distance measures from anatomical landmarks provides valuable spatial context, particularly beneficial in complex anatomical regions where traditional intensity-based classification proves insufficient (67). This multi-dimensional approach, while computationally more intensive than single-dimensional transfer functions, enables more nuanced tissue differentiation and improved boundary detection in medical visualisation applications (66).

Transfer function design employs several methodological approaches, ranging from manual specification to automated techniques. The most straightforward approach involves direct specification, where colour and opacity values are manually defined for specific scalar ranges based on standardised tissue-specific Hounsfield Units, though this requires considerable expertise and iterative refinement (68). More sophisticated approaches leverage histogram analysis to identify peaks corresponding to distinct tissue types, facilitating automatic or semi-automatic transfer function generation (69). Recent advances have introduced data-driven approaches utilising machine learning techniques trained on expert-annotated datasets, enabling the incorporation of domain-specific medical knowledge (70). Feature-based classification methods extend beyond simple scalar value mapping by

incorporating derived measures such as gradient magnitude, enabling enhanced boundary detection and structure differentiation - particularly valuable for complex anatomical regions where tissue boundaries may be subtle or gradual (71). These various approaches offer different trade-offs between automation, accuracy, and computational complexity, with the choice of method often guided by specific clinical requirements and computational constraints (72).

1.4.1.3 Practical Implementation: Discrete Ray Casting

In practical implementations, the continuous model of light interaction within the volume is approximated using numerical methods. One predominant approach is ray casting, where rays are projected from the observer's viewpoint through each pixel of the image plane into the volumetric dataset.

1.4.1.3.1 Ray Casting Process

1. **Ray Initialization**: For each pixel on the image plane, a ray is generated starting from the observer's eye position and passing through the pixel into the volume.
2. **Sampling**: Along each ray, the volume is sampled at discrete intervals. At each sample point, the scalar data value is retrieved, often through interpolation of the surrounding voxel data.
3. **Opacity and Colour Assignment**: The scalar values are mapped to optical properties—opacity and colour—using the **transfer function**.
4. **Compositing**: The contributions from each sample are accumulated along the ray to compute the final pixel colour. Starting from the nearest point to the observer, the colour and opacity of each sample are combined, considering how previous samples have attenuated the light. This process continues until the ray exits the volume or the accumulated opacity becomes high enough that further contributions are negligible.

1.4.1.3.2 Optimisation Techniques

Rendering high-resolution volumetric datasets interactively poses significant computational challenges. To achieve the performance necessary for practical applications, especially in clinical settings, various optimisation strategies are employed.

1. ***Early Ray Termination***

Early ray termination leverages the observation that once the accumulated opacity along a ray becomes sufficiently high, additional contributions to the pixel colour are minimal.

Therefore, the processing of a ray can be halted early, reducing computational workload without significantly affecting image quality. This optimisation is particularly effective in regions with dense structures, such as bones in CT scans, where opacity accumulates quickly (73).

2. ***Empty Space Skipping***

Empty space skipping involves identifying regions within the volume that do not contribute meaningfully to the final image, such as areas outside the object of interest or regions of uniform intensity. By bypassing these regions during ray traversal, computational resources are focused on processing relevant data. Techniques such as space leaping and the use of bounding volumes help in efficiently skipping over empty spaces, improving rendering performance (73).

3. **Acceleration Structures**

Spatial data structures like octrees or k-d trees are used to organize the volumetric data hierarchically, enabling efficient traversal and sampling. These acceleration structures facilitate rapid identification of empty or homogeneous regions and support adaptive sampling strategies. By adjusting the sampling rate based on the complexity of the data in different regions, computational efficiency is improved without compromising image quality (73).

4. **GPU-Accelerated Volume Rendering**

The emergence of programmable Graphics Processing Units (GPUs) has fundamentally transformed volume rendering capabilities through massive parallelism and enhanced memory bandwidth (74). Modern implementations leverage shader programming and texture mapping functionalities to perform ray casting operations directly on GPU hardware, enabling real-time rendering of substantial datasets (75). Volume bricking techniques address memory constraints by partitioning datasets into manageable blocks, loading only view-relevant data segments (76,77).

1.4.2 Surface Rendering

In contrast to direct rendering methods, surface rendering relies on creating a polygon mesh intermediary form of the dataset, which is subsequently rendered. This approach is labelled

'indirect' because it relies on a representation separate from the original dataset. Unlike volume rendering, which directly converts volume data into images, surface rendering uses an indirect approach by creating a polygon mesh representation. This mesh can be derived by isolating an isosurface from the original volume data or modifying segmentation results. A polygon mesh comprises an interconnected network of vertices, edges, and faces, shaping the structure of a polyhedral object. Vertices represent a position in three-dimensional Euclidian space. When a straight-line links two vertices, they form an edge, the basic mesh geometry unit. The faces of the mesh, which are the flat surfaces, are constructed by connecting these edges. Typically, a face is either a triangle, formed by three vertices and their respective edges, or a quadrangle (often referred to as 'quads'), which involves four vertices and four edges (78).

1.4.2.1 Historical context and evolution of surface rendering

The historical development of surface rendering in medical imaging reflects the interplay between technological constraints and clinical requirements. Initially adopted primarily for its computational efficiency, surface rendering emerged as the predominant approach to three-dimensional medical visualisation during an era of limited computational resources (61). The technique's ability to generate interpretable images with clear depth cues and illumination proved particularly valuable in early medical visualisation applications, where immediate visual comprehension was paramount (79).

The advent of modern graphics processing units (GPUs) and parallel computing architectures has fundamentally altered the computational landscape of medical visualisation. Contemporary GPUs support hardware-accelerated ray casting and texture-based volume rendering, enabling real-time processing of large volumetric datasets (80). These advances have substantially diminished the original performance advantages that drove the adoption of surface rendering techniques. However, rather than rendering surface rendering obsolete, these technological developments have enabled more sophisticated applications of the technique.

Despite the diminished computational advantages, surface rendering remains important in medical visualisation due to several factors:

(a) Interactive Visualisation on Web and Mobile Platforms

Surface rendering favours interactive visualisation on web and mobile platforms because of its lower memory requirements and reduced computational demands (79). Web-based applications using technologies like WebGL can efficiently render and manipulate surface meshes in browsers without specialised hardware (81). This accessibility is crucial for telemedicine, remote consultations, and educational purposes.

(b) Requirement for 3D Printing

Surface mesh models are essential for 3D printing applications in medicine. The process of additive manufacturing relies on geometric representations of structures to fabricate physical models (82).

(c) Biomedical Virtual Simulation Using Game Engines

Biomedical simulations using computer game engines require surface mesh models to produce deformable objects with physical properties (79). Game engines like Unity and Unreal Engine provide physics simulations, collision detection, and interactive environments where anatomical models can be "digitally dissected" or manipulated (83,84). Surface meshes enable these engines to apply finite element methods and other computational models for realistic simulations.

(d) Advanced Model Manipulation in Commercial Graphics Software

Most commercial computer graphics software operates with surface meshes, allowing for advanced model manipulation techniques. These include:

- **Digital Sculpting:** Programmes like ZBrush enable detailed sculpting of anatomical features, adding fine details beyond the resolution of imaging data (85).
- **Division of Structures:** Meshes can be segmented into subcomponents, facilitating focused studies on specific anatomical regions.
- **Colourisation and Transparency:** Surface meshes support per-vertex or per-face colour assignments, enabling detailed colouring and transparency effects to highlight structures.
- **Realistic Texturing:** Textures and materials can be applied to meshes to simulate realistic organ appearances, enhancing visual comprehension (86).

1.4.3 Surface rendering methods

1.4.3.1 Mesh extraction using marching cubes algorithm.

The marching cubes algorithm is utilised to reconstruct surfaces from 3D volumetric datasets. Developed in 1987 by William Lorensen and Harvey Cline, this computer graphics technique efficiently extracts an isosurface as a triangular mesh model (87).

It operates by partitioning the volume data into a grid of cubic cells, each defined by eight corner vertices (voxels). By evaluating the scalar field/segmentation label at these vertices against a chosen isovalue, the algorithm determines the topology of the isosurface within each cell (88).

The marching cubes algorithm adeptly handles previously segmented data. As described above, each voxel contains a discrete label rather than continuous density. To reconstruct a surface, voxel labels are checked against the label of interest rather than an isovalue threshold (79).

The core algorithm is unchanged. Cubes are processed cell-by-cell, analysing labelling patterns at the corners. Instead of density gradients, intersections now lie at label boundaries. These transitions are triangulated into surface facets within each cell (79). Pre-segmentation simplifies surface selection and reduces noise. It also isolates individual structures without visualising all tissue boundaries. But the critical process remains identical - marching through the volume in cubes, tabulating edge intersections via lookup tables, and connecting triangular patches.

This versatility to handle raw and segmented data makes marching cubes vital for medical imaging. As segmentation algorithms improve, it provides an efficient path to visualise labelled volumes in 3D.

1.4.3.2 Post-Processing of Extracted 3D Geometry

Converting volumetric scan data into 3D surface models involves key post-processing steps to optimise visual appearance, functionality, and performance.

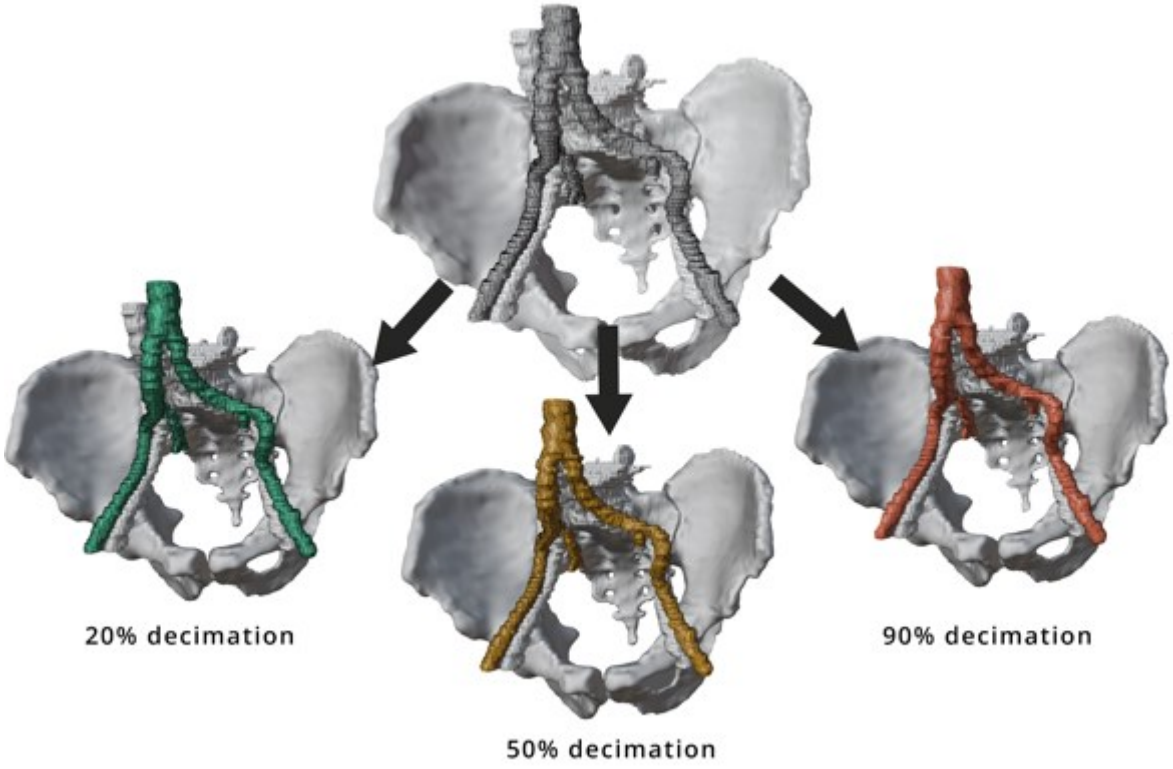
Two essential techniques are decimation and smoothing. However, where clinical applications demand high anatomical accuracy, post-processing should be limited owing to the potential distortion of the original geometry.

1.4.3.3 Decimation

The marching cubes algorithm, while effective at extracting surface geometry, typically generates meshes comprising hundreds of thousands of polygons from high-resolution medical scans, far exceeding the requirements for practical visualisation. Decimation addresses this limitation through systematic reduction of mesh complexity, selectively removing vertices and faces while preserving anatomical fidelity and critical features. (87). This optimisation proves particularly crucial for web-based and mobile applications, where rendering performance directly impacts usability. The target performance of 60 frames per second, considered optimal for smooth interaction, necessitates careful balance between visual quality and geometric complexity (89).

Various decimation strategies exist, each offering different trade-offs between processing speed and geometric accuracy. Error-quadric based approaches evaluate the impact of each potential vertex removal on the overall surface geometry, prioritising operations that minimise visible changes. Local approaches focusing on edge collapse operations offer faster processing but may sacrifice some geometric accuracy. The degree of decimation must be carefully calibrated for different anatomical structures; while relatively planar regions may tolerate aggressive simplification, complex structures such as vascular networks require more conservative approaches to maintain anatomical accuracy (90).

Figure 1-5 Demonstrating the effect of different levels of decimation.



1.4.3.4 Smoothing

Smoothing eliminates jagged surfaces and staircase artefacts to improve visual quality. The marching cubes produce noticeable sharp discontinuities between adjacent cubes. Smoothing blends these seams for more natural surfaces (91). Most smoothing approaches do not alter the number of vertices but instead change their position and are therefore deemed topology-preserving (79).

Common approaches iteratively adjust vertex positions based on surrounding geometry. For example, Laplacian smoothing moves vertices to the average location of their neighbours (91). Low-pass filters can also be applied in the normal or domains (92). These methods improve appearance but can shrink and distort geometry.

Alternative edge-preserving filters like bilateral smoothing better maintain fidelity (93). GUIDOS also shows promise for selective smoothing of medical models (94). Smoothing must balance visual improvement against anatomical accuracy requirements in medical use cases.

1.4.3.5 Colourisation

The application of colour is essential for distinguishing anatomical structures and aiding in user comprehension.

- Hue - Unique hues like red, blue, and yellow are more easily discriminated than shades.
- Value - Lighter and brighter colours stand out against darker backgrounds.
- Complementary colours - Pairing opposite hues like blue/orange maximises contrast.
- Context - Consideration of the semantic meaning colour can hold.

Adhering to established medical illustration colour conventions also capitalises on existing user familiarity. For example, arteries are red, veins are blue, nerves are yellow, etc. Selective colourisation focusing on structures of interest reduces visual clutter. The judicious use of colour is critical for effectively communicating complex 3D relationships (95).

1.4.4 Advanced 3D modelling techniques

Advanced computer graphics techniques, originally developed for visual effects and gaming industries, have been adapted for medical visualisation to create highly detailed, photorealistic anatomical models. These approaches utilise sophisticated software pipelines, integrating specialised applications such as ZBrush, Maya, and Blender, each offering complementary capabilities for model enhancement, texture generation, and material definition. The application of these techniques to medical visualisation represents a significant advancement over traditional approaches, enabling the creation of models that combine anatomical accuracy with enhanced visual comprehension through photorealistic rendering (96).

1.4.4.1 Complex 3D Modelling and Digital Sculpture

Complex polygon modelling in specialised software provides powerful mesh manipulation with tools to separate, extrude, and animate components (97). This enables dividing models into distinct regions and adding thickness to surface-only structures like vessels (86). Animation tools are valuable for illustrating motion and function.

Digital sculpture facilitates detailed organic modelling ideal for anatomy (85). Sculpting introduces fine surface details like muscle striations, challenging traditional techniques. Adaptive subdivision enables high-poly sculpting projected as normal maps onto low-poly

models, combining detail and performance (98). This workflow allows adding high-frequency details while retaining low polygon counts for efficiency.

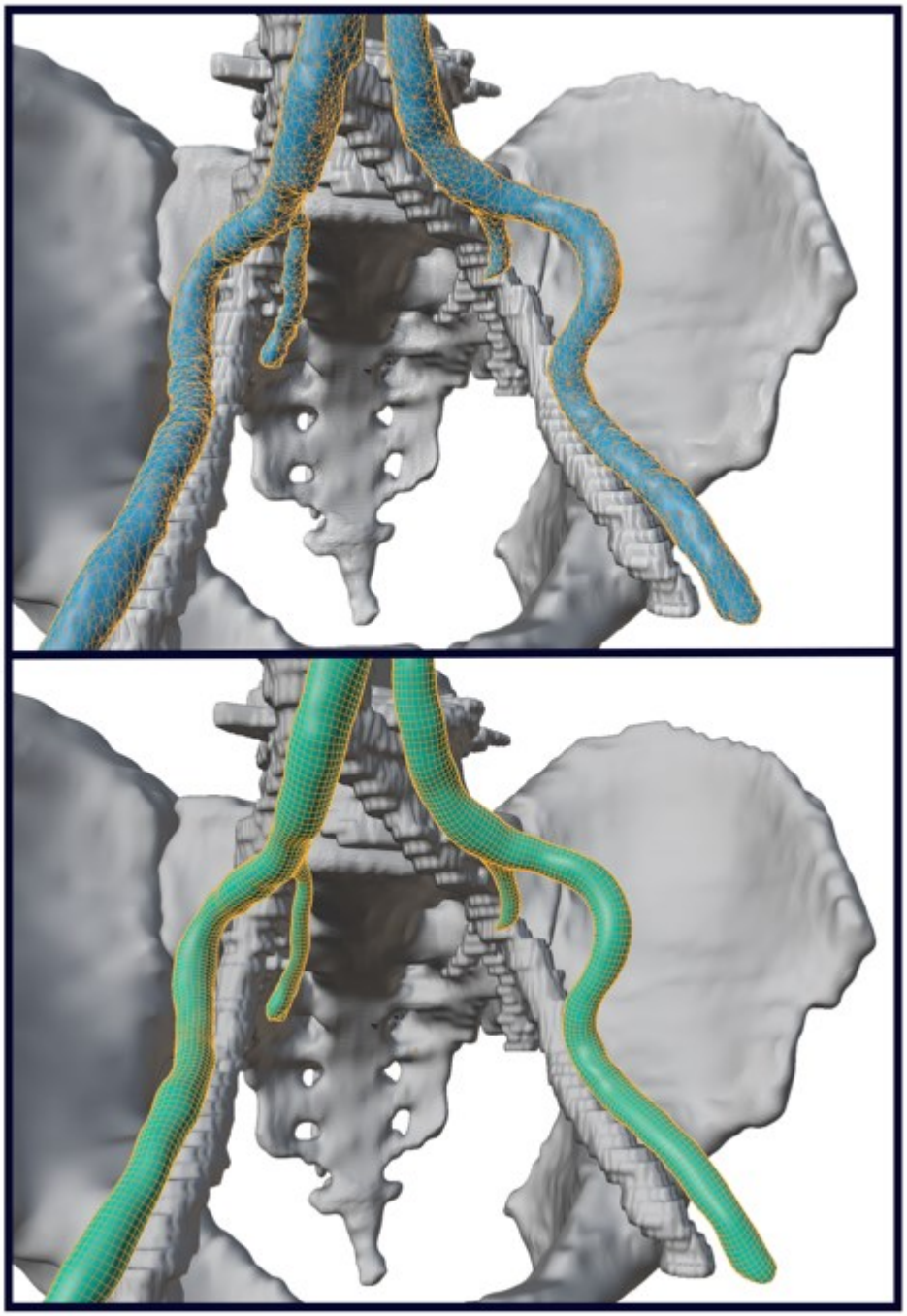
1.4.4.2 Retopology and Quad Remeshing

Segmented medical models contain triangle meshes. Quad remeshing converts these into quad-based meshes better suited for optimisation, texturing, and animation (99). Most software provides rapid retopology tools and quad-focused algorithms to rebuild the model with primarily quads instead of triangles.

Quad meshes are preferred in many applications because they:

- **Facilitate Deformation:** Quads deform more predictably during animation or simulation (100).
- **Support Subdivision Surfaces:** Quads are compatible with subdivision algorithms that smooth meshes while preserving shape, enabling multi-resolution modelling (78).
- **Enhance Edge Flow:** Proper edge flow aligns with the natural contours of the anatomy, improving visual quality and facilitates placement of UV seams (see below) (99).

Figure 1-6 Tri to Quad retopology



1.4.4.3 UV Unwrapping

UV unwrapping maps 3D coordinates onto a 2D texture space and is a fundamental requirement for texture application. Each vertex in the 3D mesh is assigned a coordinate (U, V) in the 2D texture space, establishing a correspondence between the 3D model and the 2D image.

Seams define how the 3D model is cut and laid out on the 2D UV grid. Seam placement is optimised for clean, minimal distortion layouts specific to each model region. UV maps should have uniform texel density (texel density refers to the level of detail present in a texture map, it is measured by the number of texels, or texture elements packed into a given area) and scale with efficient use of space. Grids verify correct unwrapping before texturing (101)

1.4.4.4 Physically based rendering and texture mapping

Physically Based Rendering (PBR) is an approach that seeks to render images in a way that models the flow of light in the real world, producing materials that react to lighting conditions realistically (26). PBR has become a standard in industries like gaming and film due to its ability to achieve consistent and plausible results under varied lighting environments.

In medical visualisation, PBR enhances the realism of anatomical models, improving depth perception and material differentiation, which is beneficial for educational and communicative purposes (27).

PBR relies on various texture maps to define the physical properties of materials. Each map describes different physical properties of a material as summarised in table 1-2.

Table 1-2 Common texture maps used in PBR rendering.

Map Type	Description
Base Colour	Defines diffuse colour without lighting. Photographic textures provide realism.
Metallic	Controls reflectance qualities - metals vs dielectrics.
Roughness	Defines microsurface irregularities diffusing reflections.
Normal	Encodes surface normals to fake geometry details (Surface normals are vectors perpendicular to a surface that indicate the orientation of the surface relative to the lighting direction) (102).
Bump	Adds simulated minor height variations.
Displacement	Alters underlying mesh vertex positions.
Specular	Controls specular reflection qualities.
Glossiness	Similar to roughness, defines surface shininess/diffusion.
Ambient Occlusion	Simulates local occlusion to add realism.
Emission	Defines self-illumination.
Transparency	Controls geometrical transparency.
Translucency	Simulates subsurface light diffusion and scattering.

1.5 Visualisation methods

The effectiveness of 3D medical models depends not only on the quality of their reconstruction but critically on how users interact with them. An understanding of user requirements and interface design is essential, as different clinical applications demand distinct forms of interaction. Surgeons planning complex procedures may require precise control over model orientation, transparency, and cross-sectional views, while patients need intuitive interfaces that facilitate understanding without technical expertise. The choice of visualisation platform therefore must consider both technical capabilities and user experience design.

Key interaction requirements typically include:

- Rotation, panning and zooming controls.
- Selective visibility of anatomical structures
- Cross-sectional viewing capabilities
- Measurement tools
- Annotation features
- Screenshot or video capture functionality.

Various platforms and technologies exist for visualising computer-generated 3D models. Each solution offers different capabilities and trade-offs between ease of use, interactive features, and development requirements.

1.5.1 WebGL and Three.js

Web-based visualisation has become increasingly sophisticated through WebGL (Web Graphics Library), a JavaScript API that enables hardware-accelerated 3D graphics rendering within modern web browsers. WebGL provides low-level access to the graphics processing unit (GPU), allowing real-time manipulation of complex 3D models without requiring additional plugins. However, its relatively complex implementation has led to the development of higher-level libraries that abstract these capabilities (81).

Three.js has emerged as a particularly valuable abstraction layer for medical visualisation applications (103). This JavaScript library simplifies WebGL implementation while maintaining performance suitable for interactive medical models. It provides built-in support for essential features such as lighting, materials, and camera controls that facilitate

anatomical visualisation. Importantly, Three.js enables the integration of custom shaders, model loaders and advanced visual effects that can enhance the representation of anatomical structures through selective transparency, highlighting, and cross-sectional views (104).

Integration with server-side frameworks (e.g. Django (105), Flask etc.) can address inherent limitations of browser-based rendering through server-side processing of large datasets, sophisticated caching strategies, and optimised data delivery pipelines. Front-end frameworks like React (106) or Vue.js (107) enhance the user interface layer, enabling responsive layouts, state management, and complex interaction patterns. This distributed architecture maintains the accessibility benefits of web-based platforms whilst facilitating sophisticated features for medical education and surgical planning applications through both client and server-side optimisations.

A key advantage of web-based platforms is their cross-platform accessibility and ease of distribution. Users can access sophisticated 3D visualisations through standard web browsers without installing specialised software. This makes web-based solutions particularly suitable for educational applications and patient communication tools. However, browser-based rendering faces certain limitations, particularly regarding memory management and processing of large datasets typical in medical imaging.

1.5.2 Game Engines

Game engines like Unreal and Unity are integrated development environments offering comprehensive tools for creating interactive real-time 3D applications. They combine rendering engines, physics simulations, audio systems, and scripting tools to facilitate sophisticated 3D visualisation and interaction possibilities.

Both engines support essential medical visualisation requirements, such as interactive 3D model manipulation, physics-based simulation, and virtual/augmented reality integration. However, Unreal Engine typically demands greater computational resources and has a steeper learning curve, while Unity may require additional development effort for complex visualisations but offers greater accessibility. The choice between these platforms ultimately depends on specific project needs, including desired visual fidelity, performance requirements, development expertise, and deployment constraints.

1.5.3 Specialised Commercial Software

Specialised medical software like 3D Slicer (108), Mimics (Materialise, 2023 (109)), Innersight labs (110) and Visible Patient (111) allows direct use of DICOM and other medical imaging formats, providing an ecosystem focused on clinical utility.

The choice of visualisation platform is guided by the specific clinical context and use cases. While visual realism can be essential and facilitate user comprehension, this should not be at the expense or neglect of required clinical functionalities.

The crucial consideration should be enabling accurate anatomy and functional simulations to inform the surgical approach, resection planning, implant design, and other clinically driven tasks.

Virtual reality (VR) for 3D model interaction has gathered recent attention, given its immersive and intuitive spatial visualisation capacity. Workflow integration of virtual and augmented reality remains limited. The practical advantage over traditional 3D planning user desktop interfaces remains debatable, and wearing an occlusive headset in the operating room poses logistical challenges (112).

1.5.4 3D printing

The rapid development of 3D printing technology in recent years has created new possibilities in surgical planning and education. Dramatic reductions in cost along with improvements in the accuracy have facilitated production of patient-specific anatomical printed models.

3D printing or additive manufacturing/rapid prototyping was originally described in 1980's and is based on the principle of sequentially layering material to construct a physical object. Each layer of material will be of equal thickness which vary between machines and techniques- the smaller the layer height the greater the accuracy/resolution of the model.

Following image segmentation and mesh processing, anatomical structures can be exported as stereolithography (STL) files, which serve as the digital blueprint for fabrication using 3D printers. These STL files are then processed by slicing software, which converts the 3D geometry into a series of two-dimensional layers and generates G-code instructions—machine-readable commands that guide the printer's movements, extrusion rates, and other operational parameters.

When selecting a particular printing method, careful consideration of its intrinsic characteristics—such as build precision, compatible materials, and overall reliability—is essential. This ensures that the final printed model accurately represents the target anatomy.

1.5.4.1 3D printing Methods

There are three main methods of 3D printing commonly used:

1) Material extrusion
    - Fused deposition modelling (FDM)
    - Fused filament fabrication (FFF)
2) Powder solidification
    - Selective laser scintering (SLS)
    - Binder Jetting (BJ)
3) Photopolymerisation
    - Stereolithography (SLA)
    - Polyjet (PJ)
    - Digital Light Processing (DLA)

Material extrusion operates by continuously feeding a thermoplastic filament through a heated nozzle. Guided by computer-controlled stepper motors, the printer head precisely deposits molten material along the horizontal plane, layer by layer, gradually building the desired object usually with the aid of 3D printed support structures. The thickness of these layers can vary between machines, and decreasing the layer height can increase both the accuracy and resolution of the printed model. Despite its accessibility and broad adoption, material extrusion has several limitations. Print times are generally slower, and the resulting parts often exhibit lower dimensional precision when compared with other additive manufacturing methods. Reliability issues may also arise, potentially limiting the technique's utility in clinical settings where accuracy and consistent quality are essential. Nonetheless, recent advancements have addressed some of these concerns. Enhanced filament materials, the capacity for multi-material printing, larger build volumes, and improved process control have collectively expanded the capabilities of material extrusion systems (113).

Powder solidification methods, including selective laser sintering (SLS) and binder jetting (BJ), convert powdered feedstock into fully formed components. In SLS, a laser beam is directed onto a thin layer of powder, causing the particles to coalesce through sintering—heat and pressure consolidate the powder without reaching a fully liquid state. After each layer is solidified, the build platform is incrementally lowered, and a fresh layer of powder is applied. As the surrounding loose powder provides inherent support for overhangs, no additional support structures are required. Binder jetting, which also relies on the sequential deposition of powder layers, instead utilises a precisely dispensed liquid binder to adhere the particles, achieving solidification without the need for localised heating.

(114).

Photopolymerisaton: In many prevalent photopolymerisation techniques, a vat of photocurable resin is selectively cured using ultraviolet (UV) light emitted from LED sources. The light is patterned through a digital mask, commonly produced by an LCD screen, which enables highly precise layer-by-layer fabrication (see Figure 4). The build platform is typically inverted and gradually elevated as each layer solidifies, following a conventional additive manufacturing approach. This method can rapidly yield extremely accurate and geometrically complex models, making it particularly well-suited for producing lattice-like vascular structures.

However, several safety considerations must be addressed when employing photopolymerisation processes. Direct contact with uncured resin may lead to severe dermatitis, and measures must be taken to mitigate exposure. In addition, proper management of volatile organic compounds (VOCs) emitted during the curing process is necessary. Adequate ventilation systems, filtering units, and appropriate personal protective equipment (PPE) are required to prevent hazardous inhalation or accumulation of VOCs. Furthermore, maintaining stable temperature and humidity levels can significantly enhance print quality and process reliability by ensuring optimal resin characteristics and curing conditions (115).

When fabricating patient-specific anatomical models, multiple considerations must be addressed. Each additive manufacturing technique requires a level of technical proficiency to diagnose and resolve common mechanical or printing errors. In a clinical environment, particularly where 3D printing is integrated into routine patient care, it may be necessary to establish a dedicated technician or department to ensure consistent and reliable production (114).

1.6 3D models in surgical practice

The potential benefits of 3D modelling in surgery are multifaceted. Patient-specific models may enhance surgeons' spatial understanding of complex anatomy, enable preoperative rehearsal of critical procedural steps, facilitate surgical education, and improve patient communication. In colorectal surgery specifically, 3D modelling shows promise for procedures involving complex anatomy like complete mesocolic excision, or pelvic exenteration for advanced rectal cancer where a comprehensive understanding of spatial relationships is paramount.

However, despite widespread enthusiasm and increasing adoption, the evidence supporting routine clinical implementation of 3D modelling remains limited. This review critically examines the current applications and evidence base for 3D modelling in surgical practice, with particular focus on colorectal surgery. I will evaluate the methodological quality of existing studies, analyse reported outcome measures, and identify key knowledge gaps that must be addressed to determine the true clinical utility of these emerging technologies.

The review is structured to first examine broad surgical applications of 3D modelling before focusing specifically on evidence in colorectal surgery across three key domains: cancer resection, inflammatory bowel disease, and surgical education. For each application, we analyse the quality of available evidence and evaluate reported benefits against implementation challenges. This systematic approach enables critical assessment of where 3D modelling may provide genuine clinical value versus areas where evidence remains insufficient to support routine use.

1.6.1 Preoperative planning

Preoperative planning encompasses activities undertaken to comprehend patient-specific anatomy and pathology, enabling informed surgical decision-making and strategy development (116).

In surgical practice, 3D modelling has been applied across four principal planning domains:

1. Anatomical Understanding Enhancement of spatial comprehension, particularly for complex or variable anatomical relationships

2. Patient-Specific Simulation
   Virtual or physical rehearsal of procedural steps and prediction of surgical outcomes
3. Resection Planning Precise delineation of surgical margins and critical structures, particularly vital in oncological surgery.
4. Reconstructive Planning Development and optimisation of reconstructive approaches, including custom implant design and surgical guide fabrication.

1.6.1.1 Anatomical understanding

Understanding three-dimensional anatomical relationships is fundamental to surgical planning and execution. While experienced surgeons regularly interpret two-dimensional cross-sectional imaging, mentally reconstructing complex spatial relationships from slice data remains challenging. Three-dimensional visualisation techniques may help overcome these cognitive demands.
Azer et al.'s systematic review of 30 studies examining 3D anatomical models in medical education revealed mixed methodological quality. Of the 30 studies 60% were randomised control trials and with remaining 40% non-randomised comparative studies. 60% utilised objective outcome measures (OSCE, written exam) as opposed to 40% in which subjective ratings were used (116). Students generally had a preference for 3D visualisation techniques over traditional teaching methods (116). However, not all studies demonstrated the superiority 3D in comparison to other teaching methods. However, heterogenous study designs and non-validated assessment methods limit definitive conclusions. The review highlighted several interacting factors affecting model effectiveness:

- Interface design and model quality
- Cognitive load and task complexity
- Individual learner characteristics, including spatial ability.
- Integration within broader educational curricula

Few studies have compared the relative effectiveness of virtual and printed models with the evidence base largely anecdotal. Kong et al.'s comparative study found both virtual and physical 3D models improved understanding of hepatic segmental

anatomy compared to traditional atlases, with no significant difference between model types. (117).

The impact of 3D models on surgeons' anatomical understanding remains relatively under-researched. Awan et al. demonstrated improved short-term identification of acetabular fracture patterns among radiology trainees using 3D printed models (117). Yang et al.'s study comparing understanding of retroperitoneal tumour anatomy across training levels found both virtual and printed 3D models superior to conventional CT for identifying retroperitoneal vascular structures (83.33%, 73.33% vs 46.67%, p=0.007), with greatest benefit among junior learners (118).

Three-dimensional visualisation appears particularly valuable for complex variable anatomy. Cromeens et al.'s study of 21 paediatric surgeons evaluating pyopagus twin anatomy found 3D printed models enabled faster and more accurate assessment of anatomical relationships compared to CT imaging alone, suggesting specific utility in challenging anatomical scenarios (119).

1.6.1.2 Patient specific simulation

Simulation based training has assumed increasing importance in surgical education in recent decades owing to reduced operative volume and patient safety concerns (120). 3D modelling has opened the possibility of patient specific rehearsal and overcomes some of the limitations of existing simulation techniques that rely on generic models lacking real world anatomical variation.

Patient-specific simulation can be categorised into two types: process simulation and outcome simulation. Process simulation involves using the model to replicate certain aspects of the surgical procedure, functioning as a form of rehearsal. Outcome simulation, on the other hand, aims to predict the results of surgery, such as aesthetic outcomes following reconstruction, blood flow, or organ function. (121).

1.6.1.2.1 Process simulation.

1.6.1.2.1.1 3D printed models and patient specific simulation.

Scale models of bony anatomy have been commonly utilised by trauma and maxillofacial surgeons for planning osteotomies and pre-shaping osteosynthesis plates. The use of 3D models is particularly advantageous in complex facial reconstructions (122) (123) (124).

Comparative studies have frequently reported reduced operative times, enhanced accuracy, and superior aesthetic outcomes when using patient-specific 3D models (125).

Recent advances in 3D printing technology have enabled the production of soft, flexible materials, addressing a key challenge in surgical simulation - particularly for procedures involving soft organs.

Coelho et al recently developed a 3D printed model with multiple materials of varying consistencies and resistances for planning frontoethmoidal meningoencephalocele surgical correction. Aside from reducing theatre time by an estimated 29%, the model facilitated multidisciplinary discussion between neurosurgeon and plastic surgeons allowing alterations of the previously defined plan (126).

In a notable feasibility study examining patient-specific models for nephrectomy procedures, Glybochko and colleagues evaluated silicone-based replicas created for five patients diagnosed with renal cell carcinoma. The surgical team reported high face validity for these models, providing positive assessments of their practical utility for surgical planning and training purposes (127).

Von Rundstedt et al. demonstrated the potential of patient-specific surgical rehearsal using soft material models. Their study validated the models' effectiveness by comparing tumour enucleation times and resected tissue volumes between simulated and actual procedures, finding strong correlations. However, while these initial results show promise, the studies lack robust objective measurements of how the simulations impact operative performance. Additionally, the current approach faces practical limitations related to production costs and time requirements (128).

1.6.1.2.1.2 Virtual patient specific simulation

Generating patient-specific, fully interactive surgical simulations based on imaging-derived three-dimensional models remains largely conceptual. The high level of complexity required—ranging from sophisticated image processing to real-time physics simulation and integration into game-engine environments—constitutes a significant barrier to widespread implementation (129).
Currently, only a handful of early feasibility studies are available. Rai et al utilised Mimics (Leuven, Belgium) 3D virtual simulation environment in order to simulate 3 partial nephrectomy cases using CT reconstructed models (130). Other preliminary studies by Head and Neck surgeons developed a virtual surgical environment for

simulating 10 endoscopic skull base procedures, demonstrating sufficient realism to allow patient specific rehearsal (131).

1.6.1.2.2 Outcome simulation

Outcome simulation aims to predict the results of surgical interventions. Four principal types have been reported in the literature: aesthetic, motion, blood flow, and structural. Aesthetic outcomes are particularly significant in facial surgery, whether addressing congenital defects or undertaking reconstructive procedures. Using finite element modelling, it is possible to accurately predict the soft tissue changes resulting from bony reconstruction of the mandible, thereby allowing for prediction of the ensuing facial appearance (132). Similarly, postoperative ranges of motion can be modelled following orthopaedic implant placement. Such modelling offers real-time feedback, enabling surgeons to virtually trial different implants and placements, thereby informing clinical decision-making (133).

For interventions involving blood flow, virtual stenting enables prediction of postoperative flow patterns. This is especially valuable in planning interventional procedures, such as endovascular treatments for aneurysms. By predicting pressure and wall stress following stent placement, the configuration can be optimised to enhance clinical outcomes (121). In orthopaedics, algorithmic approaches can predict the structural integrity of implants and their interaction with host anatomy. Surgeons can visualise the forces and stresses acting on implants, thereby allowing implant configurations to be optimised (134).

1.6.1.3 Tumour Resection planning

Achieving an R0 (tumour-free) resection margin remains a key predictor of long-term disease-free survival in patients with hepatobiliary malignancies (135). Three-dimensional (3D) reconstructions derived from standard radiological imaging have increasingly been employed to assist in pre-operative planning for liver resection (136). Their use aims to strike a balance between securing adequate tumour margins and preserving sufficient functioning liver parenchyma, thus reducing the risk of post-resection liver failure. Identification of vascular tributaries is fundamental aspect of surgical planning to preserve healthy liver.

Several studies suggest that 3D imaging may confer technical advantages compared with CT alone. These include significant reductions in both operative time and intraoperative blood loss, as well as the accurate prediction of specimen volume and surgical margins (137). In one cohort study of 305 patients, pre-operative 3D planning led to alterations in the surgical strategy in 49 of 131 complex cases, and reclassified 15 patients initially deemed unresectable based on 2D imaging as amenable to curative resection (138). Integrating perfusion data into such models can further enhance decision-making by providing automated calculations of resection volumes, functional liver reserve, and predicted dysfunctional volumes, all critical factors in determining hepatectomy feasibility (3).

Despite these technical benefits, the direct impact of 3D-assisted planning on oncological outcomes remains uncertain. Findings from non-randomised comparative studies have been conflicting, and at least one investigation found no significant difference in R0 resection rates between 2D and 3D imaging groups in the context of hilar cholangiocarcinoma (139). Beyond hepatobiliary surgery, 3D models have been utilised for pre-operative planning of minimally invasive partial nephrectomy in renal cell carcinoma. Here, detailed understanding of the renal hilar vessels is essential to maximise functional renal preservation (140). One randomised controlled trial by Shirk et al. demonstrated that 3D reconstruction use during robotic partial nephrectomy was associated with significantly reduced operative times, estimated blood loss, and vessel clamp times (141). Similar findings were reported by Porpiglia et al. and Wang et al., indicating consistent perioperative benefits (142,143).

Similarly, in video-assisted thoracoscopic surgery (VATS) lobectomy—an anatomically complex, lesion-oriented procedure—3D reconstructions have been employed to elucidate the relationships between tumours, blood vessels, and bronchi, thus aiding in procedural planning (144). Collectively, while the incorporation of 3D visualisation strategies into surgical planning shows considerable promise in improving procedural efficiency and anatomical delineation, robust evidence delineating its direct impact on long-term oncological and functional outcomes remains limited. Further high-quality, comparative studies are needed to clarify these effects, refine integration strategies, and determine the true clinical value of 3D-based pre-operative planning.

1.6.1.4 Reconstruction

Oral and maxillofacial surgery (OMFS) provides an illustrative example of how three-dimensional (3D) modelling can facilitate surgical planning and execution in the context of complex reconstructive procedures. OMFS commonly addresses injuries and congenital defects of the craniofacial skeleton, where both functional restoration and aesthetic precision are crucial due to the high visibility of the affected anatomical region and the associated psychosocial implications for patients (145). Notably, the geometrical complexity of the craniofacial skeleton and the stringent demands on aesthetic and functional outcomes suggest that 3D imaging may offer substantial advantages.

Multiple applications of 3D visualisation in OMFS are reported, ranging from improved characterisation of deformities to accurately planning osteotomies and virtually or physically rehearsing complex reconstructions (145). Modelling postoperative soft tissue changes is also feasible, enabling surgical teams to anticipate aesthetic results (146). Moreover, three-dimensional printing of patient-specific cutting guides and custom implants further refines operative precision and may reduce operative time (147), ultimately resulting in improved surgical efficiency and aesthetic outcomes (148).

In cases of facial trauma, detailed spatial localisation of bone fragments is fundamental to restoring the normal facial contour and occlusion. Here, 3D computed tomography (CT) permits accurate planning of symmetrical corrections and optimal implant placement. Evidence supports the value of 3D CT visualisation in managing displaced midfacial and mandibular fractures, where accurate reconstruction is essential for both functional recovery and cosmetic appearance(149).

Similarly, 3D imaging techniques have been employed in the evaluation and treatment of craniofacial anomalies, including craniofacial clefts and craniosynostoses. By revealing subtle asymmetries and accurately delineating abnormal suture lines, 3D CT can guide more precise classification and intervention strategies in conditions such as craniosynostosis, ultimately informing surgical

planning and improving clinical outcomes (150). Three-dimensional printing further enhances these applications by facilitating detailed surgical simulation and precise osteotomy site planning.

A systematic review by Lin et al. identified 78 studies over a ten-year period that employed 3D printing to translate virtual surgical plans into clinical practice. Applications included occlusal splints, osteotomy and repositioning guides, fixation plates, implants, spacers, and patient-specific models, with most studies comprising small prospective case series (median 10 patients) focusing primarily on accuracy as the outcome measure (151). Randomised controlled trials (RCTs) remain relatively scarce. One such RCT by Ayoub et al. assessed computer-assisted mandibular reconstruction using vascularised iliac crest bone grafts compared with conventional approaches. Among 40 patients, the computer-assisted technique reduced both transplant ischaemia time and donor site defect size (152), underscoring the potential clinical benefits of integrating 3D planning tools into reconstructive workflows.

Despite these advances, larger, high-quality studies are needed to establish the broader clinical efficacy of 3D-assisted planning and reconstruction in OMFS. Such evidence would help to refine best practices, validate outcomes, and guide the future integration of 3D visualisation and printing into routine surgical practice.

1.6.2 3D model surgical navigation

3D model navigation can be accomplished by solely displaying the model on an additional digital device for the operating surgeon's reference. The video transmission from a distinct device can be displayed as a secondary screen within the console, enabling the surgeon to reference it right next to the live operating view (for instance, using the TilePro feature available on the daVinci platform) (153).

Augmented reality (AR) surgical navigation involves integrating computer-generated information derived from preoperative imaging directly into the surgeon's view during procedures. In this method, the 3D model is overlaid onto the live surgical view, providing

real-time guidance and visualisation of underlying structures that would otherwise be obscured.

1.6.2.1 Principles and Implementation of Surgical AR Navigation

The implementation of augmented reality navigation in surgery represents a complex integration of spatial computing, computer vision, and surgical workflow considerations. While the fundamental goal is straightforward - overlaying virtual information onto the surgical field - the technical requirements for achieving this safely and effectively in clinical practice are substantial (154).

a) Registration Methodology

In augmented reality (AR) surgical navigation, registration is the process of aligning virtual models with the patient's actual anatomy to ensure accurate guidance. Approaches vary in complexity and level of automation. Manual registration relies on the surgeon's judgement and interaction with the model, often through software controls, to achieve basic alignment but can be less precise (achieving accuracy of 4-6mm) (155). Point-based registration operates through the correspondence of fiducial points between virtual and physical spaces. This method employs either anatomical landmarks or artificial markers, requiring both preoperative and intraoperative point selection. Various technological modalities, including optical tracking, medical imaging, and camera systems, facilitate point localization (155). Surface registration refines this further, using algorithms to align the patient's external contours or internal surfaces captured by imaging data. Surface data acquisition occurs through various modalities, including 3D scanning devices and stereo camera systems. While capable of achieving accuracies of 2-3mm, this approach faces challenges in partial surface matching and accommodation of tissue deformation (155). Marker-based registration introduces artificial markers placed near target structures, simplifying the alignment process by providing easily trackable reference points. Finally, calibration-based registration leverages the complementary strengths of different imaging modalities—such as ultrasound and computed tomography—by determining their relative transformations and applying these to the patient's anatomy. Taken together, these techniques enhance AR-guided surgery by improving the spatial coherence between virtual and real-world views, ultimately supporting safer and more precise interventions.

The selection of registration method requires careful consideration of accuracy requirements balanced against workflow disruption. While fiducial-based approaches typically provide higher initial accuracy, they necessitate additional preoperative planning and setup time. Marker-less approaches offer superior workflow integration but may sacrifice some degree of precision.

b) Tracking Systems and Real-time Updates

Tracking compensates for any movement of the patient or the AR system, ensuring accurate superimposition of virtual elements onto the surgical field. Continuous tracking represents perhaps the most challenging aspect of surgical AR navigation. The tracking system must maintain sub-millimetre accuracy while accommodating patient movement (both voluntary and involuntary), surgical instrument manipulation, tissue deformation, and changes in surgical field exposure (156).

Current tracking technologies encompass optical, electromagnetic, and hybrid systems. Marker-based optical tracking uses specialised cameras (often infrared) to detect and track either active or passive markers. Active markers emit their own infrared signal, while passive markers reflect infrared light emitted by the tracking system (155). While these offer excellent precision, they require maintained line-of-sight. Electromagnetic systems utilise field generators and sensors, eliminating the line-of-sight requirement but introducing susceptibility to interference from metallic objects. Hybrid systems attempt to overcome individual limitations by combining multiple tracking modalities, often incorporating inertial measurement units (155).

c) Visualisation Approaches and Human Factors

The method of delivering augmented reality content in surgery typically employs one of three main approaches: video see-through (VST), optical see-through (OST), or projection-based systems (157).

Video see-through, predominantly used in robotic and endoscopic surgery, integrates virtual content with the live surgical video feed. This approach allows precise control over the virtual overlay through image processing but introduces latency as video must be captured, processed, and displayed. The primary advantage is that synchronisation between real and virtual content can be precisely controlled since both are presented through the same digital display pipeline.

Optical see-through systems use transparent displays, typically in the form of commercial head-mounted devices like Microsoft's (now discontinued) HoloLens Meta’s Quest and Apple’s Vision Pro (158). These systems attempt to overlay virtual content onto the surgeon's direct view of the surgical field. However, they face significant technical challenges including limited field of view, poor virtual object visibility in bright operating room conditions, and substantial latency in updating virtual overlays. The ergonomic burden of wearing head-

mounted displays during lengthy procedures presents another significant barrier to adoption (159).

Projection-based systems directly project navigational information onto the surgical field or patient. While this eliminates the need for wearable displays, it limits visualisation to visible surfaces and can suffer from occlusion by instruments or personnel. Image clarity depends heavily on surface geometry and ambient lighting conditions (155).

1.6.2.2 Current state of AR surgical navigation

The current evidence supporting the application of augmented reality (AR) in surgical navigation, particularly within the context of abdominal procedures, remains preliminary and methodologically constrained (160,161). Although isolated case reports, small pilot studies, and limited feasibility investigations have begun to illustrate the potential advantages of integrating three-dimensional (3D) anatomical overlays and real-time imaging guidance into complex operative fields, the overall quality and robustness of this literature are lacking (156). Many existing studies are non-comparative, often involving heterogeneous patient populations and employing subjective endpoints, thereby hindering the ability to draw definitive conclusions regarding the clinical impact of AR on surgical accuracy, complication rates, or long-term patient outcomes (162).

In the setting of abdominal surgery, the inherent challenges posed by dynamic anatomical landscapes—such as respiratory-induced organ motion, shifting topography during laparoscopic or robotic manipulation, and variable patient positioning—further complicate the use of AR (157,163). Achieving stable and precise image-to-patient registration is especially difficult when key reference landmarks cannot be consistently maintained. The sensitivity of AR overlays to slight positional changes can lead to subtle yet clinically meaningful misalignments, potentially obscuring critical anatomical structures or providing surgeons with misleading spatial information. Moreover, the limited field of view, potential ergonomic constraints of current head-mounted or console-based displays, and difficulties integrating multiple data streams into a coherent and intuitive user interface exacerbate the cognitive load on the operating surgeon (161). The net result is an environment in which the theoretical advantages of AR—improved visualisation, navigation, and decision-making—may be offset by distractions, inaccuracies, or delayed adoption due to perceived complexity and insufficient validation (158,160,161).

From an evidence perspective, the paucity of well-structured randomised controlled trials and large-scale prospective cohorts remains a significant barrier to establishing AR as a

standard adjunct in abdominal surgery (162,164). The relative scarcity of objective measures and consensus-derived performance metrics underlines the urgent need for standardized protocols, validated scoring systems, and interdisciplinary collaboration (165). Future research efforts must focus on producing rigorous comparative data that isolate the incremental benefit of AR over conventional imaging and navigation modalities. Such studies should evaluate not only technical parameters—such as the accuracy of tumour localization or vascular delineation—but also patient-centred outcomes, operative efficiency, cost-effectiveness, and the learning curve associated with AR system implementation.

In summary, while preliminary evidence suggests that AR holds promise for enhancing surgical navigation in abdominal procedures, the current body of literature remains insufficient to support widespread clinical adoption. It is essential that future investigations incorporate methodologically sound designs, objective endpoints, and robust statistical analyses to accurately assess the role of AR in improving surgical precision, outcomes, and safety. Only through such dedicated, high-quality research can the true clinical value of AR in abdominal surgery be elucidated, guiding its safe and effective integration into routine surgical practice.

1.6.3 3D models in surgical patient education

Patient education is a fundamental element of informed consent and shared decision-making (166), yet the effectiveness of current practices is often limited. Multiple studies have highlighted that patients frequently have a poor understanding of their forthcoming surgical procedures (167) (52–55). Presentation style significantly influences comprehension and retention of information (56). Against this backdrop, three-dimensional (3D) models have been introduced as communication aids. One of the principal benefits reported for 3D visualisation is the enhancement of anatomical understanding (116,119). Thus, compared with standard medical illustrations, 3D representations may offer patients a clearer grasp of their condition, which can be particularly valuable for those facing complex, high-risk interventions.

Research exploring the use of 3D models in patient education has yielded promising results. For instance, Yoon et al. reported that personalised printed models enhanced patient-reported knowledge and satisfaction during consent for stage I lung cancer resections (160). Similarly, when employed in education before robot-assisted partial nephrectomy, 3D-printed models led to increased patient satisfaction (168). In addition, objective improvements in patient understanding have been observed. Bernhard et al. found that patients who reviewed

personalised 3D kidney models demonstrated improved understanding of renal physiology (by 16.7%), anatomy (50%), tumour characteristics (39%), and the planned procedure (44.6%) (169). Parents of paediatric patients undergoing hepatectomy also displayed better objective knowledge when 3D-printed models were introduced during the consent process (8).

Despite these encouraging findings, the studies published to date have primarily compared the use of 3D models with conventional educational methods, while employing a variety of outcome measures that have not been rigorously validated. Further research employing validated tools and consistent metrics is necessary to establish the definitive impact of 3D models on patient comprehension and informed decision-making.

1.7 The Application of Three-Dimensional Modelling in Colorectal Surgery

1.7.1 Three-Dimensional Modelling in Preoperative Planning

1.7.1.1 Vascular Mapping in Colon Cancer Surgery

Three-dimensional reconstructions derived from computed tomography have been employed to aid surgical planning for both standard oncological colorectal resections and complete mesocolic excision. Complete mesocolic excision (CME), first described by Hohenberger et al., represents a standardised surgical approach comprising three fundamental principles: dissection along embryological planes maintaining an intact mesocolic envelope, sufficient longitudinal bowel resection, and central vascular ligation with excision of the central D3 lymph nodes (170–172).

The successful execution of CME depends on the surgeon's ability to navigate complex and variable mesenteric vascular anatomy. Consequently, vascular injury remains a concern and has led to the application of 3D models as a planning/intraoperative navigation adjunct (173).

Mari et al.'s (2013) randomised controlled trial evaluated three-dimensional CT angiography reconstructions in laparoscopic colorectal surgery across 112 patients undergoing standard colorectal resections. The intervention group (3DCT) accessed reconstructions before and during surgery, while the control group viewed reconstructions only postoperatively (NO-3DCT) (174).

The study found that operative times were significantly lower in the 3DCT group for all three types of procedures. Additionally, the 3DCT group experienced fewer instances of difficulty identifying mesenteric vessels (5 cases vs. 23 cases in the NO-3DCT group; $p < 0.0001$) and a lower incidence of intraoperative haemorrhage requiring haemostasis (6 cases vs. 19 cases; $p = 0.006$). These results indicate that preoperative visualisation of 3D reconstructed images of mesenteric vessels is associated with improved surgical efficiency and safety. However, the study was conducted at a single centre with all procedures performed by four surgeons, which may affect the generalizability of the findings. Furthermore, the study did not assess long-term oncological outcomes or lymph node harvest, which are essential factors in evaluating the overall efficacy of surgical interventions in cancer treatment (174).

Miyamoto et al. (2017) investigated the impact of 3D vascular imaging on laparoscopic-assisted surgery for right-sided colon cancer. In their retrospective study involving 46 patients who underwent laparoscopic resection with preoperative 3D imaging reconstructed

from multidetector CT (MDCT) scans, they compared outcomes with a control group of 20 patients who underwent LACS without 3D imaging. The 3D reconstructions provided detailed visualisation of critical vessels, including the ileocolic artery (ICA), ileocolic vein (ICV), right colic artery (RCA), and the gastrocolic trunk (GCT) (175).

The study found that intraoperative blood loss was significantly lower in the group utilizing 3D imaging (mean blood loss: 21.0 mL) compared to the control group (mean blood loss: 53.0 mL; $p = 0.013$). This reduction suggests that enhanced preoperative visualisation of vascular anatomy may contribute to safer surgical dissection and haemostasis. However, no significant differences were observed in operative time, conversion rate, or postoperative complications between the groups. While these findings highlight the potential benefits of 3D imaging in reducing intraoperative blood loss, the retrospective nature of the study and potential selection biases limit the strength of the conclusions. Additionally, the control group consisted of patients unable to undergo contrast enhanced MDCT due to renal dysfunction or allergies, which may confound the results.

Luzón et al. (2018) conducted a prospective study to assess the accuracy and clinical utility of 3D-printed models of the superior mesenteric vessels for surgical planning in D3 right hemicolectomy. Twenty-two patients were included, and high-resolution CT angiography was used to create both virtual 3D models and physical 3D-printed models using stereolithography. Measurements of vascular structures were compared across virtual models, printed models, and intraoperative findings (176).

The study reported a strong correlation for inter-arterial distances between the models and intraoperative measurements (correlation coefficient $r = 0.997$, $p < 0.001$), indicating high accuracy in representing arterial anatomy. However, the correlation for inter-venous distances was weaker ($r = 0.580$, $p = 0.005$), possibly due to the variability and compressibility of veins during surgery. These findings suggest that 3D-printed models can accurately replicate arterial anatomy, aiding in preoperative planning for complex vascular dissections.

Despite the promising results, the study's limitations include a relatively small sample size and the lack of a control group or randomization. Additionally, the study did not evaluate clinical outcomes such as operative time, intraoperative complications, or postoperative recovery, which are crucial for determining the practical benefits of incorporating 3D models into surgical practice (176).

A recent retrospective cohort study by Kearns et al. (2024) investigated the implementation of three-dimensional virtual models (3DVMs) in laparoscopic complete mesocolic excision (CME) with central vessel ligation (CVL) for right-sided colonic cancer. The authors

evaluated outcomes in 26 patients who underwent laparoscopic CME with 3DVM guidance against 49 historical controls who received standard mesocolic excision without central vessel ligation or 3DVM assistance (177).

The study demonstrated high anatomical accuracy of the 3DVMs, with 96% concordance between the reconstructed models and intraoperative findings. These surface-rendered models, produced by a third-party company from preoperative CT mesenteric angiograms, provided detailed visualisation of the mesenteric vasculature and surrounding anatomical structures. Notably, no intraoperative complications were reported in the CME group utilising 3DVMs (177).

However, significant methodological limitations undermine the ability to draw meaningful conclusions about the efficacy of 3DVM implementation. The primary limitation stems from the non-equivalent control group. CME with CVL, as defined by Hohenberger, represents a fundamentally different operative approach compared to standard mesocolic excision, incorporating three distinct elements: intact mesocolic package excision, adequate longitudinal bowel resection, and D3 lymphadenectomy with central vessel ligation. Therefore, the observed difference in operative times between groups (mean 226 minutes for CME versus 170 minutes for controls, $p < 0.001$) cannot be meaningfully attributed to 3DVM utilisation, as it likely reflects the inherent technical complexity and learning curve associated with the CME technique itself (177).

Furthermore, the study's focus on perioperative outcomes neglects crucial long-term oncological data and postoperative morbidity metrics. These parameters are essential for comprehensively evaluating any novel surgical approach or technological adjunct. While the authors observed a reduction in operative times as experience accumulated, suggesting potential workflow optimisation, the study design precludes definitive conclusions regarding the specific contribution of 3DVMs to surgical outcomes. Future research would benefit from prospective randomised trials comparing CME procedures with and without 3DVM assistance, enabling more robust assessment of this promising technological adjunct.

Collectively, these studies suggest that 3D modelling and imaging techniques can enhance anatomical visualisation and potentially improve surgical outcomes in colon cancer surgery. Preoperative 3D vascular mapping appears to facilitate better surgical planning, reduce intraoperative blood loss, and decrease the difficulty in identifying mesenteric vessels. However, several methodological limitations are evident across the studies.

Firstly, many studies have small sample sizes and retrospective designs, limiting statistical power and introducing potential biases. The lack of control groups or use of non-equivalent historical controls, as seen in Kearns et al. (2024), complicates the interpretation of results

due to potential confounding variables. Specifically, comparing CME with 3DVMs to standard mesocolic excision without 3DVMs is problematic because the two procedures differ fundamentally in extent and complexity, making it difficult to attribute observed differences solely to the use of 3DVMs (177).

Secondly, variability in 3D modelling techniques and absence of standardized protocols make it challenging to compare results across studies. Differences in imaging modalities, reconstruction software, and surgeon experience with 3D technologies can influence outcomes. Moreover, the time and resources required to produce high-quality 3D models may limit their practicality in routine clinical settings and are generally under reported.

Thirdly, the impact of 3D modelling on key clinical outcomes such as long-term survival, recurrence rates, or quality of life has not been comprehensively evaluated. Most studies focus on immediate intraoperative metrics, such as blood loss or operative time, without assessing long-term oncological efficacy. Additionally, it is likely that 3D models would principally affect the time taken for vessel dissection rather than the overall operative time, suggesting that focused assessments on this specific metric would be more informative.

1.7.2 Three-Dimensional Modelling in Rectal Cancer Surgery

1.7.2.1 Pelvic Anatomy Visualisation and Nerve Preservation

Hojo et al. (2020) evaluated the utility of patient-specific 3D-printed pelvic models for lateral pelvic lymph node dissection (LPLND) in rectal cancer. The study included 22 patients, and 3D models were created from enhanced multidetector CT scans. Thirty colorectal surgeons assessed the models using a questionnaire, rating their usefulness in understanding pelvic anatomy and aiding surgical planning (178).

Surgeons reported that the 3D models significantly improved their spatial comprehension of pelvic anatomy, with an average Likert score of 4.68 out of 5. The models were felt to be particularly beneficial in cases with clinically diagnosed metastatic lateral pelvic lymph nodes offering improved spatial comprehension allowing surgeons to execute the dissection with greater precision. Surgeons preferred the physical 3D models over traditional 2D imaging and virtual 3D images displayed on screens (178).

Despite the positive feedback, the study's reliance on subjective assessments introduces potential bias. The absence of objective measures such as an objective assessment of anatomical understanding or clinical outcome measures limits the ability to evaluate the

clinical impact of the 3D models. Additionally, the study did not include a control group, which is necessary to attribute observed benefits directly to the intervention (178).

Wijsmuller et al. (2018) investigated the feasibility of creating a 3D map of pelvic nerves using high-resolution MRI. In their prospective observational study involving 20 healthy volunteers, the researchers utilized specific MRI sequences to enhance the visibility of pelvic nerves and manually segmented the images to create 3D reconstructions (179).

The study demonstrated that most pelvic nerves at risk during rectal surgery could be identified and accurately mapped. The validation by an anatomist and a radiologist showed high inter-observer agreement (Mean 95%; range 85-100%; for hypogastric, sacral splanchnic and obturator nerves), suggesting reliability in the nerve identification process. The potential application of this technique lies in preoperative planning to preserve autonomic nerves and reduce postoperative dysfunction (179).

However, the study's limitations include the use of healthy volunteers rather than patients with rectal cancer, who may have altered anatomy due to tumour presence or previous treatments. Additionally, the study did not evaluate the integration of the 3D nerve maps into surgical navigation systems or measure the impact on surgical outcomes, making it difficult to assess clinical relevance (179).

Bertrand et al. (2014) explored the use of MRI to visualise the autonomic nervous system within the pelvis. Utilizing cadaver models, the researchers applied various MRI sequences to generate detailed 3D reconstructions of pelvic nerves. They compared MRI measurements with anatomical dissection findings to validate the accuracy of the imaging techniques (180).

The study found that MRI could effectively visualise the pelvic autonomic nerves, with measurements closely matching those obtained from dissection. This suggests that MRI-based 3D modelling could serve as a valuable tool for understanding individual pelvic nerve anatomy preoperatively (180).

While these findings are promising, the study's use of cadavers may not fully replicate in vivo conditions, such as tissue characteristics and dynamic changes during surgery. Additionally, the practical application of this technique in a clinical setting was not assessed, and the study did not explore the impact on surgical planning or outcomes.

The application of 3D modelling in rectal cancer surgery has the potential to enhance anatomical understanding and aid in nerve preservation strategies. However, the current literature is predominantly based on feasibility studies and subjective assessments, lacking

robust clinical evidence. The studies reviewed did not incorporate objective outcome measures or assess the long-term benefits of integrating 3D models into surgical practice.

1.7.2.2 Image-Guided Navigation Systems in Rectal Cancer Surgery

Sahnan et al. explored the application of three-dimensional modelling derived from magnetic resonance imaging for planning transanal total mesorectal excision (TaTME) (181). Through two illustrative cases, the authors demonstrated the feasibility of generating detailed anatomical reconstructions from standard T2-weighted MRI sequences using open-source software and manual segmentation by specialist radiologists. The authors described an improved appreciation of surgical anatomy and proposed potential applications in surgical training and patient education, the small case series design without formal outcome measures limits meaningful conclusions about clinical utility (181).

Two subsequent studies more rigorously evaluate the use of 3D model navigation in rectal cancer surgery. Kok et al. conducted a prospective, non-randomised controlled trial to investigate whether image-guided navigation during rectal cancer resection improves complete resection rates compared with surgeries without navigation. The study included 33 patients who underwent resection with image-guided navigation (navigation cohort) and compared them with a historical cohort of 142 patients (182).

The navigation system used preoperative 3D reconstructions integrated with an electromagnetic stereotactic navigation system. Intraoperative cone-beam CT was employed to register the model to the patient, and fiducial markers were used for tracking (182).

The study found that in patients with recurrent rectal cancer, the navigation cohort showed significantly lower tumour-positive margin rates compared with the historical cohort (21.1% vs. 51.2%; P = 0.047). No significant difference was observed in locally advanced primary rectal cancer. No navigation system–associated complications occurred (182).

While these findings suggest a potential benefit of image-guided navigation in recurrent rectal cancer surgery, several limitations must be considered. The non-randomised design and use of a historical control group introduce potential biases, such as differences in surgical techniques, patient selection, and perioperative care over time. The small sample size of the navigation cohort limits statistical power, and the study did not account for variables such as surgeon experience or the quality of the total mesorectal excision specimen, which could influence resection margins.

It should be noted that the R0 resection rates in the historical control group would be lower than the current reported rates in the pelvic exenteration literature. The authors do not state

their prior experience with performing pelvic exenteration. It is possible the improvements in R0 resection rates in comparison to the historical cohorts could be as the result of the learning curve rather than the use of 3D navigation. The lack of randomisation and potential confounders make it challenging to attribute the observed improvement in resection margins solely to the use of image-guided navigation. Further studies in high volume pelvic exenteration centres would be needed to corroborate these findings of oncological superiority.

Nijkamp et al. conducted a prospective feasibility study on the safety and practicality of an electromagnetic (EM) navigation system for pelvic surgery. The study included 33 patients with pelvic malignancies scheduled for open surgery (183).

The navigation system utilized preoperative imaging to create a patient-specific 3D roadmap, registered intraoperatively using cone-beam CT. A tracked pointer was used for intraoperative guidance (183).

The navigation system was successfully used in 94% of cases, with mean target registration errors of 4.0 mm and 6.3 mm for different patient positions. Surgeons reported that the system facilitated faster tumour localization and improved decisiveness. No adverse events were attributed to the navigation system (183).

As a feasibility study, the findings demonstrate that EM-based navigation systems can be safely integrated into pelvic surgeries. However, the study did not include a control group or assess clinical outcomes such as operative time reduction, complication rates, or long-term patient outcomes. The involvement of the system's developers and the single-institution setting may limit generalizability. Future studies should focus on evaluating the clinical efficacy and potential benefits of such navigation systems in randomised controlled trials.

1.7.3 Three-Dimensional Modelling in Inflammatory bowel disease

1.7.3.1 Application in Crohn's Perianal Disease

Crohn's disease often presents with complex perianal fistulas that are challenging to manage due to their complex anatomy and association with high morbidity. Accurate visualisation of fistula tracts is crucial for effective surgical intervention.

Two recent studies have explored the application of three-dimensional modelling in complex perianal Crohn's disease. Sahnan et al. (2018) first demonstrated the technical feasibility of generating interactive three-dimensional reconstructions from standard MRI sequences

using manual segmentation and open-source software (184). Their workflow enabled visualisation of fistula tracts and associated anatomical structures through a mobile platform. However, as a technical report without formal outcome measures or control groups, the clinical utility of their approach remains unproven (184).

Jeri-McFarlane et al. (2023) attempted to advance this work by implementing artificial intelligence-assisted segmentation to automate model generation. Their prospective study of four patients suggested that automated approaches could feasibly create detailed reconstructions of perianal anatomy (185). However, crucial details regarding the neural network architecture and training methodology are absent from their report. The authors' statement that only three segmented scans were used for training raises significant concerns, as this sample size would likely be inadequate for developing a robust and generalizable deep learning model. This technical limitation, combined with the study's extremely small clinical cohort and lack of outcome measures, prevents meaningful evaluation of the proposed benefits in surgical planning and sphincter preservation (185).

Building on these feasibility studies, Verkade et al. (2024) examined 15 patients with transsphincteric and intersphincteric fistulas, comparing surgeons' assessments of 3D printed models to MRI interpretations by a GI radiologist. Two colorectal surgeons independently evaluated the models, assessing fistula classification, complexity, internal orifice location, and the extent of external sphincter involvement in transsphincteric cases (186).

Using Cohen's Kappa statistic and intraclass correlation coefficients (ICC), the researchers found almost perfect agreement ($\kappa = 0.87$) between radiologists and surgeons for fistula classification, and substantial agreement for both complexity and internal orifice location ($\kappa = 0.73$). Agreement regarding external anal sphincter involvement was moderate (ICC = 0.63 and 0.52). Inter-surgeon agreement was substantial across all parameters, with kappa values ranging from 0.73 to 0.75, and an ICC of 0.77 for sphincter involvement assessment. These findings demonstrate strong concordance between three-dimensional model interpretation and traditional radiological assessment (186).

This strong concordance across key surgical planning parameters suggests that 3D models can effectively convey complex anatomical relationships to surgeons. However, the study did not directly compare surgeons' performance using traditional imaging versus 3D models therefore it is unknown whether 3D models conferred any advantage. While Verkade et al. improved on previous reports with a larger sample size and structured evaluation, it shared limitations such as not examining clinical outcomes or surgical performance metrics (186).

These studies collectively show the progression of 3D modelling in complex perianal disease from basic feasibility to validated anatomical representation. The next step is to conduct studies that directly compare surgical planning and outcomes using traditional imaging versus 3D models.

1.7.3.2 Patient specific simulation in Ulcerative colitis

Yokose et al. (2023) conducted a retrospective study using patient-specific, deformable 3D-printed models to assist in surgical planning for ileal pouch-anal anastomosis (IPAA) in ulcerative colitis (UC) patients (187). They compared two surgical techniques:

- **Ileal pouch-anal handsewn anastomosis (IAA)**: In this procedure, the ileal pouch is directly sutured to the anus after performing a mucosectomy. The technique has the advantage of reducing the
- **Ileal pouch-anal canal double-stapled anastomosis (IACA)**: this technique connects the pouch to the anal canal using surgical staples. It preserves a portion of the anal transition zone and rectal mucosa.

By creating flexible models from CT scans—printed at 70% of actual size—they aimed to simulate the procedures more realistically. Measurements taken on these models, such as the distance from the tip of the ileal artery to the coccyx, were used to assess the feasibility of IAA (187).

The study's findings suggested that ileal pouch proximity to the anus, which was shorter in the IAA group compared to the IACA group, could potentially inform surgical planning. However, several significant limitations undermine the study's conclusions. These include its retrospective design, extremely limited sample of 11 male patients, and technical difficulties in accurately modelling vascular structures and tissue properties. The resource-intensive nature of model production, requiring approximately 70 hours and USD $20 per model, raises feasibility concerns. Moreover, the study's focus on pouch length as a primary determinant of surgical approach appears oversimplified, particularly given evidence suggesting superior outcomes with stapled versus handsewn anastomoses in many clinical settings (188,189). In recent years there has been a shift towards the stapled technique with several contemporary studies advocating for the use of stapled anastomosis as the standard approach for IPAA in UC limiting the wider utility of models as a decision making aid (190).

1.7.4 Impact on Surgical Education and Training

1.7.4.1 Virtual Simulators and Educational Tools

Three-dimensional (3D) modelling offers innovative approaches to colorectal surgical education by providing interactive and realistic representations of anatomy and surgical procedures. Hassinger et al. (2010) assessed the usability and perceived effectiveness of a virtual pelvic anatomy simulator among medical students and surgical residents (191). Participants interacted with the simulator and completed surveys evaluating its educational value. The study found that users considered the simulator easy to use and beneficial for understanding pelvic anatomy. However, the reliance on subjective feedback and a small sample size of ten participants limit the strength of these conclusions. The absence of objective measures—such as pre- and post-intervention tests assessing knowledge acquisition or skill enhancement—makes it difficult to quantify the simulator's actual educational impact. Without these metrics, it's challenging to determine whether the simulator genuinely improves understanding or if the positive feedback is influenced by user enthusiasm for novel technology.

Similarly, Pellino et al. (2018) described a case where cadaveric simulation and 3D imaging were integrated for preoperative planning in a patient with a retro rectal tumour (192). The surgical team used 3D models to understand the tumour’s relationship with surrounding structures and practiced the surgical approach on cadaver specimens. This approach allowed for the identification of optimal dissection planes and the anticipation of potential challenges, enhancing surgical preparedness. While this case report showcases the practical benefits of combining 3D modelling with hands-on simulation, it remains anecdotal and lacks empirical validation. The approach was applied to a single patient case without a control group or comparison to standard preoperative planning methods. This limits the ability to attribute any improvements in surgical preparedness or patient outcomes directly to the use of 3D modelling and cadaver simulation.

Integrating 3D modelling into surgical education offers opportunities for enhanced learning experiences. However, the current literature is constrained by a very limited number of studies with small sample sizes, subjective assessments, and a lack of objective educational metrics. Future studies should incorporate validated assessment tools to measure the impact of 3D modelling on knowledge retention, skill acquisition, and clinical performance.

2 Development of Advanced 3D Visualisation Tools for Complex Colorectal Cancer Surgery

2.1 Introduction

Modern colorectal cancer surgery increasingly employs complex operative techniques that demand precise anatomical understanding and effective communication of surgical concepts. Two procedures particularly exemplify these challenges: Complete Mesocolic Excision (CME) and pelvic exenteration. CME requires precise identification and management of variable mesenteric vasculature, while pelvic exenteration involves highly morbid multi-organ pelvic resections where patient comprehension is crucial for informed consent. Despite advances in cross-sectional imaging providing detailed anatomical data, significant barriers persist in translating this information into clinically meaningful visualisations that serve both surgical planning and patient education needs.

The dual requirements of technical precision and effective communication present distinct visualisation challenges. Surgeons performing CME must mentally reconstruct complex three-dimensional vascular relationships from cross-sectional imaging, while patients considering pelvic exenteration must understand extensive anatomical concepts to make informed decisions about life-altering surgery. Current visualisation approaches inadequately address these complementary but distinct needs, highlighting the requirement for specialised technical solutions.

2.2 Background and requirements

2.2.1 Clinical context

2.2.1.1 Surgical Planning in CME

CME, introduced by Hohenberger and colleagues, necessitates a more radical resection than a 'standard' hemicolectomy and represents a technically challenging procedure—the technical CME centres primarily on managing mesenteric vasculature not ordinarily encountered during a 'standard' hemicolectomy (170). Mesenteric blood vessels exhibit complex and variable anatomical patterns, making each case unique. Surgeons rely on conventional 2D CT imaging to understand these complex vascular relationships. This requires them to perform challenging mental reconstructions, translating multiple cross-sectional images into a comprehensive three-dimensional understanding of the patient's vascular anatomy. This cognitive burden is particularly significant given that anatomical variations in mesenteric vessels are common, making each case distinct and requiring careful individual assessment.

2.2.1.2 Patient Education in Pelvic Exenteration

Modern healthcare focusses on patient-centred care, reinforced by the Montgomery ruling, necessitates a comprehensive patient understanding of any proposed surgical intervention (193). However, research indicates significant gaps in patient comprehension of surgical procedures, with many unable to recall major complications or demonstrate adequate procedural understanding (194). These challenges are particularly acute in pelvic exenteration, where surgery is highly morbid and understanding complex anatomical relationships is crucial for informed decision-making.

2.2.2 Need analysis.

A comprehensive needs analysis was conducted to inform the development of visualisation tools for both CME surgical planning and pelvic exenteration patient education. This structured approach identified critical requirements through stakeholder engagement and systematic evaluation of technical constraints.

2.2.2.1 CME Surgical Planning Requirements

The requirements for CME surgical planning were established through consultation with expert CME surgeons (n=2) and analysis of existing surgical workflows. Three primary domains of requirements emerged:

1. **Anatomical Visualisation Requirements**
    - Accurate representation of mesenteric vasculature including:
        - Superior mesenteric vein and artery
        - Ileocolic vessels
        - Right colic vessels (when present)
        - Middle colic vessels
        - Constituent vessels of Henle's trunk
    - Clear delineation of tumour mass and lymph nodes
    - Contextual anatomical structures (colon, stomach, duodenum, and pancreas) for intraoperative reference
2. **Technical Performance Requirements**
    - Real-time interactive response
    - Compatibility with standard clinical/personal hardware
    - Integration with existing healthcare IT infrastructure
    - Minimal additional computational resource requirements
    - Capacity for intra-operative use
3. **Interface Requirements**
    - Standardised anatomical colour coding
    - Essential navigation controls (pan, tilt, rotate, zoom)
    - Selective transparency control for individual anatomical components
    - Web-based accessibility across multiple devices
    - Operation within institutional network constraints

2.2.2.2 Pelvic Exenteration Patient Education Requirements

Requirements for patient education models were derived through structured interviews with multiple stakeholder groups:

1. Patient Stakeholder Input (n=4) Key requirements identified through patient consultation included:
    - Patient-specific anatomical representations
    - Clear visualisation of disease extent

    - Independent model exploration capability
    - Clearly labelled anatomical structures
    - Intuitive interface design suitable for varied technical abilities.
2. Clinical Team Requirements (n=3) Surgical team members (two consultant surgeons and one specialist nurse) identified the need for:
    - Accurate representation of surgical anatomy
    - Compatibility with standard NHS computing infrastructure
    - Web-based accessibility for virtual consultations
    - Clear tumour visualisation
    - Structure manipulation capabilities (hide/reveal/transparency)

2.2.2.3 Technical Feasibility Assessment

Technical feasibility was evaluated against institutional constraints and available resources:

1. Infrastructure Constraints

    - Standard NHS computing hardware
    - Variable network bandwidth
    - Institutional security protocols
    - Cross-platform compatibility requirements

2. Development Resources

    - Available software development tools
    - Image processing capabilities
    - 3D visualisation frameworks
    - Quality assurance tools

2.2.2.4 Synthesis of Requirements

Analysis of stakeholder input and technical constraints led to the identification of core development priorities:

1. For CME Surgical Planning

    - Emphasis on anatomical accuracy and spatial precision
    - Efficient automated mesh processing for real-time interaction
    - Web-based deployment for accessibility

- Modular development approach for maintainability

2. For Patient Education

    - Focus on visual clarity and comprehension.
    - Intuitive interface design
    - Realistic anatomical representation
    - Interactive exploration capabilities

This needs analysis provided the foundation for subsequent technical development decisions and informed the selection of appropriate methodologies for each application. The contrasting requirements of surgical planning and patient education necessitated distinct technical approaches while maintaining a cohesive overall development strategy.

2.3 Research Aims and Objectives

2.3.1 Primary Aim

The primary aim of this chapter is to develop and implement 3D visualisation workflows from standard imaging data to meet the technical and communicative needs of advanced colorectal cancer surgery, specifically in CME and pelvic exenteration. This work seeks to support surgeons' anatomical and spatial understanding while enhancing patient engagement and understanding.

2.3.2 Specific Objectives

1. Design and implement an automated surface mesh processing pipeline that:

    - Converts segmented CT data into web-accessible 3D visualisations.
    - Preserves critical anatomical relationships in mesenteric vasculature and associated anatomy.
    - Maintains mesh quality while optimising computational efficiency.

2. Establish and validate quality assurance protocols for:

    - Surface mesh accuracy and fidelity
    - Anatomical relationship preservation

- Computational performance metrics

3. Develop a standardised PBR workflow for patient education models that:

    - Leverages surface rendering for optimal visual clarity
    - Maintains anatomical accuracy while supporting interactive exploration.
    - Integrates advanced texturing techniques for enhanced comprehension.

4. Create web-based visualisation platforms that:

    - Support clinical workflow integration.
    - Enable cross-device accessibility.
    - Provide real-time interaction capabilities.

2.4 Methodology Overview

The development and validation of visualisation tools for complex colorectal cancer surgery demanded distinct methodological approaches, reflecting the differing requirements of surgical planning and patient education. This methodological framework encompassed both technical development and comprehensive clinical validation through structured studies.

2.4.1 Development Philosophy

The contrasting requirements of surgical planning and patient education necessitated complementary methodological approaches. The CME surgical planning tools required precise anatomical reconstruction with demonstrable geometric accuracy and underwent rigorous clinical validation. The pelvic exenteration patient education models, while maintaining anatomical accuracy, prioritised effective communication and underwent systematic evaluation of their impact on patient understanding and decision-making.

2.4.1.1 Development Environment

The technical implementation required a robust and reproducible development environment that could support both complex medical image processing and interactive web-based visualisation. Visual Studio Code (Microsoft) was selected as the integrated development environment, utilising Python 3.9 for the core processing pipeline. The selection of dependencies was driven by the need for scientific rigour, computational efficiency, and maintainable code architecture.

The backend processing pipeline relied on established scientific computing libraries. NumPy 1.24.3 (195) and SciPy 1.11.3 (196) provided the mathematical foundation for array operations and spatial algorithms, essential for mesh processing and geometric transformations. Medical image processing was implemented through Nibabel 5.2.0 (197), chosen for its robust handling of neuroimaging data formats, particularly NIFTI files. The scikit-image 0.21.0 library facilitated advanced image processing operations, notably the marching cubes algorithm implementation for surface mesh generation.

Mesh processing and analysis capabilities were provided by Trimesh 4.0.5 and Open3D 0.17.0, offering complementary functionality for mesh manipulation and optimisation. The web application framework Flask 3.0.0, coupled with Werkzeug 3.0.1, enabled efficient server-side processing and RESTful API implementation.

For frontend development, Three.js r158 was employed as the WebGL rendering engine. This choice was informed by its mature ecosystem, comprehensive documentation, and optimised performance for web-based 3D graphics. The implementation utilised core Three.js modules including orbit controls for camera manipulation, GLTFLoader for efficient model loading, and optimised WebGL rendering capabilities.

This carefully curated technology stack ensured consistency across development and deployment phases while maintaining the flexibility required for future enhancements. The combination of established scientific computing libraries with modern web technologies provided the necessary foundation for developing both precise surgical planning tools and interactive patient education models.

2.4.1.2 Validation Framework

The validation strategy comprised three distinct workstreams:

1. CME Model Validation

    - Inter-rater and intra-rater reliability study examining impact on anatomical understanding among expert CME surgeons (chapter 4)
    - Clinical feasibility study assessing anatomical accuracy against intraoperative findings (chapter 5)
    - Evaluation of surgical utility and collection of key outcome measures for future validation work

2. Patient Education Model Validation (chapter 6)

    - Initial pilot study (n=10) collecting structured user feedback
    - Randomised study evaluating impact on:
        - Decisional conflict
        - Procedural understanding
    - Qualitative interviews exploring patient experience.
- Technical Validation (current chapter)
    - Geometric accuracy assessment for CME models
    - Computational efficiency metrics

2.4.1.3 Iterative Design Implementation

The development process followed an evidence-based iterative methodology, with each cycle informed by rigorous validation and structured feedback. This project required the acquisition of advanced technical skills spanning medical image processing, computer graphics, and web development - competencies not typically part of surgical training.

The technical learning journey was structured through formal and self-directed education. Core programming skills were developed through completion of Imperial College's Python programming modules, supplemented by online resources focused on scientific computing libraries and web development frameworks. Proficiency in 3D modelling was systematically developed through structured online courses in ZBrush and Substance Painter, progressing from basic mesh manipulation to advanced anatomical modelling and physically based rendering techniques. This multi-faceted approach to skill acquisition proved essential for implementing a complex processing pipeline that bridged clinical and technical domains.

Each development iteration comprised three distinct phases:

1. Development Phase The technical implementation phase involved translating anatomical knowledge into computational solutions:

- Development of mesh processing algorithms and visualisation features
- Enhancement of existing functionality based on validation findings.
- Basic interface development focused on essential functionality.
- Progressive integration of advanced features as technical capabilities matured.

2. Evaluation Phase A systematic evaluation protocol assessed primarily technical and clinical aspects:

- Integration and analysis of clinical study findings

- Quantitative assessment of technical performance metrics
- Informal user feedback on interface functionality
- Critical analysis of technical limitations to guide further development.

3. Optimisation Phase The refinement process focused on technical performance and clinical utility:

- Technical optimisation guided by quantitative validation metrics.
- Basic interface refinements based on user feedback.
- Performance optimisation based on computational profiling.
- Implementation of advanced features reflecting growing technical expertise

This iterative methodology was effective in managing the transition from clinical expertise to technical implementation, allowing for the systematic development of increasingly sophisticated features as programming and 3D modelling capabilities evolved. While the approach successfully delivered functional tools for both surgical planning and patient education, formal user interface evaluation and human-computer interaction assessment represent important areas for future development. A structured evaluation of interface design principles and user experience metrics would enhance future iterations of these tools.

2.4.1.4 Quality Assurance Protocol

A comprehensive quality assurance framework encompassed:

1. Geometric Accuracy Metrics The preservation of anatomical geometry was systematically logged for each mesh:
    - Initial and final vertex counts
    - Initial and final face counts
    - Mean edge length pre-processing
    - Bounding box comparisons pre- and post-processing
    - Surface normal verification
2. Clinical Quality
    - Expert/intra-operative anatomical verification
    - Surgical workflow integration
    - Patient comprehension assessment

2.5 Technical approach

Following the methodological framework outlined above, this chapter details the development and implementation of two complementary visualisation approaches for colorectal cancer surgery. Both approaches utilise established computer graphics and mesh processing techniques, adapted and validated for specific clinical applications.

The technical implementation was driven by practical considerations that directly impact clinical utility. Surface rendering methodology was selected as the foundational approach for both applications, informed by several key factors. Surface-rendered models, constructed from triangulated mesh geometries, offer significant computational advantages over volumetric approaches. The reduced memory requirements enable real-time interaction on standard clinical hardware, eliminating the need for specialised computational resources - a crucial consideration for NHS clinical environments where high-end hardware may not be available and where responsive performance is essential for practical utility.

The implementation comprises two distinct but complementary approaches:

2.5.1 Automated Visualisation Framework for Complete Mesocolic Excision

This framework establishes an automated processing pipeline for reconstructing and visualising 3D models of mesenteric vasculature and associated structures. The implementation combines optimised mesh processing techniques with web-based rendering to convert segmented CT data into interactive 3D visualisations. The processing pipeline incorporates differential mesh optimisation parameters for vascular and solid organ structures, ensuring preservation of critical anatomical relationships while maintaining computational efficiency. The following sections detail the technical specifications, mesh processing pipeline development, quality assurance protocols, and clinical workflow integration.

2.5.2 Patient-Specific Educational Models for Pelvic Exenteration

The second implementation applies physically based rendering (PBR) techniques to create patient-specific educational models. This approach emphasises visual clarity and anatomical accuracy while ensuring accessibility for patient education and virtual consultation. The PBR workflow incorporates advanced texturing techniques, anatomically accurate materials, and

optimised lighting models to enhance visual comprehension (198). Subsequent sections cover the model development methodology, material creation workflow, and implementation strategy.

Both implementations leverage web-based visualisation frameworks through standardised formats such as GLB, enabling efficient deployment across various platforms and devices through standard web browsers. This accessibility proves essential for both in-person and remote clinical applications, supporting modern healthcare delivery requirements including telemedicine consultations. The GLB format was specifically chosen for its efficient binary encoding, comprehensive material support, and native scene graph implementation - crucial features for maintaining anatomical relationships and interactive performance.

A critical consideration in both workflows was the current limitation of automated segmentation methods for abdominal-pelvic imaging. Given these constraints, manual segmentation, though time-intensive, was adopted as the most reliable approach for generating accurate three-dimensional models. This approach enables precise extraction of distinct mesh files for each anatomical structure, facilitating manipulation of visual properties including opacity and colourisation. Manual segmentation was performed using ITK-SNAP (20), followed by custom Python processing pipelines utilising established scientific computing libraries for mesh generation and optimisation.

The visualisation layer employs WebGL-based rendering through Three.js (103), enabling broad compatibility while maintaining high-quality visual output. This technical framework prioritises practical clinical utility while ensuring the accuracy and reliability necessary for surgical applications. Surface-rendered polygon models provide broad functionality with various 3D technologies, making them highly suitable for virtual and augmented reality platforms whilst enabling the option to 3D print models. Their compatibility with professional 3D modelling software allows for the integration of advanced visualisation techniques, such as anatomical animation and physically based rendering.

The technical implementations detailed in the following sections prioritise practical clinical utility while ensuring the accuracy and reliability necessary for surgical applications. Their clinical validation and assessment are addressed in subsequent chapters.

2.6 Technical implementation: Image segmentation

The generation of three-dimensional models requires the segmentation of Digital Imaging and Communications in Medicine (DICOM) datasets. Segmentation involves the systematic classification of individual voxels within the imaging data, with each voxel being assigned a unique label corresponding to specific anatomical structures. Given the current limitations of automated algorithms in accurately segmenting pelvic imaging, all segmentation was performed manually using ITK-SNAP, an open-source software platform (20).

2.6.1 Complete mesocolic excision

For mesenteric vascular reconstruction, we utilised standard clinical staging CT imaging. The imaging protocols encompassed:

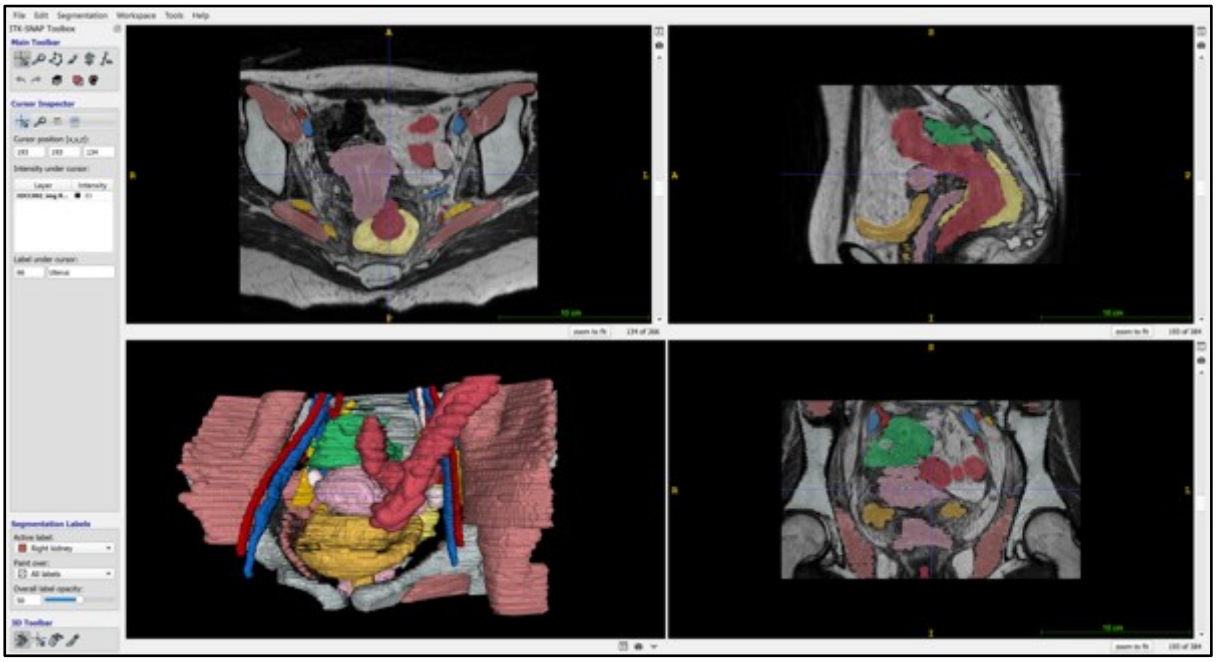
- Porto-venous phase CT
- CT angiography
- CT colonography

Image quality was maintained with slice thickness ranging from sub-millimetre to 2.5mm, ensuring adequate spatial resolution for accurate vessel delineation. A detailed breakdown of segmentation times and anatomical accuracy can be found in Chapter 5 which documents the clinical feasibility study.

The following anatomical structures were systematically segmented in each scan:

- Mesenteric vasculature (arteries and veins)
- Colon
- Stomach and duodenum.
- Pancreas
- Tumour mass and associated pathology

Figure 2-1 Example segmentation of pelvic MRI in ITK SNAP



2.6.2 Pelvic exenteration

The segmentation protocol for pelvic exenteration cases employed a multimodal imaging approach, leveraging the complementary strengths of CT and MRI:

- Standard portovenous CT provided superior spatial resolution for osseous structures and vascular anatomy, enabling precise delineation of the complete bony pelvis and its associated vasculature.
- T2-weighted MRI offered superior soft tissue contrast resolution for primary anatomical structures of interest, though its narrower field of view precluded complete visualisation of the bony pelvis.

This dual-modality approach compensated for the inherent limitations of each imaging technique. Imaging selection prioritised scans demonstrating maximal disease extent, as these were crucial for planning patient-specific R0 resection procedures.

Anatomical Classification System

Segmented structures were categorised into three distinct groups:

1. **Tumour Components**
    - Primary tumour mass
    - Tumour deposits
    - Pathological lymph nodes
2. **Target Structures**
    - Anatomical structures requiring resection for R0 status.
3. **Context Anatomy**
    - Supporting anatomical structures
    - Included to enhance patient comprehension of spatial relationships.

Where necessary/applicable, resultant anatomical mesh files from each imaging modality were manually integrated within the 3D modelling software platform.

2.7 Technical Implementation: CME Visualisation

2.7.1 Mesh Extraction

The first stage of the pipeline utilises the Python scientific computing stack to extract surface meshes from volumetric segmentation data. The process begins with loading NifTI format segmentation files using python library NiBabel (v4.0.2) (197), which provides access to the volumetric data and associated metadata, including voxel dimensions and spatial transformations.

2.7.1.1 Marching Cubes algorithm implementation

We employ the marching cubes algorithm implemented in scikit-image for each label in the segmentation volume to generate initial surface meshes. The marching cubes algorithm is a fundamental technique used in medical visualisation to generate surface meshes from volumetric imaging data.

The algorithm processes binary masks created by thresholding each label value to generate vertex coordinates and face indices that define the surface boundary. Medical imaging datasets often have non-uniform voxel dimensions, where the resolution within each slice (x and y axes) differs significantly from the slice thickness (z-axis). The coordinates are scaled

based on voxel dimensions retrieved from the NIfTI header to correct this anisotropy, ensuring that the model accurately reflects real-world proportions.

2.7.1.2 Global transformation and mesh standardisation

Preserving spatial relationships between different mesh components is crucial for maintaining the overall anatomical accuracy of the resulting model. Our normalisation pipeline implements a global transformation approach that simultaneously applies identical operations across all meshes, thereby preserving their relative positions and anatomical relationships.

1) Global Scene Centralisation
2) The process begins by calculating a unified scene centre by aggregating all vertex positions across the constituent meshes. This approach ensures that the centralisation transformation considers the anatomical structure rather than treating each component separately, thereby preserving critical spatial relationships between anatomical structures.
3) Standardised Anatomical Orientation: A standardised -90-degree rotation around the X-axis is applied uniformly across all meshes. This transformation aligns the model with conventional anatomical cranial-caudal orientation.
4) Uniform scale normalisation
5) Surface Normal Standardisation: The pipeline concludes with the standardisation of surface normals, ensuring a consistent outward-facing orientation across all mesh surfaces. Surface normals, which are unit vectors perpendicular to the tangent plane of a surface, are essential for rendering and visualising the model accurately, as they determine how light interacts with the surface.

We adopted this approach after our initial mesh extraction methodology failed to preserve anatomical spatial relationships. The original implementation processed each anatomical structure independently, applying transformations and optimisations at the individual component level. This approach introduced systematic errors that compromised the spatial integrity of the final model.

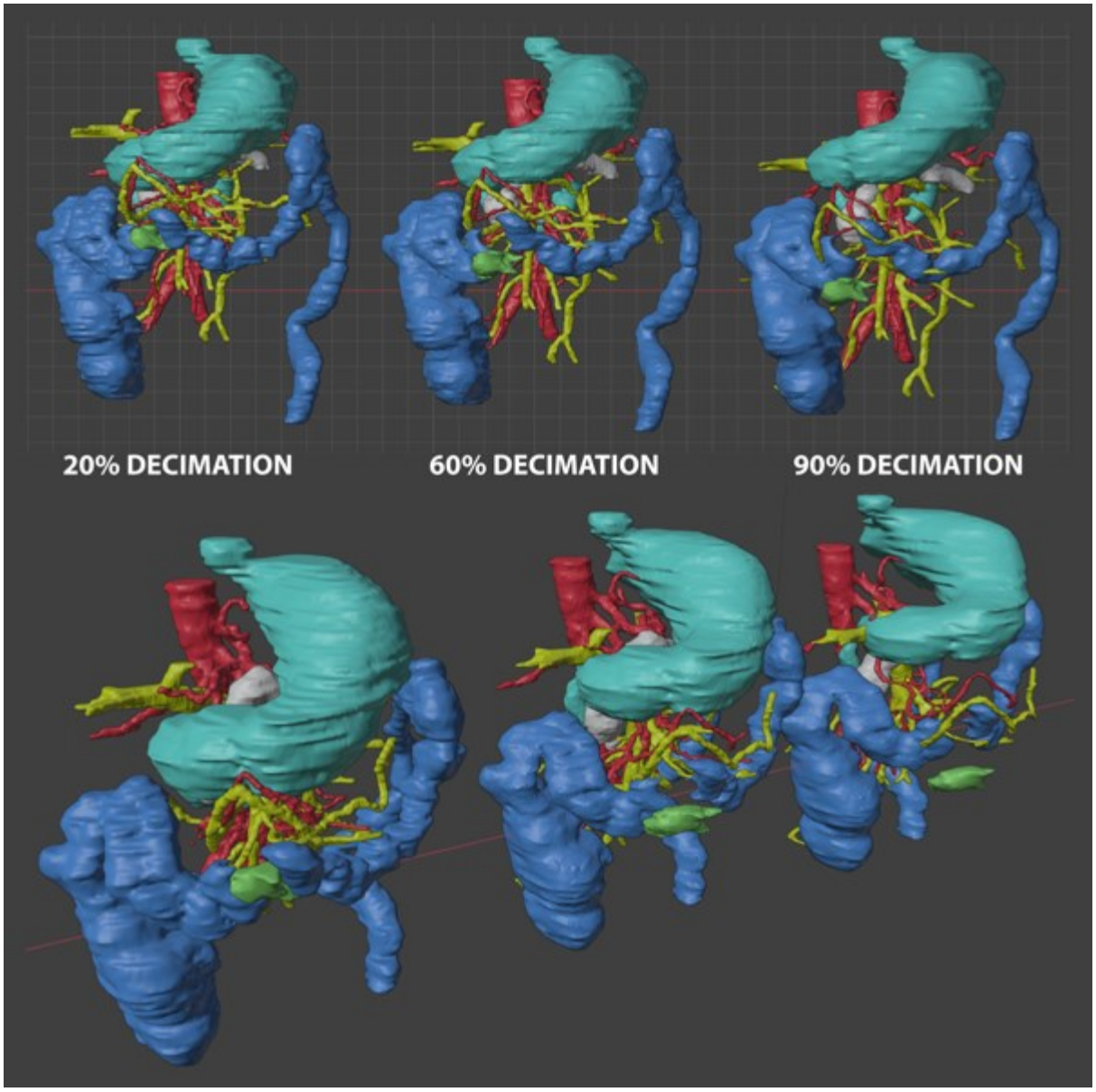
The independent centring of each mesh established different reference frames for each anatomical structure, leading to progressive spatial misalignment. Subsequent processing steps, such as decimation and smoothing, further exacerbated this misalignment, with the magnitude of displacement correlating with the degree of mesh decimation.

The spatial disruption occurred in three primary ways:

1. **Reference Frame Inconsistency**: Independent centring resulted in multiple inconsistent reference points, causing cumulative transformation errors across components.
2. **Non-uniform Vertex Distribution**: Mesh decimation altered vertex distributions differently for each component, leading to centroid shifts proportional to the decimation level.
3. **Differential Smoothing Effects**: Separate smoothing operations caused inconsistent boundary modifications and varying degrees of volume preservation between adjacent structures.

The relative position shifts were quantified with each method by calculating the distance between the centroid of each mesh with respect to one another.

Figure 2-2 Relative shifts of each anatomical mesh with initial mesh extraction and transformation method.



2.7.1.3 Affine transformation for scale preservation

While the refined mesh processing methodology successfully maintained the relative spatial relationships between anatomical structures, it did not preserve the real-world dimensions present in the source NIFTI data. This limitation, although acceptable for purely conceptual visualisations, posed potential constraints for future applications requiring accurate spatial measurements, such as surgical planning or quantitative anatomical studies.

To address this limitation, we implemented an enhanced mesh extraction process that incorporates the NIFTI file's affine transformation matrix. The affine transformation encodes the mapping between voxel coordinates and real-world space, encompassing scaling, rotation, and translation components. By applying this matrix during mesh extraction, we ensured that the resultant meshes retained the true spatial dimensions and orientations inherent in the original imaging data.

Figure 2-3 Python code implementation of 3D mesh extraction from segmentation file with affine transformation and scene centring and rotation to ensure correct relative positioning

```
def extract_transformed_mesh(filepath):

    nii = analyze_nifti(filepath)
    data = nii.get_fdata()
    original_affine = nii.affine

    # Extract raw meshes
    raw_meshes = []
    for label in range(1, 7):
        if np.any(data == label):
            logger.info(f"\nExtracting label_{label}")
            vertices, faces, _, _ = marching_cubes(data == label)

            # Apply affine transformation to vertices
            homogeneous_vertices = np.hstack((vertices, np.ones((vertices.shape[0], 1))))
            transformed_vertices = np.dot(homogeneous_vertices, original_affine.T)[:, :3]

            raw_meshes.append({
                'vertices': transf'rmed_vertices,
                'faces': 'aces,'
                'label': 'abel
'           })

    # Calculate scene center
    all_vertices = np.vstack([mesh['vertices'] for mesh in raw_meshes])
    scene_center = np.mean(all_vertices, axis=0)
    logger.info(f"\nScene center in real-world coordinates: {scene_center}")

    # rotate -90 degrees around X axis
    angle_x = -np.pi/2
    rotation_matrix = np.array([
        [1, 0, 0, 0],
        [0, np.cos(angle_x), -np.sin(angle_x), 0],
        [0, np.sin(angle_x), np.cos(angle_x), 0],
        [0, 0, 0, 1]])

    # Process each mesh
    scene = trimesh.Scene()
    processed_meshes = []

    for mesh_data in raw_meshes:
        label = mesh_data['label']
        logger.info(f"\nProcessing label_{label}")

        # Create mesh
        mesh = trimesh.Trimesh(
```

```
    vertices=mesh_data['vertices'],
    faces=mesh_data['faces'])


# Flip normals outward
mesh.invert()

# Centre + rotate scene
center_transform = np.eye(4)
center_transform[:3, 3] = -scene_center

transform = np.dot(rotation_matrix, center_transform)
mesh.apply_transform(transform)
```

Each model was scaled to ensure uniform proportions required for the subsequent 3D visualisation of the model in Three.js (see below).

2.7.2 Mesh optimisation and processing.

A primary limitation of the marching cubes algorithm is that it generates dense meshes, mainly when applied to high-resolution medical imaging data. Each intersected cube creates multiple triangles, leading to hundreds of thousands for typical DICOM volumes (e.g., 256×256×256 voxels). Rendering dense meshes in real time requires significant computational resources, leading to degraded frame rates by end users during real-time visualisation, particularly when multiple meshes are visualised simultaneously.

Furthermore, raw mesh outputs by marching cubes often contain stair-step artefacts resulting from the discrete voxel grid of the input data. Additionally, redundant triangulation in regions of low curvature or flat surfaces contributes to unnecessary complexity without significantly improving geometric accuracy.

To address the computational burden and aesthetic limitations of the raw mesh derived from segmentation, we developed an optimisation pipeline in Python that includes decimation, smoothing, and an optional shrink-wrapping method.

2.7.2.1 Selective Mesh Decimation

Decimation is implemented using quadric metric reduction algorithm. The well-established quadric error metrics algorithm by Garland and Heckbert (1997) (90) functions to:

1. Compute error quadrics for each vertex.
2. Iteratively collapses edges based on minimal error.
3. Maintains mesh topology during reduction.

This approach is useful because it prioritises the preservation of sharp features and areas of high curvature while more aggressively simplifying flatter, less detailed regions.

Figure 2-4 Python implementation of decimation using decimation submodule from the Trimesh library. The implementation decimated different labels to ensure adequate fidelity in the final mesh (Label 1= artery, 2=Vein, 3= Stomach/Duodenum, 4= Colon, 5= Pancreas, 6=Tumour).

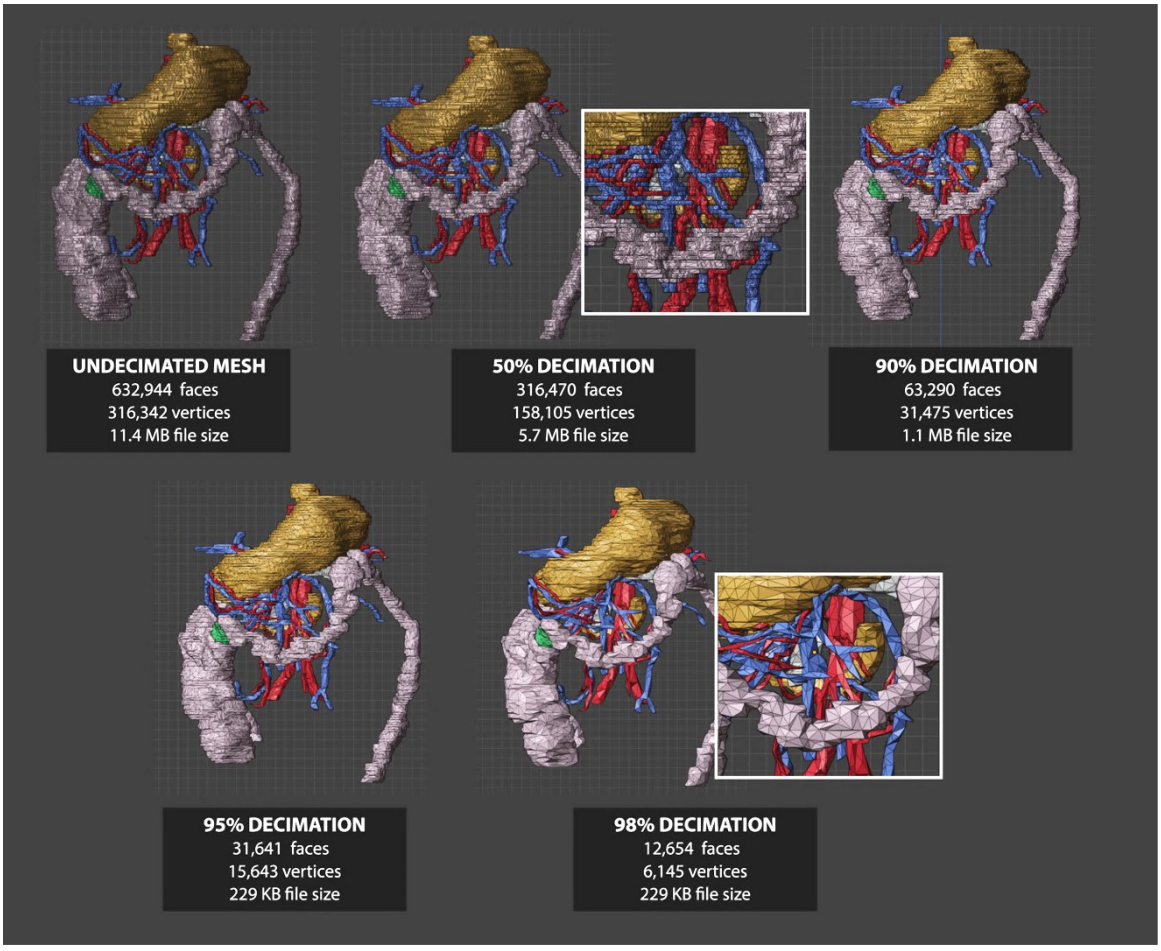
```
# Decimation
    if label in [1, 6]:
        target_percent = 0.7
        logger.info(f"Label {label}: Decimating to 70% of original faces.")
    elif label == 2:
        target_percent = 0.8
        logger.info(f"Label {label}: Decimating to 80% of original faces.")
    else:
        target_percent = 0.2
        logger.info(f"Label {label}: Decimating to 20% of original faces.")
    target_faces = int(len(mesh.faces) * target_percent)

    if len(mesh.faces) > 1000:
        logger.info(f"Decimating label_{label} from {len(mesh.faces)} to {target_faces} faces")
        mesh = mesh.simplify_quadric_decimation(target_faces)
```

The degree of decimation varied depending on the specific mesh being processed. Mesenteric vessels were decimated less to preserve the mesh integrity and fine vessel detail. Experiments were conducted with models at varying levels of decimation to determine the correct balance between reduced polygon counts and maintaining sufficient mesh integrity and detail.

The result was a reduced mesh that maintains the most visually and geometrically important characteristics of the original model.

Figure 2-5 Effect of different degrees of decimation on overall model topology. Each mesh can be decimated to 90% without any significant distortions.



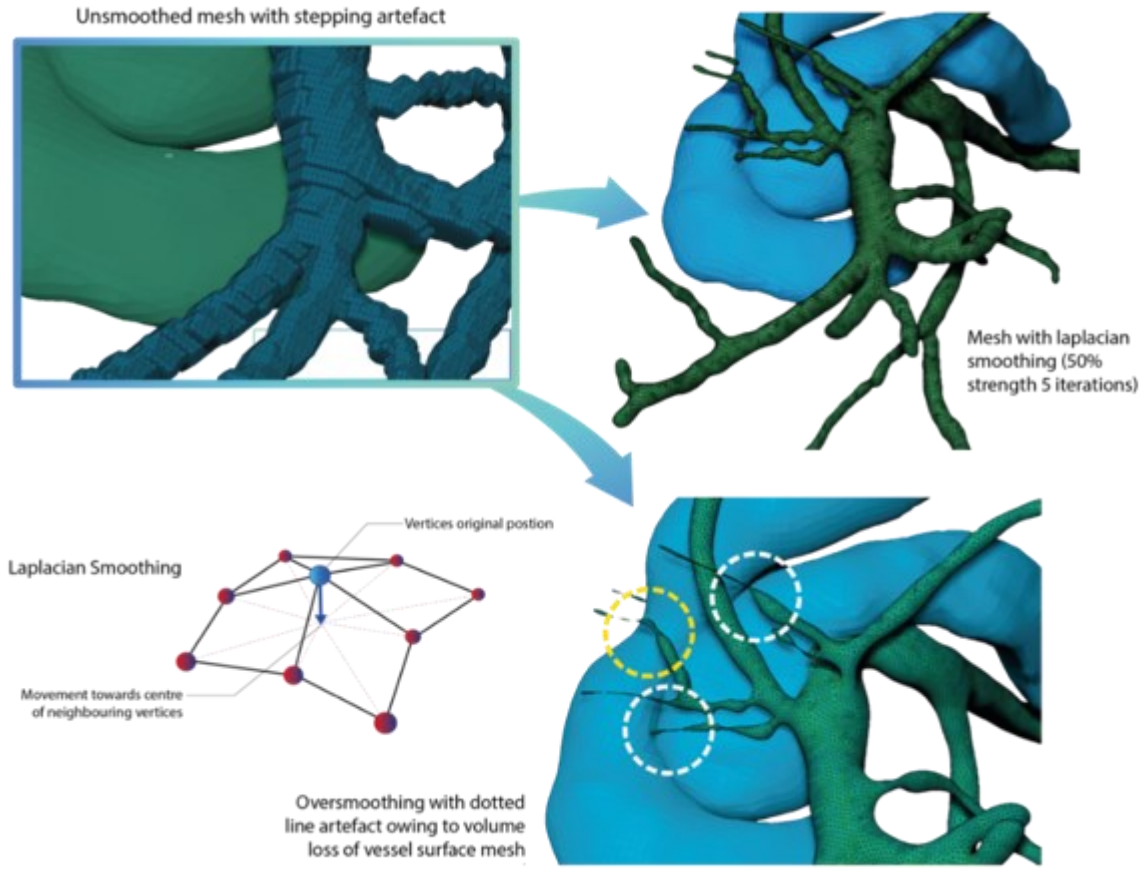
2.7.2.2 Volume-Preserving Laplacian Smoothing

Laplacian smoothing was applied to the decimated mesh components to help reduce the stepping artefact. This smoothing technique adjusts the positions of vertices iteratively based on their local neighbourhood, effectively moving each vertex toward the average position of its connected neighbours (91). Iterative adjustment helps to even out irregularities and produce smoother surface transitions.

We utilised the *Trimesh* Laplacian smoothing, which includes a volume preservation constraint to minimise mesh shrinkage—a common side effect of smoothing algorithms (199). Recognising the need to preserve fine details in certain structures, we adopted a differential smoothing approach. Specifically, vascular structures were smoothed less than larger organs to maintain their intricate features. Smoothing was employed after decimation,

as each mesh had fewer vertices representing the same surface. With fewer vertices, the effect of smoothing is more pronounced, as each vertices have a greater influence on the overall geometry.

Figure 2-6 Laplacian mesh smoothing with illustration of mesh shrinkage and 'dotted-line' artefact.



Parameter optimisation was conducted across 111 anatomical models to determine optimal mesh processing parameters while maintaining anatomical accuracy. The study evaluated mesh decimation percentages ranging from 10% to 90% combined with Laplacian smoothing iterations from 0 to 20, maintaining consistent smoothing strength ($\lambda = 0.3$).

Surface deviation was quantified using bidirectional mean surface distance calculations between original raw mesh from segmentation and processed meshes. This approach utilised k-dimensional (KD) tree data structures for efficient nearest-neighbour distance calculations between point sets (200). The bidirectional calculation ensured comprehensive

surface comparison by computing the mean distance from the original to the processed surface and vice versa, then averaging these values.

Accuracy thresholds were established based on anatomical significance, with vascular structures (arteries and veins) and tumour requiring mean surface distances changes below 1.0 mm, while other anatomical structures permitted deviations up to 3.0 mm. Analysis of the mean surface distances revealed optimal parameters for each anatomical category. Vascular structures achieved optimal results with 20% mesh decimation and four iterations of Laplacian smoothing ($\lambda = 0.3$- moderate smoothing coefficient). The remaining anatomical structures maintained adequate accuracy with 80% decimation and 14 iterations of Laplacian smoothing ($\lambda = 0.3$). These parameters successfully balanced mesh simplification requirements with anatomical accuracy constraints while remaining within the specified surface distance thresholds.

Figure 2-7 and 2-8 illustrates the effect of combined decimation and smoothing parameters on the overall model topology for each label.

Figure 2-7 Heat map plot demonstrating the effect of smoothing and decimation on the mean surface distance in comparison to the unprocessed meshes for each anatomical structure across the 111 patient data set. Such metrics allowed selection of appropriate processing parameters to achieve predetermined levels of mesh accuracy.

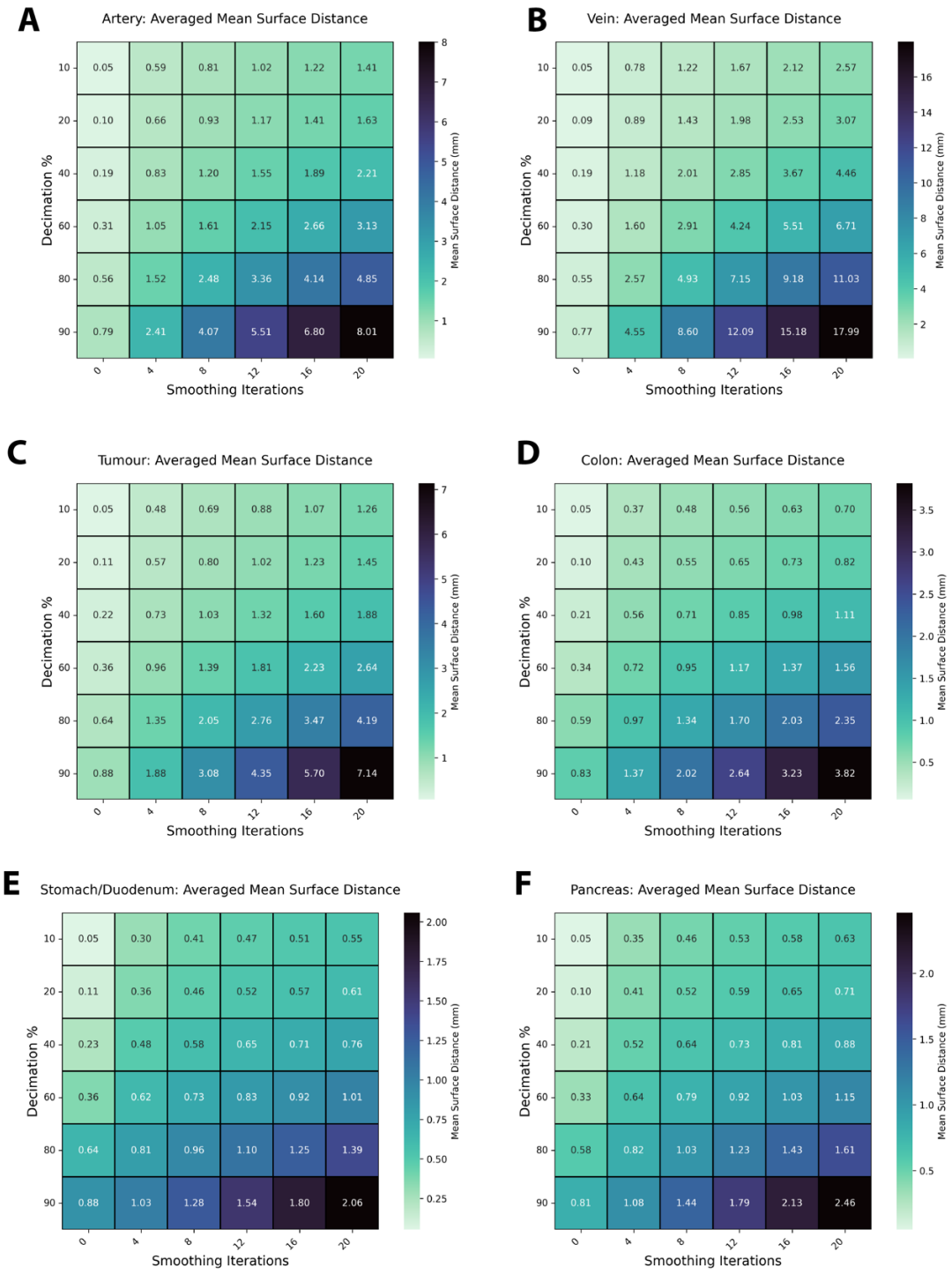
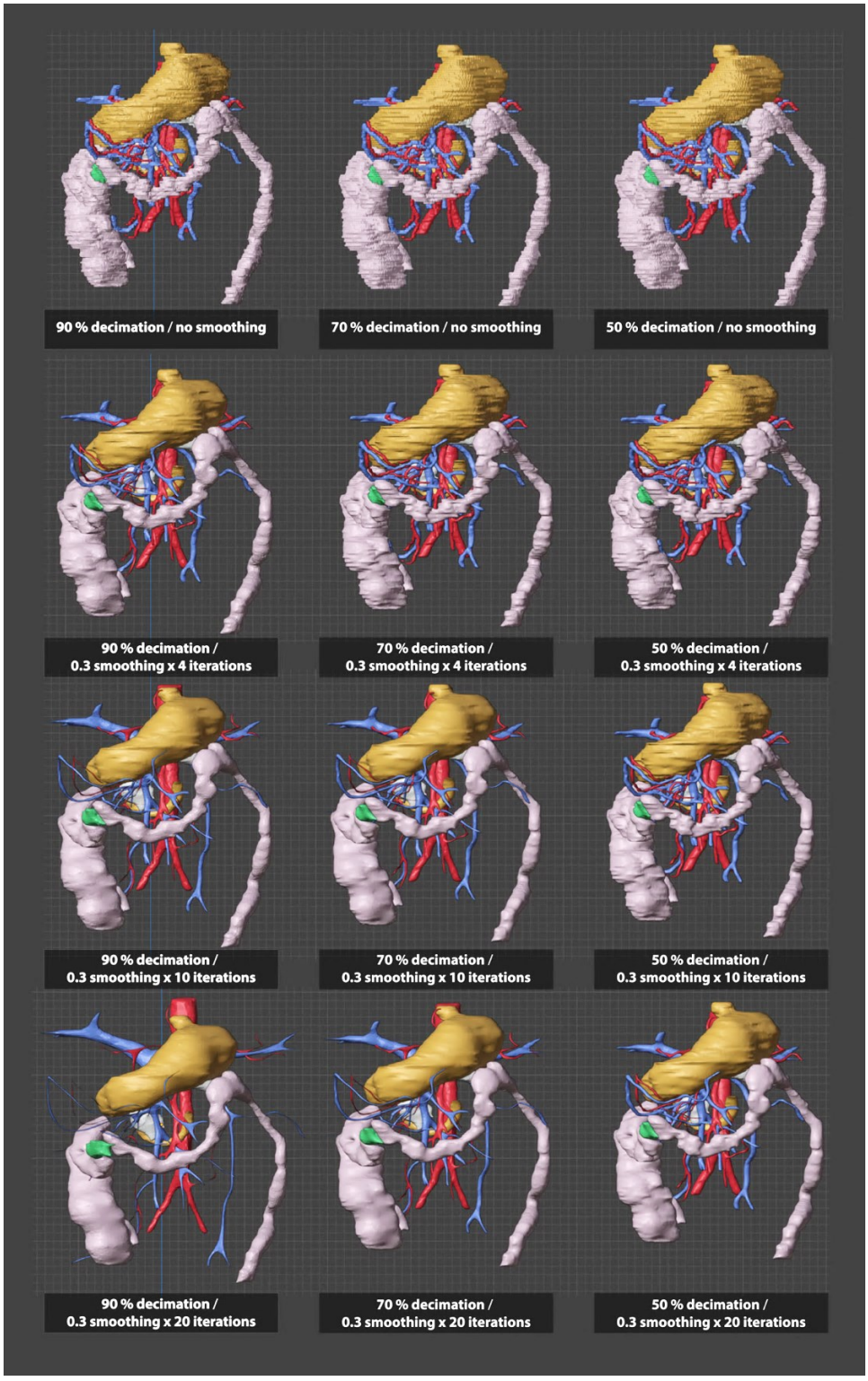


Figure 2-8 Visual comparison of the effect on mesh topology for combinations of smoothing and decimation. As decimation increases (and vertices count reduce) the model will tolerate less smoothing before unacceptable alterations in mesh topology occur. The model in the bottom left corner representing 90% decimation with 20 iterations of smoothing with a coefficient of 0.3 demonstrates the significant degradation in model fidelity that occur.



2.7.2.3 Shrink Wrapping

The shrink-wrap method serves as a final optional stage in our mesh optimisation pipeline, designed to maintain geometric accuracy following decimation and smoothing operations. This method utilises spatial computation algorithms implemented through the Trimesh and SciPy libraries to project vertices of the processed mesh onto the surface of the original, unprocessed mesh (201).

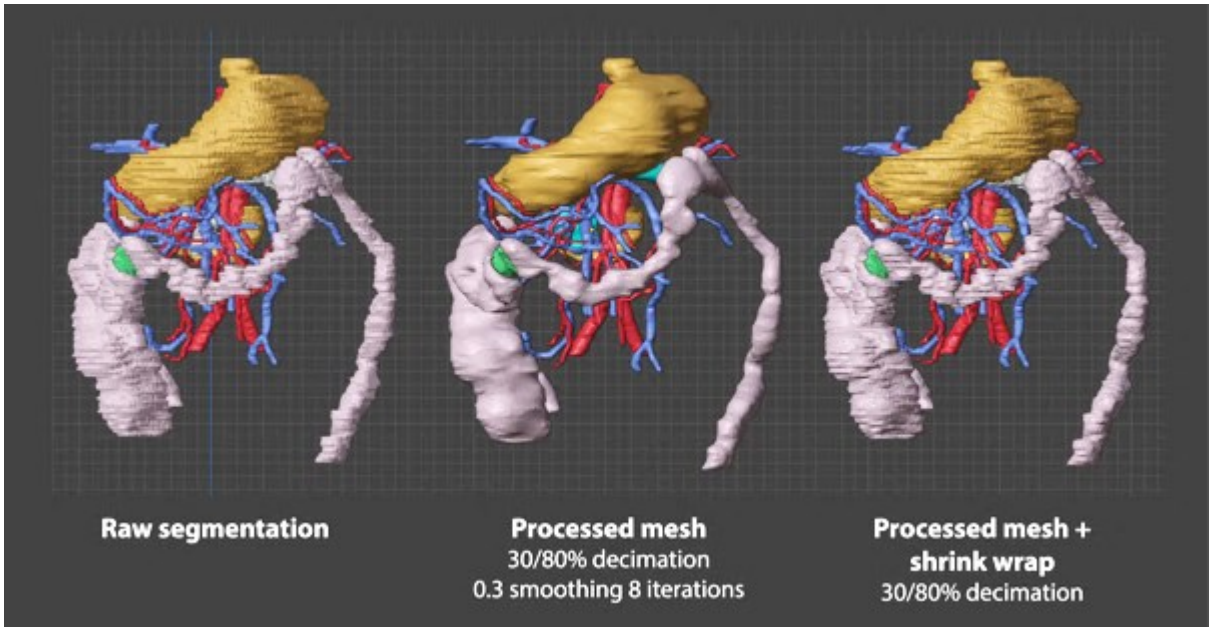
The method begins by constructing a k-dimensional tree (KD-tree) data structure using SciPy's KDTree class, initially focusing on the target mesh's vertices. This spatial indexing structure enables efficient nearest neighbour searches and facilitates rapid identification of the closest vertices on the target mesh for each vertex in the source mesh (202).

Following the initial vertex proximity assessment, a second KD-tree is constructed using the centroids of the target mesh's faces. This secondary spatial index enables more precise surface projection by considering the actual geometry of the mesh surface rather than merely vertex positions. The face centroids are computed as the arithmetic mean of each triangle’s positions:

Projection of each vertex of the processed mesh onto the nearest face of the original mesh was accomplished by calculating the normal for the closest face on the target mesh and using the dot product to calculate how far the source vertex is from the target mesh.

While our use case does not require such millimetre precision, other applications may require this level of accuracy, e.g. for tumour resection where distortions of the tumour with the surrounding anatomy would cause potential interpretation errors.

Figure 2-9 Visual illustration of the effects of model processing and subsequent shrink wrapping. The shrink wrap function restores the original topology of the unprocessed high polygon mesh derived from the segmentation file.



2.7.3 3D model file format exports

The processed meshes are assembled into a scene using the Trimesh library, with each mesh assigned a unique identifier corresponding to its segmentation label. The scene is then exported in GLB format. The GLB format, developed by the Khronos Group, is a binary version of the GL Transmission Format (glTF) designed for efficient transmission and loading of 3D content, particularly for web-based visualisation using Three.js.

OBJ is a traditional text-based 3D file format that, while widely used, presents limitations in the context of our model application. GLB offers several advantages over OBJ in the context of web-based visualisation.

- **File Size**: GLB's binary encoding results in files that are significantly smaller compared to OBJ's text-based files (50% reduction in file size for the same model).
- **Material Management**: Unlike OBJ, which lacks native material management, GLB supports UV mapping and Physically Based Rendering (PBR) textures, allowing for

more sophisticated material rendering and control over individual mesh properties (e.g., transparency).

- **Scene Graph Implementation**: GLB's hierarchical scene graph enables the preservation of complex structural relationships, maintaining individual component identifiers and material definitions for enhanced user control (203).

Table 2-1 Comparison of different 3D file formats

Feature	GLB Format	OBJ Format	FBX Format
Data Representation	Binary format: compact and efficient	Text-based, redundant, and inefficient	Binary/text-based; versatile but complex
File Size	Smaller due to binary encoding	Larger due to text-based structure	Medium; can be larger due to extensive features
Parsing Speed	Faster parsing, low computational overhead	Slow parsing, higher computational demands	Moderate; extensive feature set may slow parsing
Web Compatibility	Highly compatible with WebGL and Three.js	Requires additional conversion for web use	Limited direct web compatibility; requires conversion
Scene Graph Support	Native scene graph supports hierarchical models	No native scene graph: manual organisation required	Supports complex scene graphs; suitable for detailed hierarchies
Memory Utilisation	Optimised for low memory usage	High memory utilisation due to text format	Moderate to high; depends on features used
Progressive Loading	Supports incremental loading for large datasets	No native support for progressive loading	Limited support; often requires custom implementation
Cross-Platform Consistency	Consistent rendering across devices	Inconsistent rendering; device-specific issues	Generally consistent but may vary due to proprietary elements
Application in Medical Context	Ideal for preserving anatomical relationships	Limited capabilities for interactive manipulation	Suitable for detailed animations but adds complexity not always needed in medical contexts

2.8 Web-Based Visualisation application

We developed a web application for visualising anatomical reconstructions using a client-server architecture. The system comprises a Flask backend server for processing medical imaging data using the workflow described above and a browser-based frontend for interactive 3D visualisation (204).

2.8.1 Architectural Overview

The system architecture consists of two main components: a client-side visualisation engine and the server-side processing pipeline. This division of responsibilities ensures efficient computational task distribution, with intensive processing managed server-side while the client side remains focused on delivering a responsive user experience.

2.8.1.1 Client-Side Architecture

The client-side implementation utilises Three.js as its core rendering engine, providing WebGL (Web Graphics Library)-accelerated 3D graphics capabilities. WebGL is a JavaScript API (Application Programming Interface) that enables hardware-accelerated rendering of interactive 2D and 3D graphics within web browsers without additional plugins (103). This choice enables hardware-accelerated rendering while maintaining broad browser compatibility. The client architecture implements:

1. Real-time 3D rendering through WebGL.
2. Asynchronous model loading and processing.
3. Interactive user interface components
4. Client-side state management

2.8.1.2 Server-Side Architecture

The server implementation employs Flask, a lightweight Python web framework chosen for its efficient integration with scientific computing libraries, ease of use, and minimal overhead. Flask is particularly suitable for applications that require integration with Python's scientific libraries (NumPy, SciPy, etc.), which are utilised in our mesh processing pipeline.

Key server-side components include:

1. RESTful API endpoints for model processing

2. Asynchronous task handling
3. Real-time processing status updates
4. Efficient file management system

2.8.1.3 Frontend Implementation

The front-end implementation combines modern web libraries to create an interactive medical visualisation platform. The system employs a component-based architecture, with distinct modules handling different aspects of the visualisation process.

2.8.1.4 Interface Components

The user interface utilises HTML5 and Tailwind CSS (205), a utility-first CSS framework designed to enable rapid and consistent UI development, implementing a responsive design pattern that adapts to various display configurations. This approach ensures consistent functionality across different devices and screen sizes while maintaining a professional appearance suitable for clinical applications. The final app can be seen in figures 2-10 and 2-11.

The full source code for the mesh processing and web app is available for review at the following GitHub repository.

https://github.com/JAFletch-surg/3D-Anatomy-viewer

Figure 2-10 Segmentation upload page. Users can drag and drop the file or upload via file directories.

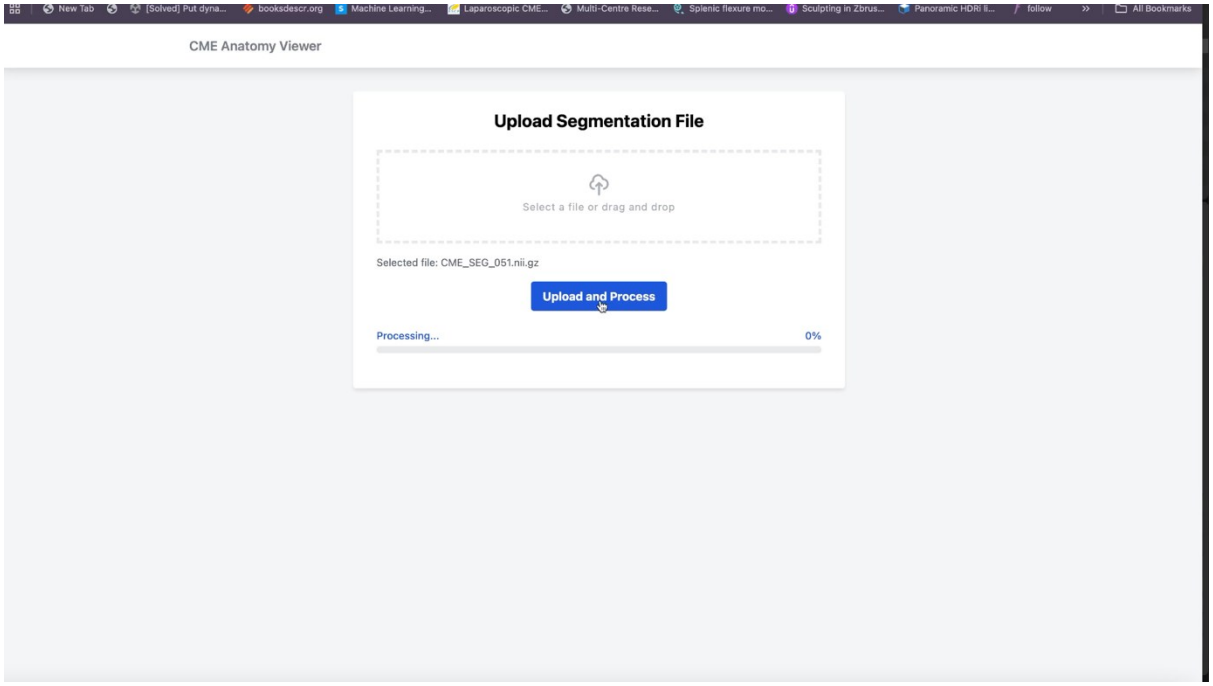
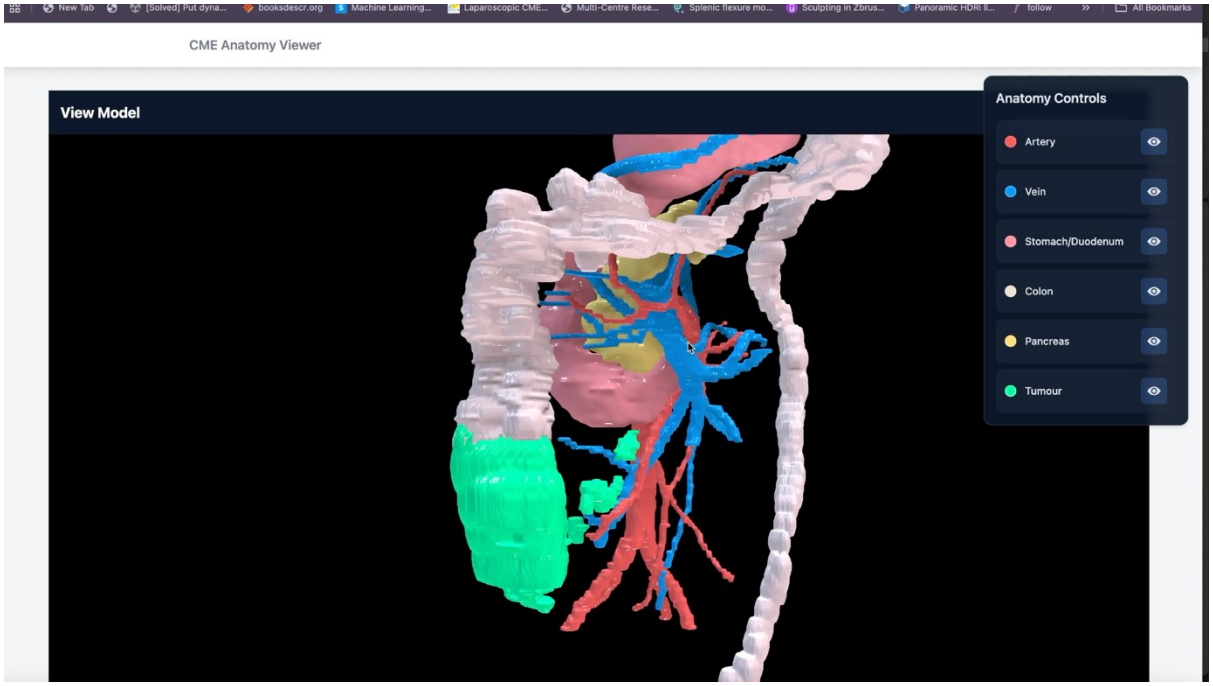


Figure 2-11 Interactive colour coded 3D model derived from user uploaded segmentation file. Transparency controls are in the upper right corner of the screen.



2.9 Technical implementation: Patient education models for Pelvic exenteration

A novel 3D model workflow was developed based on the initial needs analysis and patient input. Starting with patient-specific imaging data, anatomical structures were segmented to generate base meshes of the relevant anatomy. These initial meshes were processed using ZBrush (Pixologic), a commercial 3D modelling and sculpting software particularly suited for manipulating complex organic structures. ZBrush's capability to handle dense meshes comprising millions of polygons makes it ideal for creating highly detailed anatomical models.

The segmented STL files were converted to FBX format before importing into ZBrush. This conversion step is crucial as FBX's hierarchical structure preserves each anatomical component as a distinct mesh while maintaining spatial relationships - unlike STL format which would require merging all structures into a single mesh. This preservation of separate anatomical structures enables independent manipulation and texturing of each component while maintaining their correct anatomical positions in Euclidean space.

For cases utilising both CT and MRI data, the meshes from these different imaging modalities required manual alignment. Typically, CT data provided superior resolution for bony structures and vessels, while MRI data was used for soft tissue structures. Following alignment, any duplicate meshes were removed to create a unified model incorporating the optimal data from each imaging modality.

2.9.1 Model Production Workflow

The process of producing the final 3D models can be divided into the following steps:

a) **Basic Smoothing**

Initial smoothing was applied to remove the stepping artefacts resulting from segmentation. This step involved flattening the angles between adjacent faces to smooth the surface.

b) **Manual 3D Modelling and Sculpting**

The workflow utilised ZBrush's comprehensive digital sculpting toolset to refine geometric accuracy and enhance anatomical detail. Two key features were central to this process: Dynamesh, which enables dynamic re-meshing to maintain consistent polygon distribution during sculpting, and Sculptris Pro, which provides adaptive tessellation - automatically increasing mesh resolution in areas requiring finer detail.

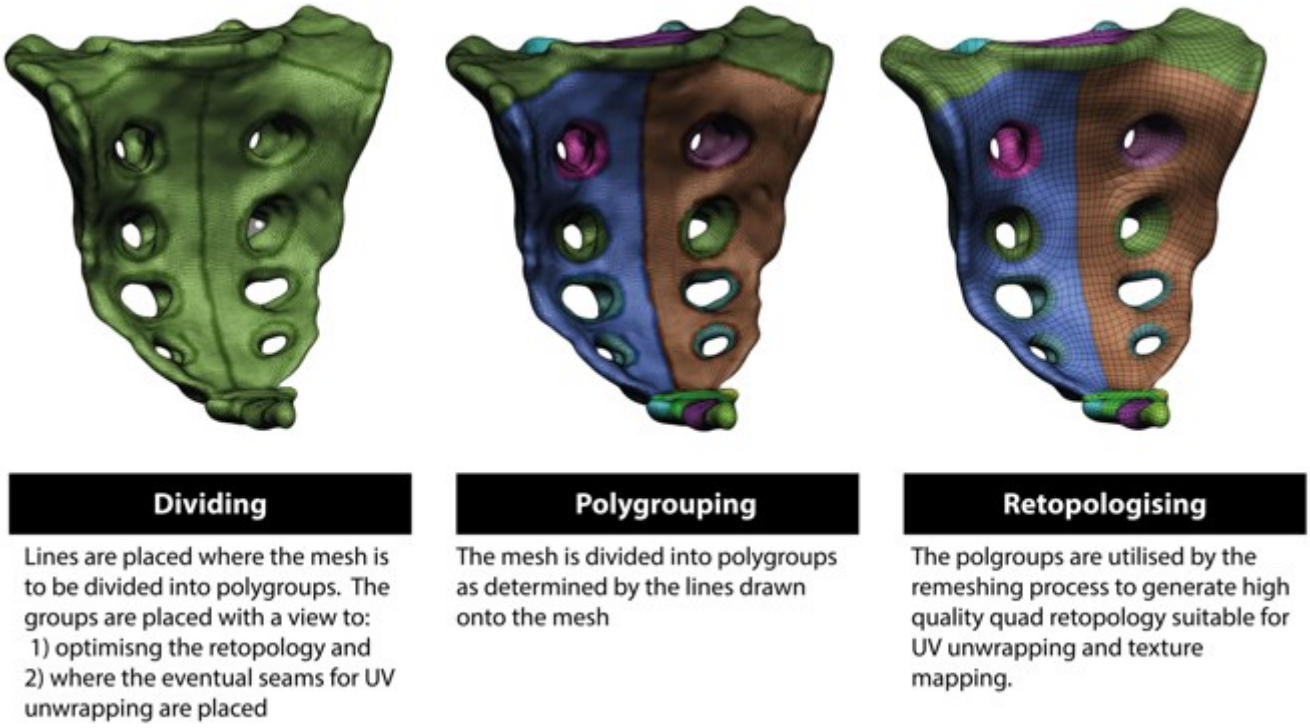
Through these tools, each anatomical structure underwent precise refinement of both volumetric form and surface detail. Dynamesh ensured the mesh remained malleable during major shape adjustments by maintaining even polygon distribution, while Sculptris Pro automatically subdivided areas requiring higher geometric detail to capture fine anatomical features (206). This combination of techniques resulted in high-resolution mesh representations that accurately captured both macro anatomical form and micro surface details.

c) **Creation of Low-Poly Copy**

To prepare for texturing, a duplicate of each high-resolution mesh underwent a structured optimisation process. First, the mesh was segmented into polygroups - distinct regions that guide subsequent processing steps. These polygroups were defined using ZBrush's masking and Pen Tool features, allowing precise control over the segmentation of complex anatomical structures. The polygroups are particularly important as they influence how ZBrush creates the flow of quadrilateral polygons across the model's surface, ensuring that edge loops follow natural anatomical contours and features.

The optimised low-polygon version was then generated using ZRemesh, a specialised retopology algorithm. ZRemesh converts the original triangular mesh into a quadrilateral-based topology while reducing overall polygon count to a specified target. The previously defined polygroups guided this retopology process, enforcing quadrilateral edge flows that respect anatomical boundaries and maintaining appropriate topology in areas of high geometric detail. Quadrilateral polygons were specifically chosen as they provide superior results in UV unwrapping and texture mapping compared to triangular topology. The polygroups boundaries also served to define UV seams, resulting in efficient texture layouts that minimise distortion in the final textured model. This process is illustrated in figure 2-12.

Figure 2-12 Process of topologizing complex anatomical mesh structures using pen and polygrouping. The model is manually divided into different polygroups which then serve to determine the quad remeshing algorithm.



d) **UV Unwrapping**

Each retopologised mesh underwent UV parameterisation, mapping the 3D surface geometry onto a 2D plane. This transformation is crucial for accurate texture application, as it defines how textures are projected onto the surface. Proper UV mapping ensures textures are not distorted, preserving the model's anatomical integrity.

The UV parameterisation process utilised ZBrush's capability to automatically generate UV seams from the polygroups boundaries. Where anatomically appropriate, polygroups were merged prior to UV unwrapping to minimise the number of UV islands, reducing texture complexity and potential visible seams. Seam placement was carefully considered, ensuring they were either hidden in naturally occurring anatomical junctions or placed in areas that would be less visible in the final model.

These optimised UV islands maintain local geometric relationships and minimise distortion, resulting in an organised texture layout with consistent Texel density, essential

for achieving uniform texture resolution across different model parts. This approach of minimal, strategically placed UV seams ensures optimal texture quality while maintaining the model's visual integrity (see Figure 2-13 and 2-14).

Figure 2-13 UV unwrapping using polygroups to determine seam placement.

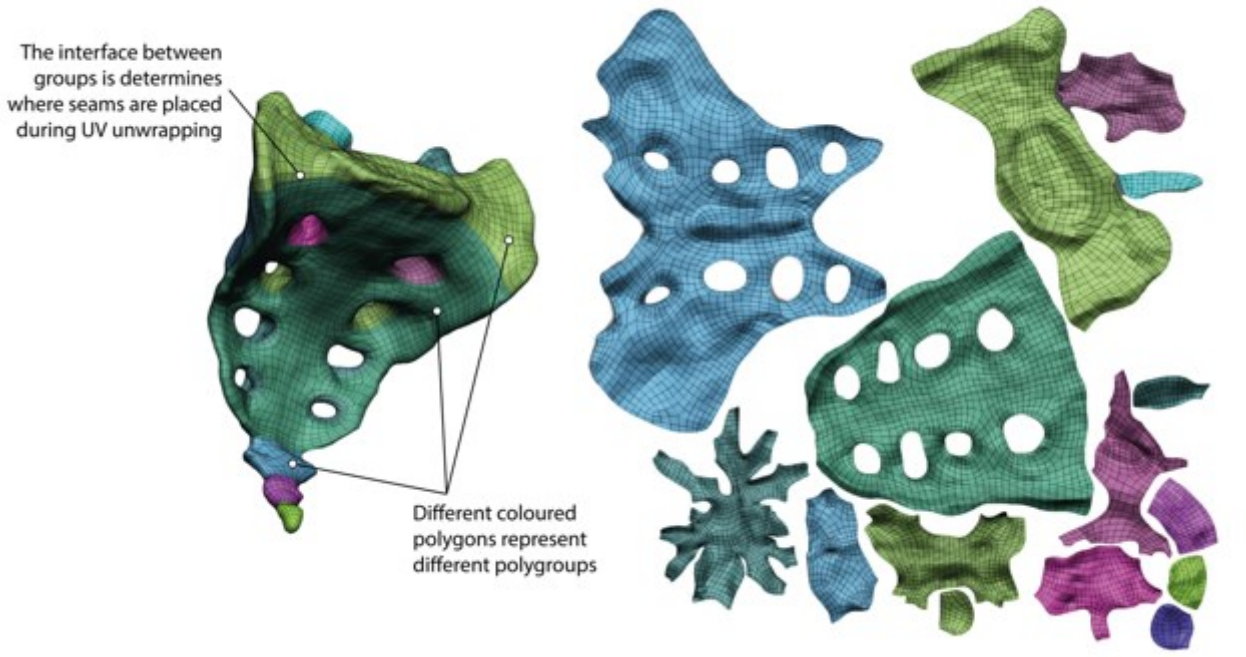
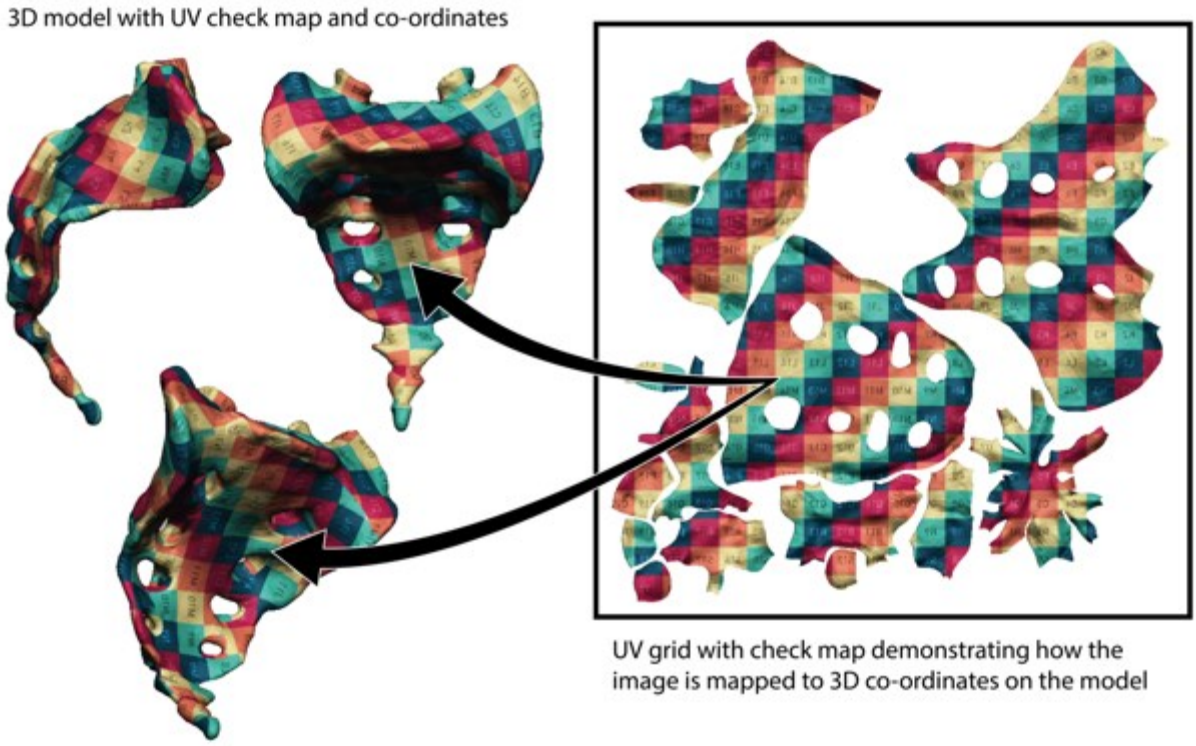


Figure 2-14 UV grid map applied to unwrapped sacrum to demonstrate how 2D texture images are applied to 3D model.

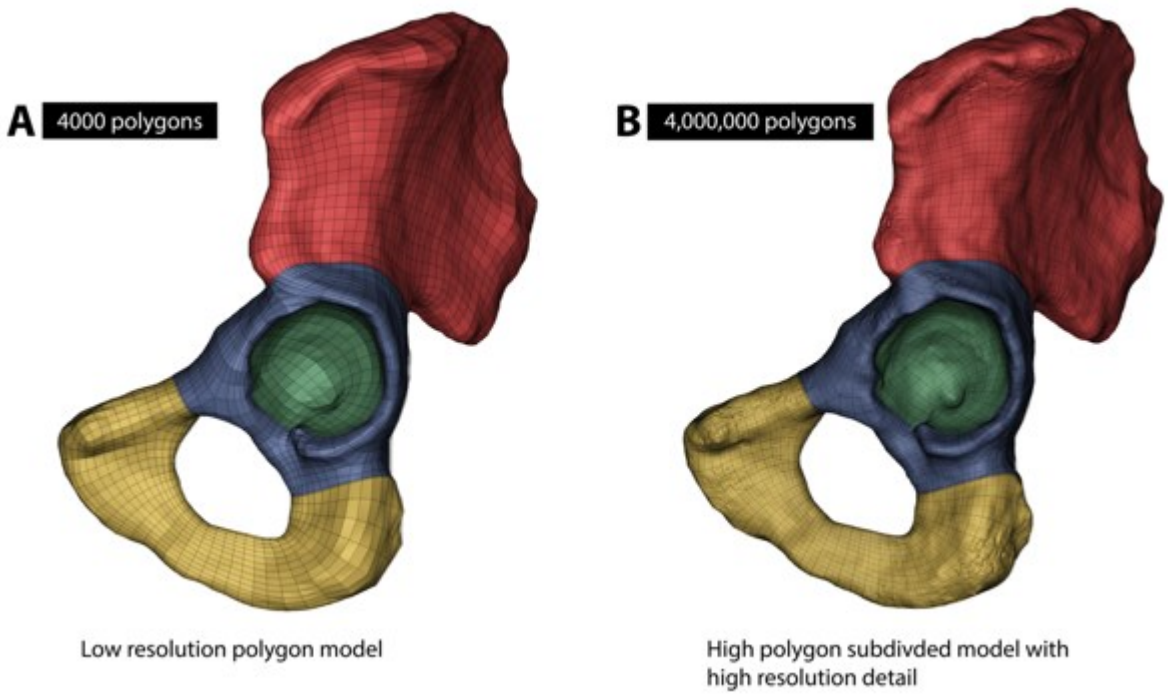


e) **Detail Projection**

The low-resolution mesh copy was subdivided 5-6 times using ZBrush's subdivision capabilities to create a model with multiple subdivision levels. This progressive subdivision provided the mesh with sufficient polygon density to capture intricate anatomical details while maintaining the efficient quad-based topology of the low-resolution mesh.

The high-resolution surface detail from the original sculpted mesh was then projected onto this subdivided model. This detail projection process transferred the fine surface features from the original high-resolution model onto the subdivided mesh, which now had adequate polygon density to accurately represent these details. This approach combines the benefits of an optimised quad-based topology for texturing with the geometric detail of the original sculpted mesh, allowing the model to retain high visual complexity and anatomical accuracy while maintaining computational efficiency through its multi-resolution structure (see Figure 2-15).

Figure 2-15 3D mesh with multiple subdivision levels.



f) **Export as FBX Files**

Both the low-polygon and high-polygon models were exported as FBX files for use in subsequent texturing workflows. The low-polygon model, with its optimised quad-based topology and UV layout, served as the base mesh for texture painting. The high-polygon model was used to generate (bake) a normal map - a specialised texture that encodes surface detail from the high-resolution geometry into an image format. When applied to the low-polygon model, this normal map recreates the fine anatomical details of the high-resolution mesh through pixel shading rather than additional geometry, maintaining visual fidelity while ensuring computational efficiency.

2.9.2 Texturing Workflow

The creation of realistic anatomical textures utilised Adobe Substance 3D Painter, an industry-standard 3D texturing software that allows direct painting onto 3D models in real-time. The software enables the creation of complex materials through a non-destructive, layer-based workflow like Adobe Photoshop, but specifically designed for 3D models. The process employed both the optimised low-polygon mesh and its high-resolution counterpart

exported from ZBrush in FBX format. The workflow began with normal map baking, which transfers surface detail from the high-resolution mesh onto the simplified low-polygon model through tangent space calculations. This technique encodes surface normal direction data within RGB channels (red for X-axis, green for Y-axis, and blue for Z-axis), enabling the simulation of complex anatomical surface details without additional geometry.

The texturing methodology implemented a comprehensive Physically Based Rendering (PBR) approach, which simulates realistic light interaction by accurately modelling surface properties such as roughness, reflectivity, and metallicity. This ensures consistent material appearance under various lighting conditions, crucial for achieving lifelike representations of anatomical structures.

Bespoke "smart materials" were developed in Substance Painter for each anatomical structure. These smart materials are sophisticated, procedural materials that combine multiple texture layers and effects that automatically respond to the model's surface properties such as curvature, height, and orientation. For instance, blood vessels received smart materials that automatically emphasise surface detail along curved areas while maintaining consistent colouration, while hollow organs were assigned materials that generate appropriate surface variation based on interior and exterior surfaces.

Substance Painter's layer-based system provided precise control over these material properties, enabling fine-tuned adjustments to surface characteristics. A significant advantage of smart materials is their reusability - once created, they can be rapidly applied to any anatomical structure of the same type across different patient models, automatically adapting to each model's unique topology while maintaining consistent anatomical appearance.

The final models utilised multiple specialised texture maps that combine to create a physically accurate, photorealistic representation. Each map controls a specific aspect of how the surface interacts with light (see figure 2-16):

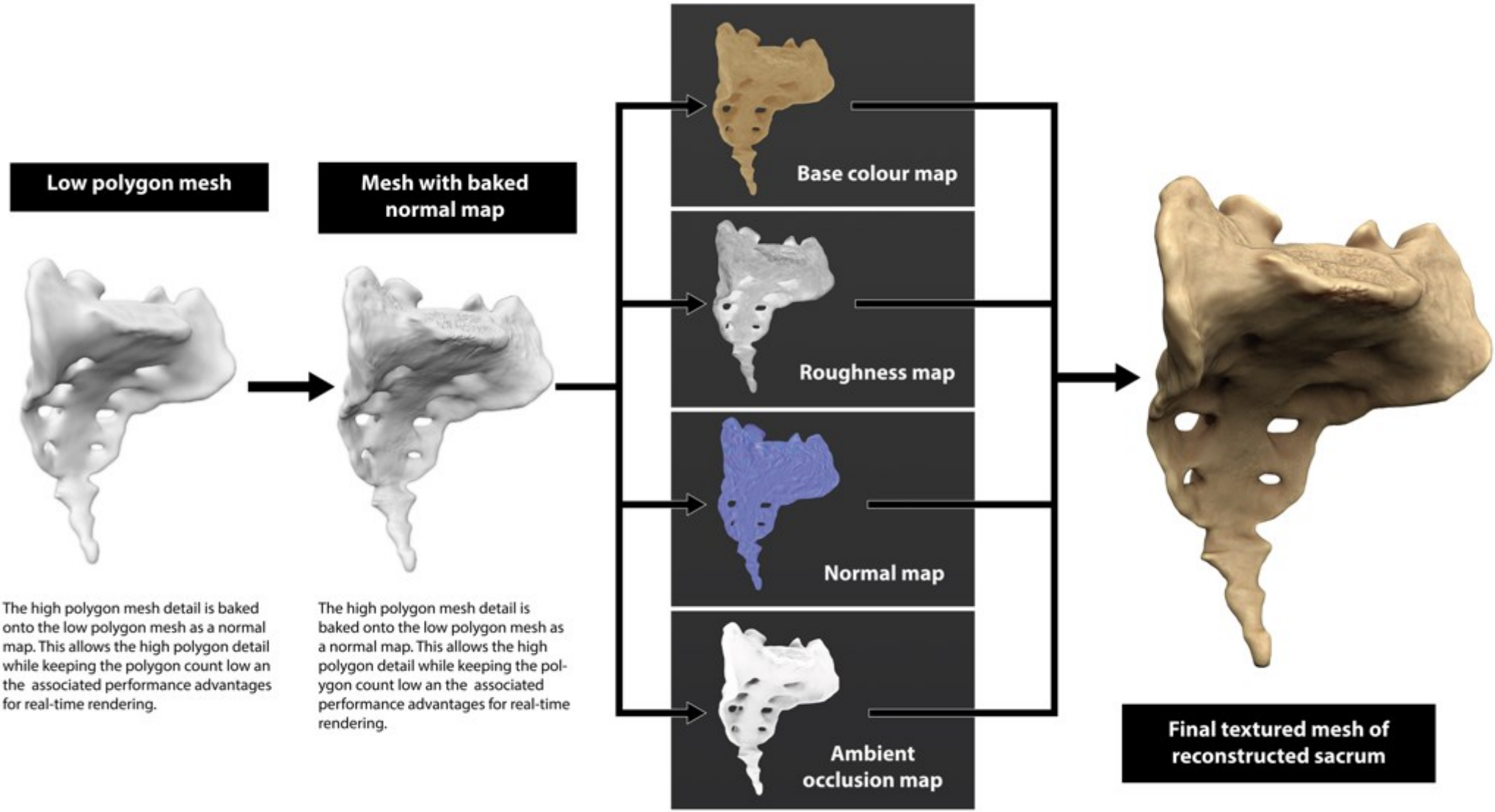
Base colour maps provide the fundamental surface colouration without any lighting information. For anatomical structures, these were carefully crafted to represent authentic tissue colours while avoiding the flat appearance typical of simple colour textures. Roughness maps control the microscopic surface detail by defining how diffuse or specular each area appears - allowing precise control over whether surfaces appear moist, dry, or glossy. This was particularly important for achieving realistic tissue appearances. Ambient occlusion maps enhance depth perception by simulating how light is occluded in crevices

and recessed areas, adding subtle shadowing that emphasises anatomical form. When combined with the base colour, these maps significantly enhance the perception of three-dimensional form. Subsurface scattering maps were crucial for achieving realistic tissue appearance, simulating how light penetrates and diffuses through organic materials - essential for replicating the translucent qualities of structures like blood vessels or membranous tissues.

Normal maps, baked from the high-resolution models, provide fine geometric detail by perturbing surface normals, creating the illusion of high-resolution surface detail without additional geometry. For specific anatomical features requiring emphasis, such as tumours or key surgical landmarks, emission maps were employed to make these structures subtly glow or stand out from surrounding tissues.

The interaction between these various maps creates a complex, physically based material representation that responds realistically to lighting changes. Opacity maps enable selective transparency, allowing the viewer to see internal structures while maintaining context - particularly useful for understanding spatial relationships between different anatomical components.

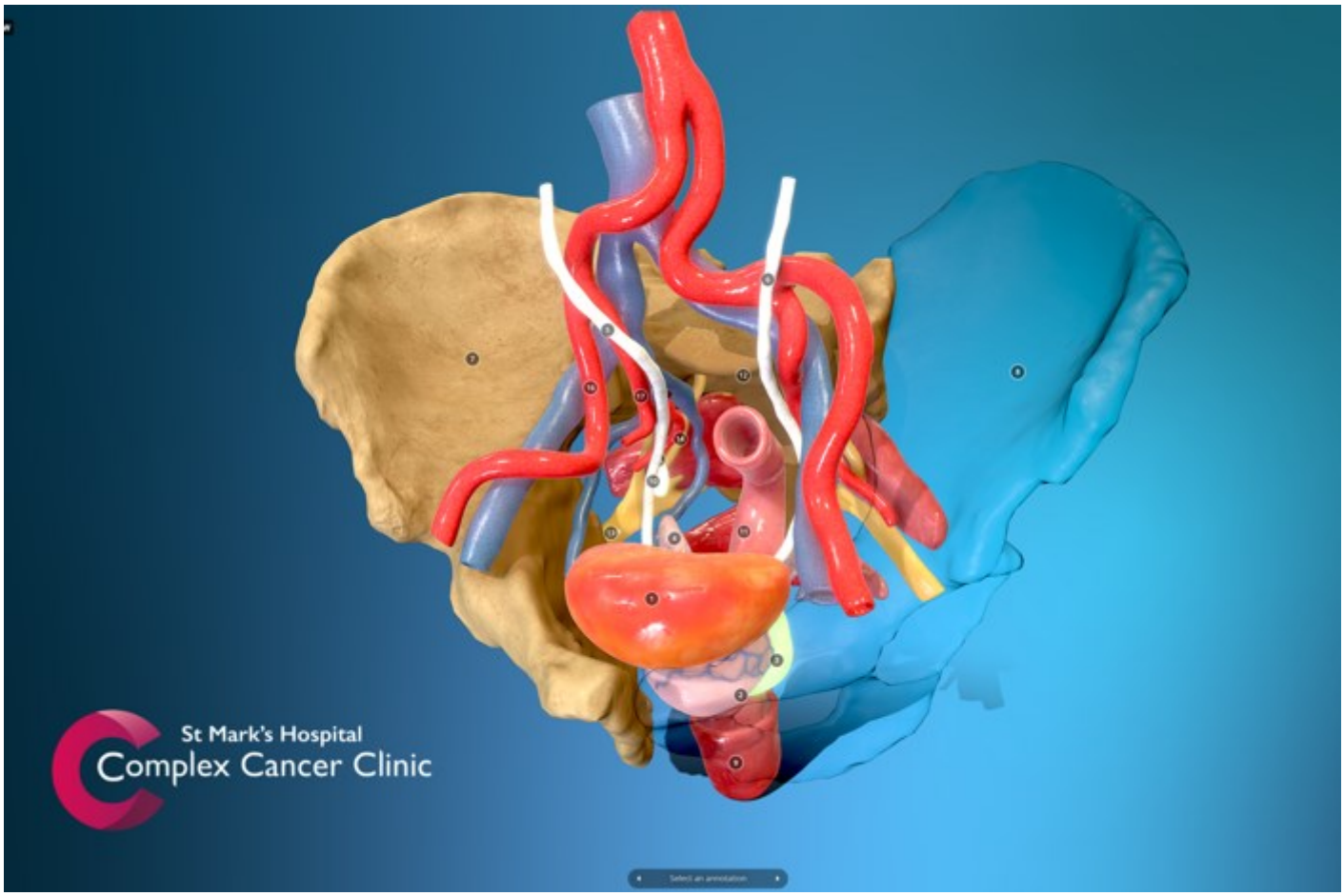
Figure 2-16 Example texture mapping components of low polygon sacrum mesh. The workflow show baking the normal map and the subsequent PBR texture maps that result in the final photorealistic bone texture (far right).



2.9.3 Online Model Visualisation and Interactive Interface

The three-dimensional anatomical models were deployed through the Sketchfab platform, with direct export from Adobe Substance 3D Painter using the built-in export API.

Figure 2-17 Advanced rectal cancer PBR rendered model derived from MR and CT imaging. The two extracted mesh were visually paired in the 3D software to enable the advantages of each imaging modality.



While the standard platform provides advanced visualisation and rendering capabilities, it limits user interaction to basic pan, tilt, and zoom functions. This restriction presents a significant limitation in clinical scenarios where the ability to selectively reveal anatomical relationships is crucial for understanding complex spatial relationships.

To address this limitation, we developed a bespoke interactive interface using the Sketchfab Viewer API (207), enhancing the clinical utility of these models by enabling more dynamic interaction.

The custom interface was implemented using HTML5, CSS3, and JavaScript, incorporating a responsive design framework to ensure compatibility across various devices. The interface implements a three-state visibility system for each anatomical structure (normal, transparent, hidden) controlled through a custom user interface. When in a transparent state, users control the opacity of individual structures using interactive sliders.

The technical implementation utilises the Sketchfab visualisation API's manipulation capabilities to dynamically adjust the visual properties of each structure. The system maintains separate material states for each anatomical component, enabling real-time adjustments to opacity levels whilst preserving the original material properties. This is achieved through programmatic manipulation of the material channels, principally opacity and subsurface scattering. Each anatomical structure is represented by a dedicated control button with an associated opacity slider, allowing users to progressively reveal or conceal specific anatomical relationships.

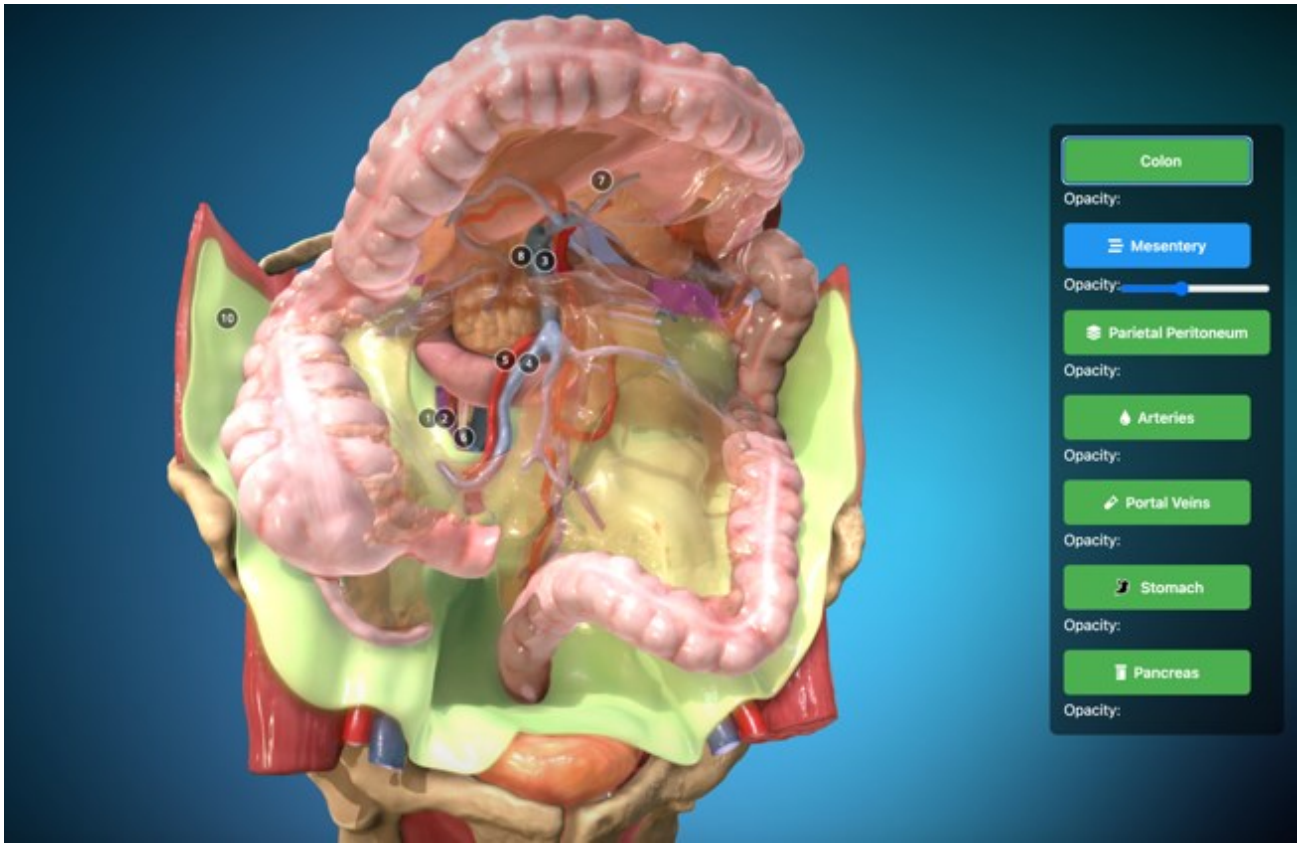
An example model (currently only optimised for desktop viewer) can be found at:

https://jafletch-surg.github.io/CME-anatomy/

Source code for the interactive model visualiser is available at the GitHub repository:

https://github.com/JAFletch-surg/CME-anatomy/blob/main/index.html

Figure 2-18 PBR Rendered model with custom UI allowing control over each component's transparency and material properties.



2.10 Quality Assurance and Validation of Mesh Processing Pipeline

To ensure the anatomical accuracy and geometric fidelity of the CME 3D reconstructions, a comprehensive quality assurance framework was implemented across the mesh processing method. Four key metrics were evaluated across 111 segmentations: mean surface distance change (mm), Hausdorff distance (mm), and edge length ratio (mm). These metrics were assessed at two critical stages: after initial decimation and following the complete processing workflow (decimation with smoothing). For the pelvic exenteration patient education models, where the primary goal was effective communication of surgical concepts, formal geometric validation was not performed.

2.10.1 Mean Surface Distance Change

The mean surface distance change quantifies the average deviation between the processed mesh and the original segmentation surface. This metric was evaluated in two stages to isolate the effects of different processing steps. Following decimation alone, the mean surface distance changes were minimal across all structures (arteries: 0.09 ± 0.02 mm; veins: 0.09 ± 0.02 mm; colon: 0.58 ± 0.12 mm; pancreas: 0.57 ± 0.10 mm; duodenum: 0.63 ± 0.14 mm; tumour: 0.11 ± 0.04 mm).

After the complete processing pipeline incorporating both decimation and smoothing, the surface distances increased but remained within acceptable clinical thresholds. Vascular structures maintained high precision (arteries: 0.64 ± 0.17 mm; veins: 0.87 ± 0.24 mm), while larger anatomical structures showed greater but clinically acceptable deviations (colon: 1.67 ± 0.66 mm; pancreas: 1.20 ± 0.30 mm; duodenum: 1.09 ± 0.25 mm). Notably, only 13% of colon cases and 9% of tumour cases exceeded the 1-3mm threshold, indicating robust preservation of anatomical geometry throughout the processing pipeline (see table 2-2 A-B).

2.10.2 Hausdorff Distance

The Hausdorff distance measures the maximum deviation between the original and processed meshes. Vascular structures and tumours maintained the lowest Hausdorff distances (arteries: 4.49 ± 1.35 mm; veins: 3.42 ± 0.78 mm; tumours: 3.79 ± 1.69 mm), reflecting the conservative processing parameters applied to these critical structures. Larger anatomical structures showed higher but expected Hausdorff distances (colon: 11.80 ± 3.93 mm; duodenum: 12.07 ± 5.40 mm; pancreas: 8.06 ± 7.15 mm), primarily attributable to their greater surface area and more aggressive optimisation parameters. Furthermore, these larger Hausdorff distances may also be influenced by artefacts in the original segmentation, particularly where significant misalignment between segmented layers can result in greater surface deviations when smoothing is applied (see Table 2-2 C).

2.10.3 Edge Length Ratio

The edge length ratio provides a quantitative measure of mesh element quality and potential geometric distortion. This metric is calculated as the ratio between the longest and shortest edges in each triangular face of the mesh, normalised across the entire structure. A ratio closer to 1.0 indicates more uniform triangulation and better preservation of the original mesh topology. Higher ratios suggest potential mesh distortion or uneven vertex distribution.

The edge length ratio serves as a measure of mesh quality and potential geometric distortion, with values closer to 1.0 indicating better preservation of the original mesh topology. Vascular structures and tumours demonstrated excellent mesh quality (arteries: 1.05 ± 0.21; veins: 1.02 ± 0.19; tumours: 1.03 ± 0.18), with no cases exceeding the critical threshold of 2.0. Larger structures showed higher edge length ratios (colon: 1.86 ± 0.29; pancreas: 1.84 ± 0.28; duodenum: 1.87 ± 0.29), with varying percentages of cases exceeding the 2.0 threshold (colon: 26%; pancreas: 11%; duodenum: 53%). This pattern reflects the more aggressive optimisation applied to larger structures, balanced against the clinical requirement for accurate visualisation (see Table 2-2 D).

These quantitative metrics demonstrate that the mesh processing pipeline successfully maintains anatomical accuracy while achieving significant mesh optimisation. The differential processing approach, applying more conservative parameters to vascular structures and tumours, effectively preserves critical anatomical features while enabling substantial mesh reduction in larger structures.

Table 2-2 A-D Quality metrics for 3D reconstructions derived from 111 segmentation files (corresponding to 111 patient cases).

A

Mean Surface distance change after decimation (mm)							
	n	Mean	Min	Max	SD	number of cases >1-3mm	% of cases
Artery	111	0.09	0.06	0.13	0.02	0	0
Colon	110	0.58	0.33	0.86	0.12	0	0
Pancreas	110	0.57	0.35	0.78	0.10	0	0
Duodenum	110	0.63	0.39	1.08	0.14	0	0
Tumour	74	0.11	0.00	0.32	0.04	0	0
Vein	111	0.09	0.06	0.13	0.02	0	0

B

Mean Surface distance change after decimation and smoothing (mm)							
	n	Mean	Min	Max	SD	number of cases >1-3mm	% of cases
Artery	111	0.64	0.33	1.09	0.17	0	0
Colon	110	1.67	0.60	3.28	0.66	14	13
Pancreas	110	1.20	0.63	2.30	0.30	0	0
Duodenum	110	1.09	0.59	2.00	0.25	0	0
Tumour	74	0.56	0.22	2.74	0.34	7	9
Vein	111	0.87	0.47	1.38	0.24	0	0

c

Hausdorff distance (mm)							
	n	Mean	Min	Max	SD		
Artery	111	4.49	2.21	8.25	1.35		
Colon	110	11.80	2.99	31.48	3.93		
Pancreas	110	8.06	3.76	79.95	7.15		
Duodenum	110	12.07	6.09	51.55	5.40		
Tumour	74	3.79	1.24	11.27	1.69		
Vein	111	3.42	1.92	5.52	0.78		

D

Edge length ratio (mm)							
	n	Mean	Min	Max	SD	number of cases >2mm	% of cases
Artery	111	1.05	0.66	1.37	0.21	0	0
Colon	110	1.86	1.29	2.38	0.29	29	26
Pancreas	110	1.84	1.25	2.38	0.28	12	11
Duodenum	110	1.87	1.20	2.43	0.29	58	53
Tumour	74	1.03	0.65	1.34	0.18	0	0
Vein	111	1.02	0.65	1.34	0.19	0	0

Figure 2-19 Box plot displaying the mean surface distance change (mm) after decimation only for different anatomical structures, including arteries, veins, tumour, colon, stomach/duodenum, and pancreas.

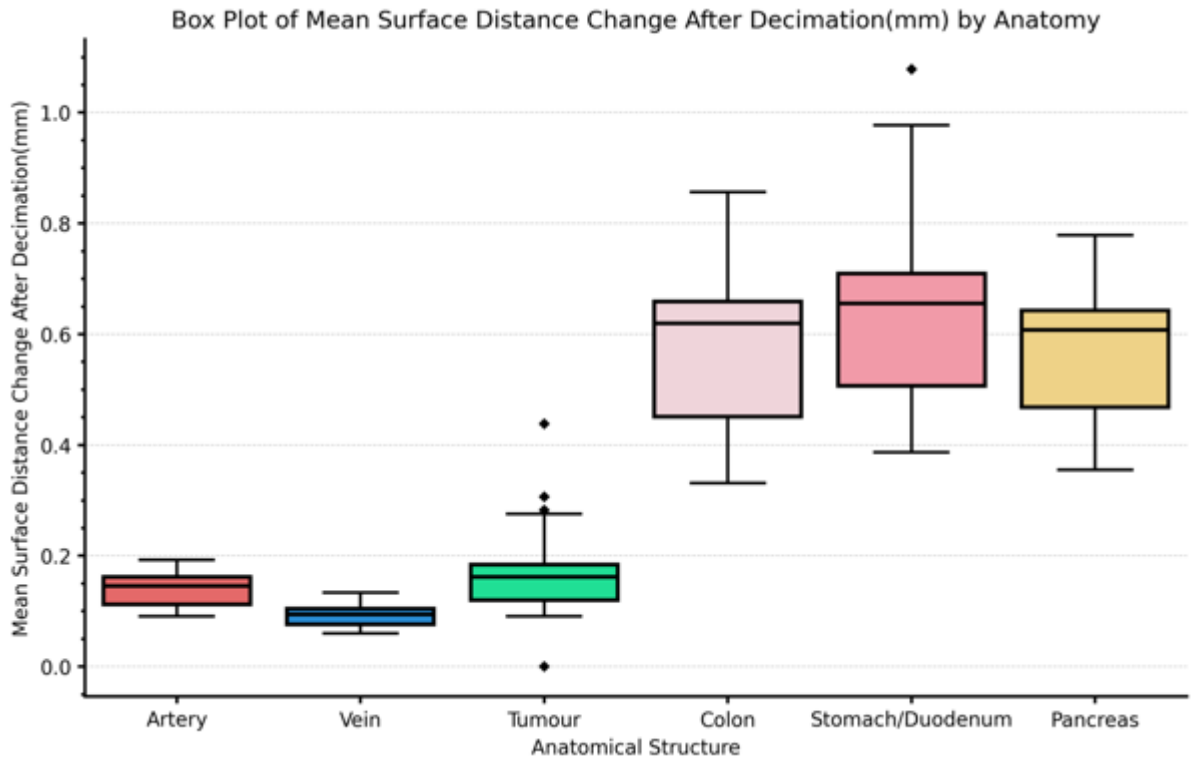


Figure 2-20 Box plot displaying the mean surface distance change (mm) after decimation and smoothing for different anatomical structures, including arteries, veins, tumour, colon, stomach/duodenum, and pancreas.

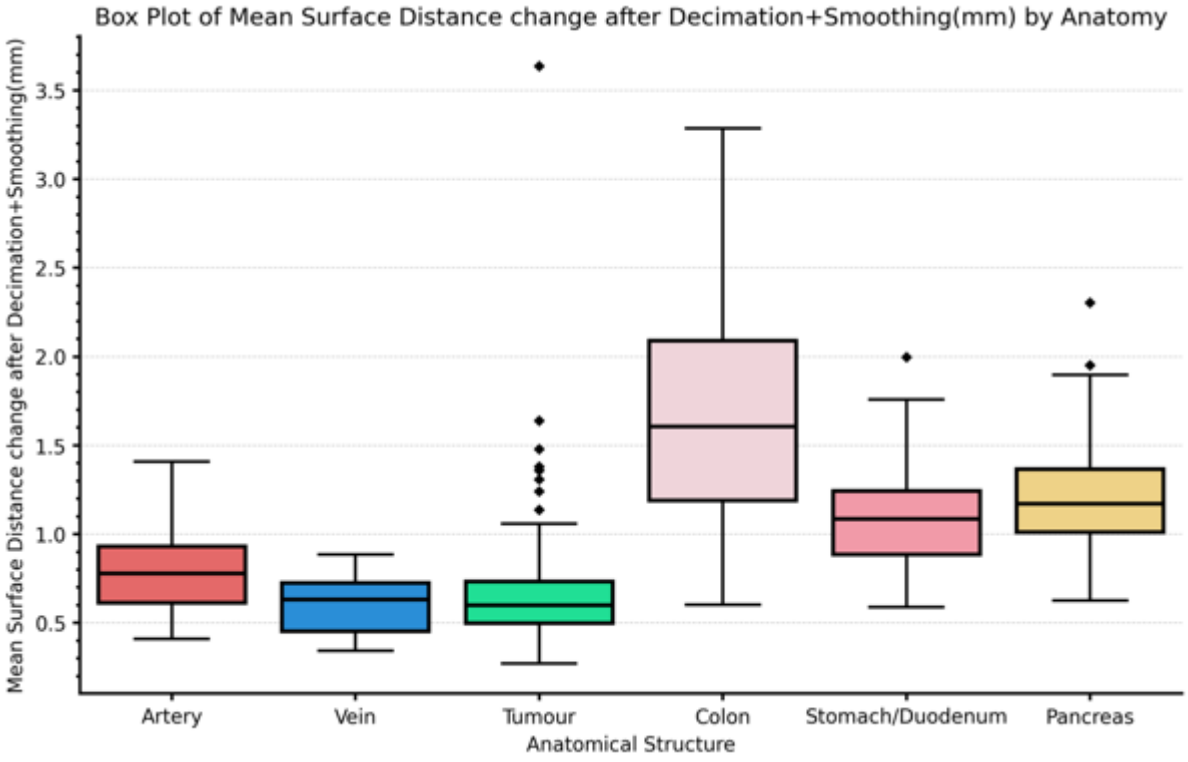


Figure 2-21 Box plot illustrating the mean edge length ratio (mm) across different anatomical structures, including arteries, veins, tumour, colon, stomach/duodenum, and pancreas. Each box represents the interquartile range, with the median indicated by a horizontal line within the box. Whiskers extend to the minimum and maximum values within 1.5 times the interquartile range, providing an overview of the mesh quality for each anatomical structure. Lower mean edge length ratios are observed for arteries, veins, and tumours, indicating a more uniform triangulation in these structures, while the colon, stomach/duodenum, and pancreas exhibit higher mean edge length ratios, reflecting greater variability in mesh element quality.

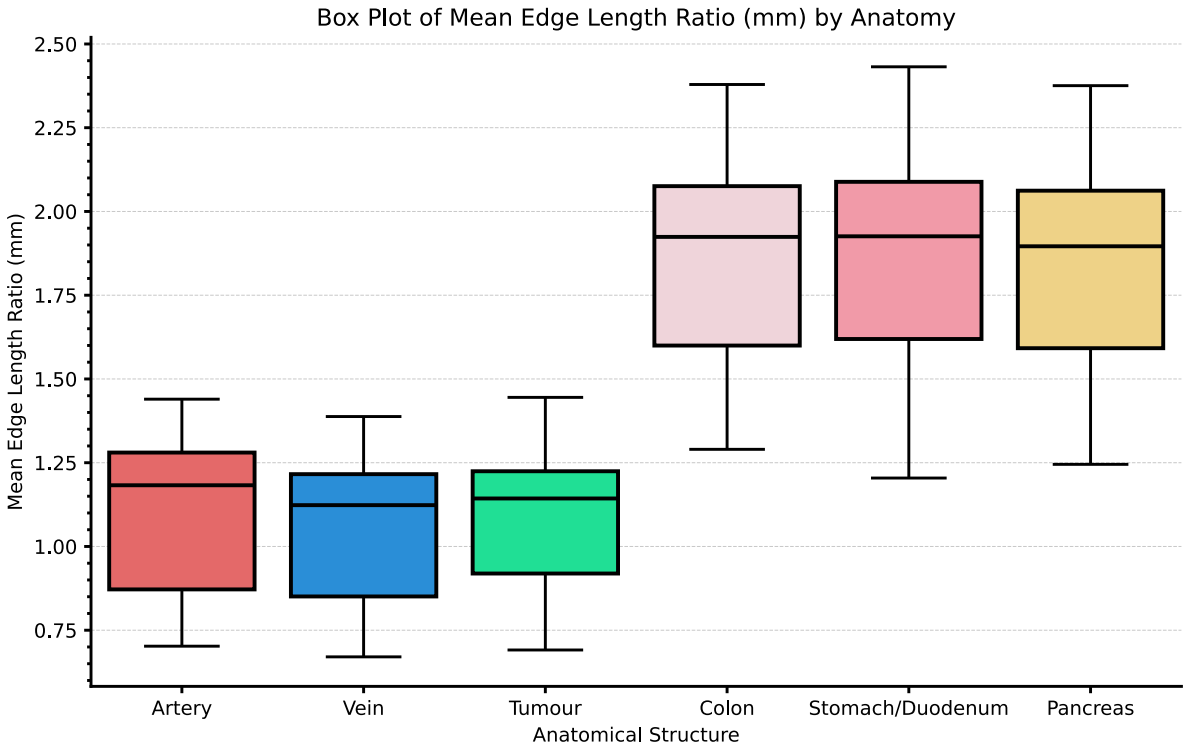
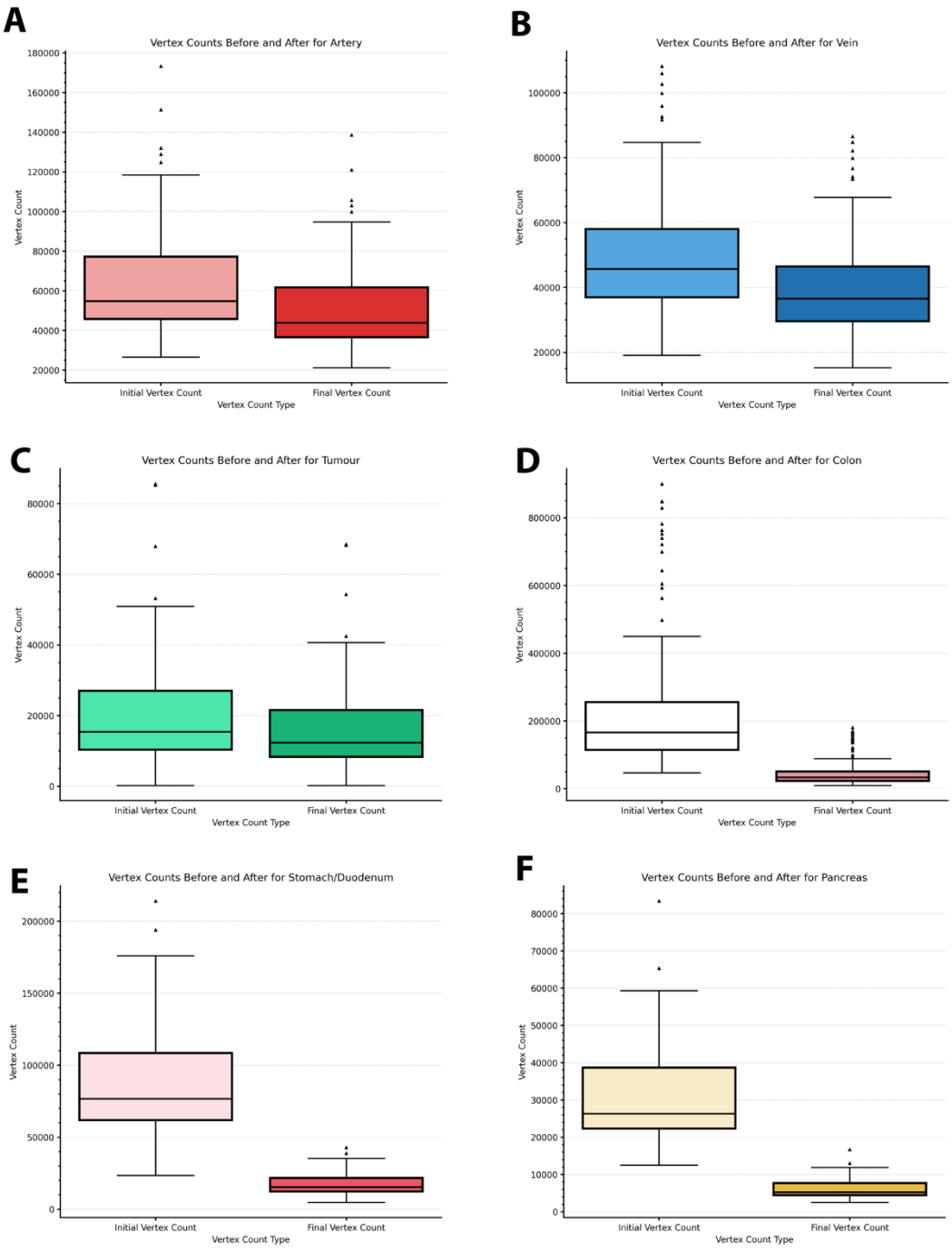


Figure 2-22 Box plots for each mesh component demonstrating vertices counts before and after decimation



2.11 Discussion

This chapter presents a systematic approach to developing patient-specific 3D visualisation tools for complex colorectal cancer surgery, addressing two distinct technical challenges: high-precision vascular modelling for CME surgical planning, and anatomically accurate yet aesthetically optimised representations for patient education in pelvic exenteration. The technical solutions implemented, particularly the differential mesh processing pipeline and physically based rendering approach, establish a foundation for integrating 3D visualisation into clinical practice.

For CME models, we present an accurate automated model workflow with a visualisation platform that meets the core surgical and technical requirements outlined in our needs analysis. The quantitative validation of mesh processing parameters across 111 anatomical models provides robust evidence for the effectiveness of our differential processing approach. The achievement of sub-millimetre accuracy in vascular structures (mean surface distance change of 0.64 ± 0.17 mm for arteries and 0.87 ± 0.24 mm for veins) while maintaining acceptable deviation in larger structures demonstrates our implementation successfully balances precision with computational efficiency. This quantitative approach to optimisation parameters represents a methodological advancement in surgical visualisation, providing objective criteria for assessing model quality.

2.11.1 Limitations and Challenges

A central limitation lies in the reliance on manual segmentation. While this method offers the anatomical precision necessary for both surgical planning and model development, it is highly time-consuming and subject to variability between different operators. The lack of scalability represents a significant barrier to widespread clinical adoption. While automated segmentation of colorectal cancer imaging is beyond this chapter's scope, we will consider it in detail in the overall thesis discussion, emphasising artificial intelligence's role (specifically artificial neural networks).

Another critical point is the divergent workflows developed for CME and pelvic exenteration models. These different approaches, necessitated by distinct clinical objectives, reveal the underlying tension between geometric precision and visual comprehensibility. The CME workflow prioritised anatomical fidelity and automation, employing a utilitarian approach to

model appearance, whereas the pelvic exenteration models focused on achieving aesthetically optimised outputs for patient education. Bridging these workflows to create a unified model capable of both surgical planning and educational use would be ideal for maximising the value proposition of 3D models in surgery.

2.11.2 Web Platform Implementation and Interface Design

The adoption of the GLB format has facilitated efficient compression and delivery of 3D anatomical models, supporting interactive visualisation requirements within a web-based platform. However, several critical limitations persist:

1. The current platform lacks optimisation for mobile and tablet devices, potentially limiting its accessibility in clinical settings

2. The absence of formal performance benchmarking across different hardware configurations and network conditions

3. Unknown impact of variable network bandwidth, latency, and computational capacity of clinical workstations

A notable omission is the lack of formal user interface evaluation. While basic functionality was implemented successfully, the absence of structured assessment of interface design principles and user experience metrics represents a significant limitation. Future work should incorporate formal UI/UX evaluation methodologies, including:

1. Systematic usability testing
2. Task completion analysis
3. User satisfaction metrics
4. Cognitive walkthrough evaluations
5. Accessibility assessment

2.11.3 Integration Challenges and Future Directions

This work must be explicitly considered as a proof of principle, requiring significant further development before clinical implementation. This includes addressing data protection concerns, ensuring compliance with relevant regulations (e.g., GDPR, HIPAA), and

integrating the visualisation platform with existing clinical systems such as PACS (Picture Archiving and Communication System).

Future development should focus on several key areas:

1. Implementation of automated segmentation techniques
2. Systematic performance benchmarking
3. Integration with clinical systems
4. Development of structured validation protocols for patient education visualisations
5. Unified workflow development bridging surgical planning and patient education applications

2.12 Conclusion

The methodologies described establish a viable, though still evolving, foundation for creating specialised surgical visualisation tools. The quantitative validation of mesh optimisation parameters and systematic evaluation of visualisation techniques provide a robust framework for future refinements. However, the reliance on manual methods, workflow divergence, and lack of formal UI evaluation underscore important limitations requiring attention for broader clinical integration.

This work demonstrates technical feasibility while highlighting areas requiring further development for clinical implementation. The subsequent chapters, evaluating clinical utility in both surgical planning and patient education, will build upon this technical foundation while acknowledging its current limitations.

3 Systematic review of the use and evaluation of 3D patient-specific model for pre-operative surgical planning

3.1 Background

3D visualisation has been highlighted as one of the key technological innovations likely to impact surgical practice in the next decade by the Royal College of Surgeons (1). Pre-operative planning is one of the principal applications suggested for 3D visualisation in surgery.

Preoperative planning is a crucial aspect of safe, effective surgery. A complete understanding of a patient's unique anatomy enables the surgeon to plan an operative strategy and anticipate potential difficulties. Pre-operative planning can be defined as any activity aimed at understanding a patient's anatomy or pathology to inform decision-making and/or determine an appropriate surgical strategy.

Current decision-making is based on the review of imaging modalities such as CT and MRI in collaboration with radiology. However, extracting the relevant 3D anatomical relationships from 2D images to apply them intra-operatively can be difficult. Intuitively, 3D reconstructions appear to have certain advantages over traditional 2D images. Patient-specific in silico models, derived from digital imaging and communication in medicine (DICOM) data, have the potential to improve understanding of gross pathology and complex structural relations. Furthermore, the advances in additive manufacturing have enabled 3D reconstructions of

patient anatomy to be printed as physical objects allowing patient specific pre-operative rehearsal of procedures (208).

3.2 Rationale.

Despite the initial optimism of early adopters, the effectiveness of 3D models in surgical planning has yet to be fully demonstrated. Ensuring 3D modelling techniques have validated clinical benefits will be essential if they are to be routinely incorporated into surgical workflows. This is particularly pertinent when considering the necessary time and resources needed to generate these images and prints. This systematic review seeks to ascertain how 3D models have been used in surgical planning, what methodologies and outcomes have been used to judge efficacy and evaluate the current level of evidence available.

3.3 Objective

We sought to determine the following through a systematic review of the literature.

1. How have 3D patient specific models been used in surgical planning?
2. What specific reconstruction/printing techniques were employed
3. What outcome measures and study designs were used to judge effectiveness
4. What is the current level of evidence for 3D planning against current standard practice?

3.4 Methods

3.4.1 Protocol

Methods of the analysis and inclusion criteria were stipulated in advance in accordance to PRISMA guidelines.

3.4.2 Eligibility criteria

Studies evaluating the use of 3D virtual or printed models for pre-operative planning in all surgical specialties between 2008 – 2020 were identified systematically. We excluded animal, cadaveric, and non-English language- studies.

We excluded irrelevant articles, letters, editorials, duplicates, abstract only papers, reviews and metanalyses or where the full text was not available. Where authors had published the same patient cohort twice as separate papers (reporting identical outcome measures) the most recent publication was included and older study excluded.

We utilised the PICOS framework to specify study eligibility characteristics.

3.4.2.1 Population

a) Participants of any age receiving surgical intervention in which a 3D model (virtual and/or printed) was used for pre-operative planning were included.

b) Dental and interventional radiology patients were excluded.

3.4.2.2 Intervention

a) We considered studies which evaluated the use of 3D virtual or printed models, reconstructed from patient imaging data for pre-operative planning.

b) Pre-operative planning was defined as any activity aimed at understanding a patient's anatomy, pathology in order to determine an appropriate clinical decision or operative strategy. Studies in which 3D reconstructions were utilised for planning activities pre-operatively and subsequently used for intra-operative navigation were also included.

c) Studies evaluating bioprinting ,3D printed custom implants, 3D ultrasound or pseudo-3D reconstruction techniques such as Maximum Intensity Projection (MIP) as the primary intervention were excluded.

3.4.2.3 Comparators

a) Comparators were broadly defined as 'standard practice'(typically review of radiographic/cross sectional imaging) for a given surgical intervention i.e. planned and performed without the aid of 3D modelling.

3.4.2.4 Outcomes

a) The given aim of this study was to systematically evaluate the outcome measures employed to evaluate 3D planning interventions. All outcome measures employed were considered eligible for inclusion.

b) We excluded studies without any defined outcome measure.

3.4.2.5 Study Designs

a) All comparative study designs were eligible for inclusion whether they were randomised or non-randomised trials, prospective/ retrospective cohort studies or cross-over studies.

b) Case reports, case series lacking any comparator, technical papers and feasibility studies (defined in this context as studies focussing on reconstruction methodology rather than clinical application) were excluded.

3.4.3 Information sources

Studies were identified by searching electronic databases and scanning reference lists of articles. Literature searches were undertaken using the OVID SP versions of the National Library of Medicine's MEDLINE database (1966-Present) and adapted for EMBASE. The last search was run 21st March 2021. In addition, we manually searched the reference lists of relevant review articles to identify any relevant studies omitted from the electronic search.

We quality controlled our review strategy by ensuring 5 studies indicative of our inclusion criteria, were included in the resulting list of abstracts.

3.4.4 Search Strategy

The search strategy was designed in accordance with the Preferred Reporting Items for Systematic reviews and Meta-Analyses (PRISMA) statement and was implemented by JF.

The specific strategy is listed below.

1 ((Three dimensional or Three-dimensional or 3d or 3 d) adj3 (print* or rapid prototype* or additive manufactur* or reconstruct* or imag* or render or virtual model*)).mp.

2 (Surger* or surgical or Operat*).mp.

3 1 and 2 (61503)

4 Pre-operative.mp.

5 Preoperative.mp.

6 Plan*.mp.

7 4 or 5 or 6

8 3 and 7

9 limit 8 to yr="2008 -2020"

10 limit 9 to yr="2013 -2020"

11 limit 10 to "review articles"

12 limit 11 to animal studies

13 11 or 12

14 10 not 13

15 remove duplicates from 14

3.4.5 Study selection process.

We used the online systematic review management platform Covidence to screen abstracts and full texts for data extraction.

Two independent reviewers screened each abstract for full text review to determine inclusion. Disagreements between authors were resolved by discussion and consensus. If consensus could not be reached the decision to include/exclude was made by the senior author (DM). Following abstract screening the full texts were reviewed by two independent reviewers for inclusion in the final review. Disagreements between authors were handled as per the process outlined for abstract screening.

3.4.6 Data collection process

We developed a data extractions sheet and pilot tested on five randomly selected studies which was subsequently refined based on user feedback. One review author extracted the data items detailed below and a second author checked the extracted data. Discrepancies were resolved by consensus discussion with the senior author (DM) making the final decision if no agreement could be met.

The key areas for data collection related to the technical aspects of 3D reconstruction; descriptions of how models were used to plan the given surgical procedure; the study design and specific the outcome measures that were employed to assess model efficacy.

3.4.7 Data items

a) technical aspects of 3D model production

Papers were reviewed for the technical aspects of 3D reconstruction. For virtual model reconstruction we extracted; the imaging modality and sequence 3D reconstructed; the rendering technique (volume versus surface rendered); the segmentation and computer graphics software; method of segmentation; who produced the model; time taken and cost; verification processes and the user interface used.

For research involving 3D printed models we recorded the specific printing technique, model of printer, and material used along with the printing time and cost time per model and whether 3D prints were sterilised for intra-operative use.

b) Specific details of model use in pre-operative planning

Details of how 3D models were utilised for planning were recorded including details of the end user (surgeon/ radiologist, level of training etc.). Planning activities were classified a priori as follows:

visualisation in which the model is primarily used to improve the anatomical understanding to determine the operative strategy/improve performance; process simulation- in which virtual/printed models were used to recreate/rehearse the entire operation or steps of the procedure; outcome simulation where models were used to predict operative outcomes (e.g. aesthetic appearance, organ function) and computer assisted planning. Computer assisted planning encompasses a variable range of activities for resection or reconstructive surgery characterised by more complex user interaction with the model. Details relating to potential use in theatre to aid intra-operative navigation were recorded.

c) Study design

We extracted details relating the characteristics of the study design including number of participants in intervention and comparator groups; selection of participants (inclusion/exclusion criteria); the specific comparator used; randomisation method or where relevant how participants were allocated to groups in non-randomised study designs; details of any power calculations to determine sample size; whether data was collected prospectively or retrospectively. The number and grade of the participating surgeons, specific surgical procedure(s) and operative indication/ underlying patient pathology were recorded.

d) Outcome measures

Outcome reporting was extracted for each study. Our aim was to ascertain the measures employed to judge the effectiveness of 3D planning including both qualitative and quantitative outcomes. Expected outcome measures included:

- Qualitative subjective measures (e.g. Likert-scale questionnaires)
- Impact on planned procedure e.g. changes to operative strategy
- Anatomical accuracy of the model
- Anatomical understanding (both subjective and quantitative)
- Diagnostic accuracy and inter/intra observer reliability.
- Accuracy of surgical plan
- Surgical performance metrics- operative time (total/procedure specific step), blood loss, intra-operative adverse events
- Clinical outcomes- quality of cancer resection (R0 rates, recurrence, survival), post-op complication rates (general and procedure specific), functional and aesthetic outcomes, length of stay.
- Time/Cost

We recorded where relevant how outcomes were measured and recorded, the individual making the measurement and any descriptor of the measurement methodology, and the time point measurements were taken with respect to the operation.

3.4.8 Data synthesis

For all studies, we have produced tables of summary statistics grouped by specialty.

We conducted a meta-analysis of those studies that met the following criteria:

- All the outcomes were comparable and pooled meaningfully.
- All the interventions and comparators are the same or similar enough to be meaningfully combined.
- Necessary data is available for the included studies (means and standard deviations). For studies reporting medians, range and/or inter-quartile range we calculated the means and standard deviations from the available data using the method proposed by Wan et al (209).

It has been proposed that two studies can be utilised for metanalysis.

We excluded any studies deemed to be critically at risk of bias and utilised a random effects model assuming different studies are estimating different, yet related intervention effects.

We conducted the metanalysis where heterogeneity was low ($I^2 < 50\%$).

3.4.9 Risk of Bias in Individual Studies

Two independent reviewers independently performed bias assessments using two validated measures of bias. Randomised control trials were assessed using version 2 of the Cochrane risk of bias for randomised trials (RoB 2) (210). Bias domains consist of bias arising from; randomisation; deviations from the intended intervention; missing data; measurement of the outcome; selection of the reported result. Each domain is assessed as at low risk, some concerns or high risk of bias. An overall risk of bias was made for each study to correspond to the worst risk of bias in any of the domains. If multiple domains were considered at risk it may be judged as at high risk of bias.

Bias in non-randomised studies was assessed using the Risk of Bias In Non-Randomised Studies -of Interventions (ROBINS-I) (211). The tool contains seven domains of bias- bias due to; confounding; selection of participants into the study; classification of interventions; deviations from the intended intervention; missing data; measurement of outcomes; selection of reported results. Each domain is rated to be at low, moderate, serious, or critical risk of bias with an overall judgement made corresponding with the worst risk in any domain.

Both assessment methods have online data collection templates that were used to collect data. Discrepancies between the two assessors were resolved by discussion and consensus with the senior author (DM) providing the final decision if an agreement could not be made.

3.4.10 Effect measures.

One of the aims of this systematic review was to identify the outcome measures used to assess the utility of 3D planning across all surgical subspecialities for a diverse range of application. We anticipated a wide range of primary outcome measures would be employed. Based on our knowledge of the existing literature we anticipated reductions in average operative times and blood loss would commonly be employed.

3.4.11 Data analysis

All data was analysed and visualisations produced using custom Python language scripts (version 3.8.7, Python Software Language) using the Anaconda distribution package and

online Jupyter Notebooks (a server-client application that allows editing and running executable code for data analysis via a web browser). We utilised the following Python libraries; NumPy (v1.19.2) (195), Pandas (1.1.3) (212), Matplotlib (v3.3.2) (213), Seaborn (v0.11.0) and the pythonmeta (v1.4.0) (214) library to perform the meta-analysis.

3.5 Results

3.5.1 Study selection.

A total of 126 studies were identified for inclusion in the review. The search of MEDLINE and EMBASE provided 8620 citations. After adjusting for duplicates 7438 studies remained. No additional studies were added because of manually reviewing review articles. We excluded 6318 studies based on review of the abstract as irrelevant or not meeting our inclusion criteria. The full text of the remaining 1120 studies were examined in further detail. 994 studies were excluded for not meeting the inclusion criteria as described. The PRISMA flow diagram breaks down reasons for exclusion (see figure 3-1). Most studies were excluded owing to being either case studies or lacking any comparator (n=260).

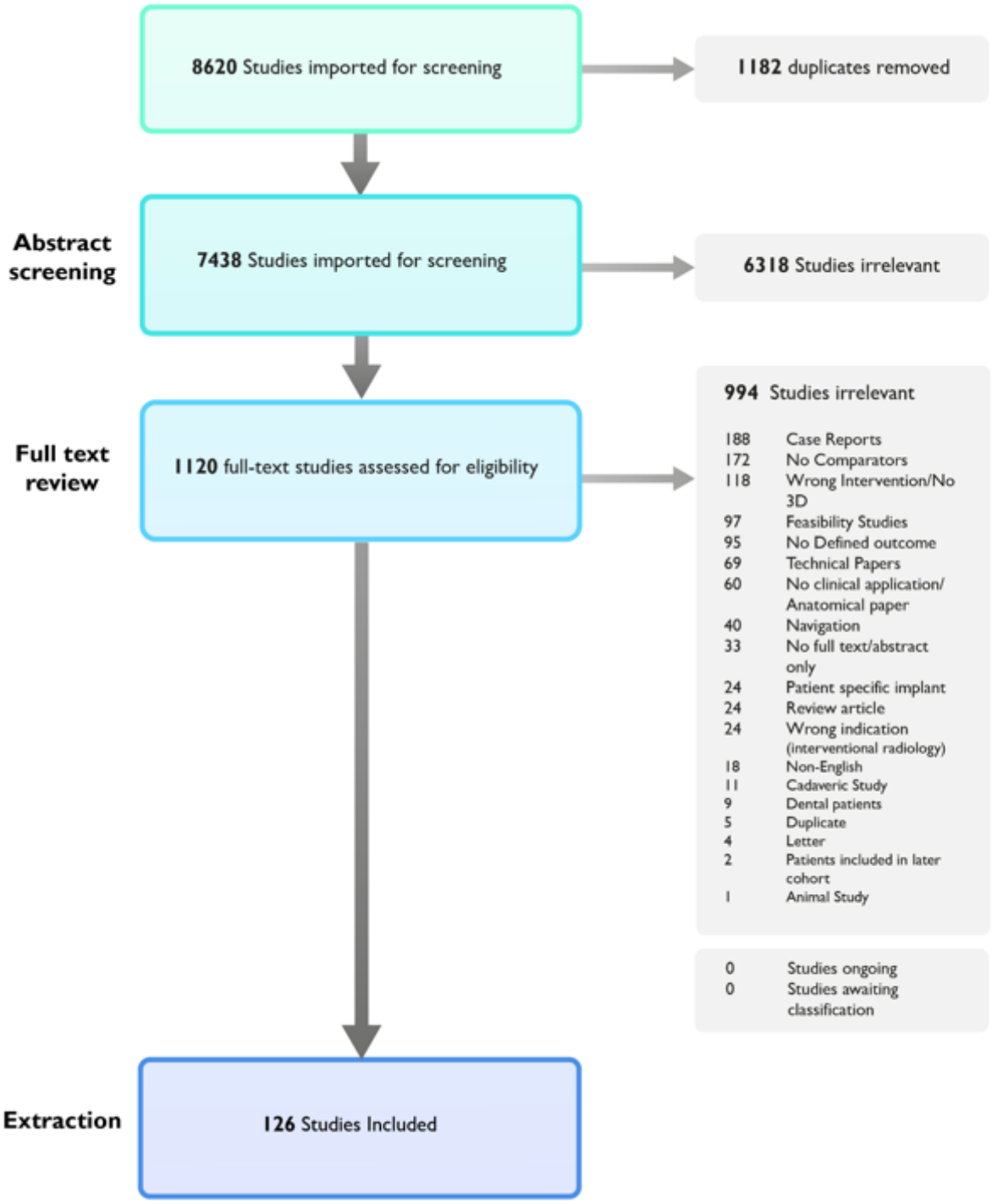


Figure 3-1 Prisma Diagram

Figure 3-2: Number of 3D planning studies published per year from 2008 -2020

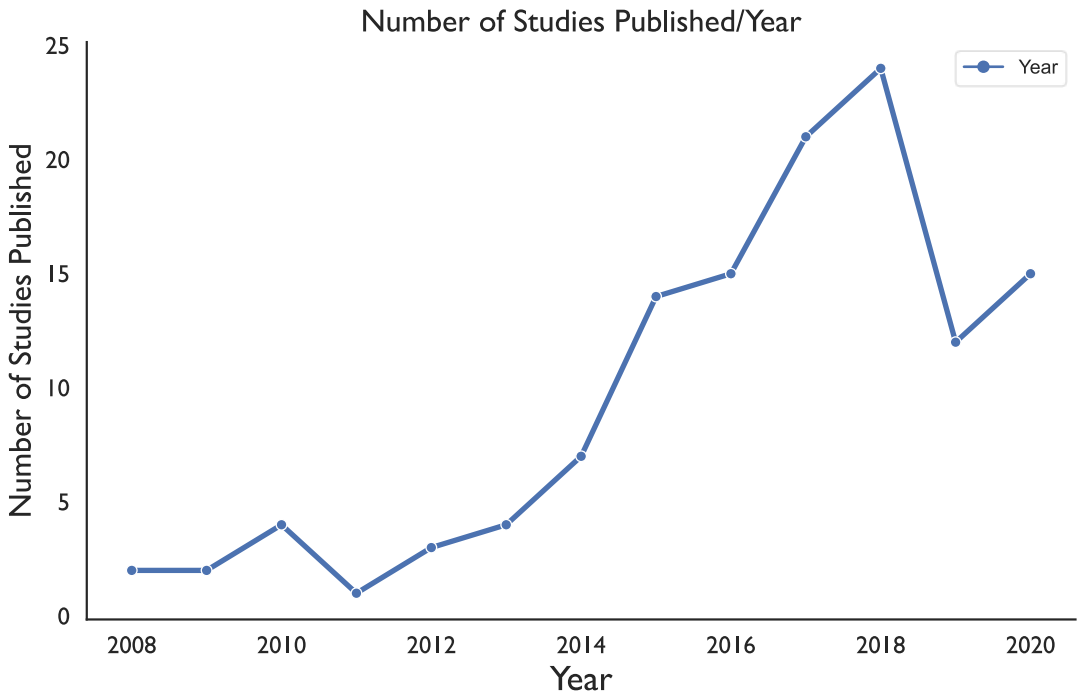


Figure 3-3 Number of 3D planning studies published by specialty between 2008-2020

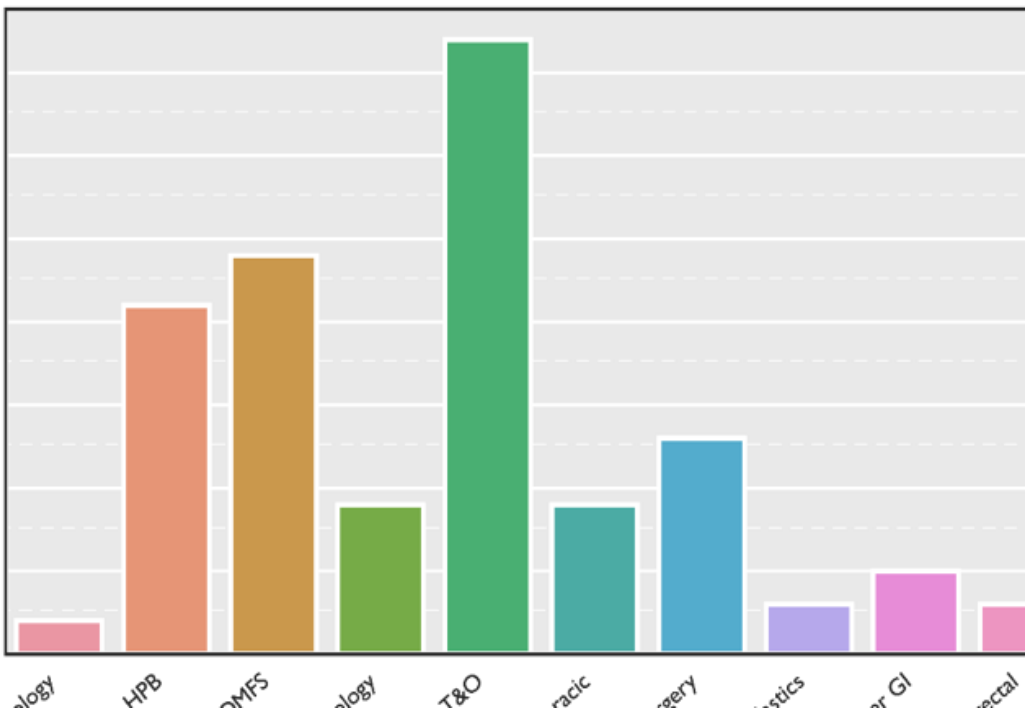
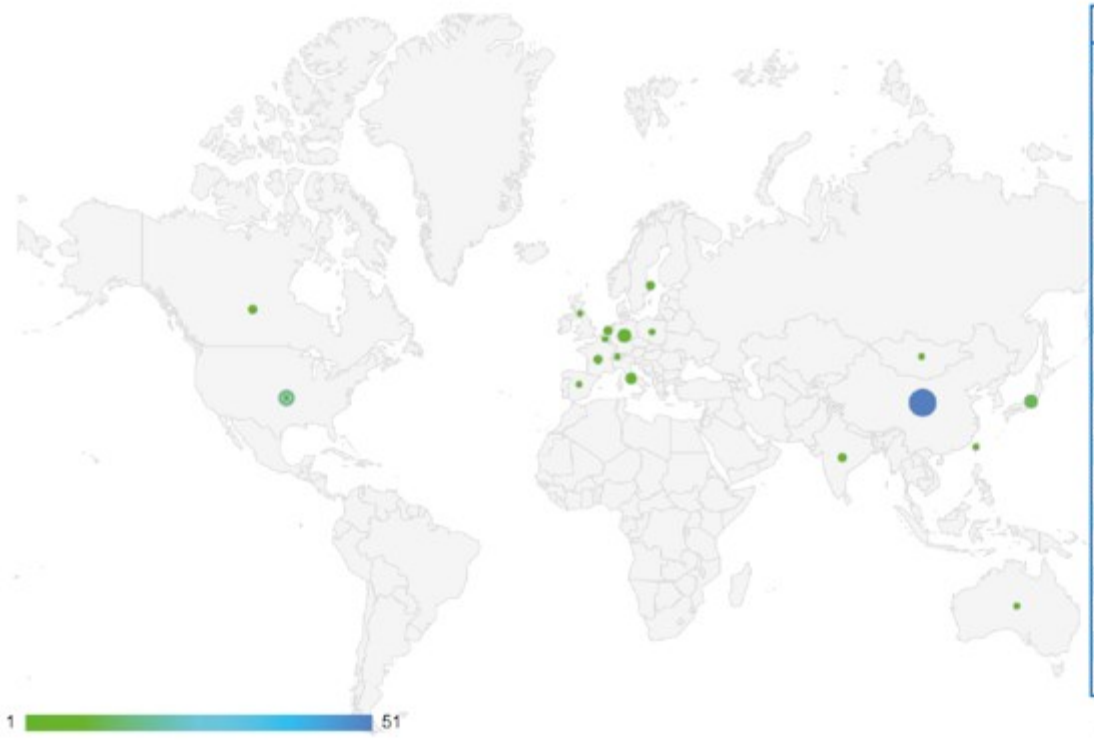


Figure 3-4 Number of 3D planning studies published by country



Country	n
China	51
USA	18
Japan	12
Germany	9
Italy	6
France	4
India	4
Netherlands	3
Sweden	3
Canada	3
Poland	2
Spain	2
Taiwan	2
Mongolia	1
Belgium	1
Australia	1
International	1
Belgium	1
UK	1
Switzerland	1

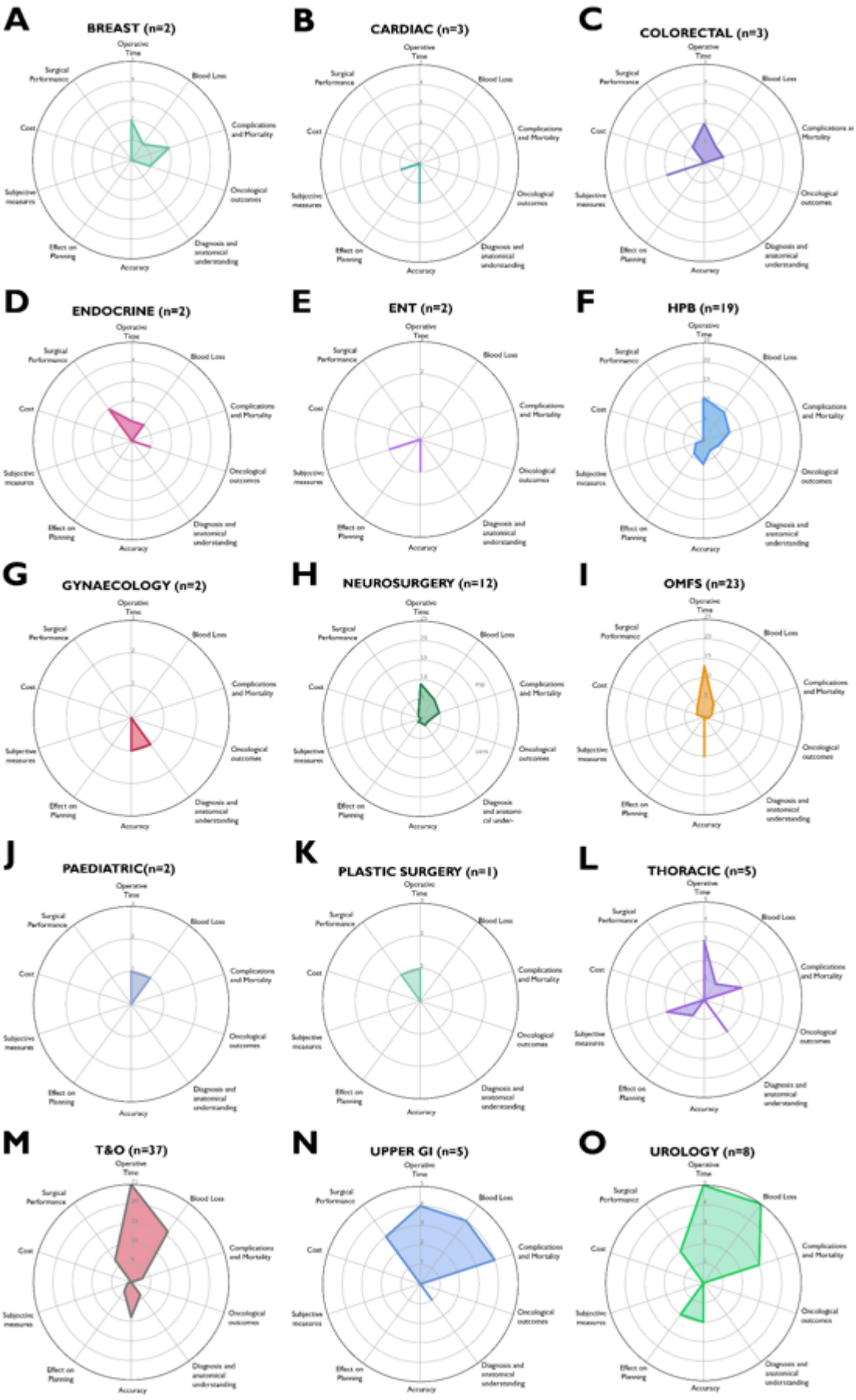


Figure 3-5 A-0 Radar plots summarising outcome measures used in all studies by surgical specialty

Table 3-1 Summary of procedures by specialty in which 3D planning was used

Specialty	Procedure	n
Breast	Breast reconstruction	2
Cardiac	Congential cardiac disease procedure	3
Colorectal	Colectomy	1
	Colorectal resection	1
	Lat. pelvic lymph node dissection	1
ENT	Otoscopy	1
	Skull base surgery	1
Gynaecology	Endometriosis	1
	Myomectomy	1
HPB	Hepatectomy	15
	Pancreaticoduodenectomy	4
	Cholecystectomy	1
	Liver transplant	1
Neurosurgery	Cervical lateral screw fixation	1
	Brain tumour resection	3
	Endonasal transphenoid pituitary resection	1
	Lamiotomy &l spinal tumour resection	1
	Lumbar discectomy	1
	Microsurgical aneurysm clipping	1
	Pediclle screw placement	1
	Posterior lumbar fusion	1
	Scoliosis Corrective surgery	1
	Trigeminal microvascular decompression	1
	Skull base surgery	1
OMFS	Mandibular resection and reconstruction	14
	Maxillary osteotomy/reconstruction	7
	Bone contouring	1
	Fronto supraorbital bar advancement	1
Plastics	Sural neurovascular island flap	1

Specialty	Procedure	n
T&O	Acetabular ORIF	4
	Pelvis MI cannulated screw	2
	Neck of femur ORIF	1
	Tibial ORIF	7
	Tibia Ilizarov frame	1
	Ankle ORIF	1
	Calcaneal ORIF	1
	Tibia, calcaneus, tibial plateau ORIF	1
	Humerus ORIF	2
	Elbow ORIF	1
	Distal radius ORIF	2
	Lumbar spine surgery	1
	Total shoulder arthroplasty	3
	Total knee replacement	2
	Total hip replacement	2
	Subtalar arthrodesis	1
	Proximal femoral osteotomy	1
	Acromioplasty	1
	Femur osteoplasty	1
	Radius Corrective osteotomy	1
	Coracoid osteotomy	1
Thoracic	Chest wall reconstruction (Nuss)	2
	VATS segmentectomy/\nlobectomy	2
	Surgical stabilization of rib fractures	2
Upper GI	Gastrectomy	4
	Oesophagectomy	1
Urology	Partial Nephrectomy	5
	PCNL	2
	Radical Nephrectomy	1
	Laparoscopic adrenalectomy	1

Table 3-2 Summary of study designs

Study design	Allocation to groups	n
Cohort study (unable to determine if pro/retrospective)	All patients assessed by each method	**1**
Comparative cohort (unable to determine if pro/retrospective)	Unclear method of group allocation	**5**
Prospective cohort	All patients assessed by 3D and comparator	**24**
Prospective cohort with retrospective controls	Time period	**9**
	Matched by patient demographics	**1**
Prospective comparative cohort	Unclear method of group allocation	**8**
	Patient choice	**3**
	Matched	**2**
	Time period	**3**
Retrospective cohort	All patients assessed by each method	**6**
	Multiple assessors of each case using 2D/3D	**1**
	Unclear	**1**
Retrospective comparative cohort	Time period	**14**
	Unclear	**15**
	Matched	**2**
	Emergency case precluding 3D printing	**1**
	No CT available for reconstruction	**1**
RCT	Simple	**27**
	Block	**1**

3.5.2 General Summary

We observe a general trend of an increasing number of 3D planning studies published per year with a peak number in 2018 (n= 24) (Figure 3-2). Trauma and Orthopaedics published the highest number of studies in the period (n=37) followed by oral maxillofacial surgery (n=23) and hepatobiliary surgery (n=19) (Figure 3-3). China, the USA and Japan account for the majority of 3D planning publications, accounting for 68% of published research (Figure 3-4).

3.5.3 Study Characteristics

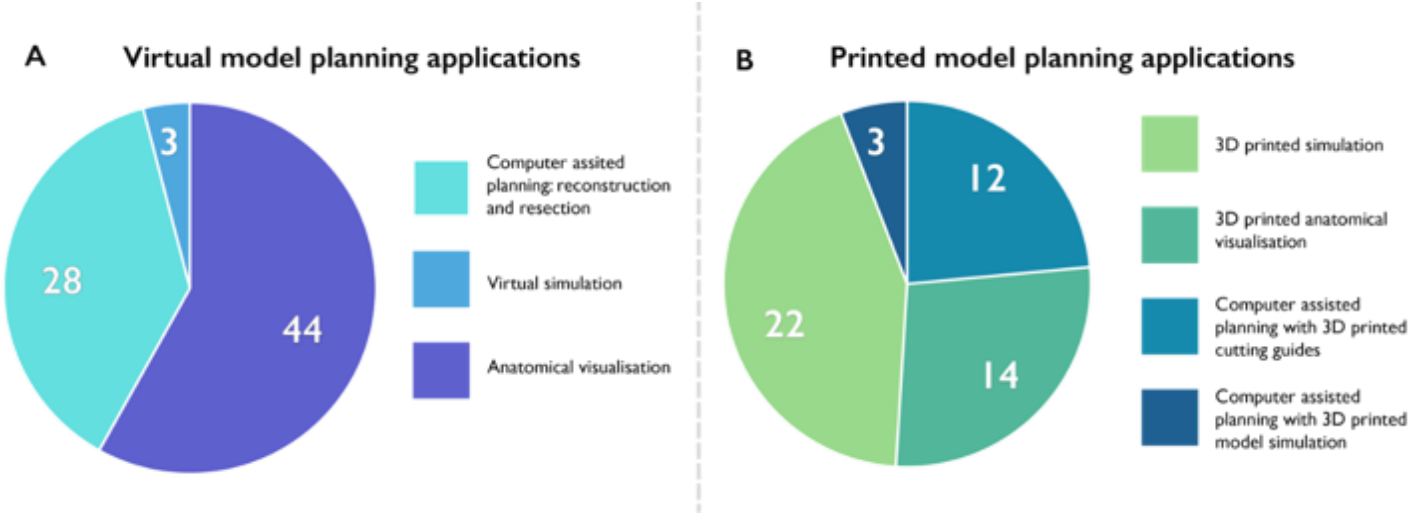
28/126 studies were randomised control trials. The remainder employed non-randomised cohort designs. 50/98 were prospective studies. In 24/50 prospective studies all the included patients were evaluated by both standard and 3D planning methods. Allocation to intervention and control groups were most frequently determined by the period patients were treated. 41 studies were retrospective. Intervention and comparator groups were most determined by time periods. In 7 studies patients both standard and 3D planning techniques were used on all patients within the cohort. In 6/98 of the non-randomised studies, we could not determine whether data was collected pro- or retrospectively (Table 3-2).

Table 3-3 Segmentation software utilised in studies

Software	n	Software	n	Software	n
Materialise Mimics	28	EOS	2	M3D MedGraphics	1
Not stated	10	SuperImage Ortho edition	1	Zed-Trauma	1
Workstation/ PACS	8	Leonardo InSpace	1	Maxilim	1
3D Slicer	7	Dolphin 3D	1	Myrian 3 dimensional volumetry	1
PACS System	6	HipPlan (Symbiosis)	1	FreeForm Modeling System	1
MI-3DVS	5	Rhino3D	1	Imascap	1
ITK-SNAP	4	iPlan CMF	1	3D Plus Body Visible System	1
Osirix X	4	Super Image Orthopaedics	1	Dextroscope	1
Synapse Vincent	3	Amira 4.1	1	MEDICAL Imaging Three Divisional Visulisation System	1
Ziostation	2	Multimodality workplace software	1	M3DICS	1
Materialise pro plan	3	Sensation64	1	3D-MIRGS	1
Hisense CAS	2	iNtellect Cranial Navigation	1	MITK ReLiver	1
IQQA-Liver	2	Visible Patient	1	HepaVision	1
Custom	2				

Most authors utilised surface rendering for 3D virtual reconstruction/ printing (70/126). 38 studies employed volumetric rendering techniques, while in the remainder the rendering method was not stated or could not be identified. A wide variety of segmentation software packages were employed as outlined in table 3-4. In most studies included it was not stated who performed the segmentation or produced the model (92/126, 73%). Surgeons produced the model in 16 studies, radiologists in 12, external companies in 5 and an in-house engineer in 1 study. Similarly, very few papers documented the time to produce the model, with only 11/126 providing any information on the time to reconstruct.

Figure 3-6 A-B Breakdown of specific planning applications for virtual and printed models.



In 75 studies virtual models were used for pre-operative planning. Models were primarily used for basic anatomical visualisation planning applications (44/77) (Figure 3-6).

In 51 studies 3D printing was used. A wide range of printing methods and specific printing models and materials were employed (table 3-5). In 32/51 studies the printing time was not documented. Documented printing/model production times ranged between 5 to 100 hours (215), (216). The cost per model was not stated in 37/51 studies. Costs ranged between as low as £1.40 and as high as £2,600 with material extrusion printing associated with the lowest costs per model where data was provided.

3D prints were sterilised and used intraoperatively in 18/51 studies. Figure 3-6 summarises the specific use of 3D printed models. In 14/51 studies models were used for pure anatomical visualisation, in 22/51 studies 3D prints were used for patient specific simulation/rehearsal-typically fracture fixation/pre-bending osteosyntheses plates in T&O, OMFS and Thoracic Surgery (accounting for 21/22 3D printed simulation applications).

Table 3-4 Summary of 3D methods, printer models and print material used for planning

Printing Method	3D Printer Model	n	Print Material	n
Color jet (CJ)	3D systems projet 660	1	Not stated	1
Material Jet (MJ)	connex 500 stratsys	1	Not stated	1
Material extrusion (FDM & FFF)	Flashforge	2	PLA	12
	Ultimaker 2	2	ABS	7
	3D ORTHO Waston Med	4	Not stated	5
	Axiom Dual Extruder	1		
	BQ witbox	1		
	Dimension BST 1200	1		
	HP Design Jet 3D	1		
	JGAurora	1		
	Lulzbot	1		
	Maker Gear M2 desktop	1		
	Mankati Fullscale XT plus	1		
	Not stated	1		
	SST1200es	1		
	UP-BOX 3D printer	3		
	WASP delta turbo	1		
	Songsun N2	1		
	MakerBot Replicator 2	1		
Polyjet (PJ)	Prismlab Rapid400	1	Photopolymer resin	3
	Polyjet Connex 350	1		
	Stratasys J750TM	1		
Stereolithography (SLA)	ProJet 660	3	Photopolymer resin	8
	Not stated	5		
Selective laser scintering (SLS)	Spectrum Z510	1	Nylon	2
	Zprinter 650	1	Polystyrene	2
	EOSINT P380	1		
	Unknown	1		
Not stated	Not stated	10	Not stated	10

Figure 3-7 radar plot summarising outcome measures used to evaluate 3D planning. Time and blood loss where the most common outcome measures employed in the included studies.

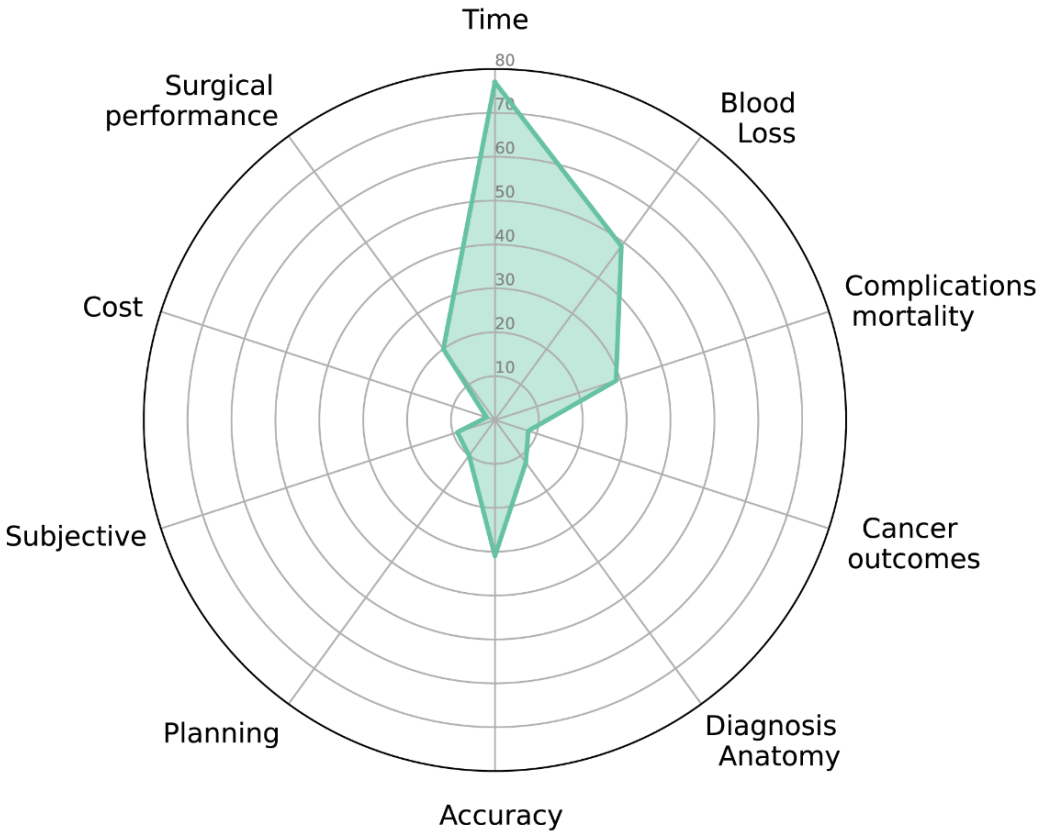
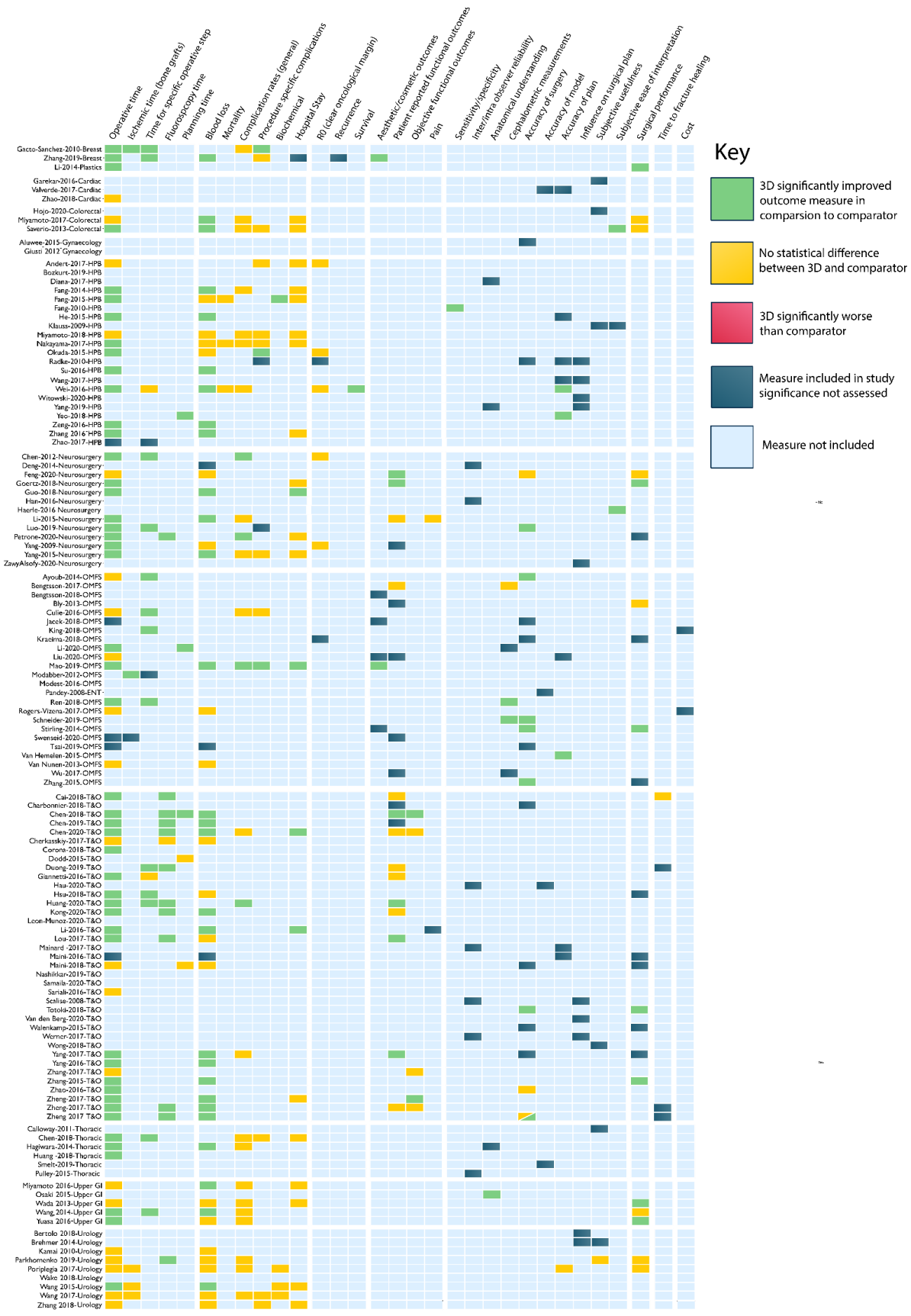


Figure 3-8 Summary of outcome measures used by each study.



3.5.4 Colorectal Surgery

Three studies in Colorectal surgery utilised virtual models to assist planning in Colorectal cancer resections (175) (217) (178). The characteristics of each study are summarised in table 3-6. Outcome measures employed in each study are summarised in figure 3-5C and figure 3-8.

3.5.4.1 Outcome measures

Two studies utilised operative time and blood loss as their main objective outcome measures. Saverino et al conducted a randomised study (3D n= 59 vs non 3D n=62) and found the use of 3D volume rendered models significantly reduced intraoperative blood loss in patients undergoing right and left hemicolectomies and anterior resection (217). In a retrospective comparative cohort study conducted by Miyamoto et al, use of 3D planning similarly significantly reduced operative blood loss for patients undergoing right sided hemicolectomies in comparison to no pre-operative imaging (175). The randomised study found a significant reduction in operative times in the 3D group; however Miyamoto et al. found no difference between 3D and non 3D planning groups. No description of the methodologies used to measure either blood loss or operative times were documented in either study. No difference in other surgical performance metrics such as lymph node yield, conversion rates or complication rates was found in either study.

Hojo et al conducted a prospective comparative cohort study of 28 patients undergoing lateral lymph node dissections in which all patients were assessed using 3D models and standard CT imaging. Using a non-validated Likert scale questionnaire 35 responding surgeons rated 3D surface rendered models as superior to a standard CT for pre-operative anatomical understanding and intraoperative navigation (178).

3.5.5 Hepatobiliary Surgery

19 studies were performed in HPB surgery. The characteristics of each study are summarised in table 3-7.

3D was primarily used for planning hepatectomies (13/19) for benign/ malignant tumours and cholangiocarcinoma and eccinococcosis. 4 studies used 3D to plan

pancreaticoduodenectomy for pancreatic cancer and the remaining two used 3d planning for liver transplant and cholecystectomy.

3.5.5.1 Interventions

11 studies utilised 3D virtual models for basic anatomical visualisation (218) (219) (220) (221) (222) (223) (224) (225) (226) (227) (228) with 2 studies utilising 3D printed models in the same capacity (216) (229). 5 studies virtually simulated resection planes and estimated resection functional volumes (230) (231) (232) (233) (234).

3.5.5.2 Outcomes

Operative time and intraoperative blood loss were the two most reported outcome measures. 8/10 reported a significant reduction in operative time in the 3D planning group (235). 5/10 studies using blood loss as an outcome measure found significantly less blood loss in the 3D group (235) (221) (227) (233,234).

6 studies met our criteria for metanalysis:

Figure 3-9 displays a forest plot summarizing the meta-analysis of six studies (Andert 2017, Fang 2015, Nakayama 2017, Wei 2016, Zeng 2016, Zhang 2016) evaluating the effect of three-dimensional (3D) model utilization on intraoperative outcomes in hepatectomy. The total sample size comprised 531 participants.

The combined mean difference of -32.53 mL (95% CI: -46.39 to -18.68) suggests that the use of 3D models is associated with a statistically significant reduction in intraoperative blood loss compared to standard practice ($z=4.60$, $p<0.001$). Heterogeneity was negligible ($Tau^2=0.000$; $Q=0.39$, $p=0.977$; $I^2=0\%$), indicating consistency across the included studies. These findings imply that 3D models may offer a statistical reduction in blood loss.

Figure 3-9 Metanalysis of the effect of 3D models on operative time (mins) of Hepatectomy

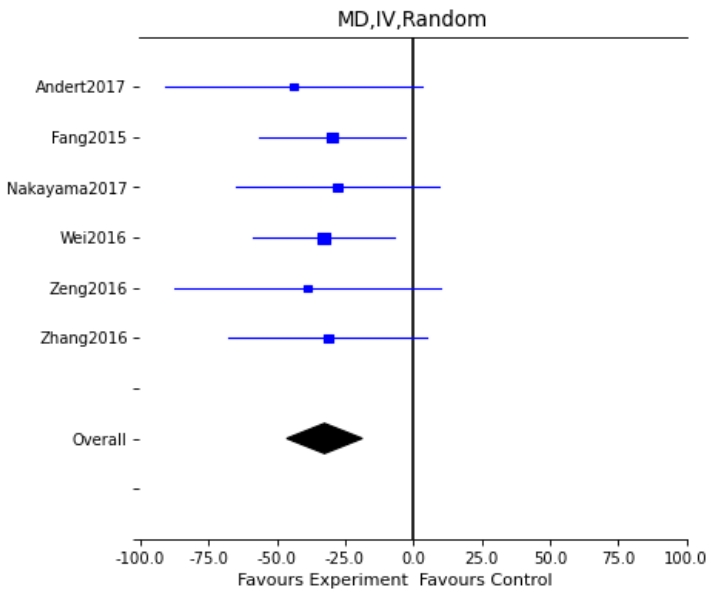
Study ID	Experiment Group			Control Group			Bias
	Mean	SD	n	Mean	SD	n	
Andert 2017	329	40.1	16	373	90.2	17	Serious
Fang 2015	294.5	61.9	60	324.3	83.1	56	Moderate
Nakayama 2017	406.5	149.9	120	434.3	144.6	120	Serious
Wei 2016	167.4	42.6	31	200.2	71.3	43	Moderate
Zeng 2016	408.6	65.9	25	447.3	99.3	22	Serious
Zhang 2016	142.18	21.87	11	173.5	54.88	10	Serious

MD,IV,Random			
Study ID	**n**	**Effect(95% CI)**	**Weight(%)**
Andert 2017	33	-44.00 [-91.17, 3.17]	8.63
Fang 2015	116	-29.80 [-56.62, -2.98]	26.71
Nakayama2017	240	-27.80 [-65.07, 9.47]	13.83
Wei 2016	74	-32.80 [-58.86, -6.74]	28.28
Zeng 2016	47	-38.70 [-87.58, 10.18]	8.04
Zhang 2016	21	-31.32 [-67.71, 5.07]	14.51
Total	**531**	**-32.53 [-46.39, -18.68]**	**100**

6 studies included (N=531)

Heterogeneity: Tau²=0.000, Q=0.39 (p=0.977), I²=0%

Overall effect test: z=4.60, p=0.000



3.5.6 Oral Maxillofacial Surgery and ENT

24 studies were performed in maxillofacial surgery. The characteristics of each study are summarised in table 3-12. 6 randomised studies (236) (237) (238) (239) (240) (241), 7 prospective cohort (242) (242) (243) (244) (245) (246) (247), and 9 retrospective cohort studies were performed (248) (249) (250) (250) (251) (252) (253) (254) (255) (256). 3D planning was primarily used for mandibular or maxillary reconstructions. Mandibular resection with fibular free flap /iliac crest/ scapular free flap reconstruction was the most common procedure for which 3D planning was evaluated (7/24) (236) (248) (257) (242) (240) (251) (253) followed by maxillary Le fort osteotomies (5/24) (237–239,241,252) .

3.5.6.1 Interventions

Most studies utilised computer assisted planning with either 3D printed cutting guides or simulation models. Computer assisted planning allows users to conduct 3D cephalometric analysis to quantify the deformity and predict outcomes. Activities include simulation of the surgical process such as osteotomies, reposition of segments, evaluation of occlusions and soft tissue response to skeletal reconstruction. 8 studies used computer assisted planning with subsequent manufacture of 3D printed cutting guides (152,240,241,243,248,254,255,257) with 6 using 3D printed models for pre-operative simulation (239,242,249,250,252).

3.5.6.2 Outcome measures

11 studies reported the operative time as an outcome measure (236,239,244,248,249,251,252,254,258–260). Of the 8 studies which compared operative times in the 3D group with standard planning controls 3 found significant reductions in operative time in the 3D planning group (249) (251). The methods of recording the operative time were not described in any of the studies with 8/11 reporting retrospective data (see table 3-12). Where time taken for specific operative steps was reported (shaping of the donor or defect site/ flap ischemia time) 4/5 found significant improvements using 3D planning. The aesthetic outcome was reported in 5 studies (152,240,242,248). Only Mao et al compared the aesthetic outcomes with a control group and found significant improvements in facial symmetry with 3D planning (249).

The accuracy of surgery was reported in 7 studies (152,241,243,252,254,257,261). Accuracy was assessed using objective post-operative assessment of interfragmentary distance, contour symmetry, number of segments in the anatomical position, deviation from the virtual plan. All four studies comparing the accuracy of 3D planning with a standard planning control group found 3D planning was significantly more accurate (152,241,253,261).

3.5.7 Trauma and Orthopaedics

37 were performed in trauma and orthopaedics (see table 3-14). 15 studies used randomised study designs (124,124,262–273). 11 studies (274–283) were prospective cohort designs in which historical controls were used in 3/11 (277,278,280) and all patients were assessed with both the 3D intervention and 2D comparator (radiograph or CT). 11 studies were retrospective cohort designs (124,284–291).

3.5.7.1 Interventions

22 studies utilised 3D planning in trauma fracture fixation applications and 7 for joint arthroplasty (see table 3-14). 20 studies utilised 3D printing in total (215,263–266,272,273,276,280,282,284,291–293,293–295). 13 studies used 3D printed models to simulate the intended procedure. Simulation tasks involved pre-bending or selection and application of plates/implants pre-operatively. 4 studies used 3D printed models purely for anatomical visualisation and 2 studies used 3D printed cutting guides to transfer a virtual plan to theatre (272,285). Computer assisted planning was used in 16/32 studies (215,262,267,269,271,272,277–279,281,283,285,286,288,289). Planning activities consisted of virtual fracture reduction, osteotomy placement, anatomical measurements, and virtual implant placement/ sizing.

3.5.7.2 Outcome measures

The most common outcome used was operative time (see Figure 3-8). 23/37 studies reported the effect of 3D planning on overall operative time (215,239,263–270,272,274,276,284,286,292–296) with 78% (18/23) finding 3D planning significantly reduced the overall operative time for the given procedure. None of the studies reported the methodology for how operative time was measured, who took the measurement and whether for randomised studies whether the rater was blinded to the intervention group. 6 studies recorded instrumentation time with 5/6 finding significant reductions in the 3D group. 3D planning was reported to reduced fluoroscopy time in 9/10 that utilised this outcome measure (215,263–265,272,285,292,293,295). Operative blood loss was recorded in 16 studies (figure 3-8). 11/16 reported 3D planning significantly reduced operative blood loss (215,264,265,269,270,270,272,273,293,295). No study recorded the method used to estimate operative blood loss or who took the measurement.

Patient reported functional outcome measures were recorded in 11 studies . A diverse range of specific measures included. Only 36% (4/11) studies found 3D planning improved functional outcomes (263,265,268,293). A wide variety of functional measurement tools were utilised (American Shoulder and Elbow Score, Subjective Shoulder Value, Simple Shoulder

Test, SF36PCS, Japanese Orthopaedic Association score, Hospital for Special Surgery Knee Score, MPES, Gartland-Werley Score, Knee society score, American Orthopaedic Foot and Ankle Score, Disabilities of the Arm Shoulder and Hand scores, Harris Hip score).

5 studies evaluated the impact on surgical performance. Totoki and Zhao both found 3D planning significantly improved the accuracy of screw placement as evaluated using post-operative CT imaging and a validated objective measure (281) (269). 3 studies evaluated the adequacy of fracture reduction (266) (268) . No significant difference between 3D and standard planning was found.

3.5.8 Neurosurgery

13 studies evaluated 3D for neurosurgical/spinal procedures (see table 3-11). Two of the studies were randomised (297) (298) with the remainder being prospective (299) (300) and retrospective comparative cohort designs. In 4/11 studies all the included patients were assessed with 3D and standard imaging methods. In one study patient choice was used to allocate to each study arm (301); in the remaining cohort studies it was unclear how patients were allocated to the intervention or comparator group (302) (303) (304) (305).

3.5.8.1 Intervention.

6 utilised 3D planning for intracranial/spinal tumours (305) (306) (307) (308) (309), 1 for microsurgical clipping of intracranial aneurysms, 3 for degenerative disc disease, 2 for corrective surgery adolescent scoliosis, and 1 to plan trigeminal microvascular decompression. 9 studies used virtual models primarily for anatomical visualisation with volumetric rendering used in 5/9 studies. 3 studies employed computer assisted planning to manufacture 3D printed cutting guides; two studies used 3D printed models for anatomical visualisation and pre-operative simulation.

3.5.8.2 Outcome measures

9/13 studies utilised operative time as the primary outcome measure, of which 8 reported 3D significantly reduced operative times (305) (302). None of the studies recorded how operative time was measured. 6 studies reported intraoperative blood loss, of which 3 found significant reductions in the 3D intervention group.

Two studies evaluated the effect of 3D planning on surgical accuracy. 3D printed cutting guides improved the accuracy of pedicle screw placement as assessed by post-operative CT scan using the Raley pedicle break classification(303).

Patient reported functional/pain outcome measures were compared in 3 studies (297) (302) (310). The Japanese orthopaedic score (JOA), modified Rankin score, Oswestry disability score, and visual analogue score (VAS). 2/3 studies reported significantly better scores in the 3D model group.

Post-operative complications were evaluated in 4 studies (305) (310) (303) (304). Two studies reported significant reductions in complication rates when 3D planning was used. Complications were reported as a combined rate and were not defined or complication classification systems such as Clavien-Dando were not used (305) (303).

3.5.9 Urology

8 studies were performed in Urology (see table 3-9). 3 were retrospective cohort studies; Bertolo et al both 3D and standard 2D CT imaging was used for all patients with 3D and 2D imaging modalities (311); Wang et al used matched controls (143) and Kamai et al allocated patients to each study arm by the time period admitted (312). The remainder were prospective studies; 2 studies compared all the included patients with both 3D and standard imaging (313) (314); 2 studies used retrospective matched controls (142) (315).

3.5.9.1 Intervention

2 studies evaluated the used of 3D for planning percutaneous nephrolithotripsy for renal calculi (313) (316). 6/8 used 3D models for planning partial/radical nephrectomy for renal cell carcinoma (311) (312) (314) (143) (315). 3D virtual models utilised for anatomical visualisation were the main intervention evaluated (7/8 studies) with 3 using volumetric rendering and 4 using surface rendering techniques. 1 study evaluated 3D printed model similarly used for anatomical visualisation (314).

3.5.9.2 Outcome measures

6 studies reported both operative time and intra-operative blood loss as outcome measures (312) (316) (142) (315) (143). Wang et al reported significant reductions in operative times and intra-operative blood loss in the 3D planning group (315), however none of the remaining studies found any statistical difference between 3D and standard planning groups. 3 Studies evaluated the effect on the ischemic kidney time with no differences between planning groups observed (142) (143) (143). The subjective usefulness was evaluated in two studies.

Metanalysis for the effect of 3D planning on partial nephrectomy for renal cell carcinoma operative times.

Figure 3-11 presents a forest plot summarising the results of a meta-analysis examining the effect of effect of 3D planning on partial nephrectomy for renal cell carcinoma operative times. Four studies (Kamai 2010, Poriplegia 2017, Wang 2015, and Wang 2017) are included, representing a total of 221 participants.

The combined effect size is a mean difference of -12.23 minutes (95% CI: -23.51 to -0.95), suggesting that, on average, the intervention group demonstrated a statistically significant improvement over the control group. Statistical measures indicate low between-study heterogeneity ($Tau^2 = 7.037$; $Q = 3.14$, $p = 0.373$; $I^2 = 4.42\%$), implying that variability in effect sizes across included studies is minimal. The overall test for effect is significant ($z = 2.13$, $p = 0.034$), favouring 3D models.

Figure 3-10 Meta-analysis of the effect of 3D models on operative time (min) of partial nephrectomy for renal cell carcinoma

Study ID	Experiment Group			Control Group			
	Mean	SD	n	Mean	SD	n	Bias
Kamai (2010)	124.80	25.70	20	149.70	34.50	20	NRCT **Serious**
Poriplegia (2017)	131.10	43.00	31	132.30	61.00	21	NRCT **Serious**
Wang (2015)	114.80	41.50	49	121.00	31.60	45	NRCT **Moderate**
Wang (2017)	159.00	148.50	21	193.20	108.00	14	NRCT **Moderate**

MD,IV,Random			
Study ID	**n**	**Effect(95% CI)**	**Weight(%)**
Kamai 2010	40	-24.90 [-43.75, -6.05]	33.25
Poriplegia 2017	52	-1.20 [-31.36, 28.96]	13.58
Wang 2015	94	-6.20 [-21.04, 8.64]	51.43
Wang 2017	35	-34.20 [-119.26, 50.86]	1.75
Total	**221**	**-12.23 [-23.51, -0.95]**	**100.00**
4 studies included (N=221)			
Heterogeneity: Tau²=7.037, Q=3.14 (p=0.373), I²=4.42%			
Overall effect test: z=2.13, p=0.034			

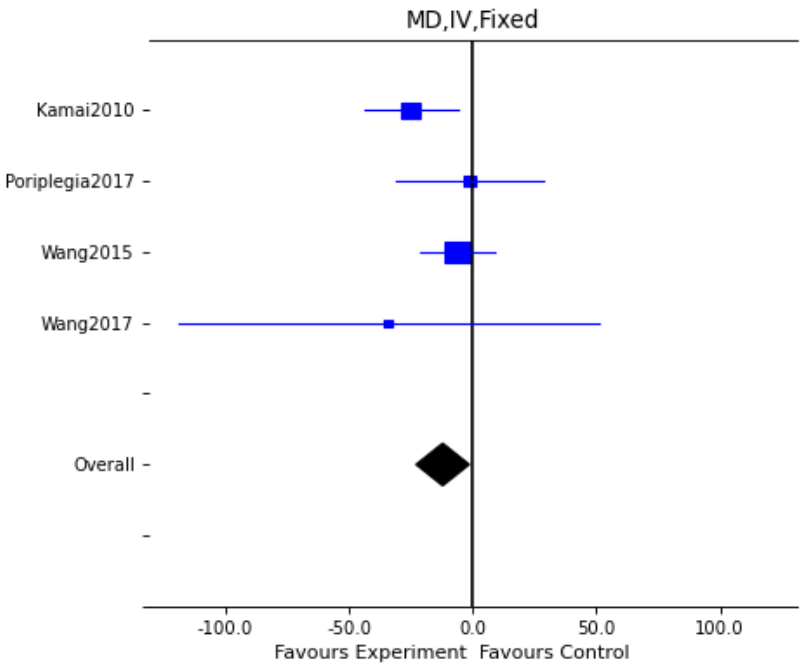


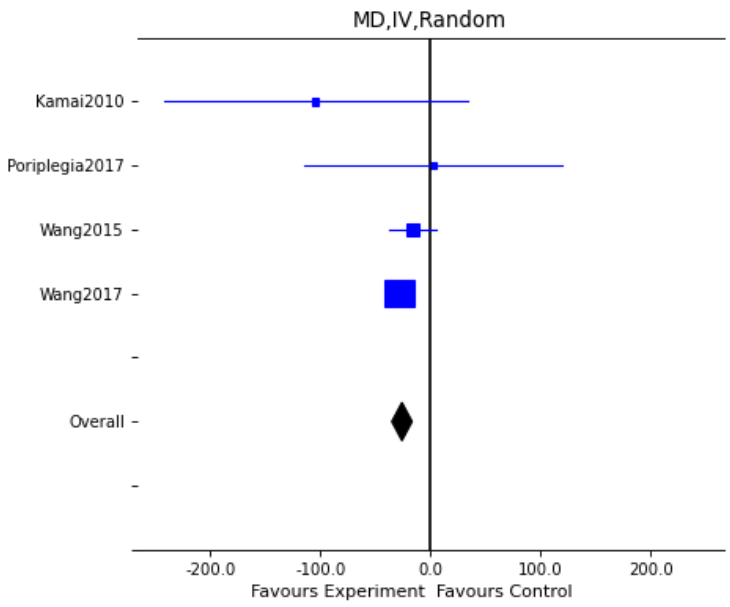
Figure 3-12 illustrates the pooled effects of 3D planning interventions on intraoperative blood loss in partial nephrectomy for renal cell carcinoma. Four studies (Kamai 2010, Poriplegia 2017, Wang 2015, and Wang 2017) with a total sample size of 221 participants were included in the meta-analysis.

The combined estimate indicates a statistically significant reduction in intraoperative blood loss when 3D planning is used, with a mean difference of -25.84 mL (95% CI: -35.12 to -16.55 mL) in favour of the experimental intervention. The test for overall effect is highly significant ($z=5.45$, $p<0.001$). Statistical measures suggest minimal between-study heterogeneity ($Tau^2=0.000$; $Q=2.49$, $p=0.478$; $I^2=0\%$), suggesting that the observed effect sizes are consistent across included studies.

Figure 3-11 Metanalysis of the studies evaluating the effect of 3D models on intra-operative blood loss (ml) in partial nephrectomy for renal cell carcinoma.

Study ID	Experiment Group			Control Group			
	Mean	SD	n	Mean	SD	n	Bias
Kamai (2010)	221.60	138.10	20	326.30	282.80	20	NRCT **Serious**
Poriplegia (2017)	131.60	246.80	31	129.00	182.00	21	NRCT **Serious**
Wang (2015)	142.60	46.60	49	158.50	57.30	45	NRCT **Moderate**
Wang (2017)	148.10	20.70	21	176.10	10.40	14	NRCT **Moderate**

MD,IV,Random			
Study ID	**n**	**Effect(95% CI)**	**Weight(%)**
Kamai 2010	40	-104.70 [-242.63, 33.23]	0.45
Poriplegia 2017	52	2.60 [-114.05, 119.25]	0.63
Wang 2015	94	-15.90 [-37.13, 5.33]	19.14
Wang 2017	35	-28.00 [-38.40, -17.60]	79.78
Total	**221**	**-25.84 [-35.12, -16.55]**	**100.00**
4 studies included (N=221)			
Heterogeneity: Tau²=0.000, Q=2.49 (p=0.478), I²=0%			
Overall effect test: z=5.45, p=0.000			



3.5.10 Upper GI

5 studies were performed in upper gastrointestinal surgery (see table 3-8). Each were comparative cohort studies with 2 retrospective (223) (317) and 2 prospective designs (318) (one of which used retrospective controls (319)), with it being unclear in the study by Osaki et al the specific study design (320). Patients were generally allocated to the 3D intervention group based on the period during which their surgery was performed. In the prospective study by Wang et al allocation to each group was by patient choice (318).

3.5.10.1 Intervention

3D was used to plan interventions for gastric cancer in 4/5 studies and oesophageal cancer. All used volumetric rendering for anatomical visualisation.

3.5.10.2 Outcomes

4/5 studies evaluated the effect of 3D planning on intraoperative blood loss and operative time (321) (319) (318) (317).

Wang et al. and Yuasa et al. found 3D planning significantly reduced intra-operative blood loss (318) (317). The method of measuring blood loss was not described in any of the included studies. 2/4 studies reported significant reductions in operative times when 3D planning was utilised (318) (321). In fours studies complication rates were reported as a combined rate with no specification of type or severity; no difference was found between 3D and non 3D groups (321) (319) (318) (317). Three studies reported the number of lymph nodes retrieved with no differences found between groups. Osaki et al evaluated the effect of 3D visualisation on anatomical understanding. Pre-operative identification of an aberrant left hepatic artery was significantly more accurate in the 3D group (non3D 75%[n=24/32] vs 3D 100 % [n=36/36]) (320).

3.5.11 Cardiac and Thoracic surgery

5 studies were conducted in thoracic and 3 in cardiac surgery (see tables 3-10 and 3-16). 4 utilised prospective cohort study designs in which both standard and 3D imaging modalities were used for all the included patients. Two retrospective cohort studies were performed with matched controls used to compare to the intervention group. For two of the included studies we cannot ascertain whether they employed a retrospective or prospective design or how patients were allocated to intervention or control groups.

3.5.11.1 Interventions

5 studies evaluated 3D printed models that were used for anatomical visualisation and pre-operative simulation. The remaining 3 studies used volumetric 3D virtual reconstructions for anatomical visualisation. 3D planning was used for planning chest wall deformity surgeries (322) (323), open rib fracture stabilisation (215), video-assisted thoracic surgery for lung cancer (323) (324), and congenital cardiac disease interventions (325) (326) (327).

3.5.11.2 Outcome measures

4 studies evaluated the effect of 3D on operative time with 3 reporting significantly reduced operative times using 3D (323) (328) (329), while Zhao et al reported 3D planning had no impact on the operative time of (327). Hagiwara et al reported significantly reduced blood loss when 3D planning was used (323).

Of the two studies which reported and compared general and procedure specific complications, 3D had no impact (329) (329).

3.5.12 Bias assessments

Bias was prominent in most of the included studies. For the non-randomised studies 52% of studies were at serious or critical risk of bias (31/98 serious; 20 critical). A further 36/98 were of moderate risk of bias. The measurement of the outcome domain was the most significant contributor of bias found identified with 30/98 studies at risk of serious or critical bias and a further 44/98 at moderate risk. Common reasons included a lack of blinding and/or no documented detail of how measurements were taken especially for blood loss or operative time outcome measures. As a visual intervention blinding poses a unique challenge to studies evaluating 3D. Confounding was the second most prominent domain contributing to overall bias with 33/98 at moderate, 22/98 at serious and 4 studies at critical risk of bias.

Randomised studies were considered at high risk of bias in 13/27 studies. The measurement of the outcome domain and selection of reported results were the most significant contributors to overall bias. 15/27 studies were judged as ‘High’ or ‘Some concerns’ risk of bias in the measurement of the primary outcome measure. Some concern/high risk of bias within the randomisation domain was found in 11 studies. Figures 12 A & B detail the bias assessments for each study included in the review.

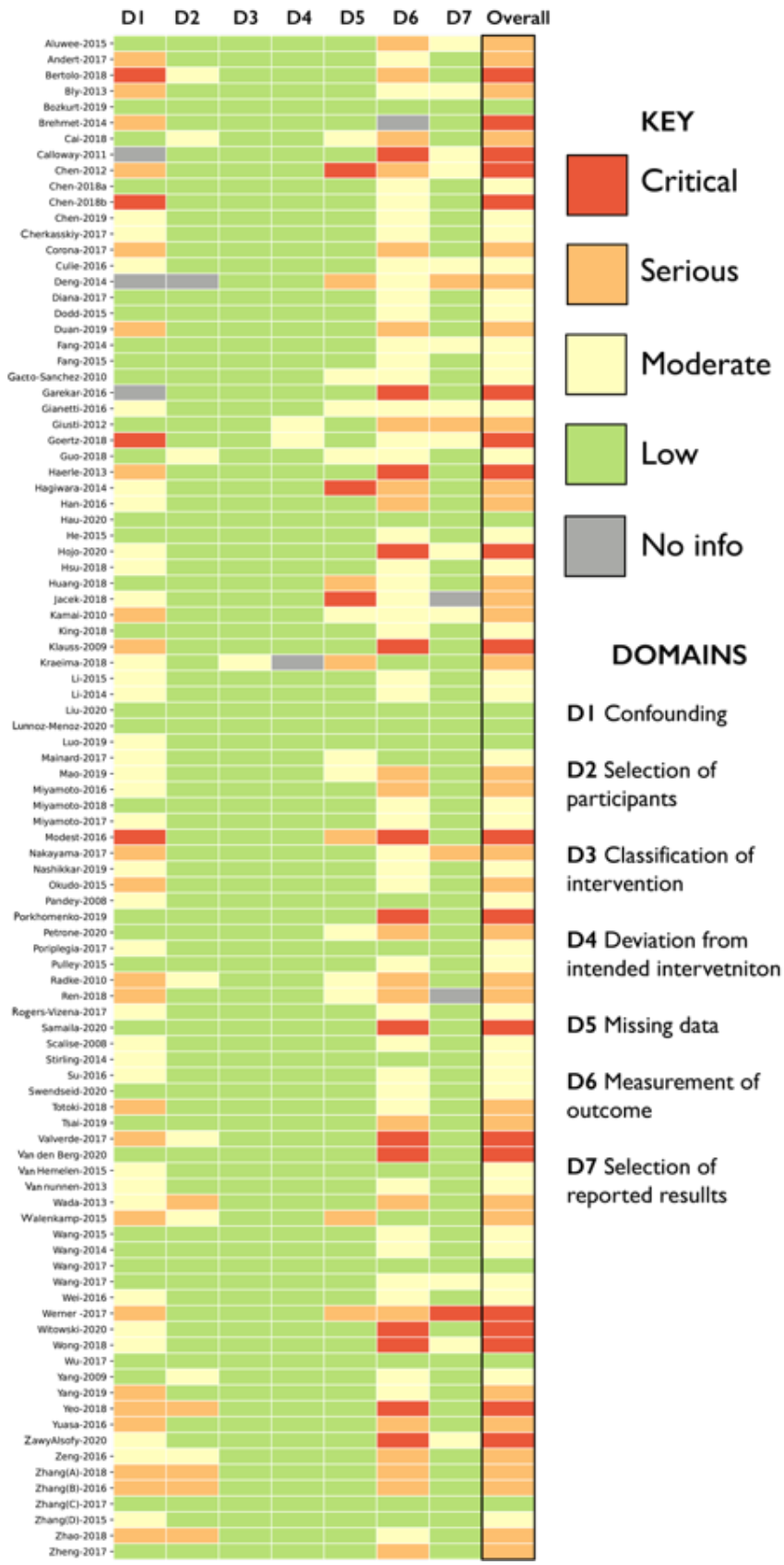
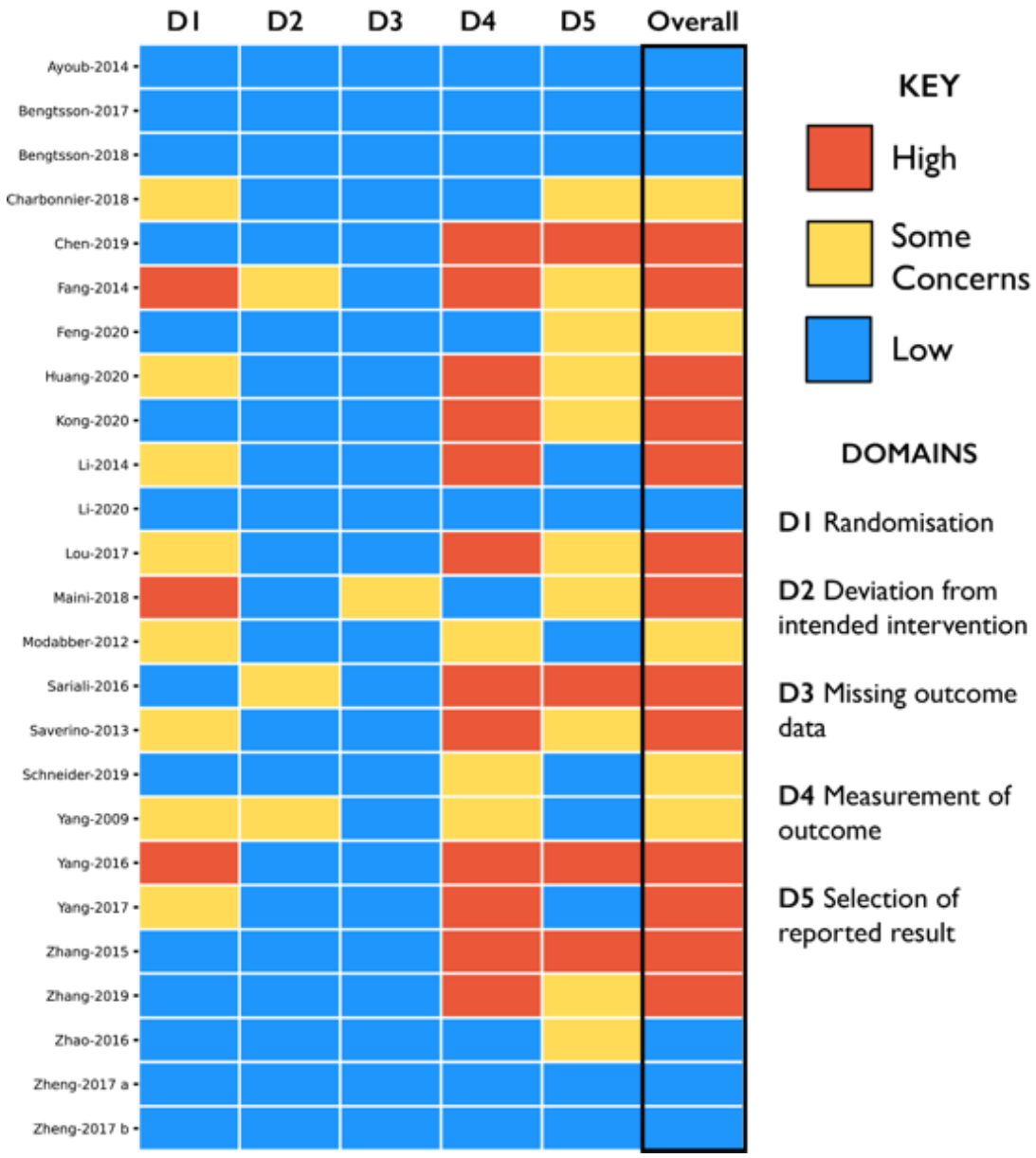


Figure 3-12 Bias Assessments of non-randomised studies using ROBBINS-2 assessment tool

Figure 3-13 Bias assessment of randomised studies using ROB 2 bias assessment tool.



3.6 Discussion

3D models have been utilised for a wide variety of planning activities in most surgical disciplines. As an emerging technology the number of publications evaluating 3D has generally increased over the included period. Despite the significant heterogeneity found between the specific procedures, 3D planning is broadly utilised for procedures involving variable complex anatomy or where precision is required for reconstructive surgery.

While we draw a line between pre-operative planning and intra-operative navigation in practice this line is more of a continuum, where models are frequently reviewed pre-operatively and subsequently brought into theatre to facilitate intra-operative decision making or 3D printed cutting jigs are manufactured to execute computer assisted planning performed for complex limb or maxillofacial reconstructions.

The specific planning activity (i.e. visualisation, computer assisted planning, simulation etc.) and the type of model (virtual versus printed) can be predicted by the specialty and procedure- with certain procedures lending themselves more readily to certain model types. 3D patient specific simulation using printed models is largely restricted to procedures involving bone. It's therefore dominated by trauma and orthopaedics and maxillofacial reconstructions owing to the ease with which hard material 3D printed models can recreate aspects of the intended surgery (e.g. sizing/ shaping implants). Procedure's involving soft tissue organs typically utilised virtual models for anatomical visualisation (i.e 3D virtual models aimed at improving pre-operative understanding).

There is a significant variation in the study designs utilised to evaluate 3D models. Comparative studies evaluating the effect of 3D planning were dominated by non-randomised cohort designs (96/126) with 3D planning often compared with historical controls, although the specific designs varied significantly. None of the included studies included a power calculation to determine sample size.

The most reported outcome was operative time recorded either as the total procedure time and/or time for a specific step (78/124). A significant proportion of studies reported 3D planning significantly reduced operative times which would be in accordance with the often-cited benefit of 3D planning within the pre-existing literature (208). However, these results must be reviewed with some degree of caution owing to the inherent limitations of non-randomised data with a lack of stated methodology for how operative time was measured. This is reflected in the high levels of observed bias within both the randomised

and non-randomised studies stemming from the measurement of the outcome measure. The significant heterogeneity of procedures in which 3D planning was used largely prohibited attempts at meta-analysis, however 3 procedures met our criteria for inclusion: acetabular fracture fixation, partial nephrectomy, and liver resections. In each case the intervention was favoured i.e. suggesting 3D reduced operative times in comparison to standard planning.

Blood loss was the second most reported outcome measure, included in 49/126 studies. Of these 49 studies, 28 found the use of 3D planning significantly reduced blood loss. We cannot make any clear conclusions with respect to the effect of 3D planning on blood loss and the relative impact will be both intervention and procedure specific. As with operative times, this outcome measure was subject to significant bias, as most studies used retrospective data and did not state any methodology on how blood loss was measured or who recorded the measurement. Furthermore, we cannot assess the clinical impact of potential reductions in blood loss. While blood loss may reach statistical significance, the effect on actual patient outcomes may be negligible.

A wide range of clinical outcome measures were utilised. 30 studies reported general and/or procedure specific complication rates out of which 6 studies reported significant reductions in complications when 3D planning was used. Of the 40 studies evaluating 3D for cancer surgery, 8 reported oncological outcomes, of which only 5 statistically compared 3D with standard planning (218) (225) (227) (298) (305). Clear oncological margins were the most commonly reported outcome (owing to the lack of long term follow up data) where 3D was not found to impact the R0 rates for resections for cholangiocarcinoma (218) (225) (227) or mengioma (298) (305) . Only Wei et al reported long term survival data finding statistically improved survival at 6,12, 18 and 24 months for patients undergoing liver resections for hepatocellular carcinoma (227).

Few of the included studies utilised outcome measures that would be specific to 3D e.g. objective measures of anatomical understanding where this was the primary purpose of pre-operative planning instead using the surrogate clinical outcomes more conveniently obtained. Reductions in operative time and blood loss could be attributed to the improved anatomical understanding, however this would be difficult to demonstrate based on the current comparative studies as only one objectively analysed anatomical understanding (320). Understanding the how and why 3D planning may be beneficial may require a mixed methods approach that incorporates narrative and qualitative outcome measures in addition to quantitative metrics. For example, the potential influence on a given operative plan e.g.

tumour respectability or the extent of the resection for liver tumours may be better evaluated qualitatively.

Evaluating the utility of 3D models in surgical planning will likely be difficult within the context of purely quantitative outcome measures as the effect size is likely to be modest and the number of patients that would need to be recruited to randomised studies prohibitive. Furthermore, if we judge 3D by the standards set by randomised control trials- which were conceived primarily to evaluate medical interventions- most studies will suffer from a significant level of bias owing to the difficulties around blinding. Given the methodological flaws of retrospective studies, future research should begin to include a greater proportion of randomised prospective designs if the level of evidence for 3D planning is to be improved.

There is a lack of consistency in the literature with respect to the technical detail of model production. While the focus on the included studies was to evaluate the clinical effectiveness of 3D, the logistics of model production is a notable absence that makes any assessment of their relative impact and feasibility difficult. Future research should not only focus on readily available clinical outcome measures, but also feasibility of implementation, workflow development of 3D model manufacturing, cost-analyses, and qualitative outcome measures on their impact on surgeons and patients.

Table 3-5 Summary of study design and 3D interventions in Colorectal Surgery

Author	Year	Pathology	Procedure	Study Design	Allocation	Total (n)	3D (n)	2D (n)	Other comp (n)	3D intervention	Rendering	Imaging	Segmentation Software	Produced	Printing method	Cost 3DP	Print time	Used in theare
Hojo (178)	2020	Rectal cancer	Lateral pelvic lymph node dissection	Prospective comparative cohort	All patients assessed by each method	28	28	28		3D printed anatomical understanding	Surface	CT not defined	Not stated	Surgeon	Material extrusion	$15	22	No
Miyamoto (175)	2017	Colorectal cancer	Colectomy	Retrospective comparative cohort	No CT available	66	24	20	22	3D Virtual: anatomical visualisation	Volumetric	CT not defined	Synapse Vincent	Not stated				
Saverio (217)	2013	Colorectal cancer	Colorectal resection	RCT	Simple	121	58	59		3D Virtual: anatomical visualisation	Volumetric	CT PV	Workstation	Not stated				

Table 3-6 Summary of study design and 3D interventions in Hepatobiliary Surgery

Author	Year	Pathology	Procedure	Study Design	Allocation	Total (n)	3D (n)	2D (n)	Other comp (n)	3D intervention	Rendering	Imaging	Segmentation Software	Produced	Printing method	Cost 3DP	Print time	Used in theare
Andert (218)	2017	Cholangiocarcinoma	Hilar en bloc resection	Prospective cohort with retrospective controls	All patients assessed by each method	33	16	17		3D Virtual: anatomical visualisation	Volumetric	CT PV	PACS System	Radiologist				
Bozkurt (230)	2019	Liver	Liver transplant	Cohort study	All patients assessed by each method	41	41	41		Computer-assisted planning- outcome simulation	Not stated	CT not defined	Myrian 3 dimensional volumetry	Surgeon				
Diana (219)	2017	Gallstones	Cholecystectomy	Prospective comparative cohort	All patients assessed by each method	58	44	54	52	3D Virtual: anatomical visualisation	Surface	MRI	Visible Patient	Not stated				
Fang (235)	2014	Pancreatic cancer	Pancreaticoduodenectomy	RCT	Randomisation	62	43	19		Computer-assisted planning- resection	Surface	CT Angio	MI-3DVS	Radiologist				
Fang (231)	2015	Hepatocellular carcinoma	Hepatectomy	Retrospective comparative cohort	Unclear	116	60	56		Computer-assisted planning- resection	Surface	CT Angio	MI-3DVS	Radiologist				
Fang (220)	2012	Pancreatic cancer	Pancreaticoduodenectomy	Prospective cohort	All patients assessed by each method	57	57	57		3D Virtual: anatomical visualisation	Surface	CT Angio	MI-3DVS	Radiologist				
He (221)	2015	Hepatic alveolar echinococcosis	Hepatectomy	Prospective comparative cohort	Unclear	106	59	47		3D Virtual: anatomical visualisation	Surface	Other	IQQA-Liver	Not stated				
Klauss (222)	2009	Pancreatic carcinoma	Pancreaticoduodenectomy	Prospective cohort	All patients assessed by each method	10	10	10		3D Virtual: anatomical visualisation	Surface	Multi-phase CT	MITK ReLiver	Radiologist				
Miyamoto (223)	2018	Pancreatic cancer	Pancreaticoduodenectomy	Retrospective comparative cohort	Time period	117	64	53		3D Virtual: anatomical visualisation	Surface	CT and MRI	Synapse Vincent	Not stated				
Nakayama (224)	2017	Hepatocellular carcinoma & intahepatic cholangiocarcinoma	Hepatectomy	Retrospective comparative cohort	Time period	240	120	120		3D Virtual: anatomical visualisation	Unclear/ Not stated	Multi-phase CT	Synapse Vincent	Surgeon				
Okuda (225)	2015	Cholangiocarcinoma	Hepatectomy	Prospective cohort with retrospective controls	Time period	118	49	69		3D Virtual: anatomical visualisation	Volumetric	Multi-phase CT	Ziostation	Not stated				
Radke (226)	2010	Hepatectomy	Hepatectomy	Prospective cohort	All patients assessed by each method	202	202	202		3D Virtual: anatomical visualisation	Surface	CT portoven ous	HepaVision	Not stated				
Su (330)	2016	Hepatoblastoma	Hepatectomy (Paeds)	Retrospective comparative cohort	Unclear	26	16	10		3D Virtual: anatomical visualisation	Surface	CT PV	Hisense CAS	Not stated				
Wang (232)	2017	Malignant and benign liver tumours	Segental hepatecotmy	Prospective cohort	All patients assessed by each method	305	305	305		3D Virtual: simulation	Surface	Multi-phase CT	IQQA-Liver	Not stated				
Wei (227)	2016	Hepatocellular carcinoma	Hepatectomy	Prospective comparative cohort	Patient choice	74	31	43		3D Virtual: anatomical visualisation	Surface	Multi-phase CT	3D Plus Body Visible System	Not stated				
Witowski (216)	2020	Hepatocellular carcinoma	Hepatectomy	Prospective cohort	All patients assessed by each method	19	19	19		3D Printed: anatomical visualisation	Surface	CT multi phase	3D Slicer	Surgeon	Material extrusion	$90	90-100	No

Yang (229)	2019	Hepatocellular carcinoma	Hepatectomy	Retrospective cohort	Multiple assessors of each case using 2D/3D	4	4	4		3D Printed: anatomical visualisation	Surface	CT multi-phase	Mimics	Surgeon	Polyjet	$1200		No
Yeo (228)	2018	Hepatocellular carcinoma	Hepatectomy	Prospective comparative cohort	Matched	10	5	5		3D Virtual: anatomical visualisation	Surface	CT not defined	3D Slicer	Not stated				
Zeng (233)	2016	Cholangiocarcinoma	Cholangiocarcinoma Resection	RCT	Simple	47	25	22		3D virtual: simulation	Volumetric	CT Angio	MI-3DVS	Not stated				
Zhang (234)	2016	Hepatoblastoma	Hepatectomy	Retrospective comparative cohort	Time period	21	11	10		3D virtual: simulation	Volumetric	CT Angio	Sensation64	Not stated				
Zhao (331)	2017	Giant hepatic mesenchymal hamartoma	Hepatectomy (Paeds)	Comparative cohort	Unclear	5	3	2		3D Virtual: anatomical visualisation	Surface	CT not specified	Hisense CAS	Not stated				

Table 3-7 Summary of study design and 3D interventions in Upper Gastrointestinal Surgery

Author	Year	Pathology	Procedure	Study Design	Allocation	Total (n)	3D (n)	2D (n)	Other comp (n)	3D intervention	Rendering	Imaging	Segmentation Software	Produced	Printing method	Cost 3DP	Print time	Used in theare
Miyamoto (321)	2016	Gastric cancer	Gastrectomy	Retrospective comparative cohort	Time period	84	42	42		3D Virtual: anatomical visualisation	Volumetric	CT not defined	Workstation	Not stated				
Osaki (320)	2015	Gastric cancer	Gastrectomy	Cohort study	Unclear	68	32	36		3D Virtual: anatomical visualisation	Volumetric	CT PV	Workstation	Not stated				
Wada (319)	2013	Oesophageal cancer	Oesophagectomy	Prospective cohort with retrospective controls	Time period	48	26	22		3D Virtual: anatomical visualisation	Volumetric	CT Angio	Workstation	Radiologist				
Wang (318)	2014	Gastric cancer	Gastrectomy	Prospective comparative cohort	Patient choice	312	231	81		3D Virtual: anatomical visualisation	Volumetric	CT Angio	PACS System	Radiologist				
Yuasa (317)	2016	Gastric cancer	Distal gastrectomy	Retrospective comparative cohort	Time period	192	115	77		3D Virtual: anatomical visualisation	Volumetric	Multi-phase CT	Ziostation	Not stated				

Table 3-8 Summary of study design and 3D interventions in Urology

Author	Year	Pathology	Procedure	Study Design	Allocation	Total (n)	3D (n)	2D (n)	Other comp (n)	3D intervention	Rendering	Imaging	Segmentation Software	Produced	Printing method	Cost 3DP	Print time	Used in theare
Bertolo (311)	2018	Renal cell carcinoma	Partial nephrectomy	Retrospective cohort	All patients assessed by each method	20	20	20		3D Virtual: anatomical visualisation	Volumetric	CT PV	PACS System	Not stated				
Brehmer (313)	2014	Renal stones	PCNL	Prospective cohort	All patients assessed by each method	35	35	35		3D Virtual: anatomical visualisation	Volumetric	CT non contrast	PACS System	Radiologist				
Kamai (312)	2010	Renal cell carcinoma	Radical Nephrectomy	Retrospective comparative cohort	Time period	80	20	60		3D Virtual: anatomical visualisation	Volumetric	CT Angio	Leonardo InSpace	Radiologist				
Parkhomenko (316)	2019	Renal Stones	PCNL	Prospective cohort with retrospective controls	Matched + all patients assessed by each method	50	25	25		3D Virtual: anatomical visualisation	Surface	CT not contrast	3D Slicer	Not stated				
Poriglia (142)	2017	Renal cell carcinoma	Partial nephrectomy	Prospective comparative cohort	Time period	52	31	21		3D Virtual: anatomical visualisation	Surface	CT not specified	M3DICS	Engineer				
Wake (314)	2018	Renal cell carcinoma	Partial nephrectomy	Prospective cohort	All patients assessed by each method	10	10	10		3D Printed: anatomical visualisation	Surface	MRI	Materialise Mimics	External company	MJ	$1000	10	0

Wang (315)	2015	Renal cell carcinoma	Partial nephrectomy	Prospective cohort with retrospective controls		21	21	14		3D Virtual: anatomical visualisation	Surface	Multi-phase CT	3D-MIRGS	Not stated				
Wang (143)	2017	Renal cell carcinoma	Partial nephrectomy	Retrospective comparative cohort	Matched	94	49	45		3D Virtual: anatomical visualisation	Surface	Multi-phase CT	MEDICAL Imaging Three Divisional Visulisation System	Not stated				
Zhang (332)	2018	Phaeochromocytoma /paraganglioma	Adrenalectomy	Retrospective comparative cohort	Unclear	36	14	22		3D Virtual: anatomical visualisation	Surface	CT Angio	FreeForm modelling system	Not stated				

Table 3-9 Summary of study design and 3D interventions in Thoracic Surgery

Author	Year	Pathology	Procedure	Study Design	Allocation	Total (n)	3D (n)	2D (n)	Other comp (n)	3D intervention	Rendering	Imaging	Segmentation Software	Produced	Printing method	Cost 3DP	Print time	Used in theare
Calloway (322)	2011	Chest wall deformity	Chest reconstruction	Prospective cohort	All patients assessed using each method	82	82	82		3D Virtual: anatomical visualisation	Volumetric	CT non contrast	Multimodality workplace software	Not stated				
Chen (329)	2018	Rib fractures	surgical stabilization of rib fractures	Retrospective comparative cohort	Unclear	51	17	34		3D Printed: simulation	Unclear/ Not stated	CT not defined	Not stated	Not stated	Material extrusion	Not stated	Not stated	No
Hagiwara (323)	2014	Lung cancer	VATS segmentectomy/ lobectomy	Case Series	All patients assessed using each method	124	124	124		3D Virtual: anatomical visualisation	Volumetric	Other	Workstation	Surgeon				
Huang (328)	2018	Pectus Excavatum	Nuss procedure	Retrospective comparative cohort	Matched	84	14	70		3D Printed: simulation	Unclear/ Not stated	CT not defined	Materialise-Mimics	Not stated	Not stated	Not stated		1
Smelt (324)	2019	Lung cancer	Video assisted thoracic surgery	Prospective cohort	All patients assessed by each method	16	16	16		3D Virtual: anatomical visualisation	Volumetric	Multi-phase CT	ITK-SNAP	Not stated	Material extrusion	Not stated	Not stated	0

Table 3-10 Summary of study design and 3D interventions in Neurosurgery

Author	Year	Pathology	Procedure	Study Design	Allocation	Total (n)	3D (n)	2D (n)	Other comp (n)	3D intervention	Rendering	Imaging	Segmentation Software	Produced	Printing method	Cost 3DP	Print time	Used in theare
Chen (305)	2012	Meningioma	Meningioma resection	Retrospective comparative cohort	Unclear	730	473	257		3D Virtual: anatomical visualisation	Volumetric	CT Angio	Workstation	Surgeon				
Deng (299)	2014	Intraspinal hemangioblastoma	Lamiotomy and microsurgical tumour resection via posterior approach	Prospective cohort	All patients assessed by each method	28	15	13		3D Virtual: anatomical visualisation	Volumetric	CT Angio	Workstation	Not stated				
Feng (297)	2020	Cervical spondylotic myelopathy	Cervical lateral screw fixation	RCT	Simple	12	6	6		Computer-assisted planning and 3D printed cutting guides	Surface	CT	Mimics	Not stated	SLS	Not stated	40	Yes
Goertz (302)	2018	Intracranial aneurysms	Microsurgical clipping	Retrospective comparative cohort	Unclear ?time	157	117	40		3D Virtual: anatomical visualisation	Volumetric	CT Angio	PACS System	Not stated				
Guo (306)	2018	Pituitary adenoma	Endonasal transphenoid pituitary resection	Retrospective cohort	Unclear	53	26	27		3D Virtual: anatomical visualisation	Unclear/ Not stated	CT non contrast	Not stated	Not stated				
Han (300)	2016	Trigeminal neuralgia	Trigeminal microvascular decompression	Prospective cohort	All patients assessed by each method	40	40	40		3D Virtual: anatomical visualisation	Surface	MRI	3D Slicer	Not stated				
Haerle (307)	2013	Pituitary lesions	Skull base surgery	Retrospective cohort	All patients assessed by each method	8	12	12		3D Virtual: anatomical visualisation	Volumetric	MRI	ITK-SNAP	Surgeon				
Li (310)	2015	Lumbar disc	Lumbar discectomy	Prospective comparative cohort	Unclear	37	15	22		3D printed: anatomical visualisation	Surface	CT non contrast	Materialise Mimics	Not stated	SLS	Not stated	Not stated	No
Luo (301)	2019	Severe congenital scoliosis	Pedicle screw placement	Prospective comparative cohort	Patient choice	32	15	17		Computer-assisted planning and 3D printed cutting guides	Surface	CT non contrast	Mimics	Not stated	SLS	Not stated	Not stated	Yes
Petrone (303)	2020	Lumbar degenerative disease	Posterior lumbar fusion	Retrospective comparative cohort	Unclear	238	43	158	37	Computer-assisted planning and 3D printed cutting guides	Surface	CT not specified	OsiriX X; Mimics	Not stated	Not stated	Not stated	Not stated	Yes
Yang (308)	2009	Skull base tumors	Skull base tumour resection	RCT	Simple	84	42	42		3D Virtual: anatomical visualisation	Volumetric	CT Angio	Dextroscope	Not stated				
Yang (304)	2015	Adolescent idiopathic scoliosis	Scoliosis Corrective surgery	Retrospective comparative cohort	Unclear	126	50	76		3D Printed: simulation	Surface	CT not defined	Not stated	Not stated	SLS	Not stated	Not stated	No
ZawyAlsofy (309)	2020	Infratentorial brain tumour	Deep infratentorial tumour resection	Retrospective cohort	All patients assessed by each method	14	14	14		3D Virtual: anatomical visualisation	Not clear	CT/MRI	3D Slicer	Surgeon				

Table 3-11 Summary of study design and 3D interventions in Oral maxillofacial surgery

Author	Year	Pathology	Procedure	Study Design	Allocation	Total (n)	3D (n)	2D (n)	Other comp (n)	3D intervention	Rendering	Imaging	Segmentation Software	Produced	Printing method	Cost 3DP	Print time	Used in theare
Ayoub (236)	2014	Mandibular deformity	Mandibular reconstruction with iliac crest graft	RCT	Simple Randomisation	20	10	10		Computer-assisted planning with 3D printed cutting guides	Unclear/ Not stated	CT non contrast	Materialise pro plan	Not stated	SLS	Not stated	Not stated	Yes
Bengtsson (237)	2017	Grade III Mandibular Malocclusion	Maxillary Le Fort osteotomy	RCT	Simple Randomisation	57	28	29		Computer-assisted planning	Surface	CT non contrast	Materialise Mimics	Not stated				
Bengtsson (238)	2018	Grade III Mandibular Malocclusion	Maxillary Le Fort osteotomy	RCT	Simple Randomisation	55	28	27		Computer-assisted planning	Surface	CT non contrast	Materialise Mimics	Not stated				
Bly (333)	2013	Orbital fractures	Orbital reconstruction	Prospective cohort with retrospective controls	Time period	113	56	57		Computer-assisted planning	Unclear/ Not stated	CT non contrast	iNtellect Cranial Navigation	Not stated				
Culie (248)	2016	Mandibular defects	Mandibular resection and fibular free flap reconstruction	Retrospective comparative cohort	Time period	29	18	11		Computer-assisted planning with 3D printed cutting guides	Surface	CT non contrast	Not stated	External company	Not stated	€25	Not stated	Yes

Jacek (257)	2018	Oral squamous cell carcinoma	Mandibular resection and scapular free flap reconstruction	Comparative cohort	Unclear	8	4	4		Computer-assisted planning with 3D printed model for simulation	Volumetric	CT non contrast	3D Slicer	Not stated	Material extrusion	Not stated	Not stated	No
King (242)	2018	Mandibular fracture	Mandibular ORIF	Prospective comparative cohort	Matched	38	19	19		3D Printed: simulation	Surface	CT not defined	IntelliSpace Portal	Not stated	Material extrusion	Not stated	Not stated	No
Kraeima (243)	2018	Oral squamous cell carcinoma	Mandibular resection and reconstruction	Prospective cohort with retrospective controls	Time period	89	34	55		Computer assisted planning with 3D Printed cutting guide	Surface	Fused CT and MRI	Materialise pro plan	External company	Not stated			
Li (239)	2020	Class III mandibular malocclusion	Le fort I osteotomy and bilateral sagittal split osteotomy	RCT	Simple randomisation	46	23	23		3D printed simulation	Surface	CT non contrast	Mimics	Not stated	SLA	Not stated	Not stated	No
Liu(244)	2020	Zygomaticomaxillary fibrous dyspllasia	Bone contouring	Prospective comparative cohort	Unclear	24	13	11		Computer-assisted planning- reconstruction	Surface	CT non contrast	ProPlan CMF					
Mao (249)	2019	Pierre robin syndrome	Bilateral mandibular distraction osteogenesis	Retrospective comparative cohort	Unclear	22	10	12		3D Printed: simulation	Surface	CT non contast	Mimics	Not stated	SLS	Not stated	Not stated	No
Modabber (240)	2012	Mandibular defects	Mandibular resection and fibular free flap reconstruction	RCT	Simple	10	5	5		Computer-assisted planning with 3D printed cutting guides	Volumetric	CT non contrast	Materialise-Mimics	Not stated	Not stated	Not stated	Not stated	Yes
Modest (250)	2016	Maxillary tumour	Maxillectomy with thoracodorsal scapular composite free-flap	Retrospective comparative cohort	Unclear	9	4	4		3D Printed: simulation	Surface	CT non contrast	Materialise Mimics	Radiologist	Polyjet	Not stated	Not stated	Yes
Pandey (245)	2008	Otitis Media	Otoscopy	Prospective cohort	All patients assessed by each method	33	33	33		3D Virtual: anatomical visualisation	Volumetric	CT non contrast	PACS System	Not stated				
Ren (251)	2018	Mandibular tumour	Mandibular resection and fibular free flap reconstruction	Retrospective comparative cohort	Time period	30	15	15		Computer-assisted planning- reconstruction	Surface	CT not specified	Materialise Mimics	Not stated				
Rogers-Vizena (252)	2017	Congenital facial deformity	Le fort III midfacial distraction	Retrospective comparative cohort	Time period	29	9	20		3D Printed: simulation	Surface	CT non contrast	Not stated	Not stated	SLS	$1000-2000	Not stated	No
Schneider (241)	2019	Retrognathism	Le fort I osteotomy	RCT	Simple	21	9	12		Computer-assisted planning and 3D printed cutting guides	Surface	CT non contrast	Dolphin 3D		SLS	$884	Not stated	Yes
Stirling (253)	2014	Mandible reconstruction	Mandibular resection and reconstruction	Retrospective comparative cohort	Unclear	28	9	19		Computer-assisted planning- reconstruction	Surface	CT non contrast	Materialise Mimics	Not stated				
Swenseid (254)	2020	Midface defects	Subscapular system free flap reconstruction	Retrospective comparative cohort	Unclear	23	9	14		Computer-assisted planning and 3D printed cutting guides	Surface/volume	CT non contrast	Mimics	Not stated	Not stated	Not stated	Not stated	Yes
Tsai (255)	2019	Cleft lip and palate	Bimaxillary osteotomies	Retrospective comparative cohort	Unclear	53	30	23		Computer-assisted planning and 3D simulation and printed cutting guides	Surface	CT non contrast	Rhino3D	Not stated	Not stated	Not stated	Not stated	Yes
Van Hemelen (246)	2015	Mandibular malocclusion	Bimaxillary osteotomy	Prospective cohort	All patients assessed by each method	66	31	35		Computer-assisted planning- reconstruction	Not stated	CT non contrast	Maxilim	Not stated				
Van Nunen (247)	2013	Non syndromic trigonocephaly	Fronto supraorbital bar advancement	Prospective cohort with retrospective controls	Time period	5				Computer-assisted planning- reconstruction	Surface	CT non contrast	Materialise Mimics	Surgeon	SLA	900 Euro/ skull	Not stated	Yes
Wu (256)	2017	Facial asymmetry	Orthagnathic surgery	Retrospective comparative cohort	Time period	60	30	30		Computer-assisted planning- reconstruction	Surface	CT non contrast	Materialise Mimics	Not stated				
Zhang (261)	2015	Maxillary defects	Maxillectomy and fibular free flap reconstruction	Comparative cohort	Unclear	27	8	19		Computer-assisted planning- reconstruction	Volumetric	CT Angio	iPlan CMF	Not stated	Not stated	Not stated	Not stated	No

Table 3-12 Summary of study design and 3D interventions in Gynaecological Surgery

Author	Year	Pathology	Procedure	Study Design	Allocation	Total (n)	3D (n)	2D (n)	Other comp (n)	3D intervention	Rendering	Imaging	Segmentation Software	Produced	Printing method	Cost 3DP	Print time	Used in theare
Aluwee (334)	2015	Uterine fibroids	Myomectomy	Prospective cohort	All patients assessed by each method	10	10	10		3D Virtual: anatomical visualisation	Surface	MRI	Custom using open source Toolkit	Radiologist				

Giusti (335)	2012	Endometriosis	Endometriosis resection	Prospective cohort	All patients assessed by each method	36	36	36		3D Virtual: anatomical visualisation	Unclear/ Not stated	MRI	ITK-SNAP	Not stated				

Table 3-13 Summary of study design and 3D interventions in Trauma and Orthopaedics

Author	Year	Pathology	Procedure	Study Design	Allocation	Total (n)	3D (n)	2D (n)	Other comp (n)	3D intervention	Rendering	Imaging	Segmentation Software	Produced	Printing method	Cost 3DP	Print time	Used in theare
Cai (292)	2018	Pelvic fracture	Pelvis MI cannulated screw	Non-RCT	Not stated	137	65	72		3D Printed: simulation	Surface	CT non contrast	Materialise Mimics	Not stated	Not stated	Not stated	Not stated	No
Charbonnier (262)	2018	Subacromial impingement	Acromioplasty	RCT	Randomisation	58	27	31		Computer-assisted planning	Surface	CT non contrast	Materialise Mimics	Surgeon				
Chen (293)	2018	Proximal humerus fractures	Proximal Humeral ORIF (plate)	Retrospective comparative cohort	Time period	131	46	53	32	3D Printed: simulation	Surface	CT non contrast	SuperImage Ortho edition	Surgeon	Material extrusion	Not stated	Not stated	No
Chen (215)	2019	Distal radius fracture	Distal radius ORIF (volar locking plate)	RCT	Simple	48	23	25		3D Printed: simulation	Surface	CT non contrast	Mimics	Not stated	Material extrusion	Not stated	5hrs	No
Chen (336)	2020	Distal radius fracture	Distal Radius ORIF (volar locking plate)	Retrospective comparative cohort	Time period	32	15	17		Computer-assisted planning- reconstruction	Volume	CT non contrast	Super Image Orthopaedics	Not stated				
Cherkasskiy (274)	2017	Slipped femoral epiphysis	Proximal femoral osteotomy	Prospective comparative cohort	Time period	15	5	5	5	3D Printed: simulation	Surface	CT non contrast	Materialise Mimics	Not stated	Material extrusion	Not stated	Not stated	No
Corona (284)	2018	Post traumatic tibial deformity	Tibia Ilizarov frame	Retrospective comparative cohort	Emergency case precluding 3D printing	10				3D Printed: simulation	surface	CT non contrast	Materialise Mimics	External company	Material extrusion	300 Euros	14.9	Yes
Dodd (275)	2015	Tibial plateau fracture	Tibial plateau ORIF (plate)	Prospective cohort	All patients assessed by each method	12	12	12		3D Virtual: anatomical visualisation	Unclear/ Not stated	CT non contrast	OsiriX X	Surgeon				
Duan (285)	2019	Subtalar arthritis	Subtalar arthrodesis	Retrospective comparative cohort	Unclear	30	14	16		Computer-assisted planning and 3D printed cutting guides	Surface	CT non contrast	Mimics	Not stated	Material extrusion	Not stated	Not stated	Yes
Giannetti (276)	2016	Tibial plateau fracture	Tibial Plateau ORIF (minimally invasive plate)	Prospective comparative cohort	Unclear	40	16	24		3D Printed: anatomical visualisation	Surface	CT not defined	OsiriX X	Not stated	SLA	98-138 euro	10	Yes
Hau (277)	2020	Knee osteoarthritis	Total knee replacement	Prospective comparative cohort	All patients assessed by each method	35	35	35		Computer-assisted planning-	Surface	CT	EOS	Not stated				
Hsu (286)	2018	Acetabular fractures	Acetabular ORIF (plate)	Retrospective comparative cohort	Time period	29	12	17		Computer-assisted planning- reconstruction	Unclear/ Not stated	CT not defined	Materialise-Mimics	Surgeon	Not stated	Not stated	612.25+/- 23.14 mins	No
Huang (263)	2020	Acetabular fractures (both column)	Acetabular ORIF (plate)	RCT	Block	40	20	20		3D printed simulation	Surface	CT	Mimics	Not stated	SLA		Not stated	No
Kong (264)	2020	Distal radius fracture	Distal Radius ORIF (distal volar plate)	RCT	Simple	32	16	16		3D printed simulation	Surface	CT	Mimics	Not stated	Not stated	Not stated	Not stated	No
Leon-Munoz (278)	2020	Knee osteoarthritis	Total knee replacement	Prospective comparative cohort	All patients assessed by each method	227	227	227		Computer-assisted planning- reconstruction	Not stated	CT	Not stated	Not stated				

Li	2016	Pelvic fracture	Pelvis ORIF (fixation method not stated)	Retrospective comparative cohort	Time period	157	76	81		3D printed: anatomical visualisation	Volumetric	CT Angio	Materialise Mimics	Not stated	Not stated	Not stated	Not stated	No
Lou (265)	2017	Tibial plateau fractures	Tibial ORIF (plate)	RCT	Simple	72	34	38		3D Printed: simulation	Volumetric	CT non contrast	Materialise Mimics	Not stated	Not stated	Not stated		No
Mainard (288)	2017	Total hip replacement	Total hip replacement	Retrospective cohort	All patients assessed by each method	31	31	31		Computer-assisted planning	Surface	CT not defined	EOS imaging	External company				
Maini (337)	2016	Acetabular fractures	Acetabular ORIF (plate)	RCT	Simple	21	11	10		3D Printed: simulation	Surface	CT non contrast	Materialise Mimics	Not stated	SLS	Not stated	0	No
Maini (294)	2018	Acetabular fractures	Acetabular ORIF (plate)	RCT	Simple	25	12	13		3D Printed: simulation	Surface	CT non contrast	Materialise Mimics	Not stated	Material extrusion	Not stated	0	Yes
Nashikkar (279)	2019	Shoulder osteoarthritis	Total shoulder arthroplasty	Prospective cohort with retrospective controls	Time period	71	35	36		Computer-assisted planning	Surface	CT	Not stated	Not stated				
Samaila (280)	2020	Intra-articular fractures of calcaneus, tibial plateau and distal radius	Distal, calcaneus, tibial plateau ORIF (screw and plate)	Prospective cohort	All patients assessed by each method	52	52	52		3D Printed: anatomical visualisation	Volume/surface	CT non contrast	OsiriX X	Not stated	Material extrusion	Not stated	Not stated	Yes
Sariali (267)	2016	Hip osteoarthritis	Total hip replacement	RCT	Simple	28				Computer-assisted planning	Surface	CT not defined	HipPlan (Symbiosis)					
Scalise (289)	2008	Total shoulder arthroplasty	Total shoulder arthroplasty	Retrospective cross-over	All patients assessed by each method	24	24	24		Computer-assisted planning	Surface	CT non contrast	Custom	Not stated				
Totoki (281)	2018	Distal radius fracture	Distal radius ORIF (volar locking plate)	Prospective comparative cohort	Time period	49	30	19		Computer-assisted planning	Surface	CT not defined	Zed-Trauma	Not stated				
Van den Berg (290)	2020	Posterior tibial plateau fractures	Tibial Plateau ORIF (plate)	Retrospective cross over	All patients assessed by each method	34	34	34		3D Virtual: anatomical visualisation	Volume	CT	Not stated	Not stated				
Walenkamp (282)	2015	Malunited radius fracture	Radius Corrective osteotomy	Prospective comparative cohort	Unclear	8	4	4		3D Printed: simulation	Surface	CT non contrast	Custom	Not stated	Material extrusion	Not stated	Not stated	No
Werner (338)	2017	Osteoarthritis	Total shoulder arthroplasty	Prospective comparative cohort	All patients assessed by each method	50	50	50		Computer-assisted planning	Surface	CT non contrast	Imascap	Not stated				
Wong (291)	2018	Femoeroacetabular impingement	Femur osteoplasty	Retrospective cohort	All patients assessed by each method	10	10	10		3D Printed: simulation	Surface	CT non contrast	3D Slicer	Not stated	Material extrusion	$3	2 hr 37 min	No
Yang (268)	2017	Humeral Condyle and radial head fracture	Elbow ORIF (plate)	RCT	Simple	40	20	20		3D Virtual: anatomical visualisation	Surface	CT non contrast	Materialise Mimics	Not stated	Material extrusion	$3	2.5hr	No
Yang (270)	2016	Trimalleolar ankle fracture	Ankle ORIF (plate)	RCT	Simple	30	15	15		3D Virtual: anatomical visualisation	Surface	CT non contrast	Materialise Mimics	Not stated	Material extrusion	$2	2.5hr	No
Zhang (296)	2017	Shoulder dislocation	Coracoid osteotomy	Retrospective comparative cohort	Unclear	78	34	44		Computer-assisted planning	Volumetric	CT non contrast	Materialise Mimics	Not stated				
Zhang (271)	2015	Tibial plateau fractures	Tibia plateau ORIF (plate)	RCT	Simple	32	14	18		Computer-assisted planning	Volumetric	CT non contrast	Materialise Mimics	Not stated				
Zhao (269)	2016	Thoracolumbar fractures, lumbar disk herniation, lumbar canal stenosis, lumbar spondylolisthesis	Lumbar spine surgery	RCT	Simple	23	23	23		Computer-assisted planning	Not stated	CT non contrast	Centricity Radiology RA 600	Not stated				
Zheng (272)	2017	Intertrochanteric proximal femoral fracture	Intramedullary hip screw	RCT	Simple	39	19	20		Computer-assisted planning and 3D printed cutting guides	Not stated	CT non contrast	M3D MedGraphics	Surgeon	Not stated	Not stated	Not stated	No
Zheng (295)	2017	Distal Humerus fractures	Humerus ORIF (plate)	RCT	Simple	91	43	48		3D Printed: simulation	Volumetric	CT non contrast	Materialise Mimics	Not stated	Not stated	Not stated	Not stated	Yes
Zheng (273)	2017	Calcaneal fractures	Calcaneal ORIF (plate and screw)	RCT	Simple	75	35	40		3D Printed: simulation	Volumetric	CT non contrast	Materialise Mimics	Not stated	Not stated	Not stated	Not stated	Yes

Table 3-14 Summary of study design and 3D interventions in Plastic/Breast Surgery

Zhao (327)	2018	Congenital cardiac disease	Congential cardiac disease procedure	Comparative cohort	Unclear	25	8	17		3D Printed: anatomical visualisation	Volumetric	CT Angio	Materialise Mimics	Not stated	Not stated	Not stated	Not stated	No
Author	Year	Pathology	Procedure	Study Design	Allocation	Total (n)	3D (n)	2D (n)	Other comp (n)	3D intervention	Rendering	Imaging	Segmentation Software	Produced	Printing method	Cost 3DP	Print time	Used in theare
Li (339)	2014	Multiple soft tissue defects	Sural neurovascular island flap	RCT	Simple	40	20	20		Computer-assisted planning	Volumetric	CT Angio	Amira 4.1	Not stated				
Gacto-Sanchez (340)	2010	Breast cancer	Mastectomy and reconstruction	Prospective cohort with retrospective controls	Time	70	35	35		Computer-assisted planning	Volumetric	CT Angio	VirSSPA					
Zhang (341)	2019	Breast ccancer	Mastectomy and reconstruction	RCT	Simple	96	52	44		Computer-assisted planning	Not clear	CT not defined	MI-3DVS					

Table 3-15 Summary of study design and 3D interventions in cardiac surgery

Author	Year	Pathology	Procedure	Study Design	Allocation	Total (n)	3D (n)	2D (n)	Other comp (n)	3D intervention	Rendering	Imaging	Segmentation Software	Produced	Printing method	Cost 3DP	Print time	Used in theare
Garekar (325)	2016	Double outlet right ventricular septal defect	Congential cardiac disease procedure	Prospective cohort	All patients assessed by each method	6	6	6		3D Printed: anatomical visualisation	Unclear/ Not stated		Not stated	Not stated	Color jet	Not stated	Not stated	No
Valverde (326)	2017	Congential cardiac disease	Congential cardiac disease procedure	Prospective comparative cohort	All patients assessed by each method	40	40	40		3D Printed: anatomical visualisation	Surface	CT and MRI	ITK-SNAP	Surgeon	Material extrusion	Not stated	35 hrs	No

4 Impact of 3D Reconstructions on Understanding of Mesenteric Vascular Anatomy

4.1 Background

Werner Hohenberger and colleagues first introduced the concept of complete mesocolic excision (CME) for colonic cancer (170). Central to the CME technique are three foundational principles: dissection along embryological planes, sufficient longitudinal bowel resection, and central vascular ligation coupled with the excision of central aspects of the mesocolon (342). CME represents an advanced surgical procedure demanding a high level of technical skill. A key challenge to CME is navigating the complex mesenteric vascular anatomy, particularly for lesions in the right and transverse colon (342).

The central dissection performed in CME contains a risk of vascular injury, which has raised concerns about the safety of adopting this technique widely beyond high-volume expert centres (343,344). Results regarding the risk of vascular injury reported in two recent randomised trials are contradictory (345,346). However, central dissection does not appear to be associated with higher morbidity and mortality (173,347).

A detailed understanding of colonic and mesenteric anatomical variations is essential for preoperative planning and performing these extensive surgical procedures (348). Traditionally, this understanding is acquired by examining computed tomography (CT) datasets. However, translating the 3D anatomical relationships inferred from 2D images for intra-operative application presents a significant challenge, even for experienced surgeons (349). Moreover, clinically relevant anatomical variations are often underreported.

The advent of 3D reconstructed models from patient imaging data has the potential to enhance anatomical comprehension (350), serving as a valuable tool for surgical planning and execution (351). These 3D reconstructions, theoretically, offer advantages over conventional 2D imaging, yet their utility and reliability in mesenteric vessel visualisation have yet to be empirically validated in trainee or expert surgeons (352,353).

Building on this background, this chapter presents two complementary studies examining the impact of three-dimensional models on understanding mesenteric vascular anatomy across different levels of surgical expertise.

Study 1 investigates whether 3D reconstructions improve anatomical understanding among surgical trainees compared to a standardized CT interpretation protocol (AMIGO). Through a randomised crossover design involving 13 surgical trainees, the study evaluates the effectiveness of 3D models versus conventional 2D imaging for identifying key vascular structures relevant to CME. The primary research question is whether 3D visualisation enhances trainees' ability to recognise and understand complex mesenteric vascular relationships compared to traditional CT-based methods.

Study 2 examines the reliability and accuracy of 3D models versus standard CT imaging among expert CME surgeons. Through a two-phase assessment of inter-rater and intra-rater reliability involving four high-volume CME surgeons evaluating 66 cases, this study investigates whether 3D reconstructions can improve consistency and accuracy in identifying critical vascular anatomy among experienced practitioners. The core research question explores if 3D visualisation technology can enhance even expert-level interpretation of mesenteric vascular configurations.

Together, these studies aim to provide comprehensive evidence regarding the utility of 3D models across the spectrum of surgical expertise, from trainees to established experts. Their findings will help determine whether 3D visualization represents a valuable tool for improving anatomical understanding and potentially enhancing the safety and effectiveness of CME procedures.

4.2 The impact of three-dimensional reconstruction and standardised CT interpretation (AMIGO) on the anatomical understanding of mesenteric vascular anatomy for planning complete mesocolic excision surgery. A randomised cross-over study.

- **Aim:** Evaluate whether trainees gain a significantly improved understanding of mesenteric vascular anatomy using 3D models versus standardised CT interpretation protocols (AMIGO).
- **Hypothesis:** Exposure to 3D models will yield statistically higher objective assessment scores compared to standard CT interpretation.

4.2.1 Methods

Thirteen senior surgical trainees were recruited into a randomised, controlled, cross-over study conducted over one month. All higher trainees in general surgery within the United Kingdom were eligible to participate. A total of fifteen retrospective CT scans were selected. Two consultant gastrointestinal radiologists jointly reviewed each scan to establish the anatomical configuration of the mesenteric blood vessels and to confirm the corresponding three-dimensional (3D) reconstruction.

The trainees were randomly divided into two groups of unequal size (Group 1: n=6; Group 2: n=7). Each participant received an illustrated manual (see appendix 4.1) on complete mesocolic excision (CME) anatomy two weeks before the study day, and this manual remained available for reference throughout all assessment rounds. The same anatomical content was also reviewed during the initial instructional anatomy workshop on the study day.

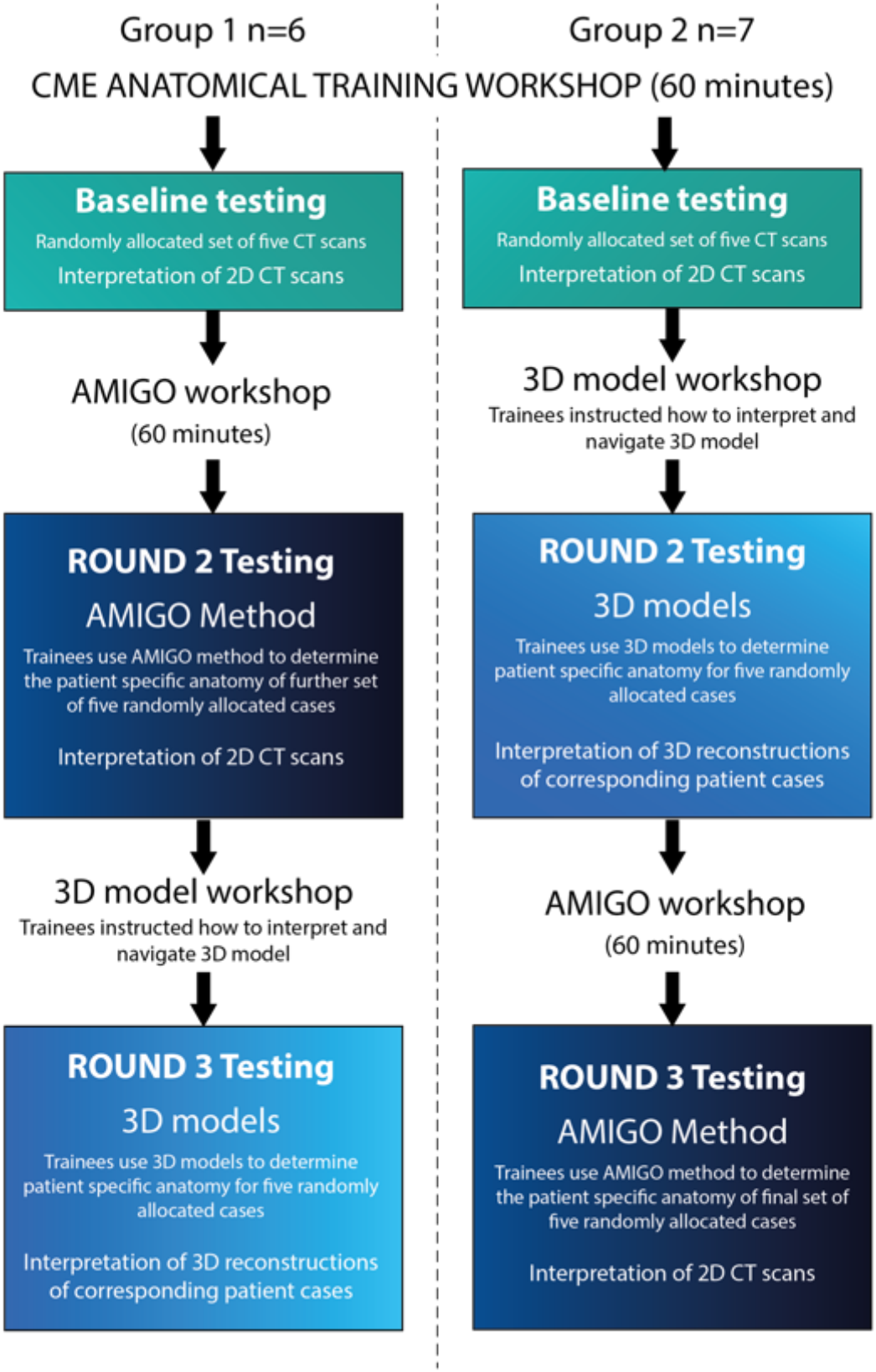
Three training workshops were provided sequentially:

1. Basic mesenteric vascular anatomy (90 minutes)
2. The AMIGO method for CT interpretation (60 minutes)
3. 3D model usage (10 minutes)

During the brief 3D model training, trainees were instructed on interacting with the model (panning, tilting, zooming). Trainees were not provided with formal interpretation guidelines or a structured approach to identifying vessels.

The fifteen patient cases were randomly assigned into three sets of five for each participant using a random sequence generator. Each set of five cases was assessed following one of the three workshops (basic anatomy, AMIGO, 3D models). Every trainee interpreted all fifteen cases, with each round of testing consisting of a randomly allocated set of five cases for each participant. No time limits were imposed on case interpretation at any stage. Figure 4-1 provides a schematic overview of the study design.

Figure 4-1 3D vs. AMIGO study flow diagram



4.2.1.1 Outcome measures

The primary outcome measure was an objective vascular anatomy knowledge score. This assessment tool was initially piloted with surgeons and radiologists external to the study to ensure its validity and reliability. The score was derived from a multiple-choice questionnaire designed by the investigators to evaluate participants' understanding of mesenteric vascular anatomy (Supplemental Data 1). Subjective user feedback using a custom Likert-scale questionnaire was a secondary outcome measure.

4.2.1.2 Sample size and power calculation.

Based on preliminary data, with an estimated effect size of 0.39, power set at 80%, and an α-level of 0.05, a sample size calculation indicated that 29 observations per group were required to detect a statistically significant difference among the three groups.

4.2.1.3 3D model production

3D surface rendered reconstructed models were produced for fifteen colon cancer patients using standard porto-venous phase computed tomography scans (1-2mm slice thickness). DICOM files were imported into segmentation software ITK-SNAP (Version 3.8, open-source). Segmentation was performed predominantly through manual methods. The larger arterial vessels (aorta, coeliac, and superior mesenteric arteries) were segmented using a region-based, algorithmic approach. In this process, segmentation was initiated from selected seed points, and adjacent voxels were iteratively included until predefined threshold parameters were no longer satisfied. In contrast, smaller-calibre vessels typically necessitated manual segmentation. Venous structures and organs were also segmented manually due to their homogeneity and indistinct boundaries within the surrounding anatomy.

All segmentations were initially completed by the primary investigator (JAF) and verified by two consultant radiologists to ensure accuracy. The mesenteric arterial and venous vessels, colon, stomach, duodenum, and pancreas were delineated for each model.

Verification consisted of a review of each scan to determine the vessel configuration, which was then matched against the segmentation results (and 3D reconstruction). Any discrepancy

between reviewers was resolved by mutual consensus. Corrections where necessary were then made to the finalised segmentation result.

PBR-rendered models with realistic texturing were produced for each case, as outlined in Chapter 2. Models were displayed on the online platform Sketchfab. At the time of the study, we had yet to utilise the Sketchfab API to give users control over model transparency; therefore, models' textures and each mesh component's opacity were static. Models can be viewed here at https://skfb.ly/prKzD.
Users could freely pan, tilt, and zoom models but lacked control over the transparency of the individual elements. The average time for segmentation was 84 minutes (range 50-120 mins) per case. Processing time and texturing ranged from 240- 350 minutes.

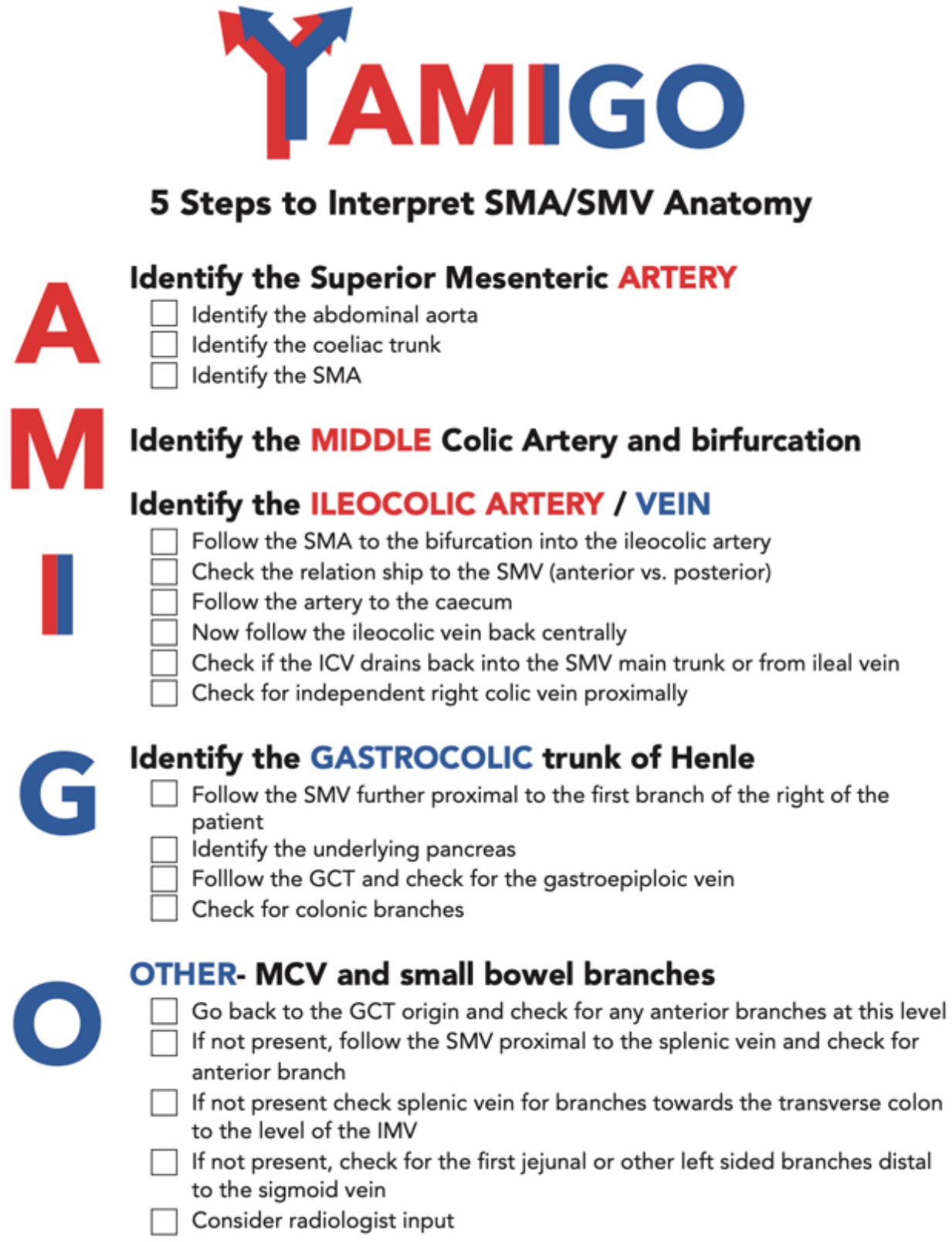
4.2.1.4 AMIGO Method

AMIGO is a mnemonic designed to facilitate the systematic analysis of mesenteric vascular anatomy for complete mesocolic excision (CME) procedures when interpreting two-dimensional (2D) cross-sectional computed tomography (CT) scans. This structured five-step checklist is applied when reviewing the CT and encompasses the following anatomical landmarks:

1. **A:** Identify the superior mesenteric **A**rtery (SMA).
2. **M:** Identify the **M**iddle colic artery (MCA).
3. **I:** Identify the Ileocolic artery and vein.
4. **G:** Identify the **G**astropancreaticocolic trunk (trunk of Henle).
5. **O:** Identify **O**ther relevant structures, such as the middle colic vein (MCV) and small bowel branches.

Prior to conducting the assessments, all participants underwent a training session with several work examples to ensure proficiency in using the AMIGO method (see Figure 4-2)

Figure 4-2 AMIGO CT interpretation checklist



4.2.1.5 Statistical Analysis

All statistical analyses were conducted using SPSS (Version 23, IBM). The Shapiro–Wilk test indicated a significant deviation from normality in the primary outcome measure ($W(195) = 0.967$, $p < 0.001$). Consequently, the differences between the median values for each group (Baseline, AMIGO, and 3D) were evaluated using the Kruskal–Wallis test.

4.2.2 Results

Thirteen general surgical trainees participated in the study. None had received formal instruction in CT interpretation; however, 11 of the 13 trainees reported informal, on-the-job training. Among the participants, five had no prior experience with complete mesocolic excision (CME), two had attended a related lecture, and six had either assisted or performed the procedure (in whole or in part). Demographic details of the trainee cohort are presented in Table 4-1.

Table 4-1 3D vs AMIGO Participant demographics

Length of training	
ST3-4	2
ST5-6	8
ST7-8	2
Post-CCT	1
Previous CT instruction	
None	2
Informal	11
Previous CME experience	
None	5
Lecture	2
Assisted	3
Performed	3

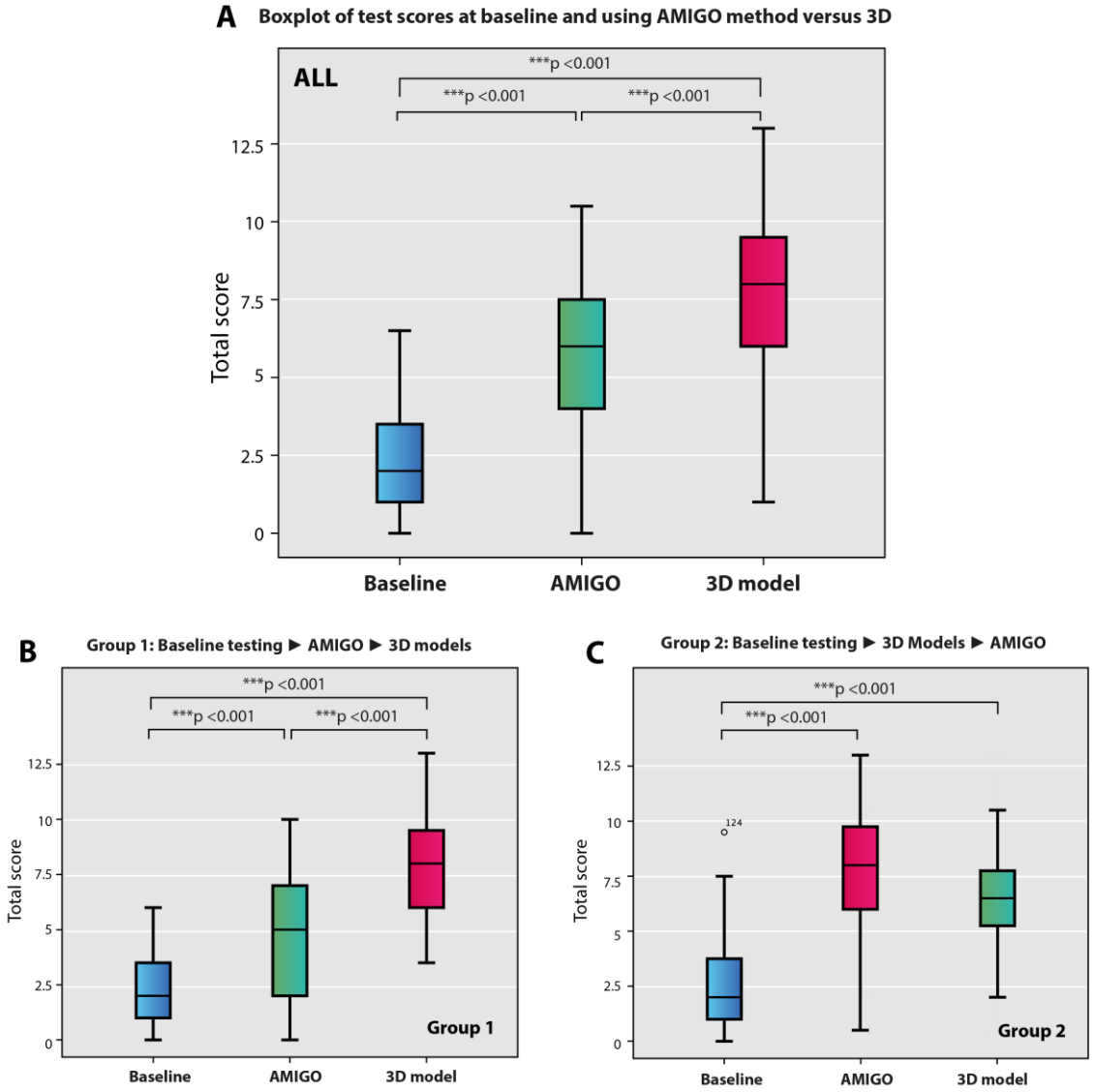
Compared with baseline testing, the use of three-dimensional (3D) models resulted in significantly improved performance, yielding a fourfold increase in median objective anatomy knowledge scores (median: 8.0 vs. 2.0, H (2) = 76.856, P < 0.001). Likewise, the AMIGO method enhanced anatomical understanding relative to baseline (median: 5.0 vs. 2.0, P < 0.001). Furthermore, trainees achieved substantially higher objective anatomy scores with 3D models compared to the AMIGO method, corresponding to a 60% improvement (median: 8 [3D] vs. 5 [AMIGO] vs. 2 [Baseline]; P < 0.001). Complete results are presented in Table 4-2.

Table 4-2 Summary of test scores overall and by study group at baseline and using AMIGO and 3D models (SD – standard deviation, maximum score = 14)

Group	Model	N case observations	Median	Range	IQR	Comparator	Average Score diff.	p-value
All	Baseline	65	2	0 -11	1.0-3.8			
	AMIGO	65	6	0-11	4.0-7.5	vs Baseline	+2.98	**<0.001**
	3D Model	65	8	1-13	6.0-9.5	vs Baseline	+5.13	**<0.001**
						vs AMIGO	+2.15	**<0.001**
1	Baseline	30	2	0-11	2.0-3.3			
	AMIGO	30	5	0-10	2.0-7.0	vs Baseline	+2.18	**0.005**
	3D Model	30	8	4-10	6.0-9.5	vs Baseline	+5.23	**<0.001**
						vs AMIGO	+3.05	**<0.001**
2	Baseline	35	2	0-10	1.0-4.0			
	AMIGO	35	6.5	2-11	5.0-8.0	vs Baseline	+3.66	**<0.001**
	3D Model	35	8	1-13	6.0-10.0	vs Baseline	+5.04	**<0.001**
						vs AMIGO	+1.39	0.066

Both the three-dimensional (3D) model approach and the AMIGO method significantly enhanced trainees' comprehension of mesenteric vascular anatomy compared with baseline assessments (see Figures 4-3B and 4C). In Group 1 (AMIGO first, then 3D), participants achieved markedly higher scores with 3D models than with AMIGO (median 8.0 vs. 5.0; p=0.001) (Figure 4-3B). Although 3D scores were also higher than AMIGO in Group 2 (3D first, then AMIGO), this difference did not reach statistical significance (median 8.0 vs. 6.5; p=0.264).

Figure 4-3 Mean scores for all candidates at baseline and using AMIGO method versus 3D models; B- Mean scores for group 1 at baseline and using AMIGO method versus 3D models; C- Mean scores for group 2 at baseline and using 3D models versus AMIGO



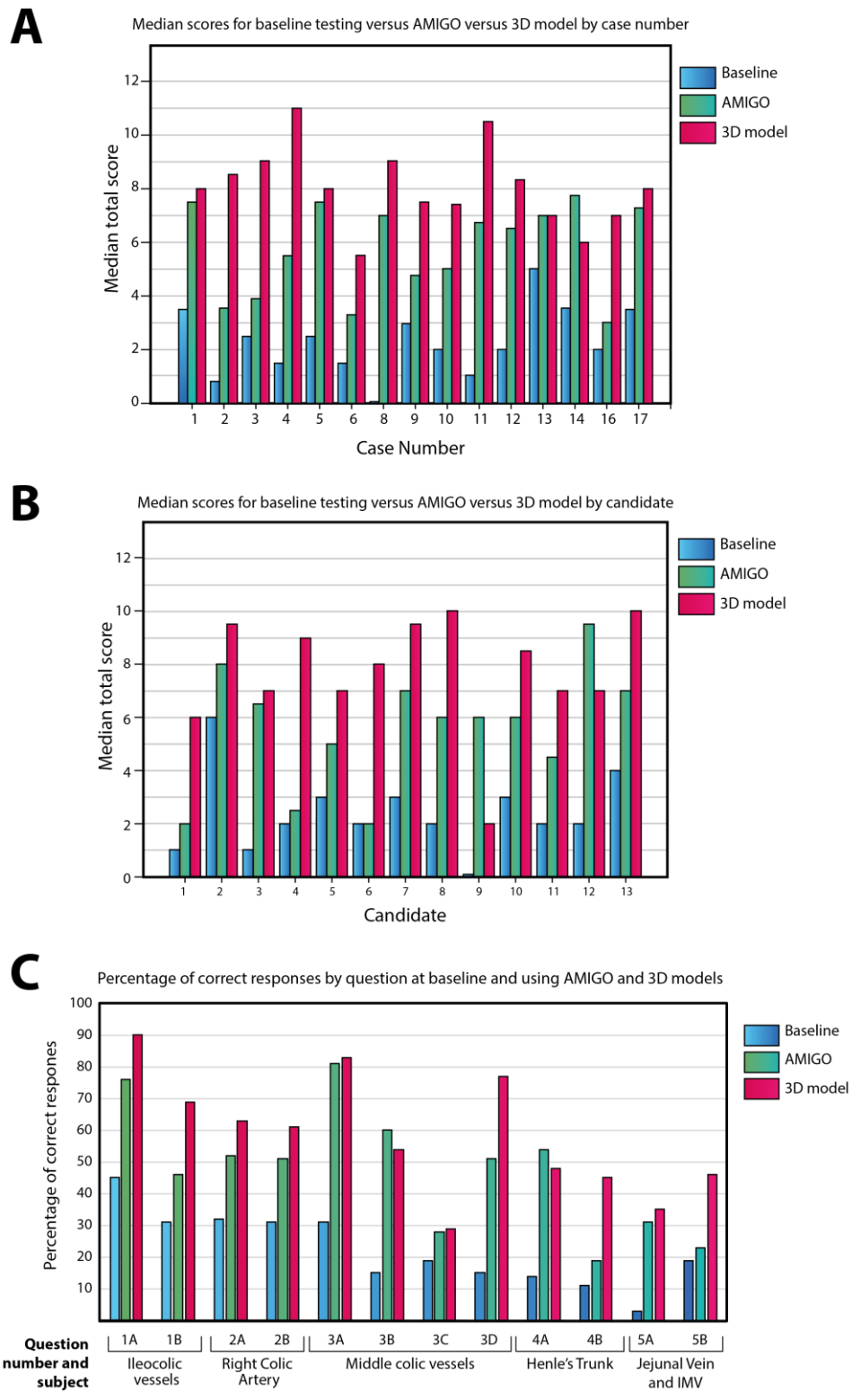
Examining the effect of 3D models by patient case, we observed a trend for improved scores for 3D over AMIGO and baseline. In 14/15 patient cases, 3D was superior to using the AMIGO method. 3D models and the AMIGO method improved anatomical understanding from baseline in each case (figure 4-4A). The median score per case improved by an average of 3.5x compared to the baseline.

All candidates improved their performance from baseline using both 3D and AMIGO. Eleven of thirteen candidates achieved higher test scores when using 3D models versus AMIGO (figure 4-4B) in both groups (table 4-2).

The percentage of correct responses varied according to the specific vessel in question and the interpretation method used (3D and AMIGO). Trainees could better identify each examined vessel using 3D and AMIGO than the baseline. However, for each vessel, the results for 3D were superior to those of AMIGO (Figure 4-4C).

At baseline, trainees correctly identified an average of 22.8% of mesenteric vessels (range: 3.1–44.6%), with substantial variation depending on the specific vessel examined. The ileocolic artery and vein were most accurately recognised, with correct identification rates increasing from 37.7% at baseline to 61.5% when using the AMIGO method and reaching 80% with 3D models. In contrast, the trunk of Henle proved more challenging, as correct responses increased from 12.4% at baseline to 36.2% with AMIGO and further improved to 61.6% with 3D.
Baseline recognition rates for the right and middle colic vessels were 31.6% and 22.3%, respectively. Using the AMIGO method, these values rose to 51.5% and 54.6%, while the introduction of 3D models led to further improvements, achieving correct identification rates of 62.3% for right colic and 60.8% for middle colic vessels.

Figure 4-4 *A) Mean scores for baseline testing versus AMIGO versus 3D model by case number; B) Mean scores for baseline testing versus AMIGO versus 3D model by the candidate; C) Percentage of correct responses by the question at baseline versus AMIGO versus 3D model*



4.2.2.1 Trainee performance by level of training and previous experience with CME

The level of trainee seniority significantly influenced overall performance on the anatomical knowledge assessment (Kruskal–Wallis $H(3) = 17.076$, $p < 0.001$). Senior trainees achieved higher objective knowledge scores than their junior counterparts (ST3–4 median: 5.25/16, IQR: 1.0–8.0; ST6 median: 5.0/16, IQR: 2.0–7.0; ST7–8 median: 6.25/16, IQR: 4.0–9.0; post-CCT fellow median: 9.0/16, IQR: 6.0–9.5).

Prior CME experience also significantly impacted performance (Kruskal–Wallis $H(3) = 16.975$, $p = 0.001$). Trainees who had previously performed CME procedures outperformed those with no hands-on CME experience (performed CME: median = 7.5/16, IQR: 5.25–9.5; attended lecture only: median = 3.25/16, IQR: 1.0–6.6, $p = 0.001$; no previous experience: median = 5.5/16, IQR: 2.0–7.0, $p = 0.004$).

4.2.2.2 Subjective user feedback

Twelve participants (92%) reported that the 3D models enhanced their understanding of mesenteric vascular anatomy. Furthermore, eleven candidates (85%) agreed or strongly agreed that using colour coding in the 3D models facilitated their comprehension. However, nine trainees indicated that they would not have been able to interpret the 3D models without prior instruction. Ten participants (77%) considered 3D models easier to interpret than the standard CT images used in the AMIGO approach, yet twelve (92%) preferred having both 2D CT scans and 3D reconstructions available in clinical practice.

As illustrated in Figure 5, ten and thirteen participants found it easier to identify most vascular structures using 3D models, reflecting the objective improvements observed in their assessment scores. On average, trainees rated all colonic vessels as more readily identifiable on 3D models (Table 4-3).

Participants were also invited to provide open-ended feedback. Key issues raised included limitations of the 3D user interface and the models themselves. Six trainees noted that the inability to adjust the transparency of individual structures hindered interpretation. Four candidates reported difficulty naming vessels that were truncated and did not extend fully to their organ of origin—an acknowledged limitation related to the imaging parameters and the inability to segment smaller-calibre vessels fully.

Table 4-3 Trainee subjective rating of ease of identifying colonic vessels using CT and 3D models

Vessel	Subjective ease of identification (Likert scale: 1 Very Difficult – 7 Very Easy)	
	Median	
	CT	3D
Superior Mesenteric Artery	5	6
Superior Mesenteric Vein	5	6
Ileocolic Artery	4	5
Ileocolic vein	4	6
Middle colic artery	3	6
Middle colic vein(s)	3	6
Henle's Trunk	2	5

4.3 Inter and intra-rater reliability of multi-slice CT and 3D Reconstructed Imaging Analysis of Mesenteric Vascular Anatomy for Planning and Performing Complete Mesocolic Excision

4.3.1 Study Aims

The objectives of the study are twofold: first, to compare the inter- and intra-rater reliability of three-dimensional (3D) models against standard computed tomography (CT) scans for evaluating mesenteric vascular anatomy relevant to complete mesocolic excision (CME), and second, to determine the accuracy of each imaging modality in identifying these vascular configurations.

4.3.2 Method

4.3.2.1 Outcome measure

The primary outcome measure was an objective vascular anatomy knowledge questionnaire (Appendix 4.3) developed by the research team to evaluate participants' comprehension of mesenteric vascular anatomy within a clinically relevant context of right-sided complete mesocolic excision (CME).

4.3.2.2 Participant Selection and Data Collection

Four expert CME surgeons were recruited for this investigation, three regularly serving as instructors for the European Society of Coloproctology Minimally Invasive Training Course (348). The fourth surgeon possessed substantial practical experience in performing CME. Information was collected regarding each surgeon's prior CME experience and standard preoperative planning practices.

Sixty-six patient cases were randomly selected for analysis from a prospectively maintained CME database containing 100 total reconstructed scans using a random number generator to create a sequence from 1 to 100. The first 66 unique numbers drawn corresponded to the

cases included in the study. Three-dimensional reconstructions were created by manually segmenting (JF) each CT scan using the open-source software ITK-SNAP (Version 3.8) (20) and subsequently validated by a consultant gastrointestinal radiologist (PL). Segmentation times were recorded to the nearest five minutes. Polygon mesh models were then generated from the segmentation files following the methodology described in Chapter 2.

Verification of each reconstruction was performed by JF and PL, drawing upon intra-operative video footage (see Chapter 5) sourced from the prospectively maintained CME database. Before the study, the participating surgeons received a detailed manual defining all relevant mesenteric vessels (Appendix 4.1 and 4.3) and a tutorial on using the 3D models. To ensure blinding, the CT data and the corresponding 3D models were assigned random identifiers, preventing the surgeons from associating any individual reconstruction with its original CT scan.

4.3.2.3 Testing Procedure and Analysis

The study was conducted in two rounds. In the first round, participants completed a multiple-choice anatomical questionnaire (see Appendix 4.2) for each of the 66 cases, using CT data and 3D models, or vice versa, resulting in 132 assessments. After a three-month washout period, a second round of testing was conducted. This time, 20 cases were randomly selected from the original 66, and participants again completed the questionnaire using both 3D models and CT imaging. Each case was re-encoded to preserve blinding so that participants could not associate the models and CT scans from the first round.

All responses were recorded electronically using Microsoft Forms (Microsoft Corp., 2023).

4.3.2.4 Data Analysis

Data analysis was conducted using Microsoft Excel (Microsoft Corp. 2023) and custom Python 3.4 scripts within a Jupyter Notebook environment (354), offering a reproducible and transparent computational framework. Data manipulation and analysis were performed using Python libraries: Numpy (195) and Pandas (355) for data handling, Matplotlib (213) and Seaborn (356) for visualisation, and SciPy (196) and Stats for statistical analysis.

Fleiss' kappa values were calculated for each single-response question to calculate inter-rater reliability in the first round. This measure is suited to assessing agreement among multiple raters. For questions requiring multiple responses, a one-hot encoding approach was applied to transform each response into binary indicators, facilitating subsequent analyses. The mean kappa value for each question was then derived to provide an overall measure of rater consensus.

Kappa results were interpreted as follows: values ≤ 0 as indicating no agreement, 0.01–0.20 as none to slight, 0.21–0.40 as fair, 0.41– 0.60 as moderate, 0.61–0.80 as substantial, and 0.81–1.00 as almost perfect agreement (357).

The average agreement was quantified as the percentage of identical responses provided by each rater for each case and question, thereby reflecting the consistency of their assessments. Intra-rater reliability for both imaging modalities—CT and 3D models—was evaluated using Cohen's kappa values, complemented by calculating average agreement (the percentage of matched responses between rounds).

The mean number of correctly identified anatomical structures per case was determined for each participant. The benchmarks for correct anatomy in each case were established through previous intraoperative observations and a review of the imaging by a GI radiologist with expertise in CME anatomical evaluation. As the data did not meet normality assumptions (as confirmed by the Shapiro–Wilk test), non-parametric statistical methods were employed for comparative analysis. Specifically, the Mann–Whitney U test was used to examine differences in anatomical identification accuracy between the 3D reconstructions and the multi-slice CT datasets.

4.3.2.5 Sample Size Determination

The study analysed data from 66 patient cases. The sample size was calculated based on an estimated kappa value of 0.7, which falls within the 'good' agreement range of 0.6 to 0.8, providing a confidence interval of ± 0.12.

4.3.3 Results

4.3.3.1 Participating surgeon demographics

The CME operative and imaging interpretation experience and preoperative planning practices of each participating surgeon are outlined in Table 4-4.

Table 4-4: *CME experience and preoperative planning practices of participating surgeons*

Surgeon	CB	EVE	AS	KS
Operative experience				
Number of years performing CME	**16**	**5**	**8**	**17**
Number of CME performed	**700**	**120**	**400**	**1100**
Open	250	0	20	100
Laparoscopic	450	0	380	1000
Robotic	0	120	0	0
Preoperative planning processes and imaging interpretation experience				
Reviews CT imaging pre-operatively to determine vascular anatomy	Yes- alone	Yes- alone	Yes-alone	Yes-alone
Does the radiology report contain any information regarding anatomical variants?	No	No	No	No
Formal training in CT interpretation for CME anatomy?	Taught on course	None	Taught on course	Taught on course
Do you use 3D reconstructed models to plan and perform CME?	No	No	No	No

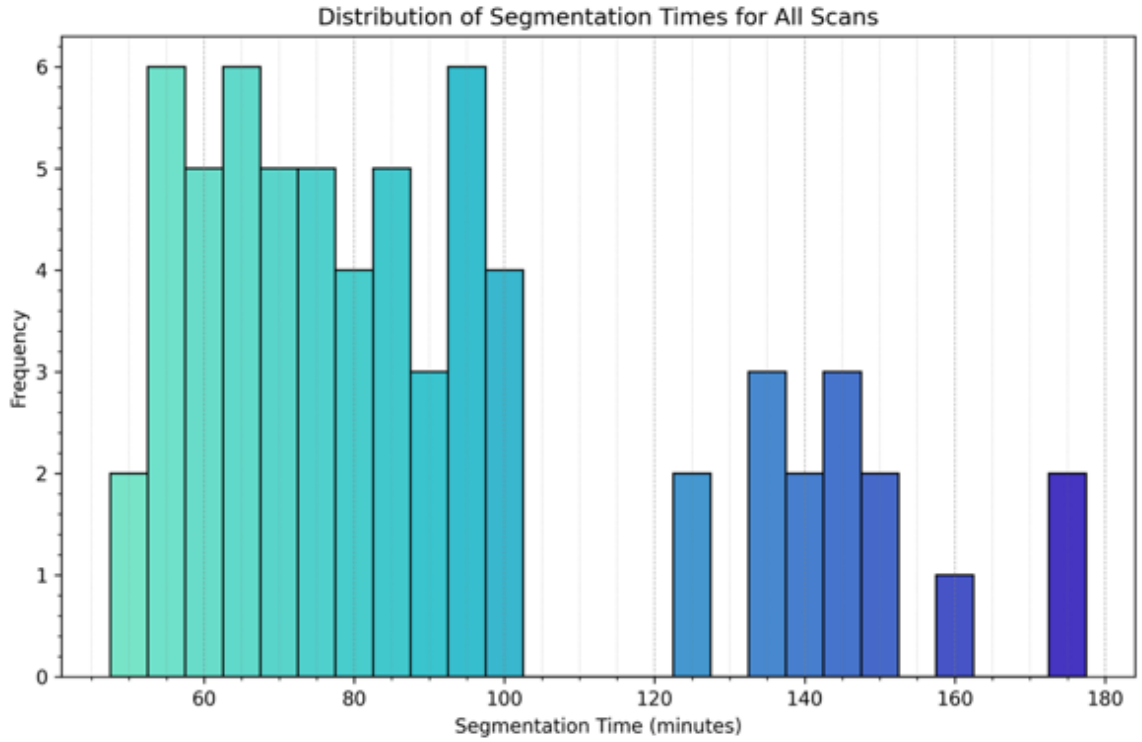
4.3.3.2 Segmentation time

Table 4-5 presents the segmentation times for each type of scan, while Figure 4-5 shows how these times were distributed across the dataset.

Table 4-5: *Segmentation times summary as per scan protocol and slice thickness*

Scan Category	n	Time (min)				Total Segmentation time (min)
		Median	IQR	Min	Max	
CT PV contrast (Slice thickness ≤1mm)	4	140	3.75	135	150	565
CT PV contrast (Slice thickness >1-≤2.5mm)	47	75	25	50	100	3600
CT PV contrast (Slice thickness >2.5mm)	4	57.5	7.5	50	65	230
CT colon	11	145	20	125	175	1615

Figure 4-5 Distribution of Time Required for 3D Model Generation. Histogram showing the frequency of cases by segmentation duration (minutes).



4.3.3.3 Inter-rater reliability

The Fleiss Kappa statistical analysis (Table 4-6) conducted for Round 1 inter-rater reliability across 66 cases demonstrated a substantially better agreement for most anatomical landmarks when the 3D models were used. The overall Fleiss Kappa was 0.6 for 3D and 0.1 for CT.

Table 4-6: Comparative Inter-Rater Reliability Measured by Fleiss' Kappa for CT and 3D Imaging Modalities During Round 1. This table enumerates the Fleiss' Kappa statistics for each anatomical question, assessing raters' agreement when using CT and 3D imaging techniques. Colour key for Fleiss' Kappa values: RED: κ = 0-<0.2 (poor agreement) ORANGE: κ = 0.21-0.40 (fair agreement) YELLOW: κ = 0.41-0.60 (moderate agreement) LIGHT GREEN: κ = 0.61-0.80 (good agreement) GREEN: κ= 0.81-1.00 (very good agreement)

Question	CT	3D
ICV Drainage	0.13	0.85
ICA trajectory	0.56	0.93
RCA present?	0.02	0.79
RCA trajectory	0.02	0.75
RCV present?	0.04	0.25
RCV Drainage	0.03	0.32
No. of MCA Trunks	0.01	0.47
Origin of MCA	0.15	0.75
No of MCV trunks	0.10	0.18
MCV drainage	0.25	0.43
Constituent vessels of Henle	0.14	0.50
Henle class	0.14	0.62
No. of ASPDV	0.05	0.59
ASPDV drainage	0.08	0.73
1st Jejunal vein trajectory	0.30	0.57

4.3.3.4 Intra-rater reliability

As measured by Cohen Kappa values, the intra-rater reliability for CT and 3D imaging modalities demonstrated a range of agreement across the anatomical structures assessed. The average Cohen Kappa values were higher for 3D when compared to CT, as shown in Table 4-7.

Table 4-7: Intra-Rater Reliability Assessment Using Cohen's Kappa for CT Versus 3D Imaging Across Anatomical Questions. This table quantifies the consistency of each rater's responses between rounds 1 and 2 by presenting Cohen's Kappa values for both CT and 3D imaging modalities. *Colour key for Fleiss' Kappa values: RED: κ = 0-<0.2 (poor agreement) ORANGE: κ = 0.21-0.40 (fair agreement) YELLOW: κ = 0.41-0.60 (moderate agreement) LIGHT GREEN: κ = 0.61-0.80 (good agreement) GREEN: κ= 0.81-1.00 (very good agreement)*

Intra-rater Cohen Kappa values for CT and 3D image modalities										
Question	Rater 1		Rater 2		Rater 3		Rater 4		Average Cohen Kappa	
	CT	3D	CT	3D	CT	3D	CT	3D	**CT**	**3D**
ICV Drainage	0.0	0.6	1.0	1.0	0.5	0.6	0.0	0.8	**0.37**	**0.76**
ICA trajectory	0.9	0.8	0.7	1.0	0.7	0.9	0.5	1.0	**0.68**	**0.92**
RCA present?	0.2	0.6	0.4	0.5	0.1	0.7	0.0	0.7	**0.18**	**0.63**
RCA trajectory	0.1	0.6	0.4	0.5	0.0	0.7	0.0	0.6	**0.13**	**0.62**
RCV present?	0.6	0.2	0.3	0.7	0.0	0.2	0.0	0.4	**0.22**	**0.37**
RCV Drainage	0.7	0.3	0.4	0.7	0.0	0.2	0.2	0.4	**0.32**	**0.42**
No. of MCA Trunks	0.0	0.6	0.0	0.6	0.0	0.5	0.1	0.7	**0.03**	**0.59**
No of MCV trunks	0.0	0.2	0.4	0.4	0.3	0.2	0.3	1.0	**0.25**	**0.46**
Henle class	0.1	0.4	0.2	0.9	0.1	0.8	0.2	0.7	**0.17**	**0.69**
ASPDV	0.0	0.7	0.4	0.8	0.3	0.7	0.4	0.7	**0.30**	**0.70**
1st Jejunal vein trajectory	0.3	0.7	0.4	0.7	0.4	0.8	0.5	0.1	**0.39**	**0.56**

4.3.3.5 Accuracy

In a direct comparison of diagnostic accuracy, three-dimensional (3D) imaging consistently produced higher correct vessel identification rates than computed tomography (CT) across all evaluators. In the first round (66 cases), the mean percentage of correct responses for CT ranged from 76% to 85%, whereas 3D imaging yielded higher mean percentages between 87% and 93% (Table 4-8, Figure 4-6). This trend persisted in the second round (20 cases), with CT yielding correct response rates of 78% to 83% and 3D imaging demonstrating improved accuracy, ranging from 87% to 90% (Table 4-8).

Table 4-8 Mean percentage of correct responses for CT and 3D imaging modalities by rater. Box and whisker plots depicting the distribution of correct responses percentages for each rater are provided in Figure 1-7.

		CT correct responses (%)				3D correct responses (%)				p-value
		Mean	Min	Max	SD	Mean	Min	Max	SD	
ROUND 1 n= 66	Rater 1	**79**	49	97	11.7	**90**	68	100	7.5	p<0.001
	Rater 2	**85**	68	100	8.7	**92**	68	100	7.9	p<0.001
	Rater 3	**76**	49	97	11.8	**93**	76	100	6.0	p<0.001
	Rater 4	**77**	51	97	9.7	**87**	60	100	10.0	p<0.001
ROUND 2 n= 20	Rater 1	**81**	70	100	8.2	**87**	70.3	100	7.2	p<0.001
	Rater 2	**83**	62	97	9.1	**90**	78.4	100	5.8	p<0.001
	Rater 3	**80**	62	97	12.0	**88**	51.4	100	11.7	p<0.001
	Rater 4	**78**	65	100	9.2	**87**	67.6	100	9.5	p<0.001

Minimum correct response rates in the first round ranged from 49% to 68% for CT and from 60% to 76% for 3D imaging. In the second round, the minimum percentages for CT increased slightly to 62%–70%, while for 3D, they were 51%–78%. Both modalities achieved maximum correct response rates of up to 100% across both rounds. The standard deviation of correct responses was consistently lower for the 3D imaging modality, indicating greater uniformity among raters when using these reconstructions. Statistically significant differences in accuracy between the two imaging techniques were observed, with all p-values below 0.001 for every rater in both rounds (Figure 4-7).

Figure 4-6 Box Plot Analysis of Average Correct Response Rates by Imaging Modality. This box plot contrasts the distribution of the average percentage of correct responses for each rater using CT (shown in blue) and 3D imaging modalities (shown in orange). The central line in each box represents the median percentage, the box itself shows the interquartile range (IQR), and the whiskers extend to the range of data points.

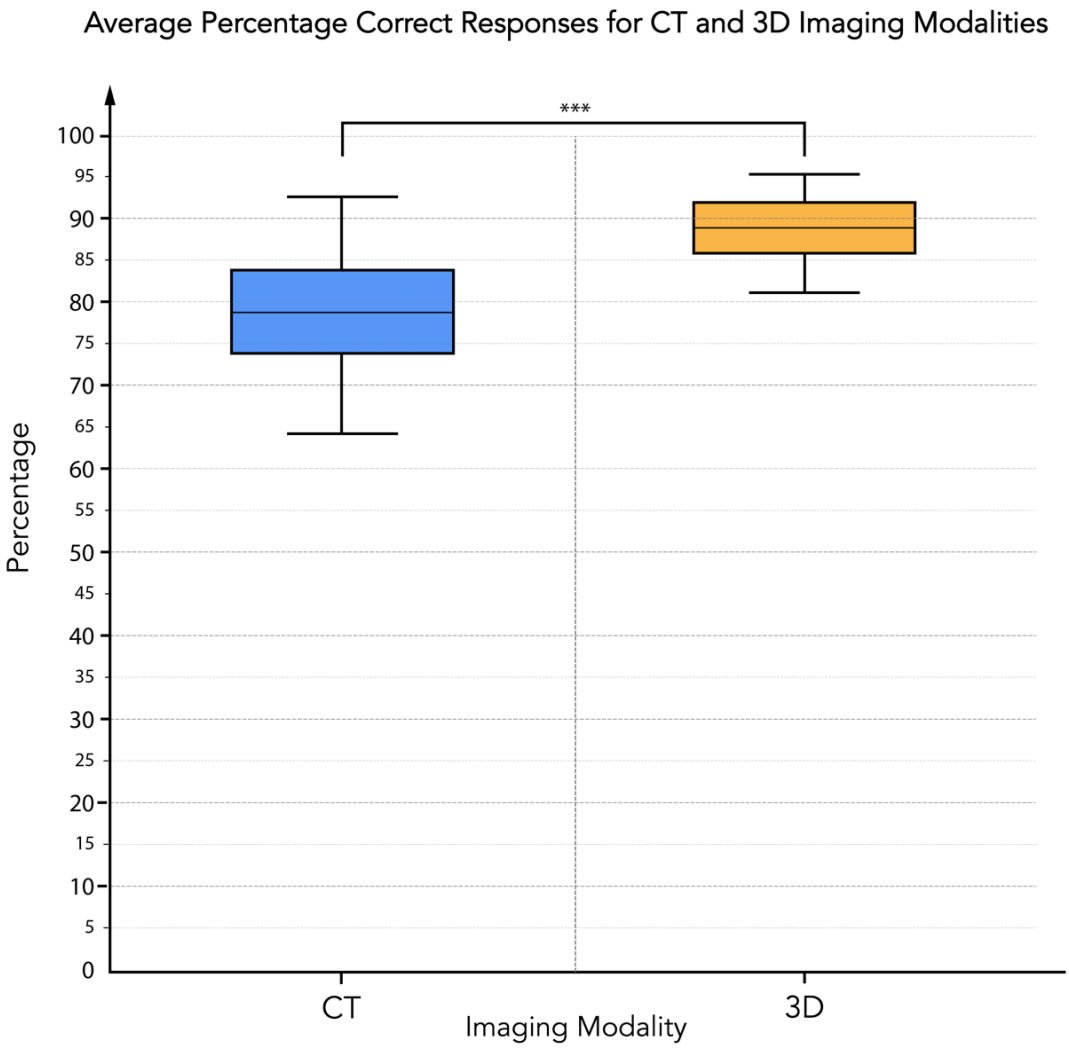
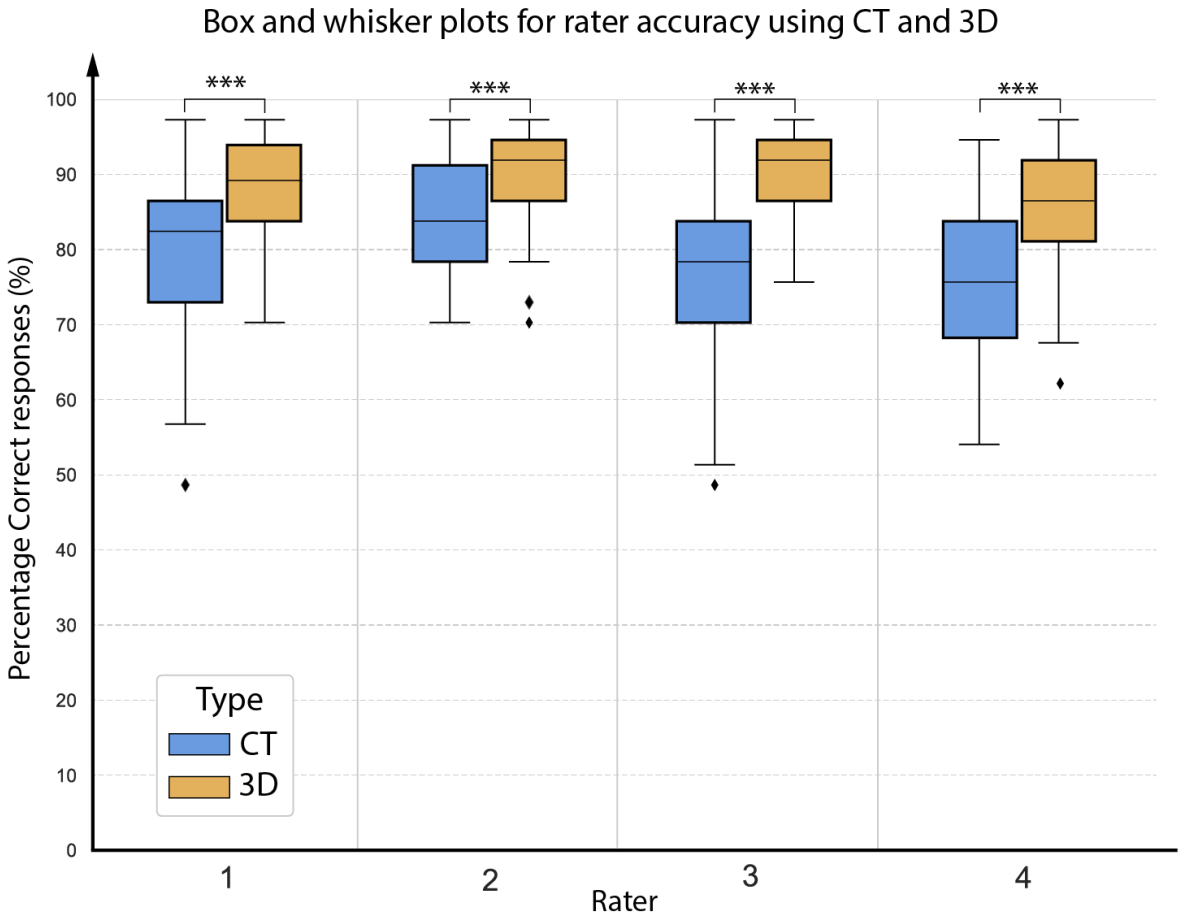


Figure 4-7 Box Plot Distribution of Rater Accuracy Using CT and 3D Imaging Modalities. The correct response for raters 1-4. Each rater has a pair of box plots where the blue box represents the distribution of correct responses when using CT imaging, and the orange box corresponds to 3D imaging. The central line in each box indicates the median accuracy, the box limits represent the interquartile range (IQR), and the whiskers extend to the furthest point within 1.5 times the IQR from the box. Outliers are represented as individual points outside the whiskers.



4.3.3.6 Performance of 3D models relative to CT imaging by case and rater

In the initial round of case assessments, three-dimensional (3D) virtual models enhanced diagnostic accuracy in 62 of the 66 cases (94%) compared with CT imaging alone. Across all raters, the median accuracy improvement was 10.1 percentage points (IQR: 10.8%). Improvements varied considerably by case, ranging from a decrease of 7.4 percentage points to an increase of 29.1 percentage points (Figure 4-8).

In the second round, comprising 20 cases, 3D reconstructions outperformed CT in 18/ 20 cases (90%). The median accuracy improvement was 7.8 percentage points (IQR: 8.5%), with a narrower range from -5.4 to +19.6 percentage points (Figure 4-9). Correct responses for each case per round of testing for each rater can be visualised in figures 4-10 and 4-11.

When examining results by individual surgeons, median accuracy enhancements ranged from 6.1 to 17.9 percentage points in the first round and from 4.8 to 10.5 points in the second round. Despite these substantial median improvements, the wide interquartile ranges indicated notable variability between different raters and the cases they assessed.

Overall, Raters 1–4 demonstrated higher accuracy using CT alone in 12%, 17%, 8%, and 14% of cases, respectively.

Figure 4-8 Differential Rater Performance in Correct Responses Using CT Imaging Versus 3D Models for Round 1. The bar chart illustrates the average absolute percentage difference in correct responses for each case, with the green bars representing the aggregated data. The overlaid scatter plot depicts individual rater performance, with each rater denoted by a unique colour and symbol.

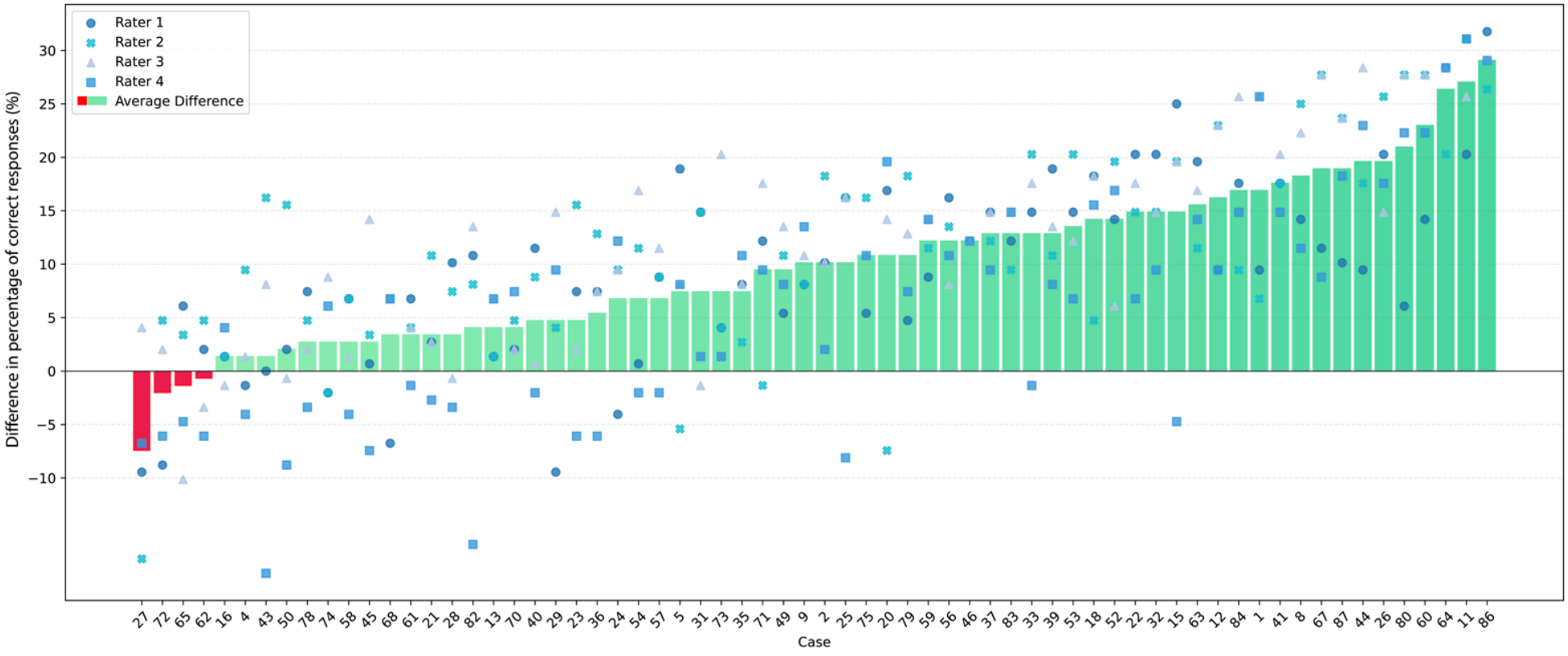


Figure 4-9 Differential Rater Performance in Correct Responses Using CT Imaging Versus 3D Models for Round 2. The bar chart illustrates the average percentage difference in correct responses for each case, with the green bars representing the aggregated data. The overlaid scatter plot depicts individual rater performance, with each rater denoted by a unique colour and symbol

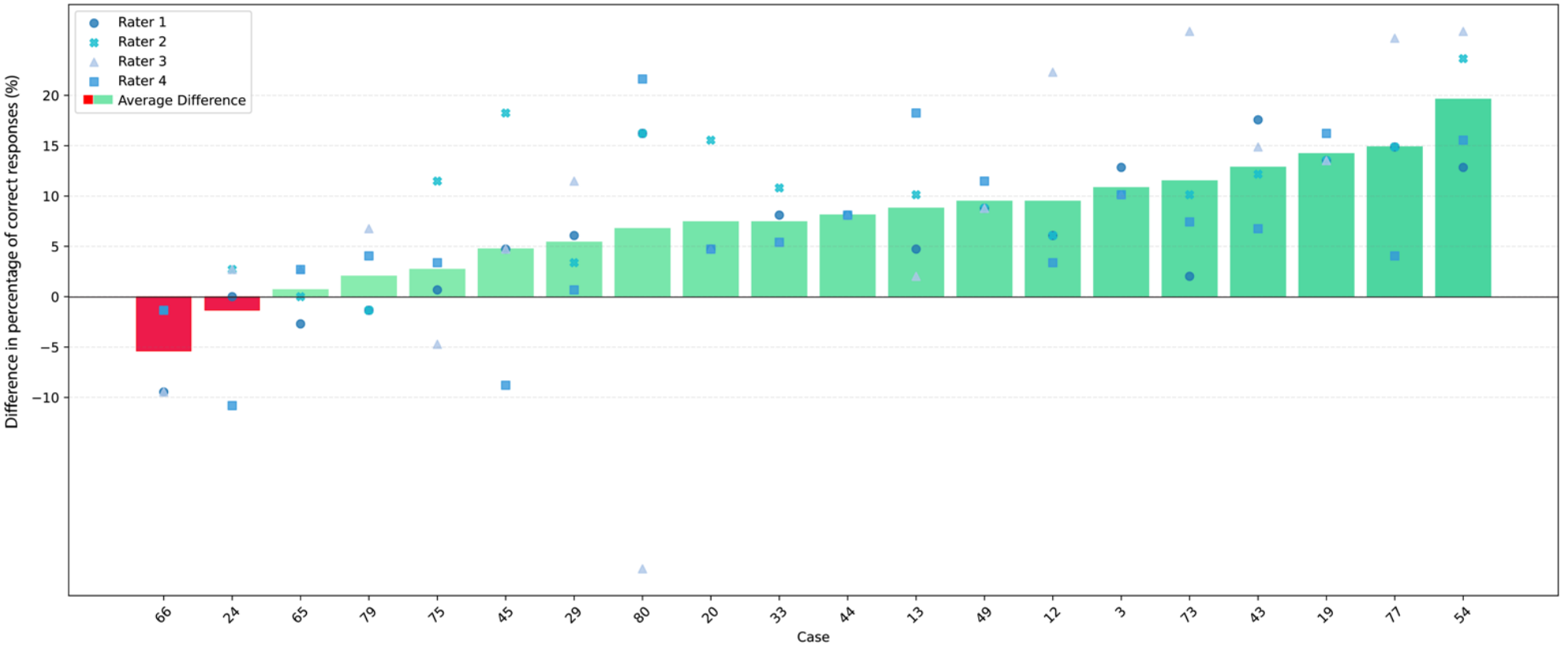


Figure 4-10 Individual Rater Accuracy Comparison by Case in ROUND 1 Using CT and 3D Models. This series of line graphs illustrates the percentage of correct responses for each case by four separate raters in the second evaluation round. The accuracy is compared between two diagnostic tools: CT imaging (depicted in blue) and 3D modelling (depicted in orange). Each graph corresponds to one of the four raters, with the x-axis representing individual cases and the y-axis showing the accuracy percentage. Data points on the lines indicate the accuracy achieved by the respective rater for each case using the specified imaging modality.

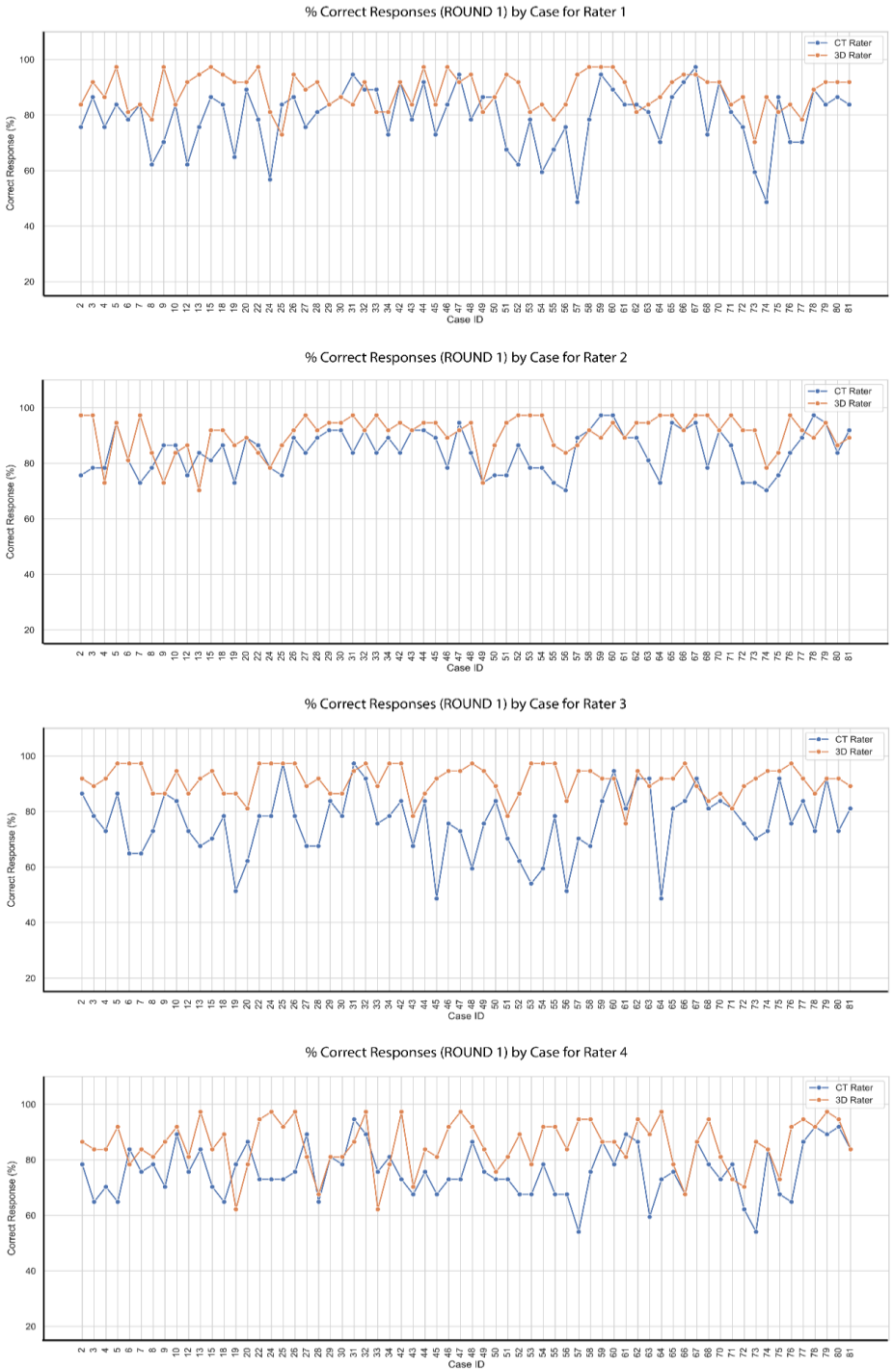
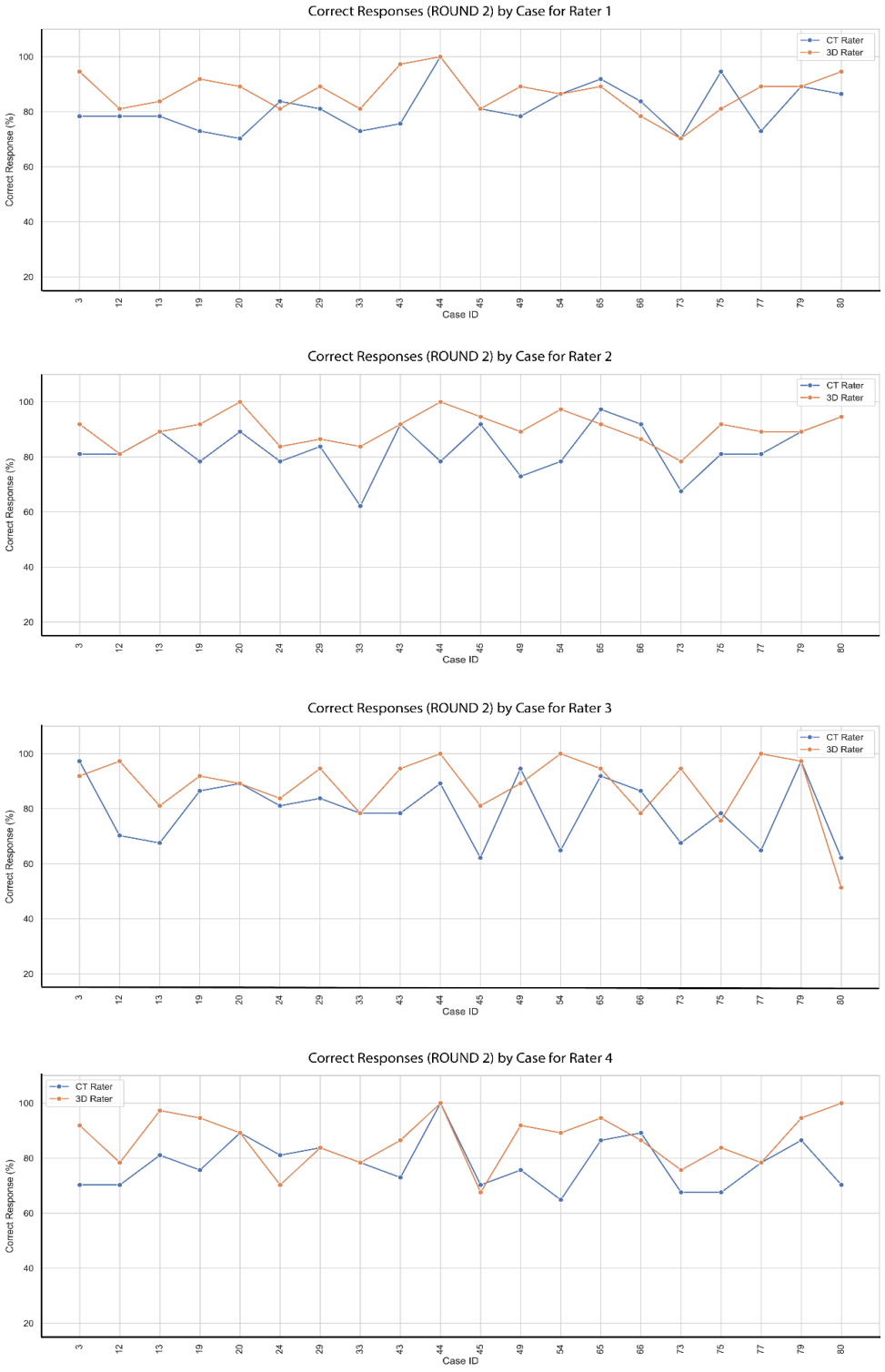


Figure 4-11 Individual Rater Accuracy Comparison by Case in ROUND 2 Using CT and 3D Models. This series of line graphs illustrates the percentage of correct responses for each case by four separate raters in the second evaluation round. The accuracy is compared between two diagnostic tools: CT imaging (depicted in blue) and 3D modelling (depicted in orange). Each graph corresponds to one of the four raters, with the x-axis representing individual cases and the y-axis showing the accuracy percentage. Data points on the lines indicate the accuracy achieved by the respective rater for each case using the specified imaging modality.



4.3.3.7 Accuracy by mesenteric vessel

Examining the percentage of correct responses per question revealed that, for most assessed anatomical features, three-dimensional (3D) imaging consistently produced higher accuracy rates than computed tomography (CT) (Table 4-9 and Figure 4-12). A Mann–Whitney U test further supported this finding, demonstrating a statistically significant difference in rater accuracy between CT and 3D approaches ($U = 62.0$, $p = 0.038$).

Table 4-10 comprehensively summarises correct responses stratified by the specific anatomical variant.

Table 4-9: Number(n) and per cent correct responses (%) for each anatomical questionnaire item for CT and 3D.

Correct response percentage for each rater using CT and 3D imaging modalities																		
Question	RATER 1				RATER 2				RATER 3				RATER 4				% average correct responses	
	CT		3D		CT		3D		CT		3D		CT		3D			
	n	%	n	%	n	%	n	%	n	%	n	%	n	%	n	%	CT	3D
ICV Drainage	60	91	64	97	66	100	65	98	53	80	65	98	58	88	65	98	**89.8**	**98.1**
ICA trajectory	58	88	64	97	66	100	66	100	55	83	66	100	51	77	64	97	**87.1**	**98.5**
RCA present?	55	83	64	97	54	82	65	98	38	58	64	97	50	76	59	89	**74.6**	**95.5**
RCA trajectory	55	83	61	92	52	79	63	95	36	55	62	94	47	71	57	86	**72.0**	**92.0**
RCV present?	29	44	20	30	22	33	13	20	15	23	17	26	18	27	23	35	**31.8**	**27.7**
RCV Drainage	30	45	46	70	44	67	51	77	36	55	48	73	41	62	43	65	**57.2**	**71.2**
No. of MCA Trunks	59	89	62	94	52	79	59	89	47	71	61	92	45	68	61	92	**76.9**	**92.0**
Origin of MCA	65	99	66	100	66	99	66	100	65	98	66	100	65	99	65	98	**98.8**	**99.6**
No of MCV trunks	35	53	45	68	39	59	45	68	29	44	46	70	30	45	37	56	**50.4**	**65.5**
MCV drainage	53	80	58	88	57	87	60	90	54	82	61	92	54	81	57	86	**82.5**	**89.0**
Constituent vessels of Henle	51	78	57	87	54	82	60	91	51	77	61	92	51	77	56	85	**78.6**	**89.0**
Henle class	30	45	54	82	38	58	57	86	32	48	57	86	29	44	46	70	**48.9**	**81.1**
No. of ASPDV	23	35	38	58	38	58	44	67	34	52	41	62	28	42	36	55	**46.6**	**60.2**
ASPDV drainage	50	76	61	93	51	77	62	94	51	77	64	96	43	66	60	91	**73.9**	**93.8**
1st Jejunal vein trajectory	50	76	54	82	56	85	60	91	45	68	61	92	46	70	46	70	**74.6**	**83.7**

Figure 4-12 Average correct responses by question using CT and 3D models.

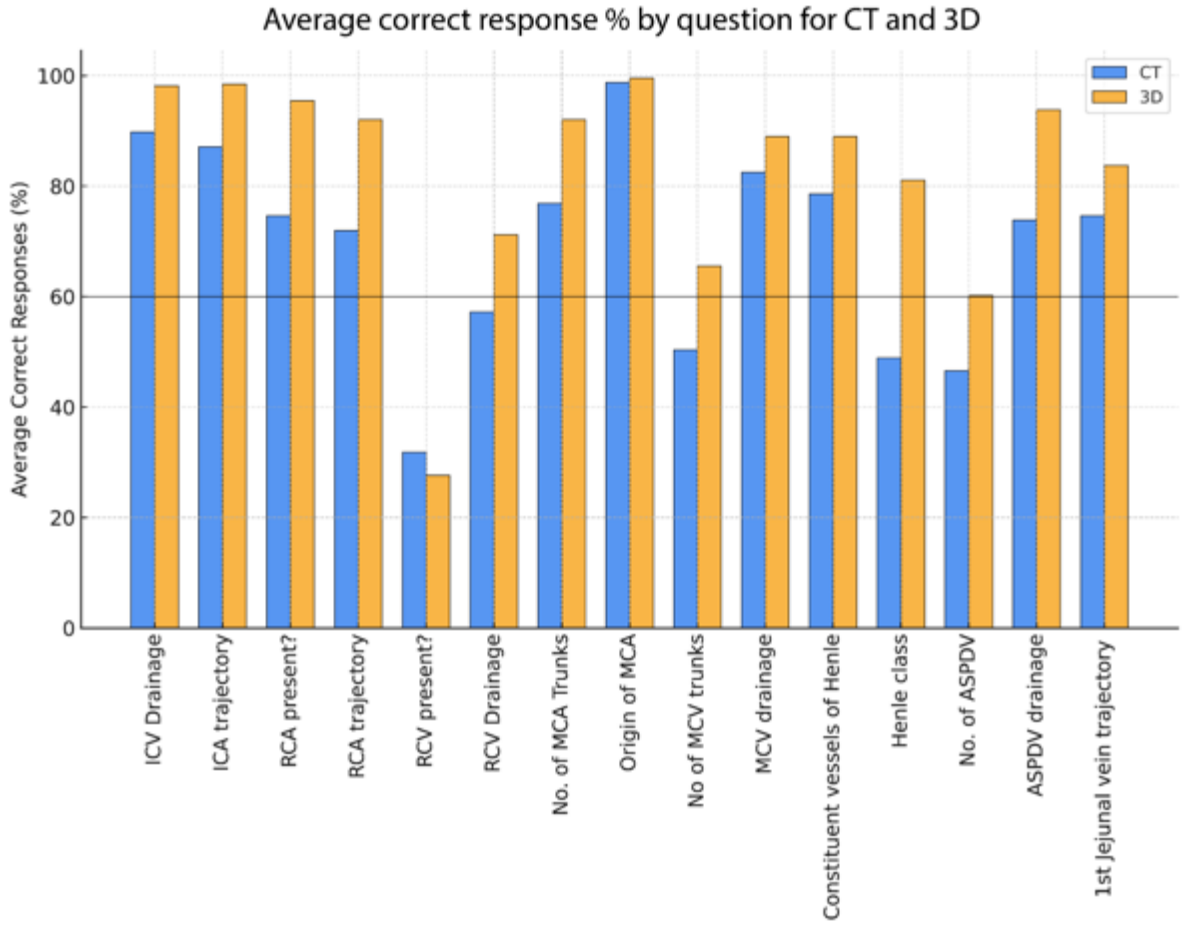


Table 4-10 Rater-Specific Diagnostic Accuracy for Anatomical Variants Using CT and 3D Imaging. This table presents a detailed breakdown of the correct response rates for each rater across various anatomical variants using CT and 3D imaging modalities. The 'Total' column indicates the number of cases for each anatomical feature, while subsequent columns provide each rater's counts (n) and percentages (%) of correct diagnoses for the two imaging methods.

Question	Answer	Total	RATER 1				RATER 2				RATER 3				RATER 4			
			3D		CT		3D		CT		3D		CT		3D		CT	
			n	%	n	%	n	%	n	%	n	%	n	%	n	%	n	%
ICV drainage	SMV	60	60	100.00	57	95.00	60	100.00	60	100.00	59	98.33	51	85.00	60	100.00	58	96.67
	HenleTrunk	5	4	80.00	3	60.00	5	100.00	5	100.00	5	100.00	2	40.00	5	100.00	0	0.00
	Jejunal Vein	1	0	0.00	0	0.00	0	0.00	1	100.00	1	100.00	0	0.00	0	0.00	0	0.00
ICA trajectory	Posterior	44	42	95.45	40	90.91	44	100.00	44	100.00	44	100.00	36	81.82	42	95.45	37	84.09
	Anterior	22	22	100.00	18	81.82	22	100.00	22	100.00	22	100.00	19	86.36	22	100.00	14	63.64
RCA Present?	No	58	56	96.55	53	91.38	57	98.28	50	86.21	56	96.55	34	58.62	52	89.66	49	84.48
	Yes	8	8	100.00	2	25.00	8	100.00	4	50.00	8	100.00	4	50.00	7	87.50	1	12.50
RCA Trajectory	Posterior	3	2	66.67	0	0.00	3	100.00	2	66.67	3	100.00	1	33.33	2	66.67	0	0.00
	Anterior	5	5	100.00	1	20.00	5	100.00	2	40.00	5	100.00	3	60.00	5	100.00	0	0.00
	N/A	56	54	96.43	54	96.43	55	98.21	48	85.71	54	96.43	32	57.14	50	89.29	47	83.93
RCV Present?	Yes	26	6	23.08	7	26.92	5	19.23	14	53.85	8	30.77	8	30.77	18	69.23	16	61.54
	No	39	14	35.90	22	56.41	8	20.51	8	20.51	9	23.08	7	17.95	5	12.82	2	5.13
RCV drainage	SMV	8	6	75.00	2	25.00	6	75.00	4	50.00	6	75.00	0	0.00	5	62.50	2	25.00
	Henle	17	13	76.47	11	64.71	14	82.35	8	47.06	11	64.71	4	23.53	2	11.76	1	5.88
	N/A	40	26	65.00	17	42.50	31	77.50	32	80.00	31	77.50	32	80.00	35	87.50	38	95.00
No. MCA Trunks	One	60	57	95.00	58	96.67	54	90.00	52	86.67	57	95.00	46	76.67	60	100.00	43	71.67
	Two	5	4	80.00	1	20.00	4	80.00	0	0.00	3	60.00	1	20.00	0	0.00	1	20.00
	No MCA	1	1	100.00	0	0.00	1	100.00	0	0.00	1	100.00	0	0.00	1	100.00	1	100.00
No MCV Trunks	One	39	34	87.18	34	87.18	32	82.05	31	79.49	30	76.92	22	56.41	33	84.62	30	76.92
	Two	27	11	40.74	1	3.70	13	48.15	8	29.63	16	59.26	7	25.93	4	14.81	0	0.00
Henle class	GPCT	31	28	90.32	25	80.65	28	90.32	25	80.65	28	90.32	20	64.52	23	74.19	17	54.84

	GCT	17	13	76.47	1	5.88	12	70.59	1	5.88	13	76.47	5	29.41	14	82.35	10	58.82
	GPT	15	11	73.33	4	26.67	14	93.33	11	73.33	13	86.67	7	46.67	9	60.00	2	13.33
	CPT	1	0	0.00	0	0.00	1	100.00	0	0.00	1	100.00	0	0.00	0	0.00	0	0.00
	N/A	2	2	100.00	0	0.00	2	100.00	1	50.00	2	100.00	0	0.00	0	0.00	0	0.00
No. ASPDV	One	49	34	69.39	21	42.86	38	77.55	37	75.51	37	75.51	33	67.35	32	65.31	27	55.10
	Two	7	4	57.14	2	28.57	6	85.71	1	14.29	4	57.14	1	14.29	4	57.14	1	14.29
Jejunal vein trajectory	Posterior	43	36	83.72	35	81.40	39	90.70	38	88.37	42	97.67	31	72.09	27	62.79	33	76.74
	Anterior	22	18	81.82	15	68.18	21	95.45	18	81.82	19	86.36	14	63.64	18	81.82	13	59.09

Figure 4-13 Comparative Analysis of Correct Response Rates by Imaging Modality Across Anatomical Variations. This paired bar chart displays the mean percentage of correct diagnoses by all evaluators, contrasting results obtained using 3D imaging (orange bars) with those from CT imaging (blue bars). Each pair of bars corresponds to a different anatomical variation as specified on the x-axis. The number of cases (n) featuring each anatomical variant is indicated atop the respective bars, reflecting the sample size for each question category.

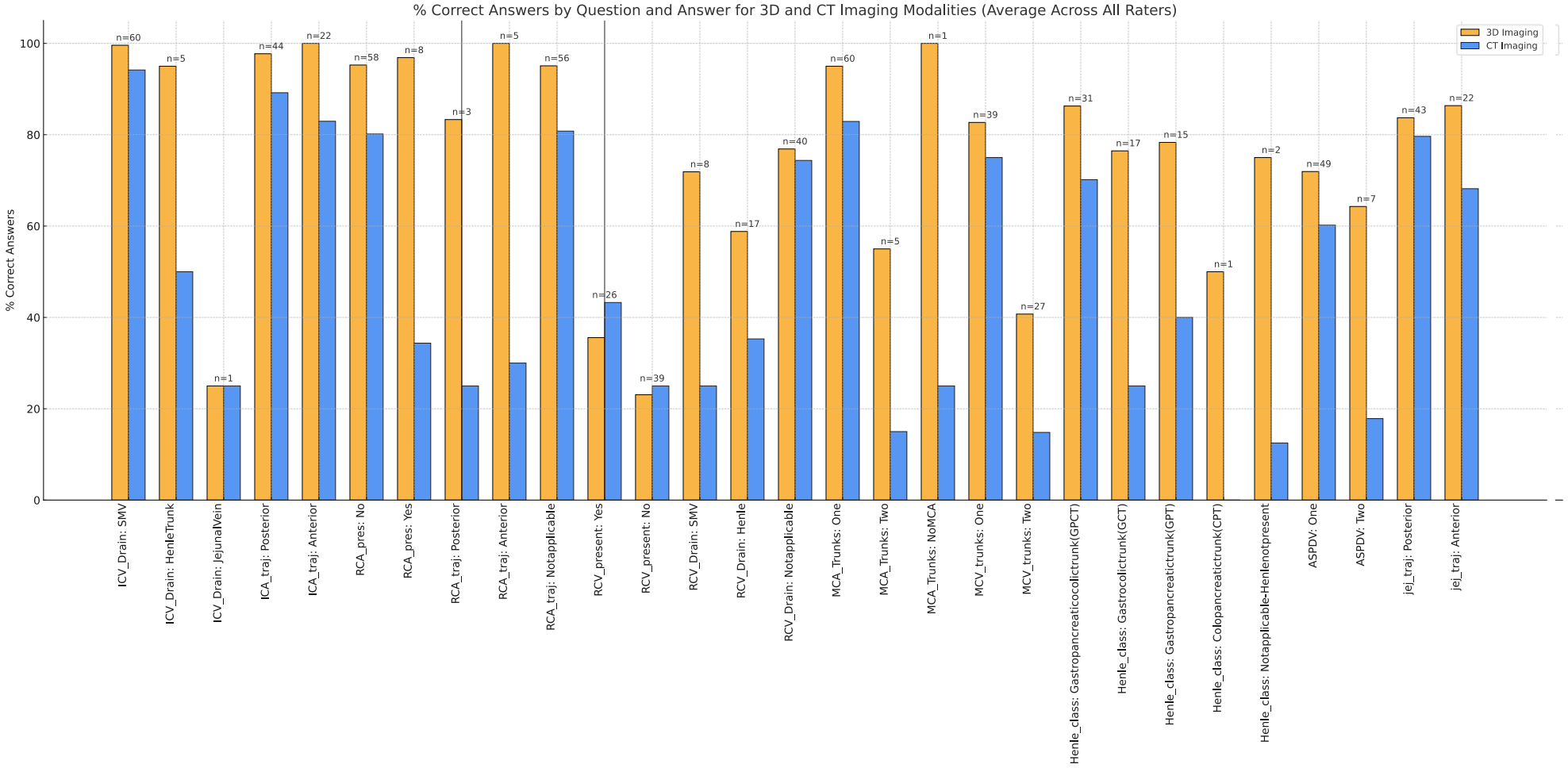
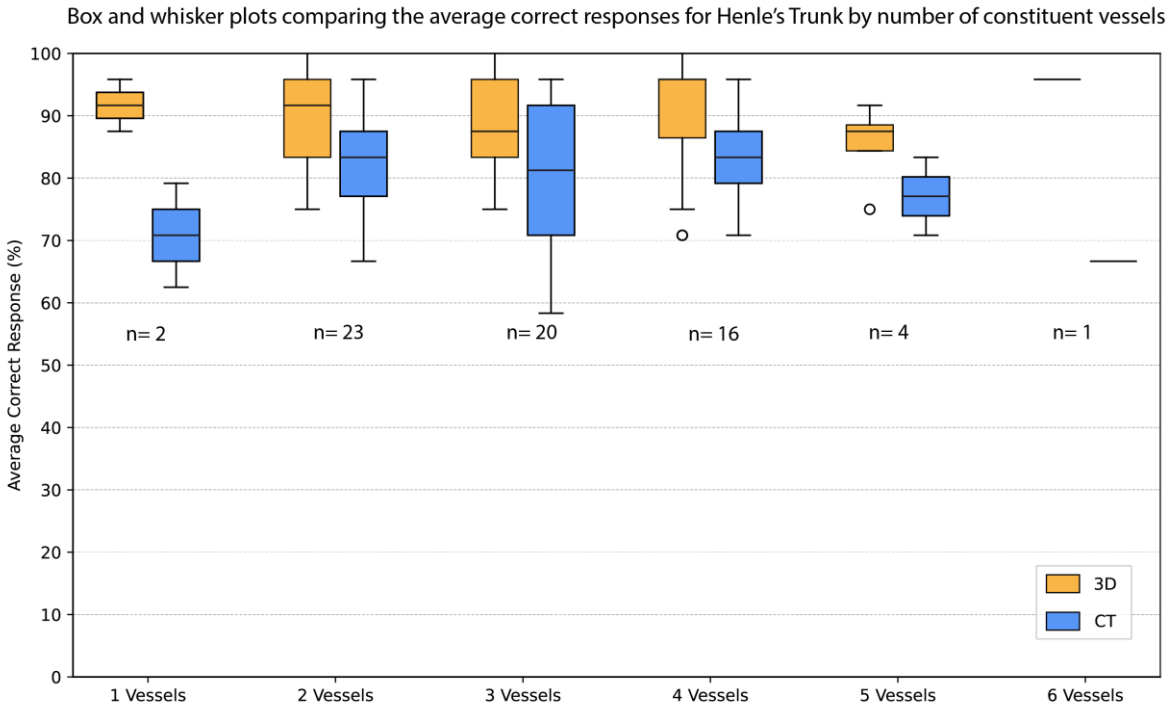


Figure 4-14 Box and whisker plots comparing the average correct responses for Henle's trunk using 3D and CT imaging modality by the number of constituent vessels. No statistical difference was found between the magnitude of the improvement of 3D over CT for the number of vessels as assessed by the Kruskall-Wallis test.



4.4 Discussion

The findings from these two complementary studies provide compelling evidence for the utility of three-dimensional visualisation in enhancing anatomical understanding for complete mesocolic excision surgery while also highlighting important considerations for clinical implementation. By examining trainee and expert surgeons, we gain valuable insights into how 3D models might benefit practitioners across the spectrum of surgical expertise.

4.4.1 Summary of Key Findings

These findings demonstrate that three-dimensional visualisation substantially enhances anatomical understanding for trainees and expert surgeons, although the extent and nature of this improvement differ with the level of surgical experience. Among trainees, using 3D models resulted in a fourfold increase in anatomical knowledge scores relative to baseline, exceeding the threefold improvement observed with the AMIGO method.

Expert surgeons also demonstrated substantial benefits from 3D visualisation, achieving median accuracy improvements of 10.1% and 7.8% in successive study phases. Moreover, inter-rater reliability notably increased with 3D models (Fleiss Kappa 0.6) compared to conventional CT imaging (Fleiss Kappa 0.1), indicating that 3D visualisation may foster more uniform interpretations of complex vascular anatomy. Although the relative improvement among expert CME surgeons was smaller than that observed in trainees, their absolute performance with both imaging modalities was already markedly high, as would be expected given their greater baseline expertise. Similarly, two trainees' overall performance was better using CT imaging rather than 3D models.

These parallel improvements in both cohorts highlight the intrinsic value of 3D visualisation. The varying degrees of benefit between trainees and experts offer insights into how best to incorporate such tools in surgical education and practice. The fact that experts, despite their familiarity with conventional imaging modalities, also showed significant enhancements underscores that 3D visualisation extends beyond reinforcing basic anatomical knowledge to improving the understanding of intricate spatial relationships.

Nevertheless, results from the inter-rater reliability study indicate that 3D reconstructions do not guarantee improved understanding in every case. Although superior in most instances, the advantages of 3D visualisation are not universal. Consequently, surgeons' skill in interpreting both 3D reconstructions and standard imaging techniques remains essential.

Rather than functioning as a stand-alone solution, 3D models should be integrated as a complementary resource to support and refine surgical planning.

4.4.2 Interpretation and Analysis of Results

4.4.2.1 Clinical implications

A significant finding across both studies was the benefit of 3D models in identifying complex or variable anatomical features.

For instance, in the study two, five cases exhibited an atypical drainage pattern where the ileocolic vein drained directly into Henle's trunk instead of the superior mesenteric vein (SMV). Expert surgeons correctly identified this variant in 95% (19 out of 20) of cases using 3D imaging, compared to only 60% with conventional computed tomography (CT). Notably, one rater failed to recognise this variant in any case using CT. The ileocolic vein is a crucial anatomical landmark, and its ligation is one of the early critical steps in CME (171). If the vein drains into Henle's trunk, it may not be encountered during the usual portion of the operation, potentially leading to unexpected bleeding or ligation of the SMV or terminal ileal branches mistaken for the ileocolic vein.

Similarly, three-dimensional (3D) imaging offers considerable advantages in identifying smaller-calibre vessels, such as the right colic artery. This vessel, defined as a distinct branch originating from the superior mesenteric artery (SMA) between the middle and ileocolic arteries, was present in eight cases. Using 3D models, expert CME surgeons accurately identified the right colic artery in 97% of instances (35 out of 36), compared with only 34% (11 out of 36) using standard CT imaging. Recognising this artery preoperatively is critical, as its unexpected presence may necessitate modifying the surgical approach and mitigates the risk of inadvertent vascular injury. Additionally, 3D models assist in detecting other potentially hazardous anatomical variants, such as a jejunal vein coursing caudally to the origin of the middle colic artery. A supplementary video demonstrates how these models can facilitate both the identification of such variants and the precise targeting of dissection, thereby supporting safer intraoperative navigation (358).

Three-dimensional (3D) models afford a more comprehensive appreciation of the spatial relationships among vascular structures than is typically achievable with conventional CT scans. For instance in one case in which three distinct colonic veins converge into the

superior mesenteric vein (SMV). In this scenario, correct identification of multiple middle colic veins was notably poor using CT alone (3–29% accuracy). In contrast, 3D models not only facilitate the recognition of each individual vessel but also provide clear insights into their relative positions and trajectories. Such enhanced spatial understanding is critical during complete mesocolic excision (CME), as it helps to prevent vascular injuries and ensures a more effective lymphadenectomy.

Translating enhanced anatomical visualisation into better patient outcomes is complex and influenced by multiple factors, including variations in surgical technique, individual surgeon experience, intraoperative decision-making, and patient-specific considerations. While our study provides evidence that 3D imaging improves anatomical identification, proving that this leads to reduced vascular injuries, decreased operation times, or enhanced surgical confidence requires further investigation. Such translational studies would necessitate large sample sizes and multi-institutional collaboration to achieve the statistical power needed for definitive conclusions, which may be challenging to obtain. Comparable studies using 3D to perform liver resections and partial nephrectomy have demonstrated use of 3D models significantly reduces blood loss and operative time (173,345,359).

Despite these limitations, our findings suggest that 3D imaging enhances agreement and accuracy concerning critical structures integral to performing safe CME. Structures such as the drainage pattern of the ileocolic vein, the trajectory of the ileocolic artery, the number and origin of the middle colic arteries, and the number and drainage patterns of the middle colic veins are pivotal for surgical planning and execution. While it is difficult to quantify precisely how many CMEs transition from 'unsafe' to 'safe' based solely on our study, the notable improvements in identifying these critical structures with 3D models indicate a potential for significant surgical and technical benefits. By pre-emptively recognising anatomical variations, surgeons can tailor their approach to each patient, potentially reducing the risk of intraoperative complications and improving overall surgical outcomes.

4.4.2.2 Experience-Dependent Effects

The relationship between surgical experience and benefit from 3D visualisation emerged as complex and multifaceted. Among trainees, those with prior CME experience showed greater improvement with 3D visualisation, suggesting that some baseline anatomical knowledge

derived from intraoperative experience may be necessary to fully exploit the benefits of 3D models.

This variation in benefit highlights an important consideration for implementation: the need to consider individual differences in spatial ability and learning style when deploying 3D visualisation tools. The finding that two participants performed better with AMIGO than 3D models suggests that different approaches may suit different learners, and that a one-size-fits-all approach to surgical imaging may be suboptimal.

4.4.3 Study Limitations

4.4.3.1 Methodological Limitations

Both studies have several limitations that warrant consideration. Firstly, despite our efforts to provide precise anatomical definitions, subjectivity in vessel classification may not have been eliminated. Incorrect responses from raters might stem from misclassification rather than a genuine lack of understanding. This issue is particularly evident with vessels such as the middle colic vein (MCV), right colic vein (RCV), and superior right colic vein (SRCV). Raters may identify a draining vein in regions like the ascending colon, hepatic flexure, or transverse colon, but variations in interpretation and naming conventions can lead to discrepancies. For example, differentiating between a superior right colic vein and a right colic vein can be challenging, potentially contributing to the observed low accuracy in identifying the RCV on 3D scans.

The variation in model types and functionalities introduces complexity when comparing outcomes between the two studies. It remains unclear how individual interface features and varying levels of model interactivity influence users' anatomical understanding. Nonetheless, trainee feedback has highlighted the importance of having the ability to adjust component transparency, suggesting that this feature may be essential for optimising the educational and practical utility of 3D models.

While the median accuracy improvements were statistically significant, they were not universal across all cases in both studies. This raises the question of how much these improvements in anatomical understanding correspond to clinical benefits. It is important to acknowledge that our assessment focused on specific facets of anatomical understanding—namely, the presence of a vessel, its origin, or drainage pattern. This does not capture other critical components such as scale, relative location, and the spatial relationships between

structures. Therefore, we may not be fully appreciating the qualitative benefits that 3D models provide in fostering a more holistic understanding of mesenteric anatomy.

The study assumes uniform high quality in both the 3D reconstructed models and CT scans across all cases. Variability in image acquisition and reconstruction quality can influence the accuracy of anatomical interpretation, potentially confounding the results. Additionally, having the same team responsible for both the 3D reconstruction and the definition of the gold standard introduces potential bias. This dual role could inadvertently align the gold standard more closely with our 3D models than if an independent team had set the standard. While we believe this bias is minimal—since all 3D models were reviewed by a consultant gastrointestinal radiologist and validated using intraoperative findings—we acknowledge its potential influence on our results. Future studies should consider involving independent teams for reconstruction and validation to enhance robustness.

The statistical measures used to evaluate inter-rater and intra-rater reliability have their limitations. Fleiss Kappa and Cohen Kappa values are sensitive to the prevalence of the attribute being measured and the bias of raters, which can lead to paradoxical situations where observed agreement is high, but kappa values are low. This phenomenon, known as the kappa paradox, can result in misinterpretation of the agreement levels among raters (360). However, the level of average intra-rater agreement observed corroborates our findings and overall conclusions.

The finding that both trainees and experts preferred having access to both conventional CT and 3D models suggests that implementation should focus on integrating 3D visualisation into existing workflows rather than replacing current imaging modalities. This hybrid approach might offer the best combination of detailed anatomical visualisation while maintaining familiarity with conventional imaging interpretation.

4.5 Conclusions

The synthesis of findings from these complementary studies provides strong evidence for the value of 3D visualisation in enhancing anatomical understanding for CME surgery, while also highlighting important areas for development. The consistent improvement in anatomical recognition across both trainee and expert cohorts suggests that these tools could play a valuable role in surgical education and planning.

However, the path to routine clinical implementation requires addressing several key challenges, particularly regarding workflow integration and technical optimisation.

The variation in benefit observed across different user groups emphasises the importance of considering individual differences in learning and practice styles when implementing these tools. A flexible approach that integrates 3D visualisation with conventional imaging while accommodating different user preferences and needs may prove most effective.

These findings represent an important step toward optimising surgical planning and education in CME, while also providing a framework for future development and implementation of 3D visualisation in complex surgical procedures more broadly.

5 Feasibility and Early Clinical Integration of 3D Models for Complete Mesocolic Excision

5.1 Aims

This multicentre, international feasibility study aims to investigate integrating patient-specific three-dimensional (3D) reconstructed models derived from preoperative imaging into the routine clinical practice of Complete Mesocolic Excision (CME) for right-sided colon cancer. The primary objectives are:

1. **To evaluate the accuracy of 3D models in predicting intraoperative mesenteric vessel anatomy.** This involves assessing the congruence between the preoperative 3D models and the actual anatomical findings during surgery.
2. **To gather surgeon feedback on the utility of 3D models.** Surgeon perceptions regarding the usability of the models, their value in preoperative planning and intraoperative guidance, and their impact on anatomical understanding will be collected using structured questionnaires.
3. **To assess the feasibility of collecting key clinical data points for future clinical trials.** This includes determining whether essential data such as operative times, intraoperative complications, and postoperative outcomes can be reliably recorded in the context of using 3D models.
4. **To create a validated, labelled dataset for future automation of the segmentation process through neural networks.** By generating high-quality segmentation data, the study aims to facilitate the development of automated tools that could streamline the creation of 3D models.

By addressing these aims, the study seeks to provide preliminary evidence on the practicality and potential benefits of integrating 3D modelling into CME surgery. The findings are expected to inform the design of larger, more definitive clinical trials and contribute to the evolving landscape of surgical innovation.

5.2 Study Population and Recruitment:

Patients aged 18 years or older, of any gender and tumour stage deemed suitable for elective, curative resection of right-sided (including extended right hemicolectomies) or transverse colon tumours were considered eligible. Exclusion criteria included pre-operative imaging not adhering to the study protocol, unsuitability for or refusal of surgery, inability to provide informed consent, or needing emergency surgery (unplanned resection within 48 hours of admission). Written informed consent was obtained from all participants.

5.2.1 Surgeon Characteristics:

Five consultant surgeons from multiple international centres participated, representing a range of CME experience. To better characterise experience, surgeons were classified into four groups:

1. Trainee Surgeon: Surgeon in training programme or post training fellowship.
2. Novice CME surgeon: Fewer than 20 completed CME cases.
3. Intermediate CME Surgeons: 20- 49.
4. Experienced: Over 50 CME cases performed.
5. Highly Experienced: >100 CME cases performed.

5.2.2 3D model workflow

5.2.2.1 Segmentation

Pre-operative staging imaging data, consisting of either CT with port venous contrast or CT colonography with port venous contrast, was utilised. Arterial phase imaging, when available, served as a reference for segmentation due to the challenge of identifying mesenteric venous structures in this phase. DICOM files were imported into ITK SNAP's open-source segmentation software (17).

Segmentation was primarily performed manually by a research team member (JF) experienced in mesenteric vessel segmentation, using a Wacom Cintiq 24Pro pen display interface. Using a threshold-based seed-growing approach, semi-automatic segmentation was employed for the colon in CT colonography data and, when feasible, for larger vessels like the aorta and superior mesenteric artery (SMA). Each segmentation was verified by a consultant gastrointestinal radiologist with extensive experience in CME anatomy. Segmentation times were prospectively recorded to the nearest 5 minutes.

5.2.2.2 3D model processing and visualisation

3D mesh extraction and visualisation were undertaken as outlined in detail in chapter 2.

5.2.3 Pre-operative Review and Intra-operative Use:

3D models were provided to the operating surgeon the day before the procedure, along with an instructional video demonstrating the user interface and model navigation. Surgeons were not given specific instructions on how or for how long to use the models. All participating surgeons reviewed the model and scan pre-operatively.

Intraoperatively, models were visualised on a separate computing device (tablet/laptop) and, for robotic CME cases, integrated into the DaVinci Xi console using the TilePro feature. For laparoscopic procedures, the model was displayed on an assistant monitor.

5.3 Outcome measures

5.3.1 Primary Outcomes:

1. Segmentation Time: Time required for manual segmentation of pre-operative imaging data to create the 3D model, measured in minutes per case.
2. Model Accuracy: Qualitative assessment of the congruence between the 3D model and intraoperative findings, with discrepancies documented using a structured reporting tool.
3. Subjective Surgeon Feedback: Perceptions of the 3D model's usability, value for pre-operative planning and intraoperative guidance, and impact on anatomical understanding were collected through a custom Likert scale questionnaire.

4. Pre-operative Planning Time: Duration of time spent by surgeons interacting with the 3D model during pre-operative planning.

5.3.2 Feasibility Assessment of Clinical Data Points:

The feasibility of collecting the following data points for future clinical trials was evaluated:

1. Objective CME Anatomy Knowledge: Change in knowledge assessed through a validated questionnaire administered before and after 3D model use.
2. Operative Times: Time taken for specific procedural steps.
3. Peri-operative Acute Haemorrhage Events: Occurrence of events defined as:
    - Blood loss exceeds an estimated 15% of circulating volume.
    - Need for intraoperative blood transfusion due to blood loss.
    - Conversion to open surgery due to bleeding.
4. Perioperative Complications: Classified using the Clavien-Dindo III system.
5. Post-operative Length of Hospital Stay: Duration in days.
6. Operative Performance: Assessed using a validated complete mesocolic excision assessment tool and video recordings.
7. Oncological Specimen Quality: Lymph node yield and CME grading evaluated from histology reports and specimen photography.
8. Practicality of Model Delivery: Assessment of logistical and practical aspects of pre-operative delivery of patient-specific 3D models.

Example study questionnaires can be viewed in Appendices 5.1 -5.3.

5.4 Sample size and patient recruitment.

Little published guidance exists on the sample size required for a pilot or feasibility trial.

The aim of the study is not to include any hypothesis testing; therefore, a power calculation is not a valid consideration for the sample size. Patients were recruited over a 18 month period.

Patients were recruited from the multidisciplinary colorectal cancer lists in each participating sites.

5.5 Results

5.5.1 Clinical Summary

Table 5-1 Patient demographic and clinical characteristics summary

Age	
Median Age yrs (IQR) Age Range	69.5 38- 88
Age category (years)	
30-50	4
51-60	15
61-70	20
71-80	28
81-90	9
Sex	
Female	25
Male	51
ASA	
1	1
2	43
3	32
Site	
St Mark's Hospital (London, United Kingdom)	29
Ikazia (Rotterdam, Netherlands)	43
Mater (Dublin, Ireland)	4
Total	76
Tumour location	

Caecum	28
Ascending colon	29
Hepatic Flexure	9
Transverse colon	10
Splenic Flexure	1
Lap/Open procedure*	
Laparoscopic	39
Robotic	29
Lap/Robotic>Open	2
Open	0
Pathology (TNM 8)	
T-stage	
No T stage	8
pT1	8
pT2	17
pT3	37
pT4a	7
pT4b	0
N-stage	
N0	44
N1a	18
N1b	8
N2a	2
N2b	5
UICC stage	
I	22
IIA	18
IIB	2
IIIA	4
IIIB	15
IIIC	6
Unknown	9
EMVI~	
Negative	58
Intramural	12
Extramural	6
Histopathology	
Adenocarcinoma well differentiated	29
Adenocarcinoma mod. differentiated	30
Adenocarcinoma poorly differentiated	8
Other	10
Lymph Node Yields	
Median Range IQR	27 11-89 16
Grading of specimen	

Mesocolic	76
WHO Subtype	
Mucinous	7
Medullary	2
Signet cell	1
Not specified	66
Adjuvant chemo	
No	56
Yes	20

5.5.2 Intraoperative haemorrhage events

No injuries to major mesenteric vessels, including the superior mesenteric vein (SMV) and superior mesenteric artery (SMA), were observed. Three episodes of unplanned intraoperative bleeding occurred, two of venous origin and one arterial, all of which were successfully controlled using an energy device and vessel clipping. One episode of significant venous bleeding necessitated conversion to an open procedure to achieve haemostasis. The source of this bleeding was identified as a short colonic vein draining into Henle's trunk, which was torn during elevation of the transverse colon. There was no requirement for intraoperative blood transfusion.

5.5.3 Morbidity and mortality

30-day morbidity and mortality were recorded for all patients recruited to the study

Results are summarised in table 5-2.

Table 5-2 Morbidity and mortality data

Length of stay (d)	**Median**	**Min**	**Max**	**IQR**
	5	2	24	6
30- mortality	0/76			
30- day morbidity	29/76 (38%) see break down below			
Readmission rate	2/76 (3%)			
Clavien- Dindo Grade				
I	11/76 (14%)	11	Ileus NG tube only	
II	11/76 (14%)	1	SMV thrombosis	
		2	Bronchopneumonia	
		8	Ileus requiring TPN	
III	6/76 (8%)	4/6	Anastomotic leak	
		1/6	Abdominal wall collection requiring IR drainage	
		1/6	Adhesions requiring laparotomy + adhesiolysis	
IV	1/76 (1%)		Fast AF requiring ITU admission	
Anastomotic leak	4/76 (5%)	1/4	1/4 Grade A antibiotics only	
		2/4	Grade B Re-laparoscopy	
		1/4	Grade C Required laparotomy + take down anastomosis	
Ileus	19/76 (25%)	11/19	NG only	
		8/19	NG and TPN	

5.5.4 Feasibility of intraoperative assessment of performance using recorded video

The intraoperative video was recorded using two principal methods.

The video feed from the robotic console or laparoscopic stack was captured locally via a video capture card and OBS Studio, an open-source, cross-platform software for video recording and live streaming. The footage was recorded in the Matroska (MKV) format, which was selected due to its ability to write in chunks. This feature was particularly beneficial because it enhanced the system's resilience to power loss and software crashes. As a result, any footage recorded in MKV was preserved even during an interruption, in contrast to MP4 formats, which result in data loss under such conditions.

The video was also captured using the online telementoring platform Proximie. The video was recorded directly to the platform's secure servers over the internet. However, the quality of the recordings was observed to fluctuate based on the available bandwidth, resulting in variable recording quality that, at times, was insufficient for effective postoperative review.

Video can be feasibly recorded. Based on this study, we found recording on local devices resulted in better quality and would be the method of choice for any further research.

The CMECAT tool has been recently been validated as an assessment tool to evaluate technical performance for video recorded minimally invasive CME cases (361).

5.5.5 Imaging and Segmentation time summary

Mean segmentation time varied depending on the specific imaging used and slice thickness.

The mean segmentation time for a 2mm porto venous CT scan was 68 minutes, with a minimum time of 55 minutes and a maximum time of 90 minutes. The average segmentation time for CT colonography with an average of 678 slices of<1mm thickness was 119 minutes. Segmentation times ranged from

The total time spent segmenting scans for all included cases was 104 hours.

Segmentation time data is summarised in table 5-3 and figure 5-1.

Table 5-3 Summary table of segmentation times by scan type and slice thickness

Scan Category	n	Slice thickness (mm)	Mean no. slices	Mean seg. Time (mins)	SD	Min seg. Time (min)	Max seg. Time (min)	Total Seg. Time (min)
CT Angio	1	≤1mm	635	135	n/a	135	135	135
CT PV contrast	5	≤1mm	677	136	5.5	130	140	680
CT PV contrast	52	>1-≤2.5mm	242	68	7.1	55	90	3545
CT PV contrast	4	>2.5mm	226	49	4.8	45	55	195
CT colon	14	≤1mm	678	119	12.0	105	140	1665

Figure 5-1 Histogram of segmentation times (minutes) per scan.

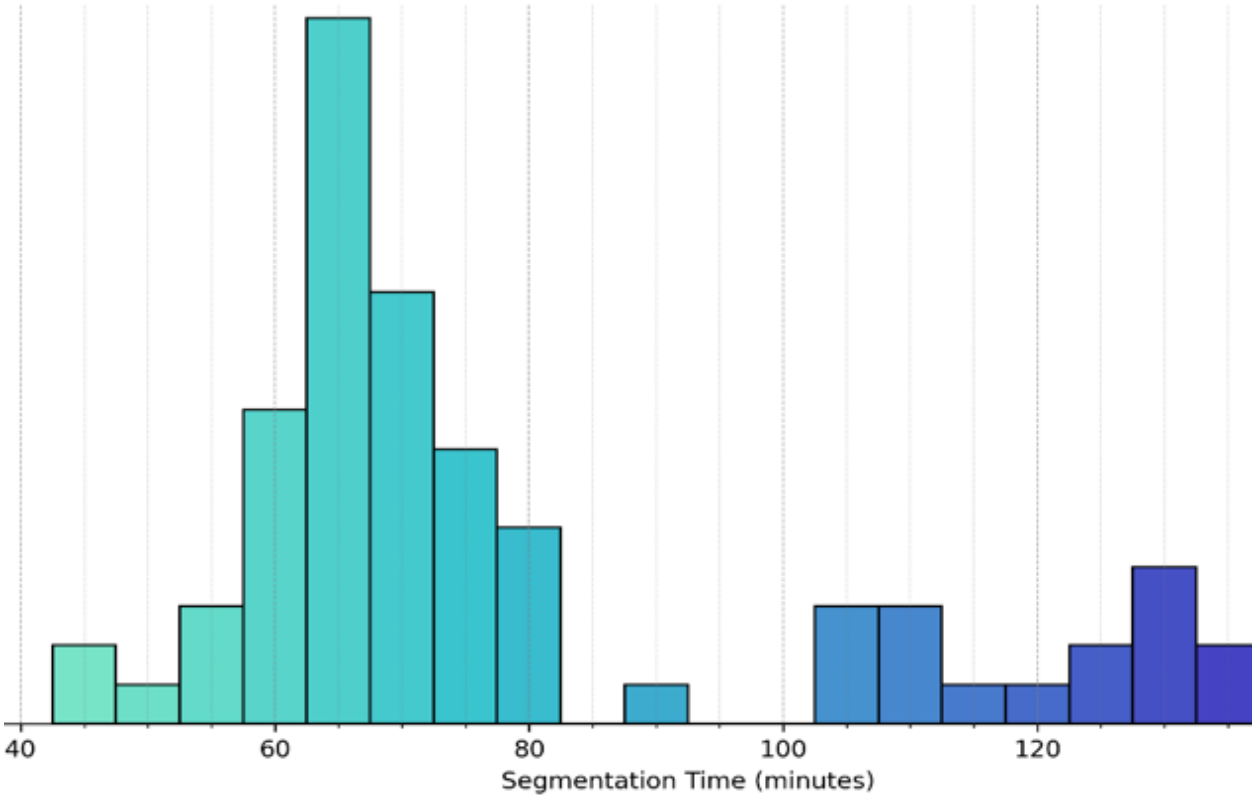


Table 5-4 Summary of imaging protocols utilised.

Scan Type	Count
CT PV contrast	61
CT colon with PV contrast	14
CT Angio	1

5.6 Anatomical Configuration of Mesenteric Vessels

5.6.1 Ileocolic Vein and Artery

In this cohort of 76 cases, the ileocolic vein (ICV) predominantly drained into the superior mesenteric vein (SMV) in 70 cases (92%). ICV drained into Henle's trunk and an ileal vein in 3 cases, respectively (4%)

The trajectory of the ileocolic artery (ICA) in relation to the superior mesenteric vein (SMV) was posterior in 51 cases (67%) and anterior in 25 cases (33%). The ICA was present in 100% of cases.

5.6.2 Right Colic Artery

The right colic artery (RCA) was defined as an independent branch emerging directly from the superior mesenteric artery to supply the right colon. RCA was absent in 62 cases (82%) and present in 14 cases (18%). Among the cases where RCA was present, the artery followed an anterior trajectory with respect to the SMV in 9 cases (64%) and a posterior trajectory in 5 cases (36%).

5.6.3 Middle Colic Veins

Regarding MCA trunks, a single trunk was observed in 61 cases (80%), and two trunks were noted in 15 cases (20%). In nearly all cases (74 cases, 97%), the middle colic artery (MCA) originated from the superior mesenteric artery (SMA). In cases with two trunks, both vessels originated from the SMA in 13/15 cases. There were two cases where the MCA shared a common trunk with the ileocolic artery (2%). In one of these chases a second MCA trunk was observed originating in the typical location of the SMA.

The Middle colic vein was defined as a branch draining the transverse colon. The middle colic vein (MCV) was most observed in a single trunk in 42 cases (54%). Two trunks were present in 29 cases (38%), and three trunks were identified in 5 cases (7%).

The middle colic vein (MCV) exhibited greater variability than the middle colic artery (MCA). The most common drainage site for MCV branches was the superior mesenteric vein (SMV), which occurred in 55 cases (72%). Henle's trunk was another frequent drainage site, observed in 21 cases (28%). Additionally, the MCV drained into the inferior mesenteric vein (IMV) in 6 cases, the jejunal vein in 5 cases, and the splenic vein in 2 cases.

Among cases with only one MCV branch, 33 out of 41 (80%) drained into the SMV, 7 cases (17%) drained into Henle's trunk, and 1 case (2%) drained into the IMV. In cases where two MCV branches were observed, both branches most commonly drained into the SMV in 11 out of 29 cases (38%). The combination of SMV and Henle's trunk drainage was the second most common, found in 5 out of 29 cases (17%).

5.6.4 Henle’s Trunk

In this cohort of 76 cases, the analysis of the vessels draining into Henle’s trunk revealed a range in the number and combinations of vessels. The total number of vessels draining into Henle's trunk per case varied from 1 to 5, with the most frequent observation being three vessels in 29 cases (38%). Two vessels were noted in 22 cases (29%), four vessels in 17 cases (22%), and five vessels in 6 cases (8%). In 2 cases (3%), there was no identifiable Henle's trunk, and the constituent vessels were observed to drain directly into the superior mesenteric vein (SMV) rather than converging into a true Henle's trunk.

In terms of the specific vessels involved, the most frequently observed vessel was the right gastroepiploic vein, identified in 71 cases (93%), followed by the anterior superior pancreaticoduodenal vein in 63 cases (83%). The superior right colic vein was present in 53 cases (70%), while the middle colic vein and right colic vein were observed in 24 cases (32%) and 15 cases (20%), respectively. The ileocolic vein was identified in 3 cases (4%).

When assessing the combinations of vessels, the most common configuration involved the right gastroepiploic vein, anterior superior pancreaticoduodenal vein, and superior right colic vein, occurring in 20 cases (26%). Another frequent combination was the right gastroepiploic vein and anterior superior pancreaticoduodenal vein, found in 14 cases (18%). Other combinations involved additional vessels such as the middle colic vein, right colic vein, and ileocolic vein, with varying frequencies across the cohort.

Table 5-5 Measured distances between mesenteric vessels landmarks.

Distance between landmarks	Count	Mean (mm)	Median	SD (mm)	Min (mm)	Max (mm)	Normality (p-value)
ICA to MCA trunk	75	26.0	24.4	10.9	10.3	64	<0.001
ICA to RCA	8	14.5	15.35	5.6	7.6	20.5	0.06
Origin of MCA to bifurcation	51	24.7	24.9	8.12	11.3	46	0.2656
ICV to Henle's trunk	59	34.1	34.6	9.42	11.6	55	0.8567
ICV to nearest MCV draining into SMV	53	37.9	37.1	11.69	9	68.1	0.945

Figure 5-2 Histogram depicting the distribution of measured distances (in millimetres) between the ileocolic artery and the middle colic artery trunk. The most frequent range of measurements is between 20–30 mm.

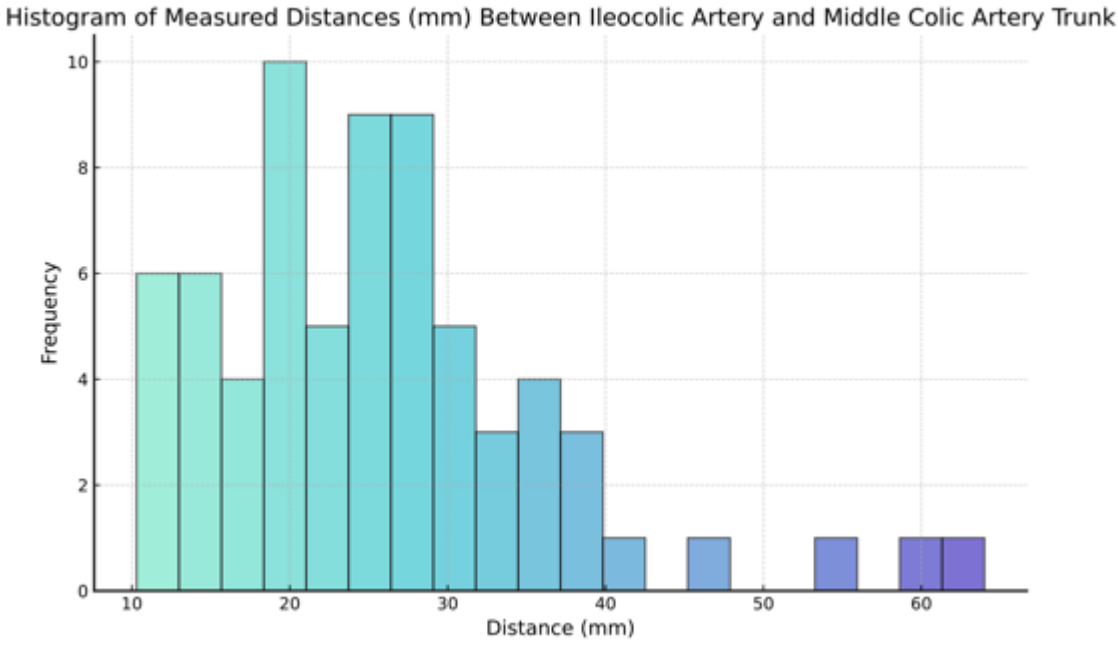


Figure 5-3 Histogram illustrating the distribution of measured distances (in millimetres) between the origin of the MCA and its bifurcation into right and left branches.

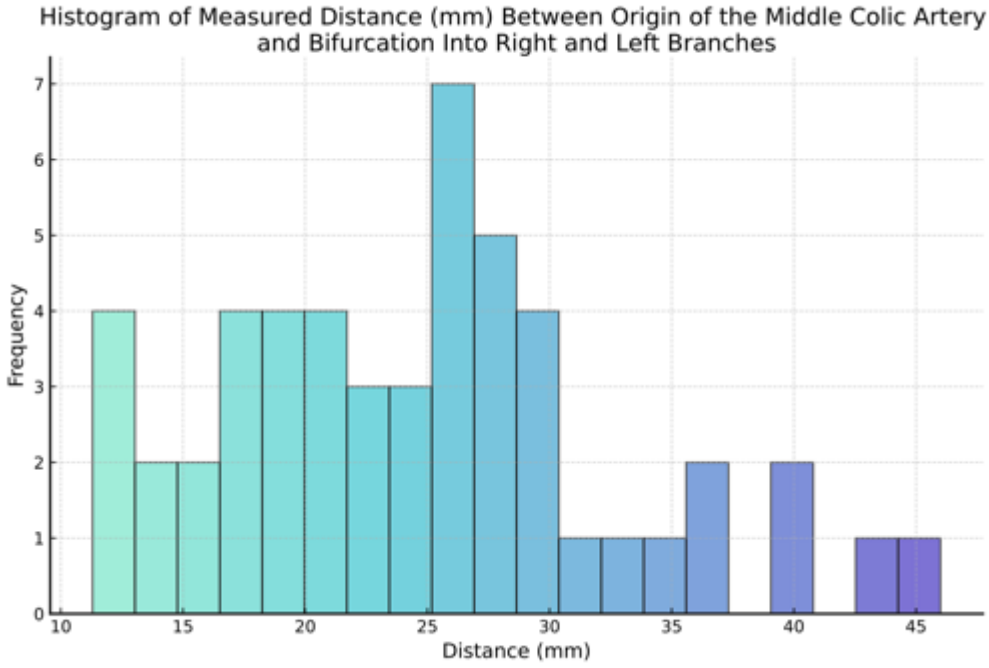


Figure 5-4 Histogram representing the distribution of measured distances (in millimetres) between the ileocolic vein and Henle's trunk. The most frequent distances fall within the 35–40 mm range.

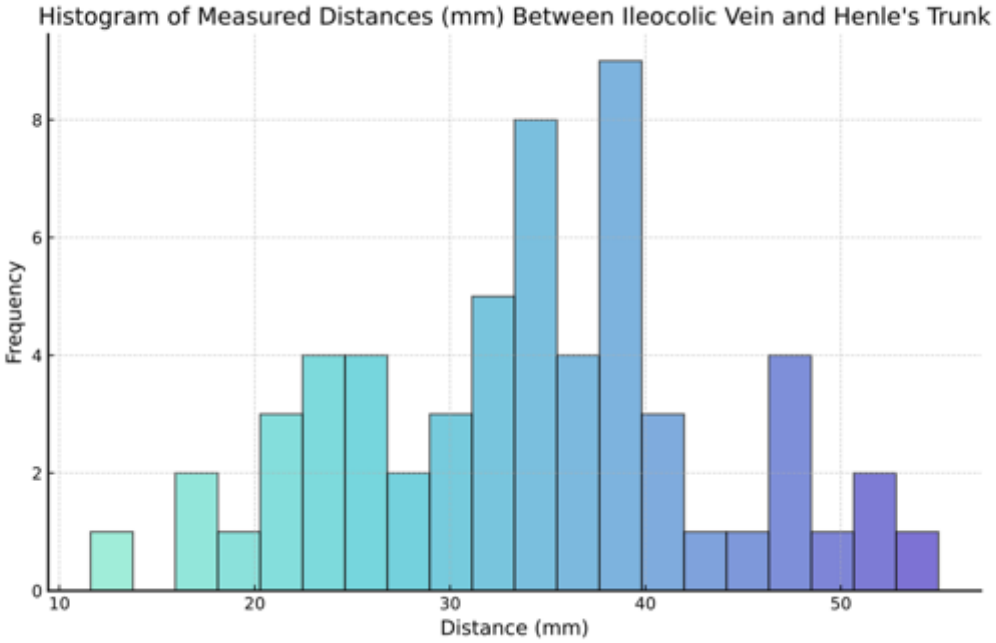
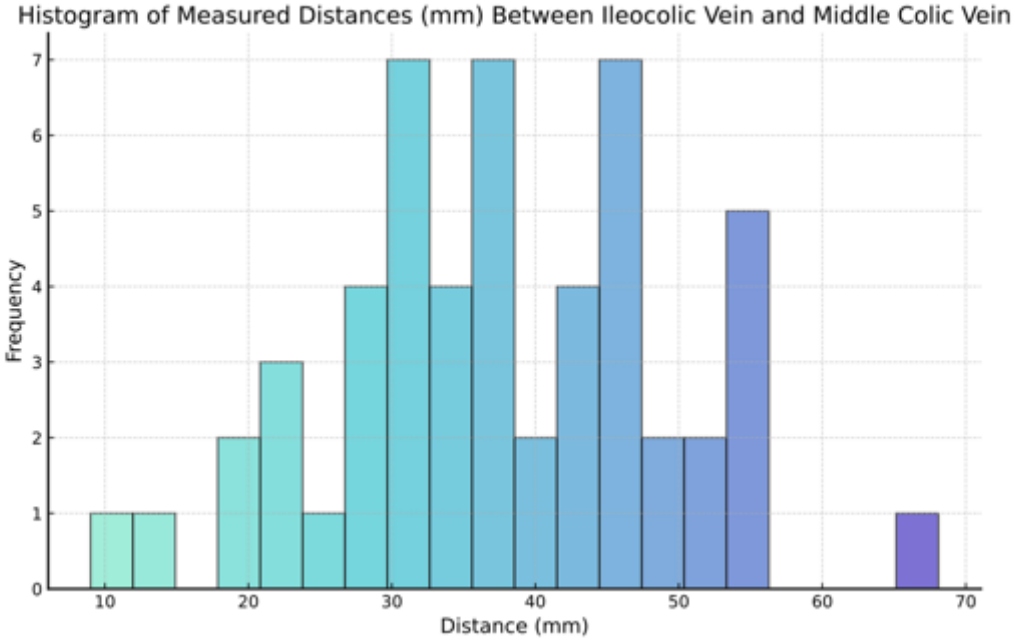


Figure 5-5 Histogram showing the distribution of measured distances (in millimetres) between the ileocolic vein and the middle colic vein.



5.7 Accuracy of Reconstructions

3D reconstructions accurately predicted the drainage of the ileocolic vein and the relationship of the ileocolic artery with respect to the superior mesenteric vein in all cases, achieving an accuracy of 100% (Table 5-6).

The 3D reconstructions demonstrated high accuracy in predicting the presence and course of the right colic artery, with an overall accuracy of 98.7%. Specifically, for detecting a right colic artery 92.9% corresponds to one case where the artery was missed on the reconstruction compared to the intra-operative findings.

Table 5-6 Reconstruction Accuracy in Predicting Vascular Anatomy: Sensitivity, Specificity, and Predictive Values Compared to Intraoperative Findings

Structure	Total cases (n)	TP	FP	TN	FN	Sen (%)	Spec (%)	PPV (%)	NPV (%)	Accuracy (%)
Drainage of the ileocolic vein	76	73	0	3	0	100	100	100	100	100
Course of ileocolic artery in relation to SMV	76	51	0	25	0	100	100	100	100	100
Presence of Right Colic Artery	76	13	0	62	1	92.9	100	100	98.4	98.7
Course of Right colic artery in relation to SMV	14	5	0	8	1	83	100	100	88.9	92.9
MCA (origin and number)						100	98.5	98.5	100	98.5

Table 5-7 Confusion matrix for prediction and presence of middle colic artery

Predicted/Actual	1 trunk	2 trunks	NV (not visualised)	Total (Predicted)
1 vessel	61 (TP)	0 (FN)	0	61
2 vessels	1 (FP)	6 (TP)	8	15
Total (actual)	61	5	10	76

The 3D reconstructions predicted the number of MCA trunks with an accuracy rate of 98.5% for cases where intraoperative visualisation was possible. In 8 cases, additional predicted vessels were not visualised intraoperatively due to exposure limitations, as dissection of these vessels was not clinically necessary. However, in such cases, middle colic vessels included in the dissection were accurately predicted in terms of origin and configuration of branching (Table 5-7).

In cases where the predicted vessels were not visualised, it is possible that these vessels were present but not detected intraoperatively. These cases were categorised as 'Not Visualised' and excluded from sensitivity and specificity calculations.

Table 5-8 Confusion matrix for prediction and presence of middle colic veins

Predicted/Actual	1 trunk	2 trunks	3 trunks	NV (not visualised)	Total Predicted
1 vessel	41 (TP)	1 (FP)	0	0	42
2 vessels	0	9	0	20	29
3 vessels	0	0	0	5	5
Total actual	61	0	0	25	76

The constituent vessels of Henle's Trunk were only sufficiently delineated in 29 cases to allow visual confirmation of accuracy. Results are summarised in table 5-9.

3D models were highly accurate in predicting intra-operative findings. 100 per cent accuracy was observed for the presence of the gastroepiploic vein and colic veins. The anterior

superior pancreatic duodenal vein was missed in two cases and incorrectly predicted as present in one case.

Figures 5-7 to 5-16 depict side-by-side comparisons of 3D reconstructions against the operative findings in 8 patients.

Table 5-9 3D Reconstruction Accuracy in Predicting Henle Trunk Vascular Anatomy: Sensitivity, Specificity, and Predictive Values Compared to Intraoperative Findings

Structure	Total cases (n)	TP	FP	TN	FN	NV (not visualised)	Sen	Spec	PPV	NPV	Accuracy
GEV	29	26	0	2	0	1	100	100	100	100	100
ASPDV	29	24	1	2	2	1	92	67	96	50	93
SRCV	29	23	0	5	0	1	100	100	100	100	100
RCV	29	5	0	25	0	0	100	100	100	100	100
MCV	29	9	0	20	0	0	100	100	100	100	100
ICV	29	1	0	28	0	0	100	100	100	100	100

Figure 5-6 Example case 1 3D model predictions versus intraoperative findings. A-B ICA passes anteriorly over SMV. MCA origin off SMA with bifurcation into right and left branches

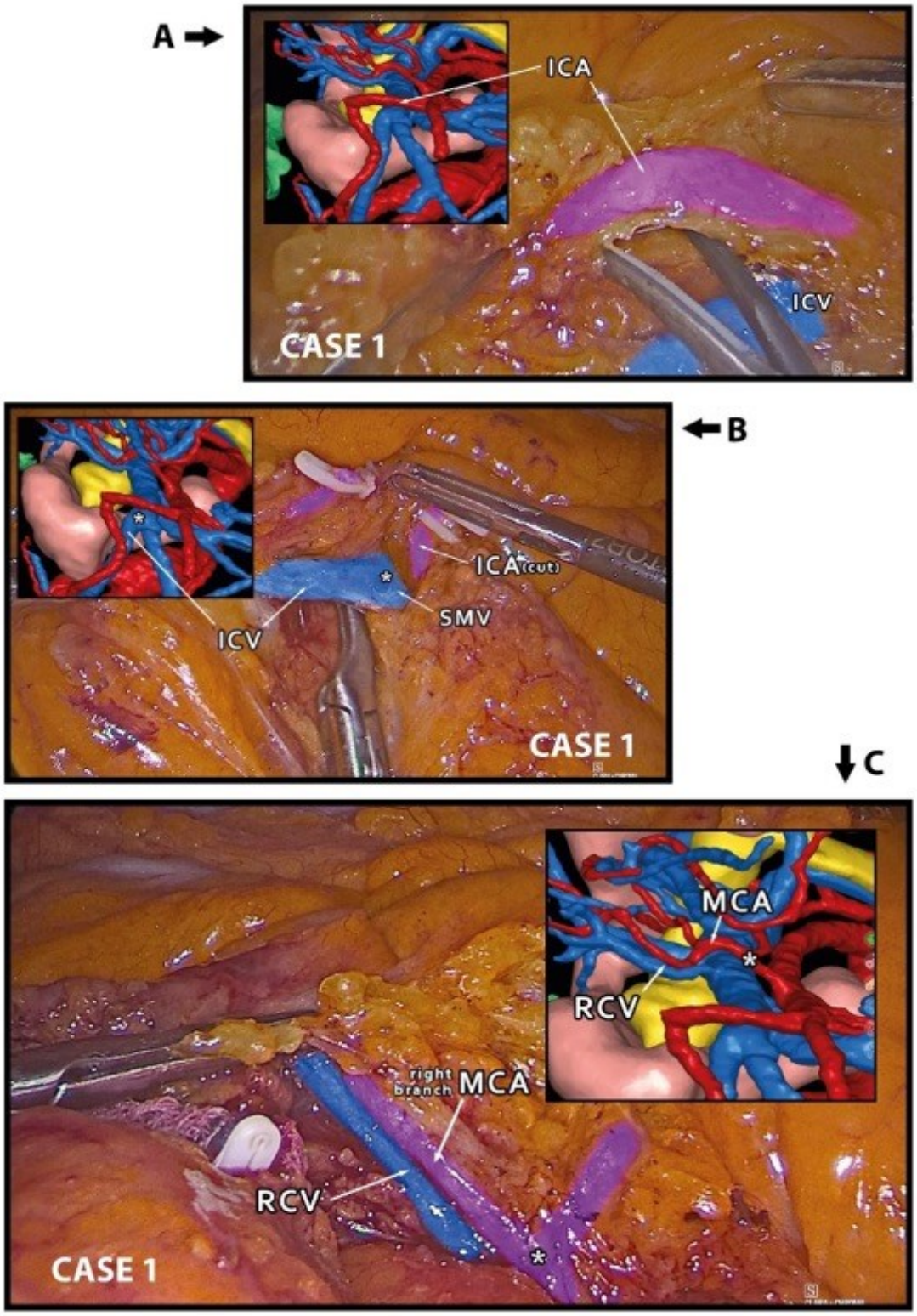


Figure 5-7 Example case 6- dissection of atypical colonic veins. Patient possessed 3 separate venous branches draining right and proximal transverse colon directly into the SMV (vessels 1-3) as predicted by 3D model. Each vessel was dissected and ligated.

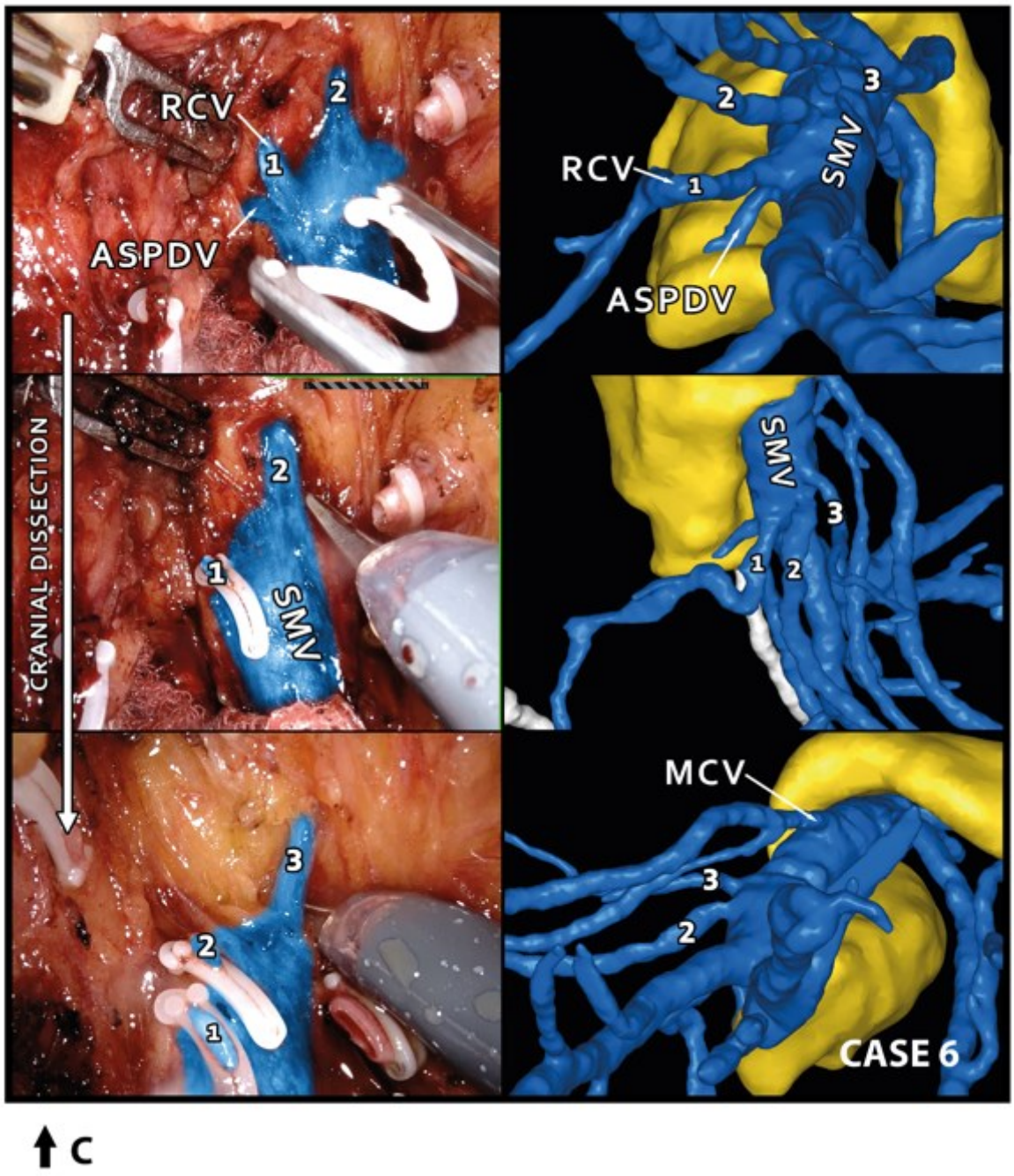


Figure 5-8 Published video abstract demonstrating intra-operative use of 3D model in case 7. The bottom image demonstrates a jejunal vein passing over SMV just caudal to the origin on the MCA. The 3D model helped identify this variant, avoid iatrogenic injury during D3 lymphadenectomy and help target dissection of the MCA trunk.

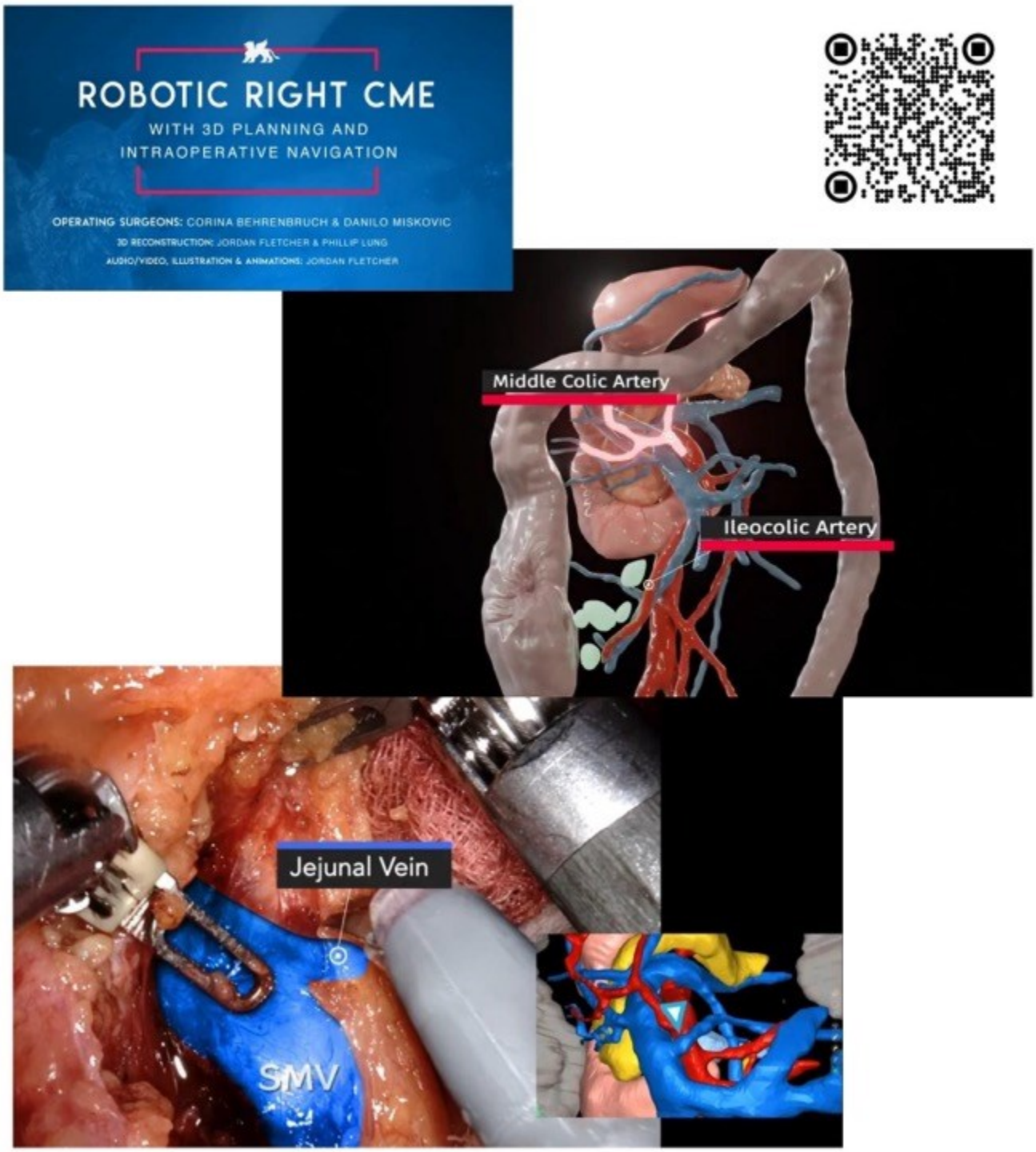


Figure 5-9 Case 12- two separate MCV veins draining directly into SMV as predicted by 3D reconstruction.

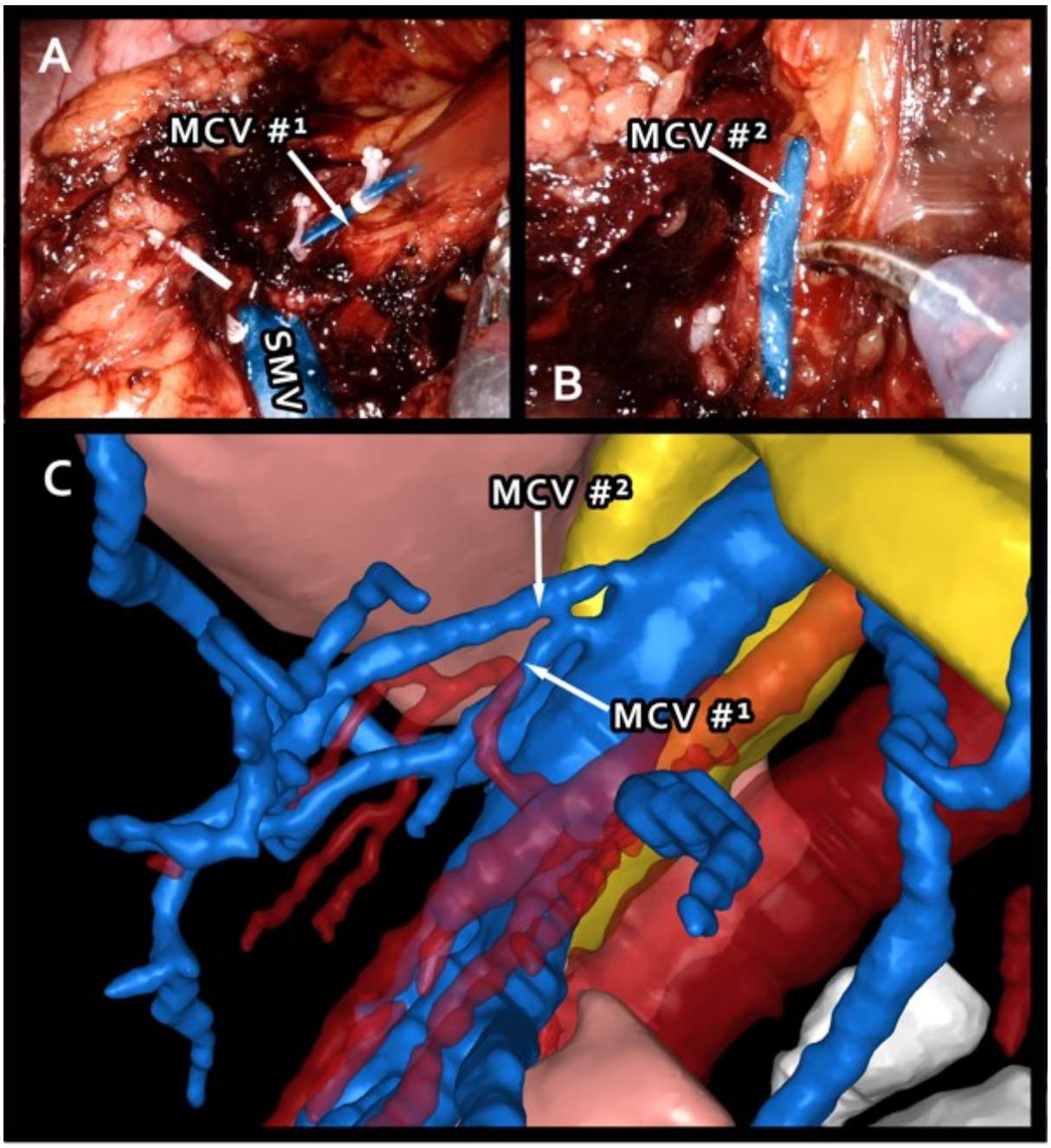


Figure 5-10 Case 12- Henle's Trunk comprised of GEV and ASPDV

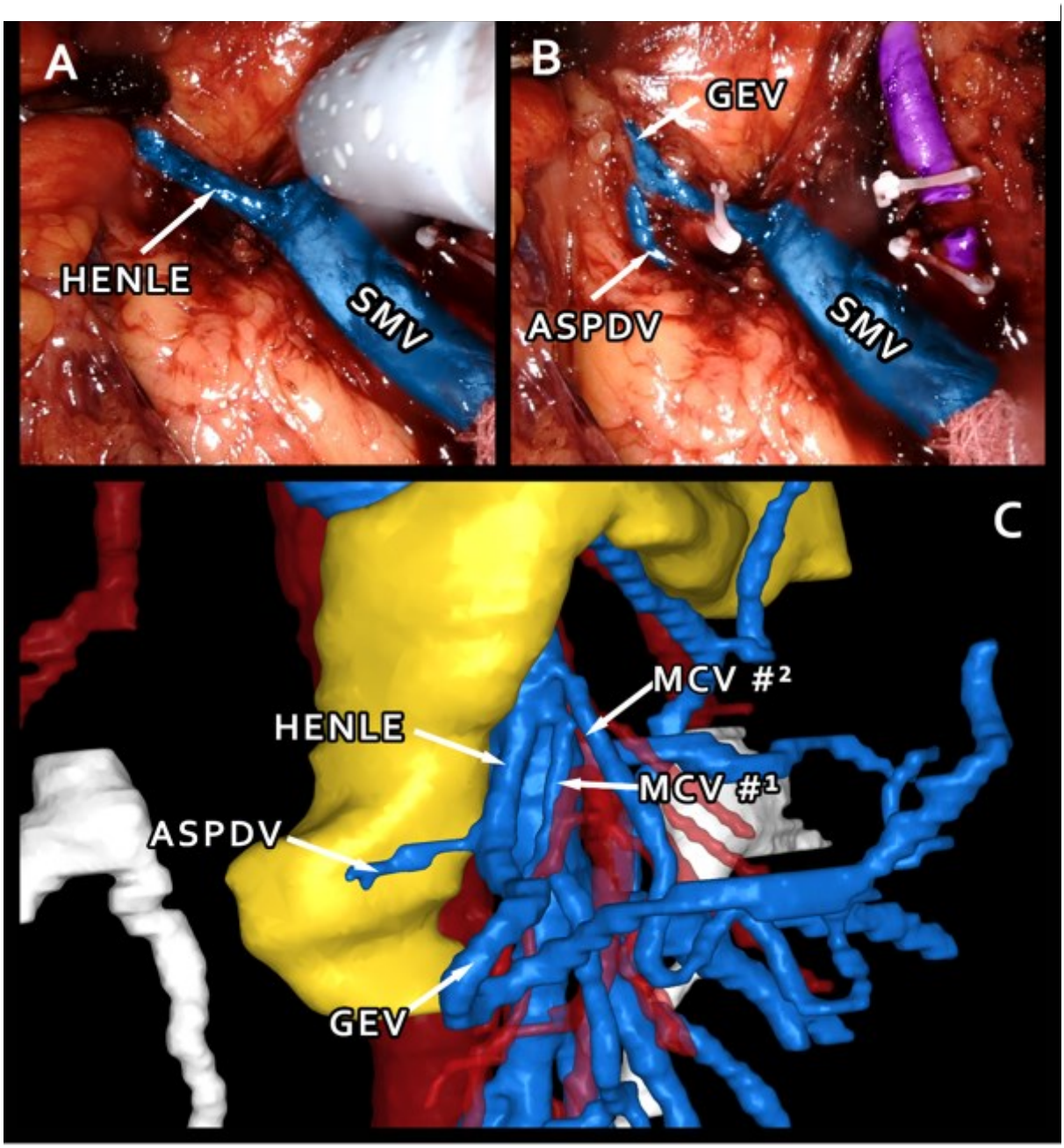


Figure 5-11 Case 49- One MCV trunk inserting into SMV. Henle's Trunk was comprised of SRCV, GEV and SRCV.

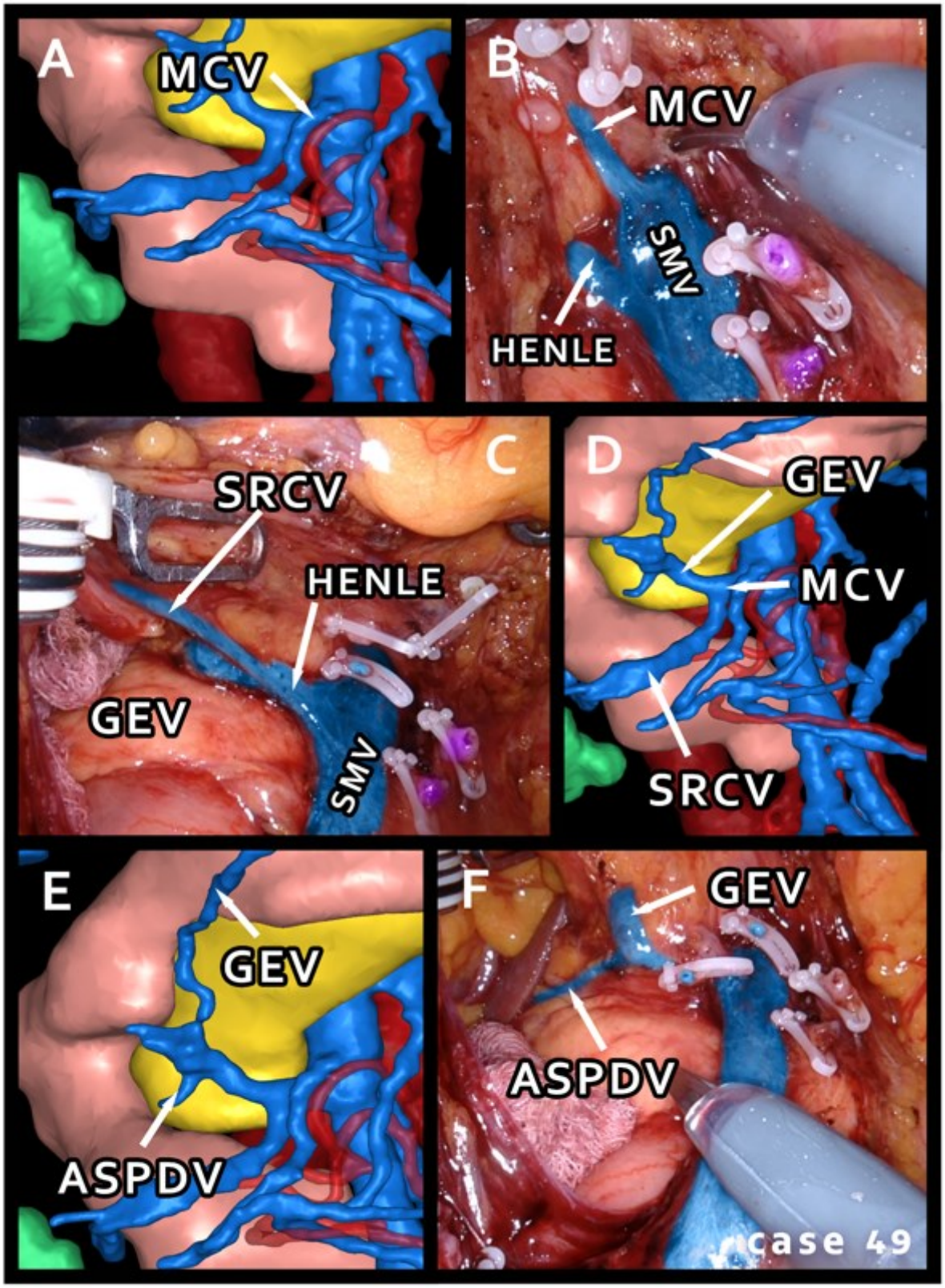


Figure 5-12 Case 69- Views demonstrating the MCA trunk and MCV trunk. Intraoperative findings were accurately predicted by the 3D model both in terms of number of trunks and their relative spatial relationships. Henle's trunk was ligated at its origin.

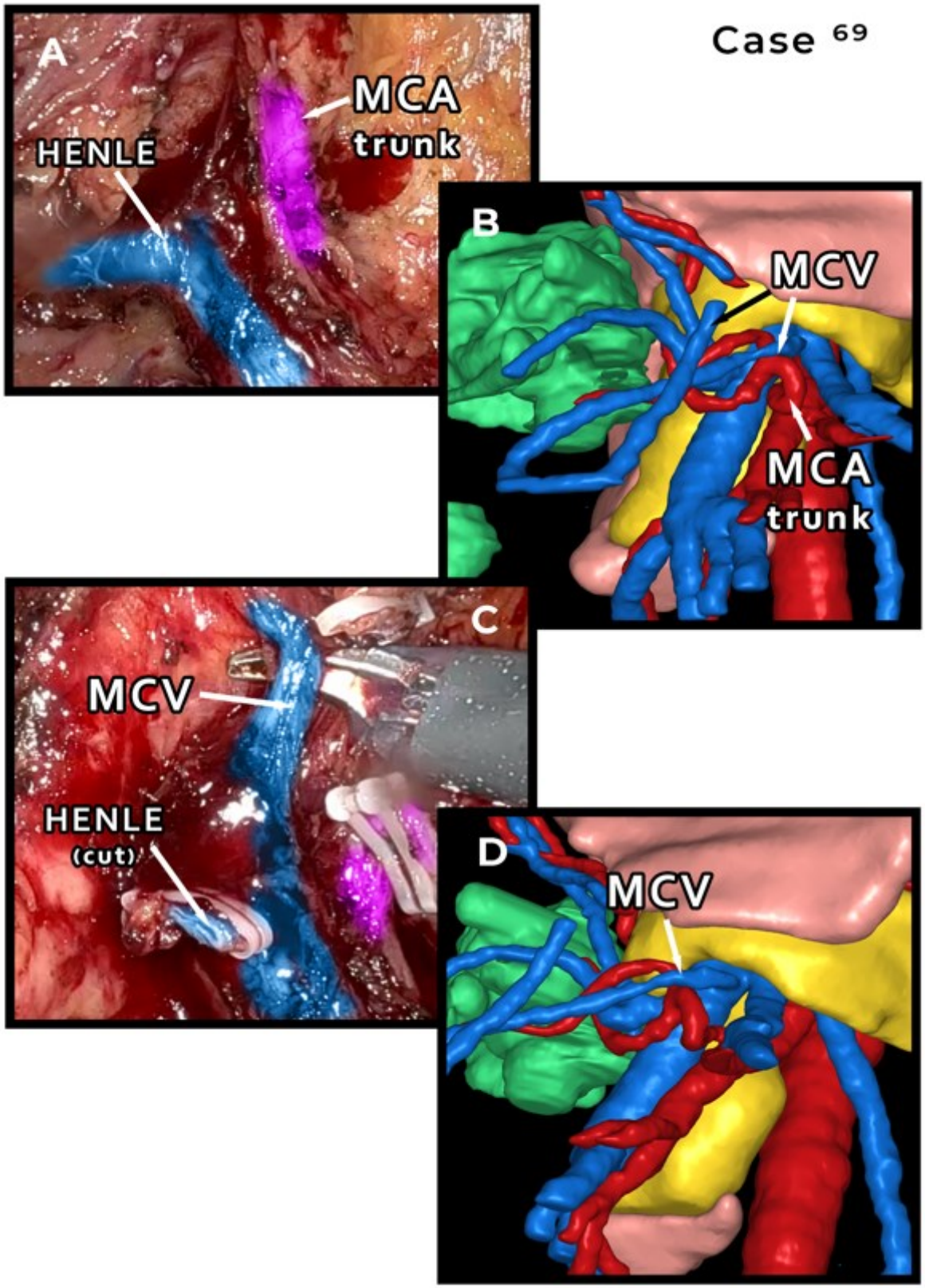


Figure 5-13 Case 85- Sequential intraoperative dissection views alongside 3D reconstruction. ICV can be viewed draining into SMV at same level as jejunal/ileal vein as can viewed on the 3D model. ICA passes posterior to SMV. The MCA trunk can be visualised with bifurcation into left and right branches.

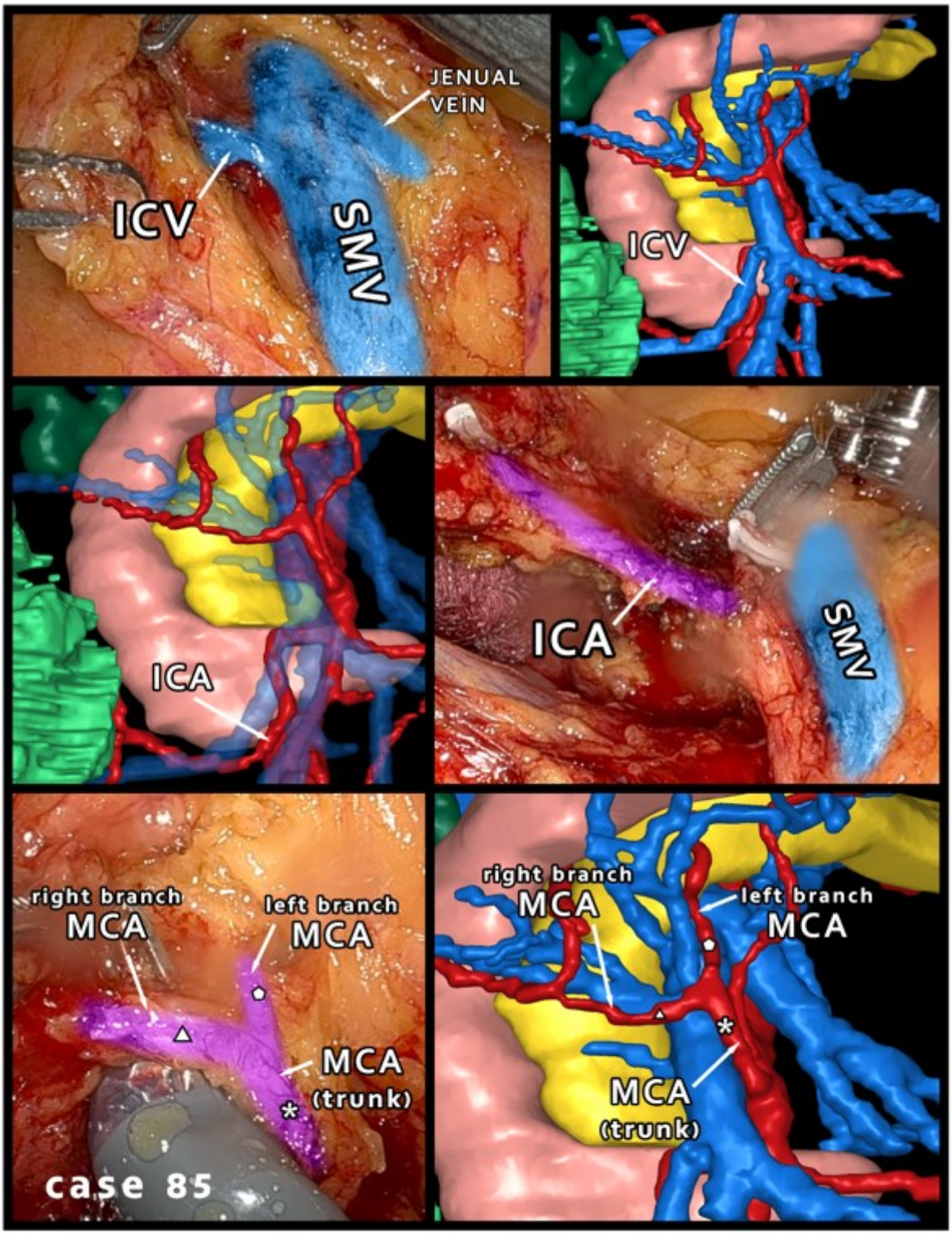


Figure 5-14 Case 85 Henle's trunk comprised of SRCV and ASPDV. GEV separate vessel draining into SMV directly.

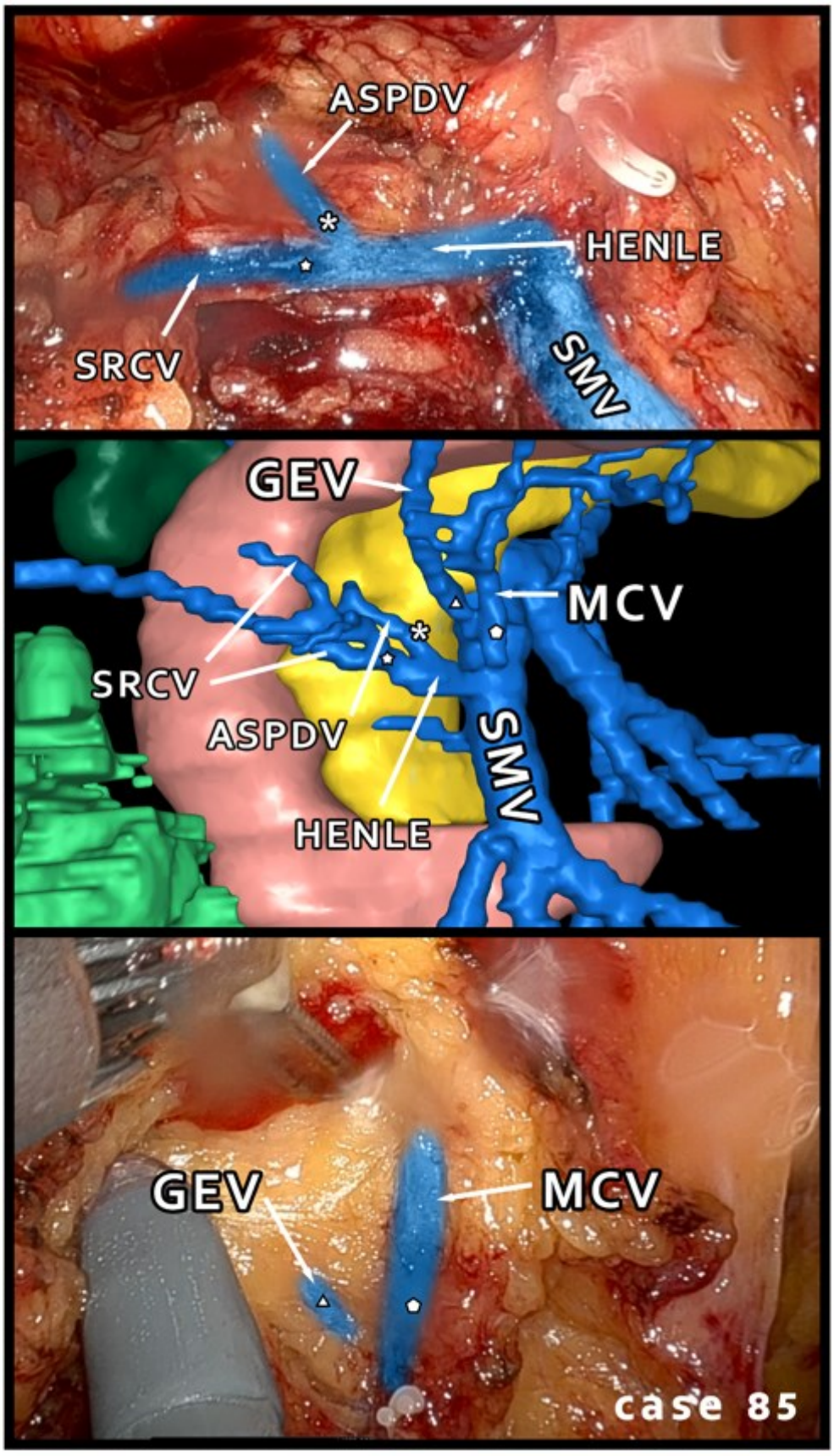


Figure 5-15 Case 87- Atypical anatomy with early bifurcation of SMV with the ICA passing between the two (star and Asterix). Model accurately predicted the vessel configuration allowing confident dissection and ligation.

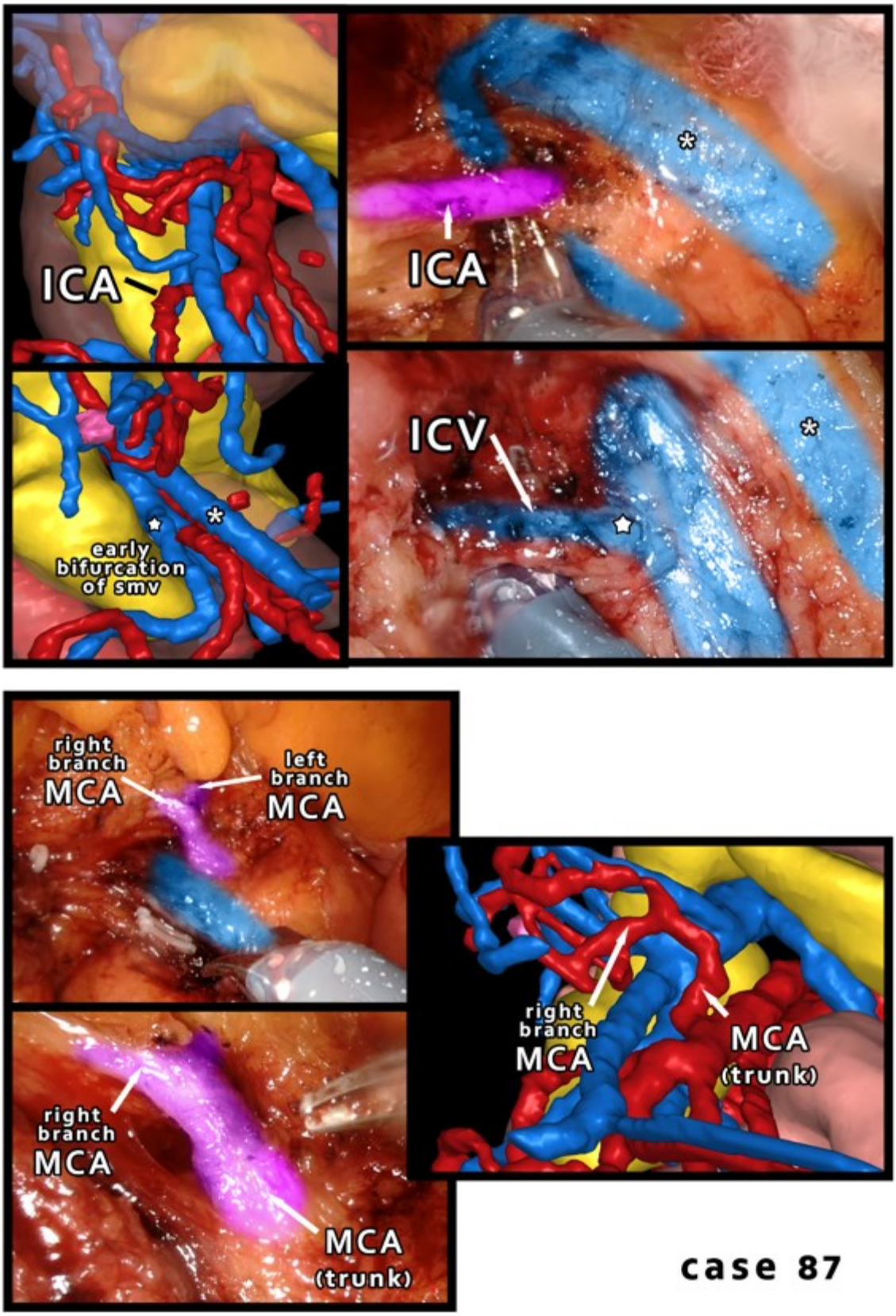
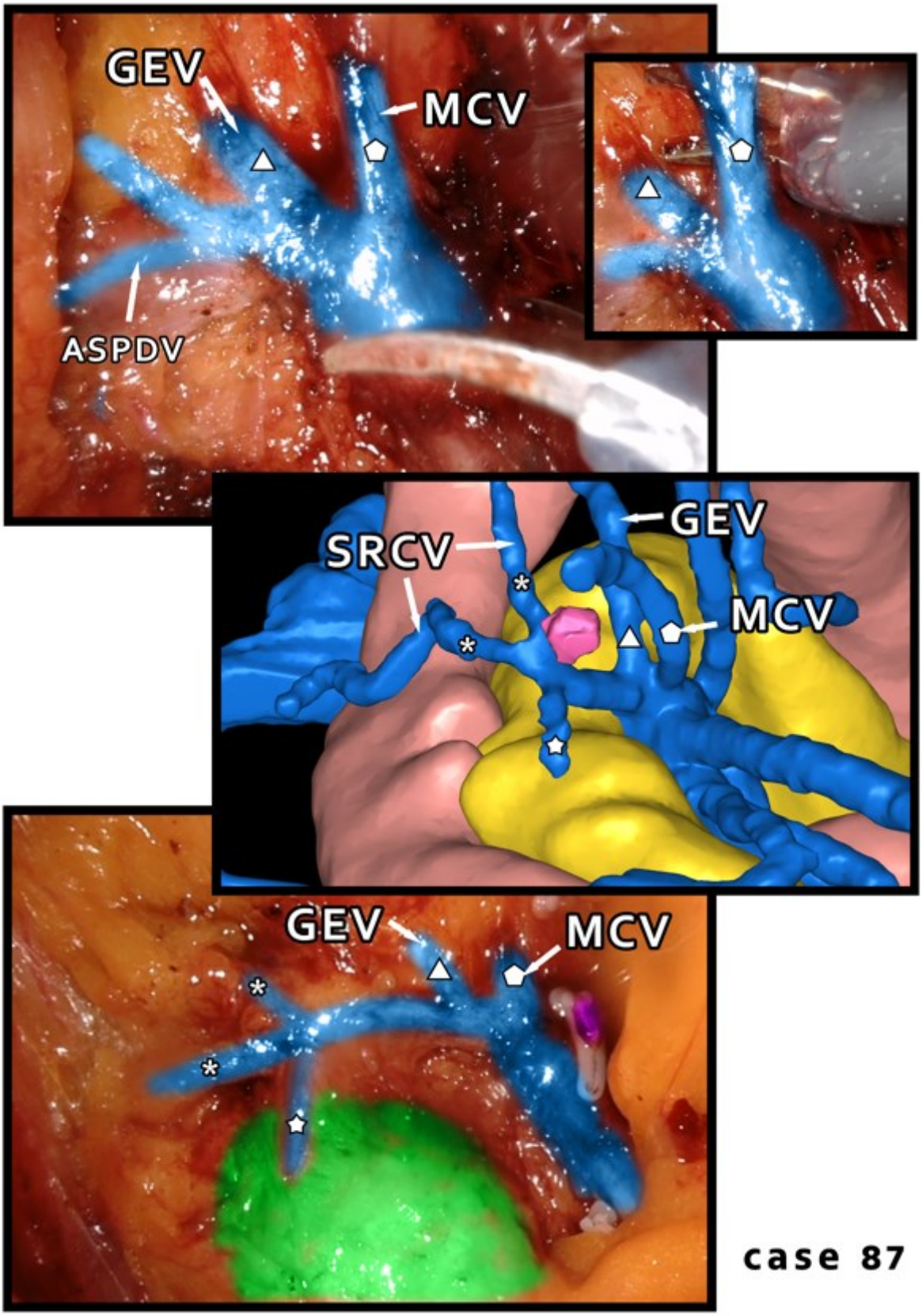


Figure 5-16 Case 87 (continued). MCV draining into SMV in proximity with the trunk of Henle with proximal drainage of GEV close to SMV. Confluence of two colonic vessels draining the hepatic flexure (SRCV) and ASPDV form the other constituent vessels of Henle.



5.7.1 Anatomical Understanding of Participating Surgeon CT versus 3D

We observe a significant enhancement in the accuracy of mesenteric vessel assessment when surgeons utilise three-dimensional (3D) models compared to conventional computed tomography (CT) scans. The overall median accuracy increased from 62% with CT scans to 87% with 3D models (p=<0.001) (see figure 5-17). Accuracy with 3D resulted in a smaller interquartile range, indicating a greater consistency.

3D models resulted in improved anatomical understanding for each of the twelve participating surgeons. The median improvement in correct responses ranged from 11-62%.

For surgeons performing over 3 case assessments, 6/10 demonstrated statistically significant improvements in accuracy when using 3D models.

No learning effect was observed in the accuracy of assessments for either imaging modality, as there was no correlation between time and performance. Participants did not demonstrate improved accuracy in later cases compared to their initial assessments (see Figure 5-18 A-H, Table 5-10).

Table 5-10 Summary statistic for percentage correct responses for each participating surgeon using CT scans and 3D models.

Surgeon			CT				3D models				
ID	CME Experience	n	median	min	max	IQR	median	min	max	IQR	p-Value
1	Trainee	12	21.5	8	53	14.5	83.5	29	100	18.5	<0.001
2	Highly Experienced	29	75	43	94	22	94	50	100	13	<0.001
3	Novice	4	65.5	50	79	12.5	76	71	86	5.25	0.2
4	Novice	21	67	21	93	24	87	60	100	29	<0.001
5	Novice	12	64	43	92	28.5	90.5	53	100	23.5	<0.01
6	Novice	7	69	44	93	26	80	58	100	24	0.249
7	Trainee	4	24	20	64	15.5	79.5	73	86	4	0.029
8	Trainee	1	18	n/a	n/a	0	59	n/a	n/a	0	N/A
9	Trainee	1	62	n/a	n/a	0	92	n/a	n/a	0	N/A
11	Novice	3	43	42	77	17.5	58	57	77	10	0.507
12	Novice	5	43	31	50	9	86	77	93	2	<0.01
13	Experienced	1	38	n/a	n/a	0	85	n/a	n/a	0	N/A
Overall		**100**	**62**	**8**	**94**	**34.5**	**87**	**29**	**100**	**24.25**	**<0.001**

Figure 5-17 Box plot comparing the percentage of correct responses for identifying mesenteric vessel configuration using CT scans (blue) and 3D reconstructions (orange). The median percentage correct for 3D reconstructions is higher than for CT, with reduced variability and fewer outliers, indicating improved consistency and accuracy in identification with the 3D modality.

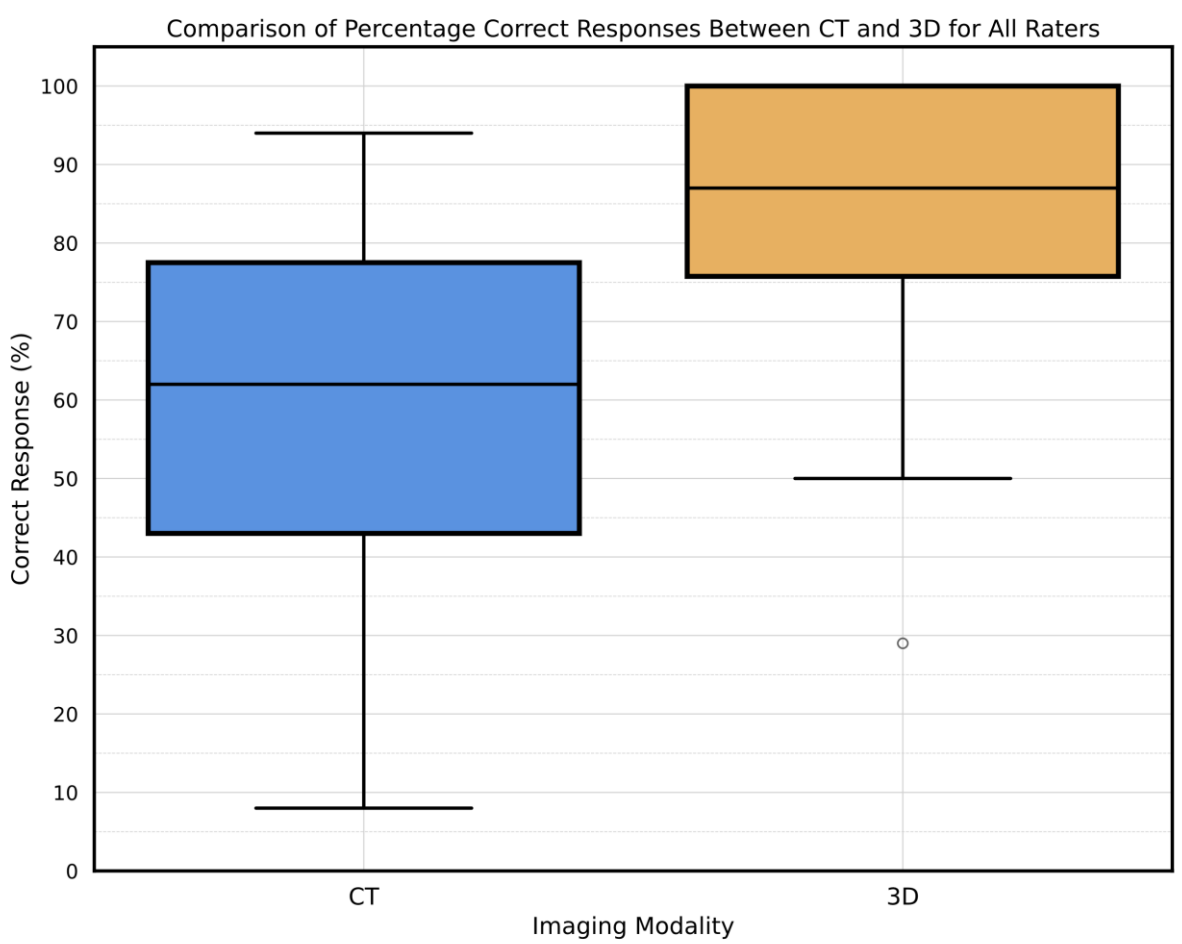
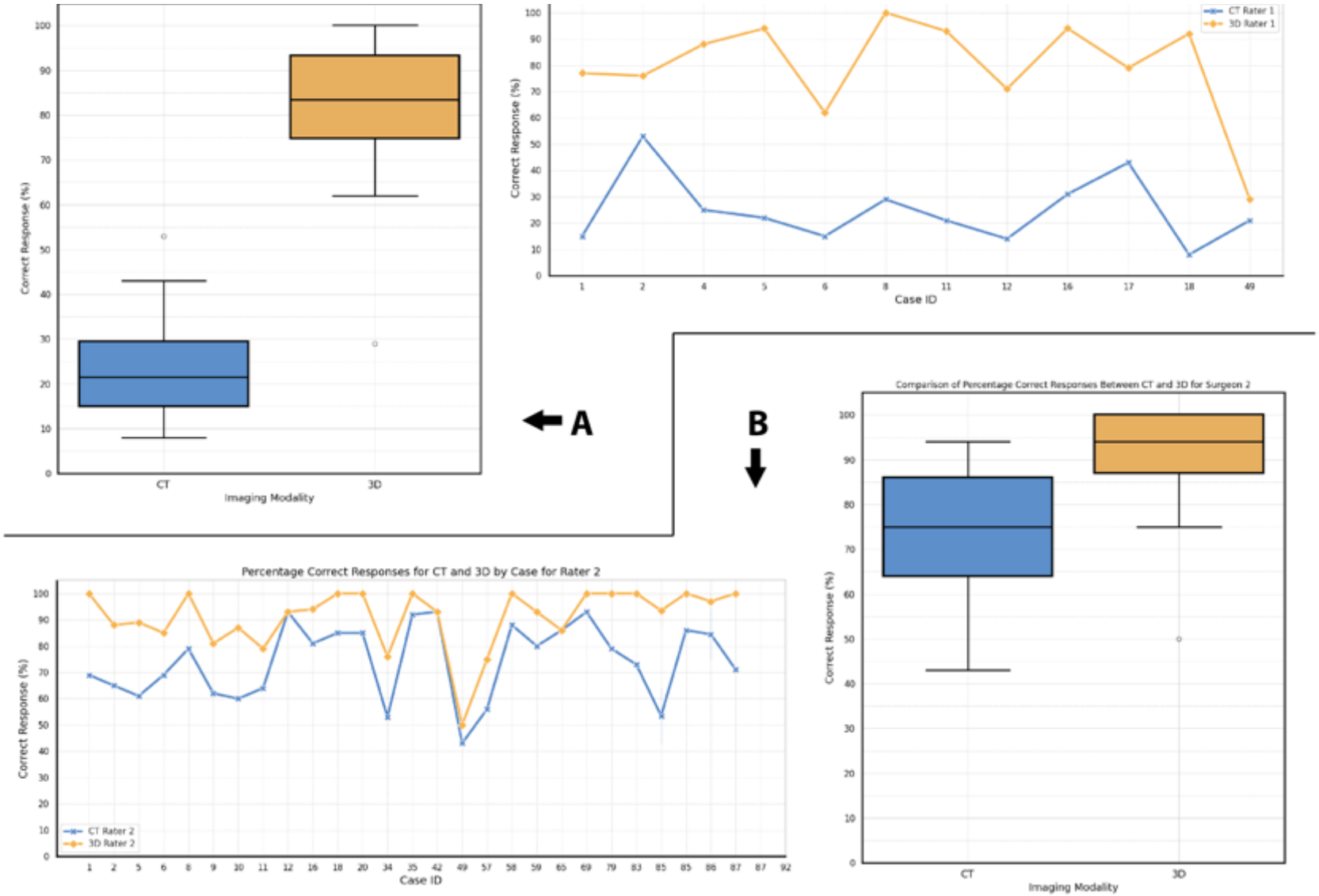
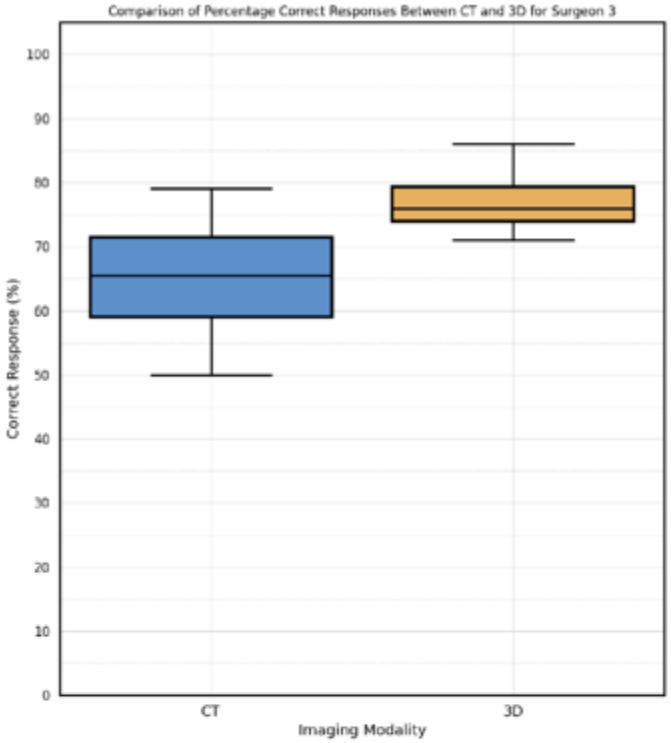
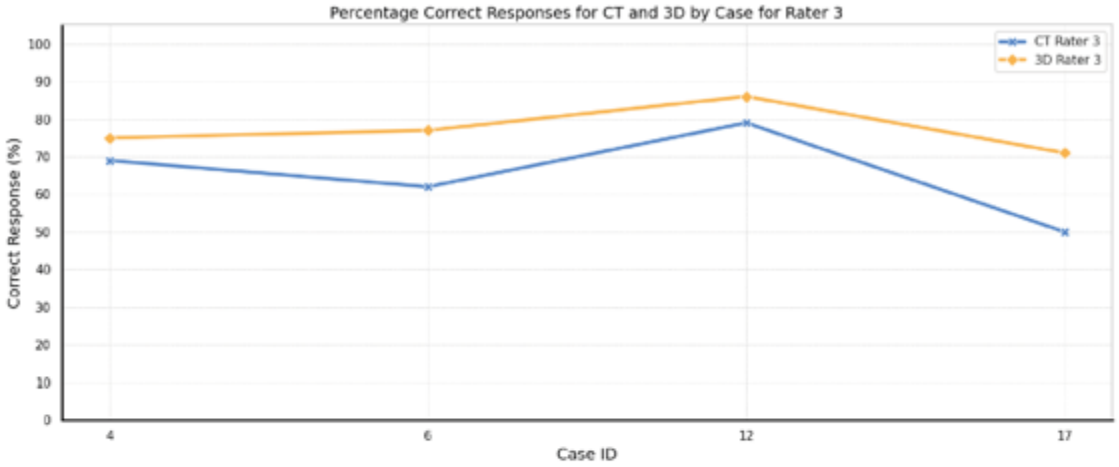


Figure 5-18 A-H Comparison of correct responses for mesenteric vessel identification using CT (blue) and 3D (orange) imaging modalities for multiple raters. Each figure (A–I) presents data for one rater who performed at least three cases. For each rater, a box-and-whisker plot compares the average percentage of correct responses between CT and 3D and a line plot shows the percentage of correct responses by case, displayed chronologically. These figures highlight both the overall improvement in accuracy with 3D reconstructions and the case-by-case variability in performance.

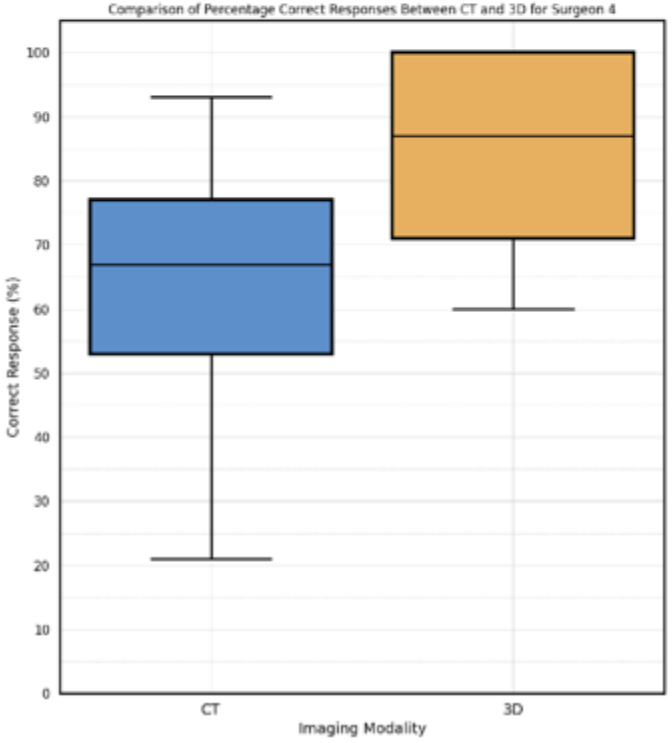


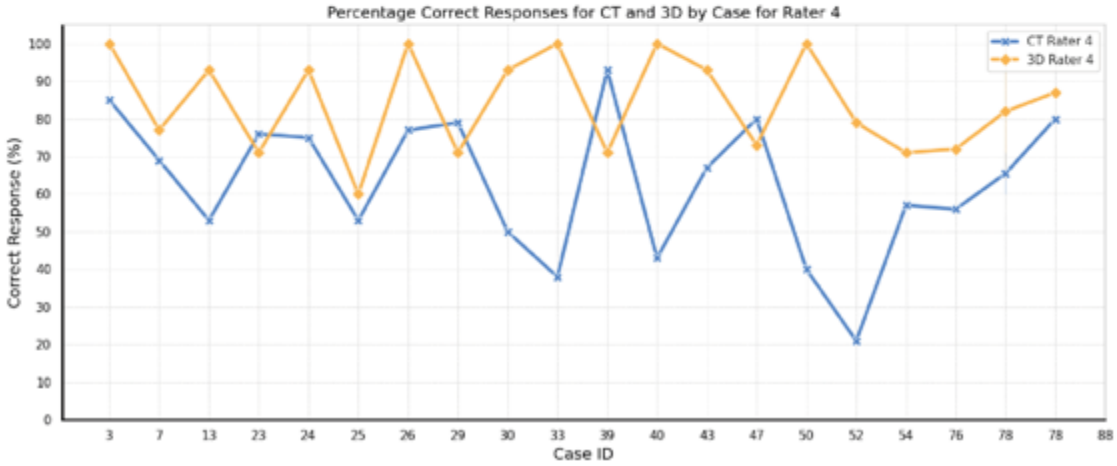

Comparison of Percentage Correct Responses Between CT and 3D for Surgeon 3
Correct Response (%)
Imaging Modality
CT
3D

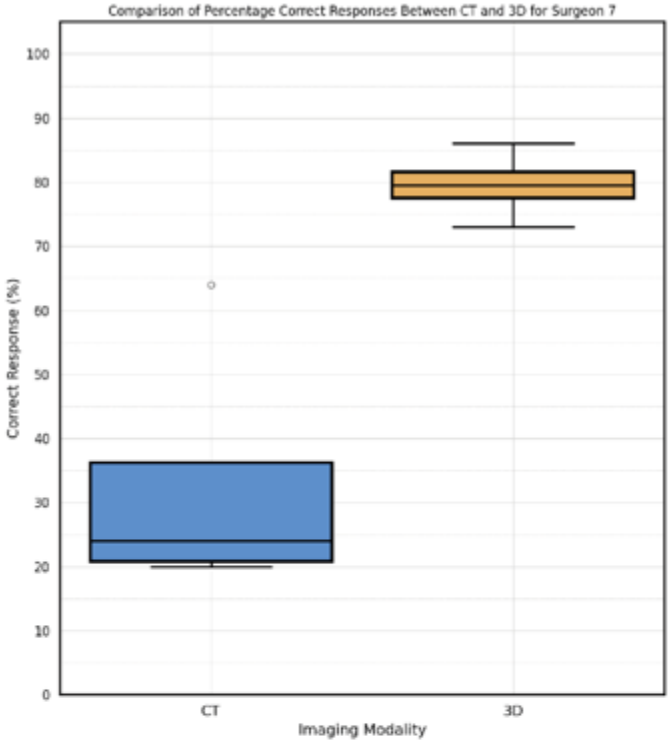

Percentage Correct Responses for CT and 3D by Case for Rater 3
CT Rater 3
3D Rater 3
Correct Response (%)
Case ID

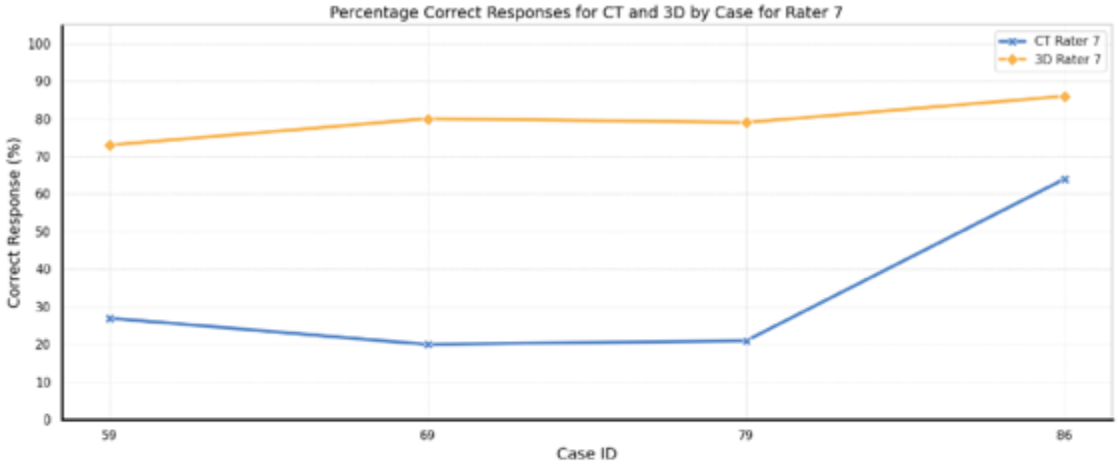
C

D


Comparison of Percentage Correct Responses Between CT and 3D for Surgeon 4
Correct Response (%)
Imaging Modality
CT
3D

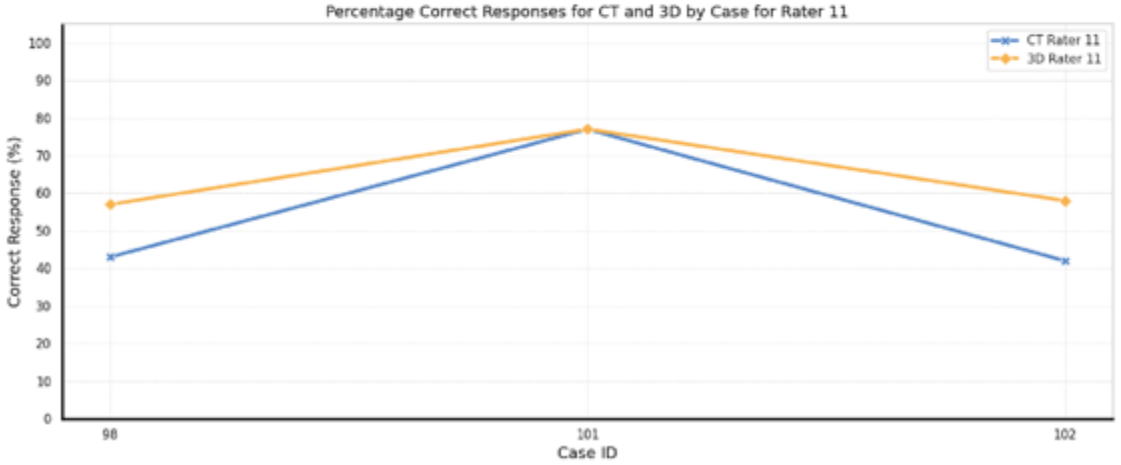

Percentage Correct Responses for CT and 3D by Case for Rater 4
CT Rater 4
3D Rater 4
Correct Response (%)
Case ID


Comparison of Percentage Correct Responses Between CT and 3D for Surgeon 7
Correct Response (%)
Imaging Modality
CT
3D


Percentage Correct Responses for CT and 3D by Case for Rater 7
CT Rater 7
3D Rater 7
Correct Response (%)
Case ID
59
69
79
86

G

H


Percentage Correct Responses for CT and 3D by Case for Rater 11
CT Rater 11
3D Rater 11
Correct Response (%)
Case ID
98
101
102

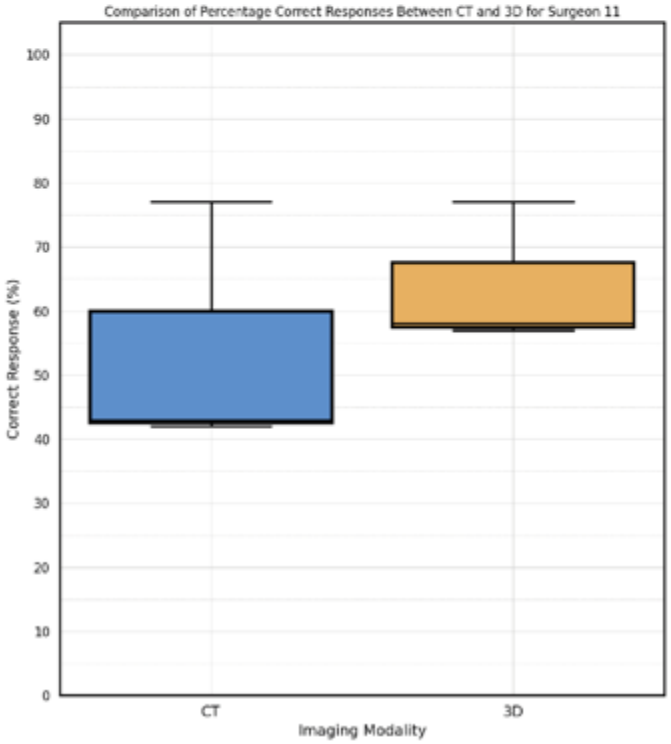

Comparison of Percentage Correct Responses Between CT and 3D for Surgeon 11
Correct Response (%)
Imaging Modality
CT
3D

Table 5-11 Comparative Percentage Differences in Correct Responses Between 3D Models and CT scans

Surgeon	n	Mean Diff.	Std Dev	Min Diff.	Max Diff.	3D Better (n)	3D Worse (n)	No diff. (n)
1	12	55	22.4	8	84	12	0	0
2	29	17	9.9	0	40	24	0	3
3	21	12	7.1	6	21	4	0	0
4	4	21	24.7	-22	62	16	4	0
5	12	22	15.6	0	50	11	0	1
9	7	30	n/a	n/a	n/a	1	0	0
8	4	41	n/a	n/a	n/a	1	0	0
7	1	47	17.5	22	60	4	0	0
6	1	12	14.8	-8	31	5	1	1
12	3	44	2.8	40	47	5	0	0
11	5	10	8.7	0	16	2	0	1
13	1	47	n/a	n/a	n/a	1	0	0
Overall		**24**	**18.4**	**-22**	**62**	**66**	**5**	**5**

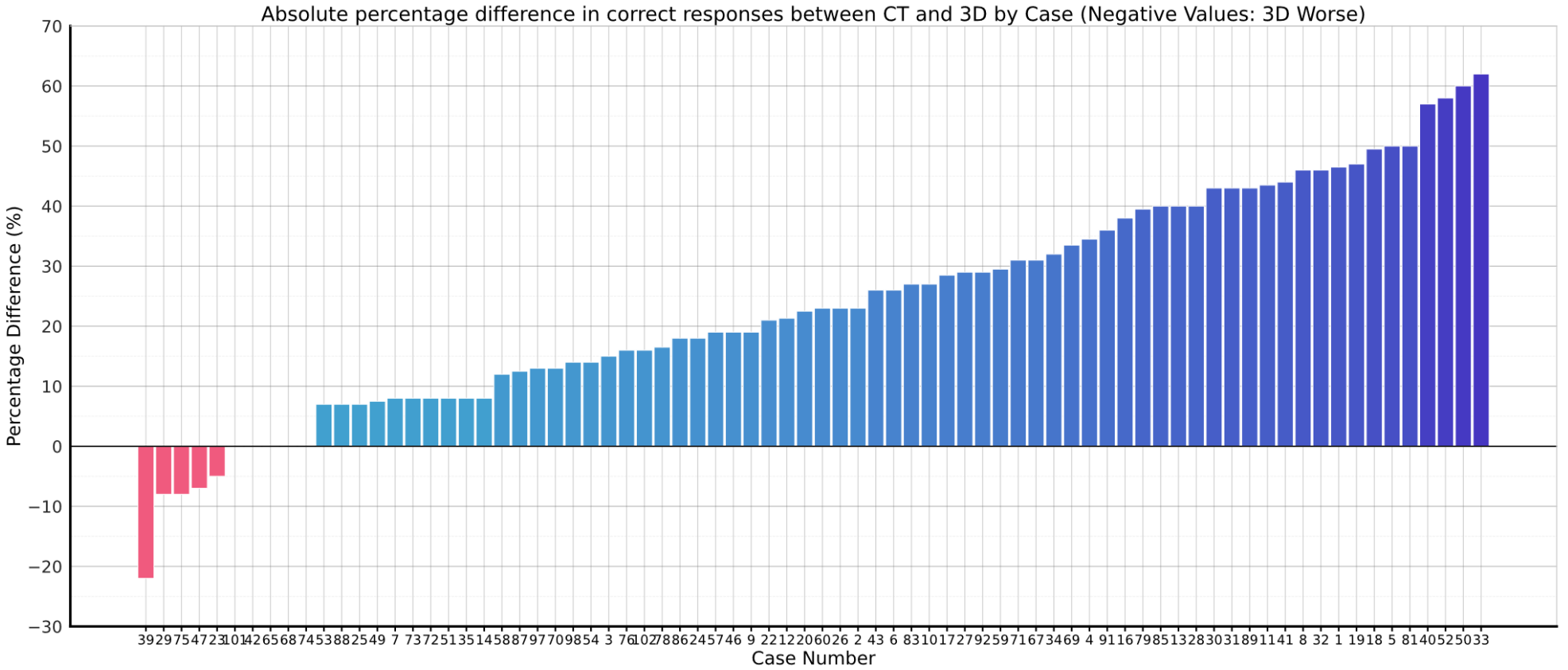
In most cases, using 3D models enhanced surgeons' anatomical understanding. Detailed results are provided in Table 5-11 and illustrated in Figures 5-19.

On average, using 3D models resulted in a 24% increase in correct responses. All participating surgeons demonstrated improvements, with individual increases ranging from 10% to 55%.

Specifically, assessments using 3D models were more accurate in 66 out of 76 cases. In five cases, the accuracy was identical between 3D models and CT scans, whilst in another five cases, CT scans proved superior.

The differences in correct responses varied widely, ranging from a decrease of 22%—indicating better performance with CT scans—to an improvement of 84% with 3D models.

Figure 5-19 Bar chart illustrating the absolute percentage difference in correct responses between CT and 3D imaging modalities for each case. Positive values indicate better performance with 3D, while negative values (in pink) represent cases where CT performed better. Most cases show improved accuracy with 3D, with only a small subset exhibiting a preference for CT.



5.7.1.1 Comparative Evaluation of Correct Responses by Mesenteric Vessel

Figure 5-20 Average correct responses by question using CT and 3D models

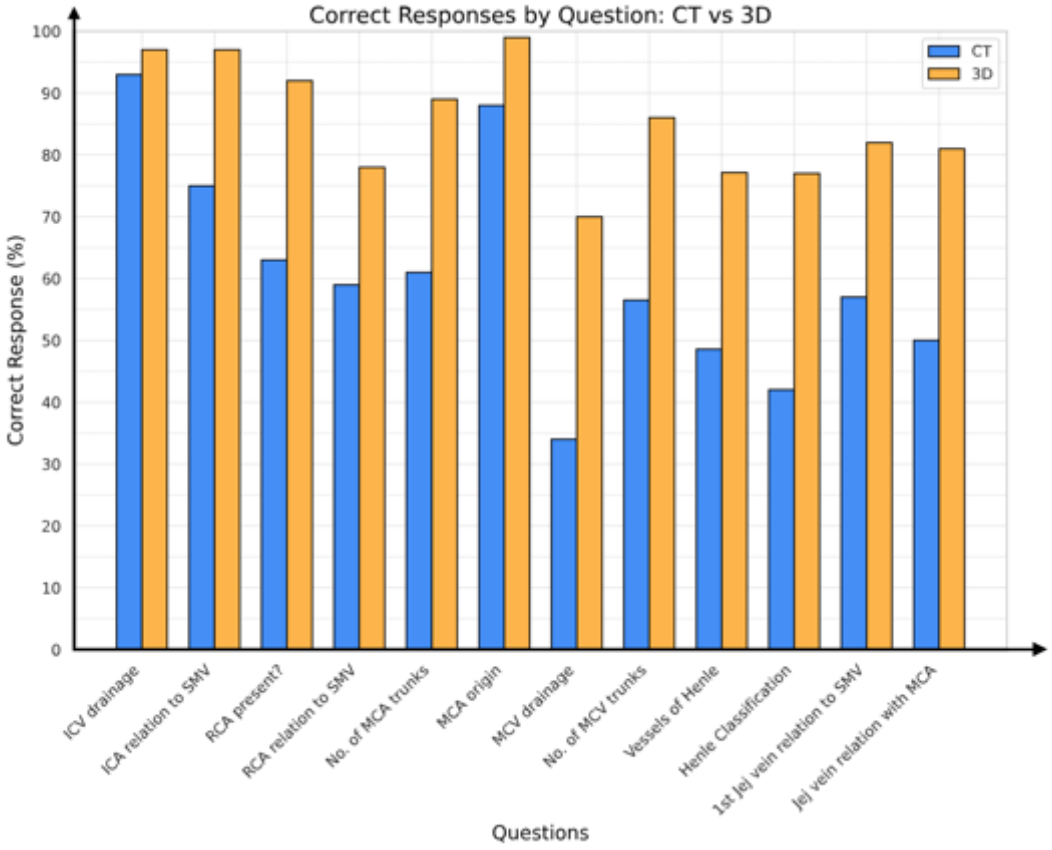


Table 5-12 Average correct response by vessel using CT and 3D

	Percentage (%) Correct Responses	
	CT	**3D**
ICV drainage	93	97
ICA relation to SMV	75	97
RCA Present?	63	92
RCA Relation to SMV	59	78
Number of MCA trunks	61	89
MCA origin	88	99
Number of MCV trunks	34	70
MCV drainage	57	86
Constituent vessels of Henle's	49	77
Henle's Classification	42	77
Jejunal vein relation to SMV	57	82
Jejunal Vein relation to MCA	50	81

The accuracy of identifying vascular structures improved when using the 3D model compared to CT imaging alone. For ICV drainage, the correct response rate increased from 93% with CT to 97% with the 3D model. The correct identification of the ICA's relation to the SMV rose from 75% with CT to 97% with the 3D model. Similarly, the presence of the RCA was correctly identified in 63% of cases using CT, which improved to 92% with the 3D model. The correct determination of the RCA's relation to the SMV increased from 59% with CT to 78% with the 3D model.

In assessing the MCA, the number of trunks was correctly identified in 61% of cases with CT, improving to 89% with the 3D model. The origin of the MCA showed a correct response rate of 88% with CT, rising to 99% with the 3D model. Identification of the number of MCV trunks improved significantly from 34% with CT to 70% with the 3D model. Correct responses for MCV drainage also increased from 56.5% with CT to 86.0% with the 3D model.

For the constituent vessels of Henle's trunk, correct responses improved from 48.6% with CT to 77.2% with the 3D model. The accuracy of the Henle classification increased from 42% with CT to 77% with the 3D model. The relation of the jejunal vein to the SMV was correctly identified in 57% of cases using CT, improving to 82% with the 3D model. Similarly, correct identification of the jejunal vein's relation to the MCA increased from 50% with CT to 81% with the 3D model.

5.7.2 Time spent on imaging interpretation.

3D models significantly reduced the amount of time surgeons required to determine the vascular anatomy by 50% (12 versus 6 minutes, p=<0-0001). Figure 5-21 depicts the distribution of time spent on each imaging modality, with results summarised in Table 5-13.

Figure 5-21 Time spent on interpretation of CT scans and 3D models to determine mesenteric vascular anatomy

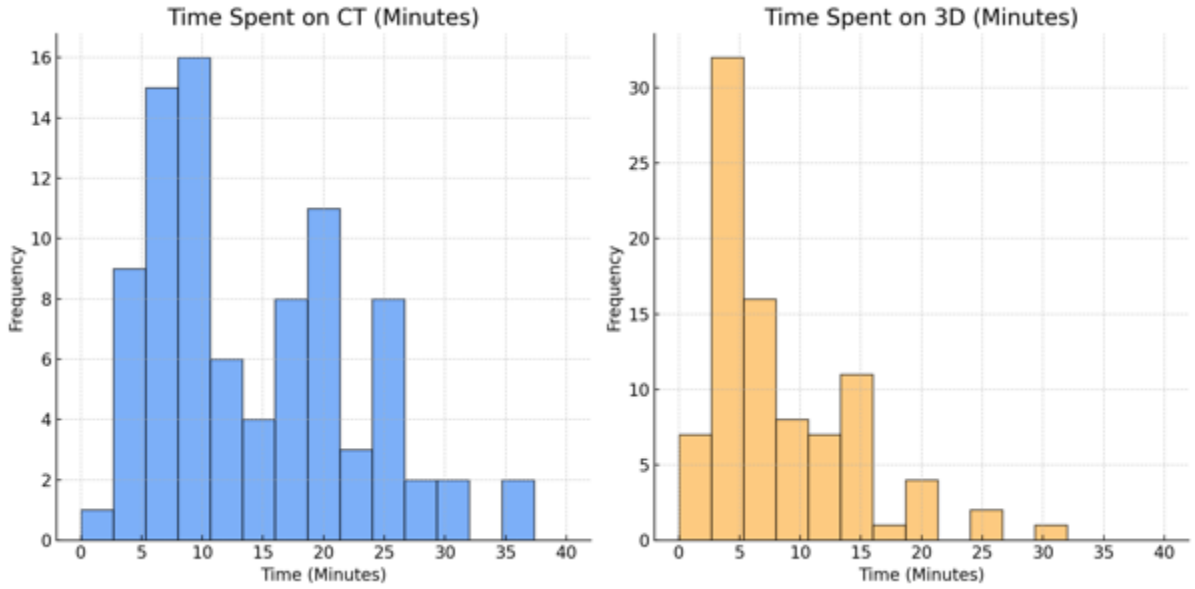
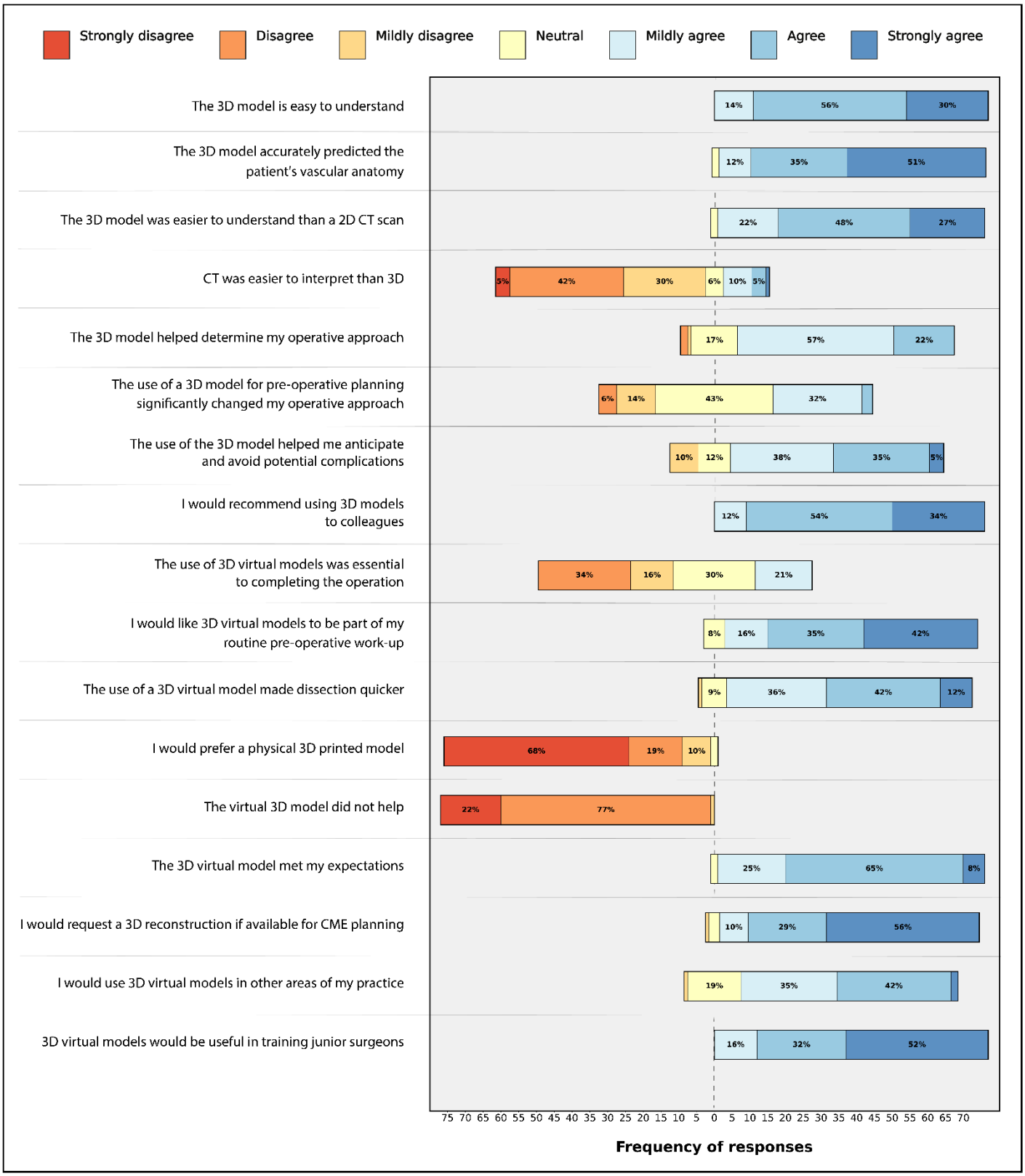


Table 5-13 Summary statistics for time spent on imaging modality interpretation.

Statistic	CT (Minutes)	3D (Minutes)
Median	12m 0s	6m 0s
Min	1m 40s	1m 20s
Max	35m 0s	30m 0s
Interquartile Range	12m 34s	7m 0s
p-Value	<0.001	

5.7.3 Subjective model feedback

Figure 5-22 Diverging bar chart of surgeon responses to Likert scale questionnaire relating to use of 3D model.



A summary of responses to the Likert subjective questionnaire can be found in figure 5-22.

Subjective feedback regarding the utility of 3D models was generally positive. A total of 87% of respondents agreed or strongly agreed that the 3D model was easy to interpret, while 85% felt that the model accurately represented patient anatomy. In comparison, 77% disagreed that conventional CT imaging was easier to understand. Additionally, 100% of respondents indicated that they would recommend the use of 3D models to colleagues, and 92% expressed a preference for incorporating 3D visualisations into their routine pre-operative planning.

Most surgeons favoured the virtual 3D model over a 3D-printed version. While 57% mildly agreed that the model informed their operative approach, no respondents strongly agreed. Surgeons demonstrated a mixed response regarding whether the model substantially altered their surgical plan, with 42% remaining neutral and 14% and 32% mildly disagreeing or mildly agreeing, respectively.

All respondents (100%) considered the 3D models to be helpful in the training of junior surgeons, suggesting potential value in educational applications.

5.8 Discussion

This study investigates the feasibility of integrating patient-specific three-dimensional (3D) reconstructed models into the preoperative planning and intraoperative guidance for CME in right-sided colon cancer. By analysing both the objective accuracy of these models in predicting mesenteric anatomy and the subjective feedback from surgeons regarding their utility, this study provides important insights into the potential clinical applications and limitations of 3D modelling in complex colorectal surgery.

5.8.1 Accuracy of 3D Reconstructions

The 3D reconstructions demonstrated high accuracy in predicting mesenteric vessels. Specifically, the models accurately predicted the drainage of the ileocolic vein and the relationship of the ileocolic artery with respect to the superior mesenteric vein (SMV) in all cases, achieving an accuracy of 100%.

For the right colic artery (RCA), the 3D reconstructions achieved an overall accuracy of 98.7%, correctly identifying its presence and course in 92.9% of cases. The single instance where the RCA was missed underscores the challenges associated with visualizing this vessel using standard Porto venous imaging phases. Even with retrospective analysis, the RCA remained exceedingly difficult to detect on imaging, suggesting that limitations in imaging modalities, rather than the reconstruction process, may account for such discrepancies.

The models also predicted the number of middle colic artery (MCA) trunks with an accuracy rate of 98.5% in cases where intraoperative visualisation was possible. However, when the middle colic vessels were included in the dissection, their origin and branching configuration were accurately predicted by the 3D models. This level of accuracy in mapping the MCA is particularly relevant given its significance in preserving adequate blood supply to the remaining colon and preventing ischemic complications.

Regarding the constituent vessels of Henle's trunk, sufficient delineation for visual confirmation was achieved in 29 cases. The 3D models attained 100% accuracy in predicting the presence of the gastroepiploic vein and colic veins. The anterior superior pancreaticoduodenal vein (ASPDV), however, exhibited lower sensitivity and specificity, being missed in two cases and incorrectly predicted as present in one case. Although the accuracy for the ASPDV was lower, this vessel is of less clinical importance compared to major vessels like the ileocolic vessels and the MCA. Its variable anatomy and smaller caliber may contribute to the challenges in accurate visualisation, and limitations in standard porto venous imaging may not adequately capture such smaller vessels.

These findings suggest that while 3D reconstructions are highly accurate for major vessels critical to CME, limitations remain in detecting smaller or less clinically significant vessels due to imaging constraints. The use of standard porto venous phase imaging may not suffice for detailed visualisation of all vascular structures, particularly smaller arterial vessels. Incorporating arterial phase imaging could potentially enhance the detection and accuracy of these vessels, as supported by previous studies demonstrating improved vascular visualisation with multiphase imaging protocols (Wang et al., 2021). Although our data doesn't allow for formal imaging recommendations, our experience suggests that a maximum slice thickness of 2mm may improve visualisation. While scans of >2m were accurately segmented there were numerous incidences where interpretation was difficult with a high degree of pre-operative uncertainty relating to some of the small calibre vessels even if the resulting model was eventually found to accurately depict the operative anatomy.

Overall, the high accuracy rates achieved for the ileocolic vessels and MCA trunks validate the clinical utility of 3D models in preoperative planning for right-sided colon cancer surgeries. As the sample cases included demonstrate not only was the presence of given vessels accurate but the models accurately depicted the configuration and spatial relationship of vascular structures.

The ability to reliably predict the course and branching patterns of these critical vessels can aid surgeons in strategising their operative approach, minimising intraoperative uncertainties, and potentially reducing the risk of vascular injuries.

5.8.2 Anatomical Understanding

The integration of three-dimensional (3D) models derived from preoperative imaging significantly enhances the understanding of mesenteric vascular anatomy compared to conventional computed tomography (CT) scans. These findings align with previous work, demonstrating an improvement in the identification of clinically important vascular structures. The use of 3D models resulted in an increase in overall median accuracy, from 62% with CT scans to 87% ($p < 0.001$), with a reduction in the interquartile range, indicating greater consistency in anatomical interpretation. Each of the twelve participating surgeons demonstrated improved understanding, with the median improvement in correct responses ranging from 11% to 62%.

Furthermore, the use of 3D models significantly reduced interpretation time, from 12 minutes with CT scans to 6 minutes ($p < 0.001$). This suggests that 3D models offer not only enhanced accuracy but also a more efficient method for assimilating anatomical information relevant to preoperative planning in CME.

Although our study was not designed to ascertain whether surgeons of different levels of experience benefit differentially from 3D models in terms of anatomical understanding, the data suggest that highly experienced surgeons with extensive CME expertise demonstrated an average improvement of 17% in anatomical understanding compared to 43.4% for trainee surgeons and 20% for consultants inexperienced in CME surgery. This implies that the absolute benefit of 3D models may diminish with increasing surgical expertise, potentially reflecting the effect of prior anatomical familiarity and experience. Additionally, differences in imaging interpretation skills could confound these findings, suggesting the need for further investigation into how experience with imaging impacts the utilisation of 3D models.

The 3D models improved recognition of each assessed vessel, with particularly pronounced improvements for complex structures. Specifically, there was a 28% improvement in

understanding the configuration of Henle's trunk and a 36% improvement in recognising the middle colic vein. Improvements were more modest for other structures, with a 4% improvement in recognising the drainage of the ileocolic vein and an 11% improvement for the origin of the middle colic artery. This differential improvement likely reflects the varying complexity and anatomical variability of these structures, with more intricate anatomical arrangements benefiting more substantially from the visual clarity offered by 3D models.

It should be noted, however, that the measure of anatomical understanding used in this study focuses primarily on specific aspects, such as the presence of a vessel, its origin, or drainage pattern. This measure does not fully capture other critical components of anatomical understanding, such as an appreciation of scale, relative location, and the spatial relationships between structures. Consequently, we may not be appreciating a significant portion of the qualitative benefits that 3D models provide in terms of a more holistic understanding of mesenteric anatomy.

5.8.3 Subjective Model Feedback

The qualitative assessment of surgeon perceptions regarding 3D model utilisation yielded predominantly positive responses, indicating a high degree of user acceptance and perceived utility. A significant majority of respondents (87%) reported that the 3D models were easily interpretable, while 85% affirmed that the models accurately represented patient-specific anatomy. These findings suggest that the 3D reconstructions not only enhanced anatomical comprehension but also provided an intuitive visualisation tool that that operating surgeon found to be clinically useful.

The universal recommendation (100%) of 3D models to colleagues and the near-unanimous desire (92%) for integration into routine preoperative planning underscore the perceived value of this technology among the participating surgeons. However, the impact of 3D models on operative approach modification was less pronounced. While a majority (57%) mildly agreed that the models influenced their surgical approach, the absence of strong agreement and the presence of neutral responses (42%) indicate that the primary benefit of 3D reconstructions may lie in facilitating dissection and enhancing intraoperative decision-making through improved anatomical landmark recognition, rather than fundamentally altering the operative strategy.

50% of surgeons disagreed with the statement that the model was required to complete the operation. This finding suggests that while 3D models are perceived as valuable adjuncts, they are not considered indispensable for performing CME procedures. This perspective aligns with the understanding that 3D reconstructions serve to augment and refine existing surgical techniques rather than introduce novel approaches.

The discrepancy between the high perceived value and the more modest impact on operative approach warrants further investigation. It may reflect a distinction between the model's utility in preoperative planning and its direct influence on intraoperative decision-making. Future studies should aim to elucidate the specific aspects of surgical planning and execution that benefit most from 3D model integration, potentially through more granular questionnaires or qualitative interviews with participating surgeons.

5.9 Conclusion and Future Research Directions:

This feasibility study demonstrates that the integration of patient-specific 3D reconstructed models into the preoperative planning and intraoperative guidance for Complete Mesocolic Excision (CME) in right-sided colon cancer is both feasible and potentially beneficial. The high accuracy of 3D reconstructions in predicting intraoperative anatomy, particularly for critical mesenteric vessels, supports their clinical utility. Furthermore, the significant improvement in surgeons' anatomical understanding and reduction in interpretation time when using 3D models compared to conventional CT scans highlights their potential to enhance preoperative planning efficiency.

However, the study also identifies several challenges that need to be addressed before widespread implementation can be considered. The time-intensive nature of manual segmentation remains a significant barrier, emphasizing the need for more efficient, automated approaches. Additionally, while subjective feedback from surgeons was overwhelmingly positive, the impact of 3D models on altering operative approaches was less pronounced, suggesting that their primary benefit may lie in enhancing anatomical understanding and intraoperative navigation rather than fundamentally changing surgical strategies.

By addressing these research areas, future studies can build upon the promising results of this feasibility study and potentially establish 3D modelling as a standard tool in the preoperative planning and execution of complex colorectal surgeries.

6 The Role of Personalised 3D Imaging in Enhancing Patient Comprehension and Decision-Making in Advanced Colorectal Cancer Treatment

6.1 Background

6.1.1 Context

The modern healthcare paradigm underscores patients' need to actively participate in healthcare decisions (362). The historical physician-driven communication models have given way to a patient-centric system prioritizing shared decision-making (363) (364) . This type of care is centred on discerning individual needs and customising treatment plans accordingly (365). Current healthcare practices strive to balance medical beneficence and the emerging emphasis on patient autonomy.

Obtaining informed consent is a mandatory step for any surgical procedure. It embodies patients' fundamental legal and ethical right to control their bodies (366). Legally, informed consent is a patient's voluntary agreement to a medical or surgical intervention, with complete comprehension of the associated risks, benefits, potential outcomes, and alternatives (367). The appropriateness of consent was formerly evaluated via the Bolam test, where a doctor's obligation to inform patients about potential risks hinged on the alignment with a responsible body of medical opinion (368). However, the Montgomery ruling has redirected the focus onto the patient’s viewpoint. Physicians are now required to disclose any risk that they believe a particular patient would consider significant. Presenting isolated percentage risks without considering the individual's context is no longer adequate (368) (369). Consequently, the demand for a patient-specific consent process has risen significantly.

Consent should not be exclusively viewed as a legal requirement despite its roots in law. Informed consent serves as an opportunity for healthcare professionals to reinforce patient autonomy (370). It is a fundamental element of ethical surgical practice, encapsulating the principle that patients are autonomous entities deserving of respect and the basic human right of self-determination (371).

Consent should not be considered a singular event but a communication process that should permeate every clinical interaction (371). Informed consent is increasingly manifested via shared decision-making (SDM) in clinical practice. This represents the reciprocal relationship between the patient and the doctor. While surgeons contribute their understanding of a treatment's pros, cons, and alternatives, patients bring their personal experiences, preferences, and healthcare objectives. Surgeons typically offer expert opinions and make suggestions that can be collaboratively agreed upon with the patient to formulate the treatment plan. Historically, patients have assumed a more passive role in surgical decision-making. Three elements have traditionally dictated the decision-making process in surgery: 1) the patient’s functional status, 2) surgeon preference, and 3) disease characteristics. Facilitating SDM may foster more informed decision-making that aligns with the patient's preferences.

The Ottawa decisional support framework presents a compelling argument for enhancing patient education. It is underpinned by cognitive, social, and organisational psychological theories and encompasses three primary components: 1) decisional needs, 2) decisional quality and 3) decisional support. A patient's decisional needs encompass any conflict regarding determining the optimal course of action, a lack of understanding of their condition or treatment (including benefits, risks, alternatives, etc.), and unrealistic expectations. If patients' decisional needs are unmet, their ability to make informed decisions decreases. Numerous research studies have indicated that well-informed patients are more likely to adhere to treatment (372), experience greater satisfaction and reduced anxiety (373), and demonstrate superior outcomes (374).

6.1.2 Contemporary Challenges in Surgical Consent and Patient Instruction

For consent to be regarded as valid, three prerequisites must be satisfied: patients must possess decision-making capacity, be provided with comprehensive information, and be free from coercion. Hence, patient instruction is integral to informed consent and shared decision-making processes (166). For patients to make genuinely informed decisions about their treatment, they need to comprehend the implications of their options. According to

Marteau and colleagues, an informed decision must rely on pertinent, high-quality information that aligns with the individual's values (166).

Nevertheless, there is concern that the prevailing consent process may not satisfy these fundamental criteria (375) (376). Multiple studies suggest that patients often lack a solid understanding of their surgical procedure (167) (377) (378) (379). For instance, Santavirta et al. discovered that 37% of patients undergoing total hip replacement could not recall a significant complication (380). Likewise, a study involving 200 patients undergoing laparoscopic cholecystectomy showed that only 51% had sufficient understanding of their operation, and fewer than 31% could identify a single potential complication (381). A qualitative interview study scrutinising informed consent in rectal cancer surgery found that none of the thirty patients felt they had a choice of surgical alternatives. This perceived absence of choice may reflect the surgeon's dominant role in decision-making (382). When asked about the primary outcomes of rectal cancer surgery, half of the patients could not remember any preoperative discussion regarding changes in bowel habits, urinary function, or sexual function (382). This is especially concerning given the value patients place on quality-of-life-related outcomes.

There are several impediments to effective communication. Interactions between physicians and patients can be compromised by linguistic, educational, and socio-economic challenges (383). Patients with limited English proficiency or poor literacy are susceptible to misunderstanding (384). Research has shown that poor health literacy negatively impacts individuals' ability to acquire and utilise health-related information (385). For example, in a study by Williams et al., 60% of 2659 patients at two US public hospitals failed to comprehend the written consent document (386).

Additionally, the information provided may not always align with patients' needs regarding content and volume. There is often a disconnect between what clinicians and patients prioritise during the consent process (387). Clinicians commonly underestimate the information patients wish to receive (388). Surgeons emphasise specific technical risks and adverse outcomes during operation discussions, potentially overlooking areas of more significant patient concern, such as functional outcomes, pain, and recovery duration (389). Another issue is translating population-based risk estimates to an individual level. Standardised consent forms may overlook individual needs and compromise patient autonomy (390). Overly systematic pre-operative instruction may make clinicians insensitive to patients' concerns (391). Aside from the legal and ethical obligations, enhancing patient understanding is correlated with increased satisfaction, better adherence to treatment, and fewer post-operative complications (392) (393) (394).

6.1.3 Evaluation of Patient-Specific 3D Models in Enhancing Patient Understanding and Decision-Making

A diverse range of interventions have been assessed to enhance patient comprehension and decision-making. These interventions encompass changes in the timing of consent, extended consultations, specialised educational initiatives (such as 'joint school' for patients due for total hip replacement (395), written resources, audio-visual tools (including videos, DVDs, websites, or software solutions), interactive multimedia, decision aids, and question prompt sheets 28. Surgical studies vary significantly in study design and outcome measures, making comparing interventions challenging. Given the intricate nature of decision-making and the individual differences among patients, potential solutions must be equally diverse and target distinct facets of the consent process (387). Ensuring comprehensive patient education is a critical component of any such solution.

The presentation of information significantly impacts patient comprehension and recall (396). Standalone oral information is often poorly retained. Visual aids can make information more comprehensible for patients than text-only formats, particularly for those with limited literacy (397). A review of the role of illustrations in health communication demonstrated that visuals enhance attention, comprehension, recall, and adherence (398). Specifically, illustrations can significantly improve the recall of conceptual knowledge and problem-solving information for lay audiences (399). In a recent randomised control trial, Rosenfeld et al. assessed the impact of standardised visual aids on the consent process for children with acute appendicitis. Multivariate analysis revealed that standardised illustrations had the most positive effect on parental comprehension and retention (with 75% correct on a knowledge-based assessment, compared to 50%; $p<0.01$) (392).

However, illustrations do not necessarily ensure comprehension. Images must be straightforward, clearly labelled with a sufficiently large font, and communicate a single concept (399) (400). Three-dimensional (3D) virtual imaging and printing may offer advantages over 2D illustrations when explaining complex anatomy and surgical procedures (401). A key reported benefit of 3D visualisation is enhanced anatomical perception (402) (403) (116) (404) (405).

Preliminary studies on using 3D models in patient education have yielded promising results. Yoon et al. reported that personalised printed models enhanced self-reported patient knowledge and satisfaction during consent for stage 1 lung cancer surgery (406). A similar

increase in satisfaction was observed when 3D-printed models were used for preoperative education for patients undergoing robot-assisted partial nephrectomy (168).

3D models have also been shown to improve patient knowledge objectively. Bernhard et al. evaluated the impact of personalised models on patients' understanding of their renal tumor using a custom questionnaire. Patients provided with a personalised 3D kidney model demonstrated an improved understanding of renal physiology by 16.7%, anatomy by 50%, tumor characteristics by 39%, and the planned procedure by 44.6% (169). Parents of children undergoing hepatectomy showed improved objective understanding when 3D-printed models were used during the consent process (8). However, these studies only compare 3D models against standard practice and use variable non-validated outcome measures. It is yet to be determined whether 3D models are superior to more straightforward multimedia solutions or visual aids. A randomised control trial investigating the effect of 3D animation versus simple hand-drawn real-time illustrations found animation superior in periodontal education (407). Patient-specific 3D virtual/printed models, if derived from a patient's scan, may also facilitate personalised consent processes. This chapter evaluates the role of such patient-specific 3D models derived from patient imaging.

6.2 Methods

6.2.1 Study Design

This prospective mixed-methods, randomised controlled study was conducted at the St Mark’s Hospital Complex Cancer Clinic, where patients with complex colorectal cancer receive specialised multidisciplinary consultations. Most patients are referred from other institutions and are thus typically aware of their diagnosis before attending the clinic. Many also require multiple appointments before surgical intervention. The study's primary objective was to evaluate the effectiveness of personalised 3D imaging in enhancing patient comprehension and informed decision-making in complex colorectal cancer treatment.

6.2.2 3D patient-specific model reconstruction

PBR 3D models were reconstructed from combinations of MR and CT data as outlined in Chapter 2.

6.2.3 Patient recruitment

Patients were recruited from the St Mark's complex clinic list.

Inclusion criteria:

- Male and female patients
- Aged ≥18
- English and non-English-speaking patients
- Locally advanced and recurrent rectal cancer patients under consideration for beyond TME or pelvic exenteration surgery (including sacrectomies and pelvic sidewall excisions)
- Possess capacity and can provide consent to participate.
- Suitable imaging available (either MRI/CT scan, depending on the specific case)

Exclusion criteria

- Patients < 18 years of age
- Emergency patients
- No suitable imaging
- Patient not under consideration for operative intervention
- Patient lacking capacity.
- Did not complete the full set of questionnaires.

Patients were invited to participate in the study and provided an information leaflet. Those who consented were randomly assigned to either the STANDARD or the 3D group.

6.2.3.1 STANDARD Group

Participants in the STANDARD group underwent the typical consultation process at the St Mark's Hospital Complex Cancer Clinic (CCC), which provides specialised multidisciplinary consultations and treatments for complex colorectal cancer. Most patients are referred from other institutions and are already aware of their diagnosis before attending the clinic. Given the complexity of their condition, many patients also require multiple appointments before undergoing surgical intervention. The Multidisciplinary Team (MDT), specialising in complex colorectal cancer care, reviews each patient's case. The team brings together consultant colorectal surgeons, gastrointestinal radiologists, cancer nurse specialists, physiotherapists,

and other relevant specialists who collectively develop a comprehensive treatment plan for each patient.

During the 30- to 40-minute consultation, the radiologist explains the patient's CT/MRI scans to enhance understanding of the disease. Based on MDT recommendations, surgical options are presented, with discussions covering potential risks and benefits specific to each patient's case. The clinic introduced telemedicine appointments in response to the COVID-19 pandemic, enabling patients to discuss their care via video calls.

6.2.3.2 3D Group

Participants in the 3D group received the same standard consultation process described above, supplemented with a personalised virtual 3D model. No strict guidelines were imposed regarding the duration or way the 3D model was to be employed; however, it was typically used after the imaging review to explain the proposed surgical treatment.

6.2.4 Randomisation and Interventions

Participants were randomised 1:1 into 3D model or standard consultation groups using a computer-generated sequence. Allocation was concealed using sequentially numbered, opaque, sealed envelopes. The 3D group received a standard consultation supplemented with a personalised 3D model, and the standard group received a conventional consultation without the 3D model. Participating surgeons received training in 3D model navigation.

6.2.5 Outcome measures

We collected basic demographic data for each patient, including age, gender, level of education, and primary language, along with details of their tumour and previous surgical interventions/ cancer treatments.

Before the consultation, patients were asked to complete the following questionnaires:

- **Control preference scale** measures the degree of control an individual wants to assume when decisions are made about medical treatment. (408)
- **Quality of Life (QOL) and Length of Life (LOL) preferences** were assessed using the four-point instrument designed by Meropol et al (409).
- **Treatment preferences** were assessed using a custom six-point Likert scale questionnaire. Patients were asked to rate how important the following treatment outcomes were:

- How important is quality of life to you?
- How important is length of life to you?
- Having control of bowels
- Minimising side effects of treatment
- Being able to spend time with friends and family.
- Maintaining sexual function
- Avoiding a stoma
- Maintaining my independence
- Getting back to work

Patients were also asked to state their pre-consultation treatment preferences by selecting a statement that best described their desired treatment preferences relating to operative interventions.

6.2.5.1 Primary objective outcome measure: Decisional conflict score

The primary outcome, decisional conflict, was measured with the 16-item, five-response category Decisional Conflict Score (DCS) instrument. The scale has previously been validated and has a robust construct validity reliability with a Cronbach alpha coefficient of over 0.78 (410). Patients were asked to complete the questionnaire before and after their consultation, and we compared the change in score pre and post-consultation between each group. Higher scores indicate increased decisional conflict, while lower scores signify confidence in decision-making (see Appendix 6.3).

6.2.5.2 Secondary objective outcome measures

6.2.5.2.1 Patient knowledge score

Patients were asked to complete a custom patient knowledge questionnaire after their consultation to assess their understanding of their proposed operation. The questionnaire was comprised of two elements.

The first component was a multiple-answer questionnaire, in which participants were asked to select the organs/structures that would be removed as part of their exenteration procedure and then asked to select the single best statement that reflected the likely functional outcomes for bowel and bladder function, stoma, mobility and sexual function. A surgical team member independently completed this questionnaire for each patient, and the level of agreement was ascertained.

6.2.5.2.2 Subjective feedback

Participants from each group were instructed to fill out a questionnaire utilising a 7-point Likert scale. This questionnaire aimed to measure their level of agreement or disagreement with a set of statements regarding their consultation and consent process. In addition to the core questionnaire, the 3D group was presented with an extra set of questions designed to assess their experience and opinion of the 3D model. These statements were carefully crafted in collaboration with the clinical team and the patients to encompass essential aspects of the clinic.

6.2.5.2.3 Semi-structured interviews

The present study utilised a mixed methods research design to understand the benefits of using personalised 3D models in clinical consent consultations for patients with advanced rectal cancer undergoing pelvic exenteration. Semi-structured interviews were utilised to ascertain patient perception and explore the potential benefits/drawbacks and how using the 3D model may have influenced their decision-making or understanding.

Data was collected using semi-structured interviews conducted over the Zoom video conferencing platform. The research team developed the interview guide based on existing literature regarding clinical consent and patient education. It was designed to explore patients' experiences with and perceptions of using 3D models in their consultations based on the data from the initial pilot study. Interviews ranged from 30 to 60 minutes and were digitally recorded and then manually transcribed verbatim for data analysis. The interviews continued until data saturation was reached, meaning no new themes emerged from the discussions.

Each interview used the following predetermined open-ended questions with the flexibility to explore themes or responses in more depth as appropriate:

1. **Introduction**: Each interview was commenced by explaining its purpose, assuring confidentiality, and asking for consent to record the conversation.
2. **Background Information**: We collected some basic demographic and background data.
    - Can you tell me a bit about your cancer diagnosis and treatment journey up to this point?
3. **Experience with Traditional Consent Consultations:**
    - Could you describe your experience with traditional consent consultations prior to your pelvic exenteration?
    - How well did you feel you understood the procedure and potential outcomes from these consultations?

4. **Experience with 3D Model-Enhanced Consultations:**
    - Can you describe your experience when a 3D model was used during the consent consultation?
    - In what ways, if any, did using the 3D model change your understanding of the procedure?
    - Why is understanding of your disease and potential treatment important?
    - How important was the personalisation of the model, i.e., showing your tumour and anatomy from your imaging data?
5. **Comparative Analysis:**
    - Could you compare your experiences with traditional consent consultations and 3D model-enhanced consultations?
    - Was seeing the scans a helpful experience? How does it compare to the 3D model?
    - How did using 3D models influence your decision-making process about the surgery?
6. **Perceived Benefits and Drawbacks:**
    - What were the benefits of having a 3D model during the consultation?
    - Were there any drawbacks or challenges related to the use of the 3D model?
    - Was the appearance of the model satisfactory?
    - How might the model be improved to facilitate your understanding better?
7. **Wrap-up:**
    - Is there anything else you think we should know about your experience with the 3D model in your consultation?

6.2.6 Data Analysis

The study's data was analysed and visualised using *Microsoft Excel* (Microsoft Corp., Redmond, WA, USA) and *Python* version 3.4 within a *Jupyter Notebook* environment (354). Custom *Python* scripts were written for data analysis. *Python* libraries utilised were *Numpy* for numerical computations (195), *Pandas* for data processing (355), *Matplotlib* (213) and, *Seaborn* (356) for graphical visualisations and *SciPy* for advanced statistical tests (196).

Descriptive statistics were used to summarise patient demographics and questionnaire responses. The *Shapiro-Wilk* test was used to assess the normality of continuous variables. The *Mann-Whitney* U test was used to compare the 3D and standard groups for continuous variables not normally distributed. The *Wilcoxon signed-rank* test was used to compare pre-

and post-intervention DCS scores within each group. Categorical variables were compared using the chi-squared test. Statistical significance was set at $p<0.05$.

6.2.7 Sample size.

For the primary qualitative objective, semi-structured interviews were conducted with 3D-group participants until thematic saturation was achieved. For the quantitative assessment of change in DCS, we targeted 20 participants per arm following recommendations by Whitehead et al. (411), which indicate this sample size provides adequate parameter estimates for future trial planning. This approach was supported by our preliminary data from 10 participants showing an effect size of -0.66 for DCS reduction with 3D models, suggesting that 20 participants per arm would provide sufficient power to detect meaningful differences.

Figure 6-1 A-H Example patient specific 3D reconstructions.

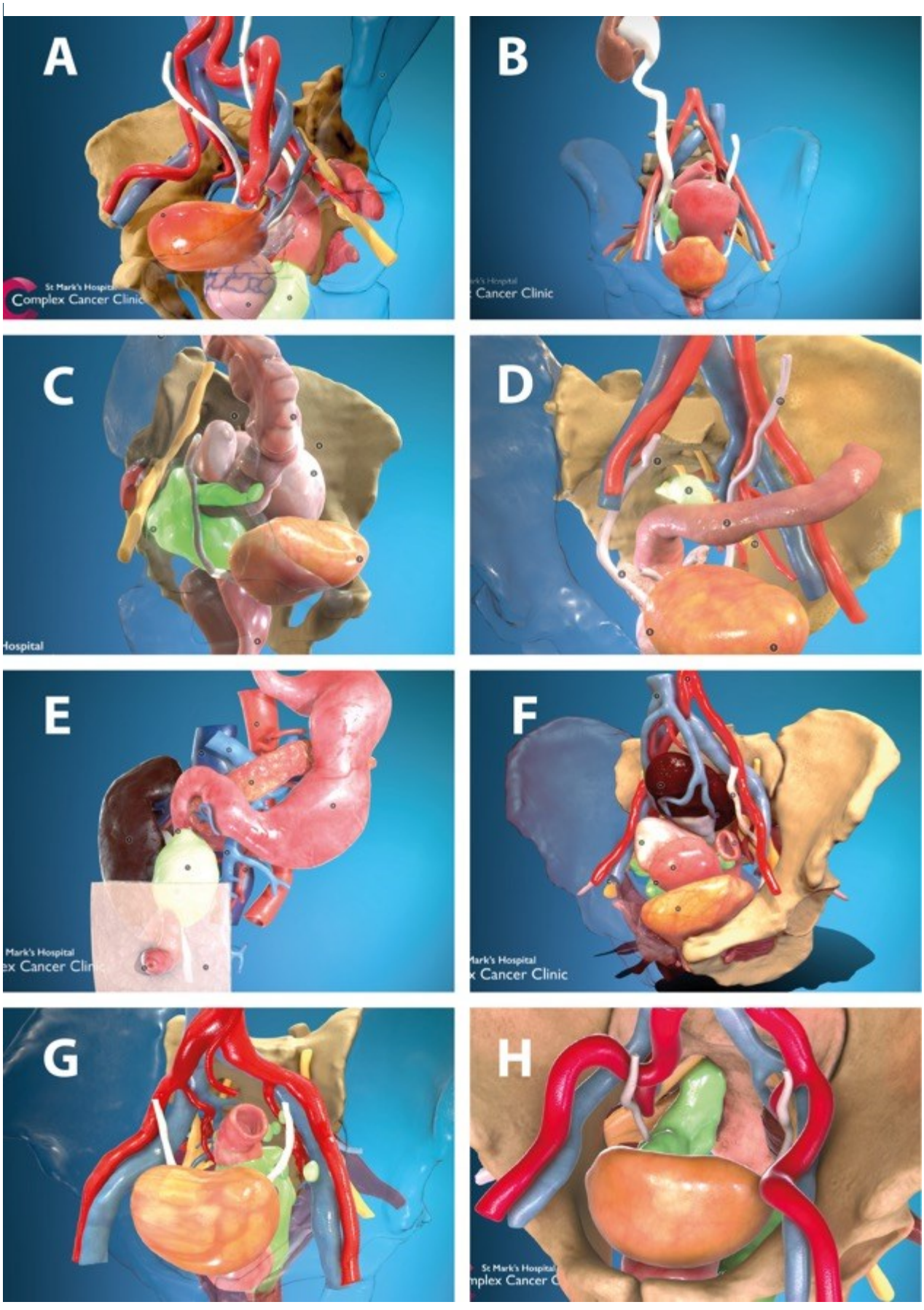
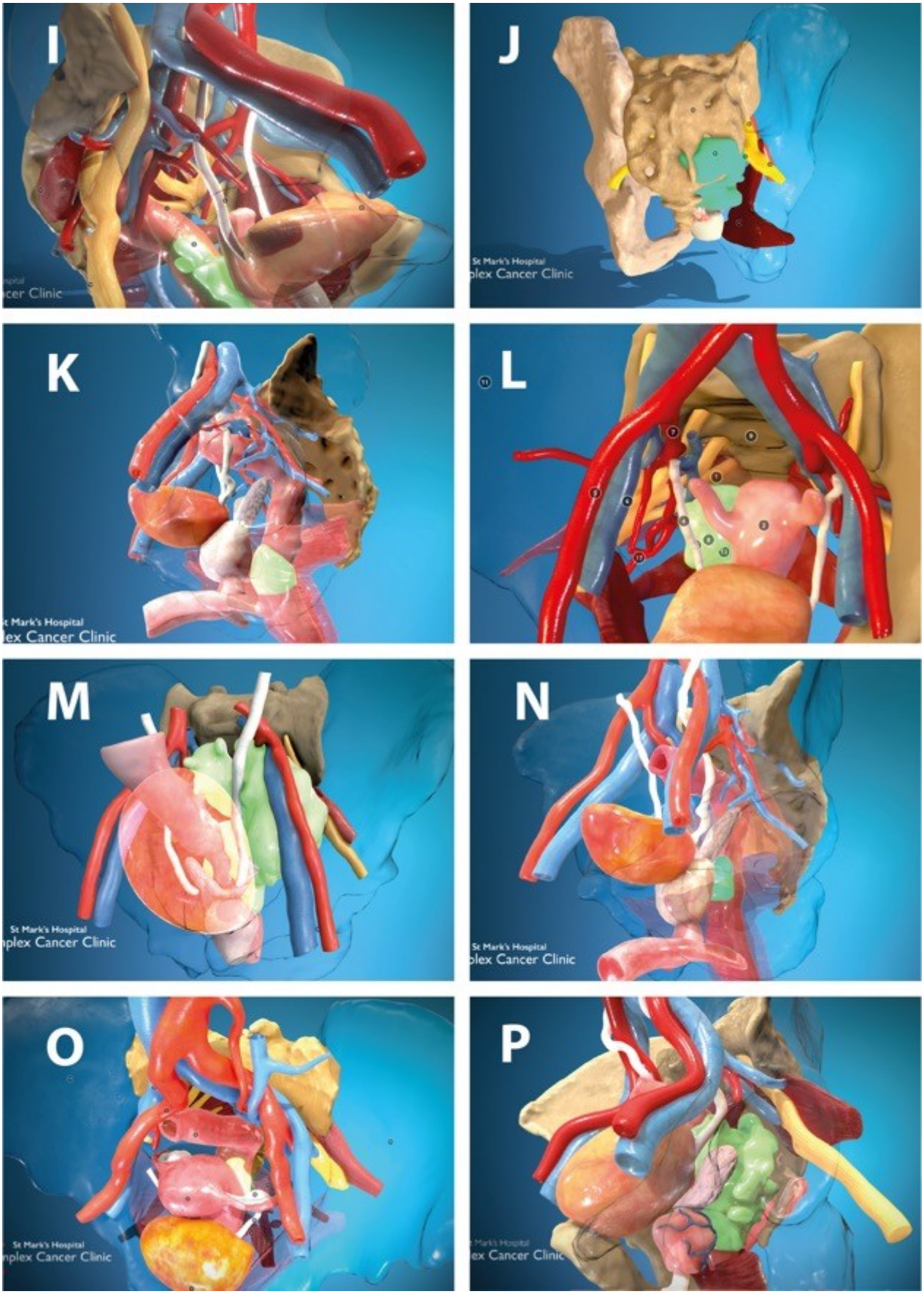
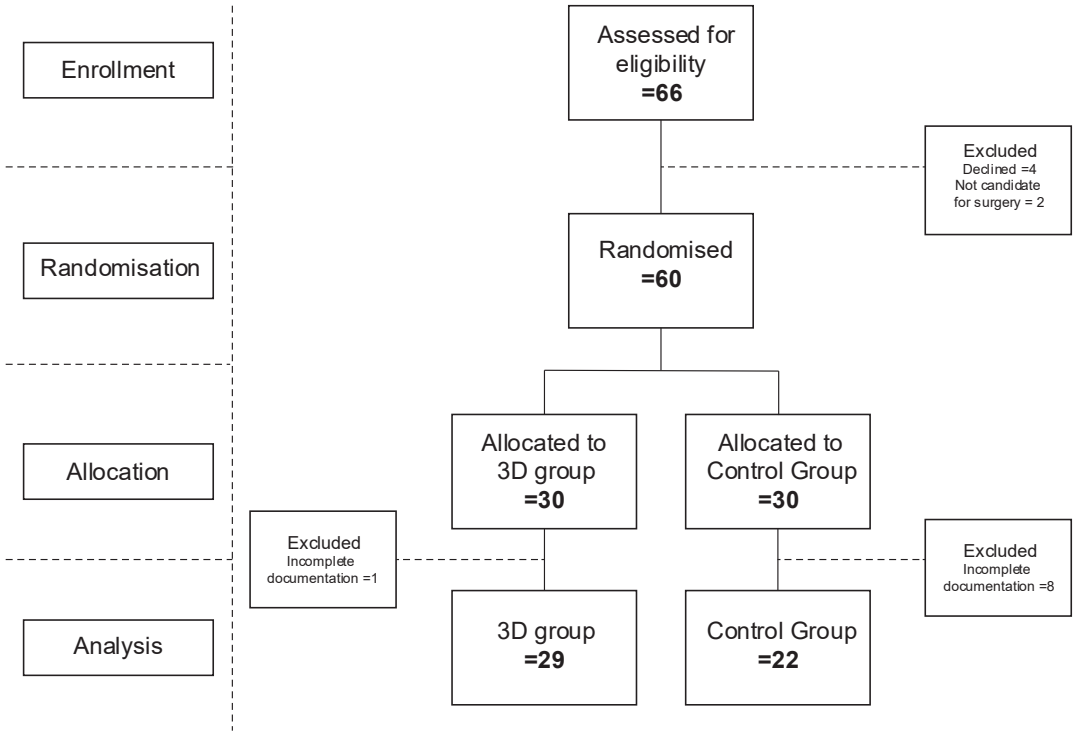


Figure 6-2 I-P Example patient specific 3D reconstructions.



6.3 Results

Figure 6-3 Consort patient flow diagram



Patient recruitment is illustrated in Figure 6-3.

The demographic data and planned pelvic exenteration procedures for each group are summarised in Table 6-1. For a detailed description of each participant, refer to Tables 6-2 and 6-3. The exenteration procedures were classified according to the Association of Coloproctologists of Great Britain and Ireland (ACPGBI) Advanced Malignancy Subcommittee and the UK Pelvic Exenteration Network (UKPEN) Pelvic Exenteration Lexicon (See Appendix 6.4).

Table 6-1 Patient demographics summary

		Standard				3D				p-value
	n	22				29				
Diagnosis	Locally advanced	12				15				0.78
	Locally Recurrent	3				9				
	Other	6				4				
	Age (years)	Median	64	Range	32-76	Median	65	Range	31-82	0.84
	Sex (M:F)	18:4 (82:18%)				18:11 (62:38%)				0.22
Referral	External institution	21				28				0.6
	Internal referral	1				1				
Appointment	First appointment	19				25				0.8
	Follow-up	3				4				
Planned exenteration	Pelvic Exent Lexicon score	Median	4.5	IQR	5	Median	8	IQR	6	***0.04**

6.3.1 Intended Exenteration Procedures

The 3D group demonstrated a median involvement of six structures in the planned resection (range: 2 - 11, interquartile range [IQR]: 3), compared to the standard group, which had a median of four structures (range: 2 - 8, IQR: 2.5). We calculated an exenteration score by numerically encoding each subcategory from the Pelvic Exenteration Lexicon and summated the scores for each patient (e.g., P1=1, P2=2, A1=1, A2=2). We found that the 3D group had a significantly higher score, representing more extensive surgery (3D median 8, IQR 6 versus standard median 4.5, IQR 5.75, p= 0.04).

Table 6-2 Detailed Demographic Characteristics and Planned Exenteration Procedures in the 3D Group

ID	Age	Sex	Group	R	App.	Previous abdominal surgery		Diagnosis	EXENTERATIVE PROCEDURE PLANNED									
									Posterior	Anterior	Central	Vessels	Nerves	PFM	Recon	Detail	Add.	Detail
1	70	M	3D	E	1st	Y	TME + L Uretectomy	R	P4		C2	SV2 L		PM1	F1	IGAP		
2	57	F	3D	E	1st	Y	TME	R	P1		C2	SV2 R	SN3 R	PM2 R				
3	33	F	3D	I	F/U	N		LA			C1							
6	41	F	3D	E	1st	N		R SCC	P2	A3	C3	SV4 R	SN4 R	PM2 R	F1;F2	IGAP; Urostomy		
7	76	F	3D	E	1st	N		LA			C2						E5	Coccy-gectomy
8	47	M	3D	E	1st	N		LA			C1	SV1 L						
9	69	M	3D	E	1st	N		LA			C2	SV2 R		PM1				
11	69	F	3D	E	1st	N	TAH BSO (endometrial cancer)	LA	P1	A2 L	C1	SV1 L					E2	
12	75	M	3D	E	F/U	Y	TME, end colostomy + L Seminal vesicle resection	R	P4	A3	C2							
13	53	F	3D	E	1st	Y		LA+ M	P1	A3	C2	SV4 R	SN4 R					
14	54	F	3D	E	1st	Y	Colectomy; proctectomy	R	P3	A3	C2	SV3 R	SN3 R		F2	Urostomy		
16	58	M	3D	E	F/U	N		LA+M		A3	C2	SV3 R						
17	57	F	3D	E	F/U	N		LA	P1		C1						E5	Left piriformis fascia
19	70	F	3D	E	1st	N		LA	P1		C2						E5	L piriformis fascia
20	73	M	3D	E	1st	N	Lap. high AR	R	P1		C2	SV1 L	SN4 L**					

24	67	M	3D	E	1st	N		LA		A3	C2	SV2 B		PM1	F1;F2	SGAP: Urostomy		
25	84	M	3D	E	1st	Y	Ultra-low TME	R	P4	A3	C2	SV3 B		PM2	F2	Urostomy		
28	74	M	3D	E	1st	Y	Defunc. colostomy	LA		A3	C2	SV2 L	SN2 L		F2	Urostomy		
30	66	M	3D	E	1st	N		LA	P2	A3	C2	SV3 R; SV2 L	SN2 L	PM1	F1;F2	SGAP; Urostomy	E5	Coccy-gectomy
31	65	F	3D	E	1st	N		LA	P3		C2							
34	71	M	3D	E	1st	Y	TME; Right nephrectomy	R		A3	C2			PM1	F1;F2	SGAP; Urostomy	E5	Penile body
37	67	M	3D	E	1st	Y	Defunc. ileostomy	LA			C2	SV2 R		PM2				
44	77	M	3D	E	1st	Y	Hartman's	R			C1						E5	Interspincteric dissection
45	55	F	3D	E	1st	N		LA			C1	SV1 R		PM1	F1	IGAP		
51	64	M	3D	E	1st	Y	Right hemi.	R Colon										
55	74	M	3D	E	1st	Y	ELAPE	R	P4	A3	C2	SV2 B	SN3 B	PM2 R	F1;F2	IGAP; Urostomy		
60	54	M	3D	E	1st	N		LA	P4	A3	C2	SV4 L		PM1	F1;F2		E5	
61	57	M	3D	E	1st	N		LA		A3	C2				F1;F2	SGAP		
68	79	M	3D	E	1st	N		LA		A3	C2	SV3 R		PM1	F1;F2	IGAP; Urostomy		

Table 6-3 Detailed Demographic Characteristics and Planned Exenteration Procedures in the STANDARD Group

ID		Age	Sex	Group	R	App.	Previous abdominal surgery		Diagnosis	EXENTERATIVE PROCEDURE PLANNED									
										Posterior	Anterior	Central	Vessels	Nerves	PFM	Recon	Detail	Add.	Detail
5		57	M	S	E	1st	Y	Defunct. colostomy	LA			C2							
10		45	M	S	E	F/U	N		NE		A3	C2	SV1		PM1				
18		51	M	S	E	1st	N		LA	P2	A3	C2	SV2 B		PM2	F2	Urostomy		
21		73	M	S	E	1st	N		LA	P2;P3		C2	SV1 B		PM2 B				
23		74	M	S	E	1st	N		LA			C2							
27		66	M	S	E	F/U	N		Anal SCC		A3	C2	SV2 L		PM1	F2	Urostomy		
32		75	F	S	E	1st	N		Stromal			C2			PM1				
35		32	F	S	I	F/U	Y	IRA	LA			C2						E5	R Ovary; small bowel
43		51	M	S	I	1st	N		PS cyst										
46		38	M	S	E	1st	Y		R										
50		57	M	S	E	1st	N		LA			C1	SV2 R						
52		69	M	S	E	1st	Y		R			C2	SV2 L						L ELSiE
53		66	M	S	E	1st	N		LA sigmoid		A2 R	C1				F2	Boari flap		
54		74	M	S	E	1st	N					C1	SV2 R; SV1 L						
56		61	M	S	E	1st	Y	TME	LA	P4	A4	C2	SV2 L	SN3 L	PM1	F1;F2	SGAP; Urostomy		
59		73	M	S	E	1st	Y	Right hemi	R colon		A1							E5	HIPEC
62		75	F	S	E	1st	N		LA	P1		C1							
67		67	M	S	E	1st	Y	EMR polypectomy	R	P4		C1	SV3 L						

71		34	F	S	E	1st	N		LA			C1			PM1			E5	Coccy-gectomy
72		75	M	S	E	1st	N		LA			C1			PM1				
73		69	M	S	E	1st	N		LA			C1			PM1				
74		78	M	S	E	1st	N		LA		A3	C2			PM1				

6.3.2 Treatment and decision making preferences

Patient responses to decision control and treatment preference and priorities are displayed in figures 6-4 to 6-13. Chi-square test revealed no statistical difference in responses between STANDARD and 3D groups.

Figure 6-4 Education level of Standard and 3D groups. No statistical difference between groups

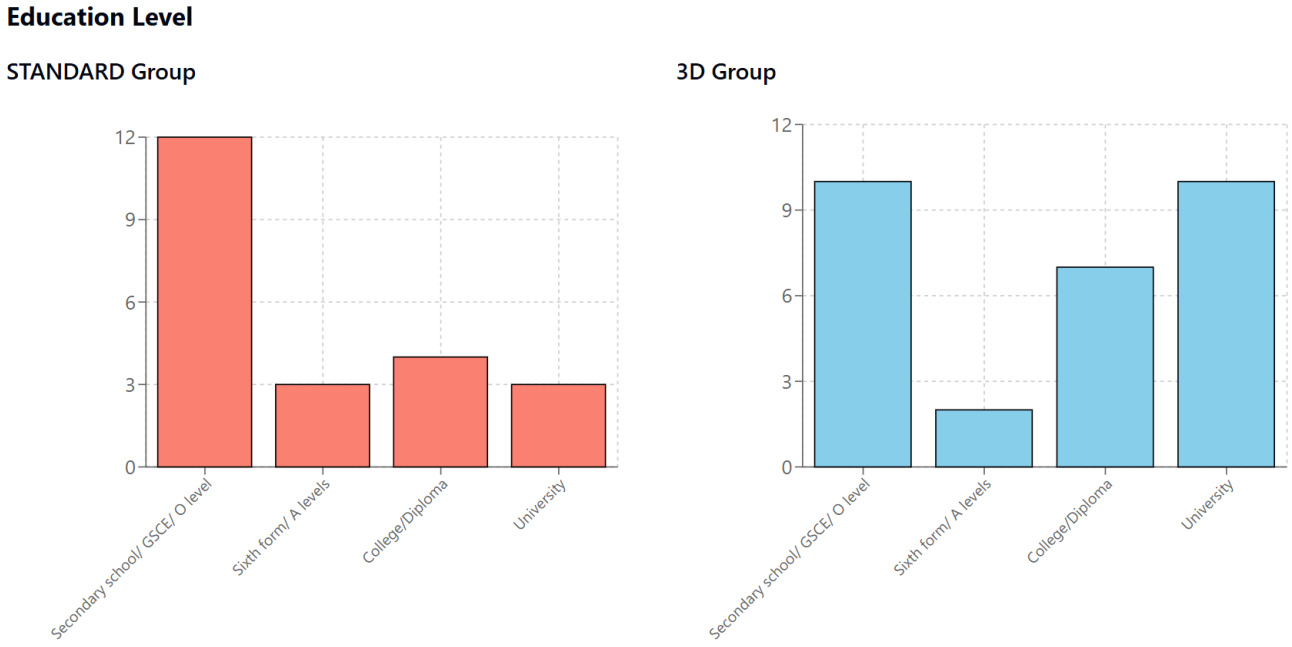


Figure 6-5 Pre-consultation treatment preferences for Standard and 3D groups.

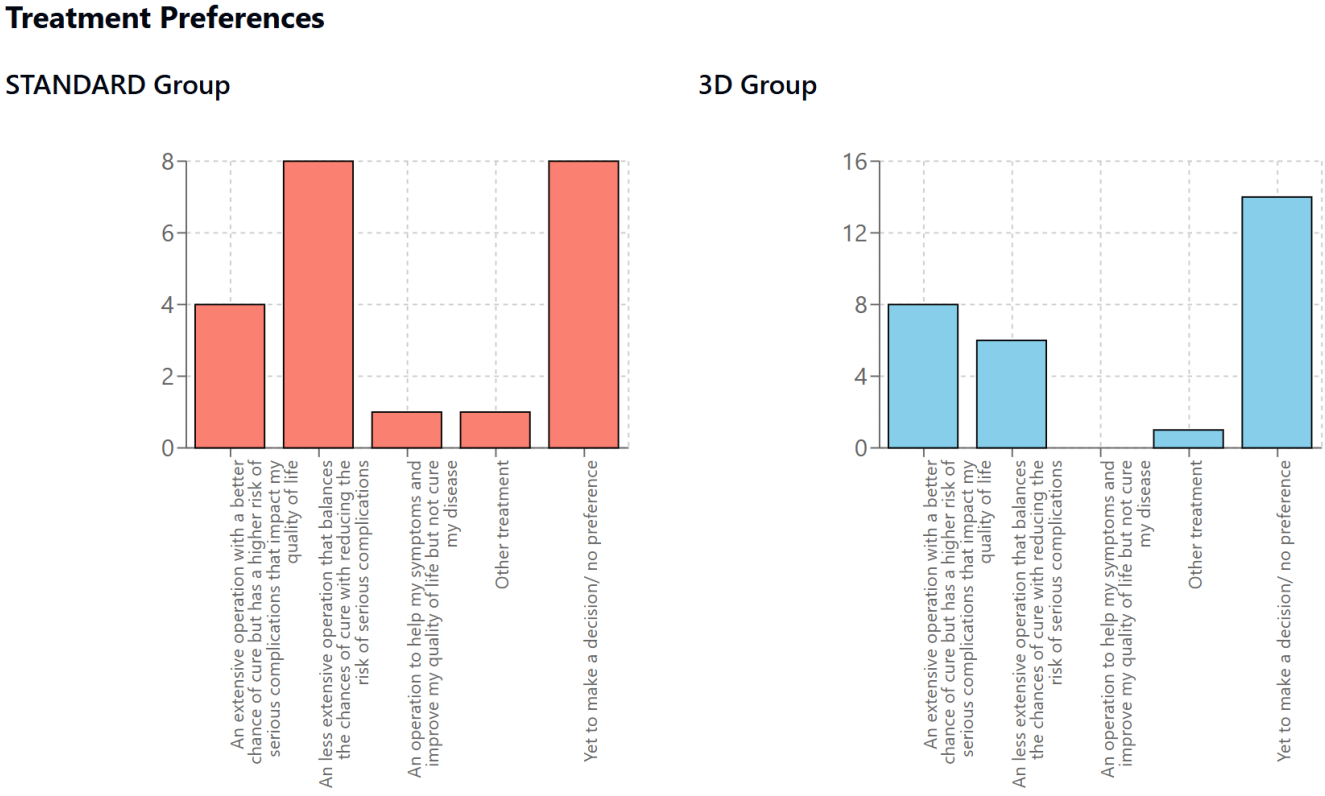


Figure 6-6 Stated decision making preferences for Standard and 3D groups.

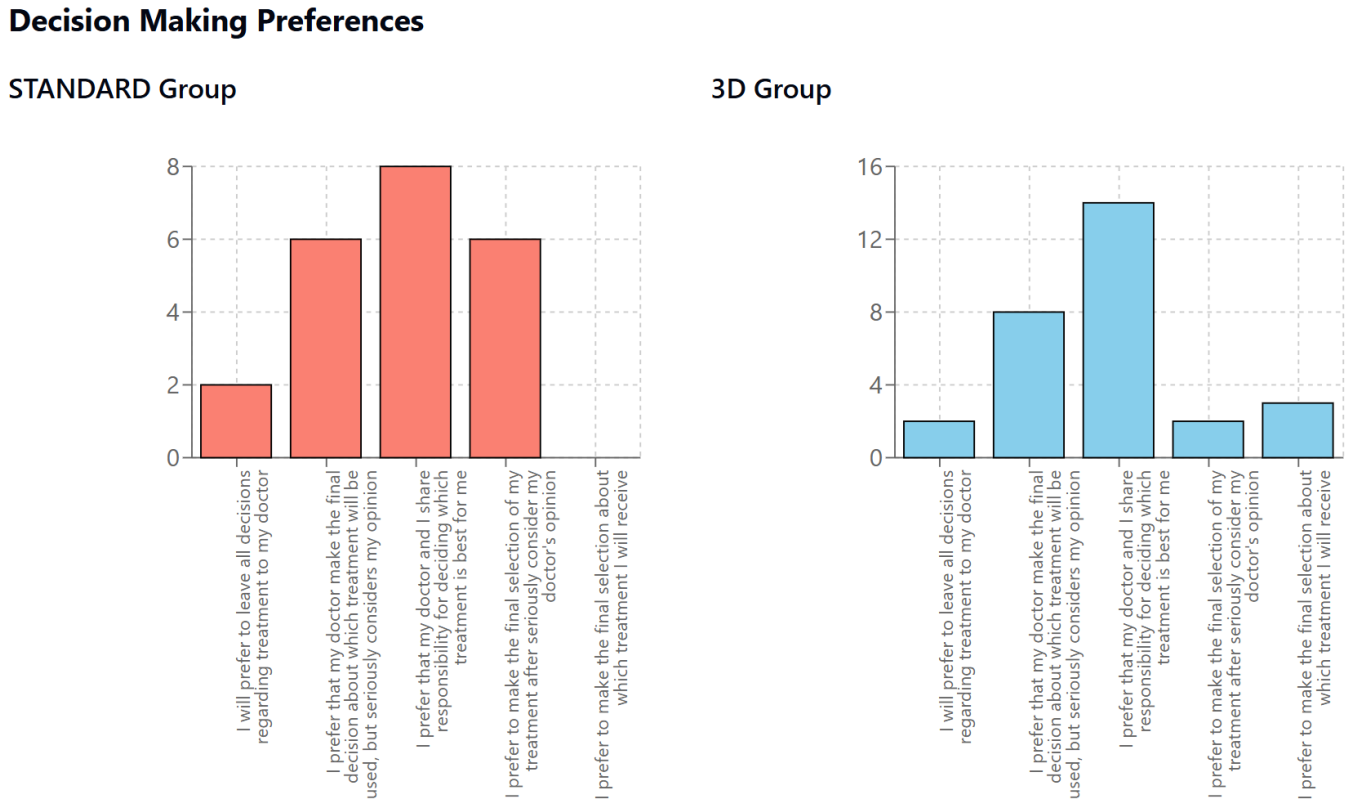


Figure 6-7 Quality and Length of life preference for Standard and 3D groups.

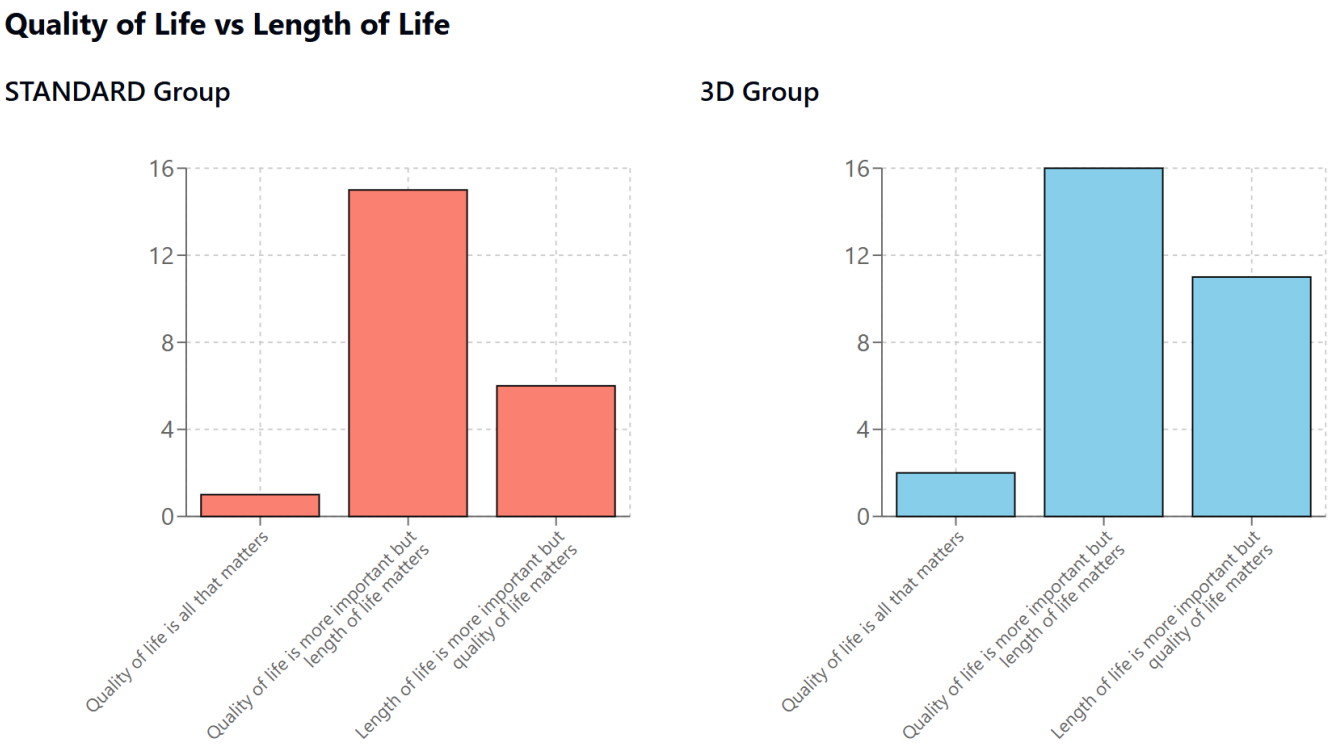


Figure 6-8 Treatment priorities: Stated importance of Avoiding Stoma- 3D versus Standard groups.

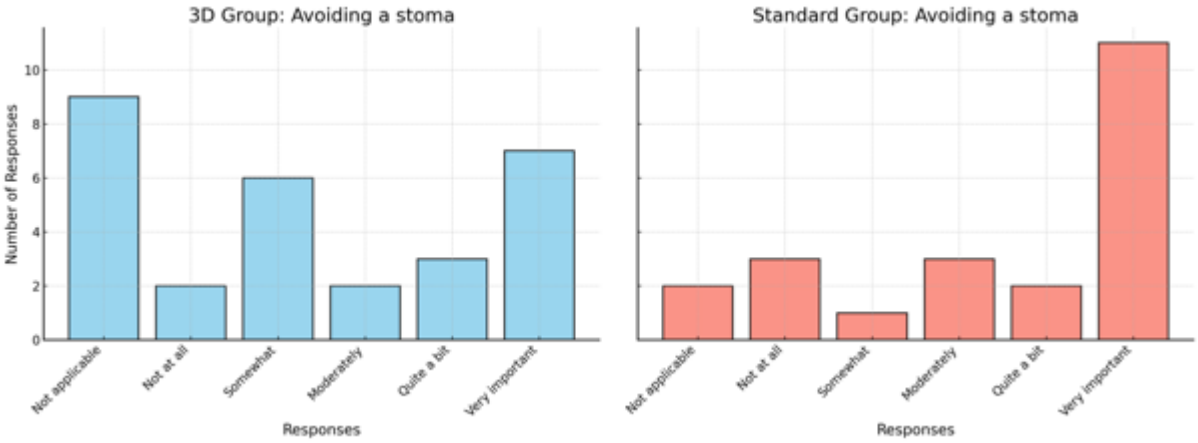


Figure 6-9 Treatment priorities: Stated importance of retaining control of bowel function 3D versus Standard Groups.

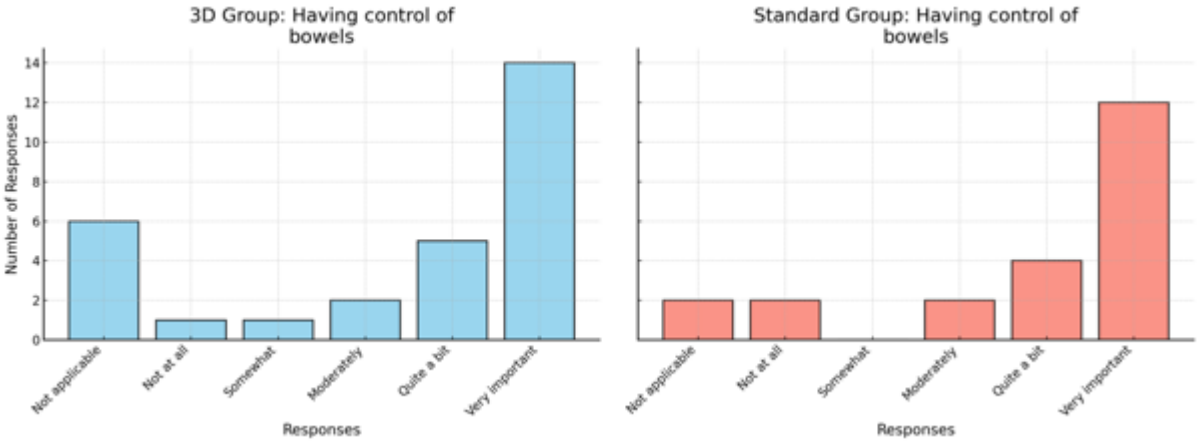


Figure 6-10 Treatment priorities Stated importance of maintaining independence 3D versus Standard Groups.

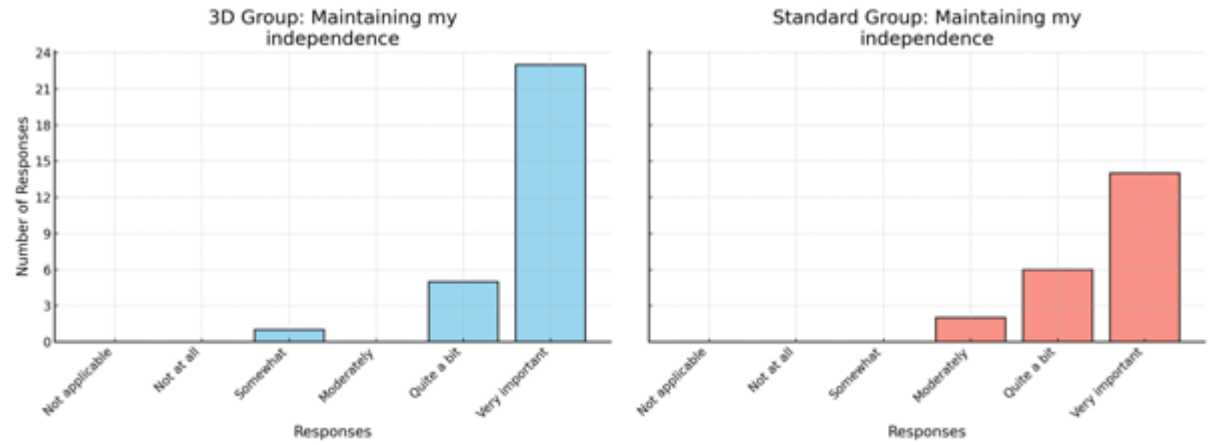


Figure 6-11 Treatment priorities: Stated importance of Minimising pain- 3D versus Standard groups.

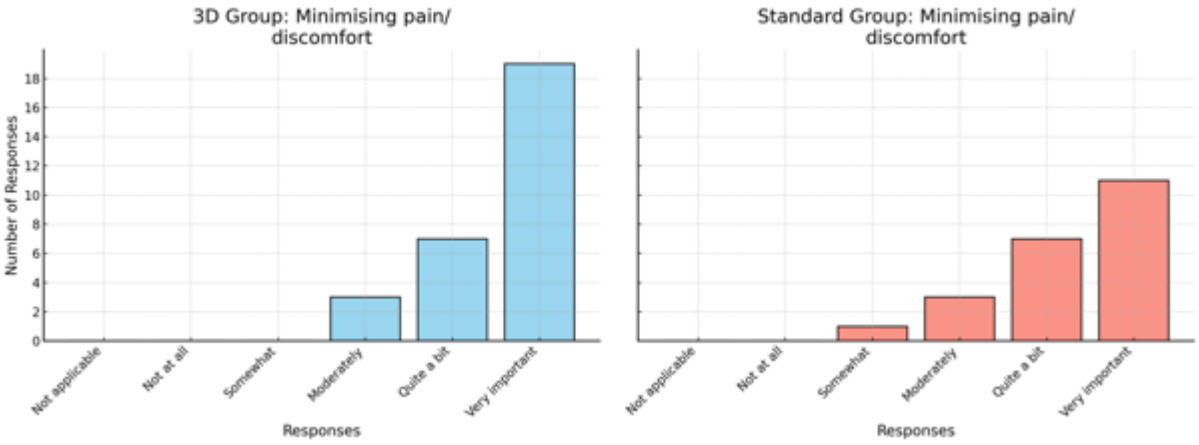
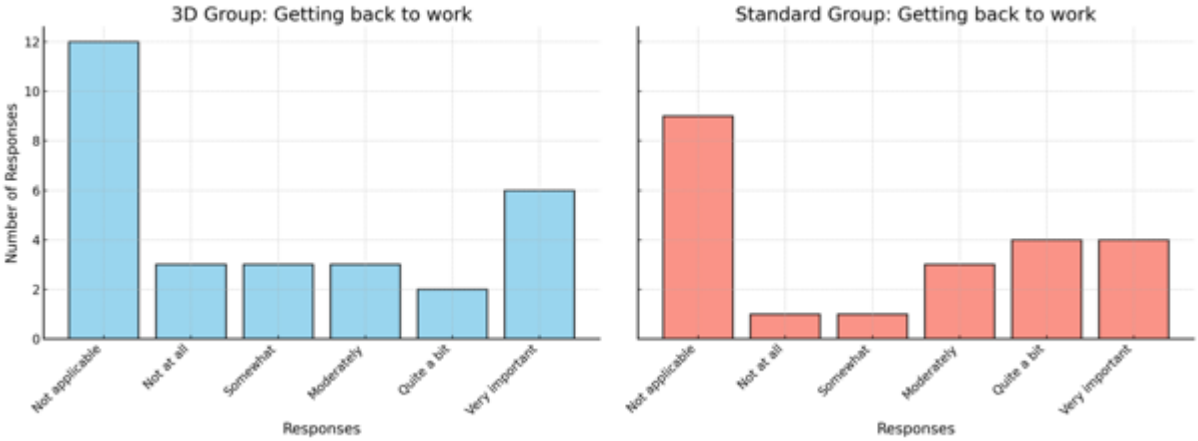


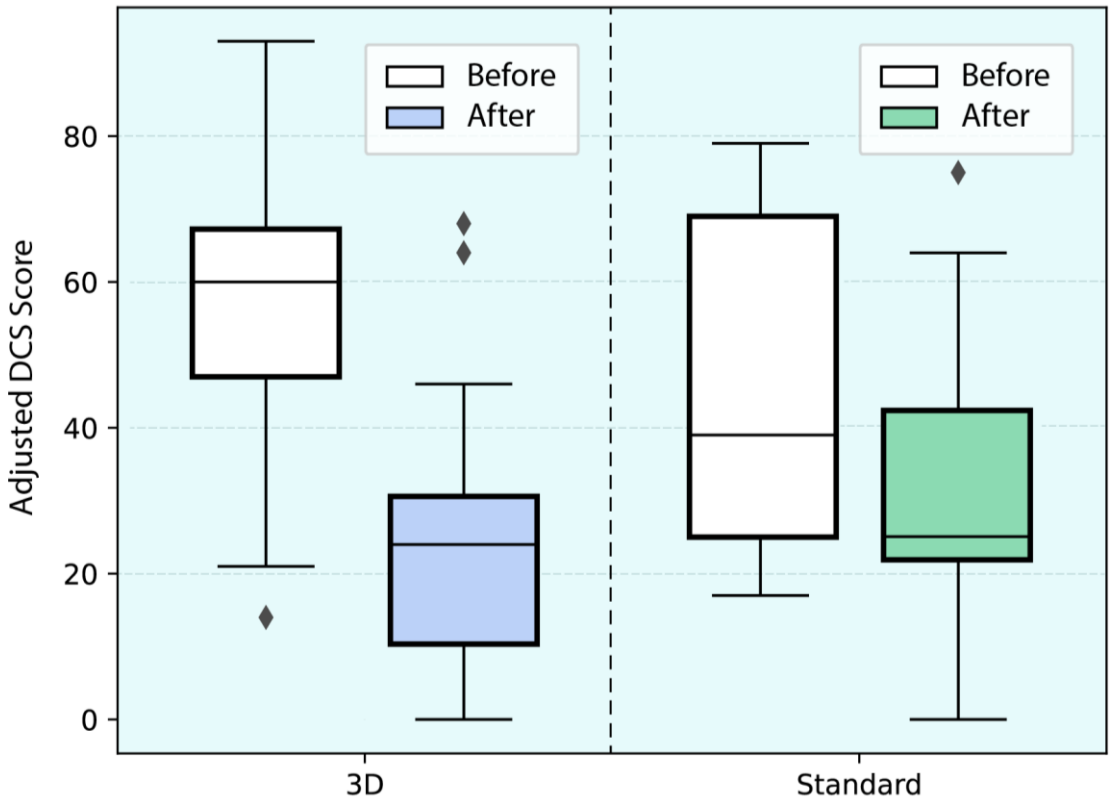
Figure 6-12 Treatment priorities Stated importance of getting back to work- 3D versus Standard groups



6.3.3 Decisional conflict score

The Decisional Conflict Scale (DCS) score was significantly reduced in both groups following the consultation (3D group: median 60 pre-consultation vs. 24 post-consultation, p<0.001; standard group: median 39 pre-consultation vs. 25 post-consultation, p=0.003). The median reduction in DCS score was significantly more significant in the 3D group compared to the standard group (-36 vs. -14, p=0.005)(see Figure 6-13).

Figure 6-13 Box plot adjusted DCS score pre and post consultation for 3D and STANDARD groups.



6.3.4 Patient knowledge questionnaire

Assessment of patient knowledge regarding anatomical structures involved in the planned surgery revealed no significant difference between the 3D and standard groups (3D median agreement 94.4%, IQR 16.7 vs. standard median agreement 88.4%, IQR 16.7; p=0.376). Table 6-4 and 6-5 detail the full breakdown of agreement/ disagreement by anatomical structure.

Table 6-4: Breakdown of agreement/discrepancies between patient and surgeon response by anatomical structure for the 3D GROUP

Anatomical Structure	**n**	**Overall agreement** Patient and surgeon gave same response	**Agreement** Included by patient and surgeon	**Agreement.** Not included by surgeon & patient	**Discrepancy** Included by Surgeon, Not by Patient	**Discrepancy** Included by patient not included by surgeon
Part of colon	29	27 (93.1%)	9 (31.0%)	18 (62.1%)	1 (3.4%)	1 (3.4%)
All of colon	29	26 (89.7%)	0 (0.0%)	26 (89.7%)	1 (3.4%)	2 (6.9%)
Rectum	29	25 (86.2%)	22 (75.9%)	3 (10.3%)	2 (6.9%)	2 (6.9%)
Anus	29	25 (86.2%)	12 (41.4%)	13 (44.8%)	2 (6.9%)	2 (6.9%)
Bladder	29	25 (86.2%)	9 (31.0%)	16 (55.2%)	2 (6.9%)	2 (6.9%)
Kidney	29	29 (100.0%)	2 (6.9%)	27 (93.1%)	0 (0.0%)	0 (0.0%)
Uterus	11	10 (90.9%)	6 (54.5%)	4 (36.4%)	1 (9.1%)	0 (0.0%)
Ovaries	11	9 (81.8%)	5 (45.5%)	4 (36.4%)	2 (18.2%)	0 (0.0%)
Part of vagina	11	10 (90.9%)	3 (27.3%)	7 (63.6%)	0 (0.0%)	1 (9.1%)
All of vagina	11	11 (100.0%)	0 (0.0%)	11 (100.0%)	0 (0.0%)	0 (0.0%)
Part of Prostate	18	16 (88.9%)	3 (16.7%)	13 (72.2%)	2 (11.1%)	0 (0.0%)
All of prostate	18	13 (72.2%)	3 (16.7%)	10 (55.6%)	1 (5.6%)	4 (22.2%)
Seminal Vesicle	18	13 (72.2%)	5 (27.8%)	8 (44.4%)	3 (16.7%)	2 (11.1%)
Bone	29	26 (89.7%)	11 (37.9%)	15 (51.7%)	1 (3.4%)	2 (6.9%)
Muscle	29	24 (82.8%)	7 (24.1%)	17 (58.6%)	2 (6.9%)	3 (10.3%)
Nerves	29	26 (89.7%)	9 (31.0%)	17 (58.6%)	1 (3.4%)	2 (6.9%)
Blood vessels	29	22 (75.9%)	1 (3.4%)	21 (72.4%)	3 (10.3%)	4 (13.8%)

Table 6-5: Breakdown of agreement/discrepancies between patient and surgeon response by anatomical structure for the STANDARD GROUP

Anatomical structure	**n**	**Overall agreement** Patient and surgeon gave same response	**Agreement** Included by patient and surgeon	**Agreement.** Not included by surgeon & patient	**Discrepancy** Included by Surgeon, Not by Patient	**Discrepancy** Included by patient not included by surgeon
Part of colon	22	15 (68.2%)	2 (9.1%)	13 (59.1%)	1 (4.5%)	6 (27.3%)
All of colon	22	20 (90.9%)	0 (0.0%)	20 (90.9%)	1 (4.5%)	1 (4.5%)
Rectum	22	15 (68.2%)	12 (54.5%)	3 (13.6%)	7 (31.8%)	0 (0.0%)
Anus	22	16 (72.7%)	3 (13.6%)	13 (59.1%)	3 (13.6%)	3 (13.6%)
Bladder	22	21 (95.5%)	4 (18.2%)	17 (77.3%)	1 (4.5%)	0 (0.0%)
Kidney	22	21 (95.5%)	0 (0.0%)	21 (95.5%)	0 (0.0%)	1 (4.5%)
Uterus	4	3 (75.0%)	1 (25.0%)	2 (50.0%)	0 (0.0%)	1 (25.0%)
Ovaries and fallopian tubes	4	4 (100.0%)	2 (50.0%)	2 (50.0%)	0 (0.0%)	0 (0.0%)
Part of vagina	4	3 (75.0%)	0 (0.0%)	3 (75.0%)	0 (0.0%)	1 (25.0%)
All of vagina	4	4 (100.0%)	0 (0.0%)	4 (100.0%)	0 (0.0%)	0 (0.0%)
Part of Prostate	18	17 (94.4%)	0 (0.0%)	17 (94.4%)	1 (5.6%)	0 (0.0%)
All of prostate	18	16 (88.9%)	1 (5.6%)	15 (83.3%)	2 (11.1%)	0 (0.0%)
Seminal Vesicle	18	15 (83.3%)	2 (11.1%)	13 (72.2%)	3 (16.7%)	0 (0.0%)
Bone	22	18 (81.8%)	0 (0.0%)	18 (81.8%)	4 (18.2%)	0 (0.0%)
Muscle	22	19 (86.4%)	0 (0.0%)	19 (86.4%)	2 (9.1%)	1 (4.5%)
Nerves	22	17 (77.3%)	0 (0.0%)	17 (77.3%)	3 (13.6%)	2 (9.1%)
Large blood vessels	22	20 (90.9%)	0 (0.0%)	20 (90.9%)	1 (4.5%)	1 (4.5%)

6.3.4.1 Functional outcome perception

Higher levels of agreement were observed in the 3D group across several functional outcomes (see Table 6-7). Specifically, bowel function agreement reached 89.6% (26/29) in the 3D group, compared with 72.7% (16/22) in the standard group. Similarly, urinary function agreement was 72.4% (21/29) in the 3D group and 63.6% (14/22) in the standard group. Notably, agreement regarding the need for a stoma was significantly higher in the 3D group (93.1%, 27/29) compared with the standard group (63.6%, 14/22). Postoperative mobility followed the same pattern, with 79.3% agreement (23/29) in the 3D group versus 40.9% (9/22) in the standard group. Male sexual function agreement was 77.8% (14/18) in the 3D group, compared with 39.0% (7/18) in the standard group.

In contrast, female sexual function showed similar levels of agreement in both groups: 54.5% (6/11) in the 3D group and 50.0% (2/4) in the standard group. Overall, the mean agreement level in the 3D group was 83.9% (n=29, range 50–100%, SD 14.42), markedly higher than the 59.8% observed in the standard group (n=22, range 0–100%, SD 26.05). This difference was statistically significant (Mann-Whitney U; $p<0.001$).

Table 6-6 Summary of the average agreement for functional outcomes in 3D and STANDARD groups

Functional outcome	Agreement: 3D		Agreement: Standard	
	Count/n	Percentage	Count/n	Percentage
Bowel Function	26/29	89.60%	16/22	72.70%
Urinary function	21/29	72.40%	14/22	63.60%
Need for stoma	27/29	93.10%	14/22	63.60%
Post op mobility	23/29	79.30%	9/22	40.90%
Male Sexual Function	14/18	77.78%	7/18	39%
Female Sexual Function	6/11	54.54%	2/4	50.00%

6.3.5 Subjective feedback

Responses to the Likert scale data are summarised in Figures 6-14 and 6-15.

6.3.5.1 3D Model Feedback:

In this cohort, most patients reported a favourable experience with the 3D model. Specifically, 63.33% strongly supported the model as a tool that enhanced understanding of their disease. In comparison, 80% indicated that the model-assisted them in making treatment decisions, including 30% who strongly agreed. The model's aesthetic appeal was highly regarded, with over 90% of patients approving of its appearance and 56.67% expressing strong agreement. Additionally, 90% of participants disagreed that the model was confusing, suggesting it offered clarity. Although 13% found the model somewhat distressing, 67% did not share this view. Personalised features of the model were broadly valued, with 96% of participants affirming its importance; of these, 87% either agreed or strongly agreed. Finally, when asked to compare the 3D model with standard imaging data, 96% demonstrated a clear preference for the 3D model.

6.3.5.2 General Feedback:

Understanding their disease and the rationale behind their operation remained crucial across both groups. In the standard group, 88% affirmed or strongly affirmed their comprehension of the operation's necessity, a figure slightly eclipsed by the 93% in the 3D group. Similarly,

96% of the standard group and 93% of the 3D group agreed or strongly agreed on the importance of understanding their disease.

When interpreting diagnostic imaging data, the 3D group reported superior comprehension. Only 10% of the 3D group agreed or mildly concurred that deciphering the scans was challenging, with no strong agreement. Conversely, the standard group contained 16% who agreed or strongly agreed with the difficulty of understanding the scan imagery.

In the standard group, a quarter of respondents disagreed or strongly disagreed with the notion that they did not comprehend the potential benefits of the operation. However, an equal fraction agreed or strongly agreed, suggesting a segment of this group grappled with understanding the operation's benefits. In contrast, 80% of the 3D group disagreed or strongly disagreed with this sentiment, indicating their perceived comprehension of the operation's benefits. This stark contrast suggests a superior grasp of the operation's benefits within the 3D group relative to the standard group.

Patient involvement in decision-making regarding their care was viewed favourably in both groups, with 79% of the standard group and 80% of the 3D group agreeing or strongly agreeing that they felt involved.

Concerning the allocation of consultation time, both groups overwhelmingly agreed or strongly agreed that the duration spent explaining their operation was appropriate (83% in the standard group and 87% in the 3D group).

The expertise of both the doctor and nurse was highly praised in both groups. The statement "I felt the doctor was knowledgeable about my procedure and treatments" was agreed or strongly agreed with by 96% of the standard group and 97% of the 3D group. Similarly, 95% in the standard group and 83% in the 3D group voiced a strong agreement with the corresponding statement about the nurse. Both groups were highly satisfied with the overall explanation of the disease and operation. 88% of the standard group agreed or strongly agreed with this statement, paralleled by 83% agreement or strong agreement within the 3D group.

Figure 6-14 3D model subjective Likert scale questionnaire responses.

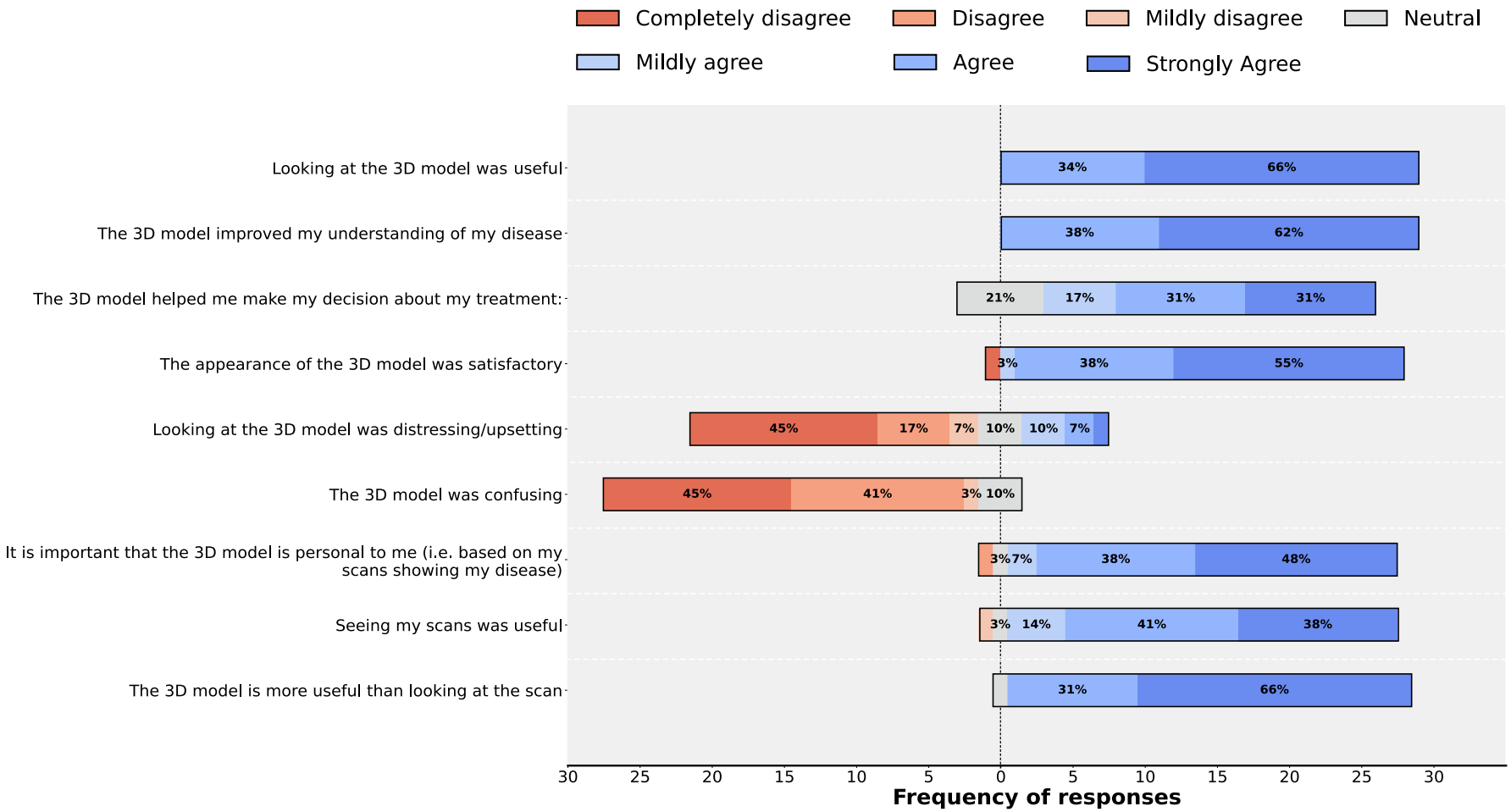


Figure 6-15 General consultation Likert scale questionnaire responses from Standard and 3D group



6.4 Interview data.

The following section presents the findings from a qualitative interview study that explored using 3D models and their impact on decision-making among patients diagnosed with advanced rectal cancer. Eighteen patients agreed to be interviewed. The interview analysis revealed several key themes. These centred on patient understanding and engagement, including the degree of personalisation in their care and quality of communication. Patients' emotional responses and coping mechanisms following their diagnosis emerged as another significant theme, as did the factors influencing their decision-making processes.

Through in-depth analysis of the interview data, these themes emerged as crucial aspects shaping patients' experiences and perceptions of the 3D models. The subsequent subsections delve into each theme, providing an in-depth exploration of the participants' perspectives and insights. By examining these themes, we gain valuable insights into the potential benefits and challenges of integrating 3D models into the decision-making process for patients with advanced rectal cancer.

6.4.1 Understanding

During the analysis of semi-structured interviews conducted with eighteen participants diagnosed with advanced rectal cancer, understanding emerged as a principal theme. Specifically, patients reported that personalised three-dimensional (3D) models offered an enhanced appreciation of their diagnosis, the rationale for complex surgery, and the interplay of anatomical structures. The following sections illustrate how participants' perspectives evolved from initial uncertainty—relying on conventional explanations and black-and-white imaging—to a more concrete, visually guided comprehension of their condition.

6.4.1.1 Comprehension of Diagnosis and Treatment

A consistent subtheme among participants was the value of the 3D model in illuminating aspects of their anatomy and tumour burden. This was particularly evident in contexts where standard two-dimensional (2D) imaging had proved difficult to interpret. For instance,

Participant #8 described initial uncertainty regarding the necessity of a specialist surgical team:

> *"Initially, when I saw my surgeon, he explained the usual procedure—resect the rectum using a robot and create a stoma. But because of these lymph nodes, it was outside the norm, and I needed a referral elsewhere. On the MRI, it looked as though the lymph nodes were quite close, so I wondered why they could not just 'move the robot a bit further.' I didn't fully understand why a specialist team was required. Once I saw the 3D model, it became clear."*

In this account, the complexity of lymph node involvement gained a visual clarity that enabled the patient to recognise why robotic resection alone was insufficient. The model served as a tangible educational resource, bridging knowledge gaps that might persist.

Participant #16 likewise emphasised the significance of seeing a 3D representation:

> *"I already expected extensive surgery, but the model let me see precisely which areas they would remove and why it was more complicated than a routine resection."*

This explanation underscores a critical function of 3D models: the ability to combine radiological findings with a patient-focused visualisation strategy, thus fostering deeper comprehension of surgical rationale. This aligns with evidence suggesting patients value accessible explanatory tools when confronted with major operative decisions.

6.4.1.2 Mental Preparedness and Acceptance

In addition to clarifying the extent of the disease, participants highlighted how an enhanced understanding improved mental preparedness. The data revealed that a vivid grasp of the anatomy, including the size of the tumour and proximity to vital structures, helped to reduce psychological distress. Participant #51 reflected:

"Does it help mentally? I think some people probably would rather Not know... But I'm probably a bit in the middle, I want to know. And then if I feel that it doesn't help me, I'll just exclude it from my mind sort of thing. But if I feel that, like, I want to know what they're doing, then I'll focus on those bits"

Similarly, Participant #11 noted:

"Maybe not so much the disease, the size of the tumour. I think I hadn't properly appreciated quite size of the tumour. And its relationship to different organs, not just the bowel, but yes. And organs, you know, how so many of them are interconnected… 'Yes, it's made me more aware of just how many because of the close proximity of so many different organs and tubes, etc, etc, in the abdomen, and the size of the tumour. And, you know, and because there is damage from the radiotherapy, just, you know, that things are not going to be straightforward."

These accounts suggest that improved understanding through 3D visualisation can facilitate psychological readiness by providing a more realistic impression of the surgical challenge. From a methodological perspective, these findings emerged consistently across transcripts, indicating that participants' sense of preparation was tied to the depth and clarity of the information they had received.

6.4.1.3 Comparison with Traditional Medical Imaging

A further subtheme under 'Understanding' was the participants' comparison of the 3D models with conventional 2D imaging. Without exception, they reported that the model offered a qualitatively different grasp of tumour location, size, and anatomical relationships. Participant #8 succinctly contrasted the two approaches:

"It's just a lot of black and white image. You know, I'm just going on the whatever the clinician says. Whereas the model brings things a bit more to life. And even without any anatomy and physiology knowledge, you can start to picture your pelvis in relation to where you're going to have an

operation and how deepens they're going. You know, and you can't get that from a 2d picture."

Likewise, Participant #7 emphasised the usefulness of colour cues:

"Because it's in colour, you notice detail you'd never spot in a black-and-white scan. It's so much clearer."

Others, including Patient #3, pointed out that 2D scans did not always allow them to form a comprehensive mental picture:

"Yeah, it's when she explained the scans step by step that helped a little. But again, like, I wasn't able to picture the whole thing."

Patient #44 emphasised the utility of having the model available at the beginning of a consultation:

"I think if that your model had been available straightaway and clearly on the screen, when I arrived at the start of that consultation, then I think the consultant would have been able, in my case thing to use that model throughout. And there wouldn't have been any questions, and it would have been a difficult situation, however, because the black and white was used, and it wasn't that clear."

Patient 8 conveyed how switching from 2D scans to a physical 3D representation created an instant "aha" moment:

"No, because to me, they're just the same but different shadows and I don't... Even though you're saying, this bit here, I'm like, well, that looks exactly the same on the other side. But is that a different shadow or...? The model's much easier to understand. Me and my mum and dad all agreed that that was so much better. Like on the first bit, where they

showed the scans, I was just like, yes. And then when they brought out the model I was like, oh I understand now, because I can see it."

Overall, participants viewed the 3D model as a tangible resource that significantly improved their understanding, communication, and experience compared to standard 2D imaging.

6.4.1.4 Summary of the 'Understanding' Theme

In summary, the 'Understanding' theme revealed that 3D models tangibly enhanced patients' comprehension of diagnosis, surgical rationale, and the topography of their disease. This enhanced comprehension frequently underpinned their ability to accept the necessity of invasive procedures. As subsequent sections indicate, personalisation, communication, emotional reassurance, and decision-making processes were often built upon this foundational understanding.

6.4.2 Personalisation

Patients consistently stated the importance of having a model based on their scans rather than a generic depiction of rectal cancer. This second theme—personalisation—encompassed participants' views on individualised care, heightened trust, and the utility of seeing their specific tumour within their unique anatomy.

6.4.2.1 Personalisation and Understanding

Many participants felt strongly that a generic model would not have conferred the same sense of pertinence or exactness. Participant #31, for instance, stressed:

"I needed to see exactly where my tumour was placed, how it touched certain organs. If it were just a general model, it wouldn't give that real-world relevance."

Participant #51 similarly added:

"You miss subtle details with a generic model—details that might matter a great deal to the patient."

The personalisation of models is inextricably linked to patient understanding. Patient #31 expressed the necessity of a personalised model to know exactly where the tumour is touching: *"I think you need to have it on a personalised basis for every person... to understand where the tumour was..".* Similarly, Patient #51 pointed out the specificities that generic models would miss: *"You wouldn't get that if it were just a general model."*

Such remarks illustrate that personalisation is not merely a preference but an integral component that strengthens the educational potential of 3D tools.

6.4.2.2 Personalisation, Comfort, and Trust

Participants also articulated how personalised 3D models contributed to feelings of reassurance and trust in the healthcare team, reflecting a perception of being treated as an individual rather than a statistical case.

Patient #8's statement, *"But I suppose it is nice that it is personalised. You feel more comfortable with 'this is you', rather than this is a model"*, reflects the emotional comfort brought about by personalised care. This sentiment is emphasised by

> *"I think it's less intimidating because you're using colour, so it's easier to understand. Somehow, it feels more personal, that you've taken the time to go, what will help this patient understand what's going on? Yes, I've got a medical problem, but I'm not just a thing with cancer, I am a person. And having a model that has taken that on board and gone, okay, we want to design something that helps you understand is much better..."*

This latter quote showcases personalisation's positive emotional impact, helping engender a sense of individual care and attention. Personalisation is about accurately representing the patient's medical condition and acknowledging and respecting their personhood. It signifies that the healthcare team sees the patient as an individual with unique needs, concerns, and emotional responses. This level of attention can significantly reduce the intimidation that patients might feel when confronted with their medical condition, contributing to a more positive patient experience.

Participant further added:

"I think there was something special about knowing that was a scan of my body. It was and yeah, I don't think it would work so well. If it had been a generic model like he described."

These accounts reflect an interactive dimension: personalisation fosters connection and validates the patient's unique experience. Notably, such a relational component of care was highlighted even by participants with strong clinical backgrounds, who nonetheless appreciated the personalised approach.

6.4.3 Communication and Engagement

The 3D model was crucial in fostering communication within the clinical setting and beyond, including with family members and friends. It also served to bridge knowledge gaps and stimulate more active patient involvement.

6.4.3.1 Facilitating Communication with Friends and Family

Participants described showing their personalised models to loved ones, who often responded with curiosity and relief. Patient #17 explained:

"Yeah, I think above all else. What it does is it helps the communication. And it helps the understanding."

Likewise, Patient #17's husband spoke about how it shaped discussions with their children:

"And certainly for me, and I think for the children, it's improved that sort of understanding and communication of what it is. And what Catherine is going through."

This testimony shows how the model has served as a communication bridge for the patient and their family, who may not have as much information or understanding. We know cancer not only impacts the patient but also their friends and family. Personalised models may help the patients' wider support network better share in their journey, as described by patient #17:

> *"We showed it to our daughters as well. And they were both fascinated... But actually, it gives that understanding of what it is. And what we're dealing with."*

Patient #9 similarly found it effective for sharing information with family, noting:

> *"It was like, a model a child would understand, you know, My son, not that he's a child, but he understood it straight away…. we sent it to my stepsons. And they came back within five minutes and asked about this and asked about that. And that is extremely important."*

6.4.3.2 Bridging the Knowledge Gap Between Physicians and Patients

The 3D model also helped correct the inherent imbalance in knowledge between clinicians and patients. Patient #16 noted:

> *"As I say, it's, I think when you just, if you're a surgeon, or a doctor describing something, you've got a very clear medical understanding of what that is, but it's very difficult to communicate it to a layperson."*

According to those interviewed, the model levelled the playing field, enabling improved understanding and allowing them ask relevant questions about their condition. This dynamic contributed to shared decision-making, as patients felt more comfortable engaging with complex information.

Patient #16 described this dynamic suggesting that the models enable a more levelled conversation between physicians and patients, making the former's explanations more accessible.

> "As I say, it's, I think when you just, if you're a surgeon, or a doctor describing something, you've got a very clear medical understanding what that is, but it's very difficult to communicate it to a lay person. Whereas when you've got some form of illustration, it's very helpful."

This situation highlights an often overlooked but critical aspect of patient care: the difficulty in translating complex medical knowledge to patients, who are, in most cases, laypersons regarding medical terminologies and practices. Here, personalised 3D models can help "level the playing field," acting as visual aids that make medical information more accessible and understandable to patients. These models might empower patients by instilling a sense of control and participation in their treatment. In turn, this enhanced understanding allows patients to engage more confidently in their healthcare decisions.

6.4.3.3 Encouraging Engagement

Some participants, such as Patient #6, admitted they previously hesitated to ask questions about 2D scans for fear of appearing uninformed:

"I thought it was really good because every time they've shown me a scan, they point to it, and I'm like, yes, I see it but I don't, actually see it. But you don't want to ask because you don't want to seem silly."

By contrast, once they saw the 3D model, they felt more confident to engage with the medical team:

"I felt like they explained it a bit more, because they actually could tell that I understood what I'm looking at, and they're showing."

Patient #9 likewise emphasised how the model prompted immediate questions from the family, underscoring its role in sparking dialogue and clarifying misconceptions.

6.4.4 Emotional Impact

Introducing personalised 3D models often elicited emotional responses ranging from relief and lowered anxiety to improved trust in the surgical team. These responses can be conceptualised through several subthemes.

6.4.4.1 Emotional Assurance and Reduced Anxiety

Some participants described the 3D model as helping them cope with the psychological burden of their illness. Patient #7 expressed relief:

“And when I saw it, it… I found it very.. what's the word.. not necessarily uplifting, but it sort of released all the tension, because I knew exactly what it was… I thought I was going to find it upsetting beforehand, once we saw it, and the way it was all explained, it just opened up.”

Patient #7 states they *"knew exactly what was happening”*, demonstrating the models' ability to reduce uncertainty and anxiety. This suggests that the visual and tangible nature of the 3D models helps patients process their situation emotionally, thus significantly reducing anxiety associated with the unknown.

6.4.4.2 Emotional Preparation and Coping Mechanisms

Patient #6 highlighted the potential impact of inadequate preoperative counselling on mental health:

“Because if you are shocked with it… I found you go really depressed. Because obviously I didn’t know I was having a stoma bag until two days before the op, and because I didn’t have time to process, I was very depressed afterwards.”

This suggests that a 3D model, introduced early enough, may allow individuals more time to adapt emotionally. Patient #14 described the model as *“less intimidating,”* reinforcing that visually oriented, detailed information can ease mental burden.

6.4.4.3 Trust and Confidence

Participants with prior negative experiences indicated that seeing a 3D model improved their confidence in the surgical team’s preparedness. Patient #68 recounted an initial operation where the surgeon seemed surprised by the disease extent on the morning of surgery:

“And in fact, I started to get worried the week before when I saw Professor x. And he was looking at his computer screen. And, you know, he obviously was realizing at that point that the whole thing was more serious than I'd been told at that point. So he started talking about seminal vesicles being affected at the margin and this and that the other obviously, I'm not

an expert, but I could just tell by his demeanour that he wasn't, you know, I mean, he was as if he was a bit surprised by the extent"

A subsequent incomplete resection margin further undermined the patient's faith, with the individual stating they should have been referred to a specialist earlier. However, seeing the 3D model in the new surgical plan restored some degree of trust:

"It's important for me to know, the scans, and the consultation and your 3d image are fantastic. You know, I've spun it around and had a look from all angles. It's great, you know, but for me, it's just so important that the team know what they what they've got to do."

Patient #8 remarked on scepticism about medical infallibility but conceded that the 3D model felt more transparent:

"I know from first-hand experience that doctors aren't infallible… I'm really sceptical about everything everybody says it's nice to have the added confidence."

These vignettes indicate that when patients see a visually detailed depiction, they gain reassurance that the surgical team is prepared and knowledgeable.

6.4.5 Decision Making

6.4.5.1

The decision-making process regarding undergoing extensive surgery, such as exenteration for advanced rectal cancer, is inherently complex and multifaceted. Personalised 3D models can significantly impact this process, aiding patients' understanding and visualization of their medical situation, but their influence on the ultimate decision to proceed with surgery is variable and context specific.

6.4.5.2 Variable influence on decision-making.

A common theme among several patients was that while the 3D model improved their comprehension of the clinical situation, it did not necessarily sway their decision to undergo surgery. Patient #61 stated, *"Probably not, in the sense that I think the information, from my perspective, that I would need to make that decision would have been more clinical... But what it does do is make the clinical understanding better."* Patient #19 expressed similar sentiments: "*I don't think it changed my decision. But I think it made it easier."* This indicates that while patients appreciate the improved understanding that 3D models provide, the decision to undertake surgery is influenced more by the clinical information and prognosis rather than the model.

The utility of personalised 3D models in facilitating decision-making relating to undergoing pelvic exenteration surgery can vary significantly among patients. This variability may depend on the complexity of the patient's pathology and the specifics of the operation they're facing.

In the case of patients facing less complex situations, the 3D model can serve as a final confirmation of understanding rather than a primary decision-making aid. Patient #10 stated: *"Yes, it was the consultation followed by the fact that the 3D model was there, if you like, ticked the last box almost."* In these scenarios, the model supplements the patient's understanding, affirming the information already discussed in the consultation.

However, in more complicated scenarios or when faced with more complex operations, patients may find the 3D model significantly more beneficial. As the same patient pointed out, *"I can see though, that for someone else, perhaps someone who has a more complex situation, an operation that was going to be really difficult, I could see it be more helpful in their situation on its own as a standalone system."*

Certain patients have expressed the sentiment of experiencing a "perceived lack of choice" regarding their final decision to undergo surgery. This perception emerges from the binary nature of their options – either to proceed with surgery (offering the prospect of a long-term cure) or to choose palliative care. However, having no "true choice" is somewhat abstract. Rather than indicating an absolute absence of options, it reflects the harsh realities of their medical situation. Patients perceive their choices as extremely limited due to the severe consequences of both alternatives, thus creating a sense of restricted autonomy in their decision-making process.

As patient #9 articulates, *"It's a bit binary; you either do or you don't do it. So, you either trust or you don't trust."* This sentiment suggests that while 3D models may give patients a deeper

understanding of their medical situation, they do not necessarily make the decision-making process any less daunting or binary.

While 3D models offer a tangible and visual representation of surgical procedures and potential outcomes, they form just one part of patients' multifaceted decision-making process when contemplating exenteration surgery. Powerful considerations, such as the balance between length of life and quality of life, often have more influence on patient decision-making.

Patient #9 acknowledges the value of professional confidence in the surgical team, suggesting that the surgery option is not difficult when the professionals exude certainty. While 3D models may provide clarity, the conversations with their medical team and the team's confidence significantly impact their decision.

"Because if the situation was a little bit different, and, and I hope the team would be honest with me, and they'd say "Look, this, this isn't easy to operate on. And the outcome is going to be very uncertain". And the option, the other options are these drugs or this radiotherapy. So you can have treatment A, B, or C. And then what decision to make if the team are telling me, you know, this is difficult, but we do it all the time. And we're confident we can get with the margin. That's clearly that's what communicated to thus far. So, I don't have a difficult decision to make at the moment."

Patient #9

Patient #61's reflection emphasizes the struggle between choosing a potentially extended life with possible post-surgery complications versus a shorter, more fulfilling life. In their case, the 3D model might provide some understanding of the surgical risks, but the emotional weight of their consideration overshadows any visualization tool.

" Is that worthwhile? Maybe yes or no. When it might actually be better just to kind of live life… and and, and live that period of least being fully functional?…

I would have to reconsider my options if the risks were too high, and if the outcome wasn't going to be long term cure, which then doesn't seem to be the case at this point in time"

Patient #61

Similarly, Patient 16's stance presents a clear 'red line.' The possibility of losing mobility and becoming a significant burden on their family surpasses any potential benefits of surgery, even if a 3D model might illustrate a successful surgical outcome. The quality of life emerges as the overriding factor in their decision-making process.

"I think one of the answers be a bit more specific, for example, you know, if there were a serious risk that I was going to be in a wheelchair, or I was going to be, you know, lose a limb use the loss of limbs, this was stuff, I would think, again, about whether the surgery was the right thing, because I don't want to become a big burden on my family, or, or Indeed, indeed, on myself, I think I'd rather, I'd rather sort of have a shorter life where I could do more, and the longer life just hanging around."

Patient #16

Patient #9 also reflects this sentiment. They stress the importance of making informed, life-altering decisions. While 3D models may add detail to their understanding, the depth of information, the grappling with quality-of-life considerations, and potential future outcomes truly influence their choices.

"for me, it facilitates maybe making choices. You know, it made us think much harder about the quality of life with the, with the possibility of that final operation and some of the some of the choices that we might have to make, you know, and, and you really shouldn't be able to make choices like that without all of the detail and all of that information."

Patient #9

An interesting facet of patient decision-making in pelvic exenteration is establishing "red lines," or absolute limits that patients express when contemplating potential surgery outcomes. However, these "red lines" are often not likely outcomes of their proposed surgery. Despite this, they carry significant weight in the patient's decision-making process.

Patients #9 and #16 statements demonstrate this concept. Both patients express clear boundaries - the risk of long-term disability or becoming a burden to their families - which they are unwilling to cross, even if it means potentially sacrificing years of life. However, it is important to note that such outcomes were not likely consequences of their likely procedure.

This raises intriguing questions about the nature of these "red lines." Are these absolute limits based on their current understanding and emotions, or might these boundaries shift when faced with the tangible prospect of their mortality? Would the detailed visualisation provided by a 3D model of their disease and proposed surgical procedure make any difference?

While 3D models can help patients better understand their medical situation, they do not necessarily affect these personal and emotional considerations. This reinforces the idea that the decision-making process around exenteration surgery is complex, involving a delicate balance of objective information, personal values, emotions, and existential considerations. It also emphasizes the importance of the healthcare team's clear, compassionate communication and support in helping patients navigate this challenging terrain.

Personalised 3D models offer a tangible and visual tool to facilitate a deeper understanding of the surgical process and its potential outcomes. They can help patients to appreciate the reality of their post-surgical life and make more informed decisions but do not fundamentally sway the decision-making process. The balance between length and quality of life, professional confidence, personal thresholds for acceptable post-operative lifestyle changes, and overall understanding of the implications of surgery are more significant influences on patient decision-making.

6.4.5.3 Influence in Specific Circumstances:

However, there may be specific scenarios where 3D models manifestly impact decision-making. For example, patient #31 was initially reluctant to consider posterior vaginectomy due to the significant impact on her sex life. The visual representation provided by the 3D model enabled her to genuinely consider this procedure as an essential step in achieving a

curative resection. She confirmed that her "understanding of the decision-making process has made much easier with that model definitely."

Similarly, Patient #3 faced a potential hysterectomy, which would significantly impact her family planning. The ability to review her model at home helped her come to terms with the necessity of this measure. She stated, "Yeah, I think that also helped and affected my decision-making." These instances indicate that in specific, complex situations, 3D models can play a vital role in the decision-making process, especially for operative interventions that negatively impact areas of great importance to the patient. The visualisation and understanding offered by 3D models may help avoid denial or cognitive dissonance regarding the necessity of a given intervention. Offering the opportunity for patients to visualise their tumour and how it involves organs/structures may help them come to terms with the radicality of their proposed surgery.

In summary, while personalised 3D models can enhance patients' clinical understanding and aid in visualizing their disease, their influence on the decision-making process for exenteration surgery in advanced rectal cancer is variable. They appear most influential in specific complex scenarios or when patients must balance potential outcomes against their quality of life. For many, the decision is heavily influenced by clinical information and prognosis, with the 3D models serving as an aid to understanding rather than a determinant in decision-making.

6.5 Discussion

The study demonstrates that personalised 3D models derived from patient imaging data can be successfully integrated into complex cancer consultations. Models significantly reduced patient decisional conflict more than with standard consultation. Furthermore, 3D models led to notable improvements in patient-perceived and measured comprehension, especially regarding functional outcomes, without directly determining final treatment decisions. This aligns with existing literature emphasising visual aids and personalisation to enhance patient education.

The semi-structured interviews reveal multifaceted patient-perceived benefits spanning enhanced understanding, communication, trust, and emotional reassurance. These interrelated themes have been less explored in past 3D modelling research on patient education. The personalised nature of the models was especially impactful and consistent

with the broader movement towards individualised care. The model's advantages should also be contextualised within the broader structure of the pre-operative counselling process, where patients have multiple appointments with a multidisciplinary team and sufficient time for discussions.

However, the models' influence on surgical decisions depended on case complexity and competing priorities like quality of life. This variable impact connects to the literature on decision-making, highlighting that choices are driven by facts and deeply personal values (412). While the models may not necessarily alter a patient's decision, they facilitate the decision-making process. This is evidenced by the significant reduction in decisional conflict scores and corroborated by patient interview testimonies.

One of the most striking findings was the marked improvement in patients' understanding of their condition and the planned surgery after utilising the 3D models. This is supported by quantitative data from knowledge questionnaires, demonstrating increased scores after consultation, and qualitative data from semi-structured interviews, where patients consistently expressed a deeper grasp of their anatomy, disease, and the likely outcomes of surgery. This enhanced understanding directly translated into a sense of patient empowerment. Patients reported feeling more in control of their decision-making, with the tangible visualisation of their bodies and the surgical intervention facilitating informed choices. This aligns with previous research highlighting the crucial role of visual aids in promoting patient understanding and autonomy in complex medical contexts (413,414).

The 3D models also served as a valuable tool for communication between patients and the healthcare team. The shared reference point provided by the model helped promote better comprehension and facilitated patient engagement in decision-making. Furthermore, 3D models offered emotional comfort to some patients. Tumour visualisation can help transform the abstract threat of cancer into something concrete and manageable. Models help reduce the knowledge gap between patients and medical professionals, potentially contributing to increased trust. This emotional benefit aligns with studies exploring the use of visualisation tools in reducing anxiety and enhancing coping mechanisms in cancer patients (7,415).

While the study demonstrates the value of 3D models in enhancing patient understanding and communication, the influence on the ultimate decision to proceed with surgery is less straightforward. The findings reveal the inherent complexity of human decision-making, particularly in the face of high-stakes choices like exenteration surgery. For some patients, the models acted as supplementary tools, confirming their understanding of the situation, and informing their choice, which often remained heavily influenced by clinical factors and prognosis. This aligns with research on decisional conflict in cancer care, emphasising the

nuanced interplay of medical information, personal values, and emotional considerations in patient choices (416). Patients often put forth compelling considerations, such as the balance between length of life and quality of life, which significantly shape their decision-making. While the 3D models offer clarity and information, the depth of conversation with their multidisciplinary team, the team's confidence, and these weighty life considerations significantly influence their decision.

The value and influence of 3D models may also be contingent on the complexity of a patient's pathology and the specifics of their surgery. Patients with less extensive procedures found 3D models useful as confirmatory aids rather than primary decision-making tools. However, in more complex scenarios, 3D models were perceived as highly beneficial, potentially serving as standalone decision aids. For example, in cases where surgery can lead to significantly negative impacts on important areas of a patient's life, such as sexual function or fertility, 3D models can aid in understanding the necessity of such interventions.

6.5.1.1 Limitations and Future Directions:

The study did not evaluate the duration or specific use of the 3D models during consultations, nor did it assess the overall 'quality' of these consultations, which could influence patient comprehension. The absence of standardised protocols for using 3D models underscores the need for further research into optimal integration strategies and training frameworks for healthcare professionals. Furthermore, addressing potential biases due to participant attrition and selection, alongside exploring generalisability through multi-institutional studies, remains essential for a comprehensive evaluation. Finally, the study does not account for the impact of 3D models on long-term knowledge retention, as testing was conducted shortly after the consultations.

Their time-consuming production process hinders the broader clinical use of models. Simpler models, though quicker to produce via algorithms from segmentation results, often lack the visual appeal and clarity of the more sophisticated methods employed in this study. Additionally, the segmentation process itself, taking 1-2 hours, remains a significant time barrier. An alternative could be using generic models that represent typical clinical scenarios. However, this would go against the patient's preference for personalised models and undermine some of their key advantages. This study does not explicitly examine whether 3D models offer distinct advantages compared to other visual aids, such as anatomical drawings. Additionally, only virtual models were employed, and no comparison was made regarding the potential benefits of printed models. However, it is important to acknowledge that 3D printing a pelvic model would be technically challenging, potentially expensive, and associated with an environmental impact (417).

Future research should explore the potential of advanced 3D modelling techniques, automated segmentation using machine learning methods, and generative AI solutions to address these technical challenges. Longitudinal studies investigating the long-term impact of 3D models on patient well-being and decisional regret, as well as research on cost-effectiveness analyses, would further strengthen the case for integrating this technology into routine clinical practice.

6.5.2 Conclusion

In conclusion, this study demonstrates the valuable role personalised 3D models can play in decision-making, enhancing patient education, communication, and empowerment in pelvic exenteration surgery. While the influence on ultimate decision-making remains nuanced, the improvements in patient understanding, emotional comfort, and engagement in the consultation process offer compelling evidence for integrating this technology into clinical practice. By addressing the identified limitations and fostering continued research and development, personalised 3D models have the potential to significantly improve patient experience and optimise surgical outcomes in this complex and challenging area.

7 Discussion

7.1 Overview

This thesis has investigated developing, implementing, and evaluating patient-specific three-dimensional visualisation tools for complex colorectal cancer surgery. The research was driven by two specific clinical challenges in advanced colorectal cancer surgery: the technical complexity of complete mesocolic excision (CME), where understanding of variable mesenteric vascular anatomy is crucial, and the need for enhanced patient comprehension when contemplating extensive pelvic exenteration procedures. While three-dimensional visualisation shows considerable promise in addressing these challenges, its implementation requires rigorous validation across multiple domains before widespread clinical adoption can be justified.

The overarching aim was to develop, validate, and evaluate patient-specific 3D anatomical models as an integrated decision-support system throughout the continuum of advanced colorectal cancer surgery. This encompassed four interrelated objectives: (1) technical innovation in generating high-quality, patient-specific models from standard imaging data; (2) establishment of standardised frameworks to evaluate model accuracy and clinical utility; (3) assessment of clinical feasibility in CME procedures; and (4) exploration of patient-centred applications, particularly in enhancing comprehension and shared decision-making for complex pelvic exenteration surgery.

Our systematic review revealed significant limitations in the existing evidence base for 3D surgical planning. Despite increasing adoption across surgical specialities, studies were characterised by methodological heterogeneity, limited outcome measures, and a high risk of bias. Such limitations highlight the need for robust validation across multiple domains before widespread clinical adoption can be justified. Consequently, this thesis employed a mixed-methods strategy, combining technical development, quantitative clinical studies, and qualitative research to provide a more complete understanding of both the technical and human factors influencing successful implementation.

The novel contributions of this work include the development of a web-based automated processing pipeline for efficient model generation and interactive visualisation; validation of 3D visualisation's impact on anatomical understanding across a range of surgical expertise for mesenteric blood vessels; demonstration of clinical feasibility of 3D model use for planning and performing CME surgery; and the first detailed investigation of how personalised 3D models influence patient decision-making in advanced rectal cancer. The research progresses systematically from technical innovation through clinical validation to patient application, providing a comprehensive evaluation framework that could inform the implementation of 3D visualisation in other surgical contexts. The project offers a robust foundation on which future work can build upon.

This discussion chapter synthesises findings across these domains, critically examining the potential of 3D visualisation to enhance surgical practice while acknowledging limitations in the work and areas for future development. It considers the immediate practical implications for colorectal cancer surgery and broader applications in surgical education, planning, and patient communication.

7.1.1 Synthesis of Key Findings in Context

This dissertation applies established computer graphics methods in a novel, targeted manner to address the specialised requirements of colorectal cancer surgery. By adapting these surgical planning and patient education techniques, the work advances the integration of visualisation technologies into this specific clinical context. This thesis unifies multiple strands of technological innovation, clinical assessment, and patient-oriented insights as it explores the role of three-dimensional (3D) modelling in advanced colorectal cancer surgery. Findings emerging from the technical development, surgeon-focused anatomical comprehension studies, clinical feasibility trials, and the patient education study collectively highlight the substantial advantages of 3D visualisation tools and the remaining obstacles that must be overcome to maximise their clinical impact.

7.1.2 Integration of Findings Across Studies

The systematic review findings helped contextualise and inform technical development and clinical implementation. The review identified significant heterogeneity in how 3D planning tools were evaluated, with most studies relying on readily available clinical metrics like operative time or blood loss using retrospective study designs rather than measures specific

to 3D visualisation. This insight influenced our approach, which seeks to validate the use of three-dimensional models in a more comprehensive, multifaceted manner. This thesis validates the technical fidelity of models with clinical verification of reconstruction accuracy and comprehensively evaluates the effect on surgical anatomical understanding and patient comprehension.

The comparative analysis of 3D model utilisation across different user groups reveals both universal benefits and group-specific advantages while highlighting important considerations for implementation. This systematic examination demonstrates how three-dimensional visualisation technology can enhance anatomical understanding and surgical planning across the spectrum of medical expertise, from trainees to experienced surgeons, while also serving as a valuable educational tool for patients.

7.2 Technical Innovation and implementation

A significant contribution of this work is the establishment of two complementary validated 3D modelling workflows that bridge the technical domains of medical image processing and computer graphics with distinct surgical and educational requirements. The methodological framework developed in Chapter 2, emphasising modular architecture, data-driven optimisation, and rigorous quality assurance protocols, provides a robust foundation for surgical planning and patient education applications.

Introducing a web-based visualisation platform further enhances the accessibility and usability of 3D models. Unlike traditional implementations that require specialised software or hardware, this platform delivers interactive 3D content directly through standard web browsers. Key features like selective transparency and standardised anatomical colour coding align with clinical requirements while streamlining integration into existing workflows. These advances bridge a longstanding gap between technical capability and practical application in surgical visualisation. Ensuring models can be generated accurately and quickly will be essential in routine widespread adoption.

Developing an automated processing workflow with quantitative validation metrics addresses a key limitation identified in our systematic review - the lack of standardised approaches to evaluating model quality. Previous studies in abdominal surgery have typically relied on subjective assessments without linking these to clinical accuracy. Our validation framework, demonstrating submillimetre accuracy for vascular structures (arteries: 0.64 ± 0.17 mm),

provides objective criteria for assessing model fidelity while adopting core visualisation principles that could be adopted across other surgical specialities.

This study represents the first application of advanced computer graphics techniques, specifically Physically Based Rendering (PBR), to create patient-specific educational models in colorectal surgery. Developing specialised PBR materials and texturing workflows has enabled the creation of photorealistic visualisations of anatomical structures. These advancements aim to enhance patient comprehension through intuitive and visually rich representations. The study establishes a reproducible pipeline capable of generating consistent, high-quality educational models by designing reusable “smart materials” for diverse tissue types and incorporating robust UV unwrapping strategies. This approach addresses a critical gap in patient education, advancing from traditional simplified illustrations to personalised, anatomically accurate, and visually sophisticated models.

Creating these patient rectal cancer models required significant manual effort and technical expertise across multiple software platforms. Considerable time was invested in digital sculpting, UV unwrapping, and texture painting. While these processes were manually executed during this project, subsequent efforts have focused on developing automation tools to streamline these tasks. Early initiatives include scripting repetitive processes using Python in Blender and ZScript in ZBrush, aiming to reduce the time required per model. These automation strategies represent promising steps toward efficiency, though further refinement is necessary to achieve full integration into clinical workflows (likely requiring a complete integrated end-to-end solution).

A patient-centred, iterative design process was central to developing these models. Regular feedback from patients informed decisions regarding colour schemes, transparency, and overall visual style. This iterative refinement ensured the models effectively addressed patient comprehension needs while balancing visual clarity with anatomical accuracy. The ongoing evolution of the visualisation pipeline remains informed by patient input, underscoring the commitment to refining the tool’s educational utility.

3D reconstruction comprises three key steps: imaging segmentation, 3D anatomical mesh extraction, processing, and visualisation. While this project has primarily advanced the latter two stages through innovative mesh processing pipelines and rendering techniques, the reliance on manual segmentation represents a significant limitation. The time-intensive nature of this process, as revealed in both the technical specifications and the clinical feasibility study, poses a considerable barrier to widespread clinical implementation. However, machine learning techniques offer the potential for a complete scan-to-model

pipeline, particularly for automating the labour-intensive segmentation stage. The creation of a validated dataset through this work provides a foundation for developing such automated solutions.

7.3 Clinical Impact and Educational Value

The findings across chapters 4, 5, and 6 demonstrate that three-dimensional visualisation can significantly enhance anatomical understanding across multiple user groups, advancing beyond previous research by providing comprehensive evidence through a systematic, multi-stakeholder evaluation approach. This work directly addresses the primary thesis aims of developing, implementing, and evaluating patient-specific three-dimensional models as an integrated decision-support system throughout the continuum of advanced colorectal cancer surgery.

Critically, this research provides robust evidence of improved understanding (Kirkpatrick Level 2) across multiple user groups - a fundamental assumption that has often been taken for granted in previous studies of surgical visualisation technologies. While many papers cite enhanced understanding as a benefit of 3D visualisation, few have systematically evaluated this claim. The fourfold improvement in anatomical knowledge scores among trainees,

For expert surgeons, despite their high baseline competence, the introduction of 3D models led to measurable improvements in both accuracy and efficiency. The enhancement of inter-rater reliability (Fleiss Kappa 0.6 vs 0.1 for CT) suggests that 3D visualisation may standardise anatomical interpretation among specialists. The 50% reduction in interpretation time (from 12 to 6 minutes) demonstrates potential workflow efficiencies, particularly valuable in time pressured clinical settings.

Across all user groups, the technology showed value in visualising complex anatomical relationships, especially vascular arrangements. The clinical feasibility work in CME surgery demonstrated consistent accuracy in predicting intraoperative findings and strong correlation with surgical anatomy which supports the validity of these models as planning tools. The efficiency gains in learning and communication suggest potential benefits for medical education and clinical practice.

Coupled with enhanced performance among expert surgeons despite their high baseline competence, suggests that 3D visualisation offers benefits across the spectrum of experience levels. This finding challenges the assumption that such tools primarily benefit

novice practitioners. Specifically, 3D imaging enables better appreciation of vessel trajectory, presence/ absence of variants and spatial understanding.

The investigation of inter-rater reliability among expert surgeons represents a particularly novel contribution. Expert CME surgeons demonstrated improved inter-rater reliability using 3D models (Fleiss Kappa 0.6 vs 0.1 for CT), suggesting these tools may foster more uniform interpretations of complex vascular anatomy.

This demonstration of improved understanding is particularly significant as it underpins many assumed benefits of 3D visualisation, such as enhanced surgical performance, better decision-making, and improved outcomes. Previous research has often attempted to evaluate these higher-level impacts without first establishing this baseline of improved comprehension (418). By providing robust evidence that 3D visualisation demonstrably enhances anatomical understanding across different user groups, this work establishes a solid foundation for future research into clinical outcomes and surgical performance.

7.4 Critical Analysis of Research Limitations

This research aimed to develop, implement, and evaluate patient-specific three-dimensional anatomical models to support the surgical planning and patient education in advanced colorectal cancer surgery. While the studies demonstrated promising results, several important limitations must be acknowledged when interpreting the findings and considering future research directions.

7.4.1 Technical Implementation Limitations

Despite automating the 3D mesh extraction, processing, and visualisation steps, the labour-intensive nature of manual segmentation remains a major limitation. Our findings reveal that even experienced segmenters using dedicated equipment require a median time of 49 to 136 minutes, depending on the imaging modality and slice thickness. This time investment, while yielding accurate models, poses challenges for integration into busy clinical workflows where rapid turnaround is often essential. It’s unlikely either surgeons or radiologists would be able to accommodate this amount of time per case within the confines of typical job plans in the U.K. context.

Furthermore, manual segmentation introduces an inherent lack of reproducibility. The accuracy of the reconstruction is heavily reliant on the subjective interpretation of the imaging data by the clinician or technician performing the segmentation. This variability underscores the need for more standardised and objective approaches to segmentation.

The web-based visualisation platform, while successfully delivering interactive 3D content, faces several technical constraints that warrant consideration. The current implementation lacks comprehensive optimisation for mobile and tablet devices - an increasingly important consideration as healthcare delivery becomes more mobile. The absence of formal performance benchmarking across different hardware configurations and network conditions leaves uncertainty about real-world performance in clinical settings. Additionally, the platform's integration with existing hospital Picture Archiving and Communication Systems (PACS) remains undefined, presenting a significant barrier to workflow integration.

The balance between model fidelity and computational efficiency required several compromises that may impact clinical utility. Aggressive mesh decimation of larger anatomical structures was necessary to maintain interactive performance, potentially sacrificing some anatomical detail. The ability to visualise very small vessels remains constrained by imaging resolution limitations, while the mesh processing pipeline may result in the loss of subtle anatomical features during optimisation. For patient education models specifically, the time demands of generating photorealistic physically based rendered (PBR) models makes the current workflow unfeasible for routine clinical implementation.

7.4.2 Clinical Validation Limitations

The clinical validation work must be interpreted within the context of its clearly defined feasibility aims. The CME study (n=76) was designed as a multi-centre international feasibility study with the primary objective of determining whether key clinical outcome measures could be reliably collected to inform future trials, rather than definitively evaluating clinical utility. The study successfully demonstrated that operative metrics, complication data, and video recordings could be consistently gathered across multiple international sites, providing crucial groundwork for future clinical evaluation. Validation of model accuracy was partially limited by the extent of the dissection and operative technique. Novice CME surgeons often did not dissect and selectively ligate the constituent vessels of Henle’s trunk or even the middle colic vessels. However, models were found to accurately predict intraoperative vessel configurations where visualised.

The reliance on manual segmentation in this study underscores a key limitation: while the high accuracy of our 3D reconstructions demonstrates that precise anatomical representations from imaging are achievable in principle, the reproducibility of these results is contingent on the expertise of the segmenters. Our findings reflect the accuracy of imaging interpretation performed by highly skilled personnel, but less experienced or non-expert segmenters may not achieve comparable outcomes. As the accuracy of the 3D model is intrinsically linked to the fidelity of imaging interpretation and segmentation, variability in expertise could compromise the consistency and reliability of model generation in broader clinical or research applications.

Additionally, this study did not formally assess the specific imaging requirements for 3D reconstruction, instead adopting a pragmatic approach that utilised the routine imaging available for each case. While subjective experience allows us to propose recommendations, the lack of a systematic evaluation of how scan protocols and slice thickness influence reconstruction quality represents a limitation in our methodology. Such an analysis would have provided valuable contributions to the literature by delineating the optimal imaging parameters required to ensure accurate and reliable model generation.

7.4.3 Methodological limitations

The patient education study (n=51) faced substantive methodological limitations. The absence of stratified randomisation resulted in an imbalance in disease complexity between the standard and 3D model groups, as reflected in significantly higher pelvic exenteration scores in the 3D group (median 8, IQR 6) compared to the standard group (median 4.5, IQR 5.75, p=0.04). This disparity complicates direct comparisons of objective outcome measures between the groups and introduces a potential bias when interpreting the results.

The study's focus on immediate post-consultation outcomes further limits its scope, as it neglects the potential influence of 3D models on longer-term metrics such as decisional regret. Decisional regret, defined as distress or remorse over a healthcare decision, offers a valuable lens for assessing the enduring impact of patient education interventions. A more informed patient is hypothesised to experience greater satisfaction with their decision-making process, given a clearer understanding of their condition, the proposed surgical approach, and associated risks. The 3D models, by providing personalised and visually

intuitive representations of patient-specific anatomy, could plausibly mitigate decisional conflict and enhance the alignment between patient expectations and surgical realities.

Incorporating decisional regret into the study would have required follow-up assessments over an extended period, capturing patients' reflections as they navigate the outcomes of their surgery. Such data could provide critical insights into the longitudinal benefits or limitations of integrating 3D models into patient education. Time constraints precluded this additional layer of evaluation, limiting the study's capacity to fully explore the long-term impact of 3D visualisation. Future research should aim to address these gaps by evaluating both short- and long-term outcomes, enabling a more comprehensive understanding of the role of 3D models in patient education and decision-making.

A key limitation of both studies is the lack of comparative evaluation between different visualisation approaches. The research examined photorealistic PBR-rendered virtual models for patient education and simpler surface-rendered models for CME planning but did not systematically compare these to alternative methods. This leaves critical questions unanswered regarding the optimal approach to 3D visualisation in colorectal cancer surgery.

For the patient education study, the exclusive use of personalised models precluded comparison with generic anatomical representations. Although patients strongly preferred personalisation, its specific value remains unquantified, particularly given the additional time required to generate personalised models. Additionally, we did not assess whether physical 3D printed models might provide benefits over virtual ones. While virtual models offer interactivity and ease of distribution, physical models could enhance understanding through tactile engagement.

In CME planning, the success of simpler automated surface-rendered models raises questions about the necessity of higher visual fidelity. Despite lacking photorealistic textures and lighting, these models accurately represented vascular anatomy and were well-received by surgeons. Whether such streamlined models could also meet patient education needs, reducing resource demands, warrants investigation. Furthermore, we did not compare 3D visualisation to traditional tools like anatomical drawings. While 3D models theoretically enhance spatial understanding, simpler methods might suffice in many contexts, particularly where resources are constrained.

7.4.4 Unmeasured Impact of Imaging Acquisition Parameters on 3D Model Fidelity

A further limitation of this work is the absence of systematic evaluation regarding how specific imaging acquisition parameters influence 3D model fidelity and clinical utility. Rather than prospectively controlling imaging protocols, this study adopted a pragmatic approach that utilised routine clinical imaging available for each case. While this strategy enhances external validity and reflects real-world implementation conditions, it precludes definitive conclusions about which imaging parameters are necessary or sufficient for reliable 3D reconstruction.

7.4.4.1

7.4.4.2 Uncontrolled Technical Variables

Multiple technical factors remained unexamined throughout this study, despite their potential impact on segmentation accuracy and downstream model quality. CT acquisition parameters including scanner vendor, slice thickness and isotropy, contrast timing and dosage protocols, radiation dose optimisation, and the presence of motion or metallic artefacts were not systematically documented or controlled. Similarly, MRI sequence selection, coil configuration, acceleration strategies, and motion correction techniques were not standardised across participating centres. This heterogeneity limits our ability to establish evidence-based imaging protocols for optimal 3D reconstruction.

The absence of comprehensive DICOM metadata capture represents a missed opportunity to retrospectively analyse the relationship between image quality parameters and segmentation performance. Quantitative image quality metrics such as signal-to-noise ratios, contrast-to-noise ratios, and modulation transfer function surrogates could have provided insights into the minimum imaging requirements for clinically acceptable model generation.

7.4.4.3 Clinical Validation Constraints

The validation approach employed in this study, while clinically relevant, introduced inherent limitations in detecting protocol-driven variations in model accuracy. Intraoperative correlation consistently confirmed the correctness of vascular and anatomical relationships predicted by the models, creating a "ceiling effect" that obscured more subtle geometric

inaccuracies. The relatively coarse nature of operative findings as ground truth verification made it difficult to detect protocol-induced degradations in model fidelity that might not manifest as grossly incorrect anatomical relationships but could nonetheless impact surgical planning precision.

For CME surgery specifically, this limitation is partially mitigated by the primacy of schematic topological accuracy over millimetric precision. The key clinical requirement is accurate representation of vascular branching patterns, spatial relationships, and anatomical variants rather than precise vessel diameter measurements. Vessel calibre naturally varies with patient hydration status, cardiac output, and vasoactive medications, making millimetric accuracy less clinically relevant than topological correctness. The successful prediction of intraoperative findings in this study suggests that routine imaging protocols may be sufficient for capturing the schematic anatomical relationships essential for CME planning.

7.4.4.4 Implications for Reproducibility and Standardisation

The reliance on heterogeneous imaging protocols across institutions limits the reproducibility of our findings and complicates efforts to establish standardised approaches to 3D model generation. Without systematic evaluation of imaging parameter effects, it remains unclear whether the observed model accuracy is attributable to favourable imaging conditions, or operator expertise.

This uncertainty has important implications for clinical implementation. Healthcare systems considering adoption of 3D surgical planning may question whether their existing imaging infrastructure is adequate, or whether protocol modifications and equipment upgrades are necessary. The absence of evidence-based imaging requirements hinders informed decision-making regarding resource allocation and infrastructure planning.

In summary, although our models proved clinically concordant with intraoperative findings, the thesis cannot specify which imaging parameters are optimal for reproducible, high-fidelity reconstruction. Defining these parameters—alongside reporting standards for acquisition, reconstruction, and quality-control metadata—should be a priority for the field. Only then can we transition from a pragmatic, “use what you have” paradigm to an evidence-based, protocol-driven standard that ensures consistent model quality across institutions and vendors.

7.5 Next steps and direction for future research

7.5.1 Clinical Validation Studies

Despite promising preliminary evidence, comprehensive clinical validation is required before 3D modelling can be considered an integral component of surgical practice. Validation must proceed along two key paths: pilot studies that refine study endpoints and assess feasibility, followed by more extensive multi-centre trials.

7.5.1.1 Pilot Studies

Small-scale, randomised trials are required to regarding the effect size and reliability of outcomes associated with 3D modelling in CME. Rather than measuring global parameters such as overall operative time, these trials should focus on technical metrics relevant to the potential benefits of 3D models- specifically vessel dissection. Emphasis on well-defined endpoints such times for specific operative steps (in line with the critical view concept) along with intraoperative errors and bleeding events allows for more meaningful effect size estimates and precise validation of assessment tools designed to capture the benefits of 3D visualisation. Studies should include qualitative elements that examine how models are utilised by surgeons to determine which cases/ scenarios they are especially useful.

Such studies also inform power calculations and optimise trial design for subsequent larger studies. Particular attention should be afforded to the influence of surgeon experience, as relative benefits of 3D models may differ for novice surgeons compared to seasoned practitioners.

7.5.1.2 Large-Scale Clinical Trials

Once pilot studies have established reliable measurement tools and preliminary efficacy, multi-centre randomised controlled trials (RCTs) will be essential to ascertain the impact of 3D modelling on technical performance and patient operative outcomes. These RCTs should stratify patients according to mesenteric vessel complexity and surgeon experience to account for variability in operative approaches. In addition to clinical and oncological outcomes, economic evaluations must be embedded to assess cost-effectiveness and feasibility of widespread adoption. Standardising model creation protocols across participating centers will enable the research community to isolate the true effect of 3D

modelling, ensuring that differences in outcomes are attributable to the technology itself rather than inter-center heterogeneity.

7.5.2 Evidence-Based Imaging Protocols

The transition from pragmatic "use what you have" approaches to evidence-based, protocol-driven standards requires comprehensive reporting of acquisition parameters and evaluation of their impact on model accuracy and quality. Future work should establish minimum acceptable, recommended, and optimal imaging protocols for different surgical applications, with clear quality control frameworks and uncertainty quantification methods.

For CME surgery, where topological accuracy supersedes absolute milimeter precision, such protocols should prioritise consistent visualisation of arterial and venous branching patterns while acknowledging that perfect geometric fidelity may be neither achievable nor clinically necessary. The development of imaging adequacy scores, analogous to pathological staging systems, could provide standardised frameworks for assessing whether available imaging is sufficient for reliable 3D reconstruction in specific clinical contexts.

A protocol-controlled evaluation is required to separate the contribution of acquisition parameters from that of segmentation expertise and post-processing. Such work should (i) prospectively standardise and systematically vary key CT/MRI parameters; (ii) capture the full DICOM metadata to permit assessment of image quality determinants and (iii) relate these to task-specific endpoints that matter for surgical planning. Appropriate quantitative targets include: (1) geometric error metrics such as surface Dice, Hausdorff distance, and centreline deviation for vessels; (2) topological correctness (e.g. preservation of small-calibre arterial branches and venous confluences); (3) segmentation time and inter-segmenter variability as operational surrogates of “useable image quality”; and (4) downstream clinical surrogates such as the need for intraoperative strategy changes attributable to model uncertainty. A multilevel mixed effects modelling framework can assign portions of the total error variance to its principal sources: the individual scanner (hardware noise and resolution), the acquisition protocol (slice thickness, reconstruction kernel, contrast timing), the anatomical region under study, and the segmentation operator.

7.5.3 Educational Impact Assessment

The potential of 3D models as an educational resource is substantial, underscoring the need for systematic investigations of how this technology can facilitate surgical training.

7.5.3.1 Learning Curve Analysis

Longitudinal studies examining 3D models' impact on surgical skill acquisition should assess multiple dimensions of learning. These include time to achieve predefined competency benchmarks, transfer of skills to clinical practice, and retention of anatomical knowledge. Cost-effectiveness analyses comparing 3D model-enhanced training against traditional methods should evaluate whether improved learning efficiency and reduced complications justify implementation costs. Such studies would provide crucial evidence for educational policy decisions regarding widespread adoption of 3D modelling in surgical training.

7.5.3.2 Experience-Dependent Benefits

The relative benefit of 3D models across different levels of surgical experience requires systematic investigation. While initial findings suggest varying advantages based on expertise, robust evidence is needed to quantify these differences. Research should examine how surgical experience influences the utility of 3D models in key areas including preoperative planning, intraoperative decision-making, and team communication. Understanding these differential benefits would enable targeted implementation strategies, optimising the use of 3D technology throughout the surgical learning curve.

7.5.4 Machine learning approach to automated segmentation

Manual segmentation remains the limiting factor in generating 3D models. As we outlined in the literature review in chapter 1, advancements in artificial intelligence (AI) offer a promising path to overcome these limitations. However, there are currently no published studies on AI-based segmentation approaches for mesenteric vessels and associated anatomy. To establish best practices and identify optimal solutions, comprehensive benchmarking studies are needed to compare the performance of different model architectures on large, well-annotated datasets.

However, the development and validation of AI-driven segmentation tools face several challenges:

- **Data Requirements:** Training robust AI models necessitates large, high-quality datasets of manually segmented scans, which are often difficult and time-consuming to acquire. This research has created a large, validated dataset for mesenteric vessels and associated anatomy which can serve to train AI.
- **Computational Demands:** Processing large volumes of CT data for AI model training requires significant computational resources, both in terms of hardware and financial investment.
- **Accuracy Assessment**: Traditional metrics like Dice coefficients and Jaccard indices, while useful, may not fully capture the clinical relevance of segmentation accuracy. The Dice coefficient and Jaccard index both measure the overlap between predicted segmentation and ground truth, ranging from 0 (no overlap) to 1 (perfect overlap). Missing or incorrectly segmented small vessels, even if not significantly impacting these metrics, could have crucial implications for surgical planning.

7.5.4.1 Development of a 3D U-Net Convolutional Neural Network

The next stage of this project employs a 3D U-Net architecture specifically designed to automate volumetric segmentation for CT imaging data. Numerous studies have shown that 3D-UNET designs perform well for volumetric imaging segmentation tasks. This initial model encompasses four encoding blocks, each comprising two consecutive three-dimensional (3D) convolutions followed by batch normalisation and rectified linear unit (ReLU) activation functions, with max pooling operations to progressively downsample and increase the receptive field. Channel depths proceed in powers of two (64→128→256→512) before reaching a 1024-channel bottleneck layer that integrates global context. On the decoder side, each corresponding upsampling step deploys transposed convolutions, skip connections to reinstate high-resolution encoder features, and the same double-convolution structure as in the encoder. A final 1×1×1 convolution layer outputs probability maps for each class (e.g., artery, vein, colon, pancreas, stomach/duodenum and tumour), effectively delivering automated segmentations.

7.5.4.2 Preliminary Validation on Synthetic and Small-Scale Datasets

Using this 3D U-Net implementation, we have conducted basic proof-of-concept experiments:

1. Synthetic Dataset: To confirm the foundational functionality of our 3D U-Net model and training scripts, we developed a simple, synthetic dataset. Within each volumetric image, we placed a single white cube in an otherwise empty (black) space, corresponding to a binary (0,1) classification task. This artificially generated arrangement allowed us to verify that the model could learn to discriminate between foreground (the cube) and background.
1. Small Clinical Cohort: A pilot collection of ten 64x64x64 scan imaging patches with corresponding arterial and venous segmentation labels. The model achieved acceptable segmentation performance on these patches, indicating promise for real-world applications. However, the limited size of this dataset restricts the generalisability of our findings and points to the need for expanded data collection.

The basic structure of our prototype model is outlined in the publicly available code repository (https://github.com/JAFletch-surg/3DCNN_CME).

7.5.5 Implementation research and technical developments

7.5.5.1 Multi-Purpose Model Development

Maximising the utility and cost-effectiveness of 3D models necessitates creating unified datasets that cater to diverse clinical and educational applications. Research should focus on developing models that integrate seamlessly with multidisciplinary team (MDT) visualisation platforms. Additional adaptations could involve tailoring models for patient consultations by incorporating interactive features and ensuring visual clarity suitable for non-specialist audiences. Furthermore, incorporating 3D models into surgical training simulators with accurate tissue properties and enabling compatibility with intraoperative navigation systems, including robotic platforms, would broaden their scope of utility. Lastly, export functionalities for augmented reality (AR) and virtual reality (VR) applications should be enhanced to ensure model fidelity across platforms.

7.5.5.2 Clinical Integration Studies

Implementation research must address the technical and workflow challenges associated with incorporating 3D models into routine clinical practice. Establishing standardised protocols for model storage and retrieval within hospital Picture Archiving and Communication Systems (PACS) is a critical first step. Further integration with electronic medical record (EMR) platforms would facilitate documentation and audit processes. Developing secure sharing protocols to enable remote access for MDT discussions and introducing version control systems to track model iterations are additional priorities. Automated reporting tools that document model usage and clinical outcomes would further streamline the process and provide valuable insights into model efficacy.

7.6 Summary conclusion

This thesis set out to develop, validate, and evaluate patient-specific three-dimensional models as an integrated decision-support system throughout the continuum of advanced colorectal cancer surgery. Through systematic investigation across technical, educational, and clinical domains, the research has demonstrated both the feasibility and value of 3D visualisation while highlighting important considerations for implementation.

The technical aims were achieved through the development of validated workflows for both surgical planning and patient education applications. The processing pipeline achieved high accuracy for vascular structures while significantly reducing model generation time. Web-based delivery enabled broad accessibility without specialist hardware requirements, though manual segmentation remains a significant barrier to routine clinical implementation.

In addressing the educational objectives, the research provided robust evidence that 3D visualisation enhances anatomical understanding across different levels of surgical expertise. The significant improvements in trainee anatomical knowledge scores and enhanced inter-rater reliability among expert surgeons demonstrates value for complex mesenteric vascular anatomy. The substantial reduction in interpretation time suggests potential workflow efficiencies.

The clinical feasibility study validated the accuracy of 3D reconstructions against intraoperative findings and established protocols for collecting key outcome measures in future trials. For patients considering pelvic exenteration, 3D models significantly reduced

decisional conflict compared to standard consultation and improved understanding of functional outcomes. The impact of model on patient decision making is complex and situation dependent.

While this work establishes a foundation for implementing 3D visualisation in colorectal cancer surgery, several challenges remain. Future research should focus on developing automated segmentation approaches, conducting large-scale clinical trials to quantify impact on surgical outcomes, and optimising integration into existing clinical workflows. Nevertheless, the comprehensive evidence presented supports the targeted implementation of 3D visualisation to enhance surgical precision and shared decision-making, particularly for complex oncological procedures where detailed anatomical understanding is paramount.

8 Bibliography

1. RCS. *Future of Surgery*. Royal College of Surgeons; 2018. https://futureofsurgery.rcseng.ac.uk/?_ga=2.127512013.158368602.1585999188-1360980048.1585999188

2. Rengier F, Mehndiratta A, von Tengg-Kobligk H, Zechmann CM, Unterhinninghofen R, Kauczor HU, et al. 3D printing based on imaging data: review of medical applications. *International journal of computer assisted radiology and surgery*. 2010;5(4): 335–341. https://0-dx-doi-org.wam.leeds.ac.uk/10.1007/s11548-010-0476-x.

3. Perica ER, Sun Z. A Systematic Review of Three-Dimensional Printing in Liver Disease. *Journal of Digital Imaging*. 2018;31(5): 692–701. https://doi.org/10.1007/s10278-018-0067-x.

4. Soon DSC, Chae MP, Pilgrim CHC, Matthew W, Spychal RT, Hunter-smith DJ. 3D haptic modelling for preoperative planning of hepatic resection : A systematic review. *Annals of Medicine and Surgery*. 2016;10: 1–7. https://doi.org/10.1016/j.amsu.2016.07.002.

5. Emile SH, Wexner SD. Systematic review of the applications of three-dimensional printing in colorectal surgery. *Colorectal Disease*. 2018; codi.14480. https://doi.org/10.1111/codi.14480.

6. Crane J, Hamed M, Borucki JP, El-Hadi A, Shaikh I, Stearns AT. Complete mesocolic excision versus conventional surgery for colon cancer: A systematic review and meta-analysis. *Colorectal Disease*. 2021;23(7): 1670–1686. https://doi.org/10.1111/codi.15644.

7. Farrell EH, Whistance RN, Phillips K, Morgan B, Savage K, Lewis V, et al. Systematic review and meta-analysis of audio-visual information aids for informed consent for invasive healthcare procedures in clinical practice. *Patient Education and Counseling*. 2014;94(1): 20–32. https://doi.org/10.1016/j.pec.2013.08.019.

8. Yang T, Tan T, Yang J, Pan J, Hu C, Li J. The impact of using three-dimensional printed liver models for patient education. *Journal of International Medical Research*. 2018;46(4): 1570–1578. http://0-dx.doi.org.wam.leeds.ac.uk/10.1177/0300060518755267.

9. Heydari MR, Taghva F, Amini M, Delavari S. Using Kirkpatrick's model to measure the effect of a new teaching and learning methods workshop for health care staff. *BMC Research Notes*. 2019;12(1): 388. https://doi.org/10.1186/s13104-019-4421-y.

10. Larobina M. Thirty Years of the DICOM Standard. *Tomography*. 2023;9(5): 1829–1838. https://doi.org/10.3390/tomography9050145.

11. Gibaud B. The DICOM Standard: A Brief Overview. In: Lemoigne Y, Caner A (eds.) *Molecular Imaging: Computer Reconstruction and Practice*. Dordrecht: Springer Netherlands; 2008. p. 229–238. https://doi.org/10.1007/978-1-4020-8752-3_13.

12. Pelberg R. Basic Principles in Computed Tomography (CT). In: Pelberg R (ed.) *Cardiac CT Angiography Manual*. London: Springer London; 2015. p. 19–58. https://doi.org/10.1007/978-1-4471-6690-0_2.

13. Grover VPB, Tognarelli JM, Crossey MME, Cox IJ, Taylor-Robinson SD, McPhail MJW. Magnetic Resonance Imaging: Principles and Techniques: Lessons for Clinicians. *Journal of Clinical and Experimental Hepatology*. 2015;5(3): 246–255. https://doi.org/10.1016/j.jceh.2015.08.001.

14. Fernandes MC, Gollub MJ, Brown G. The importance of MRI for rectal cancer evaluation. *Surgical Oncology*. 2022;43: 101739. https://doi.org/10.1016/j.suronc.2022.101739.

15. Sharma N, Aggarwal L. Automated medical image segmentation techniques. *Journal of medical physics / Association of Medical Physicists of India*. 2010;35: 3–14. https://doi.org/10.4103/0971-6203.58777.

16. Preim, Bernhard, Botha, Charl. Chapter 4 Image Analysis for Medical Visualisation. In: *Visual Computing for Medicine Theory, Algorithms, and applications*. 2nd ed. Morgan Kaufmann Publishers Inc.; p. 111–174.

17. Byrne N, Velasco Forte M, Tandon A, Valverde I, Hussain T. A systematic review of image segmentation methodology, used in the additive manufacture of patient-specific 3D printed models of the cardiovascular system. *JRSM Cardiovascular Disease*. 2016;5: 204800401664546. https://doi.org/10.1177/2048004016645467.

18. *Automatic abdominal multi-organ segmentation using deep convolutional neural network and time-implicit level sets | SpringerLink*. https://link.springer.com/article/10.1007%2Fs11548-016-1501-5 [Accessed 29th April 2021].

19. Akhil M, Aishwarya R, Lal V, Mahesh S. Comparison and Evaluation of Segmentation Techniques for Brain MRI using Gold Standard. *Indian Journal of Science and Technology*. 2016;9(46). https://doi.org/10.17485/ijst/2016/v9i46/106495.

20. Yushkevich PA, Piven J, Hazlett HC, Smith RG, Ho S, Gee JC, et al. User-guided 3D active contour segmentation of anatomical structures: Significantly improved efficiency and reliability. *NeuroImage*. 2006;31(3): 1116–1128. https://doi.org/10.1016/j.neuroimage.2006.01.015.

21. Ghorpade H, Jagtap J, Patil S, Kotecha K, Abraham A, Horvat N, et al. Automatic Segmentation of Pancreas and Pancreatic Tumor: A Review of a Decade of Research. *IEEE Access*. 2023;11: 108727–108745. https://doi.org/10.1109/ACCESS.2023.3320570.

22. Lamba R, McGahan JP, Corwin MT, Li CS, Tran T, Seibert JA, et al. CT Hounsfield Numbers of Soft Tissues on Unenhanced Abdominal CT Scans: Variability Between Two Different Manufacturers' MDCT Scanners. *AJR. American journal of roentgenology*. 2014;203(5): 1013–1020. https://doi.org/10.2214/AJR.12.10037.

23. Boas FE, Fleischmann D. CT artifacts: causes and reduction techniques. *Imaging in Medicine*. 2012;4(2): 229–240.

24. Almohammed HI, Elshami W, Hamd ZY, Abuzaid M. Optimizing CT Abdomen–Pelvis Scan Radiation Dose: Examining the Role of Body Metrics (Waist Circumference, Hip Circumference, Abdominal Fat, and Body Mass Index) in Dose Efficiency. *Tomography*. 2024;10(5): 643–653. https://doi.org/10.3390/tomography10050049.

25. Beets-Tan RGH, Lambregts DMJ, Maas M, Bipat S, Barbaro B, Curvo-Semedo L, et al. Magnetic resonance imaging for clinical management of rectal cancer: Updated recommendations from the 2016 European Society of Gastrointestinal and Abdominal Radiology (ESGAR) consensus meeting. *European Radiology*. 2018;28(4): 1465–1475. https://doi.org/10.1007/s00330-017-5026-2.

26. Caruso D, Rosati E, Panvini N, Rengo M, Bellini D, Moltoni G, et al. Optimization of contrast medium volume for abdominal CT in oncologic patients: prospective comparison between fixed and lean body weight-adapted dosing protocols. *Insights into Imaging*. 2021;12(1): 40. https://doi.org/10.1186/s13244-021-00980-0.

27. Zhu S, Xia X, Zhang Q, Belloulata K. An Image Segmentation Algorithm in Image Processing Based on Threshold Segmentation. In: *2007 Third International IEEE Conference on Signal-Image Technologies and Internet-Based System*. 2007. p. 673–678. https://doi.org/10.1109/SITIS.2007.116. [Accessed 8th December 2024].

28. Kaur, Dilpeet, Kaur, Yadwinder. Various Imaging Segmentation Techniques: A review. *International Journal of Computer Science and Mobile Computing*. 2014;3(5): 809–814.

29. Bandyk MG, Gopireddy DR, Lall C, Balaji KC, Dolz J. MRI and CT bladder segmentation from classical to deep learning based approaches: Current limitations and lessons. *Computers in Biology and Medicine*. 2021;134: 104472. https://doi.org/10.1016/j.compbiomed.2021.104472.

30. Savant S. A Review on Edge Detection Techniques for Image Segmentation. 2014;5.

31. Iglesias JE, Sabuncu MR. Multi-atlas segmentation of biomedical images: A survey. *Medical Image Analysis*. 2015;24(1): 205–219. https://doi.org/10.1016/j.media.2015.06.012.

32. von Siebenthal M, Székely G, Gamper U, Boesiger P, Lomax A, Cattin P. 4D MR imaging of respiratory organ motion and its variability. *Physics in Medicine and Biology*. 2007;52(6): 1547–1564. https://doi.org/10.1088/0031-9155/52/6/001.

33. Hornik K. Approximation capabilities of multilayer feedforward networks. *Neural Networks*. 1991;4(2): 251–257. https://doi.org/10.1016/0893-6080(91)90009-T.

34. LeCun Y, Bengio Y, Hinton G. Deep learning. *Nature*. 2015;521(7553): 436–444. https://doi.org/10.1038/nature14539.

35. Krizhevsky A, Sutskever I, Hinton GE. ImageNet classification with deep convolutional neural networks. *Communications of the ACM*. 2017;60(6): 84–90. https://doi.org/10.1145/3065386.

36. Driss SB, Soua M, Kachouri R, Akil M. A Comparison Study Between MLP and Convolutional Neural Network Models for Character Recognition. 2017;10223: 1022306. https://doi.org/10.1117/12.2262589.

37. Lecun Y, Bottou L, Bengio Y, Haffner P. Gradient-based learning applied to document recognition. *Proceedings of the IEEE*. 1998;86(11): 2278–2324. https://doi.org/10.1109/5.726791.

38. Yamashita R, Nishio M, Do RKG, Togashi K. Convolutional neural networks: an overview and application in radiology. *Insights into Imaging*. 2018;9(4): 611–629. https://doi.org/10.1007/s13244-018-0639-9.

39. HECHT-NIELSEN R. III.3 - Theory of the Backpropagation Neural Network**Based on “nonindent” by Robert Hecht-Nielsen, which appeared in Proceedings of the International Joint Conference on Neural Networks 1, 593–611, June 1989. © 1989 IEEE. In: Wechsler H (ed.) *Neural Networks for Perception*. Academic Press; 1992. p. 65–93. https://doi.org/10.1016/B978-0-12-741252-8.50010-8.

40. Gu J, Wang Z, Kuen J, Ma L, Shahroudy A, Shuai B, et al. Recent advances in convolutional neural networks. *Pattern Recognition*. 2018;77: 354–377. https://doi.org/10.1016/j.patcog.2017.10.013.

41. Simonyan K, Zisserman A. *Very Deep Convolutional Networks for Large-Scale Image Recognition*. 2015. https://doi.org/10.48550/arXiv.1409.1556.

42. Yang S, Xiao W, Zhang M, Guo S, Zhao J, Shen F. *Image Data Augmentation for Deep Learning: A Survey*. 2023.

43. Goodfellow I, Bengio Y, Courville A. *Deep Learning*. MIT Press; 2016.

44. Boureau YL, Ponce J, LeCun Y. A theoretical analysis of feature pooling in visual recognition. In: *Proceedings of the 27th International Conference on International Conference on Machine Learning*. Madison, WI, USA: Omnipress; 2010. p. 111–118.

45. Çiçek Ö, Abdulkadir A, Lienkamp SS, Brox T, Ronneberger O. *3D U-Net: Learning Dense Volumetric Segmentation from Sparse Annotation*. 2016.

46. Glorot X, Bordes A, Bengio Y. Deep Sparse Rectifier Neural Networks. In: *Proceedings of the Fourteenth International Conference on Artificial Intelligence and Statistics*. JMLR Workshop and Conference Proceedings; 2011. p. 315–323. https://proceedings.mlr.press/v15/glorot11a.html [Accessed 25th November 2024].

47. Nwankpa C, Ijomah W, Gachagan A, Marshall S. *Activation Functions: Comparison of trends in Practice and Research for Deep Learning*. 2018. https://doi.org/10.48550/arXiv.1811.03378.

48. Ramachandran P, Zoph B, Le QV. *Searching for Activation Functions*. 2017. https://doi.org/10.48550/arXiv.1710.05941.

49. Hendrycks D, Gimpel K. *Gaussian Error Linear Units (GELUs)*. 2023. https://doi.org/10.48550/arXiv.1606.08415.

50. Milletari F, Navab N, Ahmadi SA. *V-Net: Fully Convolutional Neural Networks for Volumetric Medical Image Segmentation*. 2016.

51. Sudre CH, Li W, Vercauteren T, Ourselin S, Cardoso MJ. Generalised Dice overlap as a deep learning loss function for highly unbalanced segmentations. In: 2017. p. 240–248. https://doi.org/10.1007/978-3-319-67558-9_28. [Accessed 8th December 2024].

52. Ronneberger O, Fischer P, Brox T. U-Net: Convolutional Networks for Biomedical Image Segmentation. 2015; 234–241. https://doi.org/10.1007/978-3-319-24574-4_28.

53. Kingma DP, Ba J. *Adam: A Method for Stochastic Optimization*. 2017. https://doi.org/10.48550/arXiv.1412.6980.

54. Siddique N, Sidike P, Elkin C, Devabhaktuni V. *U-Net and its variants for medical image segmentation: theory and applications*. 2020. https://doi.org/10.48550/arXiv.2011.01118.

55. Zhang S, Niu Y. LcmUNet: A Lightweight Network Combining CNN and MLP for Real-Time Medical Image Segmentation. *Bioengineering*. 2023;10: 712. https://doi.org/10.3390/bioengineering10060712.

56. Drozdzal M, Vorontsov E, Chartrand G, Kadoury S, Pal C. *The Importance of Skip Connections in Biomedical Image Segmentation*. 2016. https://doi.org/10.48550/arXiv.1608.04117.

57. He K, Zhang X, Ren S, Sun J. *Deep Residual Learning for Image Recognition*. 2015. https://doi.org/10.48550/arXiv.1512.03385.

58. Takahashi S, Sakaguchi Y, Kouno N, Takasawa K, Ishizu K, Akagi Y, et al. Comparison of Vision Transformers and Convolutional Neural Networks in Medical Image Analysis: A Systematic Review. *Journal of Medical Systems*. 2024;48(1): 84. https://doi.org/10.1007/s10916-024-02105-8.

59. Vaswani A, Shazeer N, Parmar N, Uszkoreit J, Jones L, Gomez AN, et al. *Attention Is All You Need*. 2023. https://doi.org/10.48550/arXiv.1706.03762.

60. Dosovitskiy A, Beyer L, Kolesnikov A, Weissenborn D, Zhai X, Unterthiner T, et al. *An Image is Worth 16x16 Words: Transformers for Image Recognition at Scale*. 2021. https://doi.org/10.48550/arXiv.2010.11929.

61. Levoy M. Display of surfaces from volume data. *IEEE Computer Graphics and Applications*. 1988;8(3): 29–37. https://doi.org/10.1109/38.511.

62. Max N. Optical models for direct volume rendering. *IEEE Transactions on Visualization and Computer Graphics*. 1995;1(2): 99–108. https://doi.org/10.1109/2945.468400.

63. Kniss J, Kindlmann G, Hansen C. Multidimensional transfer functions for interactive volume rendering. *IEEE Transactions on Visualization and Computer Graphics*. 2002;8(3): 270–285. https://doi.org/10.1109/TVCG.2002.1021579.

64. Greenway K. *Hounsfield unit | Radiology Reference Article | Radiopaedia.org*. Radiopaedia. https://doi.org/10.53347/rID-38181. [Accessed 30th December 2024].

65. Kindlmann G, Durkin JW. Semi-automatic generation of transfer functions for direct volume rendering. In: *IEEE Symposium on Volume Visualization (Cat. No.989EX300)*. 1998. p. 79–86. https://doi.org/10.1109/SVV.1998.729588. [Accessed 26th November 2024].

66. Kniss J, Kindlmann G, Hansen CD. 9 - Multidimensional Transfer Functions for Volume Rendering. In: Hansen CD, Johnson CR (eds.) *Visualization Handbook*. Burlington: Butterworth-Heinemann; 2005. p. 189–209. https://doi.org/10.1016/B978-012387582-2/50011-3. [Accessed 26th November 2024].

67. Correa CD, Ma KL. Size-based transfer functions: a new volume exploration technique. *IEEE transactions on visualization and computer graphics*. 2008;14(6): 1380–1387. https://doi.org/10.1109/TVCG.2008.162.

68. Ljung P, Krüger J, Groller E, Hadwiger M, Hansen CD, Ynnerman A. State of the Art in Transfer Functions for Direct Volume Rendering. *Computer Graphics Forum*. 2016;35(3): 669–691. https://doi.org/10.1111/cgf.12934.

69. Bernhard Preim, Botha, Charl. Chapter 9. Volume Interaction. In: *Visual Computing for Medicine*. 2nd ed. Morgan Kaufmann Publishers Inc.; 2014. p. 323–368.

70. Nasim Saravi A, Horacsek J, Alim U, Silva JD. Transferring transfer functions (TTF): A guided approach to transfer function optimization in volume visualization. *Computers & Graphics*. 2024;124: 104067. https://doi.org/10.1016/j.cag.2024.104067.

71. Lundstrom C, Ljung P, Ynnerman A. Local Histograms for Design of Transfer Functions in Direct Volume Rendering. *IEEE Transactions on Visualization and Computer Graphics*. 2006;12(6): 1570–1579. https://doi.org/10.1109/TVCG.2006.100.

72. Lawonn K, Smit N n., Bühler K, Preim B. A Survey on Multimodal Medical Data Visualization. *Computer Graphics Forum*. 2018;37(1): 413–438. https://doi.org/10.1111/cgf.13306.

73. Preim, Bernhard, Botha, Charl. Chapter 7. Direct Volume Visualisation. In: *Visual Computing for Medicine*. 2nd ed. Morgan Kaufmann Publishers Inc.; 2014.

74. Kruger J, Westermann R. Acceleration techniques for GPU-based volume rendering. In: *IEEE Visualization, 2003. VIS 2003.* 2003. p. 287–292. https://doi.org/10.1109/VISUAL.2003.1250384. [Accessed 10th November 2023].

75. Beyer J, Hadwiger M, Pfister H. State-of-the-Art in GPU-Based Large-Scale Volume Visualization. *Computer Graphics Forum*. 2015;34(8): 13–37. https://doi.org/10.1111/cgf.12605.

76. Muigg P, Hadwiger M, Doleisch H, Hauser H. Scalable Hybrid Unstructured and Structured Grid Raycasting. *IEEE Transactions on Visualization and Computer Graphics*. 2007;13(6): 1592–1599. https://doi.org/10.1109/TVCG.2007.70588.

77. Agrawal A, Kohout J, Clapworthy GJ, Mcfarlane NJ, Dong F, Viceconti M, et al. Enabling the interactive display of large medical volume datasets by multiresolution bricking. *J. Supercomput.* 2010;51(1): 3–19. https://doi.org/10.1007/s11227-009-0289-2.

78. *Tris, Quads & N-Gons*. 3D Modeling Resources. https://resources.turbosquid.com/training/modeling/tris-quads-n-gons/ [Accessed 17th November 2023].

79. Preim B, Botha C. Surface Rendering. In: *Visual Computing for Medicine*. 2nd Edition. Morgan Kaufmann Publishers Inc.; p. 229–266.

80. El Seoud MSA, Mady AS. A Comprehensive Review on Volume Rendering Techniques. In: *Proceedings of the 8th International Conference on Software and Information Engineering*. New York, NY, USA: Association for Computing Machinery; 2019. p. 126–131. https://doi.org/10.1145/3328833.3328878. [Accessed 30th December 2024].

81. *Getting started with WebGL - Web APIs | MDN*. https://developer.mozilla.org/en-US/docs/Web/API/WebGL_API/Tutorial/Getting_started_with_WebGL [Accessed 26th November 2024].

82. C. L, T.F. C, V.C. F, K.M. S, C.W.Y. W. Applications of three-dimensional printing in surgery. *Surgical Innovation*. 2017;24(1): 82–88. http://0-dx.doi.org.wam.leeds.ac.uk/10.1177/1553350616681889.

83. Technologies U. *Real-Time 3D Development Platform & Editor| Unity*. https://unity.com/products/unity-engine [Accessed 16th November 2023].

84. *Unreal Engine | The most powerful real-time 3D creation tool*. Unreal Engine. https://www.unrealengine.com/en-US [Accessed 16th November 2023].

85. Spencer S. *ZBrush Digital Sculpting Human Anatomy*. Wiley; 2010. https://books.google.co.uk/books?id=nBTJev9ummgC

86. Ebert DS, Musgrave FK, Peachey D, Perlin K, Worley S. *Texturing and Modeling: A Procedural Approach*. Elsevier Science; 2002. https://books.google.co.uk/books?id=fXp5UsEWNX8C

87. Lorensen WE, Cline HE. Marching Cubes: A High Resolution 3D Surface Construction Algorithm. *SIGGRAPH Comput. Graph.* 1987;21(4): 163–169. https://doi.org/10.1145/37402.37422.

88. Bloomenthal J. Polygonization of implicit surfaces. *Computer Aided Geometric Design*. 1988;5(4): 341–355. https://doi.org/10.1016/0167-8396(88)90013-1.

89. Janzen B, Teather R. Is 60 FPS better than 30? The impact of frame rate and latency on moving target selection. *Conference on Human Factors in Computing Systems - Proceedings*. 2014; https://doi.org/10.1145/2559206.2581214.

90. Garland M, Heckbert PS. Surface simplification using quadric error metrics. In: *Proceedings of the 24th annual conference on Computer graphics and interactive techniques*. USA: ACM Press/Addison-Wesley Publishing Co.; 1997. p. 209–216. https://doi.org/10.1145/258734.258849. [Accessed 12th November 2023].

91. Vollmer J, Mencl R, Uller HM, Dieser Z. Improved Laplacian Smoothing of Noisy Surface Meshes Improved Laplacian Smoothing of Noisy Surface Meshes. In: 1999. https://api.semanticscholar.org/CorpusID:14577723

92. Taubin G. A Signal Processing Approach to Fair Surface Design. In: *Proceedings of the 22nd Annual Conference on Computer Graphics and Interactive Techniques*. New York, NY, USA: Association for Computing Machinery; 1995. p. 351–358. https://doi.org/10.1145/218380.218473.

93. Jones TR, Durand F, Desbrun M. Non-Iterative, Feature-Preserving Mesh Smoothing. *ACM Trans. Graph.* 2003;22(3): 943–949. https://doi.org/10.1145/882262.882367.

94. Deschamps T, Cohen LD. Fast extraction of tubular and tree 3D surfaces with front propagation methods. In: *2002 International Conference on Pattern Recognition*. 2002. p. 731–734 vol.1. https://doi.org/10.1109/ICPR.2002.1044862.

95. Hodges ERS. The Guild handbook of scientific illustration.

96. Erolin C, Reid L, McDougall S. Using virtual reality to complement and enhance anatomy education. *Journal of Visual Communication in Medicine*. 2019;42(3): 93–101. https://doi.org/10.1080/17453054.2019.1597626.

97. Parent R. *Computer Animation: Algorithms and Techniques*.. 3rd ed. San Francisco, CA, USA: Morgan Kaufmann Publishers Inc.; 2012.

98. Luft T, Colditz C, Deussen O. Image Enhancement by Unsharp Masking the Depth Buffer. *Also publ. as paper in: International Conference on Computer Graphics and Interactive Techniques (SIGGRAPH), Boston, Massachusetts, 2006, pp. 1206-1213*. 2006;25. https://doi.org/10.1145/1179352.1142016.

99. Bommes D, Levy B, Pietroni N, Puppo E, Silva C, Zorin D. State of the Art in Quad Meshing. 2012;

100. *Quad-Based Topology*. 3D Modeling Resources. https://resources.turbosquid.com/training/modeling/quad-based-topology/ [Accessed 30th December 2024].

101. Denham T. *What is UV Mapping & Unwrapping?*. Concept Art Empire. https://conceptartempire.com/uv-mapping-unwrapping/ [Accessed 14th November 2023].

102. Tatarchuk N. Practical parallax occlusion mapping with approximate soft shadows for detailed surface rendering. *ACM SIGGRAPH 2006 Courses*. 2006; https://api.semanticscholar.org/CorpusID:18481952

103. *Three.js – JavaScript 3D Library*. https://threejs.org/ [Accessed 16th November 2023].

104. Dirksen J. *Learning Three.js: The JavaScript 3D Library for WebGL*. Packt Publishing; 2015. https://books.google.co.uk/books?id=Bem9zQEACAAJ

105. *Django*. Django Project. https://www.djangoproject.com/ [Accessed 30th December 2024].

106. *React*. https://react.dev/ [Accessed 30th December 2024].

107. *Vue.js*. https://vuejs.org/ [Accessed 30th December 2024].

108. *3D Slicer image computing platform*. 3D Slicer. https://slicer.org/ [Accessed 16th November 2023].

109. *Materialise Mimics | 3D Medical Image Processing Software*. https://www.materialise.com/en/healthcare/mimics-innovation-suite/mimics [Accessed 16th November 2023].

110. *Innersightlabs | Interactive 3D model for pre-operative planning and procedure*. https://www.innersightlabs.com/ [Accessed 16th November 2023].

111. *First online laboratory for 3D modelling of medical images*. Visible Patient. https://www.visiblepatient.com/en/ [Accessed 16th November 2023].

112. Barsom EZ, Graafland M, Schijven MP. Systematic review on the effectiveness of augmented reality applications in medical training. *Surgical Endoscopy and Other Interventional Techniques*. 2016;30(10): 4174–4183. https://doi.org/10.1007/s00464-016-4800-6.

113. Hodgdon T, Danrad R, Patel MJ, Smith SE, Richardson ML, Ballard DH, et al. Logistics of Three-dimensional Printing: Primer for Radiologists. *Academic Radiology*. 2018;25(1): 40–51. https://doi.org/10.1016/j.acra.2017.08.003.

114. Garcia J, Yang Z, Mongrain R, Leask RL, Lachapelle K. 3D printing materials and their use in medical education: a review of current technology and trends for the future. *BMJ Simulation and Technology Enhanced Learning*. 2017; bmjstel-2017-000234. https://doi.org/10.1136/bmjstel-2017-000234.

115. *Risk Mitigation: Safety Considerations When Buying a Resin 3D Printer*. Formlabs. https://formlabs.com/uk/blog/formlabs-resin-3d-printers-safer/?srsltid=AfmBOoq3ixoWhaY5ssGKL2AGrZw-lhvZJaSjNsGrTGgWk-7J7Xlkkk9P [Accessed 30th December 2024].

116. Azer SA, Azer S. 3D Anatomy Models and Impact on Learning: A Review of the Quality of the Literature. *Health Professions Education*. 2016;2(2): 80–98. https://doi.org/10.1016/j.hpe.2016.05.002.

117. Kong X, Nie L, Zhang H, Wang Z, Ye Q, Tang L, et al. Do Three-dimensional Visualization and Three-dimensional Printing Improve Hepatic Segment Anatomy Teaching? A Randomized Controlled Study. *Journal of surgical education*. 2016;73(2): 264–269. https://0-dx-doi-org.wam.leeds.ac.uk/10.1016/j.jsurg.2015.10.002.

118. Yang T, Lin S, Tan T, Yang J, Pan J, Hu C, et al. Impact of 3D Printing Technology on Comprehension of Surgical Anatomy of Retroperitoneal Tumor. *World Journal of Surgery*. 2018;42(8): 2339–2343. https://doi.org/10.1007/s00268-018-4489-x.

119. Cromeens BP, Ray WC, Hoehne B, Abayneh F, Adler B, Besner GE. Facilitating surgeon understanding of complex anatomy using a three-dimensional printed model. *The Journal of surgical research*. 2017;216: 18–25. https://0-dx-doi-org.wam.leeds.ac.uk/10.1016/j.jss.2017.04.003.

120. de Montbrun S, MacRae H. Simulation in Surgical Education. *Clinics in Colon and Rectal Surgery*. 2012;25(03): 156–165. https://doi.org/10.1055/s-0032-1322553.

121. Preim B, Botha CP. *Visual Computing for Medicine*.. 2nd ed. New York: Morgan Kaufmann; 2014.

122. Fan B, Chen H, Sun YJ, Wang BF, Che L, Liu SY, et al. Clinical effects of 3-D printing-assisted personalized reconstructive surgery for blowout orbital fractures. *Graefe's Archive for Clinical and Experimental Ophthalmology*. 2017;255(10): 2051–2057. https://doi.org/10.1007/s00417-017-3766-y.

123. Ciocca L, Mazzoni S, Fantini M, Persiani F, Marchetti C, Scotti R, et al. CAD / CAM guided secondary mandibular reconstruction of a discontinuity defect after ablative cancer surgery. *Journal of Cranio-Maxillofacial Surgery*. 2012;40(8): e511–e515. https://doi.org/10.1016/j.jcms.2012.03.015.

124. Zheng W, Su J, Cai L, Lou Y, Wang J, Guo X, et al. Application of 3D-printing technology in the treatment of humeral intercondylar fractures. *Orthopaedics and Traumatology: Surgery and Research*. 2018;104(1): 83–88. https://doi.org/10.1016/j.otsr.2017.11.012.

125. Crafts TD, Ellsperman SE, Wannemuehler TJ, Bellicchi TD, Shipchandler TZ, Mantravadi A V. Three-Dimensional Printing and Its Applications in Otorhinolaryngology–Head and Neck Surgery. *Otolaryngology - Head and Neck Surgery*. 2017;156(6): 999–1010. https://doi.org/10.1177/0194599816678372.

126. Coelho G, Chaves TMF, Goes AF, Del Massa EC, Moraes O, Yoshida M. Multimaterial 3D printing preoperative planning for frontoethmoidal meningoencephalocele surgery. *Child's Nervous System*. 2018;34(4): 749–756. https://doi.org/10.1007/s00381-017-3616-6.

127. Glybochko PV, Rapoport LM, Alyaev YG, Sirota ES, Bezrukov EA, Fiev DN, et al. Multiple application of three-dimensional soft kidney models with localized kidney cancer: A pilot study. *Urologia*. 2018;85(3): 99–105. https://0-dx-doi-org.wam.leeds.ac.uk/10.1177/0391560317749405.

128. von Rundstedt FC, Scovell JM, Agrawal S, Zaneveld J, Link RE. Utility of patient-specific silicone renal models for planning and rehearsal of complex tumour resections prior to robot-assisted laparoscopic partial nephrectomy. *BJU International*. 2017;119(4): 598–604. https://doi.org/10.1111/bju.13712.

129. Zhang J, Chang J, Yang X, Zhang JJ. Virtual reality surgery simulation: A survey on patient specific solution. *Lecture Notes in Computer Science*. 2017; 220–233. https://doi.org/10.1007/978-3-319-69487-0_16.

130. Rai A, Scovell JM, Xu A, Balasubramanian A, Siller R, Kohn T, et al. Patient-specific Virtual Simulation—A State of the Art Approach to Teach Renal Tumor Localization. *Urology*. 2018;120: 42–48. https://doi.org/10.1016/j.urology.2018.04.043.

131. Won T Bin, Hwang P, Lim JH, Cho SW, Paek SH, Losorelli S, et al. Early experience with a patient-specific virtual surgical simulation for rehearsal of endoscopic skull-base surgery. *International Forum of Allergy and Rhinology*. 2018;8(1): 54–63. https://doi.org/10.1002/alr.22037.

132. Westermark A, Zachow S, Eppley BL. Three-dimensional osteotomy planning in maxillofacial surgery including soft tissue prediction. *Journal of Craniofacial Surgery*. 2005;16(1): 100–104. https://doi.org/10.1097/00001665-200501000-00019.

133. Digioia AM, Jaramaz B, Nikou C, Labarca RS, Moody JE, Colgan BD. Surgical navigation for total hip replacement with the use of HipNav. *Operative Techniques in Orthopaedics*. 2000;10(1): 3–8. https://doi.org/10.1016/S1048-6666(00)80036-1.

134. Dick C, Georgii J, Burgkart R, Westermann R. Stress tensor field visualization for implant planning in orthopedics. *IEEE Transactions on Visualization and Computer Graphics*. 2009;15(6): 1399–1406. https://doi.org/10.1109/TVCG.2009.184.

135. Shaikh I, Holloway I, Aston W, Littler S, Burling D, Antoniou A, et al. High subcortical sacrectomy: A novel approach to facilitate complete resection of locally advanced and recurrent rectal cancer with high (S1-S2) sacral extension. *Colorectal Disease*. 2016;18(4): 386–392. https://doi.org/10.1111/codi.13226.

136. Xiang N, Fang C, Fan Y, Yang J, Zeng N, Liu J, et al. Application of liver three-dimensional printing in hepatectomy for complex massive hepatocarcinoma with rare variations of portal vein: preliminary experience. *International journal of clinical and experimental medicine*. 2015;8(10): 18873–18878.

137. Tian F, Wu JX, Rong WQ, Wang LM, Wu F, Yu WB, et al. Three-dimensional morphometric analysis for hepatectomy of centrally located hepatocellular carcinoma: a pilot study. *World journal of gastroenterology*. 2015;21(15): 4607–4619. https://0-dx-doi-org.wam.leeds.ac.uk/10.3748/wjg.v21.i15.4607.

138. Wang XD, Wang HG, Shi J, Duan WD, Luo Y, Ji WB, et al. Traditional surgical planning of liver surgery is modified by 3D interactive quantitative surgical planning approach: a single-center experience with 305 patients. *Hepatobiliary & pancreatic diseases international : HBPD INT*. 2017;16(3): 271–278.

139. Andert A, Bruners P, Heidenhain C, Ulmer F, Klink CD, Alizai PH, et al. Impact of Preoperative Three-Dimensional Computed Tomography Cholangiography on Postoperative Resection Margin Status in Patients Operated due to Hilar Cholangiocarcinoma. *Gastroenterology research and practice*. 2017;2017: 1947023. https://0-dx-doi-org.wam.leeds.ac.uk/10.1155/2017/1947023.

140. Russo P, Goetzl M, Simmons R, Katz J, Motzer R, Reuter V. Partial nephrectomy: The rationale for expanding the indications. *Ann Surg Oncol*. 2002;9(7): 8.

141. Shirk JD, Thiel DD, Wallen EM, Linehan JM, White WM, Badani KK, et al. Effect of 3-Dimensional Virtual Reality Models for Surgical Planning of Robotic-Assisted Partial Nephrectomy on Surgical Outcomes: A Randomized Clinical Trial. *JAMA Network Open*. 2019;2(9): e1911598–e1911598. https://doi.org/10.1001/jamanetworkopen.2019.11598.

142. Porpiglia F, Fiori C, Checcucci E, Amparore D, Bertolo R. Hyperaccuracy Three-dimensional Reconstruction Is Able to Maximize the Efficacy of Selective Clamping During Robot-assisted Partial Nephrectomy for Complex Renal Masses. *European Urology*. 2018;74(5): 651–660. https://doi.org/10.1016/j.eururo.2017.12.027.

143. Wang Z, Qi L, Yuan P, Zu X, Chen W, Cao Z, et al. Application of Three-Dimensional Visualization Technology in Laparoscopic Partial Nephrectomy of Renal Tumor: A Comparative Study. *Journal of Laparoendoscopic & Advanced Surgical Techniques*. 2017;27(5): 516–523. https://doi.org/10.1089/lap.2016.0645.

144. Iwano S, Usami N, Yokoi K, Naganawa S. Segmentectomy simulation using a virtual three-dimensional safety margin. *The Annals of thoracic surgery*. 2012;93(2 PG-e37-9): e37-9. https://0-dx-doi-org.wam.leeds.ac.uk/10.1016/j.athoracsur.2011.09.050.

145. Herlin C, Charles J, Bigorre M, Cheikh H, Captier G. Computer-assisted midface reconstruction in Treacher Collins syndrome part 1 : Skeletal reconstruction. 2013;41: 670–675.

146. Van Hemelen G, Van Genechten M, Renier L, Desmedt M, Verbruggen E, Nadjmi N. Three-dimensional virtual planning in orthognathic surgery enhances the accuracy of soft tissue prediction. *Journal of cranio-maxillo-facial surgery : official publication of the European Association for Cranio-Maxillo-Facial Surgery*. 2015;43(6): 918–925. https://0-dx-doi-org.wam.leeds.ac.uk/10.1016/j.jcms.2015.04.006.

147. Day KM, Gabrick KS, Sargent LA. Applications of Computer Technology in Complex Craniofacial Reconstruction. *Plastic and reconstructive surgery. Global open*. 2018;6(3): e1655. https://0-dx-doi-org.wam.leeds.ac.uk/10.1097/GOX.0000000000001655.

148. Chin SJ, Wilde F, Neuhaus M, Schramm A, Gellrich NC, Rana M. Accuracy of virtual surgical planning of orthognathic surgery with aid of CAD/CAM fabricated surgical splint—A novel 3D analyzing algorithm. *Journal of Cranio-Maxillofacial Surgery*. 2017;45(12): 1962–1970. https://doi.org/10.1016/j.jcms.2017.07.016.

149. Hanasono MM, Jacob RF, Bidaut L, Robb GL, Skoracki RJ. Midfacial reconstruction using virtual planning, rapid prototype modeling, and stereotactic navigation. *Plastic and reconstructive surgery*. 2010;126(6): 2002–2006. https://0-dx-doi-org.wam.leeds.ac.uk/10.1097/PRS.0b013e3181f447e1.

150. Strumas N, Antonyshyn O, Caldwell CB, Mainprize J. Multimodality Imaging for Precise Localization of Craniofacial Osteomyelitis. *Journal of Craniofacial Surgery*. 2003;14(2): 215–219. https://doi.org/10.1097/00001665-200303000-00015.

151. Lin HH, Lonic D, Lo LJ. 3D printing in orthognathic surgery − A literature review. *Journal of the Formosan Medical Association*. 2018;117(7): 547–558. https://doi.org/10.1016/j.jfma.2018.01.008.

152. Ayoub N, Ghassemi A, Rana M, Gerressen M, Riediger D, Hölzle F, et al. Evaluation of computer-assisted mandibular reconstruction with vascularized iliac crest bone graft compared to conventional surgery: A randomized prospective clinical trial. *Trials*. 2014;15(1). https://doi.org/10.1186/1745-6215-15-114.

153. Volonté F, Pugin F, Bucher P, Sugimoto M, Ratib O, Morel P. Augmented reality and image overlay navigation with OsiriX in laparoscopic and robotic surgery: Not only a matter of fashion. *Journal of Hepato-Biliary-Pancreatic Sciences*. 2011;18(4): 506–509. https://doi.org/10.1007/s00534-011-0385-6.

154. Linte CA, White J, Eagleson R, Guiraudon GM, Peters TM. Virtual and augmented medical imaging environments: enabling technology for minimally invasive cardiac interventional guidance. *IEEE reviews in biomedical engineering*. 2010;3: 25–47. https://doi.org/10.1109/RBME.2010.2082522.

155. Ma L, Huang T, Wang J, Liao H. Visualization, registration and tracking techniques for augmented reality guided surgery: a review. *Physics in Medicine and Biology*. 2023;68(4). https://doi.org/10.1088/1361-6560/acaf23.

156. Eckert M, Volmerg JS, Friedrich CM. Augmented Reality in Medicine: Systematic and Bibliographic Review. *JMIR mHealth and uHealth*. 2019;7(4): e10967. https://doi.org/10.2196/10967.

157. Wijsmuller AR, Romagnolo LGC, Consten E, Melani AEFM, Marescaux J. Navigation and Image-Guided Surgery. In: *Digital Surgery*. 1st ed. Springer; 2021. p. 137–143.

158. Gsaxner C, Li J, Pepe A, Jin Y, Kleesiek J, Schmalstieg D, et al. The HoloLens in medicine: A systematic review and taxonomy. *Medical Image Analysis*. 2023;85: 102757. https://doi.org/10.1016/j.media.2023.102757.

159. D'Amato R, Cutolo F, Badiali G, Carbone M, Lu H, Hogenbirk H, et al. Key Ergonomics Requirements and Possible Mechanical Solutions for Augmented Reality

Head-Mounted Displays in Surgery. *Multimodal Technologies and Interaction*. 2022;6(2): 15. https://doi.org/10.3390/mti6020015.

160. Yoon JW, Chen RE, Kim EJ, Akinduro OO, Kerezoudis P, Han PK, et al. Augmented reality for the surgeon: Systematic review. *The International Journal of Medical Robotics and Computer Assisted Surgery*. 2018;14(4): e1914. https://doi.org/10.1002/rcs.1914.

161. Bertolo R, Hung A, Porpiglia F, Bove P, Schleicher M, Dasgupta P. Systematic review of augmented reality in urological interventions: the evidences of an impact on surgical outcomes are yet to come. *World Journal of Urology*. 2020;38(9): 2167–2176. https://doi.org/10.1007/s00345-019-02711-z.

162. Qian L, Wu JY, Maio S, Navab N, Kazanzides P. A Review of Augmented Reality in Robotic-Assisted Surgery. *IEEE Transactions on Medical Robotics and Bionics*. 2019;PP: 1–1. https://doi.org/10.1109/TMRB.2019.2957061.

163. Onda S, Okamoto T, Kanehira M, Fujioka S, Suzuki N, Hattori A, et al. Short Rigid Scope and Stereo-scope Designed Specifically for Open Abdominal Navigation Surgery: Clinical Application for Hepatobiliary and Pancreatic Surgery. *Journal of Hepato-Biliary-Pancreatic Sciences*. 2012;20(4): 448–453. https://doi.org/10.1007/s00534-012-0582-y.

164. Khor WS, Baker B, Amin K, Chan A, Patel K, Wong J. Augmented and virtual reality in surgery—the digital surgical environment: applications, limitations and legal pitfalls. *Annals of Translational Medicine*. 2016;4(23): 454–454. https://doi.org/10.21037/atm.2016.12.23.

165. Malhotra S, Halabi O, Dakua SP, Padhan J, Paul S, Palliyali W. Augmented Reality in Surgical Navigation: A Review of Evaluation and Validation Metrics. *Applied Sciences*. 2023;13(3): 1629. https://doi.org/10.3390/app13031629.

166. Marteau T, Dormandy E, Michie E. A measure of informed choice. *Health Expectations*. 2001;4(2): 99–108.

167. Mark JS, Spiro H. Informed Consent for Colonoscopy. *Archives of Internal Medicine*. 1990;150(4): 777. https://doi.org/10.1001/archinte.1990.00390160049011.

168. Teishima J, Takayama Y, Iwaguro S, Hayashi T, Inoue S, Hieda K, et al. Usefulness of personalized three-dimensional printed model on the satisfaction of preoperative education for patients undergoing robot-assisted partial nephrectomy and their families. *International urology and nephrology*. 2018; https://0-dx-doi-org.wam.leeds.ac.uk/10.1007/s11255-018-1881-2.

169. Bernhard J, Isotani I, Matsugasumi T, Duddalwar V, Hung A, Suer E, et al. Personalized 3D printed model of kidney and tumor anatomy: a useful tool for patient education. *World journal of urology*. 2016;34(3): 337–345. http://0-dx.doi.org.wam.leeds.ac.uk/10.1007/s00345-015-1632-2.

170. Hohenberger W, Weber K, Matzel K, Papadopoulos T, Merkel S. Standardized surgery for colonic cancer: Complete mesocolic excision and central ligation - Technical notes and outcome. *Colorectal Disease*. 2009;11(4): 354–364. https://doi.org/10.1111/j.1463-1318.2008.01735.x.

171. Strey CW, Wullstein C, Adamina M, Agha A, Aselmann H, Becker T, et al. Laparoscopic right hemicolectomy with CME: standardization using the “critical view” concept. *Surgical Endoscopy*. 2018;32(12): 5021–5030. https://doi.org/10.1007/s00464-018-6267-0.

172. Bertelsen CA. Complete mesocolic excision. *Techniques in Coloproctology*. 2014;18(9): 773–774.

173. Crane J, Hamed M, Borucki JP, El-Hadi A, Shaikh I, Stearns AT. Complete mesocolic excision versus conventional surgery for colon cancer: A systematic review and meta-analysis. *Colorectal Disease*. n/a(n/a). https://doi.org/10.1111/codi.15644.

174. Mari FS, Nigri G, Pancaldi A, De Cecco CN, Gasparrini M, Dall’Oglio A, et al. Role of CT angiography with three-dimensional reconstruction of mesenteric vessels in laparoscopic colorectal resections: a randomized controlled trial. *Surgical Endoscopy*. 2013;27(6): 2058–2067. https://doi.org/10.1007/s00464-012-2710-9.

175. Miyamoto R, Tadano S, Sano N, Inagawa S, Adachi S, Yamamoto M. The impact of three-dimensional reconstruction on laparoscopic-assisted surgery for right-sided colon cancer. *Videosurgery Miniinv*. 2017;12(3): 251–256. https://doi.org/10.5114/wiitm.2017.67996.

176. Luzon JA, Andersen BT, Stimec BV, Fasel JHD, Bakka AO, Kazaryan AM, et al. Implementation of 3D printed superior mesenteric vascular models for surgical planning and/or navigation in right colectomy with extended D3 mesenterectomy: comparison of virtual and physical models to the anatomy found at surgery. *Surgical endoscopy*. 2018;32(2): 567–575. https://0-dx-doi-org.wam.leeds.ac.uk/10.1007/s00464-018-6332-8.

177. Kearns EC, Moynihan A, Dalli J, Khan MF, Singh S, McDonald K, et al. Clinical validation of 3D virtual modelling for laparoscopic complete mesocolic excision with central vascular ligation for proximal colon cancer. *European Journal of Surgical Oncology*. 2024;50(11). https://doi.org/10.1016/j.ejso.2024.108597.

178. Hojo D, Murono K, Nozawa H, Kawai K, Hata K, Tanaka T, et al. Utility of a three-dimensional printed pelvic model for lateral pelvic lymph node dissection. *International Journal of Colorectal Disease*. 2020;35(5): 905–910. https://doi.org/10.1007/s00384-020-03534-w.

179. Wijsmuller AR, Giraudeau C, Leroy J, Kleinrensink GJ, Rociu E, Romagnolo LG, et al. A step towards stereotactic navigation during pelvic surgery: 3D nerve topography. *Surgical Endoscopy and Other Interventional Techniques*. 2018;32(8): 3582–3591. https://doi.org/10.1007/s00464-018-6086-3.

180. Bertrand MM, Macri F, Mazars R, Droupy S, Beregi JP, Prudhomme M. MRI-based 3D pelvic autonomous innervation: a first step towards image-guided pelvic surgery. *European Radiology*. 2014;24(8): 1989–1997. https://doi.org/10.1007/s00330-014-3211-0.

181. Sahnan K, Pellino G, Adegbola SO, Tozer PJ, Chandrasinghe P, Miskovic D, et al. Development of a model of three-dimensional imaging for the preoperative planning of TaTME. *Techniques in Coloproctology*. 2018;22(1): 59–63. https://doi.org/10.1007/s10151-017-1724-7.

182. Kok END, van Veen R, Groen HC, Heerink WJ, Hoetjes NJ, van Werkhoven E, et al. Association of Image-Guided Navigation With Complete Resection Rate in Patients With Locally Advanced Primary and Recurrent Rectal Cancer: A Nonrandomized Controlled Trial. *JAMA Network Open*. 2020;3(7): e208522–e208522. https://doi.org/10.1001/jamanetworkopen.2020.8522.

183. Nijkamp J, Kuhlmann KFD, Ivashchenko O, Pouw B, Hoetjes N, Lindenberg MA, et al. Prospective study on image-guided navigation surgery for pelvic malignancies. *Journal of Surgical Oncology*. 2019;119(4): 510–517. https://doi.org/10.1002/jso.25351.

184. Sahnan K, Adegbola SO, Tozer PJ, Gupta A, Baldwin-Cleland R, Yassin N, et al. Improving the Understanding of Perianal Crohn Fistula Through 3D Modeling. *Annals of Surgery*. 2018;267(6): e105–e107. https://doi.org/10.1097/SLA.0000000000002629.

185. Jeri-McFarlane S, García-Granero Á, Ochogavía-Seguí A, Pellino G, Oseira-Reigosa A, Gil-Catalan A, et al. Three-dimensional modelling as a novel interactive tool for preoperative planning for complex perianal fistulas in Crohn's disease. *Colorectal Disease: The Official Journal of the Association of Coloproctology of Great Britain and Ireland*. 2023;25(6): 1279–1284. https://doi.org/10.1111/codi.16539.

186. Verkade C, Brouwers L, Stijns J, van Dal V, Wasowicz DK, de Kiefte M, et al. Validation of a 3D-printed model of cryptoglandular perianal fistulas. *Techniques in Coloproctology*. 2024;28(1): 59. https://doi.org/10.1007/s10151-024-02925-3.

187. Yokose S, Murono K, Nozawa H, Sasaki K, Emoto S, Matsuzaki H, et al. Preoperative Simulation of Ileal Pouch-Anal Anastomosis in Patients With Ulcerative Colitis Using a 3-Dimensional Printed Model. *Inflammatory Bowel Diseases*. 2023;29(12): 1865–1870. https://doi.org/10.1093/ibd/izac283.

188. Hahnloser D, Pembérton JH. Long-term Outcome After Ileal Pouch-anal Anastomosis for Ulcerative Colitis. *Australian and New Zealand Journal of Surgery*. 2016;86(10): 741–742. https://doi.org/10.1111/ans.13717.

189. Fukui R, Nozawa H, Sakamoto A, Sasaki K, Murono K, Emoto S, et al. Temporal Changes in Functional Outcomes of Stapled and Hand-sewn Ileal Pouch-anal Anastomosis for Ulcerative Colitis and Familial Adenomatous Polyposis. *Colorectal Disease*. 2022;25(3): 396–403. https://doi.org/10.1111/codi.16397.

190. Miller-Ocuin JL, Dietz DW. The Evolution of Pelvic Pouch Surgery: Optimal Pouch Design for an Ileal Pouch Anal Anastomosis. *Clinics in Colon and Rectal Surgery*. 2022;35(06): 453–457. https://doi.org/10.1055/s-0042-1758135.

191. Hassinger JP, Dozois EJ, Holubar SD, Camp JC, Farley DR, Fidler JL, et al. Virtual Pelvic Anatomy Simulator: A Pilot Study of Usability and Perceived Effectiveness. *Journal of Surgical Research*. 2010;161(1): 23–27. https://doi.org/10.1016/j.jss.2009.06.016.

192. Pellino G, García-Granero A, Fletcher-Sanfeliu D, Navasquillo-Tamarit M, Frasson M, García-Calderon D, et al. Preoperative surgical planning based on cadaver simulation and 3D imaging for a retrorectal tumour: description and video demonstration. *Techniques in Coloproctology*. 2018;22(9): 709–713. https://doi.org/10.1007/s10151-018-1854-6.

193. *Montgomery and informed consent - The MDU*. https://www.themdu.com/guidance-and-advice/guides/montgomery-and-informed-consent [Accessed 27th December 2024].

194. Besson A, Deftereos I, Chan S, Faragher IG, Kinsella R, Yeung JM. Understanding patient-reported outcome measures in colorectal cancer. *Future Oncology*. 2019;15(10): 1135–1146. https://doi.org/10.2217/fon-2018-0723.

195. Harris CR, Millman KJ, van der Walt SJ, Gommers R, Virtanen P, Cournapeau D, et al. Array programming with NumPy. *Nature*. 2020;585(7825): 357–362. https://doi.org/10.1038/s41586-020-2649-2.

196. Virtanen P, Gommers R, Oliphant TE, Haberland M, Reddy T, Cournapeau D, et al. SciPy 1.0: fundamental algorithms for scientific computing in Python. *Nature Methods*. 2020;17(3): 261–272. https://doi.org/10.1038/s41592-019-0686-2.

197. Brett M, Markiewicz CJ, Hanke M, Côté MA, Cipollini B, McCarthy P, et al. *nipy/nibabel: 5.2.1*. Zenodo; 2024. https://doi.org/10.5281/zenodo.10714563. [Accessed 8th October 2024].

198. McDermott W. *The PBR guide*. Allegorithmic; 2018. https://academy.substance3d.com/courses/the-pbr-guide-part-2

199. *trimesh.smoothing module - trimesh 4.5.3 documentation*. https://trimesh.org/trimesh.smoothing.html [Accessed 27th December 2024].

200. *Using K-D Trees to Calculate Nearest Neighbors in 3D Vector Space*. Krumware. https://blog.krum.io/k-d-trees/ [Accessed 27th December 2024].

201. Dawson-Haggerty M. *mikedh/trimesh*. 2024. https://github.com/mikedh/trimesh [Accessed 8th October 2024].

202. *KDTree — SciPy v1.14.1 Manual*. https://docs.scipy.org/doc/scipy/reference/generated/scipy.spatial.KDTree.html [Accessed 27th December 2024].

203. Iqbal K. *GLB*. https://docs.fileformat.com/3d/glb/ [Accessed 27th December 2024].

204. *Welcome to Flask — Flask Documentation (3.1.x)*. https://flask.palletsprojects.com/en/stable/ [Accessed 27th December 2024].

205. *Tailwind CSS - Rapidly build modern websites without ever leaving your HTML.* https://tailwindcss.com/ [Accessed 27th December 2024].

206. *Sculptris Pro*. https://help.maxon.net/zbr/en-us/Content/html/user-guide/3d-modeling/modeling-basics/creating-meshes/sculptris-pro/sculptris-pro.html [Accessed 27th December 2024].

207. *Viewer API - Introduction*. Sketchfab. https://sketchfab.com/developers/viewer [Accessed 30th December 2024].

208. Martelli N, Serrano C, Van Den Brink H, Pineau J, Prognon P, Borget I, et al. Advantages and disadvantages of 3-dimensional printing in surgery: A systematic review. *Surgery (United States)*. 2016;159(6): 1485–1500. https://doi.org/10.1016/j.surg.2015.12.017.

209. Wan X, Wang W, Liu J, Tong T. Estimating the sample mean and standard deviation from the sample size, median, range and/or interquartile range. *BMC Medical Research Methodology*. 2014;14(1): 135. https://doi.org/10.1186/1471-2288-14-135.

210. Sterne JAC, Savović J, Page MJ, Elbers RG, Blencowe NS, Boutron I, et al. RoB 2: a revised tool for assessing risk of bias in randomised trials. *BMJ*. 2019;366: l4898. https://doi.org/10.1136/bmj.l4898.

211. Sterne JA, Hernán MA, Reeves BC, Savović J, Berkman ND, Viswanathan M, et al. ROBINS-I: a tool for assessing risk of bias in non-randomised studies of interventions. *BMJ*. 2016;355: i4919. https://doi.org/10.1136/bmj.i4919.

212. McKinney W. Data Structures for Statistical Computing in Python. 2010; 6.

213. Hunter JD. Matplotlib: A 2D Graphics Environment. *Computing in Science Engineering*. 2007;9(3): 90–95. https://doi.org/10.1109/MCSE.2007.55.

214. Hongyong 邓宏勇Deng. *PythonMeta: A Python module of Meta-Analysis, usually applied in systemtic reviews of Evidence-based Medicine.* http://www.pymeta.com [Accessed 26th April 2021].

215. Chen C, Cai L, Zheng W, Wang J, Guo X, Chen H. The efficacy of using 3D printing models in the treatment of fractures: a randomised clinical trial. *BMC musculoskeletal disorders*. 2019;20(1): 65. https://doi.org/10.1186/s12891-019-2448-9.

216. Witowski J. Decision-making based on 3D printed models in laparoscopic liver resections with intraoperative ultrasound: a prospective observational study. *Eur Radiol*. 2020; 7.

217. Saverio F, Giuseppe M, Alessandra N, Nicola C, Marcello DC, Anna G, et al. Role of CT angiography with three-dimensional reconstruction of mesenteric vessels in laparoscopic colorectal resections : a randomized controlled trial. 2013; 2058–2067. https://doi.org/10.1007/s00464-012-2710-9.

218. Andert A, Bruners P, Heidenhain C, Ulmer F, Klink CD, Alizai PH, et al. Impact of Preoperative Three-Dimensional Computed Tomography Cholangiography on Postoperative Resection Margin Status in Patients Operated due to Hilar Cholangiocarcinoma. 2017;2017. https://doi.org/10.1155/2017/1947023.

219. Diana M, Soler L, Agnus V, D'Urso A, Vix M, Dallemagne B, et al. Prospective Evaluation of Precision Multimodal Gallbladder Surgery Navigation: Virtual Reality, Near-infrared Fluorescence, and X-ray-based Intraoperative Cholangiography. *Annals of Surgery*. 2017;266(5): 890–897. https://doi.org/10.1097/SLA.0000000000002400.

220. Fang C hua, Zhu W, Wang H, Xiang N, Fan Y, Yang J, et al. A new approach for evaluating the resectability of pancreatic and periampullary neoplasms. *Pancreatology : official journal of the International Association of Pancreatology (IAP) ... [et al.]*. 2012;12(4): 364–371. https://doi.org/10.1016/j.pan.2012.05.006.

221. He Y biao, Bai L, Aji T, Jiang Y, Zhao J ming, Zhang J hui, et al. Application of 3D reconstruction for surgical treatment of hepatic alveolar echinococcosis. 2015;21(35): 10200–10207. https://doi.org/10.3748/wjg.v21.i35.10200.

222. Klauss M, Schobinger M, Wolf I, Werner J, Meinzer HP, Kauczor HU, et al. Value of three-dimensional reconstructions in pancreatic carcinoma using multidetector CT: initial results. *World journal of gastroenterology*. 2009;15(46): 5827–5832.

223. Miyamoto R, Oshiro Y, Sano N, Inagawa S, Ohkohchi N. Three-dimensional surgical simulation of the bile duct and vascular arrangement in pancreatoduodenectomy: A retrospective cohort study. *Annals of Medicine and Surgery*. 2018;36: 17–22. https://doi.org/10.1016/j.amsu.2018.09.043.

224. Nakayama K, Oshiro Y, Miyamoto R, Kohno K, Fukunaga K, Ohkohchi N. The Effect of Three-Dimensional Preoperative Simulation on Liver Surgery. *World Journal of Surgery*. 2017;41(7): 1840–1847. https://doi.org/10.1007/s00268-017-3933-7.

225. Okuda Y, Taura K, Seo S, Yasuchika K, Nitta T, Ogawa K, et al. Usefulness of operative planning based on 3-dimensional CT cholangiography for biliary malignancies. *Surgery (United States)*. 2015;158(5): 1261–1271. https://doi.org/10.1016/j.surg.2015.04.021.

226. Radtke A, Sotiropoulos GC, Molmenti EP, Schroeder T, Peitgen HO, Frilling A, et al. Computer-Assisted Surgery Planning for Complex Liver Resections: When Is It Helpful? A Single-Center Experience Over an 8-Year Period. *Annals of Surgery*. 2010;252(5): 876–883. https://doi.org/10.1097/SLA.0b013e3181fdd012.

227. Wei XB, Xu J, Li N, Yu Y, Shi J, Guo WX, et al. The role of three-dimensional imaging in optimizing diagnosis, classification and surgical treatment of hepatocellular carcinoma with portal vein tumor thrombus. *HPB : the official journal of the International Hepato Pancreato Biliary Association*. 2016;18(3 PG-287–95): 287–295. https://0-dx-doi-org.wam.leeds.ac.uk/10.1016/j.hpb.2015.10.007.

228. Yeo CT, MacDonald A, Ungi T, Lasso A, Jalink D, Zevin B, et al. Utility of 3D Reconstruction of 2D Liver Computed Tomography/Magnetic Resonance Images as a Surgical Planning Tool for Residents in Liver Resection Surgery. *Journal of Surgical Education*. 2018;75(3): 792–797. https://doi.org/10.1016/j.jsurg.2017.07.031.

229. Yang T, Lin S, Xie Q, Ouyang W, Tan T, Li J, et al. Impact of 3D printing technology on the comprehension of surgical liver anatomy. *Surgical Endoscopy*. 2019;33(2): 411–417. https://doi.org/10.1007/s00464-018-6308-8.

230. Bozkurt B, Emek E, Arikan T, Ceyhan O, Yazici P, Sahin T, et al. Liver Graft Volume Estimation by Manual Volumetry and Software-Aided Interactive Volumetry: Which is Better?. *Transplantation proceedings*. 2019;51(7): 2387–2390. https://doi.org/10.1016/j.transproceed.2019.01.152.

231. Fang CH, Tao HS, Yang J, Fang ZS, Cai W, Liu J, et al. Impact of three-dimensional reconstruction technique in the operation planning of centrally located hepatocellular carcinoma. *Journal of the American College of Surgeons*. 2015;220(1): 28–37. https://doi.org/10.1016/j.jamcollsurg.2014.09.023.

232. Wang XD, Wang HG, Shi J, Duan WD, Luo Y, Ji WB, et al. Traditional surgical planning of liver surgery is modified by 3D interactive quantitative surgical planning approach: a single-center experience with 305 patients. *Hepatobiliary & Pancreatic Diseases International*. 2017;16(3): 271–278. https://doi.org/10.1016/S1499-3872(17)60021-3.

233. Zeng N, Tao H, Fang C, Fan Y, Xiang N, Yang J, et al. Individualized preoperative planning using three-dimensional modeling for Bismuth and Corlette type III hilar cholangiocarcinoma. *World journal of surgical oncology*. 2016;14(1): 44. https://doi.org/10.1186/s12957-016-0794-8.

234. Zhang G, Zhou XJ, Zhu CZ, Dong Q, Su L. Usefulness of three-dimensional(3D) simulation software in hepatectomy for pediatric hepatoblastoma. *Surgical oncology*. 2016;25(3): 236–243. https://doi.org/10.1016/j.suronc.2016.05.023.

235. Fang CH, Kong D, Wang X, Wang H, Xiang N, Fan Y, et al. Three-dimensional reconstruction of the peripancreatic vascular system based on computed tomographic angiography images and its clinical application in the surgical management of pancreatic tumors. *Pancreas*. 2014;43(3): 389–395. https://doi.org/10.1097/MPA.0000000000000035.

236. Ayoub N, Ghassemi A, Rana M, Gerressen M, Riediger D, Hölzle F, et al. Evaluation of computer-assisted mandibular reconstruction with vascularized iliac crest bone graft compared to conventional surgery: A randomized prospective clinical trial. *Trials*. 2014;15(1). https://doi.org/10.1186/1745-6215-15-114.

237. Bengtsson M, Wall G, Greiff L, Rasmusson L. Treatment outcome in orthognathic surgery-A prospective randomized blinded case-controlled comparison of planning accuracy in computer-assisted two- and three-dimensional planning techniques (part II). *Journal of cranio-maxillo-facial surgery : official publication of the European Association for Cranio-Maxillo-Facial Surgery*. 2017;45(9): 1419–1424. https://doi.org/10.1016/j.jcms.2017.07.001.

238. Bengtsson M, Wall G, Larsson P, Becktor JP, Rasmusson L. Treatment outcomes and patient-reported quality of life after orthognathic surgery with computer-assisted 2- or 3-dimensional planning: A randomized double-blind active-controlled clinical trial. *American journal of orthodontics and dentofacial orthopedics : official publication of the American Association of Orthodontists, its constituent societies, and the American Board of Orthodontics*. 2018;153(6 PG-786–796): 786–796. https://0-dx-doi-org.wam.leeds.ac.uk/10.1016/j.ajodo.2017.12.008.

239. Li K, Li J, Du W, Xu C, Ye B, Luo E. Computer-Aided Design and Manufacturing Cutting and Drilling Guides with Prebent Titanium Plates Improve Surgical Accuracy of Skeletal Class III Malocclusion. *Plastic & Reconstructive Surgery*. 2020;145(5): 963e–974e. https://doi.org/10.1097/PRS.0000000000006794.

240. Modabber A, Legros C, Rana M, Gerressen M, Riediger D, Ghassemi A. Evaluation of computer-assisted jaw reconstruction with free vascularized fibular flap compared to conventional surgery: a clinical pilot study. *The international journal of medical robotics + computer assisted surgery : MRCAS*. 2012;8(2): 215–220. https://doi.org/10.1002/rcs.456.

241. Schneider D, Kammerer PW, Hennig M, Schon G, Thiem DGE, Bschorer R. Customized virtual surgical planning in bimaxillary orthognathic surgery: a prospective randomized trial. *Clinical oral investigations*. 2018; https://0-dx-doi-org.wam.leeds.ac.uk/10.1007/s00784-018-2732-3.

242. King BJ, Park EP, Christensen BJ, Danrad R. On-Site 3-Dimensional Printing and Preoperative Adaptation Decrease Operative Time for Mandibular Fracture Repair. *Journal of Oral and Maxillofacial Surgery*. 2018;76(9): 1950.e1-1950.e8. https://doi.org/10.1016/j.joms.2018.05.009.

243. Kraeima J, Dorgelo B, Gulbitti HA, Steenbakkers RJHM, Schepman KP, Roodenburg JLN, et al. Multi-modality 3D mandibular resection planning in head and neck cancer using CT and MRI data fusion: A clinical series. *Oral oncology*. 2018;81(cu5, 9709118): 22–28. https://doi.org/10.1016/j.oraloncology.2018.03.013.

244. Liu S, Zhang WB, Yu Y, Wang T, Peng X. Three-Dimensional Accuracy of Bone Contouring Surgery for Zygomaticomaxillary Fibrous Dysplasia Using Virtual Planning and Surgical Navigation. *Journal of oral and maxillofacial surgery : official journal of the American Association of Oral and Maxillofacial Surgeons*. 2020;78(12): 2328–2338. https://doi.org/10.1016/j.joms.2020.07.208.

245. Pandey AK, Bapuraj JR, Gupta AK, Khandelwal N. Is there a role for virtual otoscopy in the preoperative assessment of the ossicular chain in chronic suppurative otitis media? Comparison of HRCT and virtual otoscopy with surgical findings. *European radiology*. 2009;19(6): 1408–1416. https://doi.org/10.1007/s00330-008-1282-5.

246. Van Hemelen G, Van Genechten M, Renier L, Desmedt M, Verbruggen E, Nadjmi N. Three-dimensional virtual planning in orthognathic surgery enhances the accuracy of soft tissue prediction. *Journal of Cranio-Maxillofacial Surgery*. 2015;43(6): 918–925. https://doi.org/10.1016/j.jcms.2015.04.006.

247. Van Nunen DPF, Janssen LE, Stubenitsky BM, Han KS, Muradin MSM. Stereolithographic skull models in the surgical planning of fronto-supraorbital bar advancement for non-syndromic trigonocephaly. *Journal of Cranio-Maxillofacial Surgery*. 2014;42(6): 959–965. https://doi.org/10.1016/j.jcms.2014.01.017.

248. Culie D, Dassonville O, Poissonnet G, Riss JC, Fernandez J, Bozec A. Virtual planning and guided surgery in fibular free-flap mandibular reconstruction: A 29-case series. *European annals of otorhinolaryngology, head and neck diseases*. 2016;133(3): 175–178. https://doi.org/10.1016/j.anorl.2016.01.009.

249. Mao Z, Zhang N, Cui Y. Three-dimensional printing of surgical guides for mandibular distraction osteogenesis in infancy. *Medicine*. 2019;98(10): e14754. https://doi.org/10.1097/MD.0000000000014754.

250. Modest MC, Moore EJ, Abel KMV, Janus JR, Sims JR, Price DL, et al. Scapular flap for maxillectomy defect reconstruction and preliminary results using three-dimensional modeling: Maxillectomy Reconstruction and 3D Modeling. *The Laryngoscope*. 2017;127(1): E8–E14. https://doi.org/10.1002/lary.26351.

251. Ren W, Gao L, Li S, Chen C, Li F, Wang Q, et al. Virtual Planning and 3D printing modeling for mandibular reconstruction with fibula free flap. *Medicina oral, patologia oral y cirugia bucal*. 2018;23(3): e359–e366. https://doi.org/10.4317/medoral.22295.

252. Rogers-Vizena CR, Sporn SF, Daniels KM, Padwa BL, Weinstock P. Cost-Benefit Analysis of Three-Dimensional Craniofacial Models for Midfacial Distraction: A Pilot Study. *The Cleft palate-craniofacial journal : official publication of the American Cleft Palate-Craniofacial Association*. 2017;54(5): 612–617. https://doi.org/10.1597/15-281.

253. Stirling Craig E, Yuhasz M, Shah A, Blumberg J, Salomon J, Lowlicht R, et al. Simulated surgery and cutting guides enhance spatial positioning in free fibular mandibular reconstruction: 3D Planning and Free Fibula Mandibular Reconstruction. *Microsurgery*. 2015;35(1): 29–33. https://doi.org/10.1002/micr.22229.

254. Swendseid BP, Roden DF, Vimawala S, Richa T, Sweeny L, Goldman RA, et al. Virtual Surgical Planning in Subscapular System Free Flap Reconstruction of Midface Defects. *Oral oncology*. 2020;101(cu5, 9709118): 104508. https://doi.org/10.1016/j.oraloncology.2019.104508.

255. Tsai CY, Chang YJ, Wu TJ, Lai JP, Chen TY, Lin SS. Blood loss and operative time associated with orthognathic surgery utilizing a novel navigation system in cleft lip and palate patients. *Journal of the Formosan Medical Association*. 2019;118(2): 588–599. https://doi.org/10.1016/j.jfma.2018.12.011.

256. Wu TY, Lin HH, Lo LJ, Ho CT. Postoperative outcomes of two- and three-dimensional planning in orthognathic surgery: A comparative study. *Journal of plastic, reconstructive & aesthetic surgery : JPRAS*. 2017;70(8): 1101–1111. https://doi.org/10.1016/j.bjps.2017.04.012.

257. Jacek B, Maciej P, Tomasz P, Agata B, Wiesław K, Radosław W, et al. 3D printed models in mandibular reconstruction with bony free flaps. *Journal of Materials Science: Materials in Medicine*. 2018;29(2): 23. https://doi.org/10.1007/s10856-018-6029-5.

258. Jacek B, Maciej P, Tomasz P, Agata B, Wieslaw K, Radoslaw W, et al. 3D printed models in mandibular reconstruction with bony free flaps. *Journal of materials science. Materials in medicine*. 2018;29(3): 23. https://doi.org/10.1007/s10856-018-6029-5.

259. Tsai CY, Chang YJ, Wu TJ, Lai JP, Chen TY, Lin SS. Blood loss and operative time associated with orthognathic surgery utilizing a novel navigation system in cleft lip and palate patients. *Journal of the Formosan Medical Association*. 2019;118(2): 588–599. https://doi.org/10.1016/j.jfma.2018.12.011.

260. van Nunen DPF, Janssen LE, Stubenitsky BM, Han KS, Muradin MSM. Stereolithographic skull models in the surgical planning of fronto-supraorbital bar advancement for non-syndromic trigonocephaly. *Journal of Cranio-Maxillofacial Surgery*. 2014;42(6): 959–965. https://doi.org/10.1016/j.jcms.2014.01.017.

261. Zhang WB, Wang Y, Liu XJ, Mao C, Guo CB, Yu GY, et al. Reconstruction of maxillary defects with free fibula flap assisted by computer techniques. *Journal of Cranio-Maxillofacial Surgery*. 2015;43(5): 630–636. https://doi.org/10.1016/j.jcms.2015.03.007.

262. Charbonnier C, Chague S, Kevelham B, Preissmann D, Kolo FC, Rime O, et al. ArthroPlanner: a surgical planning solution for acromioplasty. *International journal of computer assisted radiology and surgery*. 2018;13(12): 2009–2019. https://doi.org/10.1007/s11548-018-1707-9.

263. Huang JH, Liao H, Tan XY, Xing WR, Zhou Q, Zheng YS, et al. Surgical treatment for both-column acetabular fractures using pre-operative virtual simulation and three-dimensional printing techniques. *Chinese Medical Journal*. 2020;133(4): 395–401. https://doi.org/10.1097/CM9.0000000000000649.

264. Kong L, Yang G, Yu J, Zhou Y, Li S, Zheng Q, et al. Surgical treatment of intra-articular distal radius fractures with the assistance of three-dimensional printing technique. *Medicine*. 2020;99(8): e19259. https://doi.org/10.1097/MD.0000000000019259.

265. Lou Y, Cai L, Wang C, Tang Q, Pan T, Guo X, et al. Comparison of traditional surgery and surgery assisted by three dimensional printing technology in the treatment of tibial

plateau fractures. *International orthopaedics*. 2017;41(9): 1875–1880. https://doi.org/10.1007/s00264-017-3445-y.

266. Maini L. Evaluation of accuracy of virtual surgical planning for patient-specific pre-contoured plate in acetabular fracture fixation. *Archives of Orthopaedic and Trauma Surgery*. : 10.

267. Sariali E, Boukhelifa N, Catonne Y, Pascal Moussellard H. Comparison of Three-Dimensional Planning-Assisted and Conventional Acetabular Cup Positioning in Total Hip Arthroplasty: A Randomized Controlled Trial. *The Journal of bone and joint surgery. American volume*. 2016;98(2): 108–116. https://doi.org/10.2106/JBJS.N.00753.

268. Yang L, Grottkau B, He Z, Ye C. Three dimensional printing technology and materials for treatment of elbow fractures. *International Orthopaedics*. 2017;41(11): 2381–2387. https://doi.org/10.1007/s00264-017-3627-7.

269. Zhao X, Zhao J, Xie Y, Mi J. The Utility of a Digital Virtual Template for Junior Surgeons in Pedicle Screw Placement in the Lumbar Spine. *BioMed research international*. 2016;2016(101600173 PG-3076025): 3076025. https://0-dx-doi-org.wam.leeds.ac.uk/10.1155/2016/3076025.

270. Yang L, Shang XW, Fan JN, He ZX, Wang JJ, Liu M, et al. Application of 3D Printing in the Surgical Planning of Trimalleolar Fracture and Doctor-Patient Communication. *BioMed Research International*. 2016;2016: 1–5. https://doi.org/10.1155/2016/2482086.

271. Zhang H, Li Z, Xu Q, Zhang Y, Xu K, Ma X. Analysis for clinical effect of virtual windowing and poking reduction treatment for Schatzker III tibial plateau fracture based on 3D CT data. *BioMed research international*. 2015;2015(101600173): 231820. https://doi.org/10.1155/2015/231820.

272. Zheng SN, Yao QQ, Mao FY, Zheng PF, Tian SC, Li JY, et al. Application of 3D printing rapid prototyping-assisted percutaneous fixation in the treatment of intertrochanteric fracture. *Experimental and therapeutic medicine*. 2017;14(4): 3644–3650. https://doi.org/10.3892/etm.2017.4991.

273. Zheng W, Tao Z, Lou Y, Feng Z, Li H, Cheng L, et al. Comparison of the Conventional Surgery and the Surgery Assisted by 3d Printing Technology in the Treatment of Calcaneal Fractures. *Journal of investigative surgery : the official journal of the Academy of Surgical Research*. 2017;(aza, 8809255): 1–11. https://doi.org/10.1080/08941939.2017.1363833.

274. Cherkasskiy L, Caffrey JP, Szewczyk AF, Cory E, Bomar JD, Farnsworth CL, et al. Patient-specific 3D models aid planning for triplane proximal femoral osteotomy in slipped capital femoral epiphysis. *Journal of children's orthopaedics*. 2017;11(2): 147–153. https://doi.org/10.1302/1863-2548-11-170277.

275. Dodd A, Oddone Paolucci E, Korley R. The effect of three-dimensional computed tomography reconstructions on preoperative planning of tibial plateau fractures: a case–control series. *BMC Musculoskeletal Disorders*. 2015;16(1): 144. https://doi.org/10.1186/s12891-015-0608-0.

276. Giannetti S, Bizzotto N, Stancati A, Santucci A. Minimally invasive fixation in tibial plateau fractures using an pre-operative and intra-operative real size 3D printing. *Injury*. 2017;48(3): 784–788. https://doi.org/10.1016/j.injury.2016.11.015.

277. Hau MYT, Menon DK, Chan RJN, Chung KY, Chau WW, Ho KW. Two-dimensional/three-dimensional EOS™ imaging is reliable and comparable to traditional X-ray imaging assessment of knee osteoarthritis aiding surgical management. *The Knee*. 2020;27(3): 970–979. https://doi.org/10.1016/j.knee.2020.01.015.

278. Leon-Munoz VJ, Lopez-Lopez M, Martinez-Martinez F, Santonja-Medina F. Comparison of weight-bearing full-length radiographs and computed-tomography-scan-based three-dimensional models in the assessment of knee joint coronal alignment. *The Knee*. 2020;27(2): 543–551. https://doi.org/10.1016/j.knee.2019.11.017.

279. Nashikkar PS, Scholes CJ, Haber MD. Computer navigation re-creates planned glenoid placement and reduces correction variability in total shoulder arthroplasty: an in vivo case-control study. *Journal of Shoulder and Elbow Surgery*. 2019;28(12): e398–e409. https://doi.org/10.1016/j.jse.2019.04.037.

280. Samaila EM, Negri S, Zardini A, Bizzotto N, Maluta T, Rossignoli C, et al. Value of three-dimensional printing of fractures in orthopaedic trauma surgery. *Journal of International Medical Research*. 2020;48(1): 030006051988729. https://doi.org/10.1177/0300060519887299.

281. Totoki Y, Yoshii Y, Kusakabe T, Akita K, Ishii T. Screw Length Optimization of a Volar Locking Plate Using Three Dimensional Preoperative Planning in Distal Radius Fractures. *The Journal of Hand Surgery (Asian-Pacific Volume)*. 2018;23(04): 520–527. https://doi.org/10.1142/S2424835518500522.

282. Walenkamp MMJ, de Muinck Keizer RJO, Dobbe JGG, Streekstra GJ, Goslings JC, Kloen P, et al. Computer-assisted 3D planned corrective osteotomies in eight malunited radius fractures. *Strategies in Trauma and Limb Reconstruction*. 2015;10(2): 109–116. https://doi.org/10.1007/s11751-015-0234-2.

283. Werner BS, Hudek R, Burkhart KJ, Gohlke F. The influence of three-dimensional planning on decision-making in total shoulder arthroplasty. *Journal of Shoulder and Elbow Surgery*. 2017;26(8): 1477–1483. https://doi.org/10.1016/j.jse.2017.01.006.

284. Corona PS, Vicente M, Tetsworth K, Glatt V. Preliminary results using patient-specific 3d printed models to improve preoperative planning for correction of post-traumatic tibial deformities with circular frames. *Injury*. 2018;49 Suppl 2(0226040, gon): S51–S59. https://doi.org/10.1016/j.injury.2018.07.017.

285. Duan X, Fan H, Wang F, He P, Yang L. Application of 3D-printed Customized Guides in Subtalar Joint Arthrodesis. *Orthopaedic Surgery*. 2019;11(3): 405–413. https://doi.org/10.1111/os.12464.

286. Hsu CL, Chou YC, Li YT, Chen JE, Hung CC, Wu CC, et al. Pre-operative virtual simulation and three-dimensional printing techniques for the surgical management of acetabular fractures. *International Orthopaedics*. 2019;43(8): 1969–1976. https://doi.org/10.1007/s00264-018-4111-8.

287. Li B, Chen B, Zhang Y, Wang X, Wang F, Xia H, et al. Comparative use of the computer-aided angiography and rapid prototyping technology versus conventional imaging in the management of the Tile C pelvic fractures. *International orthopaedics*. 2016;40(1): 161–166. https://doi.org/10.1007/s00264-015-2800-0.

288. Mainard D, Barbier O, Knafo Y, Belleville R, Mainard-Simard L, Gross JB. Accuracy and reproducibility of preoperative three-dimensional planning for total hip arthroplasty using biplanar low-dose radiographs : A pilot study. *Orthopaedics & traumatology, surgery & research : OTSR*. 2017;103(4 PG-531–536): 531–536. https://0-dx-doi-org.wam.leeds.ac.uk/10.1016/j.otsr.2017.03.001.

289. Scalise JJ, Codsi MJ, Bryan J, Brems JJ, Iannotti JP. The Influence of Three-Dimensional Computed Tomography Images of the Shoulder in Preoperative Planning for Total Shoulder Arthroplasty: *The Journal of Bone and Joint Surgery-American Volume*. 2008;90(11): 2438–2445. https://doi.org/10.2106/JBJS.G.01341.

290. Van den Berg J, Struelens B, Nijs S, Hoekstra H. Value of three-dimensional computed tomography reconstruction in the treatment of posterior tibial plateau fractures. *The Knee*. 2020;27(1): 3–8. https://doi.org/10.1016/j.knee.2019.11.001.

291. Wong TT, Lynch TS, Popkin CA, Kazam JK. Preoperative Use of a 3D Printed Model for Femoroacetabular Impingement Surgery and Its Effect on Planned Osteoplasty. *American Journal of Roentgenology*. 2018;211(2): W116–W121. https://doi.org/10.2214/AJR.17.19400.

292. Cai L, Zhang Y, Chen C, Lou Y, Guo X, Wang J. 3D printing-based minimally invasive cannulated screw treatment of unstable pelvic fracture. *Journal of orthopaedic surgery and research*. 2018;13(1): 71. https://doi.org/10.1186/s13018-018-0778-1.

293. Chen Y, Jia X, Qiang M, Zhang K, Chen S. Computer-Assisted Virtual Surgical Technology Versus Three-Dimensional Printing Technology in Preoperative Planning for Displaced Three and Four-Part Fractures of the Proximal End of the Humerus. *The Journal of bone and joint surgery. American volume*. 2018;100(22): 1960–1968. https://doi.org/10.2106/JBJS.18.00477.

294. Maini L, Verma T, Sharma A, Sharma A, Mishra A, Jha S. *Evaluation of accuracy of virtual surgical planning for patient-specific pre-contoured plate in acetabular fracture fixation*. Berlin/Heidelberg: Springer Berlin Heidelberg; 2018. https://doi.org/10.1007/s00402-018-2868-2.

295. Zheng W, Su J, Cai L, Lou Y, Wang J, Guo X, et al. Application of 3D-printing technology in the treatment of humeral intercondylar fractures. *Orthopaedics & traumatology, surgery & research : OTSR*. 2018;104(1): 83–88. https://0-dx-doi-org.wam.leeds.ac.uk/10.1016/j.otsr.2017.11.012.

296. Zhang H, Gong J, Xie M, Tang K. Individualized coracoid osteotomy and 3D congruent arc reconstruction of glenoid for the treatment of recurrent anterior shoulder dislocation. *Journal of Orthopaedic Surgery and Research*. 2017;12(1): 193. https://doi.org/10.1186/s13018-017-0687-8.

297. Feng S, Lin J, Su N, Meng H, Yang Y, Fei Q. 3-Dimensional printing templates guiding versus free hand technique for cervical lateral mass screw fixation: A prospective study. *Journal of Clinical Neuroscience*. 2020;78: 252–258. https://doi.org/10.1016/j.jocn.2020.04.008.

298. Yang DL, Xu QW, Che XM, Wu JS, Sun B. Clinical evaluation and follow-up outcome of presurgical plan by Dextroscope: a prospective controlled study in patients with skull base tumors. *Surgical neurology*. 2009;72(6): 682–689. https://doi.org/10.1016/j.surneu.2009.07.040.

299. Deng X, Wang K, Wu L, Yang C, Yang T, Zhao L, et al. Intraspinal hemangioblastomas: analysis of 92 cases in a single institution: Clinical article. *Journal of Neurosurgery: Spine*. 2014;21(2): 260–269. https://doi.org/10.3171/2014.1.SPINE13866.

300. Han K wei, Zhang D feng, Chen J gang, Hou L jun. Presurgical visualization of the neurovascular relationship in trigeminal neuralgia with 3D modeling using free Slicer software. *Acta Neurochirurgica*. 2016;158(11): 2195–2201. https://doi.org/10.1007/s00701-016-2936-8.

301. Luo M, Wang W, Yang N, Xia L. Does Three-dimensional Printing Plus Pedicle Guider Technology in Severe Congenital Scoliosis Facilitate Accurate and Efficient Pedicle Screw Placement?. *Clinical orthopaedics and related research*. 2019;477(8): 1904–1912. https://doi.org/10.1097/CORR.0000000000000739.

302. Goertz L, Kabbasch C, Borggrefe J, Hamisch C, Telentschak S, von Spreckelsen N, et al. Preoperative Three-Dimensional Angiography May Reduce Ischemic Complications During Clipping of Ruptured Intracranial Aneurysms. *World neurosurgery*. 2018;120(101528275): e1163–e1170. https://doi.org/10.1016/j.wneu.2018.09.026.

303. Petrone S, Marengo N, Ajello M, Lavorato A, Penner F, Cofano F, et al. Cortical bone trajectory technique's outcomes and procedures for posterior lumbar fusion: A retrospective study. *Journal of Clinical Neuroscience*. 2020; 6.

304. Yang M, Li C, Li Y, Zhao Y, Wei X, Zhang G, et al. Application of 3D Rapid Prototyping Technology in Posterior Corrective Surgery for Lenke 1 Adolescent Idiopathic Scoliosis Patients. *Medicine*. 2015;94(8): e582. https://doi.org/10.1097/MD.0000000000000582.

305. Chen JQ, Guan Y, Li G, Li XH, Zhan YF, Li XY, et al. Application of 3D-computed tomography angiography technology in large meningioma resection. *Asian Pacific journal of tropical medicine*. 2012;5(7): 577–581. https://doi.org/10.1016/S1995-7645(12)60102-3.

306. Guo Z, Liu C, Hou H, Li R, Su J, Zhang F, et al. Preoperative Computed Tomography (CT) Evaluation of Anatomical Abnormalities in Endonasal Transsphenoidal Approach in Pituitary Adenoma. *Medical science monitor : international medical journal of experimental and clinical research*. 2018;24(dxw, 9609063): 1268–1275.

307. Haerle SK, Daly MJ, Chan HHL, Vescan A, Kucharczyk W, Irish JC. Virtual surgical planning in endoscopic skull base surgery: Surgical Planning in Skull Base Surgery. *The Laryngoscope*. 2013;123(12): 2935–2939. https://doi.org/10.1002/lary.24004.

308. Yang DL, Xu QW, Che XM, Wu JS, Sun B. Clinical evaluation and follow-up outcome of presurgical plan by Dextroscope: a prospective controlled study in patients with skull base tumors. *Surgical Neurology*. 2009;72(6): 682–689. https://doi.org/10.1016/j.surneu.2009.07.040.

309. Zawy Alsofy S, Sakellaropoulou I, Stroop R. Evaluation of Surgical Approaches for Tumor Resection in the Deep Infratentorial Region and Impact of Virtual Reality Technique for the Surgical Planning and Strategy. *Journal of Craniofacial Surgery*. 2020;Publish Ahead of Print. https://doi.org/10.1097/SCS.0000000000006525.

310. Li C, Yang M, Xie Y, Chen Z, Wang C, Bai Y, et al. Application of the polystyrene model made by 3-D printing rapid prototyping technology for operation planning in revision lumbar discectomy. *Journal of orthopaedic science : official journal of the Japanese Orthopaedic Association*. 2015;20(3): 475–480. https://doi.org/10.1007/s00776-015-0706-8.

311. Bertolo R, Autorino R, Fiori C, Amparore D, Checcucci E, Mottrie A, et al. Expanding the Indications of Robotic Partial Nephrectomy for Highly Complex Renal Tumors: Urologists' Perception of the Impact of Hyperaccuracy Three-Dimensional Reconstruction. *Journal of laparoendoscopic & advanced surgical techniques. Part A*. 2018;(9706293, c0d). https://doi.org/10.1089/lap.2018.0486.

312. Kamai T, Furuya N, Kambara T, Abe H, Honda M, Shioyama Y, et al. Single minimum incision endoscopic radical nephrectomy for renal tumors with preoperative virtual navigation using 3D-CT volume-rendering. *BMC urology*. 2010;10(100968571): 7. https://doi.org/10.1186/1471-2490-10-7.

313. Brehmer M, Beckman MO, Magnusson A. Three-dimensional computed tomography planning improves percutaneous stone surgery. *Scandinavian journal of urology*. 2014;48(3): 316–323. https://doi.org/10.3109/21681805.2013.876552.

314. Wake N, Bjurlin MA, Rostami P, Chandarana H, Huang WC. Three-dimensional Printing and Augmented Reality: Enhanced Precision for Robotic Assisted Partial Nephrectomy. *Urology*. 2018;116: 227–228. https://doi.org/10.1016/j.urology.2017.12.038.

315. Wang D, Zhang B, Yuan X, Zhang X, Liu C. Preoperative planning and real-time assisted navigation by three-dimensional individual digital model in partial nephrectomy with three-dimensional laparoscopic system. *International Journal of Computer Assisted Radiology and Surgery*. 2015;10(9): 1461–1468. https://doi.org/10.1007/s11548-015-1148-7.

316. Parkhomenko E, O'Leary M, Safiullah S, Walia S, Owyong M, Lin C, et al. Pilot Assessment of Immersive Virtual Reality Renal Models as an Educational and Preoperative Planning Tool for Percutaneous Nephrolithotomy. *Journal of Endourology*. 2019;33(4): 283–288. https://doi.org/10.1089/end.2018.0626.

317. Yuasa Y, Okitsu H, Goto M, Kuramoto S, Tomibayashi A, Matsumoto D, et al. Three-dimensional CT for preoperative detection of the left gastric artery and left gastric vein in laparoscopy-assisted distal gastrectomy: Gastric vessel detected by 3-D CT in LADG. *Asian Journal of Endoscopic Surgery*. 2016;9(3): 179–185. https://doi.org/10.1111/ases.12280.

318. Wang JB. Role of 3DCT in laparoscopic total gastrectomy with spleen-preserving splenic lymph node dissection. *World Journal of Gastroenterology*. 2014;20(16): 4797. https://doi.org/10.3748/wjg.v20.i16.4797.

319. Wada T, Takeuchi H, Kawakubo H, Nakamura R, Oyama T, Takahashi T, et al. Clinical utility of preoperative evaluation of bronchial arteries by three-dimensional computed tomographic angiography for esophageal cancer surgery: Preoperative evaluation of

bronchial artery. *Diseases of the Esophagus*. 2013;26(6): 616–622. https://doi.org/10.1111/dote.12012.

320. Osaki T, Saito H, Murakami Y, Miyatani K, Kuroda H, Matsunaga T, et al. Usefulness of Preoperative Assessment of Perigastric Vascular Anatomy by Dynamic Computed Tomography for Laparoscopic Gastrectomy. *Yonago acta medica*. 2015;58(4): 157.

321. Miyamoto R, Inagawa S, Nagai K, Maeda M, Kemmochi A, Yamamoto M. Three-dimensional reconstruction of vascular arrangement including the hepatic artery and left gastric vein during gastric surgery. *SpringerPlus*. 2016;5(1): 835. https://doi.org/10.1186/s40064-016-2583-9.

322. Calloway EH, Chhotani AN, Lee YZ, Phillips JD. Three-dimensional computed tomography for evaluation and management of children with complex chest wall anomalies: useful information or just pretty pictures? *Journal of Pediatric Surgery*. 2011;46(4): 640–647. https://doi.org/10.1016/j.jpedsurg.2010.10.013.

323. Hagiwara M, Shimada Y, Kato Y, Nawa K, Makino Y, Furumoto H, et al. High-quality 3-dimensional image simulation for pulmonary lobectomy and segmentectomy: results of preoperative assessment of pulmonary vessels and short-term surgical outcomes in consecutive patients undergoing video-assisted thoracic surgery†. *European Journal of Cardio-Thoracic Surgery*. 2014;46(6): e120–e126. https://doi.org/10.1093/ejcts/ezu375.

324. Smelt JLC, Suri T, Valencia O, Jahangiri M, Rhode K, Nair A, et al. Operative Planning in Thoracic Surgery: A Pilot Study Comparing Imaging Techniques and Three-Dimensional Printing. *Annals of Thoracic Surgery*. 2019;107(2): 401–406. https://doi.org/10.1016/j.athoracsur.2018.08.052.

325. Garekar S, Bharati A, Chokhandre M, Mali S, Trivedi B, Changela VP, et al. Clinical Application and Multidisciplinary Assessment of Three Dimensional Printing in Double Outlet Right Ventricle With Remote Ventricular Septal Defect. *World journal for pediatric & congenital heart surgery*. 2016;7(3): 344–350. https://doi.org/10.1177/2150135116645604.

326. Valverde I, Gomez-Ciriza G, Hussain T, Suarez-Mejias C, Velasco-Forte MN, Byrne N, et al. Three-dimensional printed models for surgical planning of complex congenital heart defects: An international multicentre study. *European Journal of Cardio-thoracic Surgery*. 2017;52(6): 1139–1148. https://doi.org/10.1093/EJCTS/EZX208.

327. Zhao L, Zhou S, Fan T, Li B, Liang W, Dong H. Three-dimensional printing enhances preparation for repair of double outlet right ventricular surgery. *Journal of Cardiac Surgery*. 2018;33(1): 24–27. https://doi.org/10.1111/jocs.13523.

328. Huang YJ, Lin KH, Chen YY, Wu TH, Huang HK, Chang H, et al. Feasibility and Clinical Effectiveness of Three-Dimensional Printed Model-Assisted Nuss Procedure. *The Annals of Thoracic Surgery*. 2019;107(4): 1089–1096. https://doi.org/10.1016/j.athoracsur.2018.09.021.

329. Chen YY, Lin KH, Huang HK, Chang H, Lee SC, Huang TW. The beneficial application of preoperative 3D printing for surgical stabilization of rib fractures. Lammi MJ (ed.) *PLOS ONE*. 2018;13(10): e0204652. https://doi.org/10.1371/journal.pone.0204652.

330. Su L, Dong Q, Zhang H, Zhou X, Chen Y, Hao X, et al. Clinical application of a three-dimensional imaging technique in infants and young children with complex liver

tumors. *Pediatric surgery international*. 2016;32(4 PG-387–95): 387–395. https://0-dx-doi-org.wam.leeds.ac.uk/10.1007/s00383-016-3864-7.

331. Zhao J, Zhou XJ, Zhu CZ, Wu Y, Wei B, Zhang G, et al. 3D simulation assisted resection of giant hepatic mesenchymal hamartoma in children. *Computer Assisted Surgery*. 2017;22(1): 54–59. https://doi.org/10.1080/24699322.2017.1358401.

332. Zhang B, Chen Z, Hu X, He Y, Li M, Liu P, et al. Application of Three-Dimensional Visualization Technology in Laparoscopic Surgery for Pheochromocytoma/Paraganglioma: A Single-Center Experience. *Journal of laparoendoscopic & advanced surgical techniques. Part A*. 2018;28(8): 997–1002. https://doi.org/10.1089/lap.2017.0704.

333. Bly RA, Chang SH, Cudejkova M, Liu JJ, Moe KS. Computer-Guided Orbital Reconstruction to Improve Outcomes. *JAMA Facial Plastic Surgery*. 2013;15(2): 113–120. https://doi.org/10.1001/jamafacial.2013.316.

334. Aluwee SAZBS, Kato H, Zhou X, Hara T, Fujita H, Kanematsu M, et al. Magnetic resonance imaging of uterine fibroids: a preliminary investigation into the usefulness of 3D-rendered images for surgical planning. *SpringerPlus*. 2015;4(101597967): 384. https://doi.org/10.1186/s40064-015-1170-9.

335. Giusti S, Forasassi F, Bastiani L, Cela V, Pluchino N, Ferrari V, et al. Anatomical localization of deep infiltrating endometriosis: 3D MRI reconstructions. *Abdominal Imaging*. 2012;37(6): 1110–1121. https://doi.org/10.1007/s00261-012-9848-8.

336. Chen S, Zhang K, Jia X, Qiang M, Chen Y. Evaluation of the computer-assisted virtual surgical technology in preoperative planning for distal femoral fracture. *Injury*. 2020;51(2): 443–451. https://doi.org/10.1016/j.injury.2019.10.085.

337. Maini L, Sharma A, Jha S, Sharma A, Tiwari A. Three-dimensional printing and patient-specific pre-contoured plate: future of acetabulum fracture fixation? *European Journal of Trauma and Emergency Surgery*. 2018;44(2): 215–224. https://doi.org/10.1007/s00068-016-0738-6.

338. Werner BS, Hudek R, Burkhart KJ, Gohlke F. The influence of three-dimensional planning on decision-making in total shoulder arthroplasty. *Journal of Shoulder and Elbow Surgery*. 2017;26(8): 1477–1483. https://doi.org/10.1016/j.jse.2017.01.006.

339. Li YG, Chen XJ, Zhang YZ, Han DZ, Yan DX, Gao GZ, et al. Three-dimensional digitalized virtual planning for retrograde sural neurovascular island flaps: a comparative study. *Burns*. 2014;40(5): 974–980. https://doi.org/10.1016/j.burns.2013.10.009.

340. Gacto-Sanchez P, Sicilia-Castro D, Gomez-Cia T, Lagares A, Collell T, Suarez C, et al. Computed tomographic angiography with VirSSPA three-dimensional software for perforator navigation improves perioperative outcomes in DIEP flap breast reconstruction. *Plastic and reconstructive surgery*. 2010;125(1): 24–31. https://doi.org/10.1097/PRS.0b013e3181c4948b.

341. Zhang P, He L, Shi F, Deng J, Fang C, Luo Y. Three-dimensional visualization technique in endoscopic breast-conserving surgery and pedicled omentum for immediate breast reconstruction. *Surgical oncology*. 2019;28(byv, 9208188): 103–108. https://doi.org/10.1016/j.suronc.2018.11.016.

342. Søndenaa K, Quirke P, Hohenberger W, Sugihara K, Kobayashi H, Kessler H, et al. The rationale behind complete mesocolic excision (CME) and a central vascular ligation for colon cancer in open and laparoscopic surgery : proceedings of a consensus conference. *International Journal of Colorectal Disease*. 2014;29(4): 419–428. https://doi.org/10.1007/s00384-013-1818-2.

343. Wang C, Gao Z, Shen K, Shen Z, Jiang K, Liang B, et al. Safety, quality and effect of complete mesocolic excision vs non-complete mesocolic excision in patients with colon cancer: a systemic review and meta-analysis. *Colorectal Disease*. 2017;19(11): 962–972. https://doi.org/10.1111/codi.13900.

344. Freund MR, Goldin I, Reissman P. Superior Mesenteric Vein Injury During Oncologic Right Colectomy: Current Vascular Repair Modalities. *Vascular and Endovascular Surgery*. 2018;52(1): 11–15. https://doi.org/10.1177/1538574417739749.

345. Karachun A, Panaiotti L, Chernikovskiy I, Achkasov S, Gevorkyan Y, Savanovich N, et al. Short-term outcomes of a multicentre randomized clinical trial comparing D2 *versus* D3 lymph node dissection for colonic cancer (COLD trial). *British Journal of Surgery*. 2020;107(5): 499–508. https://doi.org/10.1002/bjs.11387.

346. Xu L, Su X, He Z, Zhang C, Lu J, Zhang G, et al. Short-term outcomes of complete mesocolic excision versus D2 dissection in patients undergoing laparoscopic colectomy for right colon cancer (RELARC): a randomised, controlled, phase 3, superiority trial. *The Lancet Oncology*. 2021;22(3): 391–401. https://doi.org/10.1016/S1470-2045(20)30685-9.

347. Díaz-Vico T, Fernández-Hevia M, Suárez-Sánchez A, García-Gutiérrez C, Mihic-Góngora L, Fernández-Martínez D, et al. Complete Mesocolic Excision and D3 Lymphadenectomy versus Conventional Colectomy for Colon Cancer: A Systematic Review and Meta-Analysis. *Annals of Surgical Oncology*. 2021;28(13): 8823–8837. https://doi.org/10.1245/s10434-021-10186-9.

348. *Laparoscopic CME programme*. European Society of Coloproctology. https://www.escp.eu.com/education/european-school-of-coloproctology/laparoscopic-cme-programme [Accessed 15th April 2020].

349. Raikos A, Smith JD. Anatomical variations: How do surgical and radiology training programs teach and assess them in their training curricula? *Clinical Anatomy*. 2015;28(6): 717–724. https://doi.org/10.1002/ca.22560.

350. Javan R, Herrin D, Tangestanipoor A. Understanding Spatially Complex Segmental and Branch Anatomy Using 3D Printing: Liver, Lung, Prostate, Coronary Arteries, and Circle of Willis. *Academic Radiology*. 2016;23(9): 1183–1189. https://doi.org/10.1016/j.acra.2016.04.010.

351. Fletcher J, Ilangovan R, Hanna G, Miskovic D, Lung P. The impact of three-dimensional reconstruction and standardised CT interpretation (AMIGO) on the anatomical understanding of mesenteric vascular anatomy for planning complete mesocolic excision surgery: A randomised crossover study. *Colorectal Disease*. 2022;24(4): 388–400. https://doi.org/10.1111/codi.16041.

352. Nesgaard JM, Stimec BV, Bakka AO, Edwin B, Ignjatovic D, Oresland T, et al. Navigating the mesentery: A comparative pre- and per-operative visualization of the vascular anatomy. *Colorectal Disease*. 2015;17(9): 810–818. https://doi.org/10.1111/codi.13003.

353. Willard CD, Kjaestad E, Stimec BV, Edwin B, Ignjatovic D, Oresland T, et al. Preoperative anatomical road mapping reduces variability of operating time, estimated blood loss, and lymph node yield in right colectomy with extended D3 mesenterectomy for cancer. *International Journal of Colorectal Disease*. 2019;34(1): 151–160. https://doi.org/10.1007/s00384-018-3177-5.

354. Kluyver T, Ragan-Kelley B, Pérez F, Bussonnier M, Frederic J, Hamrick J, et al. Jupyter Notebooks—a publishing format for reproducible computational workflows.

355. team T pandas development. *pandas-dev/pandas: Pandas*. Zenodo; 2024. https://doi.org/10.5281/zenodo.10957263. [Accessed 18th April 2024].

356. Waskom M. seaborn: statistical data visualization. *Journal of Open Source Software*. 2021;6(60): 3021. https://doi.org/10.21105/joss.03021.

357. McHugh ML. Interrater reliability: the kappa statistic. *Biochemia Medica*. 2012;22(3): 276–282.

358. Fletcher J, Behrenbruch C, Lung P, Miskovic D. Robotic right complete mesocolectomy with patient-specific three-dimensional modelling for planning and intra-operative navigation – a video vignette. *Colorectal Disease*. 2021;23(8): 2211–2212. https://doi.org/10.1111/codi.15738.

359. Benz S, Stricker I, Tam Y, Tannapfel A. CME or traditional surgery for right-sided colon cancer? *Coloproctology*. 2017;39(3): 184–189. https://doi.org/10.1007/s00053-017-0158-z.

360. Bexkens R, Claessen FM, Kodde IF, Oh LS, Eygendaal D, van den Bekerom MP. The kappa paradox. *Shoulder & Elbow*. 2018;10(4): 308. https://doi.org/10.1177/1758573218791813.

361. Haug TR, Ørntoft MBW, Miskovic D, Iversen LH, Johnsen SP, Valentin JB, et al. Technical assessment in minimally invasive complete mesocolic excision: Is the complete mesocolic excision competency assessment tool valid and reliable? *Colorectal Disease: The Official Journal of the Association of Coloproctology of Great Britain and Ireland*. 2023;25(11): 2139–2146. https://doi.org/10.1111/codi.16756.

362. Institute of Medicine. *Crossing the quality chasm: a new health system for the 21st century*. 2001.

363. Chin JJ. Doctor-patient relationship: from medical paternalism to enhanced autonomy. *Singapore Medical Journal*. 2002;43(3): 152–155.

364. Kunneman M, Montori VM. When patient-centred care is worth doing well: Informed consent or shared decision-making. *BMJ Quality and Safety*. 2017;26(7): 522–524. https://doi.org/10.1136/bmjqs-2016-005969.

365. Wear S. *Informed consent: patient autonomy and physician beneficence within clinical medicine*. 1993.

366. Schenker Y, Fernandez A, Sudore R, Schillinger D. Interventions to improve patient comprehension in informed consent for medical and surgical procedures: A systematic review. *Medical Decision Making*. 2011;31(1): 151–173. https://doi.org/10.1177/0272989X10364247.

367. General Medical Council. Consent: patients and doctors making decisions together. 2008; 1–64. https://doi.org/978-0-901458-31-5.

368. Reynard J, Marsh H. The development of consent from Bolam to Chester : what you need to know and what your patients are entitled to know. 2009; 1458–1461. https://doi.org/10.1111/j.1464-410X.2009.08605.x.

369. Chan SW, Tulloch E, Cooper ES, Smith A, Wojcik W, Norman JE. Montgomery and informed consent: Where are we now? *BMJ (Online)*. 2017;357(May): 10–12. https://doi.org/10.1136/bmj.j2224.

370. Shahu A, Schwartz J, Perez M, Bernheim SM, Krumholz HM, Spatz ES. Discerning quality: an analysis of informed consent documents for common cardiovascular procedures. *BMJ Quality and Safety*. 2017;26(7): 569–571. https://doi.org/10.1136/bmjqs-2016-005663.

371. Bernat J, Peterson L. Patient-centered informed consent in surgical practice. *Archives of Surgery*. 2006;141(1): 86–92.

372. Roter DL, Hall JA, Merisca R, Nordstrom B, Cretin D, Hall A. to Improve Patient Compliance Effectiveness of Interventions A Meta-Analysis. *Medical Care*. 2009;36(8): 1138–1161.

373. D Bertakis K. *The Communication of Information from Physician to Patient: A Method for Increasing Patient Retention and Satisfaction*. The Journal of family practice. 1977.

374. Robinson a. Variability in patient preferences for participating in medical decision making: implication for the use of decision support tools. *Quality in Health Care*. 2001;10 Suppl 1(Suppl I): i34-8.

375. Braddock CH, Fihn SD, Levinson W, Jonsen AR, Pearlman RA. How Doctors and Patients Discuss Routine Informed Decision Making in the Outpatient Setting. 1995; 339–345.

376. Matiasek J, Wynia MK. Reconceptualizing the Informed Consent Process at Eight Innovative Hospitals. *The Joint Commission Journal on Quality and Patient Safety*. 2008;34(3): 127–137. https://doi.org/10.1016/S1553-7250(08)34015-X.

377. Lavelle-jones C, Byrne DJ, Rice P, Cuschieri A. Factors affecting quality of informed consent. *BMJ : British Medical Journal*. 2009;306: 885–890.

378. Lemaire R. Informed consent – a contemporary myth ? *The Journal of bone and joint surgery*. 2006;88: 1–7. https://doi.org/10.1302/0301-620X.88B1.16435.

379. Fink AS, Prochazka A V, Henderson WG, Bartenfeld D, Nyirenda C, Webb A, et al. Predictors of Comprehension during Surgical Informed Consent. *ACS*. 2010;210(6): 919–926. https://doi.org/10.1016/j.jamcollsurg.2010.02.049.

380. Santavirta N, Lillqvist GUN. Teaching of patients undergoing total hip replacement surgery. 1994;31(2).

381. Kriwanek S, Armbruster C, Beckerhinn P, Blauensteier W, Gschwantler M. Patients' Assessment and Recall of Surgical Information after Laparoscopic Cholecystectomy. *Digestive Surgery*. 1998;15(6): 669–673. https://doi.org/10.1159/000018675.

382. Chan BPK, O'Connor AM, Mamazza J, Moloo H, Boushey RP, Poulin EC, et al. The Myth of Informed Consent in Rectal Cancer Surgery. *Diseases of the Colon & Rectum*. 2012;55(9): 970–975. https://doi.org/10.1097/dcr.0b013e31825f2479.

383. Dahl A, Sinha M, Rosenberg DI, Tran M. Assessing Physician-Parent Communication During Emergency Medical Procedures in Children An Observational Study in a Low-Literacy Latino Patient Population. 2015;31(5): 339–342.

384. Schenker Y, Wang F, Selig SJ, Ng R, Fernandez A. The Impact of Language Barriers on Documentation of Informed Consent at a Hospital with On-Site Interpreter Services. : 294–299. https://doi.org/10.1007/s11606-007-0359-1.

385. Engel KG, Smith DM, Robinson CH, Forman JH, Ubel PA. Patient Comprehension of Emergency Department Care and Instructions : Are Patients Aware of When They Do Not Understand ? *YMEM*. 53(4): 454-461.e15. https://doi.org/10.1016/j.annemergmed.2008.05.016.

386. Williams M V, Parker RM, Baker DW, Parikh NS, Pitkin K, Coates WC, et al. *Inadequate Functional Health Literacy Among Patients at Two Public Hospitals* . JAMA . 1995. p. 1677–1682. https://doi.org/10.1001/jama.1995.03530210031026.

387. Kinnersley P, Phillips K, Savage K, Mj K, Farrell E, Morgan B, et al. Interventions to promote informed consent for patients undergoing surgical and other invasive healthcare procedures (Review) Interventions to promote informed consent for patients undergoing surgical and other invasive healthcare procedures. 2013;(7): 10–13. https://doi.org/10.1002/14651858.CD009445.pub2.Copyright.

388. Degner LF, Kristjanson LJ, Bowman D, Sloan JA, Carriere KC, O'Neil J, et al. Information Needs and Decisional Preferences in Women With Breast Cancer. *JAMA*. 1997;277(18): 1485–1492. https://doi.org/10.1001/jama.1997.03540420081039.

389. Jefford M, Tattersall MHN. Review Informing and involving cancer patients in their own care. 2002;3(October): 629–637.

390. Habiba M, Jackson C, Akkad A, Kenyon S, Dixon-Woods M. Women's accounts of consenting to surgery: is consent a quality problem ? 2004; 422–427. https://doi.org/10.1136/qshc.2004.010652.

391. Picano E. Informed consent and communication of risk from escape from a communication inferno. 2000; 849–851.

392. Rosenfeld EH, Lopez ME, Yu YR, Justus CA, Borges MM, Mathai RC, et al. Use of standardized visual aids improves informed consent for appendectomy in children: A randomized control trial. *American Journal of Surgery*. 2018; https://doi.org/10.1016/j.amjsurg.2018.07.032.

393. Berkman ND, Sheridan SL, Donahue KE, Halpern DJ, Crotty K. Annals of Internal Medicine Review Low Health Literacy and Health Outcomes : An Updated. 2014;(May). https://doi.org/10.1059/0003-4819-155-2-201107190-00005.

394. Bendok B, El Tecle N, El Ahmadieh T, Koht A, Gallagher T, Carroll T, et al. Advances and innovations in brain arteriovenous malformation surgery. *Neurosurgery*. 2014;74: 60–73. http://0-dx.doi.org.wam.leeds.ac.uk/10.1227/NEU.0000000000000230.

395. The Robert Jones and Agnes Hunt Orthopaedic Hospital NHS Foundation trust. *https://www.rjah.nhs.uk/Patient-Visitors/Coming-into-Hospital/Joint-School.aspx*.

396. Bui D, Nakamura C, Bray BE, Zeng-Treitler Q. Automated illustration of patients instructions. *AMIA Symposium*. 2012; 1158–1167.

397. Collier R. Educating patients with pictures. *CMAJ : Canadian Medical Association journal = journal de l'Association medicale canadienne*. 2011;183(15): 3967. https://doi.org/10.1503/cmaj.109-3967.

398. Houts PS, Doak CC, Doak LG, Loscalzo MJ. The role of pictures in improving health communication: A review of research on attention, comprehension, recall, and adherence. *Patient Education and Counseling*. 2006;61(2): 173–190. https://doi.org/10.1016/j.pec.2005.05.004.

399. Mayer RE, Gallini JK. When Is an Illustration Worth Ten Thousand Words? *Journal of Educational Psychology*. 1990;82(4): 715–726. https://doi.org/10.1037/0022-0663.82.4.715.

400. Rohret L, Ferguson KJ. Effective use of patient education illustrations. *Patient Education and Counseling*. 1990;15(1): 73–75. https://doi.org/10.1016/0738-3991(90)90010-I.

401. Martelli N, Serrano C, Van Den Brink H, Pineau J, Prognon P, Borget I, et al. Advantages and disadvantages of 3-dimensional printing in surgery: A systematic review. *Surgery (United States)*. 2016;159(6): 1485–1500. https://doi.org/10.1016/j.surg.2015.12.017.

402. S. M, L. P, M. B, A. P, E. C, S. L, et al. Value of 3D printing for the comprehension of surgical anatomy. *Surgical Endoscopy and Other Interventional Techniques*. 2017;31(10): 4102–4110. http://0-dx.doi.org.wam.leeds.ac.uk/10.1007/s00464-017-5457-5.

403. Brazina D, Fojtik R, Rombova Z. 3D Visualization in Teaching Anatomy. *Procedia - Social and Behavioral Sciences*. 2014;143: 367–371. https://doi.org/10.1016/j.sbspro.2014.07.496.

404. Wang L, Huang L, Li X, Zhong D, Li D, Cao T, et al. Three-dimensional printing PEEK implant: a novel choice for the reconstruction of chest wall defect. *The Annals of thoracic surgery*. 2018;

405. Yang T, Lin S, Tan T, Yang J, Pan J, Hu C, et al. Impact of 3D Printing Technology on Comprehension of Surgical Anatomy of Retroperitoneal Tumor. *World Journal of Surgery*. 2018;42(8): 2339–2343. https://doi.org/10.1007/s00268-018-4489-x.

406. Yoon SH, Park S, Kang CH, Park IK, Goo JM, Kim YT. Personalized 3D-Printed Model for Informed Consent for Stage I Lung Cancer: A Randomized Pilot Trial. *Seminars in Thoracic and Cardiovascular Surgery*. 2018; 3–5. https://doi.org/10.1053/j.semtcvs.2018.10.017.

407. Cleeren G, Quirynen M, Ozcelik O, Teughels W. Role of 3D animation in periodontal patient education: A randomized controlled trial. *Journal of Clinical Periodontology*. 2014;41(1): 38–45. https://doi.org/10.1111/jcpe.12170.

408. Degner L, Sloan J, Venkatesh P. The control preference scale. *Canadian Journal of Nursing Research*. 1998;29(3): 21–43.

409. Meropol NJ, Egleston BL, Buzaglo JS, Benson AB, Cegala DJ, Diefenbach MA, et al. Cancer Patient Preferences for Quality and Length of Life. *Cancer*. 2008;113(12): 3459–3466. https://doi.org/10.1002/cncr.23968.

410. O'Connor A. Validation of a decisional conflict scale. *Medical decision making*. 1995;15(1): 25–30. https://doi.org/10.1177/0272989X9501500105.

411. Whitehead AL, Julious SA, Cooper CL, Campbell MJ. Estimating the sample size for a pilot randomised trial to minimise the overall trial sample size for the external pilot and main trial for a continuous outcome variable. *Statistical Methods in Medical Research*. 2016;25(3): 1057–1073. https://doi.org/10.1177/0962280215588241.

412. Salek M, Silverstein A, Tilly A, Gassant PY, Gunasekera S, Hordofa DF, et al. Factors influencing treatment decision-making for cancer patients in low- and middle-income countries: A scoping review. *Cancer Medicine*. 2023;12(17): 18133–18152. https://doi.org/10.1002/cam4.6375.

413. Pratt M, Searles GE. Using Visual Aids to Enhance Physician-Patient Discussions and Increase Health Literacy. *Journal of Cutaneous Medicine and Surgery*. 2017;21(6): 497–501. https://doi.org/10.1177/1203475417715208.

414. Mbanda N, Dada S, Bastable K, Ingalill GB, Ralf W. S. A scoping review of the use of visual aids in health education materials for persons with low-literacy levels. *Patient Education and Counseling*. 2021;104(5): 998–1017. https://doi.org/10.1016/j.pec.2020.11.034.

415. Nguyen MH, Smets EMA, Bol N, Bronner MB, Tytgat KMAJ, Loos EF, et al. Fear and forget: how anxiety impacts information recall in newly diagnosed cancer patients visiting a fast-track clinic. *Acta Oncologica*. 2019;58(2): 182–188. https://doi.org/10.1080/0284186X.2018.1512156.

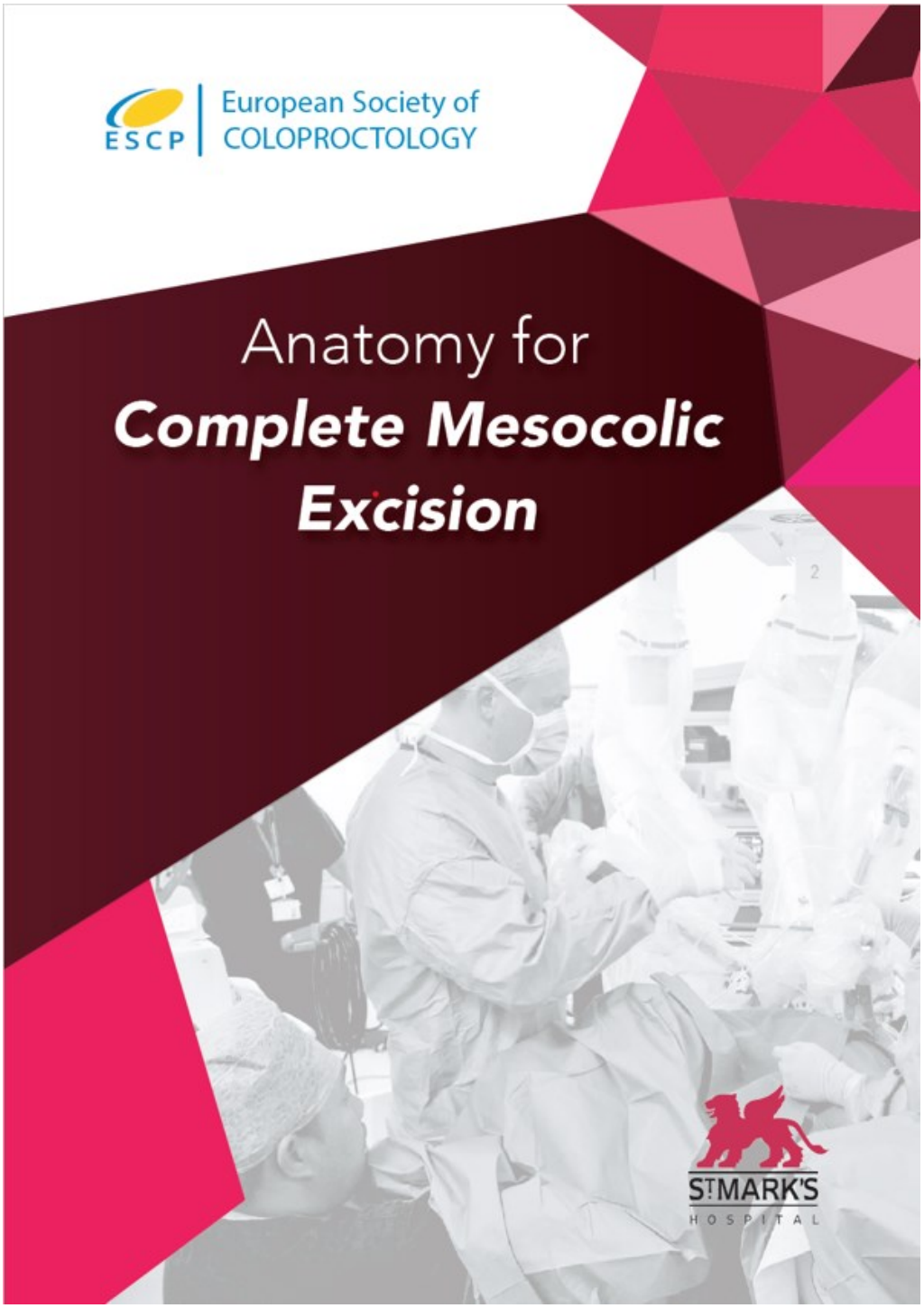
416. Lee YH, Chou XY, Lai YH, Liang YH, Hung CT, Hsaio CC, et al. Decisional conflict and its determinants among patients with cancer undergoing immunotherapy combined with chemotherapy or targeted therapy: a cross-sectional study. *Scientific Reports*. 2023;13(1): 12715. https://doi.org/10.1038/s41598-023-39280-6.

417. Ganguli A, Pagan-Diaz GJ, Grant L, Cvetkovic C, Bramlet M, Vozenilek J, et al. 3D printing for preoperative planning and surgical training: a review. *Biomedical Microdevices*. 2018;20(3). https://doi.org/10.1007/s10544-018-0301-9.

418. Przedlacka A, Pellino G, Fletcher J, Bello F, Tekkis PP, Kontovounisios C. Current and future role of three-dimensional modelling technology in rectal cancer surgery: A systematic review. *World Journal of Gastrointestinal Surgery*. 2021;13(12): 1754–1769. https://doi.org/10.4240/wjgs.v13.i12.1754.

9 Appendices

Appendix 4.1 CME Anatomy manual



4 Rationale for Complete Mesocolic Excision

Complete mesocolic excision was first defined by Werner Hohenberger [3], although the individual components had been described by previous authors.

Complete mesocolic excision can be conceptualized as a colonic corollary of the total mesorectal excision (TME) principle in rectal cancer surgery. TME is based on a more radical dissection along embryological planes of the dorsal mesentery yielding a specimen containing the entire intact vasculo-lymphatic network. TME reduces the risk of an involved circumferential resection margin (CRM) and resulted in dramatically reduced recurrence rates and improved survival [10].

Traditionally, rectal cancer was associated with a worse prognosis than colonic tumours. However, since the 1980's and the adoption of TME surgery with multi-modal treatment strategies a shift in prognosis favouring the former has been noted. As a result, there has been increasing interest in using a similar philosophy as employed in TME, in order to reduce local recurrence rates and improve survival in colonic malignancies.

Complete mesocolic excision was first defined by Werner Hohenberger [3], although the individual components had been described by previous authors. CME is based on 3 key principles:

1. Mesocolic plane dissection

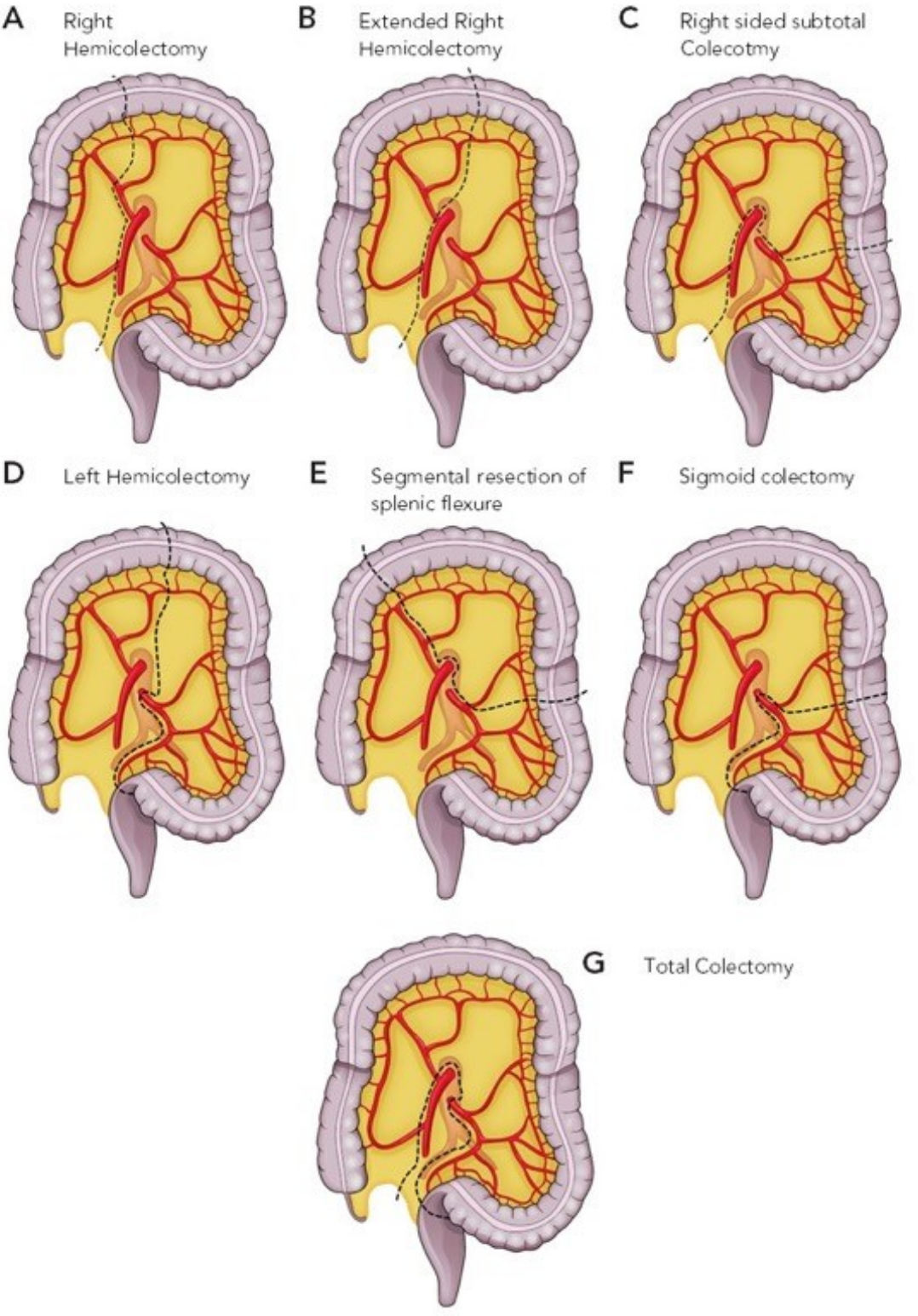
- The main component of CME involves dissection along embryological planes to remove a complete mesocolic envelope in order to excise all lymph nodes draining the tumour.
- The mesenteric vessels are surrounded by two fascia's, one ventral and one dorsal- together they act as an envelope.
- Lymph node metastases very rarely invade beyond the mesocolic plane. By adhering to the mesocolic plane all lymph node and cancer cells will be removed in virtually all specimens.

2.Central Lymph Node Dissection

- Central spread occurs along the feeding vessels. The second component of CME is therefore central vascular ligation in order to remove all the central D3 lymph nodes in a vertical direction [11 12].
- The bowel resection and D3 lymph node dissections are performed in accordance to the principles outlined in table.
- The concept of D3 metastases has mostly been evaluated from the perspective of caecal, right sided and transverse colon tumours.
- Metastases have been found in up to 11% of cases, however the figure usually reported to a range of 0-5.8%. In the MRC CLASICC trial of laparoscopic vs. open surgery for colon cancer, the Dukes C2 rate is 6.5% [13]
- A review of inferior mesenteric artery involvement reported an involvement of <5% [14 15].
- True skip metastases i.e. metastases in the D3 area without D1 or D2 involvement have been found in 0.8-2% of cases [16].

3. Longitudinal Resection

- The final component is resection of an adequate length of bowel
- Adequate longitudinal resection is considered to be 10cm proximal and distal to the tumour (the risk of involvement of D1 lymph nodes beyond this is around 2%) [17].
- This applies to the terminal ileum for caecal tumours. For distal sigmoid tumours 5cm should be sufficient [12].


A Right Hemicolectomy
B Extended Right Hemicolectomy
C Right sided subtotal Colecotmy
D Left Hemicolectomy
E Segmental resection of splenic flexure
F Sigmoid colectomy
G Total Colectomy

6 Anatomy of the Colon and Mesocolon

COLON

The colon is located intraperitoneally, though segments are fixated to the retroperitoneum. The proximal limit of the colon is well defined at the ileocaecal valve. The caecum is the colonic pouch inferior to the upper edge of the ileocaecal valve and, as the ICD10 classification is used in European and American literature, the rest of the colon divided into the following segments: the ascending colon, the hepatic flexure, the transverse colon, the splenic flexure, the descending colon and the sigmoid colon. A uniform definition of the limits of this practical division is inherently impossible. The right colon (midgut derived) and the left colon (hindgut derived) are divided by an undefined line between the right two-thirds and the left third of the transverse colon. The distal limit of the colon is the recto-sigmoid junction which is located at the level of third sacral vertebra (anatomical definition) or at the sacral promontory (surgical definition) [18]. Although the length of the colon depends on an person's height, the length of the rectum and hence the level of the distal colonic margin is often referred to as 15 cm from the anal verge measured by a rigid rectoscope [18].

MESOCOLON

The colon derives from the midgut and hindgut which develops from the endodermal yolk sac. The midgut and hindgut are initially connected only to the posterior abdominal wall by the dorsal mesentery, which similarly to the rest of the endodermal yolk sac is covered by the splanchnic mesodermal layer. Whilst the dorsal mesentery becomes the mesocolon, the splanchnic mesodermal layer becomes the mesocolic fascia covering the entire colon and mesocolon. The intraperitoneal part of the mesocolic fascia is usually referred to as the serosa and visceral peritoneum. The mesocolon is a continuum from the small bowel mesentery to the mesorectum without any distinct demarcation lines, and it contains the vessels, lymphatic structures, and nerves of the colon .

During the 6th-10th gestational weeks the midgut rotates 180° counter clockwise around the axis of the superior mesenteric artery. The ascending and descending colon adhere to the posterior abdominal wall to fixate the loop created by the rotation. A layer of hairy fibres called Toldt's fascia or the mesocolic plane is formed between the mesocolic fascia and the retroperitoneal interface [19]. As a consequence the colon and mesocolon is topographically related to the liver and spleen, the retroperitoneal organs and structures (the kidneys, ureters, gonadal vessels), and most intimately to the duodenum and the pancreas.

VASCULAR SUPPLY OF THE COLON

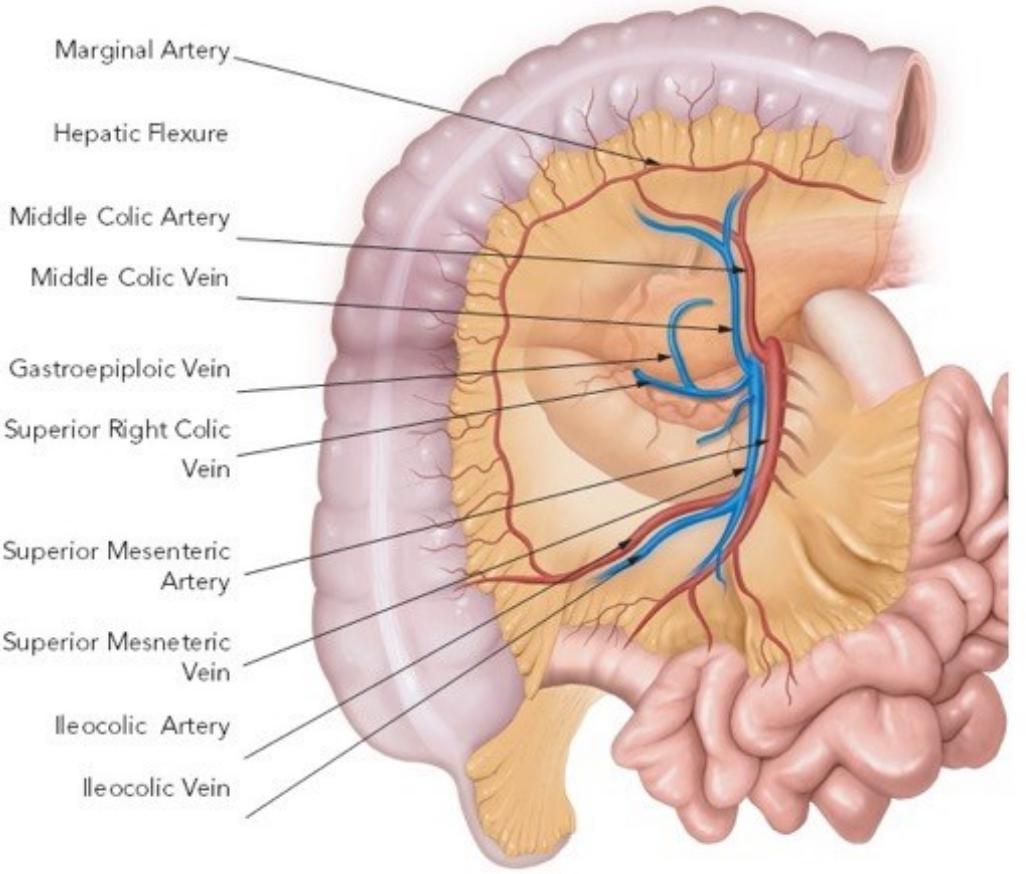
The right colon is supplied by the ileocolic artery (ICA) and middle colic artery (MCA) both of which originate from the superior mesenteric artery (SMA).

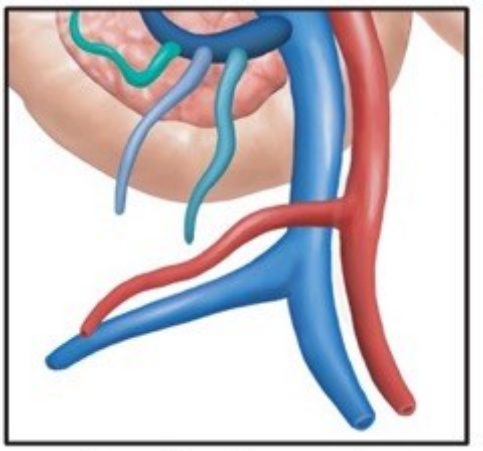
The inferior mesenteric artery supplies the left and sigmoid colon originating directly from the aorta. The branches of these three main branches form the marginal arcades (arteries of Drummond) which supply the colon.

ILEOCOLIC ARTERY AND VEIN

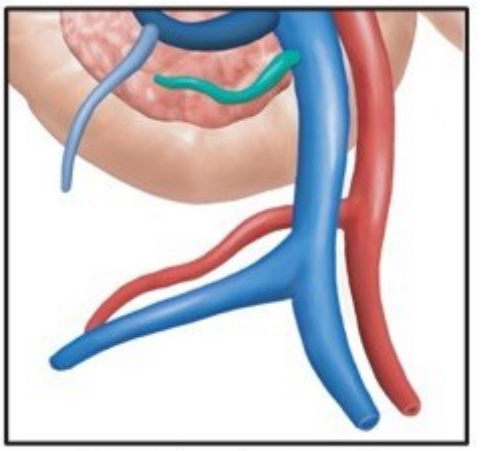
- The ileocolic vessels are the most consistent anatomical structure with a pooled prevalence of 99.7% and 99.8% for the ileocolic vein and artery respectively.
- The ileocolic vein drains into the SMV in 97.6%, into Henle's trunk in 1.9% and the jejunal trunk in 0.5% of patients [20].
- With respect to the SMV the ICA had a posterior trajectory 57.4% of cases and passed anteriorly in 42.6% of cases. This may be contingent on the ethnicity with a posterior position occurring less often in Asian studies compared with 2/3 of European studies [21 22 23].
- The ileocolic vein is relatively consistent and usually follows the course of the ICA and drains into the SMV on its right lateral surface. Variations do occur with drainage into Henle's trunk (1.9%) and jejunal veins (0.5%). The ICV can insert into the SMV up to 3cm cranial to the crossing of ICA over SMV.

Blood supply of Right Colon 7



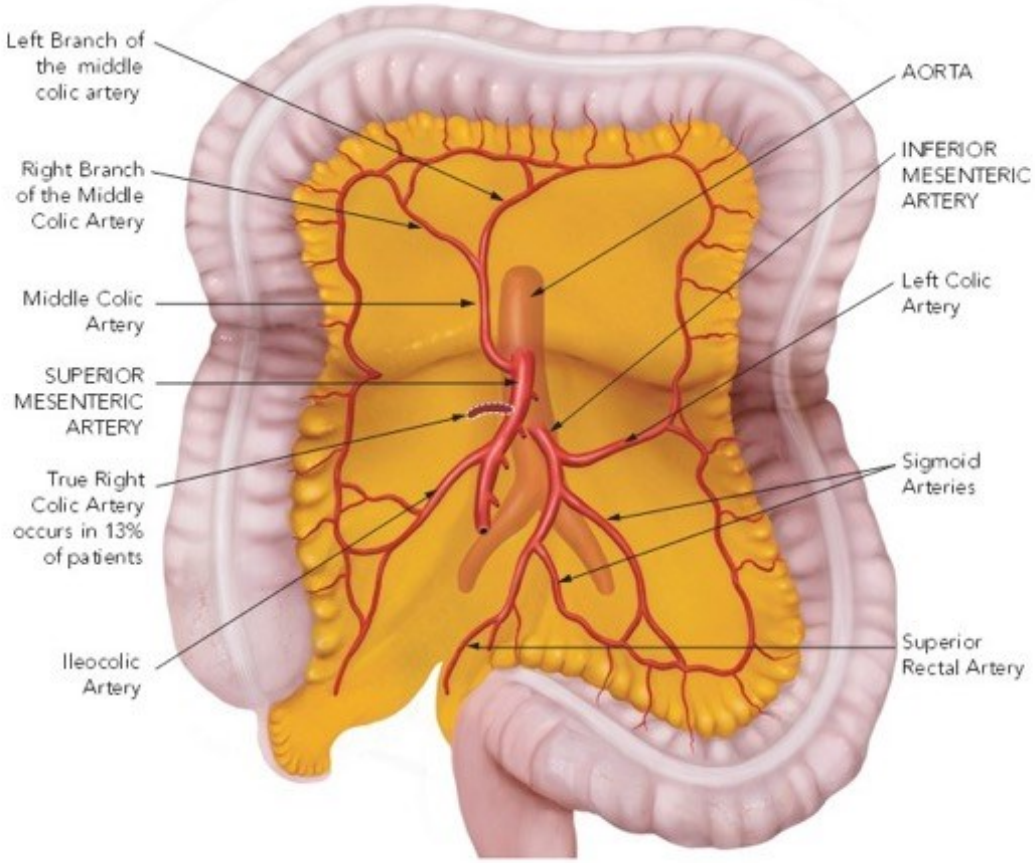


Ileocolic artery passing anteriorly to SMV (40% of patients)

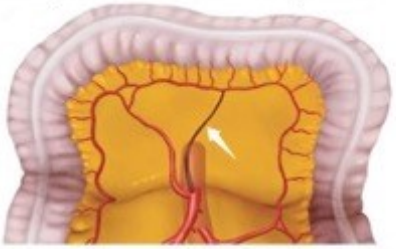


Ileocolic artery passing posteriorly to SMV (60% of patients)

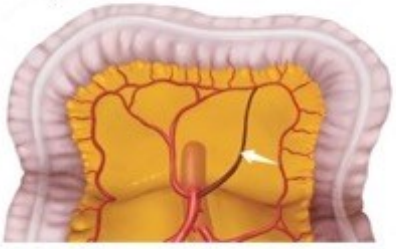
8 Vascular Anatomy of the Colon



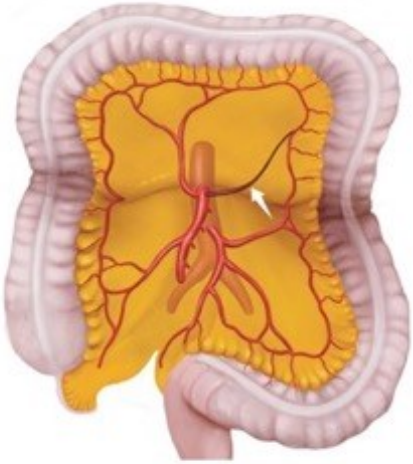
Artery to the Transverse colon with artery to the right angle occurs in around 12% of patients



Accessory artery to the transverse colon occurs in 2% of patients



Accessory to the left colic artery originating from the SMA occurs in 7% of patients



RIGHT COLIC ARTERY

The prevalence of the right colic artery varies significantly depending on the definition used. The three most commonly employed are:

1. An independent branch of the SMA between the MCA and ICA
2. A right branch of the MCA or separate MCA branch arising of the SMA
3. A branch of the ICA

If considered to be an independent branch directly emerging from the SMA, supplying the middle portion ascending colon and running inferiorly to the avascular plane overlying the duodenum, the RCA is only present in 15% of patients.

MIDDLE COLIC VESSELS

The middle colic artery is almost consistent and present in 94.6% of cases. In around 3-36% it has more than one branch arising from the SMA. In a systematic review by Negoi et al. which examined 6090 specimens from 45 separate studies (using CT imaging and cadaveric dissection) there was one MCA in 88.4%, two in 10.6% and three in 1% of cases. The number of MCAs is also dependent on the nomenclature used- i.e. whether the MCA is defined by its origin from the SMA or the colonic territory supplied [20].

The MCA arises from the right SMA in the majority of cases, however there are reports of other parent vessel origins (ICA, RCA, common hepatic artery, coeliac trunk, inferior pancreaticoduodenal artery).

The MCA crosses anteriorly to the SMV, however a rare retromesenteric course has been described 24. In 4-36% of individuals a separate accessory artery arising from the SMA supplies the transverse colon [25].

The Middle Colic Vein has been described as a highly variable vein of the right colon. The nomenclature is unfortunately not uniform. The definition used by Kuzu et al in which the MCV is defined as the marginal veins draining the right two thirds of the transverse colon is perhaps the most surgically useful definition when performing central lymph node dissections [26].

The number of middle colic veins vary with one seen in 70%, two in 26% and three in only 2-4% of patients 20.

The MCV drains into the SMV in the majority of cases (62% - 83.2%). The MCV can also drain into Henle's Trunk, inferior mesenteric vein, jejunal vein, or the splenic vein.

10 Henle's Trunk

HENLE'S TRUNK

The concept of a gastrocolic trunk venous trunk was first proposed by Henle in 1861, who recognised the structure formed by the right gastroepiploic and superior right colonic veins [27]. In practice, a simple gastrocolic trunk as originally described by Henle is rarely observed. The more accurate term of Henle's trunk is formed by the confluence of the right gastroepiploic vein (REV) with/without the anterior superior pancreatico-duodenal veins (ASPDV) and one, two or rarely 3-4 colonic veins (right colic vein [RCV], superior right colic vein [SRCV], middle colic vein [MCV] or ileocolic veins [ICV])

A right colic vein (RCV) is not always present. It is reported to drain into the SMV in up to 25-30% [20,26], but we observe this variation much less commonly in our patients. Rarely, two RCVs draining to the SMV can be present. In 64% of individuals, the RCV drains into the GPCT [26].

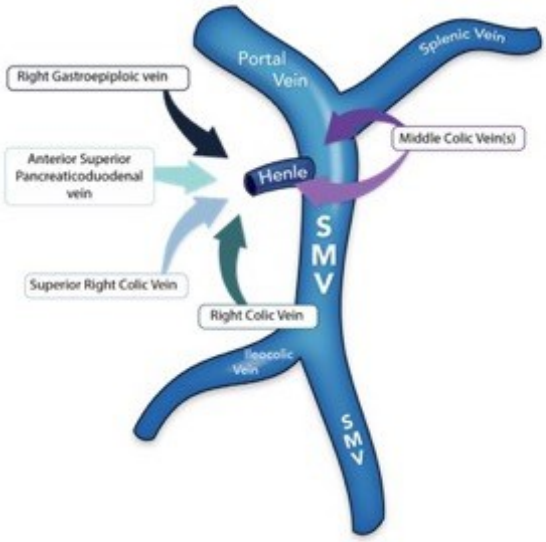
The superior right colic vein (SRCV) is, like the RCV, not consistent, and in some patients it can be difficult to distinguish it from either the ICV or one of more middle colic veins (MCV). The SRCV has been observed in 29%; joining the GPCT in most individuals and only in a few percent of individuals directly into the SMV [26].

Henle's trunk connects the blood supplies of the stomach, pancreas, duodeunum and colon.

Henle's trunk has four main subtypes proposed based on the specific confluence of constituent veins:

1. Gastro-colic Trunk (GCT)
   - (RGEV + SRCV)
2. Gastro-pancreatico Trunk (GPT)
   - (RGEV + ASPDV)
3. Gastro-pancreatico-duodenal colic Trunk (GPCT)
   - (RGEV + ASPDV + 1 colic RCV)
   - (RGEV + ASPDV + 1 colic SRCV)
   - (RGEV + ASPDV + 1 colic MCV)
   - (RGEV + ASPDV + 2 colic SRCV + RCV)
   - (RGEV + ASPDV + 2 colic SRCV + MCV)
   - (RGEV + ASPDV + 2 colic RCV + MCV)
   - (RGEV + ASPDV + 2 colic RCV + ICV)
   - (RGEV + ASPDV + 3 colic RCV + SRCV + MCV)
   - (RGEV + ASPDV + 3 colic RCV + SRCV + MCV)
   - (RGEV + ASPDV + 3 colic RCV + SRCV + ICV)
4. Colo-pancreatico Trunk (CPT)
   - (ASPDV + SRCV)

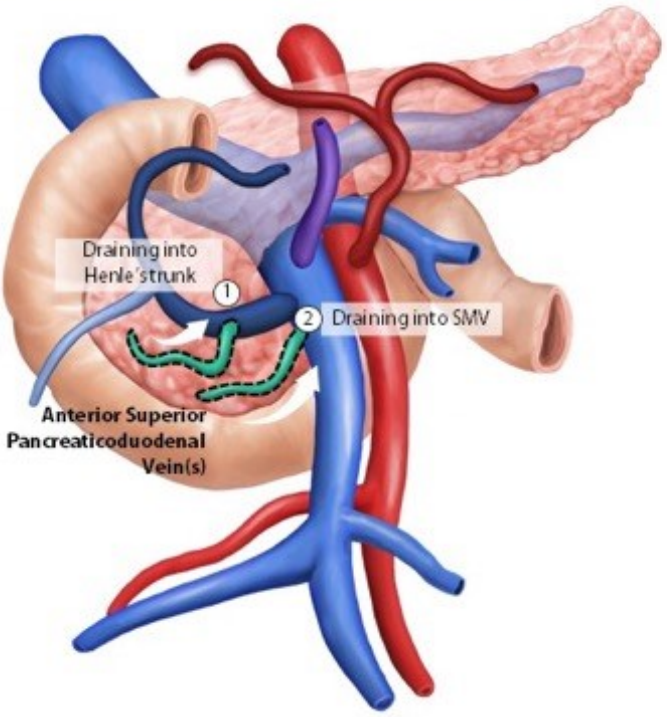
However, attempts to try and classify Henle's trunk may be not be the best approach. Surgeons performing CME surgery must appreciate that constituent vessels may or may not be present and can drain into a variety of locations in a wide variety of combinations (see Tables 1 and 2). Therefore, adequate pre-operative planning using CT imaging (+/- 3D reconstructions) and careful intra-operative dissection is essential.

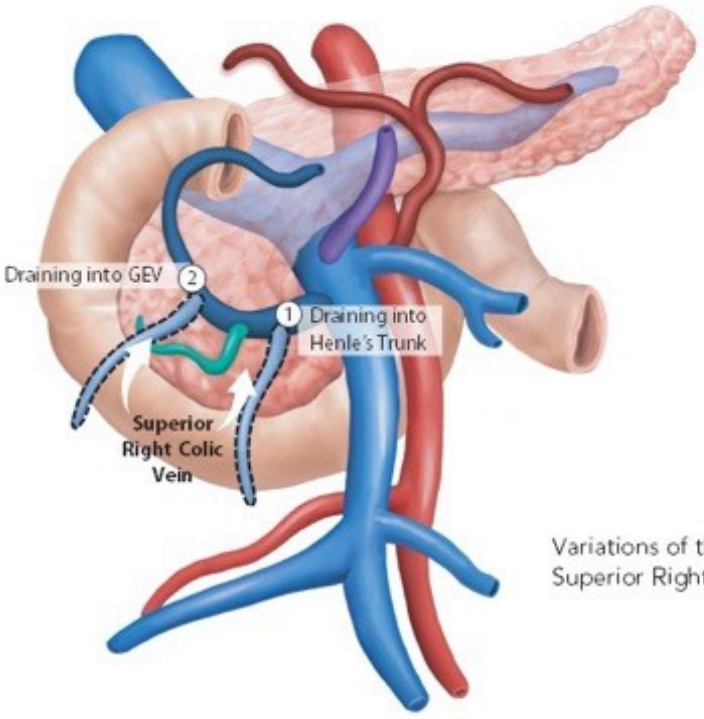


Schematic diagram of henle's trunk and venous drainage of right/transverse colon

12 Henle's Trunk

Variations of the drainage of the Anterior Superior Pancreaticoduodenal Vein(s)





Variations of the drainage of the Superior Right Colon Vein

16 Lymphatic Drainage of the Colon

LEFT SIDED COLONIC ARTERIAL SUPPLY

The anatomy of the left sided colonic blood supply is simpler, though variations exist. The inferior mesenteric artery supplies the left colonic arterial supply. The left colic artery (LCA) arises from the IMA around 25-40mm from its origin from the aorta. The LCA is present in 95% of cases, supplying the descending colon and splenic flexure. An accessory left colonic artery arising from the SMA is observed in 7% of patients [39].
The IMA continues in the sigmoid mesocolic package giving off one to five sigmoid artery branches before terminating as the superior rectal artery.

The sigmoid artery (SA) most frequently originates as a direct branch of the IMA (type1), occurring in 41-58% of individuals. Alternatively, the SA can originate from the LCA (type 2; 27-45%) or at the origin of the LCA from the IMA (type 3; 9-15%). The most common number of sigmoid arteries is two (21-40%), three (32-50%) and four (7-25%) [11 40].

An arcade, known as the arcade Riolin, located centrally to the marginal artery connecting the MCA and IMA or LCA is rarely observed. It is a tortuous artery running close to the inferior mesenteric vein [41].

The venous drainage of the left colon follows the peripheral arteries and ultimately drains into the inferior mesenteric vein (IMV). The IMV follows the IMA for a short distance before ascending cranially parallel to the aorta and dorsally to the. Pancreas before ultimately draining into the splenic vein. In 5-20% the IMV drains into the SMV and in 5-10% into the confluence of the SMV and splenic vein. Surgically, this is important as it can result in an IMV more medial than expected [35].

LYMPHATIC DRAINAGE OF THE COLON

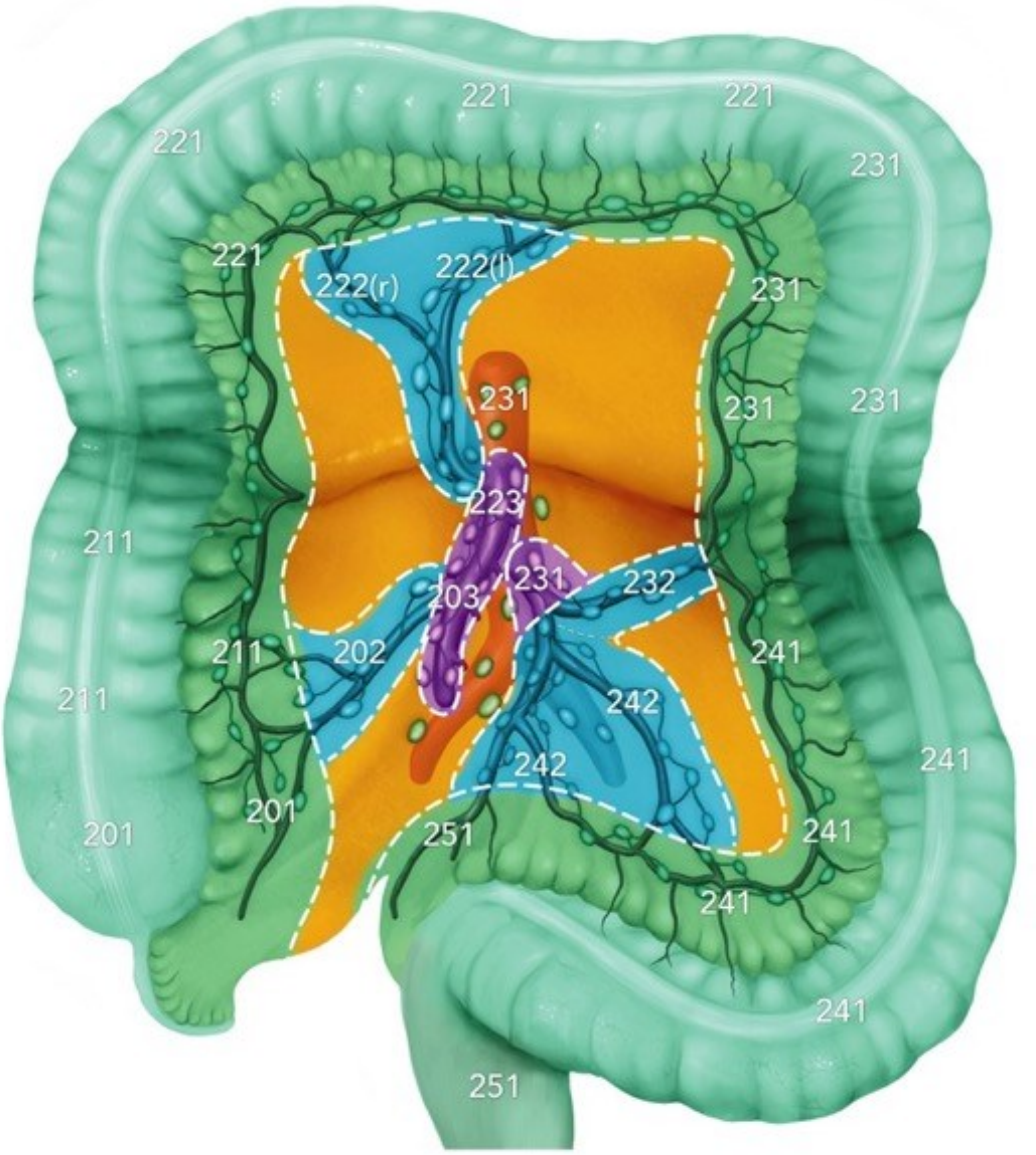
The lymphatic drainage and nodes develop embyologically alongside the arterial vessels supplying the colon. Lymphatic nodes at risk of metastatic involvement can be divided into mesocolic or extramesocolic [11].

The mesocolic lymph nodes are contained within the mesocolic envelope and can be divided by location into three groups as described by the Japanese Society for Cancer of the Colon and Rectum (JSCCR) [42](see table and figure opposite). The prefix of D is used to describe the extent of the surgical dissection to avoid confusion with the N of the TNM classification.

The extent of the lymph node dissection- according to JSCCR 11

D1	Complete dissection of the epicolic lymph nodes attached to the colon and paracolic lymph nodes along the marginal artery in the relevant colonic section along tumour-supplying arteries.
D2	Intermediate lymph nodes along the tumour-supplying artery (ileocolic, right, middle, left colic, sigmoid, or inferior mesenteric arteries from the origin of last sigmoid artery to origin of left colic artery.)
D3	Complete dissection of D1 to D2 and central lymph nodes. For left sided tumours along the inferior mesenteric artery between the aorta and left colic artery. For right sided (including up to mid transverse tumours) lymph nodes along the SMV and lateral to SMA
D4	Beyond level D3 i.e. para-aortal and along SMA between its origin from aorta and MCA.

The lymphatic drainage of the transverse colon and mesocolon with the greater omentum and pancreas can converge. This is as a result of embryonic fusion of these structures- consequently the infrapyloric and gastroepiploic LN are considered local lymph nodes [11].



Green = D1 Lymph nodes
Blue = D2 Lymph nodes
Purple = D3 Lymph nodes

18 Nervous supply of the Colon

NERVES

The right colon is innervated through the nerve plexus surrounding the SMA. It is a continuation of the coeliac nerve plexus and ganglions of the superior mesenteric nerve plexus [43,44]. The sympathetic innervation is supplied from the 5th to 12th thoracic segments, and the parasympathetic innervation from the vagus nerve [44].

The left colon's sympathetic innervation is supplied by lumbar segments through the inferior mesenteric nerves plexus and nerves running along the IMA. The inferior mesenteric nerve plexus' relation to the origin of the IMA may vary [45,46]. The parasympathetic innervation is supplied by the 2nd to 4th sacral segments though nerves from the inferior and superior hypogastric plexus running though the mesorectum and sigmoid mesocolon to the colon wall [43,44].

The sympathetic innervation is responsible for colonic wall relaxation and contraction of ileocolic valve and vascular musculature. The parasympathetic innervation is responsible for increased secretion and bowel motility. The colonic afferent autonomic nerves are responsible for sensation of pain and distension [44].

REFERENCES

1. Bokey, E. L. et al. Surgical technique and survival in patients having a curative resection for colon cancer. Dis. Colon Rectum 46, 860–866 (2003).

2. Jagoditsch, M. et al. Long-term prognosis for colon cancer related to consistent radical surgery: Multivariate analysis of clinical, surgical, and pathologic variables. World J. Surg. 24, 1264–1270 (2000).

3. Hohenberger, W., Weber, K., Matzel, K., Papadopoulos, T. & Merkel, S. Standardized surgery for colonic cancer: Complete mesocolic excision and central ligation - Technical notes and outcome. Color. Dis. 11, 354–364 (2009).

4. Bertelsen, C. A. et al. Disease-free survival after complete mesocolic excision compared with conventional colon cancer surgery: A retrospective, population-based study. Lancet Oncol. 16, 161–168 (2015).

5. Storli, K. E. et al. Short term results of complete (D3) vs. standard (D2) mesenteric excision in colon cancer shows improved outcome of complete mesenteric excision in patients with TNM stages I-II. Tech. Coloproctol. 18, 557–64 (2014).

6. Bertelsen, C. A. Complete mesocolic excision an assessment of feasibility and outcome. Dan. Med. J. 64, pii: B5334 (2017).

7. Bertelsen, C. A. et al. The risk of long-term bowel dysfunction after resection for sigmoid adenocarcinoma: a cross-sectional survey comparing complete mesocolic excision with conventional surgery. Color. Dis. 1–11 (2018). doi:10.1111/codi.14318

8. Bertelsen, C. A. et al. Long-term Functional Outcome After Right-Sided Complete Mesocolic Excision Compared With Conventional Colon Cancer Surgery. Dis. Colon Rectum 61, 1063–1072 (2018).

9. Thorsen, Y. et al. Bowel function and quality of life after superior mesenteric nerve plexus transection in right colectomy with D3 extended mesenterectomy. Tech. Coloproctol. 20, 445–453 (2016).

10. Knol, J. J., D'Hondt, M., Souverijns, G., Heald, B. & Vangertruyden, G. Transanal endoscopic total mesorectal excision: technical aspects of approaching the mesorectal plane from below—a preliminary report. Tech. Coloproctol. 19, 221–229 (2015).

11. Bertelsen, C. A. Complete mesocolic excision. Tech. Coloproctol. 18, 773–774 (2014).

12. Søndenaa, K. et al. The rationale behind complete mesocolic excision (CME) and a central vascular ligation for colon cancer in open and laparoscopic surgery: Proceedings of a consensus conference. Int. J. Colorectal Dis. 29, 419–428 (2014).

13. Jayne, D. G. et al. Randomized trial of laparoscopic-assisted resection of colorectal carcinoma: 3-Year results of the UK MRC CLASICC trial group. J. Clin. Oncol. 25, 3061–3068 (2007).

14. Kang, J., Hur, H., Min, B. S., Kim, N. K. & Lee, K. Y. Prognostic impact of inferior mesenteric artery lymph node metastasis in colorectal cancer. Ann. Surg. Oncol. 18, 704–710 (2011).

15. Titu, L. V., Tweedle, E. & Rooney, P. S. High tie of the inferior mesenteric artery in curative surgery for left colonic and rectal cancers: A systematic review. Dig. Surg. 25, 148–157 (2008).

16. Tan, K. Y. et al. Distribution of the first metastatic lymph node in colon cancer and its clinical significance. Color. Dis. 12, 44–47 (2010).

17. Y., S. et al. Benefit of three-dimensional printing in robotic laparoscopic renal surgery: Tangible surgical navigation using a patient-based three-dimensional printed kidney. Eur. Urol. Suppl. 13, e1124 (2014).

18. Guidelines for the Management of Colorectal Cancer. 3rd edition. (2007).

19. Culligan, K., Remzi, F. H., Soop, M. & Coffey, J. C. Review of nomenclature in colonic surgery – Proposal of a standardised nomenclature based on mesocolic anatomy. Surg. 11, 1–5 (2012).

20. Negoi, I., Beuran, M., Hostiuc, S., Negoi, R. I. & Inoue, Y. Surgical anatomy of the superior mesenteric vessels related to colon and pancreatic surgery: A systematic review and meta-analysis. Sci. Rep. 8, 1–15

9.1.1.1.1.1.1.1 Appendix 4.2 Link to interrater reliability study online questionnaire



https://forms.office.com/r/VSjWb4qgLZ

9.1.1.1.1.1.1.2 Appendix 4.3 Mesenteric vessel defnition

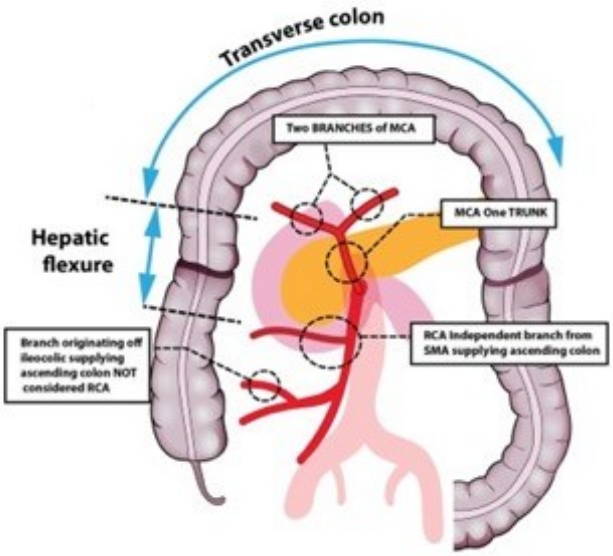
3DCME: Inter/Intra rater reliability study

Vessel Definitions and Terminology

Vessel classification with review of literature and what is deemed to be most clinically useful. Naming of vessels largely determined by the segment of colon supplied or drained.

The transition between the caecum and ascending colon is delineated by the ileocaecal valve. In lieu of any robust radiological/anatomical precise definitions delineating the hepatic flexure, transverse colon and splenic flexure we leave it to the discretion of each reviewer.

Ileocolic Artery and Vein



Highly consistent vessel present in over 99% of patients. Supplies and drains the caecum and proximal ascending colon

Right Colic Artery

In the literature has a highly varied definition. For this study an Right colic artery is defined as an independent branch arising from the SMA to supply the ascending colon.

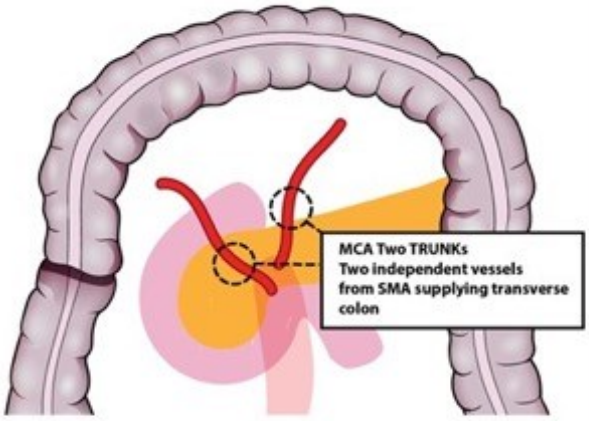
Branches arising from the ileocolic artery that supply the ascending colon should not be considered an RCA for the purposes of the study questionnaires.

Middle Colic Arteries

Middle colic arteries are defined as branches arising from the SMA to supply the transverse colon.

In the typical configuration the MCA will consist of one trunk and will bifurcate into two branches.

Figure two depicts two independent MCA trunks arising from the SMA



3DCME: Inter/Intra rater reliability study

Vessel Definitions and Terminology

Right Colic Vein

Drains the ascending colon.

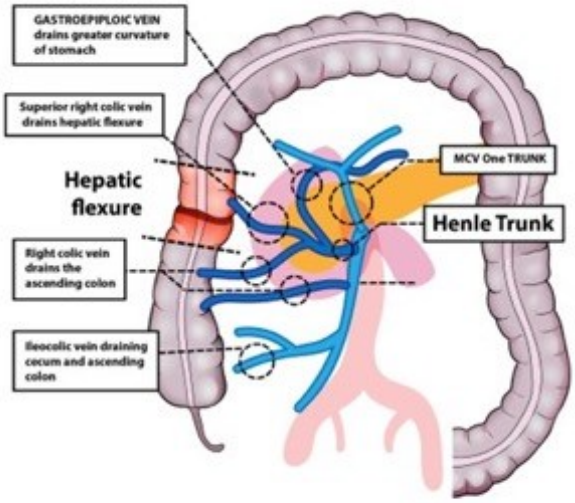
Superior Right Colic Vein

Drains the hepatic flexure

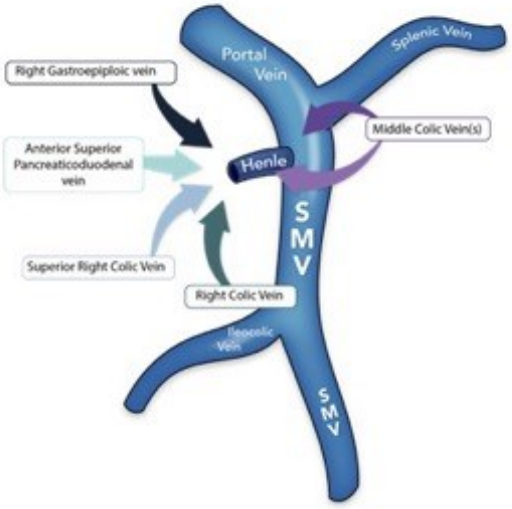
Anterior superior pancreatico duodenal vein

Drains the pancreatic head and duodenum

Henles' Trunk



Defined as the confluence of the right gastroepiploic vein (REV) with/without the anterior superior pancreatico-duodenal veins (ASPDV) and one, two or rarely 3-4 colonic veins (right colic vein [RCV], superior right colic vein [SRCV], middle colic vein [MCV] or ileocolic veins [ICV]). Henle is generally present in most cases but may be absent with each vessel draining directly into the SMV as separate vessels.



We have classified Henle by the constituent vessels:

1. Gastro-colic Trunk (GCT)
   - (RGEV + SRCV)
2. Gastro-pancreatico Trunk (GPT)
   - (RGEV + ASPDV)
3. Gastro-pancreatico-duodenal colic trunk (GPCT)
   - (RGEV + ASPDV + 1 colic RCV)
   - (RGEV + ASPDV + 1 colic SRCV)
   - (RGEV + ASPDV + 1 colic MCV)
   - (RGEV + ASPDV + 2 colic SRCV + RCV)
   - (RGEV + ASPDV + 2 colic SRCV + MCV)
   - (RGEV + ASPDV + 2 colic RCV + MCV)
   - (RGEV + ASPDV + 2 colic RCV + ICV)
   - (RGEV + ASPDV + 3 colic RCV + SRCV +MCV)
   - (RGEV + ASPDV + 3 colic RCV + SRCV +MCV)
   - (RGEV + ASPDV + 3 colic RCV + SRCV + ICV)
4. Colo-pancreatico Trunk (CPT)
   - (ASPDV + SRCV)

9.1.1.1.1.1.1.3 Appendix 5.1 Example anatomy questionaire used in feasibility study

Complete Mesocolic Excision
Pre-operative Planning Questionnaire

Case Number: 3DCME003

Surgeon Name: Toorenvliet

Time spent on Scan/ 3D model interpretation (Minutes): 15

CT Scan ■ 3D virtual model ☐

Where does the Ileocolic Vein drain?	■ SMV	☐ Henle Trunk	☐ Not Sure
	☐ Jejunal vein	☐ Not present	
What is the Ileocolic Artery trajectory related to the SMV?	■ Anterior	☐ Posterior	
	☐ Not present	☐ Not sure	
Is the RCA present? (RCA defined as an artery originating independently from the SMA between the ICA and MCA)	☐ Yes	■ No	
	☐ Not sure		
What is the RCA trajectory related to the SMV?	☐ Anterior	☐ Posterior	
	■ Not applicable	☐ Not sure	
What is the origin of the MCA? (please tick all that apply- you may select more than one)	■ SMA	☐ Left colic artery	
	☐ Splenic Artery	☐ Ileocolic artery	
	☐ Hepatic Artery	☐ Coeliac artery	
	☐ MCA absent	☐ Not sure	
How many trunks does the MCA have?	☐ No MCA	☐ One	☐ Not sure
	■ Two	☐ Three	
Number of MCV trunks?	☐ No MCV	■ One	☐ Not sure
	☐ Two	☐ Three	
Where does the MCV drain into? (please tick all that apply- you may select more than one)	■ SMV	☐ Splenic Vein	☐ Not sure
	☐ Henle's Trunk	☐ IMV	

3DCME Study

Version 2 Oct 2019

Please select the structures which form Henle's Trunk?

(please tick all that apply- you may select more than one)

- [x] Right Gastroepiploic Vein
- [x] Anterior Superior Pancreatico-duodenal Vein
- [ ] Superior Right Colic Vein
- [ ] Right Colic Vein
- [ ] Ileocolic Vein
- [ ] Middle Colic Vein
- [ ] Not sure

Which Henle's trunk type is present?

(please tick all that apply- you may select more than one)

- [ ] Gastrocolic Trunk (GCT)
- [x] Gastropancreatic Trunk (GPT)
- [ ] Gastropancreaticocolic Trunk (GPCT)
- [ ] Colopancreatic Trunk (CPT)
- [ ] Not sure

What is the trajectory of the first jejunal vein/trunk related to the SMA as it drains into the SMV?

- [ ] Anterior
- [x] Posterior
- [ ] Not sure

Where does the first jejunal vein/trunk lie with respect to the MCA origin

- [x] Above/Cranial
- [x] Below/caudal
- [ ] Not sure

9.1.1.1.1.1.1.4 Appendix 5.2 Example clinical proforma

Patient ID 3DCME003

NHS London North West University Healthcare NHS Trust

CME patient demographics and tumour proforma

Operating Surgeon: Nonner / Toorenvliet

Hospital: Ikazia

Patient No.	Age	Sex	BMI
3DCME003	57	Male	27

Co-morbidities

Previous MI/IHD ☐	COPD ☐	Hemiplegia ☐
Heart failure ☐	Peptic Ulcer Disease ☐	Moderate-severe CKD ☐
Stroke/TIA ☐	Liver disease Mild ☐	Solid tumour ☐
Dementia ☐	Severe ☐	Leukemia ☐
	Diabetes Mild ■	AIDS ☐
	End organ damage ☐	

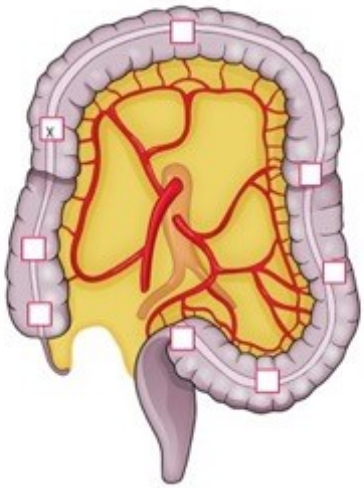
ASA: 2

Previous intra-abdominal operations?	Please specify: No
Other colonic pathology	☐ IBD ☐ Polyposis syndrome ☐ Lynch (Hereditary nonpolyposis colorecal cancer syndrome)

Procedure:

☐ Total Colectomy	☐ Transverse Mesocolectomy
☐ Subtotal Colectomy	☐ Left Hemimesocolectomy
■ Right Hemimesocolectomy	☐ Sigmoid Mesocolectomy
☐ Extended Right Mesocolectomy	☐ Segmentectomy

Tumour Location



Histopathology

- [■] Adenocarcinoma
  - [ ] Well differentiated
  - [ ] Moderately differentiated
  - [■] Poorly Differentiated

WHO SUBTYPE

- [■] Not otherwise specified
- [ ] Mucinous
- [ ] Cribriform comedo-type
- [ ] Serrated
- [ ] Medullary
- [ ] Micropapillary
- [ ] Colloid
- [ ] Signet ring cell

- [ ] Neuroendocrine
- [ ] Spindle cell
- [■] Undifferentiated
- [ ] Squamous cell
- [ ] Adenosquamous
- [ ] Other

TNM staging

Primary Tumour		
Tx	Primar tumour cannot be assessed	☐
Tis	Carcinoma in situ: Intraepthelial or invasion of lamina propria	☐
T1	Tumour invades submucosa	☐
T2	Tumour invades muscularis propria	☐
T3	Tumour invades through muscularis propria into pericolorectal tissues	☑
T4a	Tumour penetrates to the surface of visceral peritoneum	☐
T4b	Tumour directly invades or is adherant to other organs or structures	☐

Regional Lymph nodes		
Nx	No regional lymph nodes cannot be assessed	☐
N0	No regional lymph node metastasis	☐
N1	Metastasis in one regional lypmph nodes	☑
N1a	Metastasis to one regional lymph node	☐
N1b	Metastasis in 2-3 regional lymph nodes	☐
N1c	Tumour deposit(s) in the subserosa, mesentery or non peritonealised pericolic or perirectal tissues without regional metastasis	☐
N2	Metastasis in 4 or more regional lymph nodes	☐
N2a	Metastases in 4-6 regional lymph nodes	☐
N2b	Metastases in more regional lymph nodes	☐

Distant metastasis		
M0	No distant metastasis	☑
M1	Distant metastasis	☐
M1a	Metastasis confined to one organ or site (e.g. liver, lung, ovary, non regional node)	☐
M1b	Metastases in one or more than one organ/site or the peritoneum	☐

Histopathology

Maximum tumour diameter (mm)	Distance of tumour to nearer longitudinal end (Longitudinal margin)	Tumour Perforation
38mm	11 cm	☐ Yes (R0) ■ No (R1)
Local Invasion	**Max. distance beyond muscularis propria (mm)**	**Complete resection (by1mm) at all margins**
		■ Yes (R0) ☐ No (R1) ☐ No (R2)
Number of Lymph nodes	**Number of involved lymph nodes**	**Highest node involved?**
37	3	☐ Yes ☐ No
Deepest venous invasion	**Deepest lymphatic invasion**	**Deepest perineural invasion**
☐ None ☐ Intramural ■ Extramural	☐ None ■ Intramural ☐ Extramural	☐ None ☐ Intramural ☐ Extramural
Separate abnormalities **Polyps**	**Polyposis syndrome**	**CME grading**
☐ Yes ■ No Site Number	☐ FAP ☐ Juvenile Polyposis Syndrome ☐ Peutz Jeghers ☐ Serrated polypois syndrome ☐ MYH associated polyposis	■ Mesocolic ☐ Intramesocolic ☐ Intra-muscularis
Histologically confirmed distant mestasis?	**Site of distant metastasis**	**Synchromous carcinoma**
☐ Yes ■ No		☐ Yes ■ No

9.1.1.1.1.1.1.5 Appendix 5.3 Subjective model feedback questionnaire

Patient ID 3

Surgeon toorenvliet

St Mark's Hospital

NHS London North West University Healthcare NHS Trust



3DCME Surgeon Feedback

This was my first experience using 3D virtual models derived from patient anatomy — Yes ☐ No ■

Do you routinely review the pre-operative imaging yourself prior to performing CME surgery? — Yes ■ No ☐

I used the model — Pre-operatively ■ Intra-operatively ☐

Please rate the following statement (circle number)

1. The 3D model is easy to understand								
Strongly Disagree	1 ○	2 ○	3 ○	4 ○	5 ○	6 ○	7 ◉	Strongly Agree
2. The 3D model improved my understanding of the patient's anatomy								
Strongly Disagree	1 ○	2 ○	3 ○	4 ○	5 ◉	6 ○	7 ○	Strongly Agree
3. The 3D model accurately predicted the patient's vascular anatomy								
Strongly Disagree	1 ○	2 ○	3 ○	4 ○	5 ○	6 ○	7 ◉	Strongly Agree
4. The 3D model was easier to understand than a 2D CT scan								
Strongly Disagree	1 ○	2 ○	3 ○	4 ○	5 ○	6 ○	7 ◉	Strongly Agree
5. Do you think the CT was more elucidative than 3D reconstructions to correctly diagnose and interpret these images								
Strongly Disagree	1 ○	2 ○	3 ◉	4 ○	5 ○	6 ○	7 ○	Strongly Agree
6. The 3D model helped determine my operative approach								
Strongly Disagree	1 ○	2 ○	3 ○	4 ○	5 ◉	6 ○	7 ○	Strongly Agree
7. The use of a 3D model for pre-operative planning significantly changed my operative approach								
Strongly Disagree	1 ○	2 ○	3 ◉	4 ○	5 ○	6 ○	7 ○	Strongly Agree
8. The use of the 3D model helped me anticipate and avoid potential complications								
Strongly Disagree	1 ○	2 ○	3 ○	4 ○	5 ◉	6 ○	7 ○	Strongly Agree

9. I would recommend the use of 3D virtual models to colleagues								
Strongly Disagree	1 ○	2 ○	3 ○	4 ○	5 ○	6 ◉	7 ○	Strongly Agree
10. The use of the 3D virtual model was essential to completing the operation								
Strongly Disagree	1 ○	2 ○	3 ◉	4 ○	5 ○	6 ○	7 ○	Strongly Agree
11. I would like 3D virtual models to be part of my routine pre-operative work-up								
Strongly Disagree	1 ○	2 ○	3 ○	4 ○	5 ○	6 ◉	7 ○	Strongly Agree
12. The use of a 3D virtual model made dissection quicker								
Strongly Disagree	1 ○	2 ○	3 ○	4 ○	5 ○	6 ◉	7 ○	Strongly Agree
13. I would prefer a physical 3D printed model								
Strongly Disagree	1 ◉	2 ○	3 ○	4 ○	5 ○	6 ○	7 ○	Strongly Agree
14. The virtual 3D model did not help								
Strongly Disagree	1 ◉	2 ○	3 ○	4 ○	5 ○	6 ○	7 ○	Strongly Agree
15. The 3D virtual model met my expectations								
Strongly Disagree	1 ○	2 ○	3 ○	4 ○	5 ○	6 ◉	7 ○	Strongly Agree
16. I would request a 3D reconstruction if available for CME planning								
Strongly Disagree	1 ○	2 ○	3 ○	4 ○	5 ○	6 ◉	7 ○	Strongly Agree
17. I would use 3D virtual models in other areas of my practice								
Strongly Disagree	1 ○	2 ○	3 ○	4 ○	5 ◉	6 ○	7 ○	Strongly Agree
18. 3D virtual models would be useful in training junior surgeons								
Strongly Disagree	1 ○	2 ○	3 ○	4 ○	5 ○	6 ○	7 ◉	Strongly Agree

Comments

9.1.1.1.1.1.1.6 Appendix 6.1 Treament and Quality of life preferences questionnaire

3DCC Study
Questionnaire 2

St Mark's Hospital

NHS
London North West University Healthcare
NHS Trust

Treatment and Quality of Life Preferences

Please tick your preference for type of treatment for your cancer

A	An extensive operation with a better chance of cure but has a higher risk of serious complications that impact my quality of life	☐
B	An less extensive operation that balances the chances of cure with reducing the risk of serious complications	☐
C	An operation to help my symptoms and improve my quality of life but not cure my disease	☐
D	Other treatment	☐

Please Select (tick) which option best describes you

A	Quality of life is all that matters	☐
B	Quality of life is more important but length of life matters,	☐
C	Length of life is more important but quality of life matters	☐
D	Length of life is all that matters	☐

Please Select (tick) which option best describes you

	Not at all	Somewhat	Moderately	Quite a bit	Very Important
How important is quality of life to you?	☐	☐	☐	☐	☐
How important is length of life to you?	☐	☐	☐	☐	☐

3DCC Study
Questionnaire 2

Please rate how important the following areas are to you:

	Not at all	Somewhat	Moderately	Quite a bit	Very Important
Getting back to work	☐	☐	☐	☐	☐
Minimising pain/ discomfort	☐	☐	☐	☐	☐
Maintaining my independence	☐	☐	☐	☐	☐
Avoiding a stoma	☐	☐	☐	☐	☐
Having control of bowels	☐	☐	☐	☐	☐
Maintaining sexual fuction	☐	☐	☐	☐	☐
Being able to spend time with friends and family	☐	☐	☐	☐	☐
Minimising side effects of any treatment	☐	☐	☐	☐	☐

9.1.1.1.1.1.1.7 Appendix 6.2 patient expected anatomical and fucntional outcome questionnaire and subjective feedback

3DCC Study
Questionnaire 3 Colorectal Cancer patient questionnaire

St Mark's Hospital

NHS London North West University Healthcare NHS Trust

Colorectal Cancer Patient Questionnaire

The planned procedure will operate on/remove
(Please tick as appropriate. You may select more than one option)

Organs

- ☐ Part of the colon
- ☐ All of the colon
- ☐ Rectum
- ☐ Anus (sewing up of the bottom)
- ☐ Bladder
- ☐ Kidney

Female

- ☐ Uterus (womb)
- ☐ Ovaries
- ☐ Part of vagina
- ☐ All of the vagina

Male

- ☐ Part of prostate
- ☐ All of prostate

Other

- ☐ Bone (e.g. tailbone)
- ☐ Muscle
- ☐ Don't know/not sure
- ☐ Nerves
- ☐ Large blood vessels

Stoma

Will you need a stoma (a bag)?

- ☐ Yes, a permanent stoma for faeces (stool)
- ☐ Yes, a permanent stoma for urine
- ☐ Yes, two stomas one for faeces (stool) and one for urine
- ☐ Yes, I will have a temporary stoma with a plan to reverse it in the future
- ☐ No stoma is planned but there is a small chance that during the operation one may need one to be formed for safety
- ☐ No

The operation may effect (please tick as appropriate- some of the options may not be relevant to you):

My mobility (ability to walk)

- ☐ No effect
- ☐ Mild effect on mobility / may require walking aid
- ☐ Likely significant impact on mobility

Bowel function

- ☐ No effect
- ☐ Not applicable I will have a stoma
- ☐ May need to go to open my bowels more often
- ☐ May have difficulty controlling stool/flatus (incontinence)

Urinary function

- ☐ No effect
- ☐ Not applicable I will have a stoma for urine
- ☐ May need to pass urine more often
- ☐ May have difficulty controlling urine (incontinence)

Sexual function

Male

- ☐ No Change
- ☐ Difficulty achieving/ maintaining an erection possible
- ☐ Difficulty acheiving/ maintaining an erection likely

Female

- ☐ No Change
- ☐ Some changes in Sexual function
- ☐ Major changes in sexual function



3DCC Study

Questionnaire 3

NHS
London North West University Healthcare
NHS Trust

I am satisfied with my understanding of my operation:

✗	**Completely Disagree**	1 ☐	2 ☐	3 ☐	4 ☐	5 ☐	6 ☐	7 ☐	**Completely Agree** ✓

I understand why my operation is being performed:

✗	**Completely Disagree**	1 ☐	2 ☐	3 ☐	4 ☐	5 ☐	6 ☐	7 ☐	**Completely Agree** ✓

I received the right amount of information:

✗	**Completely Disagree**	1 ☐	2 ☐	3 ☐	4 ☐	5 ☐	6 ☐	7 ☐	**Completely Agree** ✓

Seeing my scans/3D model was helpful:

✗	**Completely Disagree**	1 ☐	2 ☐	3 ☐	4 ☐	5 ☐	6 ☐	7 ☐	**Completely Agree** ✓

It was difficult to understand what the scan/3D model showed:

✗	**Completely Disagree**	1 ☐	2 ☐	3 ☐	4 ☐	5 ☐	6 ☐	7 ☐	**Completely Agree** ✓

Understanding my disease is important to me:

✗	**Completely Disagree**	1 ☐	2 ☐	3 ☐	4 ☐	5 ☐	6 ☐	7 ☐	**Completely Agree** ✓

The right amount of time was spent explaining my operation:

✗	**Completely Disagree**	1 ☐	2 ☐	3 ☐	4 ☐	5 ☐	6 ☐	7 ☐	**Completely Agree** ✓

I felt involved with the decsion making around my care:

✗	**Completely Disagree**	1 ☐	2 ☐	3 ☐	4 ☐	5 ☐	6 ☐	7 ☐	**Completely Agree** ✓

NHS
London North West
University Healthcare
NHS Trust

I don't understand the potential benefits of the operation:

	1	2	3	4	5	6	7	
Completely Disagree	☐	☐	☐	☐	☐	☐	☐	**Completely Agree**

I understand the potential complications:

	1	2	3	4	5	6	7	
Completely Disagree	☐	☐	☐	☐	☐	☐	☐	**Completely Agree**

I am clear about the expected recovery time:

	1	2	3	4	5	6	7	
Completely Disagree	☐	☐	☐	☐	☐	☐	☐	**Completely Agree**

I understand how the operation may effect my quality of life:

	1	2	3	4	5	6	7	
Completely Disagree	☐	☐	☐	☐	☐	☐	☐	**Completely Agree**

I feel less worried about the operation after my consultation:

	1	2	3	4	5	6	7	
Completely Disagree	☐	☐	☐	☐	☐	☐	☐	**Completely Agree**

I feel the consultation was personal to me:

	1	2	3	4	5	6	7	
Completely Disagree	☐	☐	☐	☐	☐	☐	☐	**Completely Agree**

I was given enough time to discuss what is important to me:

	1	2	3	4	5	6	7	
Completely Disagree	☐	☐	☐	☐	☐	☐	☐	**Completely Agree**

The consultation met my emotional needs:

	1	2	3	4	5	6	7	
Completely Disagree	☐	☐	☐	☐	☐	☐	☐	**Completely Agree**

3DCC Study

Questionnaire 3

I was made aware of other options for treating my disease:

✗	**Completely Disagree**	1 ☐	2 ☐	3 ☐	4 ☐	5 ☐	6 ☐	7 ☐	**Completely Agree** ✓

I felt the doctor was knowledgeable about my procedure and treatments:

✗	**Completely Disagree**	1 ☐	2 ☐	3 ☐	4 ☐	5 ☐	6 ☐	7 ☐	**Completely Agree** ✓

I felt the nurse was knowledgable about my operation and treatments:

✗	**Completely Disagree**	1 ☐	2 ☐	3 ☐	4 ☐	5 ☐	6 ☐	7 ☐	**Completely Agree** ✓

Overall I am satisfied by how my disease and operation has been explained:

✗	**Completely Disagree**	1 ☐	2 ☐	3 ☐	4 ☐	5 ☐	6 ☐	7 ☐	**Completely Agree** ✓

9.1.1.1.1.1.1.8 Appendix 6.3 Traditional Decisional Conflict score

3DCC Study
Questionnaire 4

St Mark's Hospital

NHS
London North West University Healthcare
NHS Trust

Traditional Decisional Conflict Score

Pre-consultation ☐ Post-consultation ☐

	Srongly Agree	Agree	Neither agree nor disagree	Disagree	Strongly Disagree
I know which options are available to me.	☐	☐	☐	☐	☐
I know the benefits of each option.	☐	☐	☐	☐	☐
I know the risks and side effects of each option.	☐	☐	☐	☐	☐
I am clear about which benefits matter most to me.	☐	☐	☐	☐	☐
I am clear about which risks and side effects matter most to me.	☐	☐	☐	☐	☐
I am clear about which is more important to me (the benefits or the risks and side effects).	☐	☐	☐	☐	☐
I have enough support from others to make a choice.	☐	☐	☐	☐	☐
I am choosing without pressure from others.	☐	☐	☐	☐	☐
I have enough advice to make a choice.	☐	☐	☐	☐	☐
I am clear about the best choice for me.	☐	☐	☐	☐	☐
I feel sure about what to choose.	☐	☐	☐	☐	☐
This decision is easy for me to make.	☐	☐	☐	☐	☐
I feel I have made an informed choice.	☐	☐	☐	☐	☐
My decision shows what is important to me.	☐	☐	☐	☐	☐
I expect to stick with my decision.	☐	☐	☐	☐	☐
I am satisfied with my decision.	☐	☐	☐	☐	☐

9.1.1.1.1.1.1.9 *Appendix 6.4 Pelvic Exenteration Lexicon definitions*

Type	Code	Description	Left (L)	Right (R)
Posterior	P1	Presacral		
	P2	HiSS (High Subcortical Sacrectomy)		
	P3	Low sacrectomy (≤S3)		
	P4	High sacrectomy (≥S2)		
	P5	Sacrectomy requiring stabilisation		
Anterior	A1	Partial cystectomy		
	A2	Ureteric resection with reimplantation		
	A3	Total cystectomy or radical cystoprostatectomy		
	A4	Cystectomy with pubic bone resection		
	A5	Cystectomy with complete penectomy		
Central	C1	Rectum or TAH/BSO		
	C2	Rectum+/-TAH/BSO/partial vaginectomy or seminal vesicle/ partial or complete prostatectomy		
	C3	Rectum + TAH/oophorectomy + total vaginectomy		
Pelvic sidewall				
Vessels	SV1	Lymphadenectomy	L	R
	SV2	Distal branches of internal iliac artery	L	R
	SV3	Proximal internal iliac artery and vein	L	R
	SV4	External iliac artery or vein +/- internal iliac artery or vein	L	R
Nerves	SN1	Obturator nerve	L	R
	SN2	Single nerve root	L	R
	SN3	Multiple nerve roots (S2 or below/partial sciatic nerve resection preserving L5/S1)	L	R
	SN4	Multiple nerve roots (S1 and below/partial sciatic nerve resection preserving L5 nerve root)	L	R
	SN5	Complete sciatic nerve including lumbosacral trunk resection (include L5 nerve root) or more extensive notch clearance	L	R
Pelvic floor/muscles	PM1	Levator Ani, sacral ligaments and muscles +Ischial spine	L	R
	PM2	Levator ani, sacra ligaments and muscles + ischial spine	L	R
	PM3	Iliacus/ iliopsoas resection/Iliac crest resection	L	R
Reconstruction	F1	Perineal flap reconstruction used, please state type		
	F2	Urological reconstruction please state type		
Additional	E1	Common iliac lymphadenectomy	L	R
	E2	Para-aortic lymphadenectomy		
	E3	Femoral nerve resection	L	R
	E4	Common iliac artery or vein resection	L	R
	E5	Other not included above, please state.		